VOLUME 18 NUMBER 6 JUNE 2012
www.nature.com/naturemedicine

nature medicine

Subverting FOXO3a to foster metastasis

Atherogenic lipoproteins inhibit angiogenesis

A culprit for diabetic pain

2012 AEGEAN CONFERENCES MEETINGS

Linking the international scientific community
Bringing the humanity scholars together

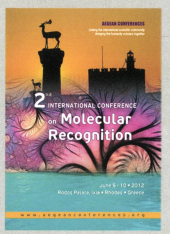

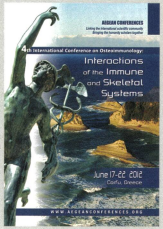

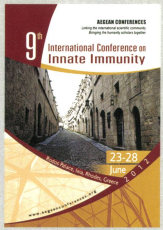

www.aegeanconferences.org

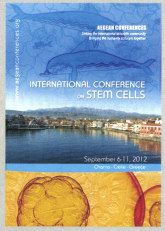

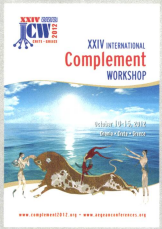

Upcoming Events

- 2nd International Conference on Molecular Recognition, June 5 - 10, 2012
- 10th International Conference on Pathways, Networks, and Systems Medicine, June 10 - 15, 2012
- 4th International Conference on Osteoimmunology: Interactions of the Immune and Skeletal Systems, June 17 - 22, 2012
- 9th International Conference on Innate Immunity, June 23 - 28, 2012
- 2nd International Conference on Model Hosts, September 1 - 6, 2012
- 1st International Conference on Stem Cells, September 6 - 11, 2012
- Tumor Microenvironment and Cellular Stress: Signaling, Metabolism, Imaging and Therapeutic Targets, October 4 - 9, 2012
- XXIV International Complement Workshop, October 10 - 15, 2012

VOLUME 18 NUMBER 6 JUNE 2012

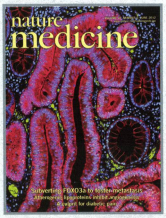

In this issue, Tenbaum *et al.* (p 892) uncover a malignant crosstalk between activated β-catenin and FOXO signaling that promotes metastasis of colon tumors, a potential negative outcome of targeted therapy. The cover shows a confocal microscopy image of a double immunofluorescence staining for β-catenin (red), FOXO3a (green) and Hoechst (blue) in a paraffin section of a human colon adenoma. Image courtesy of Irene Chicote and Héctor G. Palmer, Stem Cells and Cancer Laboratory, Vall d'Hebron Institute of Oncology, Barcelona, Spain.

Researchers unleash a species-spanning approach to biomedicine (p 847)

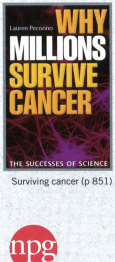

Surviving cancer (p 851)

nature publishing group

nature medicine

EDITORIAL

835 **Beyond cost considerations**

NEWS

837 **Clinical trial website struggles to serve as research data hub**
838 **Pharma backs latest attempt at a global health R&D treaty**
839 **Paper reveals new channels for worry over long QT syndrome**
839 **Panel proposes framework for FDA to evaluate drug risks**
840 **Drugs targeting mGluR5 receptor offer 'fragile' hope for autism**
841 **Recommendation of HIV test brings diagnostic dilemma home**
842 **Sequencing cells one at a time offers singular insight into cancer**
842 **Cancer drug's survivin suppression called into question**
843 **A history of drugs on the weight list**
844 **NEWS IN BRIEF**
846 **Q&A:** Joseph Schwartz
847 **NEWS FEATURE:** The vetting process
850 **OPINION:** Take Russia to 'task' on bioweapons transparency

BOOK REVIEW

851 **Why Millions Survive Cancer: The Successes of Science**
Lauren Pecorino
Reviewed by Bruce Zetter

NEWS AND VIEWS

853 **Melanoma exosomes: messengers of metastasis**
Rajasekharan Somasundaram & Meenhard Herlyn ▸*see also p 883*

854 **FOXO3a and β-catenin co-localization: double trouble in colon cancer?**
Yibing Yan & Mark R Lackner ▸*see also p 892*

856 **Nicotine: linking smoking to abdominal aneurysms**
Koichi Sugamura & John F Keaney Jr ▸*see also p 902*

858 **Peroxiredoxin sets the brain on fire after stroke**
Lidia Garcia-Bonilla & Costantino Iadecola ▸*see also p 911*

860 **New clues to bariatric surgery's benefits**
David A Sarruf, Susan Bonner-Weir & Michael W Schwartz ▸*see also p 950*

861 **Ephrin receptor: a door to KSHV infection**
Chris Boshoff ▸*see also p 961*

Nature Medicine (ISSN 1078-8956) is published monthly by Nature Publishing Group, a trading name of Nature America Inc. located at 75 Varick Street, Fl 9, New York, NY 10013-1917. Periodicals postage paid at New York, NY and additional mailing post offices. **Editorial Office:** 75 Varick Street, Fl 9, New York, NY 10013-1917. Tel: (212) 726 9325, Fax: (212) 683 5751. **Annual subscription rates:** USA/Canada: US$225 (personal), US$4,048 (institution). Canada add 7% GST #140911795rt001; Euro zone: €287 (personal), €3,214 (institution); Rest of world (excluding China, Japan, Korea): £185 (personal), £2,077 (institution); Japan: Contact NPG Nature Asia-Pacific, Chiyoda Building, 2-37 Ichigayatamachi, Shinjuku-ku, Tokyo 162-0843, Tel: 81 (03) 3267 8751, Fax: 81 (03) 3267 8746. **POSTMASTER:** Send address changes to *Nature Medicine*, Subscriptions Department, 75 Varick Street, 9th Floor, New York, NY 10013-1917. **Authorization to photocopy** material for internal or personal use, or internal or personal use of specific clients, is granted by Nature Publishing Group to libraries and others registered with the Copyright Clearance Center (CCC) Transactional Reporting Service, provided the relevant copyright fee is paid direct to CCC, 222 Rosewood Drive, Danvers, MA 01923, USA. Identification code for *Nature Medicine*: 1078-8956/04. **Back issues:** US$45, Canada add 7% for GST. CPC PUB AGREEMENT #40032744. Printed on acid-free paper by The Sheridan Press, Hanover, PA, USA. Copyright © 2012 Nature Publishing Group. Printed in USA.

SciCafé 2012

nature biotechnology

nature medicine

SciBX
Science-Business eXchange

Exclusive forum for the investment community that showcases the very best up and coming research.

Congratulations to the presenters at Nature Publishing Group's SciCafe!
San Francisco, March 1st, 2012

Daniel Nomura –
University of California,
Berkeley

Salvatore Albani –
Sanford Burnham Medical
Research Institute

We would like to acknowledge the generous support from

MERCK & CO., INC.
Whitehouse Station, N.J., U.S.A.

AMGEN

Investigators in the Boston, San Francisco or London areas interested in presenting at the SciCafé should send their applications to **scicafe@us.nature.com**. Applications should provide in 1,000 words a clear and brief description of the commercial potential of your work and any associated intellectual property, three peer-reviewed papers most relevant to your research and contact details.

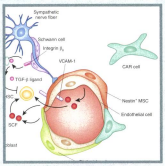

A closer look at the hematopoietic niche (p 864)

BETWEEN BEDSIDE AND BENCH

THE SECRETS OF THE BONE MARROW NICHE

864 **Enigmatic niche brings challenge for HSC expansion**
Yuya Kunisaki & Paul S Frenette

865 **Metabolic priming for AML**
Rushdia Z Yusuf, Ying-Hua Wang & David T Scadden

868 **RESEARCH HIGHLIGHTS**

REVIEW

871 **Taming lupus—a new understanding of pathogenesis is leading to clinical advances**
Z Liu & A Davidson

ARTICLES

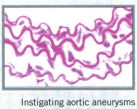

Instigating aortic aneurysms (pp 856 and 902)

883 **Melanoma exosomes educate bone marrow progenitor cells toward a pro-metastatic phenotype through MET**
H Peinado, M Alečković, S Lavotshkin, I Matei, B Costa-Silva, G Moreno-Bueno, M Hergueta-Redondo, C Williams, G García-Santos, C M Ghajar, A Nitadori-Hoshino, C Hoffman, K Badal, B A Garcia, M K Callahan, J Yuan, V R Martins, J Skog, R N Kaplan, M S Brady, J D Wolchok, P B Chapman, Y Kang, J Bromberg & D Lyden
see also p 853

892 **β-catenin confers resistance to PI3K and AKT inhibitors and subverts FOXO3a to promote metastasis in colon cancer**
S P Tenbaum, P Ordóñez-Morán, I Puig, I Chicote, O Arqués, S Landolfi, Y Fernández, J R Herance, J D Gispert, L Mendizabal, S Aguilar, S R y Cajal, S Schwartz Jr, A Vivancos, E Espín, S Rojas, J Baselga, J Tabernero, A Muñoz & H G Palmer *see also p 854*

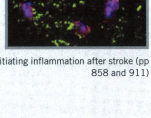

Initiating inflammation after stroke (pp 858 and 911)

902 **Activation of AMP-activated protein kinase α2 by nicotine instigates formation of abdominal aortic aneurysms in mice *in vivo***
S Wang, C Zhang, M Zhang, B Liang, H Zhu, J Lee, B Viollet, L Xia, Y Zhang & M-H Zou
see also p 856

911 **Peroxiredoxin family proteins are key initiators of post-ischemic inflammation in the brain**
T Shichita, E Hasegawa, A Kimura, R Morita, R Sakaguchi, I Takada, T Sekiya, H Ooboshi, T Kitazono, T Yanagawa, T Ishii, H Takahashi, S Mori, M Nishibori, K Kuroda, S Akira, K Miyake & A Yoshimura *see also p 858*

918 **Retinaldehyde dehydrogenase 1 regulates a thermogenic program in white adipose tissue**
F W Kiefer, C Vernochet, P O'Brien, S Spoerl, J D Brown, S Nallamshetty, M Zeyda, T M Stulnig, D E Cohen, C R Kahn & J Plutzky

926 **Methylglyoxal modification of $Na_v1.8$ facilitates nociceptive neuron firing and causes hyperalgesia in diabetic neuropathy**
A Bierhaus, T Fleming, S Stoyanov, A Leffler, A Babes, C Neacsu, S K Sauer, M Eberhardt, M Schnölzer, F Lasischka, W L Neuhuber, T I Kichko, I Konrade, R Elvert, W Mier, V Pirags, I K Lukic, M Morcos, T Dehmer, N Rabbani, P J Thornalley, D Edelstein, C Nau, J Forbes, P M Humpert, M Schwaninger, D Ziegler, D M Stern, M E Cooper, U Haberkorn, M Brownlee, P W Reeh & P P Nawroth

nature REVIEWS CANCER

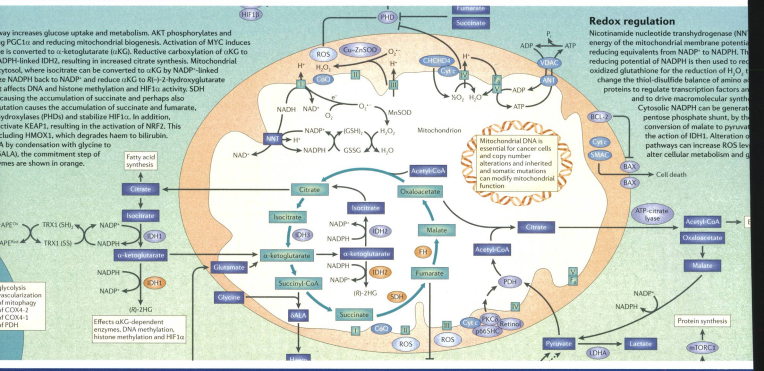
Redox regulation
Nicotinamide nucleotide transhydrogenase (NN
energy of the mitochondrial membrane potentia
reducing equivalents from NADP+ to NADPH. Th
reducing potential of NADPH is then used to re
oxidized glutathione for the reduction of H2O2 t
change the thiol–disulfide balance of amino a
proteins to regulate transcription factors an
and to drive macromolecular synth
Cytosolic NADPH can be generat
pentose phosphate shunt, by th
conversion of malate to pyruva
the action of IDH1. Alteration o
pathways can increase ROS lev
alter cellular metabolism and g
Mitochondrion
Mitochondrial DNA is essential for cancer cells and copy number alterations and inherited and somatic mutations can modify mitochondrial function
Cell death
Fatty acid synthesis
Effects αKG-dependent enzymes, DNA methylation, histone methylation and HIF1α
Protein synthesis

FREE POSTER

Mitochondrial function and cancer

Author: Douglas C. Wallace

This Poster highlights some recent discoveries that have led to a renewed interest in the function of mitochondria in cancer cells. Mitochondria carry out a number of crucial functions in cells and these can be altered through mutations in either the nuclear DNA or the mitochondrial DNA.

Access the Poster FREE online!
www.nature.com/nrc/posters/mitochondria

This Poster is freely available thanks to sponsorship from

abcam® discover more

nature publishing group npg

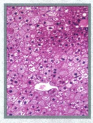

Epigenetic control of glucose production (p 934)

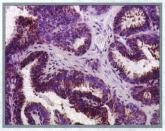

An entry receptor for a herpesvirus (pp 861 and 961)

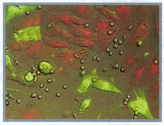

Directing immune killing of cancer (p 980)

934 **Hepatic Hdac3 promotes gluconeogenesis by repressing lipid synthesis and sequestration**
Z Sun, R A Miller, R T Patel, J Chen, R Dhir, H Wang, D Zhang, M J Graham, T G Unterman, G I Shulman, C Sztalryd, M J Bennett, R S Ahima, M J Birnbaum & M A Lazar

943 **NF-κB–inducing kinase (NIK) promotes hyperglycemia and glucose intolerance in obesity by augmenting glucagon action**
L Sheng, Y Zhou, Z Chen, D Ren, K W Cho, L Jiang, H Shen, Y Sasaki & L Rui

LETTERS

950 **Jejunal nutrient sensing is required for duodenal-jejunal bypass surgery to rapidly lower glucose concentrations in uncontrolled diabetes**
D M Breen, B A Rasmussen, A Kokorovic, R Wang, G W C Cheung & T K T Lam
see also p 860

956 **A high-throughput drug screen for *Entamoeba histolytica* identifies a new lead and target**
A Debnath, D Parsonage, R M Andrade, C He, E R Cobo, K Hirata, S Chen, G García-Rivera, E Orozco, M B Martínez, S S Gunatilleke, A M Barrios, M R Arkin, L B Poole, J H McKerrow & S L Reed

961 **The ephrin receptor tyrosine kinase A2 is a cellular receptor for Kaposi's sarcoma–associated herpesvirus**
A S Hahn, J K Kaufmann, E Wies, E Naschberger, J Panteleev-Ivlev, K Schmidt, A Holzer, M Schmidt, J Chen, S König, A Ensser, J Myoung, N H Brockmeyer, M Stürzl, B Fleckenstein & F Neipel *see also p 861*

967 **ApoB-containing lipoproteins regulate angiogenesis by modulating expression of VEGF receptor 1**
I Avraham-Davidi, Y Ely, V N Pham, D Castranova, M Grunspan, G Malkinson, L Gibbs-Bar, O Mayseless, G Allmog, B Lo, C M Warren, T T Chen, J Ungos, K Kidd, K Shaw, I Rogachev, W Wan, P M Murphy, S A Farber, L Carmel, G S Shelness, M L Iruela-Arispe, B M Weinstein & K Yaniv

TECHNICAL REPORTS

974 **Development of a new hydrogen peroxide–based vaccine platform**
I J Amanna, H-P Raué & M K Slifka

980 **Monoclonal TCR-redirected tumor cell killing**
N Liddy, G Bossi, K J Adams, A Lissina, T M Mahon, N J Hassan, J Gavarret, F C Bianchi, N J Pumphrey, K Ladell, E Gostick, A K Sewell, N M Lissin, N E Harwood, P E Molloy, Y Li, B J Cameron, M Sami, E E Baston, P T Todorov, S J Paston, R E Dennis, J V Harper, S M Dunn, R Ashfield, A Johnson, Y McGrath, G Plesa, C H June, M Kalos, D A Price, A Vuidepot, D D Williams, D H Sutton & B K Jakobsen

NATURE MEDICINE CLASSIFIED

See back pages.

nature.com scientificreports

Keep your research moving

Publishing technically sound, open-access research articles on nature.com, *Scientific Reports* is the fast, efficient way to get your paper noticed – whatever your subject area.

Submit today!

nature.com/scientificreports

nature publishing group npg

nature medicine

www.nature.com/naturemedicine

EDITORIAL OFFICE medicine@us.nature.com
75 Varick Street, Fl 9, New York, NY 10013-1917
Tel: (212) 726 9325, Fax: (212) 683 5751
Chief Editor: Juan Carlos López
Senior News Editor: Roxanne Khamsi
News Editor: Elie Dolgin
Editorial Intern, News: Rebecca Hersher
Associate Editors, Reviews and News and Views: Carolina Pola, Meera Swami
Senior Editors, Research Manuscripts: Michael Basson, Eva Chmielnicki, Alison Farrell, Randy Levinson
Associate Editors, Research Manuscripts: Victoria Aranda, Kevin Da Silva
Editor, Technical Reports: Diane Gershon
Copy Editors: Katherine Gora, Heidi Reinholdt
Senior Production Editor: Matt Hansen
Production Editor: Junel Wooten
Senior Illustrator/Cover Design: Katie Vicari
Illustrator: Marina Corral
Editorial Assistant: Somaliyah Al-Mahdi

MANAGEMENT OFFICES
NPG New York
75 Varick Street, Fl 9, New York, NY 10013-1917
Tel: (212) 726 9200, Fax: (212) 696 9006
Publisher: Melanie Brazil
Executive Editor: Veronique Kiermer
Chief Technology Officer: Howard Ratner
Commercial Director/EVP of Sales: Dean Sanderson
Head of Nature Research & Reviews Marketing: Sara Girard
Marketing Manager: Samantha Sarullo
Production Coordinator: Diane Rios
Head of Web Services: Anthony Barrera
Web Production Editor: Eddie Jones

NPG London
The Macmillan Building, 4 Crinan Street, London N1 9XW
Tel: 44 207 833 4000, Fax: 44 207 843 4996
Managing Director: Steven Inchcoombe
Publishing Director: Alison Mitchell
Editor-in-Chief, Nature Publications: Philip Campbell
Director of Web Publishing: Dan Pollock

NPG Nature Asia-Pacific
Chiyoda Building, 2-37 Ichigayatamachi, Shinjuku-ku, Tokyo 162-0843
Tel: 81 3 3267 8751, Fax: 81 3 3267 8746
Publishing Director — Asia-Pacific: David Swinbanks
Associate Director: Antoine E. Bocquet
Manager: Koichi Nakamura
Operations Director: Hiroshi Minemura
Marketing Manager: Masahiro Yamashita
Asia-Pacific Sales Director: Kate Yoneyama
Asia-Pacific Sales Manager: Ken Mikami

DISPLAY ADVERTISING display@us.nature.com (US/Canada)
display@nature.com (Europe)
nature@natureasia.com (Asia)
Global Head of Advertising and Sponsorship: Andrew Douglas, Tel: 44 207 843 4975, Fax: 44 207 843 4996
Global Head of Display Advertising and Sponsorship: Gerard Preston, Tel: 44 207 843 4965, Fax: 44 207 843 4749
Asia-Pacific Sales Director: Kate Yoneyama, Tel: 81 3 3267 8765, Fax: 81 3 3267 8746
Display Account Managers:
New England: Sheila Reardon, Tel: (617) 399 4098, Fax: (617) 426 3717
New York/Mid-Atlantic/Southeast: Jim Breault, Tel: (212) 726 9334, Fax: (212) 696 9481
Midwest: Mike Rossi, Tel: (212) 726 9255, Fax: (212) 696 9481
West Coast: George Lui, Tel: (415) 781 3804, Fax: (415) 781 3805
Germany/Switzerland/Austria: Sabine Hugi-Fürst, Tel: 41 52761 3386, Fax: 41 52761 3419
UK/Ireland/Scandinavia/Spain/Portugal: Evelina Rubio-Hakansson, Tel: 44 207 843 4079, Fax: 44 207 843 4749
France/Belgium/The Netherlands/Luxembourg/Italy/Israel/Other Europe: Nicola Wright, Tel: 44 207 843 4959, Fax: 44 207 843 4749
Asia-Pacific Sales Manager: Ken Mikami, Tel: 81 3 3267 8765, Fax: 81 3 3267 8746
Greater China/Singapore: Gloria To, Tel: 852 2811 7191, Fax: 852 2811 0743

SPONSORSHIP g.preston@nature.com
Global Head of Sponsorship: Gerard Preston, Tel: 44 207 843 4965, Fax: 44 207 843 4749
Business Development Executive: David Bagshaw, Tel: (212) 726 9215, Fax: (212) 696 9591
Business Development Executive: Patrick Murphy, Tel: (617) 475 9216, Fax: (617) 494 4960
Business Development Executive: Reya Silas, Tel: 44 207 843 4977, Fax: 44 207 843 4996
Business Development Manager: Will Piper, Tel: 44 207 014 4181

NATUREJOBS naturejobs@us.nature.com (US/Canada)
naturejobs@nature.com (Europe)
nature@natureasia.com (Asia)
US Sales Manager: Ken Finnegan, Tel: (212) 726 9248, Fax: (212) 696 9482
European Sales Manager: Dan Churchward, Tel: 44 207 843 4966, Fax: 44 207 843 4596
Asia-Pacific Sales & Business Development Manager: Yuki Fujiwara, Tel: 81 3 3267 8765, Fax: 81 3 3267 8752

SITE LICENSE BUSINESS UNIT
Americas: Tel: (888) 331 6288 institutions@us.nature.com
Asia/Pacific: Tel: 81 3 3267 8751 institutions@natureasia.com
Australia/New Zealand: Tel: 61 3 9825 1160 nature@macmillan.com.au
India: Tel: 91 124 2881054/55 npgindia@nature.com
ROW: Tel: 44 207 843 4759 institutions@nature.com

CUSTOMER SERVICE www.nature.com/help
Senior Global Customer Service Manager: Gerald Coppin
For all print and online assistance, please visit www.nature.com/help
Purchase subscriptions:
Americas: *Nature Medicine*, Subscription Dept., 75 Varick Street, Fl 9, New York, NY 10013-1917, USA. Tel: (866) 363 7860, Fax: (212) 334 0879
Europe/ROW: *Nature Medicine*, Subscription Dept., Macmillan Magazines Ltd., Brunel Road, Houndmills, Basingstoke RG21 6XS, United Kingdom. Tel: 44 1256 329 242, Fax: 44 1256 812 358
Asia-Pacific: *Nature Medicine*, NPG Nature Asia-Pacific, Chiyoda Building, 2-37 Ichigayatamachi, Shinjuku-ku, Tokyo 162-0843. Tel: 81 3 3267 8751, Fax: 81 3 3267 8746
India: *Nature Medicine*, NPG India, 3A, 4th Floor, DLF Corporate Park, Gurgaon 122002, India. Tel: 91 124 2881054/55, Fax: 91 124 2881052

REPRINTS reprints@us.nature.com
Nature Medicine, Reprint Department, Nature Publishing Group, 75 Varick Street, Fl 9, New York, NY 10013-1917, USA.
For commercial reprint orders of 600 or more, please contact:
UK Reprints: Tel: 44 1256 302 923, Fax: 44 1256 321 531
US Reprints: Tel: (617) 494 4900, Fax: (617) 494 4960

EDITORIAL

nature medicine

Beyond cost considerations

Novartis's recent legal action against the UK National Health Service to prevent the off-label use of Avastin for macular degeneration challenges the current regulatory structures ensuring accountability for the safety and quality of drugs.

In April, Novartis announced that it would seek a judicial review to overturn reimbursement for Avastin (bevacizumab), a monoclonal antibody from Genentech/Roche that is prescribed by the UK National Health Service (NHS) for the treatment of the eye condition wet age-related macular degeneration (AMD). Avastin isn't officially approved for this condition in the UK, and Novartis asserts that its use for AMD undermines regulations meant to ensure patient safety.

Yet, since 2011, the NHS has allowed the reimbursement of off-label Avastin as a cheaper alternative to the licensed AMD therapy Lucentis (ranibizumab). Lucentis, also developed by Genentech and marketed outside of the US by Novartis, costs approximately £1,250 ($1,950) per injection, in contrast to the £30–50 cost per injection of Avastin.

Avastin and Lucentis are both monoclonal antibodies targeting vascular endothelial growth factor, which drives the pathological growth of abnormal blood vessels in AMD. While Lucentis was being developed, some ophthalmologists prescribed Avastin (which had already been approved for intravenous use as a cancer therapy) for AMD with encouraging results. Even after the approval of Lucentis, Avastin continued to also be used as an AMD therapy in many countries because of its lower cost. In the US, decisions about the use of Avastin and Lucentis have depended on individual circumstances and the policies of health insurance providers, leading to increasing use of Avastin (*BMJ* **344**, e2941, 2012).

In the UK, Lucentis is recommended for the treatment of wet AMD by the National Institute for Health and Clinical Excellence (NICE), which makes its recommendations on drugs approved for a particular indication. Until very recently, no large comparative-efficacy trials for Lucentis and Avastin had been carried out. Typically, comparative-efficacy trials would be carried out with the assistance of an industry partner, but Roche has been unwilling to consider licensing Avastin for AMD or to conduct clinical studies to compare Lucentis and Avastin. But two such publicly funded trials have now indicated that both therapies have similar safety and efficacy profiles (*Ophthalmology* doi:0.1016/j.ophtha.2012.03.053, 2012; *Ophthalmology* doi:10.1016/j.ophtha2012.04.015, 2012).

Novartis has argued that the higher incidence of side effects in the individuals treated with Avastin (40%) compared with Lucentis (32%) in one of the trials raises serious safety concerns for using Avastin for AMD. But it's unclear whether these differences can be attributed to the treatments, as the trial was carried out in patients with a median age of over 80 years old, who may be prone to other medical problems. So, further comparative efficacy trials will be necessary to satisfy all parties. Nevertheless, in the UK, NICE has already been asked to consider a formal appraisal of Avastin for AMD, using the data from the two recent trials in this evaluation.

This isn't the first time Novartis has taken legal action to restrict Avastin use: they previously attempted to block off-label use of Avastin for AMD in Germany. In the US, Genentech tried to stop the supply of Avastin to pharmacies that were reformulating the drug for use in AMD and has also made payments to US doctors who administer large numbers of Lucentis injections to discourage the use of Avastin (http://www.nytimes.com/2010/11/04/business/04eye.html?pagewanted=all 3 November 2010). In response to the latest comparative trial results, Novartis is in discussions with the Department of Health and NICE about pricing Lucentis in the UK more competitively. In these discussions, Novartis may ask NICE to widen reimbursement for Lucentis for its approved uses in other eye conditions, such as diabetic macular edema and macular edema secondary to retinal vein occlusion, conditions for which NICE currently does not support reimbursement.

These attempts of drug companies to protect their revenue stream seem hard to swallow. The NHS could save an estimated £84.5 million a year by switching from Lucentis to Avastin for the treatment of AMD. Given the current economic climate, healthcare providers should be allowed to investigate the possibility of more cost-effective options without obstructions from companies.

This case points to a gray area in the existing regulatory and access process for drugs. Typically, regulatory agencies such as the US Food and Drug Administration (FDA) and the European Medicines Agency (EMA) play a key part in evaluating drug efficacy and safety but do not necessarily make calls on access to drugs. Instead, health technology assessors, such as NICE in the UK and the Centers for Medicare and Medicaid Services (CMS) in the US, make recommendations about drug coverage on the basis of cost-benefit considerations. Although these organizations helped spur support for the two publically funded comparative trials, their interests are distinct from those of drug regulatory agencies: the cost of a drug is ignored by the FDA and EMA but is a major factor for the CMS and NICE.

If access to Avastin for AMD treatment is broadened, a regulatory structure will be needed to ensure accountability for the safety and efficacy of this type of off-label use, as well as guidelines to allow clinicians and patients to make informed choices about the potential treatment options. Although drug regulatory agencies could have a potential role in devising such frameworks, under the current system, it is difficult to see how they can intervene to evaluate off-label use without a pharmaceutical sponsor submitting its product for expanded licensing. Who should take on these responsibilities? Collaborative efforts from many different parties, including healthcare providers, health technology assessors and perhaps also professional bodies such as the UK Royal College of Ophthalmologists, will be required to ensure that these responsibilities to prescribing physicians and to patients are met.

nature REVIEWS DRUG DISCOVERY

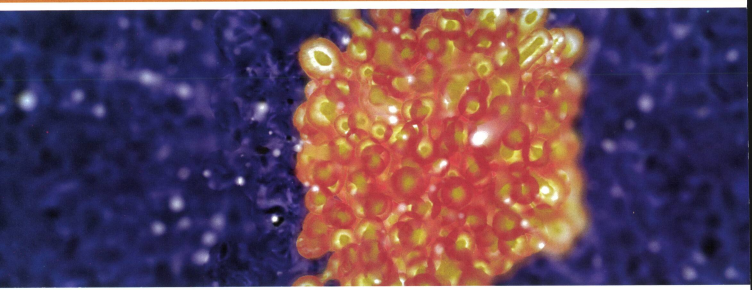

Poster and Video Animation on Cancer Immunotherapies

Efforts to harness the immune system to treat cancer have been pursued for more than a century, dating back to William B. Coley's discovery in 1898 that bacteria and bacterial products can induce antitumour immunity. Progress was slow for many decades, but the recent clinical success of several anticancer immunotherapies has provided a boost to the field. Approaches to induce an antitumor response can be broadly subdivided into non-antigen-specific or antigen-specific categories. Examples of anticancer therapeutics in both categories — such as the immune checkpoint inhibitor ipilimumab and the therapeutic vaccine sipuleucel-T — have recently received regulatory approval, and several other agents are in clinical trials.

This poster and video describe various immunotherapeutic strategies, including non-antigen-specific approaches such as nonspecific immune stimulation and immune checkpoint blockade, and antigen-specific approaches such as adoptive cell transfer and vaccination approaches.

Access the poster and video by visiting:
www.nature.com/nrd/posters/cancerimmuno

Sponsored by BAVARIAN NORDIC Dendreon

nature publishing group npg

Home schooled:
Over-the-counter test offers in-home HIV diagnosis

Weight watchers:
A timeline of antiobesity drugs in the US

A zoo out there:
A new species-spanning approach to biomedical research

Clinical trial website struggles to serve as research data hub

It's been 15 years since the US government mandated the creation of ClinicalTrials.gov, and the registry website has hit some growing pains in its teens. The web portal—a crucial resource for physicians wanting to place a patient in a trial or researchers doing meta-analyses on drug effectiveness—struggles to get researchers to report results and is being outshone by more dynamic trial-recruitment sites run by patient advocacy groups. Now, new legislation has been proposed to institute harsher penalties for failing to upload the outcomes of certain types of trials in the registry.

A report published earlier this year found that only 22% of the 738 registered trials on the website that wrapped up in 2009 and were required to report results within a year actually did so (*BMJ* **344**, 7373–7379, 2012). The US Food and Drug Administration (FDA) maintains that the study overestimated noncompliance, based on data only the agency has access to, but criticisms continue. In May, an editorial published in the *Journal of the American Medical Association* deemed the registry to be "coming up short" on the requirements for data collection, as stipulated in the FDA Amendments Act of 2007 (*JAMA*, **307**, 1861–1864, 2012).

In the same issue of *JAMA*, an analysis by a group that includes Deborah Zarin, director of ClinicalTrials.gov and assistant director for clinical research projects at the US National Library of Medicine in Bethesda, Maryland, paints a rosier picture of progress. For instance, the percentage of trials not reporting either enrollment number or type decreased from 34% between October 2004 and late 2007 to less than 2% between late 2007 and September 2010. However, the same paper also found that the proportion of studies that lacked information about their primary objectives inched up from around 5% to nearly 7% over the same time period (*JAMA*, **307**, 1838–1847, 2012).

Individuals concerned about missing data in ClinicalTrials.gov say better enforcement of the current regulations, as well as harsher penalties for failing to follow regulations, could make a difference. Currently, "penalties are tiny and not enforced," says Kay Dickersin, director of the Center for Clinical Trials at Johns Hopkins University Bloomberg School of Public Health in Baltimore and coauthor of the *JAMA* editorial.

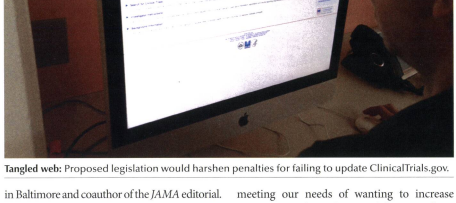

Roxanne Khamsi

Tangled web: Proposed legislation would harshen penalties for failing to update ClinicalTrials.gov.

Last month, Congressman Tom Reed, a Republican from New York, introduced legislation in the US House of Representatives that would oblige all clinical trials to register and report results regardless of whether the outcome of the trial was positive or negative—not just those related to drugs approved by the FDA, as currently required. The proposed bill would also revoke federal funds from applicants that failed to comply and deem them ineligible from receiving future federal grants until they complied with the regulations.

Zarin, for her part, told *Nature Medicine* that the US Department of Human Health and Services is currently in the process of developing proposed additional regulations that it plans to make available for public comment this month.

Impatient patients

To ensure their members have the most up-to-date information, some patient advocacy groups and nonprofit organizations have already taken matters into their own hands, creating disease-specific registries that help people with specific disorders find trials to enroll in. For example, the Alzheimer's Association runs a portal called TrialMatch, and the Michael J. Fox Foundation for Parkinson's Research recently launched its Fox Trial Finder to match patients with Parkinson's to trials.

"We didn't feel that ClinicalTrials.gov was meeting our needs of wanting to increase the number of people in trials," says William Thies, chief medical and scientific officer of the Alzheimer's Association, based in Chicago. The disease advocacy group uses ClinicalTrials.gov to populate its own registry, he explains, but follows up with the trials to make sure the data are accurate and up to date. TrialMatch also includes smaller trials that aren't listed in ClinicalTrials.gov.

Thies doesn't see TrialMatch or other trial registries as taking over from ClinicalTrials.gov, but rather as being supplementary, providing information that is beyond the scope of the government-run site. "The size of ClinicalTrials.gov would make it difficult for patients to navigate," he says, "so we've tried to add a user-friendly front end."

Ultimately, improving ClinicalTrials.gov is in everyone's best interest, says Andrew Prayle, the lead author of the *BMJ* study and a clinical research fellow at the University of Nottingham in the UK. Clinical trial registries prevent the duplication of clinical research, enable meta-analyses and prevent suppression of trial results, he argues.

"Registries are improving," he notes, "but if progress is halted, the goal of a fully transparent and open medical literature and the resulting benefits for evidence-based medicine will not be achieved."

Monica Heger

Pharma backs latest attempt at a global health R&D treaty

Philanthropists, drugmakers and governments all agree: the world's poor are in dire need of new drugs for neglected diseases, but there is not enough money available to develop innovative treatments. Now, a promising global treaty looks set to find a solution—and, unlike previous attempts to reach a similar agreement, this one seems to have the backing of most major players involved in the drug development process.

"A global R&D agreement used to be a crazy idea," says James Love, an advocate for affordable medicines and director of Knowledge Ecology International, a social justice nonprofit based in Washington, DC. "Now it looks more and more inevitable."

The US government is far and away the largest supporter of global health research and development (R&D). According to an April report from the Sydney-based nonprofit research group Policy Cures and the Washington, DC–based umbrella organization Global Health Technologies Coalition, the US contributes around 45% of all money spent on neglected diseases and 70% of all government investment in the area worldwide. Still, that expenditure—around $1.4 billion per year—represents only around 0.01% of the country's gross domestic product (GDP), a tiny fraction that policy experts and health economists hope the rest of the 193 member states of the World Health Organization (WHO) will be willing to match.

Delegates discussed this idea at the WHO's annual assembly in Geneva in late May. Such a move, if adopted, would double the amount of government funding spent internationally on global health R&D, from around $3 billion each year today to more than $6 billion annually. The proposed convention, outlined on 15 May by members of the WHO's Consultative Expert Working Group on Research and Development (CEWG), also calls for participating drug companies that are funded through the initiative to share data about early-stage treatments for neglected disease and for countries to pool their contributions into a central WHO fund, rather than allocating donations individually (*PLoS Med.* **9**, e1001219, 2012).

Commitment issues

Similar treaties were proposed in 2005 and 2009, but both efforts failed to get off the ground after drug companies lobbied hard against proposed patent reforms that could have opened the door to more generics for a wide variety of drugs, even top sellers in the developing world. This time around, however, the proposed treaty would only loosen patent protection on treatments for diseases largely absent in rich nations, such as malaria, Chagas disease or dengue fever. What's more, the latest proposal includes financial incentives for the pharmaceutical industry, including funding to advance early-stage products for neglected diseases that companies already have in their pipelines.

WHO

From treaty to treatments: A global accord through the WHO could help.

Importantly, big pharma now seems to back the measure. "Industry is willing to contribute resources to early stage R&D," says CEWG member Paul Herrling, head of corporate research at the Swiss drug giant Novartis and board chairman of the Singapore-based Novartis Institute for Tropical Diseases. "But to bring those products all the way to the market, they need more than private donors can give."

With pharma largely on board, most global health researchers agree that the main barrier remains persuading the individual member nations to rally around the cause—a difficult task at a time of global austerity measures and belt tightening. "Now we need firm financial commitments from governments," says John-Arne Røttingen, a health economist at the University of Oslo's Institute for Health and Society and chair of the CEWG.

Then comes the challenge of turning talk into action. "We will have to figure out how to build in incentives to make countries comply," says Suerie Moon, a health policy researcher at the Harvard School of Public Health in Boston who coauthored a commentary, also published last month in *PLoS Medicine* (**9**, e1001218), in support of the proposed treaty.

The fate of the CEWG's proposal was still unclear as *Nature Medicine* went to press. But most people involved in the initiative expected the proposal to weather the initial round of discussions at last month's WHO meeting and move toward a committee that will draft formal treaty language based on the CEWG analysis. A full vote could then happen before the end of the year.

Rebecca Hersher

Corrections

In the March 2012 issue, the article entitled "Korea okays stem cell therapies despite limited peer-review data" (*Nat. Med.* **18**, 329, 2012), failed to convey that the 26% improvement in knee function was an additional gain compared to the control group. The sentence should have read: "In an 89-person Korean clinical trial, 26% more people who received the Medipost treatment experienced an improvement in knee function on a widely used cartilage repair assessment scale compared with those who underwent knee surgery alone." The piece also referred to Francis Han by her Korean name, Han Sung-ho, and did not specify that she is in charge of research and development strategy. The error has been corrected in the HTML and PDF versions of the article. Additionally, as a clarification, the cells referred to as 'banked' in the piece are frozen-stored and do not require donor-recipient matching.

In the May 2012 issue, in the piece "New biologic drugs get under the skin of psoriasis'" (*Nat. Med.* **18**, 638, 2012), sales numbers mistakenly cited for the US psoriasis market were actually sales numbers for the G7 (US, UK, France, Germany, Italy, Spain and Japan) markets. The correct numbers for the US market are $2.6 billion in 2010 and more than $5.6 billion in 2020 (rather than $3.9 billion in 2010 and more than $7.4 billion in 2020). The error has been corrected in the HTML and PDF versions of the article.

Paper reveals new channels for worry over long QT syndrome

A new study suggests that the way certain medications trigger a hazardous side effect known as 'long QT syndrome' is more complex than previously thought—a finding that could necessitate changes to drug candidate screening.

Long QT syndrome (LQTS) is a condition marked by a lengthening of the QT interval on an electrocardiogram, typically indicating an excessive lapse between the depolarization and repolarization of the lower chambers of the heart when the organ recharges before the next beat. Worryingly, this condition puts people at higher risk for a kind of irregular heartbeat called torsade de pointes, which can lead to fainting, palpitations and even sudden death.

Some people develop LQTS because they carry one of more than 700 mutations in at least 13 genes. Others, however, develop it after taking certain drugs, especially those that inhibit the enzyme tyrosine kinase. For example, a recent retrospective analysis of 81 trial participants taking Tasigna (nilotinib), a tyrosine kinase inhibitor marketed by the Swiss pharma giant Novartis for the treatment of chronic myeloid leukemia, found that the drug increased the incidence of QT prolongation from 5% at baseline to 11% after treatment (*Haematologica*, doi:10.3324/haematol.2011.058776, 2012).

For years, drugs were thought to induce LQTS because they blocked potassium ion channels in heart cells, thereby delaying the repolarization process through which the heart resets after each beat. But Ira Cohen, a molecular cardiologist from Stony Brook University in New York State, thought the story might be more complicated. "It seemed to us reasonable to ask what other channels might be involved," Cohen says.

He and his colleagues exposed canine heart muscle cells to tyrosine kinase inhibitors and a handful of other drugs known to cause LQTS and discovered that the drug-induced QT prolongation was actually due to inhibition of the phosphoinositide 3-kinase (PI3K) signaling pathway, which affects multiple ion channels, not just the potassium one. Reporting in April in *Science Translational Medicine* (**4**, 131ra50, 2012), they also confirmed the finding by showing that mice bred to have reduced PI3K signaling showed QT prolongation.

"This is a fantastic example of a very complex mechanism underlying acquired long QT that is probably not addressed in safety testing," says Eckhard Ficker, a molecular physiologist at the Case Western Reserve University in Cleveland who was not affiliated with the paper.

Beyond potassium

Currently, the preclinical tests required by the US Food and Drug Administration to screen for QT prolongation primarily focus on potassium channel blocking. Cohen's team's paper may mean that the pharmaceutical industry will have to develop completely new assays. What's more, the findings could also spell trouble for drugs that inhibit PI3K, which is involved in cell division and is a natural target for cancer treatments.

But before the drug industry moves to make sweeping changes to drug screening, scientists should attempt to replicate this PI3K-inhibiting effect with the other drug classes known to cause LQTS, says Dan Roden, a clinical pharmacologist at Vanderbilt University School of Medicine in Nashville, Tennessee. The data from Cohen's paper "are quite strong," Roden says, "but the generalization to the universe of all drug induced-long QT is premature."

In the study, Cohen's team managed to reverse the effects of PI3K inhibition in heart muscle cells by adding the second messenger in the pathway, phosphatidylinositol 3,4,5-triphosphate (PIP3). That raises the possibility that one strategy for counteracting induced LQTS would be to develop an adjuvant that increases PI3K signaling.

If such an adjuvant is successful, that could not only ensure continued use of current medications, but could mean that drugs and drug candidates that were shelved for prolonging the QT interval could be dusted off and reintroduced. "There might be a real renaissance in terms of new drug candidates," Cohen says.

Roxanne Palmer

Panel proposes framework for FDA to evaluate drug risks

The withdrawal of the painkiller Vioxx and other drugs from the market highlights a central challenge faced by regulatory authorities: how to ensure that life-saving therapeutics are available in a timely fashion while still guaranteeing the medicines are safe. It's a difficult task, but one that might be made easier with a more centralized and comprehensive system for drug safety monitoring, according to the US Institute of Medicine (IOM), an independent, nongovernmental organization in Washington, DC.

Under a proposal outlined by the IOM last month, the US Food and Drug Administration (FDA) would compile risk assessments, evidence about adverse side effects, relevant studies and regulatory actions related to each drug on the market in a single, publicly accessible document known as a benefit-risk assessment management plan (BRAMP). (At present, such information is scattered throughout the agency, making it difficult for consumers and health providers to readily access it.) The IOM report also calls for therapies approved on the basis of trials that used surrogate endpoints such as blood pressure, rather than clinical endpoints such as heart attacks, to receive extra scrutiny after they reach pharmacy shelves.

"We should be looking at drugs during their entire market lifetime, with the intensity of scrutiny based on the potential for patient or population harm, periodically revisiting them to make sure there haven't been changes in the risk profiles," says Steven Goodman, co-chair of the IOM committee and a biostatistician at the Stanford University School of Medicine in California.

Current FDA pharmacovigilance efforts don't do a good enough job of anticipating risk, leaving regulators scrambling for information when concerns arise, says Goodman, who notes, "We can't wait for the fires to put them out because there are few good—or fast—options in a moment of crisis."

In a statement, the FDA said that the IOM report mirrored the agency's current programs but that implementing a public repository would pose a financial challenge that might compromise other "critical regulatory activities." FDA officials would not elaborate on what recommendations from the report it might implement or how. "We are now in the process of fully analyzing the report to determine how to implement changes that will have the largest positive impact on public health," Sandy Walsh, FDA spokeswoman, wrote in an email to *Nature Medicine*.

But even if the agency does adopt the IOM plan, that won't completely eliminate problems, says Michael Carome, deputy director for health research at Public Citizen, a research-based advocacy group in Washington, DC. "These recommendations won't [protect against] drugs that end up having serious safety problems from reaching the market because [their] premarket studies were small and not sufficiently powered to detect uncommon or rare safety problems," he says.

Trevor Stokes

Drugs targeting mGluR5 receptor offer 'fragile' hope for autism

A group of drugs that are already racing through clinical trials to treat fragile X syndrome, a rare inherited syndrome that causes both intellectual disability and autistic behaviors, may have even broader usage. Mounting evidence suggests that the drugs, which block a glutamate receptor in the brain called mGluR5, might also work in certain forms of autism that have no known cause. In recent weeks, studies have reported that mGluR5 drugs alleviate some symptoms in mouse models of autism and have found numerous genetic mutations in proteins downstream of mGluR5's signaling in people with the disorder.

"From the beginning, our hope was that insights into the pathophysiology of fragile X would apply to idiopathic autism," says Mark Bear, a neuroscientist at the Massachusetts Institute of Technology in Cambridge who reported in April that blocking mGluR5 reversed the signs of fragile X in a mouse model of the disease (*Neuron* **74**, 49–56, 2012). "So we're thrilled."

In fragile X syndrome, mutations in a signaling molecule known as fragile X mental retardation protein (FMRP) prevent it from performing its normal role of damping mGluR5's activity, among other effects. The resulting constant activation of the receptor, Bear has shown, leads to excess protein production in neurons. This excess protein synthesis—although not fully understood—causes alterations in the structure and function of the neurons. Drugs that target mGluR5 work by putting the brakes back on the receptor and dialing down protein production. And companies see promise in this approach: Roche, Novartis and Seaside Therapeutics—a company founded by Bear—all have mGluR5 antagonists in clinical trials for fragile X.

Until recently, the idea that mutations in mGluR5—or proteins downstream from the receptor—could cause autism independently of fragile X was only a hunch. Now, the idea has become a theory with data to back it up.

In the 25 April issue of *Science Translational Medicine* (**4**, 131ra51, 2012), a team of scientists from the US National Institute of Mental Health (NIMH) in Bethesda, Maryland and the New York–based drug giant Pfizer reported that GRN-529, an mGluR5 antagonist, decreased symptoms of autism in two different mouse models of the disease. The first type of mouse used in the study, an inbred strain, typically shows repetitive grooming—seen by scientists as symbolic of the repetitive behaviors of children with autism—and tend to vocalize and socialize less than other mice. When treated with GNR-529, the mice spent a quarter less time grooming themselves and showed some improvements in social interactions. The second group of mice tested are known for repetitive jumping, also viewed as indicative of the repetitive behaviors seen in people with autism, and jumped less than a third as much after treatment with the mGluR5 antagonist.

"Drugs targeting mGluR5 could have broader applicability in autism."

But, since it's unknown whether either type of mouse has an mGluR5 mutation, the mechanism by which GRN-529 helps them remains unproven. The drug could have broad antianxiety effects, for example, that alleviate some symptoms of autism even if they're not targeting particular mutations in the mGluR5 pathway. "This means that we don't know yet, in humans, which patients would be helped by drugs that work through the mGluR5 pathway," says Jacqueline Crawley, head of the NIMH's Laboratory of Behavioral Neuroscience, who led the study.

Notably, recent sequencing studies on autistic children have also turned up mutations in a number of genes in the mGluR5 network. Publishing in *Neuron* (**74**, 285–299, 2012) on 26 April, geneticist Michael Wigler and his colleagues at the Cold Spring Harbor Laboratory in New York State analyzed the overlap between autism susceptibility genes and those already implicated as being misregulated in fragile X syndrome. They analyzed the overlap between autism susceptibility genes and those already implicated as being misregulated in fragile X syndrome. Of 59 new autism genes they discovered, 14 were associated with FMRP, which is both the protein mutated in fragile X and the upstream regulator of the gene encoding mGluR5.

Variation on a theme

Raymond Kelleher, a neuroscientist at the Massachusetts General Hospital in Boston, took a more targeted look at the issue, inspecting the single-nucleotide variants in 18 mGluR5 pathway genes in 209 people with autism and 300 ethnically matched controls. His team reported in April that the idiopathic autism cases had higher burdens of mGluR5 variants. Three genes in the mGluR5 pathway that were previously implicated in autism associated with diseases such as fragile X and tuberous sclerosis—*TSC1*, *TSC2* and *SHANK3*—were confirmed to be significantly different in the idiopathic autism population. They also found a fourth gene, never before implicated in autism, to be relevant. The gene, *HOMER1*, produces a protein that interacts in the cell with both the SHANK3 protein product and mGluR5 (*PLoS One* 7, e35003, 2012).

"This fits right in with our hypothesis that genetic variation in any members of this pathway could be overrepresented in autism," Kelleher says. "And if modulation of the mGluR5 pathway turns out to be successful in treating fragile X, these sorts of results suggest that the treatment could have broader applicability in autism."

The next step for uncovering the role of mGluR5, researchers agree, is to test inhibitors of the receptor in mouse models of autism that contain genes known to be implicated in the human disease, rather than inbred mouse strains designed for the behavioral phenotype (see *Nat. Med.* **17**, 1324, 2011). But whatever the outcome of those experiments, it's likely that mGluR5 drugs, once approved for fragile X syndrome, will be studied in human clinical trials for autism.

"Mice are not humans, and it would be a mistake to assume that an alteration in mouse behavior predicts human outcomes," says Bear. "But, that being said, right now we have an extremely strong rationale to test these drugs in humans and to cast a very wide net when we do."

Sarah C P Williams

Fragile promise: mGluR5 antagonists in the clinic for the treatment of fragile X.

Company	Drug	Phase
Novartis	AFQ056	3
Roche	RO4917523	2
Seaside Therapeutics	STX107	2

Recommendation of HIV test brings diagnostic dilemma home

Last month, patient advocates hailed the unanimous vote by an advisory committee to the US Food and Drug Administration that recommended that the agency approve the OraQuick In-Home HIV test, an over-the-counter diagnostic that can be taken without medical supervision. If approved, the OraQuick test would be the first home test approved for an infectious disease. But concerns remain about whether the price will render it out of reach of those who need it most and what the test will mean for the handful of individuals participating in HIV vaccine trials.

The OraQuick test, from Pennsylvania-based OraSure Technologies, is a home version of a rapid HIV test already used in many medical centers. The kit includes an instructional booklet and a test stick, which the user swipes along his or her upper and lower gums and contains molecules that react against HIV-specific antibodies produced by the body. Results are ready just 20 minutes later. Two lines on the dipstick signify a positive result, which must be confirmed by a more sensitive test at a clinical laboratory. The company plans to provide a 24-hour hotline so that customers can ask questions or receive counseling, but the phone call is optional.

FDA approval of OraQuick would probably pave the way for other in-home HIV tests. Chembio Diagnostic Systems, based just outside New York City, already plans to seek approval for a home version of its rapid 'Sure Check HIV' test, which requires a drop of blood. Although over-the-counter tests for HIV and hepatitis C are already available from Illinois-based Home Access Health Corporation, both require the consumer to send a blood specimen to a laboratory for analysis and results.

No test is perfect, however, and one major concern is that people who test negative using the OraQuick kit might actually have HIV. In a recent phase 3 trial, OraSure gave the prototype to 5,662 individuals to use in their homes. The results, made public by the company in filing for approval, indicate that only 93% of the 114 individuals infected with HIV received a positive test result. In the clinical setting, the same test is 99% accurate. Why the home test missed so many infections isn't clear. Because the OraQuick test detects HIV-specific antibodies, recently infected individuals may test negative. False positives seemed to be less of a problem; only one uninfected study participant tested positive.

Despite the concern, the committee decided to support the test. "We shouldn't let the perfect be the enemy of the good," J. Brooks Jackson, a committee member and director of pathology at the Johns Hopkins University School of Medicine in Baltimore, said at the FDA advisory committee meeting on 15 May. However, committee members did suggest several changes to the language in the test kit. For example, Susan Buchbinder, a committee member and HIV researcher at the University of California, San Francisco, urged OraSure to clearly state that individuals who have been involved in an HIV vaccine trial should not take the test. A 2010 study found that 42% of HIV vaccine trial participants tested positive for the virus even though they were uninfected, as immunization prompts certain antibodies that are picked up by diagnostics (*JAMA* **304**, 275–283, 2010). Some in the AIDS research community have also noted that the in-home test could jeopardize the scientific integrity of such vaccine trials by making it easier for participants to determine whether they have received the vaccine or a placebo.

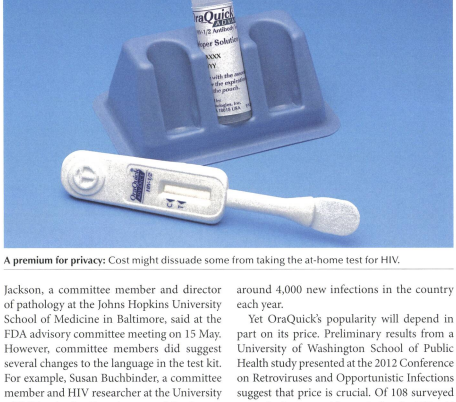

Associated Press

A premium for privacy: Cost might dissuade some from taking the at-home test for HIV.

Dollars and sense

OraSure expects the FDA to make a decision in the coming months, although no formal timeline has been set. The agency isn't required to follow an advisory committee's recommendation, but it typically does. Ultimately, the extent to which OraQuick will improve public health hinges on whether high-risk groups buy the test. An FDA analysis presented at the committee meeting found that, if one in every 100 Americans uses the test, OraQuick could newly identify up to 45,000 HIV-positive individuals and prevent around 4,000 new infections in the country each year.

Yet OraQuick's popularity will depend in part on its price. Preliminary results from a University of Washington School of Public Health study presented at the 2012 Conference on Retroviruses and Opportunistic Infections suggest that price is crucial. Of 108 surveyed men who have sex with men in Seattle, 13% said they would only take the test if it was free, and another 45% reported that they wouldn't pay more than $20.

OraSure currently sells the test to clinics for $17.50, but the version sold directly to consumers for home testing is likely to be more expensive (although the company has not yet given details). At the committee meeting, Stephen Lee, OraSure's chief scientific officer, noted that the price will be "substantially lower" than the price of Home Access's HIV test, which he said retails for about $60.

David Paltiel, a public health researcher at the Yale University School of Medicine in New Haven, Connecticut, points out that individuals with the highest risk of HIV tend to be in the lowest income brackets, and OraQuick may cost more than they are willing to pay. So he expects its consumers will probably be well-off individuals "composed disproportionately of HIV-uninfected, 'worried well' persons and very recently infected, undetectable cases."

The availability of an in-home test "is not going to hurt," Paltiel says, stressing the benefit to individuals. "But I don't think it's going to help" from a public health standpoint, he notes.

Cassandra Willyard

Sequencing cells one at a time offers singular insight into cancer

COLD SPRING HARBOR, NEW YORK — At last count, the international research community had sequenced close to 4,000 individual cancer samples, with plans in the works to study at least 21,000 more tumor genomes by the end of 2014. These genomic data sets, which span some 50 different cancer types covering nearly every organ in the body, have opened the door to a number of new targeted treatment options by identifying major genetic changes that distinguish cancer cells from normal cells. To date, however, almost all cancer genomes have come from bulk tumor samples containing many different cells, and this cellular lumping can mask some of the fine-grained complexity of the disease that underpins much of drug resistance and susceptibility.

"The best way to begin studying populations of cancer cells is to look at what happens in single cells," says Timour Baslan, a geneticist at the Cold Spring Harbor Laboratory (CSHL) in Long Island, New York, who published a protocol last month for how to analyze copy number variation of single cancer cells (*Nat. Protoc.* **7**, 1024–1041, 2012).

To enable cancer genomics at the individual tumor cell level, in December 2010 Life Technologies, based in Carlsbad, California, announced a $1 million prize to the first team that could sequence the entire genome and RNA content of a single cancer cell. And now, many researchers are getting close to that goal.

At the CSHL Meeting on The Biology of Genomes here last month, Nicholas Navin, a geneticist at the MD Anderson Cancer Center in Houston, presented new data on the genetics of breast cancer at single-cell resolution. Previously, Navin had looked at copy number variants in 100 individual cells in each of two human breast cancer cases and showed that one such tumor contained three distinct subpopulations of cells, whereas the other cancer was made up of a genetically identical pool of cells (*Nature* **472**, 90–94, 2011). Now, Navin has honed his technology to make it sensitive enough to detect single nucleotide differences, and he has found in a set of four cells from a single invasive breast cancer tumor that the individual cells often contain dozens of rare mutations that typically go undetected by bulk tumor-sequencing methods.

"It's my hope that these new tools can be used to improve diagnosis and treatment," Navin says.

"They could become very powerful at detecting remaining cancer cells that can linger in the body for months or years," as well as guide the appropriate course of adjuvant or chemotherapy, he notes.

Of a single mind

Meanwhile, Baslan and others at CSHL scanned for copy number variation in100 cells each from 12 breast cancer tumors both before and after chemotherapy. Reporting at the meeting on the first three such tumors, the researchers found that some people's cancers had gained genetic material after the treatment, whereas other tumors showed signs of chromosomal rearrangements. Although such analyses are possible with bulk sequencing, "this type of evaluation has been traditionally overlooked in cancer studies," says Baslan.

Cancer drug's survivin suppression called into question

There are no prizes for guessing the cellular function of the protein survivin. It was named for its ability to promote cell survival in cancer by blocking programmed cell death—and it's a protein that has become steadily more familiar in the cancer field in recent years. Since its discovery in 1997, survivin has emerged as one the most commonly found proteins in tumor cells. Take into account its rarity in healthy tissue, and you can understand why several companies have invested heavily in putative antisurvivin agents, with a handful already in clinical testing. The lead compound—YM155 from Japan's Astellas Pharma—has already completed phase 2 trials for various forms of cancers. However, new data are emerging from preclinical tests to suggest that the drug might not be working exactly as first anticipated.

The first hint of trouble came in April, when researchers from the Biological Testing Branch of the US National Cancer Institute's Developmental Therapeutics Program in Bethesda, Maryland performed a barrage of *in vitro* tests on YM155, known chemically as sepantronium bromide, and on a similar in-house compound called NSC80467. They found that both agents kill cells primarily by inducing DNA damage, not by suppressing survivin directly—a finding that suggests that any effect on survivin is probably a secondary event caused by general deactivation of gene expression (*Cancer Chemother. Pharmacol.* doi:10.1007/s00280-012-1868-0, 2012).

Then, last month, a team from the University of Pittsburgh School of Medicine published the results of a large chemical screen for small molecules that could kill an aggressive form of skin cancer caused by the Merkel cell polyomavirus. Of more than 1,300 compounds tested, including many standard chemotherapeutic drugs, only YM155 was able to destroy Merkel cell carcinomas, yet not for the reasons suspected (*Sci. Transl. Med.* **4**, 133ra56, 2012).

"We anticipated that YM155 would cause apoptosis; instead, we saw it causes a profound inhibition of DNA synthesis," says study author Patrick Moore, director of the Molecular Virology Program at the University of Pittsburgh Cancer Institute. Indeed, notes Bill Chang, a pediatric oncologist at the Oregon Health & Science University in Portland who was not involved in the work, "we still do not quite understand the mechanism of survivin inhibition, and, further, any drug that inhibits expression of survivin may have off-target effects."

Mechanistic melee

The findings contradict Astellas's own preliminary data, which suggested that "YM155 is not a DNA-damaging agent," says Aya Kita, an Astellas scientist who has led the drug's development.

Regardless of the drug's mechanism of action, the company is forging ahead with its clinical development of YM155—currently the only small-molecule drug in human testing that purportedly blocks survivin expression. YM155 has already been tested as a single agent to treat patients with melanoma, lung cancer, prostate cancer or lymphoma. Although the drug seems to be safe and well tolerated, its efficacy to date has been modest at best. In a recent study of 41 people with diffuse large B cell lymphoma, only one person had a complete remission and an additional two participants had a significant response after the therapy (*Cancer* doi:10.1002/cncr.26510, 2011).

Those findings don't worry Kita, who insists that the real test will come when the drug is combined with other therapies to simultaneously inhibit different cell-survival pathways. In cell culture and mouse models, Kita and her colleagues have shown that YM155 in combination with rituximab, a

Baslan and his colleagues started out by studying copy number variation because this method requires less starting material than is needed for full sequencing—and single cells don't have much DNA to begin with. In March, however, scientists from the BGI genomics center in Shenzhen, China reported a way to amplify the DNA three-million-fold, creating enough starting material to decode the entire protein-coding portion of the genome down to the single nucleotide level for individual cancer cells (*Cell* **148**, 873–885, 2012).

Future single-cell sequencing projects should also become easier thanks to the creation last month of a new single-cell genomics center at the Broad Institute in Cambridge, Massachusetts, with equipment and staff support from Fluidigm Corporation, a microfluidics technology company based in South San Francisco. According to Fluidigm's president and chief executive Gajus Worthington, the new center will begin by focusing on cancer stem cells and circulating tumor cells. "We hope that studying these cells will lead to a new type of biopsy that identifies from the start whether a tumor will spread or is drug resistant," he says.

Jeanne Erdmann

---

monoclonal antibody directed against the CD20 protein found on the surface of B cells, results in significant improvements in tumor regression and survival (*Leuk. Res.* **35**, 787–792, 2011). Trials of YM155 in combination with carboplatin plus paclitaxel chemotherapy to treat patients with lung cancer and other solid tumors are ongoing.

Meanwhile, alternative strategies to suppress survivin have also entered early clinical testing, including vaccines to generate an antigen-specific immune response against tumor cells that express survivin and several antisense oligonucleotides. The latter—which include products from Indiana's Eli Lilly, New Jersey's Enzon Pharmaceuticals and Denmark's Santaris Pharma—should in theory be able to silence the *BIRC5* gene, which codes for survivin, with more precision than small molecules such as YM155.

Nonetheless, Anthony Tolcher, director of clinical research at South Texas Accelerated Research Therapeutics in San Antonio, who has led trials involving both YM155 and antisense therapies, expects that delivery challenges associated with getting antisense molecules into the target cancer cells will most likely mean that YM155 or another small-molecule drug yet to enter the clinic will be the first such agent to hit the market. Whether or not that drug hits survivin directly, however, remains to be seen.

David Holmes

A history of drugs on the weight list

Antiobesity medications have a weighty history in the US. Throughout the post-war era, amphetamines were widely touted for their appetite-suppressing effects until their addictive potential prompted the US Food and Drug Administration (FDA) to ban their use as a weight-loss aid in 1979. The mid-1990s then saw the surge in popularity of fen-phen—a combination of the two anorectics, fenfluramine and phentermine—before that diet pill, too, was pulled from the market due to concerns over serious heart valve problems. More recent attempts haven't fared much better: Meridia, Acomplia and Ephedra all had to be yanked from pharmacy shelves owing to spotty safety records.

Will the latest obesity remedies—Lorqess (lorcaserin) and Qnexa (a combination of phentermine and topiramate)—stand the test of time? In 2010, the FDA, worried about dangerous side effects, rejected both agents. But in February, FDA advisors reviewed new data and recommended granting market approval to Qnexa, a drug from Mountain View, California–based Vivus that combines an appetite suppressant and an antiepileptic, as an obesity treatment. And last month, the same committee ruled in favor of licensing Lorqess, a serotonin receptor agonist from San Diego–based Arena Pharmaceuticals.

If the FDA follows its panel's advice—decisions are expected before mid-July—these drugs would be the first new prescription antiobesity pills to reach the US market in 13 years. Here we give the skinny on the recent checkered past of weight-loss drugs.

Elie Dolgin

Nov 1997

Abbott's Meridia (sibutramine), a neurotransmitter reuptake inhibitor, wins FDA approval.

Meridia was withdrawn from the US market in October 2010 after clinical trials revealed an increased risk of heart attack and stroke.

Apr 1999

Roche's Xenical (orlistat), which reduces intestinal fat absorption by inhibiting pancreatic lipase, receives FDA approval. It remains the only prescription antiobesity medication approved for long-term use.

Apr 2004

The FDA bans the sale of ephedra-containing dietary supplements, citing heart-rate and blood-pressure abnormalities, leading to strokes and sudden deaths.

Jun 2006

The European Medicines Agency approves Sanofi's cannabinoid receptor blocker Acomplia (rimonabant), a decision the agency reversed in 2009 owing to psychiatric risks. The FDA never approved Acomplia.

Feb 2007

The FDA approves GlaxoSmithKline's Alli, an over-the-counter formulation of orlistat.

Oct 2010

The FDA rejects both Lorqess and Qnexa. Less than two years later, advisory panels recommend in favor of approving both medicines, arguing that the benefits outweigh the risks.

Feb 2011

Despite an earlier advisory panel's recommendation in favor of approval, the FDA rejects Orexigen Therapeutics's Contrave, a combination of the antidepressant bupropion and the opioid receptor blocker naltrexone, citing concerns about possible cardiovascular risks.

Feb 2012

The FDA's Endocrinologic and Metabolic Drugs Advisory-Committee (EMDAC) votes 20–2 in favor of approving Qnexa.

May 2012

The EMDAC backs Lorqess in an 18-4 vote.

Biomedical briefing

POLICY

French facelift

As part of the fallout from the scandal over the diabetes medicine Mediator (benfluorex), France is overhauling and renaming its agency responsible for regulating drugs and medical devices. On 1 May, the French government dissolved the Health Products Safety Agency (AFSSAPS) and replaced it with the National Agency for the Safety of Medicines and Health Products (ANSM). Dominique Maraninchi, an oncologist who moved to AFSSAPS last year from the French National Cancer Institute, will lead the new agency. "Reaching out to somebody like him was a big signal that they wanted someone totally independent," says Thomas Ricketts, a health policy researcher at the University of North Carolina–Chapel Hill who runs the politics and administration program at the French School of Public Health in Paris and Rennes.

Biotech blueprint

On 26 April, the US government outlined a master plan for bolstering the country's life sciences industry that includes increased investment in basic research and development, reduced regulatory burdens and support for transitioning discoveries from the bench to the market. Building on a number of existing programs, the 'National Bioeconomy Blueprint', released by the White House, also details new initiatives, including an effort to develop genomics-based methods for cataloguing biosecurity threats and a proposal to improve information technology and medical device training at the country's Food and Drug Administration (FDA).

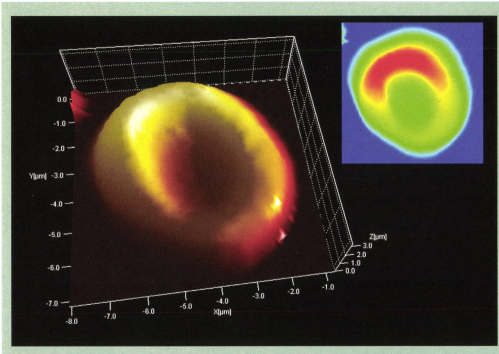

Center of Smart Interfaces, Technical University of Darmstadt, Germany (Janko Diehl)

World's oldest known blood found in iceman's wounds

You cannot get blood from a stone, but it turns out you can get it from a 5,300-year-old ice mummy. That's the conclusion of a paper published last month describing the shape and molecular composition of red blood cells isolated from the wounded right hand and back of Ötzi the Iceman, who was excavated in the Italian Alps in 1991 (*J. R. Soc. Interface* doi:10.1098/rsif.2012.0174, 2012). "This is something that people were looking for ever since the Iceman was discovered 20 years ago," says Albert Zink, of the Institute for Mummies and the Iceman in Bolzano, Italy, who led the work. Although Ötzi's blood was healthy, Zink says the findings should prompt scientists to examine blood cells of other ancient human remains to look for signs of illnesses such as malaria and sickle cell anemia.

Student support

In an effort to double the number of South African graduate students trained in biomedical research, on 26 April the nation's Department of Health launched a 500 million rand ($65 million) initiative to enroll 1,000 new doctoral students in the life sciences by 2022. "We are going to create a leadership with enormous capacity," says Bongani Mayosi, a cardiologist at the University of Cape Town and the chairman of South Africa's National Health Research Committee. In the future, the so-called 'National Health Scholars Programme' also aims to fund postdocs, midcareer fellows and research chairs in the health sciences.

Old drugs, new tricks

In what Francis Collins, director of the US National Institutes of Health, described as the "first signature initiative" of the agency's nascent drug development hub, the National Center for Advancing Translational Sciences (NCATS) has reached a deal with three major pharmaceutical companies to find new uses for a cache of 24 abandoned compounds. Under the terms of the agreement, unveiled on 3 May, the three firms involved—Pfizer, AstraZeneca and Eli Lilly—will retain ownership of the drugs, and NCATS-funded scientists will own any intellectual property stemming from their discoveries. NCATS is putting up $20 million of its $575 million annual budget next year toward the effort. In December, AstraZeneca made a similar pact with the UK Medical Research Council to share 22 compounds.

A taxing issue

California voters went to the polls this month to decide more than the fate of the Republican Party's presidential nominee. On 5 June, residents of the Golden State voted whether to impose an additional $1 tax on cigarette

packs that would go to support smoking-cessation efforts as well as research on cancer, heart disease and other tobacco-related illnesses. The fate of the ballot initiative was still unknown as *Nature Medicine* went to press.

PEOPLE

Lone Star resignation

Alfred Gilman announced plans last month to step down as chief scientific officer of the Austin-based Cancer Prevention and Research Institute of Texas (CPRIT), citing problems with the peer-review process at the $3 billion state agency. "Your most critical concern will be to keep the external peer review system intact," Gilman wrote in a resignation letter, dated 8 May, to CPRIT executive director William Gimson. "Negative actions would […] be extremely harmful to the research community's view of science in Texas and, thus, on the ability to recruit scientists to the state." Gilman, a Nobel prize–winning biochemist, plans to leave the three-year-old institute in October.

Free from smallpox

The American epidemiologist who led the US Centers for Disease Control's campaign to eradicate smallpox in the 1970s has been tapped to receive one of the nation's highest civilian honors. On 26 April, the White House named former CDC director William Foege as one of the 13 recipients of this year's Presidential Medals of Freedom. Among his many accomplishments, Foege (pictured) served as executive director of the Carter Center in Atlanta, as a medical advisor to the Seattle-based Bill & Melinda Gates Foundation and as executive director of the Task Force for Child Survival and Development, a nonprofit headquartered in Atlanta.

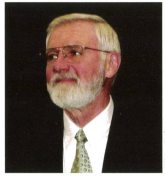

Wikimedia Commons

BUSINESS

Bye-bye baby

Pfizer is following through on its plans, announced last year, to focus on its core business and divest its divisions devoted to infant nutrition and animal health. On 23 April, the New York–based drugmaker sold its baby-food business to Switzerland's Nestlé for close to $12 billion, a price that exceeded most analysts' expectations. "Pfizer should be happy about the way the sale worked out," says Damien Conover, who covers the pharmaceutical industry for Morningstar in Chicago. Pfizer is expected to spin off its animal-health unit by the end of the summer.

Carrot and stick

US regulators have, for the first time, given the go-ahead to a human biologic manufactured in plant cells. On 2 May, the Israeli company Protalix Biotherapeutics and its partner, Pfizer, won approval for Elelyso (taliglucerase alfa), an enzyme-replacement therapy for the treatment of Gaucher's disease. Because Elelyso is made using genetically engineered carrot cells, the recombinant protein can be produced at a much lower cost than existing Gaucher's drugs, which are manufactured in mammalian cells (see *Nat. Med.* **18**, 5, 2012).

Good grief

Five and a half years after Pfizer pulled the plug on torcetrapib—a drug designed to elevate blood levels of high-density lipoprotein (HDL), or 'good' cholesterol—Roche is now making a similar move. On 7 May, the Swiss pharma giant announced plans to halt development of its own HDL-raising compound, dalcetrapib, after an interim review of the company's pivotal 15,000-person trial found no signs of clinically meaningful efficacy. Despite Roche's negative findings, some experts still believe that other HDL modulators in clinical testing, including Merck's anacetrapib and Eli Lilly's evacetrapib, will hold therapeutic promise. "It would be a mistake to close the door on this class of compounds," says Robert Rosenson, director of cardiometabolic disorders at the Mount Sinai Heart Institute in New York.

Faster than Viagra

A pill that helps men achieve erections within 15 minutes won US approval in late April. As a phosphodiesterase type 5 inhibitor, the new drug, known as Stendra (avanafil), falls into the same class as other erectile dysfunction medicines but is supposed to work at least twice as fast as existing agents such as Pfizer's Viagra (sildenafil citrate). Stendra is the sole product on the market from Mountain View, California–based Vivus, which is awaiting a decision from US regulators in mid-July on its weight-loss pill Qnexa (see page 843).

Clopidogrel clones

Another megablockbuster drug has tumbled off the patent cliff. On 17 May, the FDA approved the first generic versions of Plavix (clopidogrel), a popular blood thinner marketed jointly by New York–based Bristol-Myers Squibb and Paris-based Sanofi. "For patients who couldn't afford Plavix previously, the cost will be much less," says Shamir Mehta, a cardiologist at McMaster University in Hamilton, Ontario. Notably, he adds, "that should improve compliance." Plavix generated an estimated $43 billion in global sales during its 15 years on the market.

More online

Infections cause one in six cancers: go.nature.com/JwHghX

Vaginal microbes vary over time: go.nature.com/YFvWkV

Cannabinoid research blunted: go.nature.com/zUjGIM

FDA outpaces its global peers at drug reviews

The FDA is often criticized for taking too long to approve new medicines. But over the past decade, the US agency actually reviewed applications and gave the nod to new drugs faster than either the European Medicines Agency (EMA) or Health Canada. "Pretty consistently the FDA was coming out on top," says Nicholas Downing, a medical student at the Yale University School of Medicine in New Haven, Connecticut, who published the findings last month in the *New England Journal of Medicine* (doi:10.1056/NEJMsa1200223, 2012). See go.nature.com/IYQn3W for more.

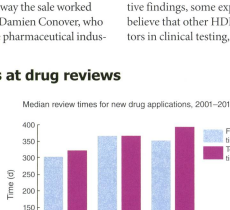

Joseph Schwartz

Straight talk with… Joseph Schwartz

On 17 May, Human Genome Sciences (HGS) formally rejected a $2.6 billion unsolicited takeover offer by GlaxoSmithKline. The Maryland-based biotech firm had long partnered with the UK drug giant to develop drugs including Benlysta (belimumab), HGS's first drug on the market and the first new medicine approved to fight lupus in 50 years. But, at $13 a share, GSK's bid was deemed "inadequate" by the HGS board. Recent history in the biotech sector shows how high the stakes are in such negotiations. Since last November, six biopharma buyouts have exceeded $1 billion each, with Gilead Sciences' purchase last year of the hepatitis C specialist Pharmasset topping the charts at a whopping $11.2 billion, the highest ever paid for a clinical-stage biotech and an 89% premium to its share price at the time. More recently, in April AstraZeneca paid $ 1.3 billion for Ardea Biosciences, a company with cancer and gout drugs in the pipeline but nothing on the market.

One person watching the upward clime of such deals is biopharma analyst Joseph Schwartz, a managing director at Leerink Swann in Boston. **Mark Ratner** sought out Schwartz, who was named the top stock picker for pharmaceuticals in the last year's FT/StarMine Analyst Awards, for his views on what's behind the recent buyout spending.

Why are drug giants paying such high premiums for biopharma assets?

All deal are financial. But more deals are strategic now, too, especially with respect to the acquirer's market position, because of scarcity issues within the sector. We always hear that the easier targets have been exploited.

There are also many more fully integrated biotech companies now at all levels of the market capitalization spectrum. In most cases, the companies will need to build or already have a sales force. Wall Street factors in the negative net present value of those expenses. The greater those synergies, the more premium a buyer can offer. Any banker will tell you that synergies and premiums are inextricably linked. There's hidden value that a pharma buyer is able to unlock.

What are some fundamental deal drivers at work now?

You have vectors on both the demand and the supply side. We think a lot of larger players are struggling for growth and have finally come to terms with the need to acquire their way to innovation. On the supply side, the emerging biotech landscape is maturing. There are now many examples of smaller companies that have developed drug candidates to an advanced enough stage to have products that could address gaps within the franchises of larger companies. The companies have a fiduciary duty to maximize shareholders' return on investment and try to add as much value as they can before they have to pass on the reins.

Can you point to a recent example from the universe of companies you cover?

Ardea Biosciences is one. I think the company has been interested in selling for a long time; that would be its natural evolution. The indication for Ardea's lead drug, gout, is a primary-care market that requires a lot of selling resources to develop. That is not Ardea's strength. The company might have left some money on the table by selling before phase 3 data. But otherwise, it could have found itself in a stalemated position: with great data yet unable to carry out an exit that would have made their shareholders as much money. In such situations, the tables turn because the biotech needs a partner more than the partner needs the biotech. AstraZeneca is buying Ardea early, well ahead of the launch, and taking some of the risk. But it was probably the best scenario for Ardea.

Is the interest in mergers and acquisitions (M&A) being reflected in increased stock prices of other biopharma companies?

There are companies we cover that people think are rational or natural takeover candidates because of the disease area they address or the business model they are pursuing. Amarin Corporation, for example, has an omega-3 fatty-acid therapy that addresses a very large potential primary-care market—if an acquirer can develop that market. Orphan drug–company models are also seen as very attractive.

Some of the more prominent deals have involved companies with drugs that treat hepatitis C virus (HCV) infections. Why is that, and which other therapy areas have been a focus of recent M&A activity?

A lot of players expect different drug combinations to be used for HCV. It's an expanding market, so it makes sense to invest there. Other areas of interest are those which would fit into the existing strengths or reinvigorate past strengths of a pharma company: areas like cardiovascular, rheumatology, neuroscience and oncology.

You mentioned rheumatology. GSK is attempting to take over Human Genome Sciences, its longtime partner in the development of the lupus drug Benlysta (belimumab). Why is GSK acting now?

Clearly, the launch of Benlysta has disappointed public investors. Human Genome Sciences' stock was approaching the mid-single-digit range, where it hadn't been since before Benlysta was de-risked with positive phase 3 data and regulatory approval. So now that expectations are low, GSK might believe it's bottomed or close to bottoming and that now is a good opportunity to buy low. By doing so, they can consolidate full rights, slash some costs to justify the investment with synergies, and perhaps participate in any upswing in Benlysta sales by owning 100% of the rights.

There's also been a lot of M&A activity in the generics space. Do you see any commonality in rationale with the buying of biotech companies?

Generics acquirers have been focused on assembling various pieces to the supply and delivery chain. Regional players are trying to become large global players by acquiring local leaders in the space: Indian companies buying European companies with established distribution capabilities, for example. Some large biotechs are thinking this way, too.

The Vetting Process

Humans and other animals suffer from many of the same ailments. Yet, aside from cases in which diseases cross the species barrier, veterinarians and physicians rarely work together to tackle common health problems. That may soon change. **Katharine Gammon** profiles one cardiologist who is pioneering a species-spanning approach to biomedical research.

To the uninitiated, Curtis Eng and Barbara Natterson-Horowitz might not seem like natural research partners. Eng, dressed in hiking books, cargo shorts and a fleece vest atop a polo shirt, looks every part the rugged animal trapper, ready to dart and transport big game on the savannahs of Africa; whereas Natterson-Horowitz, clad in her teal medical scrubs, appears to have just stepped out of a hospital room.

Yet, despite the wardrobe differences, both Eng, chief veterinarian at the Los Angeles Zoo and Botanical Gardens, and Natterson-Horowitz, a cardiologist at the University of California–Los Angeles (UCLA) David Geffen School of Medicine, share a common passion: to unite the fields of veterinary and human medicine toward the goal of better understanding disease and designing new therapeutics that move across species barriers.

On this Tuesday morning in April, the two have just finished medical rounds at the zoo, and they're discussing the similarities in their respective approaches to patient care. Standing in the zoo pharmacy, Eng points out the various items lining the shelves, all of which could easily be found at any local drugstore. There's a box of pregnancy tests to be used in the great apes, pill jars full of antibiotics and a bottle of powdered laxative. "Millions of years of divergent evolution and we've all got issues with constipation," laughs Natterson-Horowitz.

Natterson-Horowitz first teamed up with Eng in 2004 after receiving a call about a chimpanzee that was suffering from the signs of a stroke. Vets at the zoo lacked experience in treating such issues, so they called in an expert—that is, an expert in human medicine—from the zoo's advisory board to perform an echocardiogram, an ultrasound test that can reveal any blood clots that might have lodged in one of the chimp's brain-feeding arteries. "It was startling to see the similarities" between the chimp's condition and those of her patients at the UCLA Medical Center, Natterson-Horowitz recalls.

Natterson-Horowitz often finds new collaborators in unexpected places. After she began her work at the zoo, her regular morning walking partner introduced her to Kathryn Bowers, a medical journalist and UCLA writing instructor, and together they started cataloging all the diagnoses common to humans and other members of the animal kingdom. They found that animals have many of the same afflictions as humans—from obesity and diabetes to musculoskeletal injuries and anorexia. Research conducted on humans had applications in the veterinary world, and the same was true of observational studies of naturally occurring disease in animals. The two ultimately came up with a name for this concept—zoobiquity—taking the Greek root *zo-* for animal and the Latin word *ubique* for everywhere. "We wanted to coin a word that

brought together two cultures," Natterson-Horowitz explains.

In January 2011, Natterson-Horowitz hosted the first 'Zoobiquity' conference at UCLA, where some 200 participants discussed case studies of humans and animals naturally experiencing the same diseases. She simultaneously launched the Zoobiquity Research Initiative to bring together interdisciplinary teams of medical and veterinary students to work on common projects. Keeping up the momentum, Natterson-Horowitz has planned a second Zoobiquity conference, scheduled for late September, and this month Knopf will publish a book she co-authored with Bowers called *Zoobiquity: What Animals Can Teach Us about Health and the Science of Healing.*

"What Barbara is doing is very important," says Randolph Nesse, a psychiatrist at the University of Michigan–Ann Arbor who, together with the evolutionary biologist George Williams, coined the term 'Darwinian medicine' in the early 1990s. "Not just to break down barriers between disciplines and to help us realize we are yet another species shaped by selection, but also because insights from diseases in other animals will be helpful in understanding, preventing and treating human diseases."

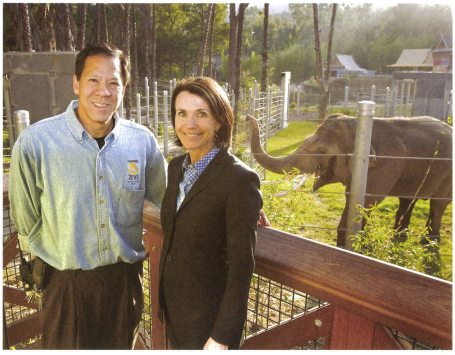

Reid Holbrook

Unexpected allies: Eng (left) and Natterson-Horowitz (right) are bridging the human-animal divide.

Am I my brother's zookeeper?

Veterinarians and doctors didn't always need a catchy name to come together. In the 1800s, it was common for one town doctor to treat both humans and animals, but around the turn of the twentieth century increasing urbanization meant that livestock weren't as important to everyday life, and the growth in academic specialization pushed veterinary schools to rural communities at the same time that medical centers were gaining distinction in wealthier cities. In reconnecting medicine between species, says Natterson-Horowitz, "Zoobiquity is a little bit back to the future."

Not that Zoobiquity isn't without recent precedent. In 2006, the American Veterinary Medical Association established the One Health Initiative, a movement to forge inclusive partnerships between physicians, veterinarians and other health specialists. And three years later, a coalition of medical, veterinary and public health groups launched the Iowa-based One Health Commission with a similar goal. However, both nonprofits are largely focused on diseases that jump from animals to humans such as West Nile virus or avian influenza. In contrast, Zoobiquity, says Natterson-Horowitz, aims to bring the shared characteristics of animal and human medicine to bear on the treatment of all manner of illness—not just zoonotic diseases. What's more, Natterson-Horowitz, through her awareness-raising efforts, hopes that scientists will rally around the idea both at the lab bench and at the bedside. "If we don't practice zoobiquitous medicine," she says, "the risk is that we are leaving nuggets along the way that could lead to life-altering therapies."

> **"Insights from diseases in other animals will be helpful in understanding, preventing and treating human diseases."**

It's natural that Natterson-Horowitz, as a cardiologist, is starting with heart disease. After an experience treating a sick tamarin monkey, Natterson-Horowitz realized that two heart problems, one afflicting humans and the other wild animals, were really one and the same condition. The human disease, known as takotsubo cardiomyopathy or broken heart syndrome, occurs in response to emotional or physical stress. The comparable animal illness, called capture myopathy, is also a stress-induced disease of the heart muscle that kills up to half of all wildlife after they are brought into captivity.

In a proposal outlined in hers and Bowers's book, Natterson-Horowitz now thinks that both illnesses should be renamed FRADE, short for fear/restraint-associated death events. By bringing the two diseases together under the same umbrella, "the benefits could extend not only to human patients at risk for sudden cardiac death but animals at risk, too," Natterson-Horowitz says. "Since human cardiologists are unaware that this happens in wild animals, such research has not occurred."

That kind of research is what the newly launched Zoobiquity Research Initiative—a collaborative project between UCLA doctors and the University of California–Davis School of Veterinary Medicine—is all about. Currently, the initiative, which is funded by the two universities and private philanthropy, has ongoing projects into the molecular basis of FRADE, the similarities between dog and human cancers and a descriptive study on collaborative potential between veterinarians and physicians on preventing zoonotic diseases in immunocompromised people.

A dog's chance for success

Independently, some other researchers are advancing many of the same concepts espoused by Natterson-Horowitz. For example, eight years ago the US National Cancer Institute (NCI) established a Comparative Oncology Program to support research into naturally occurring cancers in dogs, cats and other household animals. By studying spontaneous forms of cancer in pets, rather than tumors

that are transplanted into lab animals or arise from genetic manipulation, NCI veterinarian Melissa Paoloni says that researchers can gain insight into the natural complexities of cancer—insights that might better translate to people. Scientists have cured cancer time and again in mice and failed to translate those results into humans, Paoloni notes. Maybe it's time to look to the animal kingdom for a better model.

Since the Comparative Oncology Program's launch, it has funded 13 large dog trials at 20 veterinary medicine centers around the country. The program, with an annual budget of around $300,000, even now has a trials consortium and a pharmacodynamic core for veterinary biomarker validation[1]. Paoloni says that one advantage to testing new treatments on canines is the particular math of dog years. "Our furry friends don't live as long as we do," she says, "so we answer some big questions in a much shorter period—say 6, 10, 12 months as compared with 5 to 10 years in humans." Plus, dogs cohabitate with us in the same houses, drink the same water and share other environmental exposures, making them good stand-ins for the human condition.

"I truly believe that the answers in unlocking puzzles about cancer is sitting right next to us, wagging his tail," says Matthew Breen, a geneticist at the North Carolina State University's School of Veterinary Medicine in Raleigh and a board member of the Canine Comparative Oncology and Genomics Consortium, a Maryland-based nonprofit. "We will discover more about the process of cancer by focusing attention on dogs than with ten times the number of people with ten times the number of cancers."

Jean Bennett's research has also gone to the dogs, so to speak. But she is using the canines to study heritable blindness. A decade ago, Bennett, a molecular ophthalmologist at the University of Pennsylvania Perelman School of Medicine in Philadelphia, showed that gene therapy could restore vision in three dogs with a naturally occurring disorder similar to Leber's congenital amaurosis, a degenerative retinal disease that affects approximately 3,000 people in the US[2]. "You would never know that they had been born blind," says Bennett. "They used to be easier to take care of when they couldn't see, but now they run around like crazy." Earlier this year, Bennett and her colleagues reported similar therapeutic success when they administered the treatment to three humans carrying the same genetic defects as the dogs[3].

Albert Magazine

Made to see: Jean Bennett and two of her genetically corrected dogs, Mercury and Venus.

Andrew Bowers

Cultural revolution: Natterson-Horowitz (left) and Bowers (right) "wanted to coin a word that brought together two cultures."

"The answer in unlocking puzzles about cancer is sitting right next to us, wagging his tail."

Hatching new ideas

Using the principles of Zoobiquity, human medicine also has something to teach veterinary science. At the Smithsonian Conservation Biology Institute (SCBI) in Front Royal, Virginia, researchers are adapting assisted reproductive techniques used in clinics around the world to try and protect and extend fertility for wild and endangered animals. For example, last year they showed that, despite waning levels of reproduction in older female cheetahs, the big cats' eggs were actually good candidates for the same *in vitro* fertilization and embryo transfer techniques that are commonly used for older human eggs[4].

But, as always, the research goes both ways: the research techniques designed for freezing, thawing and grafting ovarian tissue for wildlife conservation have helped more than 30 women give birth to healthy babies after fertility-compromising cancer treatments, according to Pierre Comizzoli, a gamete biologist at the SCBI's Center for Species Survival. "The diversity of species on the animal side brings fundamental knowledge that is useful for humans," he says.

To some working in the field, however, Zoobiquity is just a new handle for an old concept. "It's comparative research, and it's a catchy term," says Michael Day, a veterinary pathologist at the University of Bristol, UK who chairs the World Small Animal Veterinary Association's One Health committee. "Unfortunately, these new words are cropping up, and I'm not sure they're necessary."

For her part, Natterson-Horowitz says she isn't looking for credit or glory; she's just glad that people are talking about comparative medicine. "We are not the only patients on the planet," she says. "An expanded perspective on illness and recognizing that disease is natural can help all patients," regardless of species. She adds, "I just want to keep the conversation going."

Katharine Gammon is a science writer in Santa Monica, California.

1. Paoloni, M., Lana, S., Thamm, D., Mazcko, C. & Withrow, S. *Vet. J.* **185**, 88–89 (2010).
2. Acland, G.M. *et al. Nat. Genet.* **28**, 92–95 (2001).
3. Bennett, J. *et al. Sci. Transl. Med.* **4**, 120ra15 (2012).
4. Crosier, A.E. *et al. Biol. Reprod.* **85**, 243–253 (2011).

Take Russia to 'task' on bioweapons transparency

Raymond A Zilinskas

Raymond A Zilinskas

In the run-up to his reelection, Russian president Vladimir Putin outlined 28 tasks to be undertaken by his administration, including one that commanded the development of weapons based on "genetic principles." Political pressure must be applied by governments and professional societies to ensure that there is not a modern reincarnation of the Soviet biological warfare program.

Last month, Vladimir Putin reclaimed his position as Russia's president, bringing about a moment of déjà-vu. For a hint of what's to come, though, one should look back to 22 March when he chaired a meeting attended by his ministers to discuss implementing 28 tasks that he had developed during his recent campaign to be undertaken by his new administration. There, Russia's Minister of Defense Anatoly Serdyukov told Putin that his office had "thoroughly studied your article [in which the tasks are listed and explained] and prepared a plan for implementing the tasks." Notably, fourth on Putin's list is a task that calls for "the development of weapons based on new physical principles: radiation, geophysical, wave, genetic, psychophysical, etc." (http://premier.gov.ru/eng/events/news/18490/; by 4 April, task 4 had been removed).

In view of Russia's history, Serdyukov's promise poses grave concerns. Developing weapons based on "genetic principles" would be a violation of the 1972 Biological and Toxin Weapons Convention (BWC), of which Russia is a State Party. According to the UN, the BWC "effectively prohibits the development, production, acquisition, transfer, retention, stockpiling and use of biological and toxin weapons." (http://www.unog.ch/bwc). In this way, the BWC serves as an important tool to prevent the proliferation of so-called weapons of mass destruction.

The convention specifies that if a member state has concerns that another party is violating the agreement, it should act "to consult bilaterally and multilaterally to solve any problems with the implementation of the BWC." Thus, BWC member states should immediately insist on consulting with Russia for the purpose of having task 4 clarified, as well as request transparency in regards to the operations of the Ministry of Defense's biological research institutes and their culture collections. Professional societies, such as the American Society for Microbiology (to which I belong), ought to support actions by governments in this regard, as it goes along with their ethical precepts.

Perhaps part of the problem is that Russia has inherited a half-hearted commitment to the BWC from the USSR. For example, while the Soviet Ministry of Foreign Affairs negotiated the BWC with the US and other governments in the early 1970s, the Soviet Central Committee was simultaneously planning to establish the world's largest and most sophisticated biological warfare program managed by a new agency called Biopreparat. Under a program code-named Ferment its main objective was to apply the recently discovered genetic-engineering technique to develop highly virulent pathogens for biological weapons.

The Soviet government ratified the BWC in 1975, thus signifying full adherence to the convention. But by then its biological weapons program was well underway, and it continued until at least 1992. At its height, Biopreparat was managing about 40 major research institutes, production plants and other industrial units, staffed by a work force of between 40,000 and 60,000 people, while the Ministry of Defense was operating three large biological research institutes and a large open-air testing facility.

Milton Leitenberg, of the University Maryland's Center for International and Security Studies in College Park, and I describe the history, work program, attributes and accomplishments of Biopreparat in exhaustive detail in a book titled *The Soviet Biological Warfare Program: A History*, which will be published by Harvard University Press next month. We describe how Biopreparat and Ministry of Defense scientists weaponized bacterial species using genetic engineering. These scientists enhanced microbes such as *Bacillus anthracis*, *Francisella tularensis* and *Yersinia pestis* by, for example, endowing them with the ability to resist multiple antibiotics and altering their cell-wall composition to resist vaccines and diagnostics used in NATO countries. A project code-named Factor sought to transfer genes coding for certain peptides into *Legionella pneumophila* that would trigger multiple sclerosis–like symptoms. Methods were developed for the mass production of variola virus and Marburg virus in cell culture, which was a vast improvement over earlier production techniques that used embryonated eggs.

Russian president Boris Yeltsin admitted early in 1992 that the USSR had operated an offensive bioweapons program in violation of the BWC. He then attempted to close down the program but was undermined by the Ministry of Defense, which kept its biological research institutes operating and their work programs secret. In September of 1992, Russia, the US and the UK signed a trilateral statement in which Russia pledged to allow its Western counterparts access to these bioweapons facilities. But, in subsequent years, it failed to deliver on the hope of transparency. Further, Yeltsin's 1992 admission was reversed by Putin after he became acting president in 1999, and Russia's official position since then is that the USSR never had an offensive bioweapons program and had only conducted defensive research as permitted by the BWC.

The three Ministry of Defense bioweapons institutes today remain as inaccessible to all foreigners and most Russians as during the Soviet era. They presumably preserve their culture collections and institutional memory, including complete 'recipes' of weaponized agents and formulations, methods of dispersal, engineering specification of munitions and many other details. This is in contrast to the actions that followed President Richard Nixon's termination of the US biowarfare program in 1969 when members of the press corps and congressional staffers were permitted to observe the destruction of biological weapons.

There are no signs that the Russian government will scale back its biological institutes that once directed the Soviet bioweapons program or destroy related culture collections. Under these conditions, Putin's task 4 is an ominous. Having been forewarned, BWC state parties must try to impress on the Putin administration that it is imperative for it to practice transparency by opening its closed bioweapons institutions to outside access, acknowledging the illegal Soviet bioweapons program of the past, revealing its accomplishments, including weaponized pathogens, and publicly destroying Soviet recipes. Unfortunately, given its past behavior on bioweapons-related issues, the Russian government is unlikely to take any of these steps. Yet, by governments and professional societies applying this kind of political pressure, task 4 is likely to at least be hindered from being realized.

Raymond A. Zilinskas is director of the Chemical and Biological Weapons Nonproliferation Program at the Monterey Institute of International Studies in Monterey, California, USA.

Surviving cancer

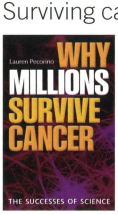

Why Millions Survive Cancer: The Successes of Science

Lauren Pecorino

Oxford University Press, 2011
256 pp., hardcover, $29.95
ISBN: 0199580553

Reviewed by Bruce Zetter

Imagine someone you know has been diagnosed with cancer. Most probably, your friend will immediately go online to search for information. He or she will find thousands of pages of notes, blogs, tweets, statistics and probabilities, as well as lists of clinical trial sites and experimental drugs. He or she may even pick up a textbook on cancer but quickly put it down, overwhelmed and confused. Where can your friend find descriptions of the disease, explanations of its biology and information about recent progress in a manageable compendium? Lauren Pecorino hopes that this book will provide the answers.

Pecorino has excellent credentials to write a book on cancer. She has a PhD in cell and developmental biology, conducted postdoctoral research at the Ludwig Institute for Cancer Research in London, lectures on cancer at the University of Greenwich in London and is the author of a textbook entitled *The Molecular Biology of Cancer*. She is clearly qualified to analyze current data on cancer incidence, outcome and prevention. She presents her analysis here, in a book aimed not at her research colleagues or even at readers of *Nature Medicine*, but squarely at the general public.

There is an openly optimistic tone to the writing, and every chapter ends with a section called "The Good News." In these sections, she tells the reader that cancer research has made many advances, that mortality rates are going down for many cancers and that individuals can take steps to reduce their cancer risk. I find all of these conclusions reasonable. Pecorino has taken on the worthy goal of promoting the positive impact of cancer research, something the cancer research community doesn't always do effectively.

Although the title may seem provocative, the writing is more nuanced, and Pecorino presents current data such that it can be digested by a casual reader. The book is short, although it could benefit from a few more pages on cancer biology. The writing is direct and concise. Documentation is provided for many of the statements, and a bibliography accompanies each chapter. The data presented are not, however, always analyzed in a critical manner that includes all possible interpretations; thus it would be possible for a nonscientist to overinterpret or misinterpret the research.

Bruce Zetter is at Children's Hospital Boston and Harvard Medical School, Boston, Massachusetts, USA. e-mail: Bruce.Zetter@childrens.harvard.edu

Many readers will open this book in the hope that they will discover new tests that detect cancers much earlier and new treatments that extend the lives of patients. What they will learn is that modern research has successfully unveiled more of the cancer cell's secrets and that certain lifestyle changes, especially those involving smoking cessation, have led to decreases in cancer incidence and mortality. New cancer drugs are appearing in clinical trials at an accelerating pace, and many extend patient survival by months or, less commonly, by years. We still await the truly effective drugs that will allow patients to live indefinitely with their disease.

In a very condensed format, Pecorino attempts to explain what cancer is, how carcinogens work and what the most important environmental risk factors are. Of the last of these, Pecorino focuses on the potential risks of radiation, chemical carcinogens, alcohol, environmental estrogen and viruses such as HPV. She devotes a relatively long and successful chapter to the risks of tobacco. I found her treatment of risks and prevention to be understandable and intriguing. The book is less successful in making the complex issues of cellular and molecular biology understandable to a general audience, and it frequently seems to dart from one subject to another without sufficient integration. Perhaps it would have benefited from a few case studies that could have combined discussions of risk factors, diagnosis, treatment, resistance and clinical trials for individual patients.

One nice touch is that the book highlights the work of "heroes," notable scientists who have made a particular impact on the understanding and treatment of cancer. This adds a human dimension and focuses attention on the enormous effort and persistence that have given rise to the advances she documents.

The author's intention is to not make her readers feel complacent about cancer. Rather, she wishes to educate the public on the biology of cancer, explain the scientific advancements of the last few decades and, most importantly, encourage individuals to take steps to reduce their likelihood of developing serious malignancies. This goal would succeed best if the book were to be read by young people who could take preventive measures early in life. It is more likely that it will be ordered by people with cancer and their friends and families. They would be wise to pass it down to their children, who might benefit from the cogent presentation of risk factors and behavioral changes that could lessen their chances of getting the disease.

Scientists often recount the difficulty of explaining their work to their friends and families: the concepts, techniques and conclusions aren't always accessible to the general public. This book approaches accessibility for the lay reader, although it will be a challenge for some. I would like to have been able to give it to my mother, who succumbed to colon cancer 40 years ago. I do believe that if she had undergone regular colonoscopies, been exposed to less tobacco smoke and had access to all of the drugs available today, she might have survived longer. The treatments and knowledge just weren't available then. But they are today, and efforts by a variety of cancer organizations to popularize this information, along with well-intentioned books such as this one, may make extended life spans a reality for many more individuals with cancer.

COMPETING FINANCIAL INTERESTS
The author declares no competing financial interests.

nature REVIEWS CANCER
nature REVIEWS IMMUNOLOGY
April 2012

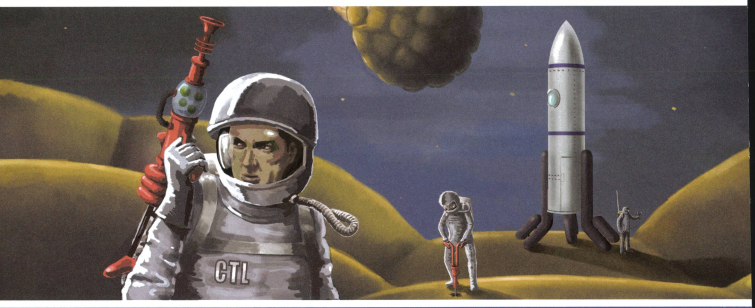

Focus on Tumour immunology & immunotherapy

Understanding how the immune system is able to protect us from cancer is an important goal for immunologists and cancer biologists alike. The progress that researchers have made in this field can be seen from the rapid expansion of new therapies that are based on boosting the immune response to tumours. This joint Focus issue from *Nature Reviews Cancer* and *Nature Reviews Immunology* features specially commissioned articles that discuss the promise of immunotherapy to treat cancer. The Focus also covers the recent insights that have been made into how key immune cells function in the tumour microenvironment — a better appreciation of this will hopefully improve the application and development of future tumour immunotherapies.

The Focus features ten articles by leading researchers, including:

The blockade of immune checkpoints in cancer immunotherapy
Drew Pardoll

Combining immunotherapy and targeted therapies in cancer treatment
Matthew Vanneman & Glenn Dranoff

Targeting natural killer cells and natural killer T cells in cancer
Eric Vivier, Sophie Ugolini, Didier Blaise, Christian Chabannon & Laurent Brossay

Access the Focus online for FREE until the end of September 2012.
www.nature.com/reviews/focus/tumourimmunology

Produced with support from Boehringer Ingelheim

nature publishing group npg

Melanoma exosomes: messengers of metastasis

Rajasekharan Somasundaram & Meenhard Herlyn

A new study shows that melanoma-derived exosomes contribute to metastatic invasion by carrying messenger proteins that direct bone marrow–derived cells toward a prometastatic phenotype. This leads to the promotion of proangiogenic events and modification of the extracellular matrix at premetastatic sites (pages 883–891).

Malignant melanoma is an aggressive form of skin cancer whose incidence continues to increase worldwide. Although a large number of primary melanomas can be cured through surgery, treatment of metastatic melanomas remains challenging[1]. In most cases, melanoma begins with the transformation of a benign nevus that develops into dysplastic lesions before progressing into a primary melanoma that can invade into the dermis and regional lymph nodes and from there disseminate to distant metastatic sites[1].

Unfortunately, in melanoma, there are no good prognostic biomarkers to predict the progression of the disease to metastasis. Genetic analyses of the primary melanomas have revealed that the invasive characteristics of the cancer are predetermined and are present in the early lesions[2]. However, the reasons for metastatic dissemination to regional lymph nodes and distant organs remain unclear. Growth factors such as vascular endothelial factor, transforming growth factor-β and tumor necrosis factor-α secreted by lymphoid and stromal cells of the uninvolved regional lymph nodes can prime their microenvironment to create a favorable 'tumor niche' for the migration of melanoma cells[3].

Exosomes were originally identified as small (30–100 nm) membrane vesicles that are actively shed by a diverse population of living normal and malignant cells[4]. These vesicles are of endosomal origin and composed of multivesicular bodies fused with the plasma membrane. Members of the Rab family of proteins are involved in the formation and secretion of exosomes[4]. Most studies have described exosomes as vesicles for excess secretion of cellular components into the extracellular milieu. Secreted components of exosomes include proteins, cell surface molecules such as human leukocyte antigens, tumor-associated antigens, co-stimulatory molecules and cytokine factors that are involved in immune regulation, and RNA molecules (both mRNAs and microRNAs)[4]. Many immunological studies have associated exosomes with the function of cross-presentation of antigens to immune cells[4].

Hood *et al.*[3] previously reported that melanoma-derived exosomes have a role in priming the lymph node environment to a proangiogenic state and also induce tumor growth–supporting extracellular matrix (ECM). However, the mechanisms by which

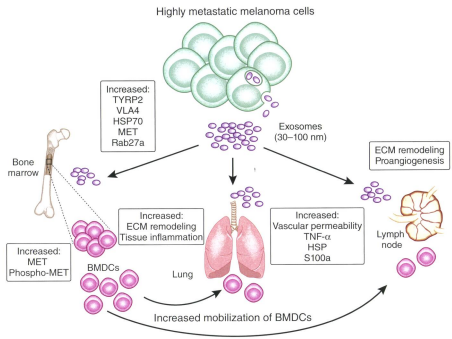

Marina Corral

Figure 1 Melanoma-derived exosomes are messengers for angiogenesis and metastatic invasion. Peinado *et al.*[5] show that tumor-derived exosomes from people with advanced metastatic melanoma contain high concentrations of TYRP2, VLA4, HSP70, MET and Rab27a proteins. They provide evidence that melanoma-derived exosomes that are shed in the extracellular milieu travel to bone marrow, lungs, lymph nodes and other organ sites of metastasis, where they are involved in the preparation of a tumor niche by altering the ECM, inducing tissue inflammation, increasing vascular permeability and promoting other proangiogenic events. They show that exosomes activate and modify the phenotype of BMDCs, inducing them to express increased amounts of the oncoprotein MET, which is phosphorylated and activated, thus resulting in the mobilization of BMDCs to the lungs and lymph nodes, where they initiate a metastatic niche. TNF-α, tumor necrosis factor-α.

Rajasekharan Somasundaram and Meenhard Herlyn are in the Tumor Microenvironment and Metastasis Program, Melanoma Research Center, The Wistar Institute, Philadelphia, Pennsylvania, USA.
e-mail: herlynm@wistar.org

increased vascularization and modification of the ECM is achieved were not addressed by this study. In the current issue of *Nature Medicine*, Peinado *et al.*[5] report that exosomes contain vital cellular components that participate in disseminating primary tumor cells to distant metastatic sites.

Peinado *et al.*[5] performed extensive studies using melanoma-derived exosomes obtained from both mouse and human melanoma cells, and, importantly, their findings may be relevant to the clinical monitoring of melanoma progression and prevention of metastasis. Using sera from patients with melanoma, the authors found that tumor-derived exosomes contain distinct proteins (TYRP2, VLA4, HSP70, MET and Rab27a (**Fig. 1**)) that constitute a 'melanoma signature'. Increased concentrations of TYRP2 and MET in circulating serum exosomes were found to be a predictor of disease progression. In addition, the authors found that patients with melanoma who had serum exosomes with high protein content had a poor prognosis when compared to patients with exosomes of low protein concentrations[5].

Peinado *et al.*[5] then used a mouse model of melanoma to show that tumor-derived exosomes promote both melanoma invasion and metastasis. They found that intravenously injected exosomes from a highly metastatic mouse melanoma cell line (B16-F10) localized in the lungs, lymph nodes and other target organs typical for B16-F10 cell metastasis and primed these sites, thus increasing vascular permeability and inflammation to promote the migration of primary tumor cells.

Exosomes can transfer molecules to recipient cells, so, to identify candidate molecules present in exosomes that could mediate the increased metastatic behavior of the primary tumor cells, the authors compared the proteomes of exosomes derived from the highly metastatic mouse melanoma cell line with those derived from a poorly metastatic melanoma cell line (B16-F1 cells). Peinado *et al.*[5] found a number of proteins that showed higher expression in the more metastatic exosomes, including MET, an oncoprotein known to be important in the migration, invasion, angiogenesis and mobilization of bone marrow cells. They then showed that the prometastatic exosomes indirectly increased the metastatic behavior of primary melanoma cells by increasing the amounts of MET and activated phospho-MET in bone marrow–derived cells (BMDCs), a process the authors termed BMDC 'education'. The reprogrammed BMDCs had a provasculogenic phenotype and were then mobilized to lungs or lymph nodes where they could aid angiogenesis, invasion and metastasis of primary tumor cells (**Fig. 1**). Notably, reducing MET expression in the tumor-derived exosomes diminished the prometastatic behavior of BMDCs.

The authors then corroborated their mouse data using human studies in which they showed that circulating BMDCs isolated from people with advanced melanoma had increased expression of MET and phospho-MET. As members of the Rab family have been implicated in exosome function, Peinado *et al.*[5] compared the expression of Rab mRNAs in human melanoma cell lines that produced high numbers of exosomes and those that produced low numbers of exosomes. They found that the cell lines with increased exosome production showed increased *RAB27A*, *RAB5B* and *RAB7* expression compared with the cell lines that produced fewer exosomes. Rab27 is known to be important in exosome release, and, consistent with this, the authors found that knockdown of Rab27a by RNAi in mouse and human melanoma cell lines resulted in decreased exosome secretion and also prevented modification of the BMDC phenotypes and their mobilization, thus preventing tumor invasion and metastasis in mice injected with these highly metastatic melanoma cells.

The results of Peinado *et al.*[5], if validated in a larger number of patients with melanoma, could have important clinical implications for the prediction and prevention of metastasis. Their work suggests that the detection of TYRP2 and the MET oncoprotein in serum exosomes could be used as a prognostic indicator for people with primary melanoma. It is also possible that metastatic events in patients with melanoma who have been identified to have exosomes with high expression of TYRP2 or MET could be prevented by designing therapeutic strategies to target MET or Rab27a. Such interventions to prevent or reduce the metastatic burden are hoped to greatly improve the likelihood of survival of patients with melanoma.

COMPETING FINANCIAL INTERESTS
The authors declare no competing financial interests.

1. Miller, A.J. & Mihm, M.C. Jr. *N. Engl. J. Med.* **355**, 51–65 (2006).
2. Chin, L., Garraway, L.A. & Fisher, D.E. *Genes Dev.* **20**, 2149–2182 (2006).
3. Hood, J.L., San, R.S. & Wickline, S.A. *Cancer Res.* **71**, 3792–3801 (2011).
4. Théry, C., Zitvogel, L. & Amigorena, S. *Nat. Rev. Immunol.* **2**, 569–579 (2002).
5. Peinado, H. *et al. Nat. Med.* **18**, 883–891 (2012).

FOXO3a and β-catenin co-localization: double trouble in colon cancer?

Yibing Yan & Mark R Lackner

Metastatic colorectal cancer is a largely incurable disease with a pressing need for targeted therapies. A new study sheds light on a surprising interaction between FOXO3a and β-catenin in metastatic colorectal cancer, suggesting new therapeutic avenues for agents targeting the PI3K-AKT pathway (pages 892–901).

Metastatic colorectal cancer is diagnosed annually in an estimated 240,000 individuals worldwide and has a five year survival rate of just 11% (ref. 1). The phosphoinositide 3-kinase (PI3K)-AKT and WNT–β-catenin signaling pathways both have prominent roles in tumorigenesis and disease progression in colorectal cancer[2,3]. Forkhead box O3a (FOXO3a) is a transcriptional regulator downstream of PI3K-AKT signaling that is normally regarded as a tumor suppressor, as it promotes cell cycle arrest and apoptosis[4]. FOXO3a is sequestered in an inactive form in the cytoplasm when phosphorylated by AKT; inhibition of AKT signaling releases FOXO3a to translocate to the nucleus, where it regulates gene expression[4] (**Fig. 1**).

In this issue of *Nature Medicine*, Tenbaum *et al.*[5] show surprising findings that suggest a previously unappreciated role for nuclear

Yibing Yan and Mark R. Lackner are in the Department of Oncology Biomarker Development, Genentech, South San Francisco, California, USA. e-mail: yyan@gene.com or mlackner@gene.com

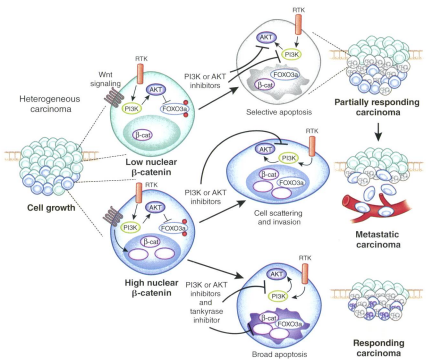

Marina Corral

Figure 1 Concomitant localization of FOXO3a and β-catenin in the nucleus mediate progression and metastasis in colorectal cancer upon PI3K or AKT inhibition. Untreated, primary colorectal cancer cells have heterogeneous levels of β-catenin (β-cat; far left). In active proliferating cells, PI3K-AKT activation results in phosphorylation of FOXO3a, restricting its localization to the cytoplasm. Treatment of colon carcinoma cells with selective PI3K or AKT inhibitors leads to translocation of FOXO3a to the nucleus. In this context, tumor cells with low nuclear β-catenin undergo apoptosis (partially responding carcinoma), whereas those with high nuclear protein levels of both β-catenin and FOXO3a become resistant to induction of apoptosis. In these resistant cancer cells, nuclear FOXO3a and β-catenin act together to regulate a defined set of target genes mediating cell scattering and metastasis. Although the tumor partially responds to treatment, the resistant cell population disseminates and contributes to treatment-induced metastasis (metastatic carcinoma). Concurrent treatment of these cells with AKT or PI3K inhibitors and WNT pathway inhibitors, such as a tankyrase inhibitor, causes enhanced apoptosis and impairs metastasis (responding carcinoma). RTK, receptor tyrosine kinase.

FOXO3a in promoting metastasis in the context of nuclear β-catenin accumulation, a common occurrence in colon cancers. Applying AKT inhibitors to tumor cells with concomitant high nuclear expression of FOXO3a and β-catenin resulted in resistance to apoptosis and promotion of the metastatic program (**Fig. 1**). The findings have important implications—a new cooperative interaction of these two fundamental pathways in the nucleus in mediating metastasis, along with clinical relevance for patients with colorectal cancer and dual elevation of FOXO3a and β-catenin, as they may respond poorly to PI3K-AKT inhibitors. These findings suggest a diagnostic strategy that may help identify nonresponsive individuals.

A notable strength of the study is the use of a combination of relevant cell line models and tumor samples with associated clinical outcome. By analyzing tumor samples, the authors found that nuclear FOXO3a and β-catenin were frequently concurrently expressed in late-stage cancers and that this was associated with poor prognostic outcome. Using cell line models, Tenbaum *et al.*[5] showed that concurrent expression of ectopic activated FOXO3a together with β-catenin promoted cell scattering *in vitro* and metastasis *in vivo*. This seemed to be due to an altered transcriptional program consisting of induction of genes involved in cell adhesion and scattering. Increased β-catenin protein amounts promoted resistance to apoptosis induced by AKT and PI3K inhibitors; moreover, inhibition of AKT signaling promoted scattering and metastasis of xenografted colon tumor cells with elevated β-catenin. Lastly, patient-derived sphere cultures and tumor xenografts showed differential sensitivity to an AKT inhibitor that was inversely correlated to their intrinsic nuclear β-catenin levels[5]. The authors therefore concluded that it will be important to investigate the subcellular localization of β-catenin and FOXO3a in tumor samples before administering AKT inhibitors to patients with colorectal cancer, as in the context of active Wnt signaling such treatment may induce malignant behavior of tumor cells.

The study adds to previous studies showing that the Wnt and PI3K-AKT pathways interact at multiple levels. For example, AKT phosphorylation of glycogen synthase kinase-3β is essential in regulating β-catenin degradation and blocking Wnt signaling[6]. Moreover, transcriptional upregulation of the kinase SGK by T cell factor–lymphoid enhancer factor–β-catenin complexes results in SGK-directed phosphorylation and retention of inactive FOXO3a in the cytoplasm[7]. In these examples, the pathways have antagonistic functions—the observation of direct cross-talk between β-catenin and FOXO3a in the nucleus and a cooperative role in triggering metastasis is therefore an unexpected aspect of the complex interplay between these pathways. It remains to be seen whether this effect is specific for PI3K-AKT signaling and unique to colorectal cancer.

A recent study suggests that elevated β-catenin activation may not be a general resistance factor for other targeted therapies that regulate FOXO3a localization in different tumor types; in particular, endogenous β-catenin is required for BRAF (an oncoprotein mutated in melanoma) inhibitor–induced apoptosis of melanoma cells harboring V600E missense mutations in the gene encoding BRAF. High nuclear β-catenin protein levels synergize with a BRAF inhibitor to induce apoptosis and decrease tumor growth, suggesting high β-catenin amounts may enhance the efficacy of BRAF-targeted therapy. Thus, the role of β-catenin in apoptosis may be context or tissue dependent. In addition, FOXO3a levels are also known to be regulated by kinases other than AKT, notably IKK and ERK[4,9]. In fact, ERK phosphorylation of FOXO3a, albeit on different sites than those regulated by AKT, drives tumorigenesis by triggering degradation of FOXO3a via a mechanism involving the E3 ubiquitin ligase MDM2 in breast cancer cell lines[9]. Therefore, blocking the BRAF-MEK-ERK axis with selective inhibitors could conceivably act analogously to AKT inhibition in terms of elevating levels of nuclear FOXO3a protein in colorectal cancer, a hypothesis that could be readily tested using the models described by Tenbaum *et al.*[5].

The findings of Tenbaum *et al.*[5] have clear clinical implications because they suggest that high nuclear FOXO3a and β-catenin amounts may predict resistance to PI3K-AKT–targeted therapies in colorectal cancer. Inhibitors of this pathway are the subject of intensive clinical investigation, and preclinical studies with the PI3K and mammalian target

of rapamycin inhibitor GDC-0980 have suggested relatively modest activity in colorectal cancer cell lines compared to breast or prostate lines[10]. The authors may have provided a clue to this observation, showing that simultaneous accumulation of β-catenin and FOXO3a not only confers poor prognosis but also seems to be predictive of a poor efficacy for AKT inhibitors. Individuals with low nuclear β-catenin protein amounts may then be the most likely to benefit from therapeutic intervention with PI3K-AKT inhibitors. Alternatively, those with high nuclear β-catenin and FOXO3a protein may require concurrent treatment with selective inhibitors of Wnt–β-catenin signaling. Indeed, the authors showed that treatment of resistant colorectal cancer cells with the tankyrase inhibitor XAV-939, which reduces nuclear β-catenin protein levels and transcriptional activity[11], resulted in increased PI3K or AKT inhibitor–mediated apoptosis[5]. However, tankyrase inhibitors have not yet entered clinical development, and dual targeting of these signaling pathways may still be a distant goal.

This study also highlights the importance of understanding interpatient tumor heterogeneity to guide administration of rationally targeted therapies. The lack of cell and tumor models that closely mimic relevant human cancers has long been recognized as a major hurdle in translating basic cancer research to the clinic. By using patient-derived tumors to assess the response to drug treatment in individual tumors, the authors have pushed the limits of this type of analysis by first testing the *in vitro* sensitivity of patient-derived colorectal cancer sphere cultures and then extending these findings to *in vivo* tumor explants[5]. The results suggest the possibility that such sphere cultures could be used immediately after surgical resection to evaluate biomarkers and assess efficacy of candidate drugs with great accuracy in real time to individualize treatment regimens. Alternatively, pharmacodynamic effects on FOXO3a nuclear levels and apoptosis could be directly assessed in pre- and post-treatment tumor biopsies, an approach several of the investigators in the current study have successfully employed with other therapeutics[12]. Though operational and technical hurdles remain, the approach of Tenbaum *et al.*[5] clearly signals a promising trend in translational research.

The work by Tenbaum *et al.*[5] suggests several additional avenues of scientific inquiry. For instance, many of the observations, although previously undescribed, remain primarily correlational. How is metastasis increased under dual activation? What are the most important effector genes induced by the combination, what is their relative biological contribution to metastasis and are any of them druggable targets? It also remains to be seen whether approved receptor tyrosine kinase inhibitors, including the epidermal growth factor–targeted antibodies cetuximab and panitumumab[13], have similar prometastatic effects, as receptor tyrosine kinase inhibition can, in some contexts, inhibit PI3K-AKT signaling.

Interesting clinical challenges lie ahead, as well. One is that colorectal cancer tumors are heterogeneous regarding amounts of elevated nuclear β-catenin protein[14], which is a continuous variable that may be challenging to dichotomize. Delineating cutoffs and the most suitable predictive diagnostic assay to define 'high' nuclear β-catenin protein are major challenges. How such an assay will be deployed and prospectively validated in the clinical setting, given that clinical trials are already underway for several inhibitors, is an equally difficult question. One might also wonder how elevated β-catenin may affect efficacy in the background of other candidate predictive biomarkers, such as *PIK3CA* mutations. Careful clinical trial design and patient stratification with mandatory biomarker assessments will be crucial in taking this story to the next level. The work by Tenbaum *et al.*[5] is a step in the right direction in the quest for more personalized therapies for patients with colorectal cancer.

COMPETING FINANCIAL INTERESTS
The authors declare no competing financial interests.

1. Howlader, N. *et al.* SEER Cancer Statistics Review, National Cancer Institute, Bethesda, MD (2008).
2. Samuels, Y. & Velculescu, V.E. *Cell Cycle* **3**, 1221–1224 (2004).
3. Zhang, Y., Gan, B., Liu, D. & Paik, J.H. *Cancer Biol. Ther.* **12**, 253–259 (2011).
4. Yang, J.Y. & Hung, M.C. *Curr. Drug Targets* **12**, 1284–1290 (2011).
5. Tenbaum, S.P. *et al. Nat. Med.* **18**, 892–901 (2012).
6. Aberle, H., Bauer, A., Stappert, J., Kispert, A. & Kemler, R. *EMBO J.* **16**, 3797–3804 (1997).
7. Dehner, M., Hadjihannas, M., Weiske, J., Huber, O. & Behrens, J. *J. Biol. Chem.* **283**, 19201–19210 (2008).
8. Biechele, T.L. *et al. Sci. Signal.* **5**, ra3 (2012).
9. Yang, J.Y. *et al. Nat. Cell Biol.* **10**, 138–148 (2008).
10. Wallin, J.J. *et al. Mol. Cancer Ther.* **10**, 2426–2436 (2011).
11. Huang, S.M. *et al. Nature* **461**, 614–620 (2009).
12. Rojo, F., *et al. J. Clin. Oncol.* **24**, 4309–4316 (2006).
13. Ciardiello, F. & Tortora, G. *N. Engl. J. Med.* **358**, 1160–1174 (2008).
14. Brabletz, T. *et al. Proc. Natl. Acad. Sci. USA* **98**, 10356–10361 (2001).

Nicotine: linking smoking to abdominal aneurysms

Koichi Sugamura & John F Keaney Jr

The link between tobacco use and aneurysms of the abdominal aorta is well established, but the specific mechanisms involved have remained elusive for decades. A new study indicates that nicotine is the major culprit in cigarette smoke and provides a common mechanism of aneurysm formation that may allow the development of drugs to treat this disease, for which currently only surgical treatments exist (pages 902–910).

Abdominal aortic aneurysm is an enlargement of the abdominal aorta that represents a difficult clinical problem because the initial symptom is often rupture of the aneurysm[1], an event with a mortality exceeding 70% (ref. 2), despite advances in surgical treatment[3]. These aneurysms start as small dilatations of the abdominal aorta that gradually expand over the course of years with the risk of rupture increasing drastically once the aneurysm reaches a diameter of 5 cm or more. The only accepted treatment for these large aneurysms is surgical open or endovascular graft placement. Early detection of smaller abdominal aneurysms is important because it enables clinicians to observe aneurysm expansion and intervene before rupture. However, prophylactic surgery for aneurysms smaller than 5 cm has not proven useful, so the current practice is watchful waiting until intervention is possible, and most aneurysms slowly expand over years.

Koichi Sugamura and John F. Keaney Jr. are in the Division of Cardiovascular Medicine, University of Massachusetts Medical School, Worcester, Massachusetts, USA.
e-mail: john.keaney@umassmed.edu

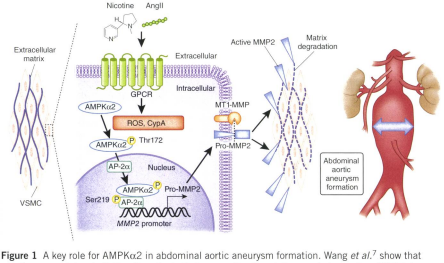

Marina Corral

Figure 1 A key role for AMPKα2 in abdominal aortic aneurysm formation. Wang *et al.*[7] show that nicotine or angiotensin II (AngII) activate their respective G protein–coupled receptors (GPCRs) on VSMCs, thus increasing the intracellular abundance of reactive oxygen species (ROS) such as $ONOO^-$ and H_2O_2 and cytokines (such as CypA, TNF-α, IL-6 and IFN-γ) that promote the activation and nuclear translocation of AMPKα2 via phosphorylation at Thr172. Nuclear AMPKα2 phosphorylates the transcription factor AP-2α at Ser219, and, collectively, these actions promote AP-2α binding to the matrix metalloproteinase-2 (*MMP2*) promoter, driving transcription and upregulation of pro-MMP2. In the VSMC cytoplasm, pro-MMP2 is cleaved by membrane type I–matrix metalloproteinase (MT1-MMP) into active MMP2, which leads to degradation and weakening of the extracellular matrix, thereby promoting abdominal aortic aneurysm formation.

Epidemiologic data have clearly linked tobacco smoking to aneurysm formation and a faster rate of expansion[1,4]. Pathological examination of human abdominal aortic aneurysm tissue has shown that it is characterized by intense oxidative stress, inflammation and matrix degradation[5,6], but the mechanistic relationship linking aneurysm formation to smoking has remained elusive.

In this issue of *Nature Medicine*, Wang *et al.*[7] break this impasse and provide new insights into the link between tobacco smoking and abdominal aortic aneurysms (**Fig. 1**). Using mouse models, they found that nicotine, the main dependence-forming ingredient of tobacco, increases aneurysm formation by stimulating the α2 isoform of AMP-activated protein kinase (AMPKα2) in vascular smooth muscle cells (VSMCs). Activation of AMPKα2, in turn, resulted in phosphorylation of activator protein 2α, a transcription factor that drives the expression of and smooth muscle cell release of matrix metalloproteinase 2, a matrix-degrading protein that functions to weaken the artery wall, thus facilitating aneurysm formation[8].

This convincing link between abdominal aortic aneurysm formation and nicotine has important implications for patients that are trying to stop smoking. A mainstay of therapy for smoking cessation is nicotine replacement, as this treatment reduces the inevitable withdrawal symptoms that occur upon discontinuation of smoking. However, the data of Wang *et al.*[7] suggest that patients with pre-existing abdominal aneurysms who are attempting to stop smoking need particular attention, as nicotine replacement therapy has the potential to exacerbate abdominal aortic aneurysm.

As AMPKα2 is required for nicotine-induced abdominal aneurysm formation and expansion, it follows that inhibition of this kinase could represent a new treatment for the disease. This premise is strengthened by additional data from the study of Wang *et al.*[7]. First, they used another common model of abdominal aortic aneurysm formation in mice, angiotensin II infusion, and observed that aneurysm formation in this model was also dependent on AMPKα2. Moreover, human abdominal aortic aneurysm tissue samples showed increased activity of AMPKα2 compared with aortic tissues from people without abdominal aortic aneurysms. Collectively, these observations suggest that AMPKα2 inhibition may help to treat early-stage abdominal aortic aneurysms and prevent their expansion and rupture. This concept is a welcome addition to the field of vascular disease, as there are currently no effective drugs to treat abdominal aortic aneurysm. Even today, smoking cessation is the mainstay of clinical management of aneurysm.

However, designing therapeutic strategies to inhibit AMPKα2 could present challenges. Overall, the AMP-activated kinases have three subunits (α, β and γ) with distinct isoforms (α1, α2, β1, β2, γ1, γ2 and γ3) and broad tissue distributions. This family of enzymes is principally involved in cellular adaptation to changing energy status (that is, metabolic stress) but also is activated in a variety of other settings that the cell may interpret as injurious. Animals lacking both catalytic isoforms of AMPK (α1 and α2) are not viable, indicating that this enzyme family is crucial in developmentally important pathways. Similarly, activation of AMPK is the mechanism for the world's most widely used diabetes treatment drug, metformin[9]. Thus, it is conceivable that AMPK inhibition for the treatment of abdominal aortic aneurysm could worsen diabetes or have other unintended consequences. Conversely, the findings of Wang *et al.*[7] suggest that patients with diabetes on metformin with known abdominal aortic aneurysms warrant close scrutiny for aneurysm dilatation.

A similar cautionary note also applies to therapeutic inhibition of activator protein 2α, the transcription factor Wang *et al.*[7] implicated in the matrix metalloproteinase upregulation that is key in aneurysm formation and dilatation. Activator protein 2α has been shown to be important for mammalian tumorigenesis, differentiation and development, and mice lacking activator protein 2α are not viable[10]. Consequently, any therapies based on inhibiting activator protein 2α will need to be scrutinized for unanticipated side effects.

In the search for new therapies using animal models, one limitation is the extent to which the animal models recapitulate the human condition. The mouse models used by Wang *et al.*[7] reproducibly generate abdominal aneurysms, but in the suprarenal aorta. In contrast, most human aneurysms are located below the renal arteries, suggesting that mice may imperfectly model the human condition. In addition, the human disease occurs in later stages of life compared to the equivalent in mice and is associated with atherosclerosis and thrombosis, conditions not prevalent in the mouse model. Thus, there are important distinctions between mouse aneurysm models and aortic aneurysms in humans, indicating there could be challenges in developing new therapies for human abdominal aortic aneurysm using mouse models.

Despite these concerns, the study by Wang *et al.*[7] provides an important molecular link between nicotine and the promotion of abdominal aortic aneurysms. This finding adds to a recent study that uncovered another molecular target of nicotine, microRNA-21 (miR-21), that is strongly upregulated in the course of aneurysm formation[11]. The upregulation of miR-21 seems to be protective, as inhibiting its expression accelerates aneurysm expansion. Collectively, these two studies begin to identify molecular targets for nicotine that provide

us with new potential therapeutic strategies for a disease that currently has no established medical therapy.

COMPETING FINANCIAL INTERESTS
The authors declare no competing financial interests.

1. Brown, L.C. & Powell, J.T. *Ann. Surg.* **230**, 289–296 (1999).
2. Cosford, P.A. & Leng, G.C. *Cochrane Database Syst. Rev.* CD002945 (2007).
3. Hoornweg, L.L. *et al. Eur. J. Vasc. Endovasc. Surg.* **35**, 558–570 (2008).
4. Wilmink, T.B., Quick, C.R. & Day, N.E. *J. Vasc. Surg.* **30**, 1099–1105 (1999).
5. Miller, F.J. Jr *et al. Arterioscler. Thromb. Vasc. Biol.* **22**, 560–565 (2002).
6. López-Candales, A. *et al. Am. J. Pathol.* **150**, 993–1007 (1997).
7. Wang, S. *et al. Nat. Med.* **18**, 902–910 (2012).
8. Longo, G.M. *et al. J. Clin. Invest.* **110**, 625–632 (2002).
9. Zhou, G. *et al. J. Clin. Invest.* **108**, 1167–1174 (2001).
10. Zhang, J. *et al. Nature* **381**, 238–241 (1996).
11. Maegdefessel, L. *et al. Sci. Transl. Med.* **4**, 122ra22 (2012).

Peroxiredoxin sets the brain on fire after stroke

Lidia Garcia-Bonilla & Costantino Iadecola

How blood-borne inflammatory cells cause tissue damage in the brain after ischemic stroke remains elusive. Peroxiredoxins, cytosolic antioxidant proteins vital for redox balance, are released extracellularly from ischemic cells, acting as potent 'danger signals' that activate macrophages and lead to a harmful cytokine response, a new study shows. The findings unveil a new culprit in the delayed phase of ischemic injury and suggest new therapeutic approaches (pages 911–917).

The World Health Organization estimates that 15 million people suffer a stroke every year. Of these, one-third dies and another third becomes permanently disabled. Despite its enormous public health burden, second only to ischemic heart diseases in high-income countries, interventions to treat stroke remain extremely limited[1]. Most strokes are caused by a sudden occlusion of a major cerebral artery (ischemic stroke) resulting in brain damage and permanent neurological impairment. Whereas energy deficit and glutamate excitotoxicity cause neuronal death immediately after ischemia, activation of brain inflammatory cells causes lingering damage that evolves over many hours[2]. In this issue of *Nature Medicine*, Shichita *et al.*[3] show that peroxiredoxins (Prxs), neuroprotective intracellular antioxidant enzymes essential for redox homeostasis, are released extracellularly after ischemia and, paradoxically, become potent proinflammatory signals that initiate a destructive immune response. The findings identify Prxs as a crucial link in the chain of events underlying post-ischemic inflammation and unveil a new powerful therapeutic target for the late stage of cerebral ischemia.

The factors responsible for the harmful inflammatory responses accompanying ischemic stroke have not been clearly defined, but activation of receptors of the innate immune system, including Toll-like receptors (TLRs) and scavenger receptors, has emerged as a key step in the signaling cascade[4,5]. These receptors are the first line of defense against infectious agents, but they also contribute to the destructive effects of 'sterile' inflammation initiated by cell damage[6]. Located predominantly on inflammatory cells, TLRs are activated by danger signals, also termed danger-associated molecular pattern molecules (DAMPs), produced during tissue injury[6]. Tissue injury generates a multitude of DAMPs, including proteins, complex lipids and nucleic acids derived from dying cells, as well as peptides produced by matrix proteolysis[6]. But the specific DAMPs responsible for TLRs activation in stroke have not been identified, an obstacle to developing much-needed therapies for the delayed phase of the injury.

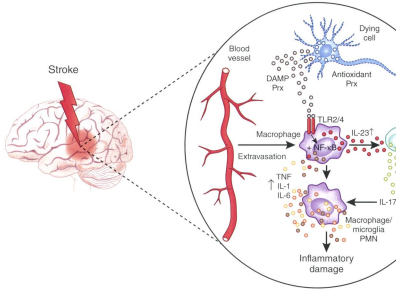

Figure 1 Release of Prxs promotes post-ischemic inflammation after stroke. Prxs are intracellular enzymes crucial for antioxidant defense. Shichita *et al.*[3] found that after stroke, Prxs are released from dying cells, lose their protective function and act as DAMPs by engaging TLR2 and TLR4 of infiltrating macrophages. The resulting nuclear factor-κB (NF-κB) activation in these immune cells leads to production of proinflammatory cytokines, which, in turn, trigger a destructive inflammatory response. One component of the inflammatory response involves IL-23, which contributes to the damage through IL-17–producing γδT cells that further enhance the activation of the inflammatory cascade.

Lidia Garcia-Bonilla and Costantino Iadecola are in the Division of Neurobiology, Department of Neurology and Neuroscience, Weill Cornell Medical College, New York, New York, USA.
e-mail: coi2001@med.cornell.edu

The authors set out to shed light on the DAMPs, receptors and downstream factors triggering post-ischemic inflammation. In a previous study, they showed that macrophages invading the ischemic brain release the cytokine interleukin-23 (IL-23) and promote IL-17 production by γδT cells[3], a T cell subset that reacts to tissue damage, which, in turn, contributes to the late phase of the injury[7]. In the present study, they found that mouse brain lysates were able to potently induce expression of IL-23 in bone marrow–derived dendritic cells (BMDCs)[3]. They found later that Prxs in the brain lysates are responsible for IL-23 induction in these cells[3].

Six mammalian Prx isoenzymes (Prxs 1–6) exist in different subcellular compartments, wherein they detoxify hydrogen peroxide and a wide range of organic hydroperoxides[7]. However, oxidation of cysteine residues on Prxs inactivates their antioxidant properties[8]. Given that Prxs activate TLR4 in peripheral macrophages[9], the authors hypothesized that after stroke Prxs may escape from damaged cells, losing their antioxidant property and becoming potent danger signals acting on TLRs. Indeed, Prx proteins were unable to induce production of IL-23 and other cytokines in TLR2- and TLR4-deficient BMDCs. After ischemic stroke in mice, Prx-positive debris-like granules were found in damaged areas, often associated with F4/80-positive phagocytic cells[3], confirming a pathogenic role during stroke *in vivo*. Furthermore, infiltrating immune cells failed to produce IL-23, and IL-17–expressing γδT cells were suppressed in TLR2- and TLR4-deficient mice after stroke.

Finally, bone marrow chimera experiments using TLR2- and TLR4-deficient marrow showed that microglia, resident macrophages of the brain that express TLRs but are not replaced by bone marrow transplantation, are not the target of Prxs and are not a source of IL-23 (ref. 3). These findings, collectively, provide convincing evidence that extracellular Prxs released from injured cells in the ischemic brain activate TLR2 and TLR4 in infiltrating immune cells, leading to production of cytotoxic cytokines, including IL-23 and IL-17 (**Fig. 1**).

But do extracellular Prxs contribute to ischemic brain injury, and, if so, what is their therapeutic potential? To address these questions, the authors developed Prx-blocking antibodies that were systemically administered to mice after cerebral ischemia[3]. Remarkably, up to 12 h after ischemia, antibodies against Prxs ameliorated both infarct growth and motor deficits in mice, indicating that the treatment was effective even when administered in the late stages of the ischemic cascade. Such a wide therapeutic window has great translational relevance because most patients reach medical attention several hours after stroke onset, when thrombolysis with tissue plasminogen activator, the only treatment for acute stroke, is no longer safe or effective[1]. The protective effect of Prx-specific antibodies was associated with a reduction in IL-23– and IL-17–producing cells in the ischemic brain; however, it was not observed in TLR2- and TLR4-null mice. Finally, by examining conserved regions among Prx proteins, they identified the domains responsible for the macrophage activation[3]. Administration of antibodies targeted against these domains was also strongly protective in the stroke mouse model. Although it remains to be determined whether these antibodies prevent the binding of Prxs to TLR2 and TLR4, the findings pinpoint a specific Prx domain that could be used for therapeutic development.

A large number of potential DAMPs, including modified lipids, heat shock proteins and β-amyloid peptides, are produced after stroke, but their role in ischemic brain injury and their therapeutic potential remain uncertain[2]. One such DAMP, the nuclear protein high-mobility group protein 1 (HMGB1) is released from ischemic cells and is endowed with proinflammatory activity[10]. However, Shichita *et al.*[3] found that HMBG1 acts predominantly in the early phase of the inflammatory cascade. In contrast, Prxs are produced later after ischemia and, as suggested by the efficacy of blocking antibodies up to 12 h after ischemia, exert their pathogenic effect in the delayed phase of the damage. Blocking Prxs also enhanced the protective effect of blocking HMGB1 (ref. 3), attesting to the more powerful role of Prx in later stages of tissue damage. HMGB1 and Prx may therefore have temporally distinct roles in post-ischemic inflammation.

Several experimental therapies suppressing inflammation protect the ischemic brain with a wide therapeutic window, including, for example, those targeting complement, the cyclooxygenase-2 pathway or inducible nitric oxide synthase and those upregulating αB-cristallin[11–14]. Therefore, the delayed protective effect of Prx-based approaches is not novel or unique. Nevertheless, counteracting Prxs is attractive because their sources, targets and pathogenic mechanisms have been clearly established[3–5,9,15]. Furthermore, the domains responsible for their proinflammatory activity have been defined, opening the way to develop therapeutic approaches with small-molecule inhibitors. In combination with other treatment strategies, such as thrombolysis or targeting early events in the ischemic cascade, Prx-based therapies may increase our chances to forestall the relentless progression of ischemic damage.

There are several issues that need to be considered in evaluating the translational potential of the Prx pathway. First, the characteristics of the protection need to be better defined according to established criteria for preclinical stroke research[16]. For example, the effectiveness in the context of a more severe ischemic insult (permanent ischemia), in females or in other species and the efficacy in the presence of stroke risk factors, such as aging, diabetes and hypertension, needs to be established. Second, inflammation is crucial for tissue reorganization and repair, and suppressing inflammation may limit the potential of the brain to recover after stroke[2]. It remains to be established whether Prx-TLR2/TLR4 signaling is involved in the recovery of the post-ischemic brain. Third, small-molecule–based approaches to neutralize the proinflammatory effect of Prx need to assure that the vital antioxidant function of the cytosolic enzymes is not impaired. These small molecules need to be cell permeable to cross the blood-brain barrier; if they penetrate into ischemic cells, they may inhibit the antioxidant activity of Prxs, which would prove devastating to the tissue at risk for infarction[15]. These considerations notwithstanding, the elegant work of Shichita *et al.*[3] provides a cogent demonstration of the powerful destructive effects of sterile inflammation in ischemic brain injury and unveils a new therapeutic target with a remarkable translational potential.

COMPETING FINANCIAL INTERESTS
The authors declare no competing financial interests.

1. Moskowitz, M.A., Lo, E.H. & Iadecola, C. *Neuron* **67**, 181–198 (2010).
2. Iadecola, C. & Anrather, J. *Nat. Med.* **17**, 796–808 (2011).
3. Shichita, T. *et al. Nat. Med.* **18**, 911–917 (2012).
4. Kunz, A. *et al. J. Neurosci.* **28**, 1649–1658 (2008).
5. Tang, S.C. *et al. Proc. Natl. Acad. Sci. USA* **104**, 13798–13803 (2007).
6. Chen, G.Y. & Nunez, G. *Nat. Rev. Immunol.* **10**, 826–837 (2010).
7. Shichita, T. *et al. Nat. Med.* **15**, 946–950 (2009).
8. Zhu, H., Santo, A. & Li, Y. *Exp. Biol. Med. (Maywood)* **237**, 143–149 (2012).
9. Riddell, J.R., Wang, X.Y., Minderman, H. & Gollnick, S.O. *J. Immunol.* **184**, 1022–1030 (2010).
10. Hayakawa, K., Qiu, J.H. & Lo, E.H. *Ann. NY Acad. Sci.* **1207**, 50–57 (2010).
11. Arac, A. *et al. Proc. Natl. Acad. Sci. USA* **108**, 13287–13292 (2011).
12. Iadecola, C., Zhang, F. & Xu, X. *Am. J. Physiol.* **268**, R286–R292 (1995).
13. Kawano, T. *et al. Nat. Med.* **12**, 225–229 (2006).
14. Gesuete, R. *et al. Ann. Neurol.* **66**, 332–342 (2009).
15. Chen, J. *et al. Antioxid. Redox Signal.* published online, doi:10.1089/ars.2011.4298 (22 February 2012).
16. Albers, G.W. *et al. Stroke* **42**, 2645–2650 (2011).

New clues to bariatric surgery's benefits

David A Sarruf, Susan Bonner-Weir & Michael W Schwartz

Bariatric surgery to treat obesity can also be effective against type 2 diabetes, but it is unclear how such surgical procedures improve glucose metabolism. A new study in rats suggests that nutrient sensing in the jejunum contributes to the antidiabetic effects of duodenal-jejeunal bypass (pages 950–955).

Several bariatric, or 'weight loss', surgical procedures are proving effective for treating not only obesity but also type 2 diabetes (T2D). As obesity is a major risk factor for T2D, it seems logical that treating the former would benefit the latter. Surprisingly, however, these surgeries seem to improve T2D through mechanisms that are at least partly independent of weight loss *per se*.

Perhaps the best-studied bariatric procedure is Roux-en-Y gastric bypass (RYGB), which both reduces the size of the stomach and bypasses the proximal small intestine (the duodenum and the proximal jejunum; **Fig. 1**). In two recently published randomized trials[1,2], RYGB was shown to fully normalize blood sugar concentrations in up to 75% of treated patients with T2D, a remarkable outcome that was not strongly related to the degree of weight loss in these individuals. Thus, rerouting of or increasing nutrient delivery to the small bowel (or both) has seemingly important potential as a diabetes treatment modality, but how this occurs remains a mystery. A related question is whether weight-loss surgery is appropriate only in the context of obesity—the condition for which it was originally developed—or whether lean people with insulin-deficient type 1 diabetes (T1D) might also benefit.

In this issue of *Nature Medicine*, Breen *et al.*[3] extend their earlier work[4] that suggested that the duodenum senses nutrients when they arrive by showing that a similar arrangement also pertains to the jejunum. Signals generated in response to nutrients in the proximal small bowel are passed on to the brain, which in turn is proposed to activate a neurocircuit innervating the liver that reduces its glucose production. This mechanism has been suggested to ensure that delivery of glucose into the bloodstream from an internal source (the liver) decreases when ingested nutrients arrive at the absorptive surface of the gut. Breen *et al.*[3] now report in normal-weight, nondiabetic rats that, analogous to what they'd previously reported for the duodenum[4], infusion of either fats or glucose directly into the jejunum activates a gut-brain-liver neurocircuit that enhances liver insulin sensitivity, thereby reducing hepatic glucose production.

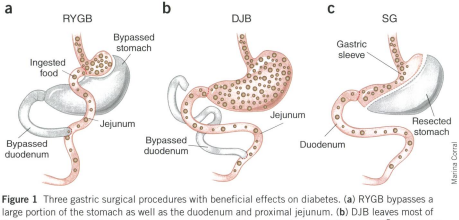

Figure 1 Three gastric surgical procedures with beneficial effects on diabetes. (**a**) RYGB bypasses a large portion of the stomach as well as the duodenum and proximal jejunum. (**b**) DJB leaves most of the stomach intact while the duodenum and proximal jejunum are bypassed. Breen *et al.*[3] now provide evidence that increased delivery of nutrients to the jejunum resulting from DJB may be important in mediating the positive effects of this form of surgery in models of T1D. (**c**) Sleeve gastrectomy (SG) removes the majority of the stomach while keeping the proximal and distal ends intact, such that intestinal nutrient flow is not altered. Ingested food is depicted with brown spheres.

Does this jejunal nutrient-sensing mechanism contribute to the antidiabetic effect of gastric bypass surgery? To investigate this question, Breen *et al.*[3] investigated the effects of duodenal-jejunal bypass (DJB, a stomach-sparing form of RYBG; **Fig. 1**) in two rat models in which diabetes is induced by the substantial destruction of pancreatic beta cells. This was achieved either by administering the beta cell–targeting toxin streptozotocin or through a genetically driven autoimmune process (in BB (BioBreeding) rats). Thus, both models are nonobese and characterized by a major loss of insulin-secreting beta cells, a situation resembling T1D rather than T2D. In both models, DJB rapidly (2 d after surgery) lowered blood glucose concentrations via a mechanism that was not explained by reduced food intake, required intact jejunal nutrient sensing, was not accompanied by increased insulin secretion and was attributable to reduced hepatic glucose production. By 14 d after the surgery, blood glucose remained at or near normal concentrations, whereas the expected marked elevation of blood glucose persisted in sham-operated diabetic rats. These findings indicate that bariatric surgery can resolve diabetes in these nonobese T1D rodent models, in addition to the earlier evidence that it can improve glucose control in a rat model of nonobese streptozotocin-induced diabetes[5] and in rat models of T2D[6,7]. More importantly, they suggest that the increased delivery of nutrients to the jejunum resulting from DJB can induce substantial lowering of glucose concentrations without increasing insulin secretion.

The notion that intestinal nutrient sensing underlies the rapid diabetes resolution induced by bariatric surgery is not without controversy. For example, many studies have implicated increased insulin secretion in the lowering of glucose concentrations observed after gastric bypass surgery in rat models of T2D[6]. Yet plasma insulin concentrations were not altered by DJB in the study of Breen *et al.*[3]. Dramatic increases in the concentrations of circulating incretin peptides (primarily glucagon-like peptide-1) have also been invoked to explain the beneficial effects of gastric bypass[7]. Although Breen *et al.*[3] observed increased

David A. Sarruf is in the Diabetes Research Unit, Novo Nordisk A/S, Maaloev, Denmark. Susan Bonner-Weir is at the Joslin Diabetes Center, Harvard Medical School, Boston, Massachusetts, USA. Michael W. Schwartz is at the Diabetes and Obesity Center of Excellence, Department of Medicine, University of Washington, Seattle, Washington, USA, and in the Division of Metabolism, Endocrinology and Nutrition, Department of Medicine, University of Washington School of Medicine, Seattle, Washington, USA. e-mail: mschwart@u.washington.edu.

circulating glucagon-like peptide-1 concentrations in response to DJB, this effect should not reduce hepatic glucose production in the absence of increased insulin (or decreased glucagon secretion, which also was not observed). The conclusion of Breen *et al.*[3] that suppression of hepatic glucose production, resulting solely from activation of a gut-brain-liver reflex arc, is sufficient to ameliorate diabetes is deserving of additional study.

Also controversial is the idea that rerouting of intestinal nutrient delivery is required for bariatric surgery to confer metabolic benefit. Data from both rats[8] and humans[2] suggest that sleeve gastrectomy, which restricts the size of the stomach but does not redirect intestinal nutrient flow (**Fig. 1**), is nearly as effective as RYGB for resolving diabetes. Combined with evidence that DJB does not improve insulin resistance or glucose tolerance in an obese rat model[9], rerouting intestinal nutrient delivery may not be essential for the effect of bariatric surgery to lower glucose concentrations—simply increasing the rate of gastric emptying may suffice. These considerations challenge the primacy of jejunal nutrient sensing as a mediator of diabetes remission induced by bariatric procedures.

Among many important unanswered questions is whether bariatric surgery can be recommended for nonobese humans with T1D. Without more data on the long-term outcomes of such procedures in obese patients with T2D, this question seems premature. Another consideration is that nonobese humans with T1D are likely to have a far greater deficit of beta cells and thus are more insulin deficient than the rat models studied by Breen *et al.*[3]. Additionally, the role of weight loss (which probably had an impact on outcomes reported by these authors, even though they took steps to minimize this effect) in diabetes resolution is complex and awaits further analysis. So, when might we consider undertaking clinical studies that address the safety, tolerability, efficacy and durability of such surgical procedures in nonobese patients with T1D? Perhaps it is not too soon to consider studies that address these questions, but the existence of a glucose-lowering neurocircuit connecting gut, brain and liver raises the possibility that we might one day develop drugs that activate this pathway without the need for surgery. This possibility offers a compelling rationale for ongoing efforts to identify the mechanisms that underlie the impressive effects of bariatric surgery on glucose homeostasis.

COMPETING FINANCIAL INTERESTS
The authors declare no competing financial interests.

1. Mingrone, G. *et al. N. Engl. J. Med.* **366**, 1577–1585 (2012).
2. Schauer, P.R. *et al. N. Engl. J. Med.* **366**, 1567–1576 (2012).
3. Breen, D.M. *et al. Nat. Med.* **18**, 950–955 (2012).
4. Cheung, G.W., Kokorovic, A. & Lam, T.K. *Cell. Mol. Life Sci.* **66**, 3023–3027 (2009).
5. Strader, A.D., Clausen, T.R., Goodin, S.Z. & Wendt, D. *Obes. Surg.* **19**, 96–104 (2009).
6. de Luis, D. *et al. Am. J. Surg.* published online, doi:10.1016/j.amjsurg.2011.07.020 (16 February 2012).
7. Kindel, T.L., Yoder, S.M., Seeley, R.J., D'Alessio, D.A. & Tso, P. *J. Gastrointest. Surg.* **13**, 1762–1772 (2009).
8. Stefater, M.A. *et al. Gastroenterology* **138**, 2426–2436 (2010).
9. Kindel, T.L. *et al. Obesity (Silver Spring)* **19**, 380–387 (2011).

Ephrin receptor: a door to KSHV infection

Chris Boshoff

Kaposi's sarcoma–associated herpesvirus is a major oncogenic virus that has been implicated in human cancers. A new study identifies ephrin receptor A2 as a key host receptor for this virus that permits infection of endothelial cells (pages 961–966).

Kaposi's sarcoma–associated herpesvirus (KSHV) causes two types of malignancies: the endothelial tumor eponymously named Kaposi's sarcoma and B cell malignancies including multicentric Castleman's disease and primary effusion lymphoma, in which the virus is associated with plasmablastic and pre–terminally differentiated B cells, respectively. Various host factors have been found to facilitate KSHV cell entry and establishment of infection (**Box 1**). However, given that these molecules are predominantly ubiquitously expressed, it is unclear how the virus is lured specifically to cells of the endothelial lineage.

Cell entry is a fundamental component of the biology of any virus. For enveloped viruses such as herpesviruses, cell entry is a multistep process that involves viral envelope glycoproteins as well as several cellular attachment and entry factors (**Fig. 1**). The virus envelope proteins have two functions: specific attachment of the virus to the cell and membrane fusion. The KSHV envelope glycoproteins H and L form a dimer (gH-gL) that is necessary for entry into the host cell.

In this issue of *Nature Medicine*, Hahn *et al.*[1] report that the ephrin receptor A2 (EphA2) tyrosine kinase specifically binds the KSHV attachment glycoproteins gH and gL, allowing virus entry (**Fig. 1**). The authors showed that EphA2 co-precipitates with gH-gL and with KSHV virions *in vitro*[1]. They then performed a number of experiments to provide convincing evidence that this host cellular molecule functions as a receptor for KSHV: knockdown or deletion of EphA2 inhibited or abolished KSHV infection of endothelial cells, and overexpression of EphA2 enhanced infection; preincubating KSHV virions with soluble EphA2 or pretreating endothelial cells with a soluble EphA2 ligand inhibited infection; and binding of KSHV gH-gL to EphA2 activated EphA2 phosphorylation and promoted endocytosis[1]. This work coincides with the observation that EphA2 is required for KSHV entry and trafficking, but not necessarily for KSHV attachment to target cells[2]. Together, these results suggest that EphA2 has a crucial role in the infection of endothelial cells by KSHV.

The first Eph receptor was discovered in 1987 in a cancer cell line called erythropoietin-producing hepatocellular[3]. Eph ligands were dubbed ephrins (Eph receptor–interacting molecules). Ephs are now the largest receptor tyrosine kinase (RTK) family, with 14 known human members. In contrast to most other ligand-RTK interactions that result in activation of the receptor, upon interaction with Eph receptors, membrane-bound ephrins are also activated to produce signals in their host cells, a phenomenon termed reverse signaling, and these signaling pathways can alternately trigger cell repulsion or attraction. In 1998 the focus of research into Ephs moved to vascular development when it was discovered that EphB4 and its ligand, ephrinB2, distinguish veins and arteries, respectively, in the developing vascular bed[4]. EphA2 was shown to be sufficient to transform mammary

Chris Boshoff is at the UCL Cancer Institute, University College London, London.
e-mail: c.boshoff@ucl.ac.uk

BOX 1 KSHV binding and entry

Virus entry is a highly regulated process involving multiple host cell surface factors that may vary according to cell type. The ubiquitous cell surface molecule heparan sulfate has been implicated as a first contact point between a KSHV envelope protein and the host cell membrane[12]. KSHV may also use DC-SIGN (CD209) to attach to hematopoietic cells (including activated B and dendritic cells)[13]. Virion binding to the integrins $\alpha V\beta 3$, $\alpha V\beta 5$ or $\alpha 3\beta 1$ initiates FAK phosphorylation, which results in the activation of downstream Src, PI3K and Akt[14,15]. The activation of these kinases is thought to be key for allowing endocytosis and therefore internalization of virions. Although FAK activation seems to be indispensable for KSHV endocytosis, the essential contribution of integrins for KSHV infection of all cell types is less well established, and Hahn *et al.*[1] could not disrupt lymphatic endothelial cell infection by neutralizing integrins. Notably, Eph kinases mediate some of their functions by negatively regulating integrins and FAK. KSHV binding to EphA2 together with heparan sulfate might be required for efficient cellular signaling, as it was suggested that the formation of Eph-ephrin complexes is directly regulated by the coexpression of heparan sulfate, where the absence of heparan sulfate results in a reduction of the functional response to the Eph ligand.

In addition to using EphA2 as a receptor, KSHV might also exploit EphA2 signaling to reorganize other cellular molecules required to establish infection. HCV, which does not bind EphA2, uses EphA2 signaling to reorganize cellular membrane CD81–claudin-1 co-receptor associations, thus permitting virus entry. xCT, the 12-transmembrane light chain of the human cystine/glutamate exchange transporter system, has also been shown to enable KSHV-cell fusion and viral entry[16]. However, xCT has not been shown to bind to any of the KSHV glycoproteins, and the overall role of xCT during KSHV entry and fusion is still unclear.

A global RNAi screen will be useful to identify the genes required for establishment of KSHV infection in cells of the endothelial lineage. Future work should also identify how heparan sulfate, integrins, FAK, PI3K and Akt signaling, xCT and EphA2 cooperate and dynamically interact to facilitate KSHV infection.

epithelial cells, indicating that EphA2 can function as an oncoprotein[5]. EphA2 is over-expressed in many human cancers, including Kaposi's sarcoma. Blocking EphA2 activation also inhibits angiogenesis in experimental tumor models[6]. More recently it was shown that EphA3 is commonly mutated in colorectal and lung cancers, where its mutated form is thought to act as a driver of oncogenesis. However, the signaling outcomes of Eph receptors might be difficult to gauge by studying one Eph in isolation, as different Eph receptors aggregate on the cell surface to signal, and this aspect may explain the conflicting reports on their functions in the literature. Relevant to Kaposi's sarcoma biology, EphA2 is expressed by lymphatic endothelial cells, and Eph receptors and ephrins have been implicated in lymphatic development and lymphangiogenesis[7,8].

Currently, the downstream signaling cascades activated specifically by the KSHV gH-gL–EphA2 interaction identified by Hahn *et al.*[1] remain unknown. Furthermore, whether KSHV binding of and signaling through EphA2 elicit endothelial cell responses involved in Kaposi's sarcoma development, including migration, recruitment, differentiation or proliferation, will need to be established.

Ephrins and their receptors have also been implicated as cellular entry molecules for other viruses[9–11]. An RNAi kinase screen identified epidermal growth factor receptor and EphA2 as host cofactors for hepatitis C virus (HCV) entry[9]. These results not only identify RTKs as HCV entry cofactors but also provide promise for exploiting RTKs to prevent viral infection (for example, after liver transplantation for HCV-related pathology) or to treat active HCV infection. EphrinB2 has been found as a cellular receptor for the emerging zoonotic paramyxovirus, Nipah virus[10,11]. Nipah virus has a broad host range, suggesting that the receptor for this virus is conserved between species. EphrinB2 is expressed on endothelial

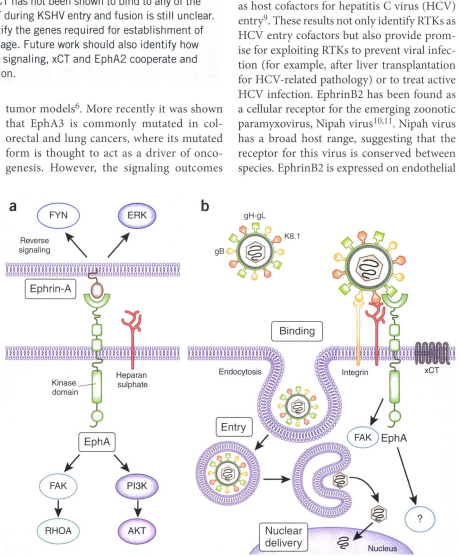

Figure 1 Ephrin signaling and KSHV entry. (**a**) Ephrin-A binding to EphA induces EphA dimerization and phosphorylation, triggering signal transduction pathways, for example, focal adhesion kinase (FAK) and phosphoinositide 3-kinase (PI3K). EphA activation is implicated in actin reorganization and cell motility. In contrast to other RTKs, ligand binding to EphA also induces reverse signaling to cells where the ligand is bound to the cell membrane, activating FYN and other kinases. (**b**) KSHV glycoproteins, including K8.1 and gB, bind endothelial cells by interacting with heparan sulfate. gB may also engage directly with integrins to induce intracellular signaling. Hahn *et al.*[1] now show that the KSHV glycoprotein complex gH-gL binds EphA2. Glycoprotein binding to this host receptor triggers intracellular signal transduction pathways including activation of FAK, creating an environment that is conducive to viral infection. Virus binding is followed by internalization and virus transport in the cytoplasm by endocytosis and fusion of the viral envelope with the endosomal membranes. Viral capsids released in the cytoplasm are transported to the perinuclear region, where viral genomes are released and enter the nucleus via nuclear pores.

cells and neurons, which could explain the *in vivo* tropism of this virus. It has been suggested that ephrinB2 engagement by this virus may act to recruit more endothelial cells to areas of Nipah virus replication. Such a mechanism could also be an attractive hypothesis for why KSHV usurps EphA2 signaling for cell entry.

In contrast to other oncogenic viruses where the respective cancer is associated with integrated or latent viral gene expression (such as human papillomavirus and cervical cancer, Epstein-Barr virus and lymphoma, and human T-lymphotropic virus type 1 and leukemia), there is ongoing lytic KSHV infection present in Kaposi's sarcoma lesions. Targeting lytic viral infection, for example by interfering with infection of endothelial cells, could be a possible therapeutic strategy. Thus, the discovery of EphA2 as a receptor for KSHV provides new insights into Kaposi's sarcoma pathogenesis, opens new avenues for further mechanistic studies and provides potential for translating this finding into clinical practice. As EphA2 has also been implicated directly in angiogenesis and lymphangiogenesis as well as in driving inflammation, processes that are relevant to Kaposi's sarcoma development, targeting this molecule might be an appealing therapeutic option to explore. RTK inhibitors and monoclonal antibodies against Ephs and their ligands are in clinical development as putative therapeutics for cancer. Thus it is hoped that the identification of Ephs and their ligands as receptors for important human pathogens such as KSHV will bolster this area of drug development.

COMPETING FINANCIAL INTERESTS
The author declares no competing financial interests.

1. Hahn, A. *et al. Nat. Med.* **18**, 961–966 (2012).
2. Chakraborty, S., Veettil, M.V., Bottero, V. & Chandran, B. *Proc. Natl. Acad. Sci. USA* **109**, 1163–1172 (2012).
3. Hirai, H., Maru, Y., Hagiwara, K., Nishida, J. & Takaku, F. *Science* **238**, 1717–1720 (1987).
4. Wang, H.U., Chen, Z.F. & Anderson, D.J. *Cell* **93**, 741–753 (1998).
5. Zelinski, D.P., Zantek, N.D., Stewart, J.C., Irizarry, A.R. & Kinch, M.S. *Cancer Res.* **61**, 2301–2306 (2001).
6. Dobrzanski, P. *et al. Cancer Res.* **64**, 910–919 (2004).
7. Wang, H.W. *et al. Nat. Genet.* **36**, 687–693 (2004).
8. Mäkinen, T. *et al. Genes Dev.* **19**, 397–410 (2005).
9. Lugberger, J. *et al. Nat. Med.* **17**, 589–595 (2011).
10. Negrete, O.A. *et al. Nature* **436**, 401–405 (2005).
11. Bonaparte, M.I. *et al. Proc. Natl. Acad. Sci. USA* **102**, 10652–10657 (2005).
12. Akula, S.M., Wang, F.Z., Vieira, J. & Chandran, B. *Virology* **282**, 245–255 (2001).
13. Rappocciolo, G. *et al. J. Immunol.* **176**, 1741–1749 (2006).
14. Akula, S.M., Pramod, N.P., Wang, F.Z. & Chandran, B. *Cell* **108**, 407–419 (2002).
15. Veettil, M.V. *et al. J. Virol.* **82**, 12126–12144 (2008).
16. Kaleeba, J.A.R. & Berger, E.A. *Science* **311**, 1921–1924 (2006).

The secrets of the bone marrow niche

The bone marrow niche keeps puzzling scientists in cancer and regenerative medicine. What elements constitute the niche and how it affects neighbor cells in different disease contexts remain to be a matter of debate and extensive investigation. The translational use of hematopoietic stem cells (HSCs) in transplantation biology poses a challenge, given the propensity of these cells to remain quiescent. Although the niche is a good candidate to exploit for reprogramming HSCs and controlling their expansion, new studies have added to its complexity. In 'Bench to Bedside', Paul S. Frenette and Yuya Kunisaki examine these studies to discuss how new players and their signals are involved in HSC maintenance and what the implications are for the development of HSC-based therapies. Among the alterations occurring in leukemias, metabolic events seem to foster cancer progression but may also be involved in cancer predisposition. Rushdia Z. Yusuf, Ying-Hua Wang and David T. Scadden peruse recent clinical and experimental studies that look at myelodysplastic syndromes and secondary leukemias and argue how metabolic changes in these cancers may not only be cell autonomous but also can emanate from the bone marrow stroma. Targeting this niche may open new avenues to reduce the risk for secondary leukemias in cancer survivors.

■ BENCH TO BEDSIDE

Enigmatic niche brings challenge for HSC expansion

Yuya Kunisaki & Paul S Frenette

The holy grail of hematopoietic stem cell (HSC) biology has been to harness self-renewal to expand stem cells for greater availability of transplantation procedures in people with cancer or hematologic diseases. Despite the advances in transplantation biology, many individuals do not have a suitable allogeneic donor. In these cases, unrelated cord blood–derived HSCs have shown promise as a source of cells for transplantation, but the number of HSCs recovered in a single cord is generally too low for adult transplantation, and infusion of two separate cords still leads to delayed hematopoietic recovery[1]. Thus, the development of methods to readily expand HSCs *in vitro* would be a major leap forward.

In-depth understanding of the identities and function of each component of the hematopoietic microenvironment at the cellular and molecular levels will be crucial to learn how to properly expand HSCs. This knowledge gap has closed substantially after the concept of a stem cell niche was enunciated more than three decades ago[2]. It has been assumed by many, perhaps wishfully, that a do-it-all niche cell exists in the mammalian bone marrow. This idea comes from the original concept by Schofield[2] and also from strong experimental work in the germline of invertebrates, where specific niche cells are thought to provide the necessary goods to maintain germline stem cells[3]. In the mammalian bone marrow, candidate niche cells including osteoblasts[4], Cxcl12-abundant reticular cells[5] and nestin-positive mesenchymal stem cells[6] have been reported, suggesting a key role for skeletal precursor cells. Two recent studies have added further complexity to the cellular makeup of putative HSC niches in bone marrow[7,8] (**Fig. 1**).

Yamazaki *et al.*[7] were searching for microenvironments enabling HSC dormancy in the bone marrow. Cell cycle quiescence is a hallmark of somatic stem cells and a key behavior to protect them from hematopoietic stresses and exhaustion[9]. Transforming growth factor-β (TGF-β) is a powerful molecule capable of inducing HSC quiescence through inhibition of the lipid-raft clustering that assembles growth factor signaling microdomains[10]. As it is secreted as an inactive form, active TGF-β is generated locally through local protease activity. If TGF-β were to be crucial in promoting HSC quiescence, one would expect that the putative niche would provide a specific environment for its activation. Yamazaki *et al.*[7] have found that glial fibrillary acidic protein (GFAP)-positive Schwann cells (which ensheath sympathetic nerve fibers) express β_8 integrin, which promotes metalloproteinase-mediated TGF-β activation. Afferent sympathetic nerves form a complex with nestin-positive cells within the bone marrow, in which the nerve itself may regulate HSC quiescence (**Fig. 1**). Unexpectedly, a reduction of HSC frequency in the bone marrow occurred when mice were surgically sympathectomized by ligation of the sympathetic trunk. The authors have suggested that the loss of Schwann cells led to HSC differentiation. Other less invasive, but also less specific, methods of sympathectomy (such as femoral and sciatic neurectomy), however, have not led to such reductions in HSC activity[11], suggesting the presence of other signals that may collaborate with those provided by the Schwann cells of sympathetic nerves. Although the latter issue still needs to be clarified, the findings support the crucial function of local sympathetic nerves in the regulation of hematopoiesis.

Another study in mice evaluated the cellular source of stem cell factor (SCF), encoded by the kit ligand gene (*Kitl*), a growth factor required for HSC maintenance in a non–cell-autonomous manner[8]. SCF exists in two forms, membrane bound and soluble, due to differential splicing and proteolytic cleavage; however, the membrane-bound form seems to play a prominent part in HSC maintenance[12]. When expressed under the *Kitl* locus, GFP expression was mostly localized in cells associated with sinusoids, the fenestrated blood vessels within the bone marrow[8]. The authors made tissue-restricted deletions of *Kitl* or knock-in expression of reporters including GFP in osteoblasts, perivascular cells expressing nestin or leptin receptor (Lepr) and endothelial cells. A reduction of HSC frequency was only found in Lepr-expressing perivascular cells and endothelial cells lacking *Kitl*, suggesting that SCF was provided by both cell types, although the contribution from the former type may be much greater. This study proposed that Lepr-expressing and nestin-expressing cells are distinct, as the deletion of *Kitl* using transgenic lines expressing Cre

Yuya Kunisaki and Paul S. Frenette are at the Ruth L. and David S. Gottesman Institute for Stem Cell and Regenerative Medicine Research and the Departments of Medicine and Cell Biology, Albert Einstein College of Medicine, Bronx, New York, USA. e-mail: paul.frenette@einstein.yu.edu

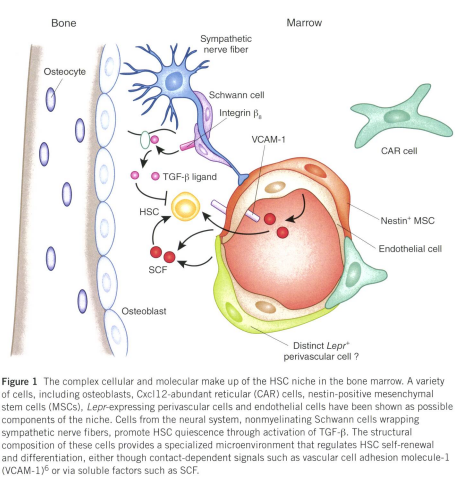

Marina Corral

Figure 1 The complex cellular and molecular make up of the HSC niche in the bone marrow. A variety of cells, including osteoblasts, Cxcl12-abundant reticular (CAR) cells, nestin-positive mesenchymal stem cells (MSCs), *Lepr*-expressing perivascular cells and endothelial cells have been shown as possible components of the niche. Cells from the neural system, nonmyelinating Schwann cells wrapping sympathetic nerve fibers, promote HSC quiescence through activation of TGF-β. The structural composition of these cells provides a specialized microenvironment that regulates HSC self-renewal and differentiation, either though contact-dependent signals such as vascular cell adhesion molecule-1 (VCAM-1)[6] or via soluble factors such as SCF.

under control of the *Nes* promoter did not elicit the same phenotype. It is important to note, however, that *Lepr* was among the top 1% most highly expressed genes in sorted nestin-positive mouse cells by microarray analysis[6], suggesting a potential overlap between the two niche cells, which will require further investigation. Thus, cells associated with the vasculature are the major source of SCF in the bone marrow under steady state. It will be important to evaluate whether the same stromal cells produce the cytokine in situations of regenerative stress, which may shed light on the requirements for building an artificial niche dedicated for HSC expansion.

These two studies bring new exciting angles that add further complexity to bone marrow niches; at the same time, they give us a reminder about the considerable hurdles ahead of us in achieving expansion of HSCs expanded HSCs for clinical use. HSCs require an array of secreted and contact factors—most of which still remain unknown—for their maintenance and proliferation. If these factors are indeed provided by distinct stromal cell types, the challenge of concocting the right ratios of niche constituents to support HSCs for clinical use becomes very substantial. By the same token, one can imagine the translational difficulty in obtaining a renewable source of a good-manufacturing-practice–grade cellular cocktail that would meet the safety thresholds for clinical cell therapy. Further studies will aim at characterizing stromal cell types and, most importantly, the molecular constituents and signals that allow HSC proliferation while maintaining self-renewal.

A major obstacle for future translational HSC-based therapeutics highlighted by the study of Yamazaki *et al.*[7] concerns the propensity of adult HSCs to remain quiescent. This natural preference was repeatedly shown in several studies where genetic mutations leading to HSC proliferation invariably produce HSC exhaustion[9]. How can we unlock HSCs from their quiescent behavior for the purpose of expansion without reaching exhaustion? It is likely that the coupling of self-renewal and quiescence is not absolute, given that it is not the case for all stem cells; for example, embryonic stem cells can both proliferate and self-renew indefinitely. The ultimate solution, through a greater understanding of the molecular basis of the niche, may lie in some sort of direct or indirect reprogramming of adult (quiescent) HSCs into fetal-like (proliferative) stem cells, a feat that will have to be achieved without increasing the risk of malignancies. Every scientific hurdle, almost by definition, can be overcome. We may be just one breakthrough away from surmounting this one.

COMPETING FINANCIAL INTERESTS
The authors declare no competing financial interests.

1. Brunstein, C.G. *et al. Blood* **116**, 4693–4699 (2010).
2. Schofield, R. *Blood Cells* **4**, 7–25 (1978).
3. Byrd, D.T. & Kimble, J. *Semin. Cell Dev. Biol.* **20**, 1107–1113 (2009).
4. Scadden, D.T. *Nature* **441**, 1075–1079 (2006).
5. Sugiyama, T., Kohara, H., Noda, M. & Nagasawa, T. *Immunity* **25**, 977–988 (2006).
6. Méndez-Ferrer, S. *et al. Nature* **466**, 829–834 (2010).
7. Yamazaki, S. *et al. Cell* **147**, 1146–1158 (2011).
8. Ding, L., Saunders, T.L., Enikolopov, G. & Morrison, S.J. *Nature* **481**, 457–462 (2012).
9. Pietras, E.M., Warr, M.R. & Passegue, E. *J. Cell Biol.* **195**, 709–720 (2011).
10. Yamazaki, S. *et al. Blood* **113**, 1250–1256 (2009).
11. Katayama, Y. *et al. Cell* **124**, 407–421 (2006).
12. Broudy, V.C. *Blood* **90**, 1345–1364 (1997).

■ BEDSIDE TO BENCH

Metabolic priming for AML

Rushdia Z Yusuf, Ying-Hua Wang & David T Scadden

Cancer survivors have recovered from a brush with death, but their battle is often not over. The rigors of their initial bout with the disease predispose them to a second round, often with a more lethal foe in the form of secondary acute myeloid leukemia (AML). The risk of these events is high after particular types of cancer therapy and in people with 'premalignant' myleodysplastic syndrome (MDS) and myeloproliferative disorder, indicating that patient groups can therefore be assessed for markers that may predict for the fight to come. Approximately 15% of all AML develops secondary to cancer chemotherapy with

Rushdia Z. Yusuf, Ying-Hua Wang and David T. Scadden are at the Massachusetts General Hospital Center for Regenerative Medicine and Cancer Center, Harvard Stem Cell Institute, Department of Stem Cell and Regenerative Biology, Harvard University, Boston, Massachusetts, USA.
e-mail: dscadden@mgh.harvard.edu

alkylating agents or topoisomerase inhibitors[1]. Alkylating agents function by adding alkyl groups to DNA, causing DNA damage. Ideally, this would result in cancer cell death; however, it can also lead to incorrect chromosome segregation in cancer cells that escape apoptosis and frequent loss of portions of chromosomes 5q and 7q (ref. 2). DNA topoisomerase inhibitors result in DNA cleavage and chromosome breakage, leading to apoptosis. However, in cancer cells where this process does not go as planned, translocations, often involving the mixed-lineage leukemia gene (*MLL*), can lead to secondary AML[3].

Historically, secondary AML was thought to be essentially untreatable. However, it is now clear that it comprises a heterogeneous group of disorders, and prognosis and choice of treatment depends upon the cytogenetic and molecular changes found in the particular case under consideration[4]. The study of those at risk for secondary AML provides a unique opportunity for capturing the molecular events driving clonal dominance that eventuates in leukemia.

By combining clinical data with gene sequencing of patient samples, researchers have been able to assess genetic changes in the predisposition setting. For example, a recent study compared whole-genome sequence data from seven individuals with *de novo* MDS and the secondary AML that emerged. All samples had clonal outgrowths, and 11 recurrently mutated genes in secondary AML were identified, including 9 that were also mutated in the precedent MDS[5]. Assessing a much larger group—bone marrow samples from 439 patients with MDS—Bejar *et al.*[6] have also recently identified somatic point mutations in 18 genes, and these genes were associated with ultimate prognostic value[6]. A previous study also described a signature of 38 genes in bone marrow cells that indicated advanced risk of MDS and AML (99.3% positive predictive value) in a selected patient group with a high frequency of therapy-related MDS and AML[1]. Together, these studies are shaping our understanding of not only the specific genes associated with risk of secondary malignancy but also the cellular processes involved. In the two studies where the genes evaluated were not preselected[1,5], there was a remarkable heterogeneity and identification of poorly annotated genes and transcriptional regulators. Rather impressive, however, is the implication of metabolism in at least one of the studies[1]. Metabolic derangement is well known in cancer but is less clearly associated with cancer predisposition.

The link between metabolic alteration and cancer was first made by Otto Warburg in the early twentieth century when he provided the provocative observation that cancer cells preferentially consume glucose and metabolize it to lactate even in the presence of oxygen[7]. Aerobic glycolysis was viewed as a corruption of the more highly efficient ATP-generating oxidative phosphorylation associated with normal cells. More modern interpretations, however, argue that the cancer cell is using a modification of metabolic pathways adaptively, shifting in favor of the production of macromolecules needed to meet the biomass demands of rapidly dividing cells[8]. This interpretation of Warburg's observation has accumulated a substantial amount of supporting experimental data.

Several studies provide evidence that at least some leukemias use the Warburg effect. PKM2 and HIF1-α, both inducers of the Warburg effect, have both been implicated in AML pathogenesis[9,10]. Isocitrate dehydrogenase 1 (*IDH1*) and *IDH2* mutations in AML are associated with promotion of aerobic glycolysis through induction of HIF1-α stability[11,12] and with production of an oncometabolite that inhibits a chromatin modifier, thereby also connecting metabolism with epigenetic control of gene expression[13].

Left unanswered is whether the metabolic events observed in cancer are always reactive to conditions imposed by transformation or can also be central to it[14]. Does cancer force a change in the way nutritive substrates are used out of the necessity proliferation imposes or is the metabolic shift a primary event, fostering the subsequent development of malignancy? Although the study by Li *et al.*[1] suggests the latter, as metabolic alterations were in the predictive gene set, other data argue that metabolic changes do little to engender cancer risk. In the case of *IDH2*, for example, germline mutations (*IDH2 R140*) in humans that are identical to those found in some human cancers do not provide a predilection to cancer in those individuals[15]. Metabolic alterations may therefore be only minor risk modifiers acting in concert with other changes, such as the epigenetic alterations effected by IDH mutations that could change gene expression such that alteration of the differentiation state would cooperate with a distinct lesion, altering cell growth. Alternatively, the metabolic change may provide the macromolecular substrates needed for new cell generation, enabling a growth-provoking mutation to circumnavigate the full reprogramming of cell metabolism that might otherwise prove limiting.

An entirely unanticipated scenario for the role of metabolism in cancer has recently emerged on the basis of a study of the metabolic interaction between malignant cells and their microenvironment. The relationship of parenchymal cells to their mesenchymal microenvironment in adult tissues is now accepted to be regulatory, in part owing to what has been learned of normal hematopoietic stem and progenitor cells and their niche. The niche concept had a controversial start when proposed in 1978 (ref. 16). At that time, the concept was in competition with an accepted wisdom that inherent randomness determined whether stem cells would differentiate, divide or self-renew—whether stem cell behavior was cell autonomous. Similarly, the notion that cancer is a cell-autonomous disease has long, perhaps reasonably, been the predominant model driving pathophysiologic evaluations of cancer. But cancer cells clearly exist in the context of tissue and may be viewed as a tissue, not a cell, gone rogue[17].

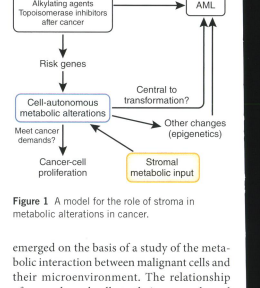

Figure 1 A model for the role of stroma in metabolic alterations in cancer.

A recent study has indicated that cancer-cell metabolism interacts with metabolic features of the bone marrow microenvironment in a fundamental way[18]. In the setting of chronic lymphocytic leukemia (CLL), bone marrow stroma conversion of cystine to cysteine was crucial for the survival of leukemia cells and their protection against oxidative damage. The authors suggest this may explain why CLL cells do not survive in *ex vivo* culture[18]. Whereas a dependence on the tumor-cell microenvironment has been proposed before, these findings directly implicate the metabolic milieu as part of the dependence. The match between the metabolic activity of therapy-damaged hematopoietic cells and perturbed microenvironmental cells may be needed to achieve the necessary ecosystem for cancer emergence. Going forward, inclusion in new investigations of studies on the microenvironmental cells of those at high risk for secondary leukemia would be of inter-

est, particularly in evaluating whether there are changes in genes that create a symbiotic relationship between the malignant cell and its supporting niche. Identification of such parameters may offer therapeutic targets to render the microenvironment less hospitable for the deranged cancer cell. Any progress in helping cancer survivors in their fight against their secondary AML would be worthy of our attention.

COMPETING FINANCIAL INTERESTS
The authors declare competing financial interests: details are available in the online version of the paper.

1. Li, L. *et al. Cancer Cell* **20**, 591–605 (2011).
2. Davies, S.M. *Med. Pediatr. Oncol.* **36**, 536–540 (2001).
3. Felix, C.A. *Med. Pediatr. Oncol.* **36**, 525–535 (2001).
4. Rowe, J.M. *Leukemia* **16**, 748–750 (2002).
5. Walter, M.J. *et al. N. Engl. J. Med.* **366**, 1090–1098 (2012).
6. Bejar, R. *et al. N. Engl. J. Med.* **364**, 2496–2506 (2011).
7. Warburg, O. *Oncologia* **9**, 75–83 (1956).
8. Vander Heiden, M.G., Cantley, L.C. & Thompson, C.B. *Science* **324**, 1029–1033 (2009).
9. Hitosugi, T. *et al. Sci. Signal.* **2**, ra73 (2009).
10. Wang, Y. *et al. Cell Stem Cell* **8**, 399–411 (2011).
11. Mardis, E.R. *et al. N. Engl. J. Med.* **361**, 1058–1066 (2009).
12. Dang, L. *et al. Nature* **462**, 739–744 (2009).
13. Figueroa, M.E. *et al. Cancer Cell* **18**, 553–567 (2010).
14. Levine, A.J. & Puzio-Kuter, A.M. *Science* **330**, 1340–1344 (2010).
15. Kranendijk, M. *et al. Science* **330**, 336 (2010).
16. Schofield, R. *Blood Cells* **4**, 7–25 (1978).
17. Greaves, M. & Maley, C.C. *Nature* **481**, 306–313 (2012).
18. Zhang, W. *et al. Nat. Cell Biol.* **14**, 276–286 (2012).

■ NEUROLOGICAL DISORDERS

The pull of the prions

Misfolded prion protein causes the buildup of voltage-gated calcium channels inside the cell, interfering with normal neuronal communication and causing motor dysfunction, according to a recent study (*Neuron* **74**, 300–313).

Mutations in the *PRNP* gene can lead to PrP protein aggregation and can cause a variety of neurological diseases in humans that are commonly linked to motor dysfunction. Assunta Senatore *et al.* found that, compared with mice expressing wild-type PrP, mice expressing mutant PrP showed reductions in glutamate release at synapses in the cerebellum, a part of the brain that controls motor function.

Voltage-gated calcium channels (VGCCs) are required at the surface of synapses for normal release of glutamate. The researchers found that mutant PrP bound VGCCs and prevented them from being delivered to the cell surface. These findings suggest that enhancing VGCC transport to synapses could ameliorate motor dysfunction in prion diseases. —*EC*

■ IMMUNOLOGY

Bugs tune gut defenses

Commensal bacteria colonize the gut mucosa, and secretion of IgA, the most abundant antibody type in mucosal secretions, by the gut is required to maintain immune homeostasis, promote tolerance and defend against pathogens in the presence of commensals.

A recent study now shows that the programmed cell death-1 (PD-1) inhibitory co-receptor regulates the microbiota by selecting the appropriate IgA repertoire (*Science* **336**, 485–489). Using mice lacking PD-1, Kawamoto *et al.* found that its deficiency perturbed the bacterial composition. Although the number of IgA-producing cells in the lamina propria, the mucosal layer that recruits immune effector cells, stayed the same, there was a change in the IgA repertoire and less coating of bacteria by IgA in PD-1–deficient mice.

The altered IgA repertoire seen in PD-1–deficient mice seems to occur because of an increased turnover of IgA-producing cells in the lamina propria, an effect that was abrogated after antibiotic treatment, suggesting that the microbiota drives selection of IgAs at this site. The authors also observed a more rapid transit of B cells through germinal centers located in lymphoid structures, where antibody affinity maturation and diversification occur. Within germinal centers, T follicular helper (T_{FH}) cells help out B cells and promote their differentiation into antibody-secreting cells or memory B cells. In the germinal centers of PD-1–deficient mice, T_{FH} cells were more abundant and had a skewed cytokine profile, which may alter the selection of B cells and cause changes in the types of gut IgAs that they produce.

As mice lacking PD-1 showed hyperactivation of the immune system and production of antibodies against commensals, these findings suggest PD-1 absence may cause loss of tolerance. Further studies should investigate the role of PD-1 in autoimmune diseases in humans and its potential as a target to modulate these diseases. —*CP*

INFECTIOUS DISEASES

NO means yes to *Listeria* infection

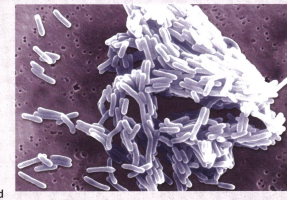

Pr Courtesy / Photo Researchers, Inc.

Listeria monocytogenes **is a food-borne pathogen that causes gastroenteritis in healthy persons and potentially fatal systemic infections in immunocompromised individuals. The bacteria are phagocytosed by macrophages and subsequently spread in a cell-to-cell manner that is crucial for their virulence. Caroline Cole *et al.* now shed light on how *L. monocytogenes* avoids innate immune responses and subverts a host cell factor to facilitate its cell-to-cell spread. (*Immunity* doi:10.1016/j.immuni.2012.03.011).**

Usually, the activation of Toll-like receptors by bacterial lipopolysaccharide (LPS) enhances the antimicrobial killing activity of macrophages, but the Gram-positive *L. monocytogenes* manages to avoid this fate. Cole *et al.* now show that even when macrophages are stimulated with LPS, their subsequent increased expression of nitric oxide synthase 2 (NOS2) and production of nitric oxide (NO) actually increases—rather than decreases—*L. monocytogenes* cell-to-cell spread.

Cell-to-cell spread of the bacteria occurs by the extrusion of pseudopods containing *L. monocytogenes* from a primary infected cell and their subsequent uptake by a recipient cell. Although the direct mechanism by which NO helps *L. monocytogenes* to spread remains unclear, the authors propose that NO delays the maturation of phagosomes that contain the bacteria, slowing their killing by the recipient cell. The researchers showed an increased escape of the bacteria into the cytosol associated with the delayed phagosome maturation and, ultimately, an increased bacterial burden. Understanding the mechanisms by which bacteria such as *L. monocytogenes* can circumvent immune responses may provide new insights into controlling the infections caused by these organisms. —*AF*

■ METABOLIC DISORDERS

BuMPing up thermogenesis

Brown adipose tissue (BAT) is coming to the forefront as a master regulator of metabolism and energy expenditure through its essential role in thermogenesis. A recent report provides clues on how this function is finely tuned by identifying bone morphogenetic protein 8B (BMP8B) as a regulator of thermogenesis that acts on both BAT and the central nervous system (*Cell* **149**, 871–885).

BMP signaling has pleiotropic effects in many tissues, but, although BMPs have been shown to promote BAT differentiation and have an emerging role in adipogenesis, a role in BAT activation was not known. Whittle *et al.* now show that BMP8B is the prevalent BMP in mature BAT cells, where it is activated by prothermogenic stimuli and signaling.

In mice lacking BMP8B, the authors observed a progressive weight gain, which was exacerbated by a high-fat diet, and linked the fat accumulation to deficient BAT activation. Interestingly, BMP8B is also present in the regions of the hypothalamus known to control thermogenesis, and in its absence the brain could not properly respond to a high-fat diet by revving up BAT metabolism.

Treatment of mice with BMP8B induced sympathetic BAT activation through the brain and also caused an increased response to thermogenic signaling in BAT adipocytes, resulting in weight loss. Further studies will

be needed to show whether this new BAT regulating mechanism is also active in humans and whether it could be explored as a relevant therapeutic target for metabolic and obesity disorders. —*VA*

■ BONE

Autoantibodies target bone

Autoantibodies against proteins marked with a type of post-translational modification called citrullination are found in people with rheumatoid arthritis and are one of the strongest risk factors for bone destruction in this disease. A recent study now directly links the formation of these antibodies to bone loss in rheumatoid arthritis, indicating that the autoantibodies act on osteoclasts, the bone cells responsible for bone resorption (*J. Clin. Invest.* **122**, 1791–1802).

Gary Gaugler/Photo Researchers, Inc.

Ulrike Harre *et al.* found that the presence of anti–citrullinated protein antibodies (ACPAs) is associated with increased amounts of serum markers of bone resorption in people with rheumatoid arthritis. They affinity-purified autoantibodies against mutated citrullinated vimentin from patients; the production of these antibodies is highly specific to people with rheumatoid arthritis. *In vitro*, these purified ACPAs bound to the surface of osteoclast progenitors and induced their differentiation into mature osteoclasts and also increased osteoclast-mediated bone resorption.

The authors then injected the purified ACPAs into immunodeficient *Rag1*$^{-/-}$ mice, leading to systemic bone loss. This bone loss seemed to be mediated through an increase in osteoclast precursor numbers and increased osteoclast differentiation in response to ACPAs. These effects may depend on tumor necrosis factor-α, as the authors observed increased amounts of this inflammatory cytokine, which is known to induce osteoclastogenesis, in the mice treated with ACPAs.

This work thus provides new insights into the interactions between the immune system, inflammation and bone in rheumatoid arthritis. —*MS*

■ GENETICS

Somatic mutations in brain

A new study highlights an intriguing role for somatic mutations restricted to the brain in a developmental brain disorder, hemimegalencephaly (HMG) (*Neuron* **74**, 41–48).

HMG is an epileptic brain disorder characterized by the enlargement and malformation of one hemisphere of the brain. Given this regional selectivity of the deformation, it has been suggested that HMG may be caused by a somatic mutation limited to the brain, and Annapurna Poduri *et al.* now provide evidence to support this hypothesis.

The authors analyzed resected brain tissue samples from eight individuals with HMG and found that two of the samples showed trisomy of chromosome 1q, but, in one of the individuals, the blood sample did not show this genetic aberration. Of the genes on chromosome 1q, Poduri *et al.* suggest *AKT3* as a strong candidate gene for HMG, because *AKT3* deletions have been previously associated with microcephaly in humans and mice. Moreover, somatic activating mutations in the related genes *AKT1* and *AKT2* have been associated with human overgrowth syndromes. The authors also found a somatic activating mutation of AKT3 (E17K) in the brain of one individual with HMG.

These results suggest that somatic mutations in the brain could have an important role in neurogenetic disease, although the mechanisms by which they occur remain to be determined. They also bring up an interesting parallel between somatic mutations in cancer and in brain disease: somatic *AKT3* mutations have also been identified in cancer, but none of the individuals studied by Poduri *et al.* had any form of cancer, suggesting that *AKT3* mutations may result in different outcomes in different cellular contexts. —*MS*

Written by Victoria Aranda, Eva Chmielnicki, Alison Farrell, Carolina Pola and Meera Swami

New from NPG

Apolipoprotein E controls cerebrovascular integrity via cyclophilin A
Bell, R.D. *et al. Nature* doi:10.1038/nature11087 (16 May).
The authors provide a mechanistic link between the *APOE4* gene and blood-brain–barrier defects by showing that *APOE4* expression in mice activates a pathway in pericytes involving cyclophilin A (CypA) activation. This leads to neuronal uptake of blood-derived neurotoxic proteins. Thus, CypA may be a potential target for treating APOE4-mediated neurovascular injury, such as in Alzheimer's disease.

PPAR-γ is a major driver of the accumulation and phenotype of adipose tissue T_{reg} cells
Cipolletta, D. *et al. Nature* doi:10.1038/nature11132 (16 May).
This study uncovers a new aspect to the action of the thiazolidinedione drug pioglitazone, used in the treatment of type 2 diabetes. The authors show that a population of regulatory T cells in the visceral fat are controlled by peroxisome proliferator–activated receptor γ (PPAR-γ) and that the expression of PPAR-γ in these cells is important for the insulin-sensitizing activity of pioglitazone.

Detectable clonal mosaicism and its relationship to aging and cancer
Jacobs, K.B. *et al. Nat. Genet.* doi:10.1038/ng.2270 (6 May).

Detectable clonal mosaicism from birth to old age and its relationship to cancer
Laurie, C.C. *et al. Nat. Genet.* doi:10.1038/ng.2271 (6 May).
Two new studies find mosaicism for large chromosomal abnormalities in peripheral blood samples from individuals in the general population. The frequency of these genetic changes increases with age and is associated with an increased risk of subsequently developing a hematological cancer.

Adolescent impulsivity phenotypes characterized by distinct brain networks
Whelan, R. *et al. Nat. Neurosci.* doi:10.1038/nn.3092 (29 April).
The authors examine the activation of brain networks in adolescents with attention-deficit hyperactivity disorder (ADHD) and those who had used drugs or alcohol using functional magnetic resonance imaging. They find that although both ADHD and substance abuse are associated with increased impulsiveness, different brain networks were activated in response to a task testing impulsiveness in these two contexts.

BoneKEy Reports

NEW TO NPG IN 2012

BoneKEy Reports: a new monthly online journal in the field of bone and mineral metabolism

Part of the *IBMS BoneKEy* platform, ***BoneKEy Reports*** serves the international community of researchers and physicians with in-depth coverage on all scientific and clinical aspects of bone health and disease.

- High-quality reviews
- **BoneKEy Watch** – weekly research highlights of key content across the bone field
- Basic science subjects such as bone cell and molecular biology
- Clinical topics including: osteoporosis diagnosis/management, genetics, and biomechanics
- Multimedia article templates

Access to *BoneKEy Reports* is available through IBMS membership, a personal subscription, or a site license through your institution.

www.nature.com/bonekeyreports

IBMS BoneKEy

nature publishing group npg

nature medicine

REVIEW

Taming lupus—a new understanding of pathogenesis is leading to clinical advances

Zheng Liu & Anne Davidson

Systemic lupus erythematosus (SLE) is an autoimmune disease that is characterized by the loss of tolerance to nuclear self antigens, the production of pathogenic autoantibodies and damage to multiple organ systems. Over the years, patients with SLE have been managed largely with empiric immunosuppressive therapies, which are associated with substantial toxicities and do not always provide adequate control of the disease. The development of targeted therapies that specifically address disease pathogenesis or progression has lagged, largely because of the complex and heterogeneous nature of the disease, as well as difficulties in designing uniform outcome measures for clinical trials. Recent advances that could improve the treatment of SLE include the identification of genetic variations that influence the risk of developing the disease, an enhanced understanding of innate and adaptive immune activation and regulation of tolerance, dissection of immune cell activation and inflammatory pathways and elucidation of mechanisms and markers of tissue damage. These discoveries, together with improvements in clinical trial design, form a platform from which to launch the development of a new generation of lupus therapies.

SLE is an autoimmune disease predominantly affecting females in which loss of tolerance to nucleic acids and their interacting proteins results in the production of pathogenic autoantibodies that cause inflammation and tissue damage. The disease often begins during childbearing years and is characterized by flares and remissions affecting multiple organs, as well as by the consequences of immunosuppressive medications used to control the disease and cumulative organ damage. A marked improvement in the survival of patients with lupus over the last 50 years is attributable largely to advances in the medical management of life threatening conditions that can occur during the course of disease, such as infections and renal impairment. In contrast, the development of targeted therapies that specifically address disease pathogenesis and progression has lagged, resulting in a limited therapeutic armamentarium of broad-spectrum immunosuppressive agents that have substantial toxicities and are not always adequate to control symptoms or prevent disease flares. Recent clinical trials based on rational hypotheses and robust preclinical effects in mouse SLE models have tested the efficacy of new biologic drugs in combination with standard-of-care therapies but have met with only limited success[1]. The recent approval by the US Food and Drug Administration (FDA) of belimumab, a monoclonal antibody that targets the B cell survival cytokine B cell activating factor (BAFF), for the treatment of moderately active lupus shows that a rational approach may be successful; however, some clinicians have reservations about belimumab because its therapeutic effect is modest and may decrease over time[2,3] (**Box 1**). One reason for the lack of a therapeutic breakthrough in SLE is the difficulty in evaluating therapeutic outcomes, largely because of its complex pathogenesis, the heterogeneity of clinical manifestations and the perceived inadequacies in clinical trial design and in the outcome instruments themselves. In addition, proof-of-concept studies using mouse models have their limitations: the mice are highly homogeneous, therapies are compared to placebo rather than the standard of care, and the timing of treatment (including the use of knockout mice) has mostly been preventive.

Despite the disappointing results of the first forays into biologic therapies for SLE, basic scientific discoveries made over the last decade have greatly enhanced our understanding of the pathogenesis of autoimmune diseases; some of these discoveries could evolve into new therapeutic strategies for SLE that complement or even replace the currently used broadly immunosuppressive treatments. These discoveries, encompassing genetics, immune-cell subsets and activation pathways, inflammation, mechanisms of tissue damage and biomarker discovery lay the foundation for improved clinical trials of new systemic and local therapies.

The current view of SLE is that it is a heterogeneous group of diseases in which environmental exposures in a genetically susceptible individual trigger activation of both innate and adaptive immune responses, resulting in loss of tolerance to ubiquitous self antigens. There may be a prolonged preclinical phase that is characterized by the accumulation of an increasing number of autoantibody specificities, followed by inflammation and tissue injury, onset of clinical symptoms, continuing immune amplification and, finally, irreversible tissue damage (**Fig. 1**). The goal of this review is to summarize recent immunologic discoveries that have a direct bearing on the

Center for Autoimmunity and Musculoskeletal Diseases, Feinstein Institute for Medical Research, Manhasset, New York, USA. Correspondence should be addressed to A.D. (adavidson1@nshs.edu).

Published online 6 June 2012; doi:10.1038/nm.2752

pathogenesis of SLE and that should form the basis of a new generation of lupus therapies that improve both longevity and quality of life in patients with lupus.

Progress in defining the genetic basis of SLE

Animal studies have shown that genetic alterations in diverse single genes or the simultaneous genetic alteration of multiple genes may lead to the development of lupus-like diseases[4,5]. In humans, a number of single genetic deficiencies, such as those affecting components of the classical complement activation pathway or intracellular nucleases, are strongly associated with SLE. More recently, genome-wide association studies (GWASs) that use millions of common single nucleotide polymorphisms as genomic markers to type increasingly large datasets of well-defined patient and control populations have definitively linked a number of genetic variants to disease susceptibility[6–8].

Although this field is still in its early stages, some fundamental concepts have emerged regarding the inheritance of autoimmunity. First, with the exception of the major histocompatibility complex (MHC), the genetic risk loci that have been identified by GWASs involve a conglomeration of relatively common alleles, each of which confers only a modest risk, with odds ratios less than two. Second, some of these polymorphisms are shared between autoimmune disorders. Third, not all of the risk genes cross major racial groups. Fourth, genetic studies have identified functional pathways that are involved in disease pathogenesis[7,8]. In SLE, three main immune pathways have been identified: aberrant clearance of nucleic-acid–containing debris and immune complexes, excessive innate immune activation involving Toll-like receptors (TLRs) and type I interferons (IFNs) and abnormal T and B lymphocyte activation[8]. In addition, genetic polymorphisms may be associated with susceptibility to target organ damage[9,10] (**Fig. 2**). These SLE-related pathways overlap with those identified in mouse lupus models and are currently leading to the development of therapeutics that target key components of these pathways.

Applying this new information to individual patients is now a major challenge. As many of the identified single nucleotide polymorphisms are not within coding regions, attribution of disease risk to a single gene requires extensive resequencing of large regions of DNA from many patients, which is a daunting and costly task. Furthermore, the risk variants identified so far account for only a small proportion of the overall heritability of disease[7], highlighting the limitations of the GWAS approach[11], which identifies only common polymorphisms with frequencies within the population of greater than 1–5%. The finding that 3′ repair exonuclease 1 (TREX1) is mutated in 0.5–2% of patients with SLE but was not identified in GWAS exemplifies the limitations of the GWAS approach for detecting variants at the lower end of this range. New methodology to identify rare variants, copy number variations and epistatic changes are being developed, but these alterations will only be found in a small fraction of affected individuals. Moreover, it is not easy to establish a link between genetic variations, gene function and disease pathogenesis. Many of the risk alleles identified by GWASs are common variants with subtle effects that are compatible with normal immunological function; some variants may even have been evolutionarily selected because they confer protection against certain pathogens. Even for genes with coding-region mutations, such as *TREX1* and *PTPN22*, functional studies have either not yet elicited definitive mechanisms by which the disease-associated polymorphism leads to increased risk for SLE or have yielded conflicting results[12,13]. More studies will be required to understand how disease-associated variants affect immune responses and interact with each other to contribute to the risk of SLE. Nevertheless, as the function of the variants is clarified and potentially pathogenic pathways are identified, personalized interventions may become possible.

BOX 1 Belimumab is the first biologic drug approved by the FDA for the treatment of SLE

Belimumab is a human monoclonal antibody against the cytokine BAFF (also known as BLyS). BAFF and its homolog APRIL are members of the trimeric TNF family and are expressed by multiple cell types. BAFF binds to three receptors, BAFF-R, TACI and BCMA (B cell maturation antigen), that are expressed by B cells at various developmental stages. BAFF-R is specific for BAFF, whereas TACI and BCMA also bind to APRIL. Strong evidence implicates BAFF, and perhaps APRIL, in the pathogenesis of SLE. In non-autoimmune mice, overexpression of BAFF is sufficient to cause lupus in a T cell–independent manner, and BAFF blockade delays disease onset. Increased serum concentrations of BAFF and APRIL have been detected in patients with SLE, and BAFF concentrations have been reported to correlate with disease activity. BAFF, through its interaction with BAFF-R, regulates selection of the naive B cell repertoire and is required for the survival of mature B cells. BAFF and APRIL, primarily through their interaction with TACI, facilitate class switching of immunoglobulin genes and are involved in the amplification of TLR-mediated signals through the interaction of the TACI signaling pathway with the MyD88 pathway. Either BAFF or APRIL is sufficient to support the survival of plasma cells through their interaction with TACI, BCMA or both, but neither is required for the survival of memory B cells. BAFF receptors are also expressed by T cells, and BAFF may have a T cell co-stimulatory role. BAFF receptors are also expressed by activated monocytes, and BAFF can facilitate the production of proinflammatory cytokines from these cells (reviewed in refs. 143,144).

The clinical efficacy of belimumab was shown at week 52 after the start of treatment in two large phase 3 clinical trials (BLISS-52 and BLISS-76) in serologically positive patients with SLE with moderately active disease but without severe renal or central nervous system involvement[2,3]. Belimumab significantly depleted the number of transitional and naive B cells but resulted in a transient increase in the number of memory cells[145] and had more of an effect on circulating IgM- than IgG-producing plasma cells[80]. Belimumab resulted in an improvement in serological activity over time[145] and, crucially, conferred both steroid-sparing effects and a decrease in severe flares; these disease features are often responsible for cumulative irreversible tissue injury. After these successful trials, belimumab was approved by the FDA, becoming the first new drug to be approved for the treatment of patients with SLE in 50 years. However, despite its clear clinical efficacy, enthusiasm for using belimumab in clinical practice has been tempered by the failure to sustain the primary efficacy outcome at 76 weeks of treatment in patients in the United States, as well as the high cost of the drug. Furthermore, because the mechanism for the efficacy of belimumab is SLE is not entirely clear, it is difficult to define the immunologic parameters of response or predict which patients will respond best[145] to treatment. Furthermore, it remains to be determined how patients with more severe manifestations will respond to belimumab.

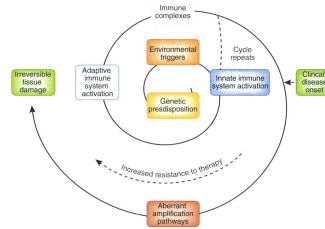

Figure 1 The spiral of disease progression in SLE. Individuals with identified genetic polymorphisms are at higher risk for SLE compared to the general population. Environmental triggers also probably contribute to the initiation and perpetuation of the disease. Activation of the innate immune system results in enhanced antigen presentation to T cells and the release of proinflammatory cytokines, including type I IFNs. These changes facilitate activation of the adaptive immune system and the development of autoantibodies. Autoantibodies bind to nucleic acids or cellular debris to form complexes that provide further stimulation to innate immune cells through TLRs. Autoreactive B cells act as antigen-presenting cells for the recruitment of more autoreactive T cells. These positive feedback loops that involve the innate and adaptive immune systems amplify clones of autoreactive lymphocytes during the preclinical stage of SLE. The onset of clinical manifestations is associated with systemic inflammation and injury of target organs, resulting in further amplification of immune activation. SLE becomes increasingly resistant to immune-modulating therapies and may eventually progress to irreversible tissue damage. The events that start to occur before or after the clinical onset are shown in green or blue, respectively.

Although the practical applicability of individual genetic profiling seems distant, pilot studies are currently underway to explore the prediction of risk in family members and the prediction of disease phenotype and severity in individual patients[10,14]. Testing is already being used in the clinic for gene variants that affect the metabolism of the immunosuppressive drug azathioprine to help predict the risk for toxicity associated with the use of this drug in patients[15]. Undoubtedly, other applications of the new genetic knowledge will be forthcoming.

The reasons for gender bias in SLE

SLE is nine times more common in women than in men. Studies in mice have shown multiple effects of both male and female sex steroids on the immune system[16]; studies in knockout mice have clearly attributed the immune-activating effects of estrogen to signaling by the estrogen receptor α. However, a clear correlation of female sex hormone concentrations and disease activity has not been established in human patients, reflecting the complexity of the contributions from genetic and environmental factors. The X chromosome harbors many genes of immunologic interest. In gonad-matched mice, the presence of XX confers a greater susceptibility to pristane-induced lupus than does XY[17]. Similarly, in humans, the XXY phenotype is associated with an increased prevalence of SLE. Although there are decreased concentrations of protective T helper type 2 (T_H2) cytokines in XX mice than in XY mice, the genetic components of the XX chromosome complement associated with lupus risk are not clear. As candidate genes on the X chromosome are identified and validated in gonad-matched mice, new therapies for female patients with SLE may emerge.

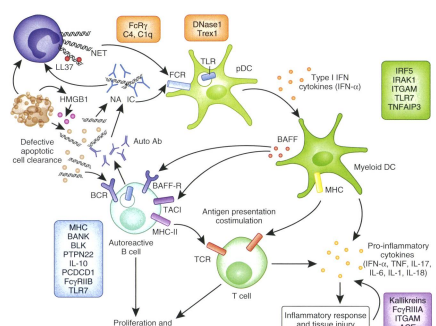

Figure 2 The role of SLE risk alleles in the pathogenesis of SLE. A panoply of genetic variations has been linked to SLE susceptibility. Polymorphisms in genes involved in the immune clearance of apoptotic particles and nucleic-acid–containing immune complexes (clearance functions, with examples shown in orange) may induce the enhanced activation of pDCs and autoreactive B cells, leading to the production of type I IFN and the expansion of autoreactive effector cells, respectively. Polymorphisms in genes involved in innate immunity (with examples shown in green) regulate the induction of, as well as the response to, type I IFN. Abnormal function of innate immune cells in turn activates the adaptive immune system. Both the innate and adaptive immune systems contribute to the inflammatory response and tissue damage. A third major group of polymorphic genes is involved in ligand recognition, receptor signaling and other immunological functions of adaptive immune cells (with examples shown in blue). Dysregulation of the adaptive immune system results in loss of tolerance and the production of autoantibodies, which in turn bind to nuclear antigens and activate innate immune cells, completing a positive feedback loop that amplifies the pathogenic processes in SLE. Polymorphic alleles may also influence the severity of organ damage (with examples shown in purple). Ab, antibody; IRAK1, interleukin-1 receptor-associated kinase 1; ITGAM, integrin α M; TNFAIP3, tumor necrosis factor, α-induced protein 3; BANK, B cell scaffold protein with ankyrin repeats; BLK, B lymphoid tyrosine kinase; PCDCD1, programmed cell death 1; NA, nucleic acid; IC, immune complex; ACE, angiotensin I converting enzyme (peptidyl-dipeptidase A) 1.

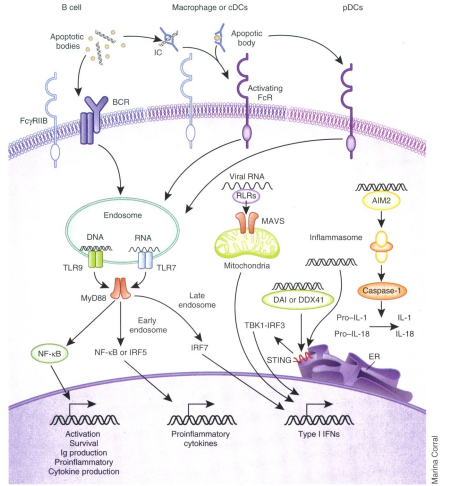

Figure 3 Recognition of nucleic acids by innate immune cells triggers cytokine production. Nucleic acids or apoptotic particles can be taken up by B cells through the BCR, and immune complexes containing these antigens are taken up by monocytes, myeloid dendritic cells and pDCs through FcR-mediated recognition and internalization. Within endosomes, DNA and RNA then interact with TLR9 and TLR7, respectively. Viral RNA can also be delivered to endosomes by autophagosome formation in pDCs. The ligation of TLRs recruits the adaptor protein MyD88, which activates the NF-κB signaling cascade in B cells and leads to B cell activation and survival, as well as various effector functions. In pDCs, the recruitment of MyD88 preferentially triggers an IRF7-mediated signaling pathway, which initiates type I IFN production. In other cell types, MyD88 recruitment in late endosomes leads to inflammatory cytokine production. Cytosolic DNA and RNA can be recognized by sensors that, through adaptors, lead to type I IFN production. Cytosolic DNA can also be recognized by AIM2, which activates caspase-1, leading to proteolytic cleavage of pro–IL-1 and pro–IL-18 into active forms. Immune complexes may signal directly through both activating and inhibitory FcRs whose relative expression on the cell surface varies with cell activation status. How these positive and negative signals are integrated with each other and with TLR-mediated signals has not yet been fully elucidated. cDC, conventional dendritic cell; RLR, RIG-I like receptors; DDX41, a member of the DEXDc family of helicases; TBK1, TANK-binding kinase 1; ER, endoplasmic reticulum; Ig, immunoglobulin.

The innate immune system is activated by nucleic acids

Safe clearance of ubiquitous cell debris is a normal immune function that is crucial for the maintenance of self tolerance; multiple pathways exist for clearing the billions of cell corpses generated daily. Apoptotic cells are engulfed by phagocytes through receptors that recognize altered cell membrane components or self antigens opsonized by 'natural' IgM autoantibodies that are present in the sera of healthy individuals, early complement components or both, inducing a suppressive program that facilitates the disposal of debris with little consequent inflammation[18]. In addition, nucleases break down circulating nucleic acids, preventing their recognition by innate receptors[19]. Defective clearance mechanisms result in secondary necrosis and an overload of self antigens that, instead of being safely consumed by phagocytes, access proinflammatory receptors, such as activating Fc receptors (FcRs) or TLRs on or inside innate immune cells.

The best studied innate cell in SLE is the plasmacytoid dendritic cell (pDC), which produces large amounts of type I IFNs in response to nucleic-acid–containing immune complexes (NA-IC) and can migrate to injured sites[20,21]. The pathogenic role of type I IFNs in SLE is supported by a signature of IFN-induced genes in the peripheral blood of patients[22], an association with risk alleles involved in TLR and IFN pathways[23], disease acceleration by exogenous IFN-α in several lupus models[24,25] and disease amelioration in some lupus-prone mouse strains that have been rendered deficient for the type I IFN receptor[26,27]. Type I IFNs have multiple proinflammatory functions in both innate and adaptive immune cells[28] and can also activate and damage endothelial cells[29]. Identification of a neutrophil signature in the blood of patients with lupus led to the recent discovery that neutrophils exposed to NA-IC are prone to die by NETosis: these dying cells extrude DNA webs (neutrophil extracellular traps, NETs) that are associated with small alarmin peptides, such as the calthelicidin LL37, that protect the DNA from nucleases. LL37-complexed DNA in turn activates pDCs, enhancing the release of type I IFNs[30,31]. It is now crucial to determine whether this amplification mechanism prevails *in vivo* and whether NET formation is required for disease to develop. Even basophils activated by IgE autoantibodies have been reported to have a proinflammatory role in lupus[32]. The relative contribution of each of these cell types to lupus pathogenesis remains to be determined.

Some TLRs are on the cell surface and interact with the circulating products of tissue injury and inflammation; in contrast, nucleic-acid–specific TLRs (TLR3, TLR7, TLR8 and TLR9) are segregated in an unprocessed form within intracellular vesicles, where they are subsequently cleaved before interacting with internalized ligands[33]. Great progress has been made in understanding the intracellular trafficking of nucleic acid antigens, TLR signaling mechanisms and downstream consequences of TLR signaling (**Fig. 3**). NA-IC and opsonized cellular debris are internalized by binding to activating FcRs on innate cells[34]; the uptake and intracellular trafficking of self antigens may be facilitated by LL37 (ref. 35) or high mobility group

box 1 (HMGB1)[36], an intracellular protein that is released by dying cells or activated monocytes and dendritic cells. Vesicles containing the internalized antigens then fuse with TLR-containing endosomes to form large autophagosomes in which processed TLRs, antigens and signaling molecules can interact[37]. On interaction with their ligands and a series of adaptor molecules, TLRs initiate transcription of either type I IFNs or inflammatory cytokines, depending on where the ligand binding occurs. In pDCs, TLR binding in early endosomes preferentially induces phosphorylation of interferon regulatory factor 7 (IRF7), which initiates the transcription of type I IFNs. In contrast, TLR ligation in late endosomes favors the activation of nuclear factor of κ light polypeptide gene enhancer in B cells (NF-κB) or mitogen-activated protein kinase (MAPK) signaling pathways, resulting in the abundant production of proinflammatory cytokines[37], such as interleukin-6 (IL-6), IL-12, tumor necrosis factor α (TNF-α) or BAFF, that serve to bridge innate and adaptive immunity, contributing to the overall inflammatory process of SLE[38]. Nucleic-acid–containing debris can also be taken up by the B cell receptor (BCR) of autoreactive B cells, resulting in cell activation and differentiation and the expression of transmembrane activator and calcium modulator ligand interactor (TACI), the receptor for the B cell survival molecules BAFF and APRIL, a proliferation ligand[39].

It is now clear that IgG antibodies to double-stranded DNA are produced only when TLR9 is accessed[40], whereas antibodies to RNA require TLR7 (ref. 40). Nevertheless, TLR9 deficiency exacerbates SLE in mouse models, perhaps because it competes with TLR7 for transport to intracellular compartments; absence of this competition skews the autoantibody specificity to a more pathogenic anti-RNA profile[41]. TLR7 deficiency has modest protective[42] effects, but full protection from disease is only achieved when both TLR7 and TLR9, or their adaptor protein myeloid differentiation primary response gene 88 (MyD88), are absent[41]. Notably, susceptibility to SLE in mice overexpressing TLR7 is conferred predominantly by excess TLR7 expression in B cells, illustrating the overlap of innate receptor function with adaptive lymphocyte populations[43]. Other nucleic acid sensors detect cytosolic DNA and RNA[44] (**Fig. 3**). Cytosolic RNA derived from viruses, a possible trigger for disease onset in some cases[45], is recognized by retinoic acid inducible receptor (RIG-I)-like family receptors, which signal through a mitochondrial adaptor protein, the mitochondrial antiviral signaling protein (MAVS), to initiate type I IFN transcription. Cytosolic DNA sensors are less well defined and may include DNA-dependent activator of interferon regulatory factor (DAI), absent in melanoma 2 (AIM2) and stimulator of interferon genes (STING). Although DAI was the first cytosolic DNA sensor identified[46], its absence does not prevent cytosolic-DNA–induced signaling, leading to considerable skepticism about its role in intracellular nucleic acid surveillance[47]. Recent studies have provided convincing results that support the role of STING as either an adaptor protein or a direct component of the cytosolic-DNA–sensing machinery that is negatively regulated by the exonuclease Trex1 (refs. 48,49). AIM2 is different from other sensors in that its interaction with DNA activates the inflammasome, leading to the production of active IL-1β and IL-18.

Although more work needs to be done to delineate how the various innate immune activation pathways interact and are regulated, and whether innate immune activation is required for both disease initiation and perpetuation, this new understanding offers opportunities for cell-specific intervention or for intervention that is targeted to shared pathways, such as TLR signaling or type I IFN release.

The adaptive immune system becomes activated in SLE

Adaptive immunity involves the clonal expansion of lymphocytes and the generation of long-lived effector T and B cells. Self-reactive lymphocytes are continuously generated by somatic gene processes that establish the large repertoire of T and B cell receptors required for protection against pathogens. Although relatively low affinity natural IgM autoantibodies, made by specific innate B cell subsets, help to prevent immune responses to the products of cell death, potentially pathogenic self-reactive lymphocytes are removed at specific developmental checkpoints (deletion), become unresponsive to external stimulation (anergy), replace their receptors (receptor editing) or are suppressed by regulatory molecules or cells[50]. In SLE, these regulatory mechanisms may be genetically defective, environmentally altered or both. Substantial evidence points to clonal expansion of autoreactive B lymphocytes in the preclinical phase of SLE[51], and most mouse studies have shown a requirement for T cells in disease initiation.

T lymphocytes are activated on recognition of a peptide–MHC complex on activated antigen-presenting cells. Polymorphisms in MHC molecules control the size and diversity of the peptide repertoire that is presented to T cells and thus have a major impact on T cell activation and the subsequent immune responses. The strongest genetic risk alleles for SLE have been mapped across the MHC region in humans[6], implying that loss of T cell tolerance in SLE might be triggered by aberrant MHC presentation of particular peptides. In addition, peripheral T cells from patients with SLE have altered signaling and a faster T cell calcium flux than those of healthy individuals as a result of replacement of the principle signaling molecule of the TCR complex, cluster of differentiation 3 ζ (CD3-ζ), by the FcR γ chain[52], resulting in the use of the adaptor molecule spleen tyrosine kinase (SYK) rather than the usual ζ chain (TCR) associated protein kinase (ZAP70) and activation of the downstream kinase calcium/calmodulin-dependent protein kinase type IV (CAMK4) that, through the transcription factor cAMP response element modulator α (CREM-α), enhances production of IL-17 and blocks production of IL-2. Other abnormalities of T cell function in SLE that contribute to excessive activation or failure of regulation include T cell mitochondrial dysfunction leading to oxidative stress[53], a decrease in the cytotoxic activity of CD8 cells[54] and increased expression of the co-stimulatory molecule CD40 ligand (CD40L) and of the adhesion molecule CD44 on $CD4^+$ T cells. CD44 ligation results in the activation of ρ-kinase coiled-coil–containing domain protein kinase (ROCK), which promotes the production of IL-17 and IL-21. The identification of key signaling molecules in SLE T cells, such as SYK, CAMK4 and ROCK, has resulted in successful proof-of-principle use of inhibitors in SLE models[55–57] that may now be translated to human use.

The role of newly discovered T cell subsets in SLE pathogenesis is also being investigated. Dysregulation of follicular T helper (T_{FH}) cells that promote B cell differentiation in germinal centers is associated with the development of SLE in mouse models[58], and expansion of a circulating T_{FH} cell population has been reported in patients with active SLE[59]. In SLE models, abundant T_{FH}-like cells are also located outside the germinal centers, where they support extrafollicular B cell differentiation[60]. Other reported abnormalities include a decrease in the number of regulatory T cells during active SLE and an expansion of the $CD3^+CD4^-CD8^-$ cell population[61] that produces the proinflammatory cytokine IL-17 and may contribute to local inflammation in the kidneys. Given the extensive heterogeneity among patients with SLE, it is plausible that genetically diverse individuals exposed to varying environments will differ in the

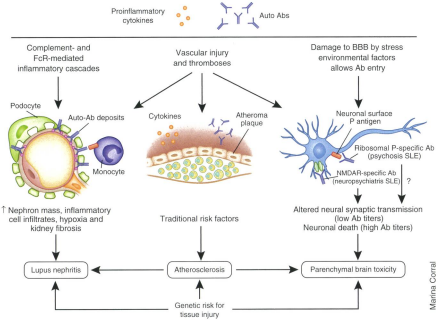

Figure 4 Mechanisms for organ damage. Organ damage is caused by immune activation and inflammation but is also influenced by genetic and nonimmunologic environmental factors. Autoantibodies and circulating inflammatory mediators trigger tissue injury in target organs by a variety of mechanisms. In the kidneys, immune complex deposition induces complement- and FcR-mediated inflammatory cascades that lead to the activation or injury of renal resident cells, which in turn release inflammatory mediators, leading to the recruitment of inflammatory cells. Long term renal damage is caused by ongoing inflammation, vascular injury by systemic and local mediators, hypoxia and fibrosis. Nephritis occurs in approximately 50% of adult and 80% of pediatric patients with SLE, and the rate of end-stage renal disease in the United States caused by SLE seems to be increasing, especially in minority patients. In the cardiovascular system, autoantibodies and soluble inflammatory mediators cause vascular endothelial injury by inducing endothelial apoptosis or activation. Recruitment of monocytes to the injured site is also crucial for plaque formation. Other proatherogenic factors in addition to traditional risk factors include oxidized low-density lipoproteins, antibodies to oxidized lipids and proinflammatory high-density lipoproteins. The 10-year risk for a coronary event or stroke is 7.5- to 17-fold increased in patients with SLE compared with healthy individuals. In the central nervous system, autoantibodies access the brain when the BBB is attenuated by inflammatory mediators or environmental factors, such as cigarette smoke or neurotransmitters released by stress. Once deposited in the brain, autoantibodies may induce neuron apoptosis or alter neuronal synaptic transmission. Neurologic injury can also result from secondary causes, such as thrombosis or infections. All these pathogenic changes lead to a wide range of neuropsychiatric manifestations of SLE, including progressive cognitive dysfunction. Neuropsychiatric manifestations may occur relatively early in the disease process, and they affect up to 40% of patients.

mechanism for disease initiation and/or the phenotype or function of dominant effector T cell subsets and will therefore require different therapeutic strategies. For example, in some individuals, excessive activation may predominate, whereas in others there may be a failure of regulation.

Defective B cell tolerance is another hallmark of SLE. Central and peripheral checkpoints that remove self-reactive immature B cells are defective in patients with SLE[50,62]. Enhanced BCR signaling can lead to autoreactivity, probably as a result of excessive B cell activation after the late transitional stage, when BCR signals start to activate the cells rather than tolerize them. Signals from several molecules, including CD19, intracellular TLRs and the BAFF receptor (BAFF-R) interact with BCR signals to enhance B cell activation and survival at this stage, and an excess of any of these molecules may predispose to SLE[63]. In addition, an SLE-susceptibility–related polymorphism in PTPN22 is associated with early B cell tolerance defects through a mechanism that has not yet been determined[64,65].

B cell tolerance can also be broken during antigen activation. An area of intense interest is the regulation of the germinal center, where clonal expansion of B cells occurs, along with somatic mutation, class switching and differentiation to long-lived effector cells. Germinal center selection is clearly defective in SLE, allowing autoreactive B cells to differentiate into pathogenic memory and plasma cells[66]. Recent live microscopy studies of secondary lymphoid organs have revealed mechanisms for the efficient sampling of antigens and the intricate orchestration of sequential reciprocal interactions between B cells, T cells and follicular dendritic cells before and during the germinal center reaction[67]. Despite the enormous gains in knowledge that have been made about the anatomy of germinal centers, a convincing explanation of how the autoreactive B cells that are inevitably generated by somatic mutation are regulated at or after the germinal center stage has yet to emerge. A recapitulation of some of the negative selection events found in early B cell development is probable. The loss of germinal center tolerance in SLE could be the result of an excess of T cell help, defects in B cell signaling or death, an excess of self antigens resulting from inadequate clearance of apoptotic cells[68] or defects in the function of various regulatory cells, including B cells[69] or T cells[70,71]. The association of SLE with an acquired decrease in the expression of the inhibitory receptor FcγRIIB has been experimentally attributed to an intrinsic failure of regulation of activated B cells in the post–germinal-center phase[72].

Autoreactive B cells can also be expanded outside germinal centers. Excess inflammatory signals, such as IL-12 (ref. 73), TLR ligation[74] or CD40 ligation[75], preferentially promote B cell expansion in extrafollicular foci in which short-lived plasma cells with a limited degree of somatic mutation arise. Little is currently known about the regulation of autoreactive B cells during the extrafollicular response or the relative contribution of this response to the pool of pathogenic effector cells in SLE.

Despite a decrease in total circulating B cells in many patients with SLE, long-lived autoreactive effector memory and plasma cells are often increased in number and, because of their quiescent state, may be resistant to immunosuppression. Molecules such as BAFF or APRIL, IL-6, transforming growth factor β (TGF-β), chemokine (C-X-C motif) ligand 12 (CXCL12) and vascular cell adhesion molecule (VCAM) contribute to bone marrow 'survival niches' that support long-lived plasma cells[76,77]. Inflamed organs express many of these molecules and can become sites for disorganized lymphoid follicles or even germinal centers in which normal regulation might be disturbed, as well as a new niche for plasma cells[78]. It is worth

noting that plasma cells are resistant to B cell depletion therapy with rituximab[78], and neither class-switched memory B cells nor long-lived plasma cells are eliminated by BAFF blockade[79,80].

Given the multiple roles of B cells in disease pathogenesis and the absolute requirement for B cells in disease initiation, a large amount of effort has been devoted to B cell–directed therapies in SLE, with phase 3 studies having been completed for the BAFF antagonist belimumab, the B cell–depleting agent rituximab (anti-CD20) and the T cell co-stimulatory antagonist abatacept (CTLA4Ig), which blocks the development of T_{FH} cells (see **Boxes 1** and **2** and **Table 1** and refs. 81–83 for comprehensive reviews). Of these, only belimumab has thus far been successful in placebo-controlled clinical trials, reflecting the complexity of treating a chronic disease in which adaptive immune system activation and clonal expansion have already occurred.

Target organ damage is mediated by diverse mechanisms

Although autoantibodies are a hallmark of SLE, the mechanisms of tissue injury by autoantibodies are variable, and the pathogenic specificities that direct autoantibodies to particular target organs can be difficult to identify. Depositing autoantibodies may directly injure or activate cells, initiate the complement cascade or activate innate receptors, leading to local inflammation. Furthermore, isotype differences in FcR and complement-binding activities influence antibody pathogenicity, and the cellular inflammatory response can vary in different organs or in patients with different genotypes, resulting in heterogeneous types of injury. This section is focused on recent advances in understanding the mechanisms that mediate injury in the brain, kidney and blood vessels (**Fig. 4**). Involvement of these vital organs contributes to substantial morbidity and mortality in SLE.

SLE is characterized by wide range of neuropsychiatric syndromes. Although many of these manifestations are the result of secondary causes, autoantibodies may directly cause vascular or parenchymal injury; the association of phospholipid-specific antibodies with intracranial clotting events is well known[84]. Recent studies have begun to unravel the pathogenic events involved in parenchymal injury. Antibodies directed to the N-methyl-D-aspartate receptor (NMDAR) and to ribosomal P protein can be detected in the cerebrospinal fluid of patients with neuropsychiatric SLE; serum P-specific antibodies are predictive of future SLE psychosis[85]. In experimental mice, a low concentration of NMDAR-specific antibody alters neural synaptic transmission, whereas a high concentration of this antibody induces neuronal death, providing some insight into the observations that cognitive dysfunction is transient in some patients and is permanent in others[86]. Neuronal damage mediated by NMDAR-specific antibody occurs without inflammation and is independent of complement activation or FcR ligation[87]. The mechanisms for tissue damage mediated by ribosomal P-specific antibodies are not as well characterized, but studies in mice have shown direct deposition of these autoantibodies in various regions of the brain and their cross reactivity with neuronal surface P antigen[88], suggesting a toxicity mechanism similar to that postulated for NMDAR-specific antibodies. Furthermore, the integrity of the brain-blood barrier (BBB) needs to be compromised for these autoantibodies to enter the brain and exert their pathogenic effects[89]. Depending on the mechanism by which the BBB is breached, autoantibodies may enter different anatomic sites, thereby causing different neuropsychiatric manifestations. These findings suggest that therapies directed at protection of the BBB and brain parenchyma may be effective in neuropsychiatric SLE.

Lupus nephritis is initiated by the deposition of immune complexes that may activate complement[90], engage activating FcRs on mononuclear cells[91] and/or activate resident renal cells, such as mesangial cells and endothelial cells, through FcRs or TLRs[92,93]. Mesangial cells produce inflammatory mediators, whereas endothelial cells either undergo apoptosis or facilitate the influx of inflammatory cells into the interstitium[94]; these infiltrating cells may then undergo local expansion and differentiation. Renal inflammation is associated with overexpression of diverse cytokines and chemokines that are upregulated at various stages of lupus nephritis and at different renal sites[95]. T_H1 and T_H17 cells have been detected in human proliferative lupus kidneys[96], and both TNF-α and IL-18 are local effector cytokines in at least some patients[97]. A relatively new development has been the identification of subsets of infiltrating renal macrophages and dendritic cells that mediate aberrant tissue remodeling and whose presence is associated with poor outcome[98,99]. As glomerular cells become injured and die, the decline of nephron mass and function is followed by the extension of the inflammatory process into the tubulointerstitium, with consequent damage to the renal tubules[100]. If the inciting injury remains active and the sites of tissue repair continue to be hypoxic, reparative processes become chronic and lead to the amplification of inflammation and fibrosis[101]. Eventually, deterioration of kidney function progresses even if the initiating inflammatory process has been adequately contained. Genetic polymorphisms may influence disease severity and the rate of progression; for example, kallikrein gene polymorphisms have recently been identified as susceptibility alleles for lupus nephritis[9], and an FcγRIIIA allele associated with excess activation confers risk for progression to end-stage disease[102]. These findings suggest that the progression of renal impairment in SLE shares many common mechanisms with other non-immune–mediated renal diseases and that strategies currently being applied in other diseases to prevent tissue hypoxia and remodeling may also be useful in SLE.

Atherosclerotic cardiovascular disease is increasingly being recognized as a major cause of death in patients with SLE; its high prevalence in SLE cannot be fully explained by traditional risk factors[103,104]. Persistent inflammation, circulating immune complexes, autoantibodies and corticosteroid use have all been proposed to contribute to the pathogenesis of atherosclerosis in SLE[105]. Vascular endothelial injury is the primary event in atherosclerosis and can be exacerbated in SLE by autoantibody- or cytokine-mediated endothelial apoptosis or by endothelial cell activation that induces the local production of pro-inflammatory cytokines and the upregulation of adhesive molecules that facilitate the local recruitment and activation of monocytes that help form plaque[105]. Another key observation in SLE is an imbalance of proinflammatory and anti-inflammatory lipids. Proinflammatory oxidized low-density lipoproteins, as well as antibodies to oxidized cardiolipin and oxidized low-density lipoproteins, have been detected in patients with SLE, with at least some subsets of these antibodies being proatherogenic[106–108]. High-density lipoproteins, instead of being protective, become proinflammatory in some patients with SLE[109]. These pathological events facilitate the development of foam cells and are linked to a high risk of plaque formation in SLE[105]. Disappointingly, initial studies of statins have failed so far to show any substantial protection from atherosclerosis progression in patients with SLE[110,111]. It is therefore imperative to determine which patients are most at risk for atherosclerosis progression and how best to protect the endothelium in these patients from inflammatory triggers.

Emerging areas in SLE

Although the last decade has brought the discovery of many new areas of knowledge relevant to the treatment of SLE, there is still a large

amount of unexplored territory. Technologic advances that allow the sequencing of individual genomes should uncover rarer variants that are associated with SLE and improve our understanding of the scope of the immune abnormalities associated with disease susceptibility, patterns and outcomes. Similarly, the delineation of the mechanisms of gene regulation is another key to understanding disease progression. Epigenetic alterations, such as DNA hypomethylation and histone modification, affect a wide range of immunological events, including cell death, cell activation and inflammation, and have been implicated in the pathogenesis of lupus[112,113]. In addition, the aberrant expression of microRNAs that regulate gene expression within normal and inflammatory environments has been associated with lupus[114,115]. More studies are needed to understand the full complement and function of microRNAs to exploit them as therapeutic targets. Systems biology approaches and high-throughput screening technologies should make all these areas more amenable to investigation using small amounts of human cells or tissue from well-phenotyped patients. Another technical advance has been the development of live-tissue imaging, which has opened up a dynamic understanding of biology within secondary lymphoid tissue and inflamed organs. Although this technology has mostly been applied to normal immune function, its application to diseased states will likely increase in the future.

The cellular regulation of immune responses is a new area of interest. The contribution of commensal gut flora to lupus is currently unknown, but the ability of particular commensal organisms to regulate proinflammatory T_H17 cell responses suggests that these organisms could influence target organ inflammation[116]. In addition, there is an ever growing repertoire of regulatory cell types whose function might be exploited *in vivo*. Finally, early studies are using both hematopoietic[117] and mesenchymal stem cells[118,119] to help reconstitute a predisease immune repertoire.

With the increasing recognition that genetic and phenotypic heterogeneity affects the clinical manifestations of SLE and patients' responses to therapies, there has been much interest in developing biomarkers for individualized disease risk prediction and prognosis, detecting impending disease flares, defining what constitutes a therapeutic response and predicting whether an individual patient is likely to mount a therapeutic response to a specific agent. This is the subject of a recent comprehensive review[120]. These types of biomarkers include measures of soluble molecules or sets of molecules in serum or urine, gene expression profiles from peripheral blood cells or tissues and functional assays of immune cell activation. Major challenges in biomarker development are the collection of longitudinal reliable and reproducible clinical data, as well as optimal specimen collection and storage. Interpretation of urine data needs to take into account the degree of proteinuria and the stability of the biomarker protein over time under conditions of variable pH, as well as the biology of the biomarker (size, tubular filtration, reabsorption and secretion characteristics, the presence of a cleaved form, and so on). Nevertheless, major methodologic advances in both generating datasets and data analysis have been made, as exemplified by the ability to group biomarkers into modules with predictive power[121,122]. In addition, several biomarkers of renal flare with somewhat improved sensitivity or specificity over the currently used serologic and urine measures have been identified in a limited number of longitudinal studies[123–125].

The promise and challenges of developing therapies for SLE

Systemic inflammation, NA-IC and tissue injury amplify immune activation in SLE by profoundly affecting both innate and adaptive immune cells. Furthermore, chronic inflammation in SLE activates aberrant signaling cascades that may impair normal regulatory control mechanisms or confer resistance to immunosuppressive drugs[126,127]. Some of these aberrant phenotypes may subsequently become fixed by epigenetic changes. With so many inflammatory pathways in play in active SLE, intense therapeutic intervention is often needed, and it can be difficult to balance the risks of prolonged or excessive immune suppression against those of smoldering inflammation. Mouse studies have shown that preventing clonal expansion of autoreactive B and T cells is effective in early disease, but this approach may fail once escalation of the immune response occurs; more aggressive drug combinations are then required to induce remission[128]. These findings suggest that earlier intervention and continuous maintenance therapy may reduce morbidity from the incremental tissue damage and drug toxicity that accompanies disease flares; the current therapeutic paradigm is to reserve immunosuppressive interventions for disease flares and withdraw the use of most medications during quiescence. As safer drugs are developed, this paradigm will probably change.

Another challenge is the variability in design and primary outcome measures in lupus clinical trials, making it impossible to compare the results of new experimental agents with each other or even to ascertain the therapeutic benefit of a single agent. One striking example

BOX 2 Reasons why clinical trials in SLE are challenging to perform and interpret

Challenges in trial design

- Outcome measures not uniform:
  - No consensus on the best way to measure responses to therapy.
  - Few validated biomarkers available.
- Disease may remit spontaneously.
- Therapies are compared with the standard of care, resulting in high response rates in the control group.

Heterogeneity in disease stage

- Pleiomorphic role for cytokines during different disease stages.
- Initiation: there may be a long preclinical phase during which the therapeutic window for some interventions may be closed.
- Progression: recruitment of long-lived effector cells, redundant inflammatory molecules, abnormal signaling pathways and epigenetic changes.
- End organ damage: irreversible tissue damage and fibrosis may progress despite immune quiescence.

Heterogeneity in disease mechanisms

- Multigenic origin with extensive intrapatient heterogeneity.
- Different pathogenic mechanisms and effector cell types among patients with lupus.
- Different injury mechanisms in various target organs, even within the same patient.

Homeostatic responses to therapy

- B cell depletion enhances B cell release from the bone marrow and impairs negative selection against autoreactivity.
- Plasma cell depletion may result in a prolonged immunoglobulin half-life.
- Depletion of naive and activated lymphocytes may lead to an increase in the number of memory cells.

Table 1 Therapeutic strategies for SLE

	Lessons from animal models of SLE[128,142]
Knockout mice can be used to study disease initiation.	Molecules involved in the clonal expansion of lymphocytes and/or germinal center functions are necessary for the initiation of disease in most models.
	Some molecules, such as type I IFNs and FcR, are involved in disease initiation or tissue damage only in certain strains, showing the effect of genetic heterogeneity on disease mechanisms.
	Some molecules, such as TLR9, TNF-α and IL-10, have pleiomorphic functions and therefore may be either protective or pathogenic, depending on the disease stage.
Specific targeting of immune pathways has proved less effective in attenuating disease than is observed in the knockouts.	Nearly all drugs are more effective at preventing disease onset than treating established disease. As disease progresses, higher drug doses and combination therapies are required to achieve remission. Different strains have different stringencies for therapeutic responses, and not all strains respond to each therapy.
	Recent approaches to SLE therapies[81–83]
Innate immunity	Approaches include targeting TLRs and their downstream signaling molecules and effector cytokines, improving clearance mechanisms using exogenous IgM and delivering exogenous DNase to compensate for intrinsic defects of this enzyme in SLE.
	Some aspects of TLR signaling are protective against autoimmunity in animal models.
	Circulating DNA in SLE may be resistant to digestion.
	These approaches are mostly experimental or are in development for human use. Phase 2 studies of IFN-α inhibition are pending.
Adaptive immunity—B cells	Approaches include B cell depletion, modulation of co-receptor function and alteration of B cell selection.
	These approaches rarely target all subsets of B cells and may lead to counterproductive homeostatic expansion of other subsets.
	Approaches that alter selection may have different effects on naive and antigen-activated immunoglobulin repertoires and may need to be given continuously to achieve clinical efficacy.
	Clinical trials have so far only shown efficacy for belimumab; new trials of individual treatments and drug combinations are underway.
Adaptive immunity—T cells	Approaches include co-stimulation blockade, cytokine inhibitors, kinase inhibitors and induction of regulatory subsets.
	Clinical trials of co-stimulatory inhibitors have so far either failed to show efficacy or were terminated because of toxicity; new trials of additional agents or drug combinations are underway.
	Effects of broad inhibitors of T cell activation may result in immune suppression.
Tissue injury and inflammation	Approaches include inhibitors of the complement cascade, cytokine blockade and nonimmunological approaches to preserve renal function.
	Nonimmunological approaches may prevent end-stage organ damage but have no effects on systemic immune dysfunction.
	Because of the pleiomorphic effects of cytokines, cytokine blockade may improve some aspects of disease but worsen others.
	Early clinical studies of cytokine blockade have produced promising results but have also shown adverse effects in several cases.
	Many new approaches are in development.

New therapies for SLE primarily target one of four major pathogenic pathways: innate immunity, B cells, T cells or tissue injury and inflammation. Although animal studies provide valuable insights into the therapeutic potential of experimental drugs for SLE, additional considerations are needed when predicting the probable outcomes of treatments in human patients.

is the different efficacy results obtained when alternative outcome measures were used to analyze the results of a trial of the T cell co-stimulatory inhibitor abatacept (CTLA4Ig) for SLE nephritis[129]. In addition, most clinical trials are of short duration, so the long-term benefits of even a modest decrease in flares or corticosteroid dose cannot be measured.

Apart from the contentious issue of trial design, heterogeneity in disease mechanisms among different individuals, disease stages and organ systems may greatly influence responses to therapeutic interventions. Given the multiple cell subsets and cytokines involved, as well as the emergence of abnormal and redundant cell activation pathways that make it difficult to achieve a therapeutic response by targeting single pathways and the capacity for ongoing organ damage even after immune quiescence, it is not surprising that the effects of new therapies in broad SLE populations compared with the current standard-of-care therapies, which have measurable efficacy, have been rather modest (**Box 2**). This highlights the need for determining whether a particular therapeutic approach will be appropriate for particular genotypic or phenotypic patient subsets; this is currently not possible, but it is an area that is ripe for exploration.

Despite these major mechanistic and logistic challenges, new immunologic discoveries have yielded a treasure trove of potential therapeutic avenues (**Table 1**). Targeting the innate immune system by enhancing clearance of DNA, RNA and cellular debris, inhibiting the activation of pattern recognition receptors or blocking downstream signaling events and cytokines may prevent cell activation by self antigens[130]. Components of the adaptive immune system are also attractive targets, which has led to the development of drugs that deplete or functionally inhibit particular B or T cell subsets or strategies that alter B cell tolerance or differentiation[54,81]. Cell-surface molecules can be targeted by monoclonal antibodies that either facilitate cell depletion or transmit activating or inhibitory signals into selected cells. Monoclonal antibodies can also target soluble molecules, particularly cytokines, thus altering the function of particular cell

subsets or inhibiting molecules that directly cause tissue damage[38]. Small molecules are being designed that enter cells and inhibit components of cell-signaling cascades[131]. Moreover, an enhanced understanding of immune regulation suggests the possibility of harnessing normal immune protective mechanisms to improve tolerance and protect target organs without the disadvantages that accompany excessive immunosuppression. As clinical trial design improves, the place of each intervention will need to be carefully determined.

In mouse models, late-stage disease that is resistant to single immune interventions can effectively be controlled with combination therapies[132,133]. Uncontrolled case series have suggested that combination therapies are also effective in humans despite concerns about toxicities, for example, the combination of rituximab, cyclophosphamide and prednisone is reportedly effective in some individuals with severe disease that are unresponsive to traditional immunosuppression[134], and a controlled trial of a combination treatment using abatacept and cyclophosphamide for nephritis is ongoing. However, it must be remembered that in humans, most clinical trials are currently designed to test new therapies on a background of standard maintenance therapies.

In addition to immune modulation, an improved understanding of the pathogenic processes in chronic organ injury is bringing new strategies to light. In a model of lupus in the central nervous system, a peptide mimic of the NMDAR receptor is able to block antibody-mediated damage to the brain parenchyma[135]. In lupus nephritis, the realization that immune complex deposition can be dissociated from renal inflammation[132,136] has prompted the exploration of mechanisms for the local recruitment of inflammatory cells and their soluble products, as well as mechanisms of tissue repair. Preserving renal function by inhibiting angiotensin activity, targeting local effector cytokines, inhibiting late complement components, addressing tissue hypoxia and using natural inhibitors of fibrosis are all avenues currently being explored to prevent chronic renal diseases[94,101,137–140]. Although optimal control of inflammation and aggressive management of traditional atherosclerosis risk factors seem to be prudent interventions in all patients, new strategies for the early detection of atherosclerotic lesions may direct potentially toxic therapies only to those patients most at risk for events[141]. Strict blood pressure control, appropriate nutrition and avoidance of environmental insults all provide long-term benefits to patients, and mechanisms need to be put in place to address the disparities that prevent delivery of this care. Furthermore, the identification of useful biomarkers may improve the ability to diagnose and treat disease flares, categorize patients for clinical trials and evaluate therapeutic responses.

Conclusions

Although SLE is a heterogeneous group of disease states linked together by the formation of autoantibodies directed to ubiquitous cellular debris, a comprehensive model of disease pathogenesis is beginning to evolve based on genetic studies and new immunologic discoveries that paint autoreactivity both as a necessity and a bane of immune responses. The disease is multigenic and involves a loss of tolerance in both innate and adaptive immune pathways that fails to be controlled by sequential regulatory mechanisms. Multiple triggers are probably involved in disease initiation and perpetuation. Tissue injury depends on antigen specificity and antigen access, as well as the degree of systemic inflammation and the strength of local inflammatory responses. Continuous exposure to excess nucleic-acid–containing material amplifies the disease process. Epigenetic changes may establish persistently aberrant activation pathways and maintain the inflammatory phenotype of long-lived effector cells. This broad range of immunologic abnormalities in SLE provides many opportunities for therapeutic intervention but is also responsible for the extensive heterogeneity and redundancy of inflammatory mechanisms that will probably require tailored or combined approaches. Improvements in clinical trial design together with the integration of genetic and biomarker information are new challenges that should be addressed as cooperative groups are formed to prioritize therapeutic approaches in the relatively limited number patients that meet the criteria for clinical trials. These strategies, together with discovery-based approaches using well-characterized human samples and the appropriate animal models, should translate into a decrease in morbidity and mortality in patients with SLE in the coming decades.

ACKNOWLEDGMENTS

This work was supported by US National Institutes of Health grants R01 DK085241-01, R01 AI083901 and R21 AR057930. The authors thank T. Rothstein and A. Boneparth for critical reading of the manuscript.

COMPETING FINANCIAL INTERESTS

The authors declare no competing financial interests.

Published online at http://www.nature.com/doifinder/10.1038/nm.2752.
Reprints and permissions information is available online at http://www.nature.com/reprints/index.html.

1. Lateef, A. & Petri, M. Biologics in the treatment of systemic lupus erythematosus. *Curr. Opin. Rheumatol.* **22**, 504–509 (2010).
2. Navarra, S.V. *et al.* Efficacy and safety of belimumab in patients with active systemic lupus erythematosus: a randomised, placebo-controlled, phase 3 trial. *Lancet* **377**, 721–731 (2011).
3. Furie, R. *et al.* A phase III, randomized, placebo-controlled study of belimumab, a monoclonal antibody that inhibits B lymphocyte stimulator, in patients with systemic lupus erythematosus. *Arthritis Rheum.* **63**, 3918–3930 (2011).
4. Morel, L. *et al.* Genetic reconstitution of systemic lupus erythematosus immunopathology with polycongenic murine strains. *Proc. Natl. Acad. Sci. USA* **97**, 6670–6675 (2000).
5. Lauwerys, B.R. & Wakeland, E.K. Genetics of lupus nephritis. *Lupus* **14**, 2–12 (2005).
6. Harley, J.B. *et al.* Genome-wide association scan in women with systemic lupus erythematosus identifies susceptibility variants in ITGAM, PXK, KIAA1542 and other loci. *Nat. Genet.* **40**, 204–210 (2008).
7. Deng, Y. & Tsao, B.P. Genetic susceptibility to systemic lupus erythematosus in the genomic era. *Nat. Rev. Rheumatol.* **6**, 683–692 (2010).
8. Flesher, D.L., Sun, X., Behrens, T.W., Graham, R.R. & Criswell, L.A. Recent advances in the genetics of systemic lupus erythematosus. *Expert Rev. Clin. Immunol.* **6**, 461–479 (2010).
9. Liu, K. *et al.* Kallikrein genes are associated with lupus and glomerular basement membrane-specific antibody-induced nephritis in mice and humans. *J. Clin. Invest.* **119**, 911–923 (2009).
10. Sanchez, E. *et al.* Phenotypic associations of genetic susceptibility loci in systemic lupus erythematosus. *Ann. Rheum. Dis.* **70**, 1752–1757 (2011).
11. Cantor, R.M., Lange, K. & Sinsheimer, J.S. Prioritizing GWAS results: a review of statistical methods and recommendations for their application. *Am. J. Hum. Genet.* **86**, 6–22 (2010).
12. Zhang, J. *et al.* The autoimmune disease-associated PTPN22 variant promotes calpain-mediated Lyp/Pep degradation associated with lymphocyte and dendritic cell hyperresponsiveness. *Nat. Genet.* **43**, 902–907 (2011).
13. Rieck, M. *et al.* Genetic variation in PTPN22 corresponds to altered function of T and B lymphocytes. *J. Immunol.* **179**, 4704–4710 (2007).
14. Taylor, K.E. *et al.* Risk alleles for systemic lupus erythematosus in a large case-control collection and associations with clinical subphenotypes. *PLoS Genet.* **7**, e1001311 (2011).
15. Askanase, A.D. *et al.* Use of pharmacogenetics, enzymatic phenotyping, and metabolite monitoring to guide treatment with azathioprine in patients with systemic lupus erythematosus. *J. Rheumatol.* **36**, 89–95 (2009).
16. Rubtsov, A.V., Rubtsova, K., Kappler, J.W. & Marrack, P. Genetic and hormonal factors in female-biased autoimmunity. *Autoimmun. Rev.* **9**, 494–498 (2010).
17. Smith-Bouvier, D.L. *et al.* A role for sex chromosome complement in the female bias in autoimmune disease. *J. Exp. Med.* **205**, 1099–1108 (2008).
18. Ravichandran, K.S. & Lorenz, U. Engulfment of apoptotic cells: signals for a good meal. *Nat. Rev. Immunol.* **7**, 964–974 (2007).
19. Martínez Valle, F., Balada, E., Ordi-Ros, J. & Vilardell-Tarres, M. DNase 1 and systemic lupus erythematosus. *Autoimmun. Rev.* **7**, 359–363 (2008).

20. Rönnblom, L. & Alm, G.V. The natural interferon-α producing cells in systemic lupus erythematosus. *Hum. Immunol.* **63**, 1181–1193 (2002).
21. Blanco, P., Palucka, A.K., Gill, M., Pascual, V. & Banchereau, J. Induction of dendritic cell differentiation by IFN-α in systemic lupus erythematosus. *Science* **294**, 1540–1543 (2001).
22. Bennett, L. *et al.* Interferon and granulopoiesis signatures in systemic lupus erythematosus blood. *J. Exp. Med.* **197**, 711–723 (2003).
23. Bauer, J.W. *et al.* Elevated serum levels of interferon-regulated chemokines are biomarkers for active human systemic lupus erythematosus. *PLoS Med.* **3**, e491 (2006).
24. Mathian, A., Weinberg, A., Gallegos, M., Banchereau, J. & Koutouzov, S. IFN-α induces early lethal lupus in preautoimmune (New Zealand Black × New Zealand White) F1 but not in BALB/c mice. *J. Immunol.* **174**, 2499–2506 (2005).
25. Ramanujam, M. *et al.* Interferon-α treatment of female (NZW × BXSB)F(1) mice mimics some but not all features associated with the Yaa mutation. *Arthritis Rheum.* **60**, 1096–1101 (2009).
26. Nacionales, D.C. *et al.* Deficiency of the type I interferon receptor protects mice from experimental lupus. *Arthritis Rheum.* **56**, 3770–3783 (2007).
27. Agrawal, H. *et al.* Deficiency of type I IFN receptor in lupus-prone New Zealand mixed 2328 mice decreases dendritic cell numbers and activation and protects from disease. *J. Immunol.* **183**, 6021–6029 (2009).
28. Banchereau, J. & Pascual, V. Type I interferon in systemic lupus erythematosus and other autoimmune diseases. *Immunity* **25**, 383–392 (2006).
29. Thacker, S.G. *et al.* The detrimental effects of IFN-α on vasculogenesis in lupus are mediated by repression of IL-1 pathways: potential role in atherogenesis and renal vascular dysfunction. *J. Immunol.* **185**, 4457–4469 (2010).
30. Garcia-Romo, G.S. *et al.* Netting neutrophils are major inducers of type I IFN production in pediatric systemic lupus erythematosus. *Sci. Transl. Med.* **3**, 73ra20 (2011).
31. Lande, R. *et al.* Neutrophils activate plasmacytoid dendritic cells by releasing self-DNA-peptide complexes in systemic lupus erythematosus. *Sci. Transl. Med.* **3**, 73ra19 (2011).
32. Charles, N., Hardwick, D., Daugas, E., Illei, G.G. & Rivera, J. Basophils and the T helper 2 environment can promote the development of lupus nephritis. *Nat. Med.* **16**, 701–707 (2010).
33. Kawai, T. & Akira, S. Toll-like receptors and their crosstalk with other innate receptors in infection and immunity. *Immunity* **34**, 637–650 (2011).
34. Boulé, M.W. *et al.* Toll-like receptor 9-dependent and –independent dendritic cell activation by chromatin-immunoglobulin G complexes. *J. Exp. Med.* **199**, 1631–1640 (2004).
35. Lande, R. *et al.* Plasmacytoid dendritic cells sense self-DNA coupled with antimicrobial peptide. *Nature* **449**, 564–569 (2007).
36. Tian, J. *et al.* Toll-like receptor 9–dependent activation by DNA-containing immune complexes is mediated by HMGB1 and RAGE. *Nat. Immunol.* **8**, 487–496 (2007).
37. Gilliet, M., Cao, W. & Liu, Y.J. Plasmacytoid dendritic cells: sensing nucleic acids in viral infection and autoimmune diseases. *Nat. Rev. Immunol.* **8**, 594–606 (2008).
38. Rönnblom, L. & Elkon, K.B. Cytokines as therapeutic targets in SLE. *Nat. Rev. Rheumatol.* **6**, 339–347 (2010).
39. Leadbetter, E.A. *et al.* Chromatin-IgG complexes activate B cells by dual engagement of IgM and Toll-like receptors. *Nature* **416**, 603–607 (2002).
40. Berland, R. *et al.* Toll-like receptor 7-dependent loss of B cell tolerance in pathogenic autoantibody knockin mice. *Immunity* **25**, 429–440 (2006).
41. Christensen, S.R. & Shlomchik, M.J. Regulation of lupus-related autoantibody production and clinical disease by Toll-like receptors. *Semin. Immunol.* **19**, 11–23 (2007).
42. Christensen, S.R. *et al.* Toll-like receptor 7 and TLR9 dictate autoantibody specificity and have opposing inflammatory and regulatory roles in a murine model of lupus. *Immunity* **25**, 417–428 (2006).
43. Fossati, L. *et al.* The Yaa gene-mediated acceleration of murine lupus: Yaa$^-$ T cells from non-autoimmune mice collaborate with Yaa$^+$ B cells to produce lupus autoantibodies *in vivo*. *Eur. J. Immunol.* **25**, 3412–3417 (1995).
44. Barbalat, R., Ewald, S.E., Mouchess, M.L. & Barton, G.M. Nucleic acid recognition by the innate immune system. *Annu. Rev. Immunol.* **29**, 185–214 (2011).
45. Harley, J.B., Harley, I.T., Guthridge, J.M. & James, J.A. The curiously suspicious: a role for Epstein-Barr virus in lupus. *Lupus* **15**, 768–777 (2006).
46. Takaoka, A. *et al.* DAI (DLM-1/ZBP1) is a cytosolic DNA sensor and an activator of innate immune response. *Nature* **448**, 501–505 (2007).
47. Ishii, K.J. *et al.* TANK-binding kinase-1 delineates innate and adaptive immune responses to DNA vaccines. *Nature* **451**, 725–729 (2008).
48. Zhang, Z. *et al.* The helicase DDX41 senses intracellular DNA mediated by the adaptor STING in dendritic cells. *Nat. Immunol.* **12**, 959–965 (2011).
49. Gall, A. *et al.* Autoimmunity initiates in nonhematopoietic cells and progresses via lymphocytes in an interferon-dependent autoimmune disease. *Immunity* **36**, 120–131 (2012).
50. Goodnow, C.C., Vinuesa, C.G., Randall, K.L., Mackay, F. & Brink, R. Control systems and decision making for antibody production. *Nat. Immunol.* **11**, 681–688 (2010).
51. Arbuckle, M.R. *et al.* Development of autoantibodies before the clinical onset of systemic lupus erythematosus. *N. Engl. J. Med.* **349**, 1526–1533 (2003).
52. Moulton, V.R. & Tsokos, G.C. Abnormalities of T cell signaling in systemic lupus erythematosus. *Arthritis Res. Ther.* **13**, 207 (2011).
53. Perl, A. *et al.* T-cell and B-cell signaling biomarkers and treatment targets in lupus. *Curr. Opin. Rheumatol.* **21**, 454–464 (2009).
54. Crispín, J.C., Kyttaris, V.C., Terhorst, C. & Tsokos, G.C. T cells as therapeutic targets in SLE. *Nat. Rev. Rheumatol.* **6**, 317–325 (2010).
55. Deng, G.M., Liu, L., Bahjat, F.R., Pine, P.R. & Tsokos, G.C. Suppression of skin and kidney disease by inhibition of spleen tyrosine kinase in lupus-prone mice. *Arthritis Rheum.* **62**, 2086–2092 (2010).
56. Ichinose, K., Juang, Y.T., Crispín, J.C., Kis-Toth, K. & Tsokos, G.C. Suppression of autoimmunity and organ pathology in lupus-prone mice upon inhibition of calcium/calmodulin-dependent protein kinase type IV. *Arthritis Rheum.* **63**, 523–529 (2011).
57. Bahjat, F.R. *et al.* An orally bioavailable spleen tyrosine kinase inhibitor delays disease progression and prolongs survival in murine lupus. *Arthritis Rheum.* **58**, 1433–1444 (2008).
58. Linterman, M.A. *et al.* Follicular helper T cells are required for systemic autoimmunity. *J. Exp. Med.* **206**, 561–576 (2009).
59. Simpson, N. *et al.* Expansion of circulating T cells resembling follicular helper T cells is a fixed phenotype that identifies a subset of severe systemic lupus erythematosus. *Arthritis Rheum.* **62**, 234–244 (2010).
60. Odegard, J.M. *et al.* ICOS-dependent extrafollicular helper T cells elicit IgG production via IL-21 in systemic autoimmunity. *J. Exp. Med.* **205**, 2873–2886 (2008).
61. Crispín, J.C. *et al.* Expanded double negative T cells in patients with systemic lupus erythematosus produce IL-17 and infiltrate the kidneys. *J. Immunol.* **181**, 8761–8766 (2008).
62. Wardemann, H. & Nussenzweig, M.C. B-cell self-tolerance in humans. *Adv. Immunol.* **95**, 83–110 (2007).
63. Liu, Z. & Davidson, A. BAFF and selection of autoreactive B cells. *Trends Immunol.* **32**, 388–394 (2011).
64. Arechiga, A.F. *et al.* Cutting edge: the PTPN22 allelic variant associated with autoimmunity impairs B cell signaling. *J. Immunol.* **182**, 3343–3347 (2009).
65. Menard, L. *et al.* The PTPN22 allele encoding an R620W variant interferes with the removal of developing autoreactive B cells in humans. *J. Clin. Invest.* **121**, 3635–3644 (2011).
66. Cappione, A. III *et al.* Germinal center exclusion of autoreactive B cells is defective in human systemic lupus erythematosus. *J. Clin. Invest.* **115**, 3205–3216 (2005).
67. Gonzalez, S.F. *et al.* Trafficking of B cell antigen in lymph nodes. *Annu. Rev. Immunol.* **29**, 215–233 (2011).
68. Kranich, J. *et al.* Follicular dendritic cells control engulfment of apoptotic bodies by secreting Mfge8. *J. Exp. Med.* **205**, 1293–1302 (2008).
69. Blair, P.A. *et al.* CD19$^+$CD24^{hi}CD38^{hi} B cells exhibit regulatory capacity in healthy individuals but are functionally impaired in systemic lupus erythematosus patients. *Immunity* **32**, 129–140 (2010).
70. Campbell, D.J. & Koch, M.A. T_{reg} cells: patrolling a dangerous neighborhood. *Nat. Med.* **17**, 929–930 (2011).
71. Kim, H.J. *et al.* CD8$^+$ T regulatory cells express the Ly49 Class I MHC receptor and are defective in autoimmune prone B6-Yaa mice. *Proc. Natl. Acad. Sci. USA* **108**, 2010–2015 (2011).
72. Brownlie, R.J. *et al.* Distinct cell-specific control of autoimmunity and infection by FcgammaRIIb. *J. Exp. Med.* **205**, 883–895 (2008).
73. Kim, S.J. *et al.* Increased IL-12 inhibits B cell differentiation to germinal center plasma cells and promotes differentiation to short-lived plasmablasts. *J. Exp. Med.* **205**, 2437–2448 (2008).
74. Herlands, R.A., William, J., Hershberg, U. & Shlomchik, M.J. Anti-chromatin antibodies drive *in vivo* antigen-specific activation and somatic hypermutation of rheumatoid factor B cells at extrafollicular sites. *Eur. J. Immunol.* **37**, 3339–3351 (2007).
75. Erickson, L.D. *et al.* Short-circuiting long-lived humoral immunity by the heightened engagement of CD40. *J. Clin. Invest.* **109**, 613–620 (2002).
76. Cassese, G. *et al.* Inflamed kidneys of NZB/W mice are a major site for the homeostasis of plasma cells. *Eur. J. Immunol.* **31**, 2726–2732 (2001).
77. Tokoyoda, K., Hauser, A.E., Nakayama, T. & Radbruch, A. Organization of immunological memory by bone marrow stroma. *Nat. Rev. Immunol.* **10**, 193–200 (2010).
78. Merrill, J.T. *et al.* Efficacy and safety of rituximab in moderately-to-severely active systemic lupus erythematosus: the randomized, double-blind, phase II/III systemic lupus erythematosus evaluation of rituximab trial. *Arthritis Rheum.* **62**, 222–233 (2010).
79. Benson, M.J. *et al.* Cutting edge: the dependence of plasma cells and independence of memory B cells on BAFF and APRIL. *J. Immunol.* **180**, 3655–3659 (2008).
80. Jacobi, A.M. *et al.* Effect of long-term belimumab treatment on B cells in systemic lupus erythematosus: extension of a phase II, double-blind, placebo-controlled, dose-ranging study. *Arthritis Rheum.* **62**, 201–210 (2010).
81. Looney, R.J., Anolik, J. & Sanz, I. A perspective on B-cell–targeting therapy for SLE. *Mod. Rheumatol.* **20**, 1–10 (2010).
82. Aringer, M. *et al.* Current state of evidence on "off label" therapeutic options for systemic lupus erythematosus, including biological immunosuppressive agents, in Germany, Austria, and Switzerland—a consensus report. *Lupus* **21**, 386–401 (2012).
83. Hahn, B.H. Targeted therapies in systemic lupus erythematosus: successes, failures and future. *Ann. Rheum. Dis.* **70** (suppl. 1), i64–i66 (2011).

84. de Laat, B., Mertens, K. & de Groot, P.G. Mechanisms of disease: antiphospholipid antibodies—from clinical association to pathologic mechanism. *Nat. Clin. Pract. Rheumatol.* **4**, 192–199 (2008).
85. Lauvsnes, M.B. & Omdal, R. Systemic lupus erythematosus, the brain, and anti-NR2 antibodies. *J. Neurol.* **259**, 622–629 (2012).
86. Faust, T.W. *et al.* Neurotoxic lupus autoantibodies alter brain function through two distinct mechanisms. *Proc. Natl. Acad. Sci. USA* **107**, 18569–18574 (2010).
87. DeGiorgio, L.A. *et al.* A subset of lupus anti-DNA antibodies cross-reacts with the NR2 glutamate receptor in systemic lupus erythematosus. *Nat. Med.* **7**, 1189–1193 (2001).
88. Matus, S. *et al.* Antiribosomal-P autoantibodies from psychiatric lupus target a novel neuronal surface protein causing calcium influx and apoptosis. *J. Exp. Med.* **204**, 3221–3234 (2007).
89. Kowal, C. *et al.* Cognition and immunity; antibody impairs memory. *Immunity* **21**, 179–188 (2004).
90. Turnberg, D. & Cook, H.T. Complement and glomerulonephritis: new insights. *Curr. Opin. Nephrol. Hypertens.* **14**, 223–228 (2005).
91. Bergtold, A., Gavhane, A., D'Agati, V., Madaio, M. & Clynes, R. FcR-bearing myeloid cells are responsible for triggering murine lupus nephritis. *J. Immunol.* **177**, 7287–7295 (2006).
92. Anders, H.J. & Schlondorff, D. Toll-like receptors: emerging concepts in kidney disease. *Curr. Opin. Nephrol. Hypertens.* **16**, 177–183 (2007).
93. Manderson, A.P., Botto, M. & Walport, M.J. The role of complement in the development of systemic lupus erythematosus. *Annu. Rev. Immunol.* **22**, 431–456 (2004).
94. Woodruff, T.M., Nandakumar, K.S. & Tedesco, F. Inhibiting the C5-C5a receptor axis. *Mol. Immunol.* **48**, 1631–1642 (2011).
95. Vielhauer, V., Anders, H.J. & Schlondorff, D. Chemokines and chemokine receptors as therapeutic targets in lupus nephritis. *Semin. Nephrol.* **27**, 81–97 (2007).
96. Kitching, A.R. & Holdsworth, S.R. The emergence of TH17 cells as effectors of renal injury. *J. Am. Soc. Nephrol.* **22**, 235–238 (2011).
97. Ernandez, T. & Mayadas, T.N. Immunoregulatory role of TNFα in inflammatory kidney diseases. *Kidney Int.* **76**, 262–276 (2009).
98. Bethunaickan, R. *et al.* A unique hybrid renal mononuclear phagocyte activation phenotype in murine systemic lupus erythematosus nephritis. *J. Immunol.* **186**, 4994–5003 (2011).
99. Hill, G.S. *et al.* Predictive power of the second renal biopsy in lupus nephritis: significance of macrophages. *Kidney Int.* **59**, 304–316 (2001).
100. Schlondorff, D.O. Overview of factors contributing to the pathophysiology of progressive renal disease. *Kidney Int.* **74**, 860–866 (2008).
101. Deelman, L. & Sharma, K. Mechanisms of kidney fibrosis and the role of antifibrotic therapies. *Curr. Opin. Nephrol. Hypertens.* **18**, 85–90 (2009).
102. Alarcón, G.S. *et al.* Time to renal disease and end-stage renal disease in PROFILE: a multiethnic lupus cohort. *PLoS Med.* **3**, e396 (2006).
103. Esdaile, J.M. *et al.* Traditional Framingham risk factors fail to fully account for accelerated atherosclerosis in systemic lupus erythematosus. *Arthritis Rheum.* **44**, 2331–2337 (2001).
104. Symmons, D.P. & Gabriel, S.E. Epidemiology of CVD in rheumatic disease, with a focus on RA and SLE. *Nat. Rev. Rheumatol.* **7**, 399–408 (2011).
105. Narshi, C.B., Giles, I.P. & Rahman, A. The endothelium: an interface between autoimmunity and atherosclerosis in systemic lupus erythematosus? *Lupus* **20**, 5–13 (2011).
106. Lopez, L.R. *et al.* Oxidized low-density lipoprotein and β2-glycoprotein I in patients with systemic lupus erythematosus and increased carotid intima-media thickness: implications in autoimmune-mediated atherosclerosis. *Lupus* **15**, 80–86 (2006).
107. Matsuura, E., Kobayashi, K., Hurley, B.L. & Lopez, L.R. Atherogenic oxidized low-density lipoprotein/β2-glycoprotein I (oxLDL/β2GPI) complexes in patients with systemic lupus erythematosus and antiphospholipid syndrome. *Lupus* **15**, 478–483 (2006).
108. Skaggs, B.J., Hahn, B.H., Sahakian, L., Grossman, J. & McMahon, M. Dysfunctional, pro-inflammatory HDL directly upregulates monocyte PDGFRβ, chemotaxis and TNFα production. *Clin. Immunol.* **137**, 147–156 (2010).
109. McMahon, M. *et al.* Dysfunctional proinflammatory high-density lipoproteins confer increased risk of atherosclerosis in women with systemic lupus erythematosus. *Arthritis Rheum.* **60**, 2428–2437 (2009).
110. Schanberg, L.E. *et al.* Use of atorvastatin in systemic lupus erythematosus in children and adolescents. *Arthritis Rheum.* **64**, 285–296 (2012).
111. Petri, M.A., Kiani, A.N., Post, W., Christopher-Stine, L. & Magder, L.S. Lupus Atherosclerosis Prevention Study (LAPS). *Ann. Rheum. Dis.* **70**, 760–765 (2011).
112. Ceribelli, A., Yao, B., Dominguez-Gutierrez, P.R. & Chan, E.K. Lupus T cells switched on by DNA hypomethylation via microRNA? *Arthritis Rheum.* **63**, 1177–1181 (2011).
113. Pan, Y. & Sawalha, A.H. Epigenetic regulation and the pathogenesis of systemic lupus erythematosus. *Transl. Res.* **153**, 4–10 (2009).
114. Dai, R. & Ahmed, S.A. MicroRNA, a new paradigm for understanding immunoregulation, inflammation, and autoimmune diseases. *Transl. Res.* **157**, 163–179 (2011).
115. Ceribelli, A. *et al.* MicroRNAs in systemic rheumatic diseases. *Arthritis Res. Ther.* **13**, 229 (2011).
116. Geuking, M.B. *et al.* Intestinal bacterial colonization induces mutualistic regulatory T cell responses. *Immunity* **34**, 794–806 (2011).
117. Illei, G.G. *et al.* Current state and future directions of autologous hematopoietic stem cell transplantation in systemic lupus erythematosus. *Ann. Rheum. Dis.* **70**, 2071–2074 (2011).
118. Choi, E.W. *et al.* Reversal of serological, immunological and histological dysfunction in systemic lupus erythematosus mice by long-term serial adipose tissue-derived mesenchymal stem cell transplantation. *Arthritis Rheum.* **64**, 243–253 (2012).
119. Liang, J. *et al.* Allogenic mesenchymal stem cells transplantation in refractory systemic lupus erythematosus: a pilot clinical study. *Ann. Rheum. Dis.* **69**, 1423–1429 (2010).
120. Mok, C.C. Biomarkers for lupus nephritis: a critical appraisal. *J. Biomed. Biotechnol.* **2010**, 638413 (2010).
121. Bauer, J.W. *et al.* Interferon-regulated chemokines as biomarkers of systemic lupus erythematosus disease activity: a validation study. *Arthritis Rheum.* **60**, 3098–3107 (2009).
122. Chaussabel, D. *et al.* A modular analysis framework for blood genomics studies: application to systemic lupus erythematosus. *Immunity* **29**, 150–164 (2008).
123. Hinze, C.H. *et al.* Neutrophil gelatinase-associated lipocalin is a predictor of the course of global and renal childhood-onset systemic lupus erythematosus disease activity. *Arthritis Rheum.* **60**, 2772–2781 (2009).
124. Rovin, B.H. *et al.* Urine chemokines as biomarkers of human systemic lupus erythematosus activity. *J. Am. Soc. Nephrol.* **16**, 467–473 (2005).
125. Rubinstein, T. *et al.* Urinary neutrophil gelatinase-associated lipocalin as a novel biomarker for disease activity in lupus nephritis. *Rheumatology (Oxford)* **49**, 960–971 (2010).
126. Guiducci, C. *et al.* TLR recognition of self nucleic acids hampers glucocorticoid activity in lupus. *Nature* **465**, 937–941 (2010).
127. Yuan, W., DiMartino, S.J., Redecha, P.B., Ivashkiv, L.B. & Salmon, J.E. Systemic lupus erythematosus monocytes are less responsive to interleukin-10 in the presence of immune complexes. *Arthritis Rheum.* **63**, 212–218 (2011).
128. Ramanujam, M. & Davidson, A. Targeting of the immune system in systemic lupus erythematosus. *Expert Rev. Mol. Med.* **10**, e2 (2008).
129. Wofsy, D.S., Shropshire, S.M., Hillson, J.L. & Diamond, B. Abatacept for lupus nephritis: alternative outcome measures support opposing interpretations of data From a multicenter, randomized, double-blind, placebo-controlled phase II/III study. ACR presentation, number 2474 (8 November 2011).
130. Lenert, P.S. Classification, mechanisms of action, and therapeutic applications of inhibitory oligonucleotides for Toll-like receptors (TLR) 7 and 9. *Mediators Inflamm.* **2010**, 986596 (2010).
131. Kyttaris, V.C. & Tsokos, G.C. Targeting lymphocyte signaling pathways as a therapeutic approach to systemic lupus erythematosus. *Curr. Opin. Rheumatol.* **23**, 449–453 (2011).
132. Schiffer, L. *et al.* Short term administration of costimulatory blockade and cyclophosphamide induces remission of systemic lupus erythematosus nephritis in NZB/W F1 mice by a mechanism downstream of renal immune complex deposition. *J. Immunol.* **171**, 489–497 (2003).
133. Daikh, D.I. & Wofsy, D. Cutting edge: reversal of murine lupus nephritis with CTLA4Ig and cyclophosphamide. *J. Immunol.* **166**, 2913–2916 (2001).
134. Ng, K.P. *et al.* B cell depletion therapy in systemic lupus erythematosus: long-term follow-up and predictors of response. *Ann. Rheum. Dis.* **65**, 1259–1262 (2007).
135. Bloom, O. *et al.* Generation of a unique small molecule peptidomimetic that neutralizes lupus autoantibody activity. *Proc. Natl. Acad. Sci. USA* **108**, 10255–10259 (2011).
136. Clynes, R., Dumitru, C. & Ravetch, J.V. Uncoupling of immune complex formation and kidney damage in autoimmune glomerulonephritis. *Science* **279**, 1052–1054 (1998).
137. Gambaro, G. & Kong, N.C. Glycosaminoglycan treatment in glomerulonephritis? An interesting option to investigate. *J. Nephrol.* **23**, 244–252 (2010).
138. Nguyen, T.Q. & Goldschmeding, R. Bone morphogenetic protein-7 and connective tissue growth factor: novel targets for treatment of renal fibrosis? *Pharm. Res.* **25**, 2416–2426 (2008).
139. Renner, B. *et al.* Binding of factor H to tubular epithelial cells limits interstitial complement activation in ischemic injury. *Kidney Int.* **80**, 165–173 (2011).
140. Tse, K.C. *et al.* Angiotensin inhibition or blockade for the treatment of patients with quiescent lupus nephritis and persistent proteinuria. *Lupus* **14**, 947–952 (2005).
141. McMahon, M., Hahn, B.H. & Skaggs, B.J. Systemic lupus erythematosus and cardiovascular disease: prediction and potential for therapeutic intervention. *Expert Rev. Clin. Immunol.* **7**, 227–241 (2011).
142. Stohl, W. *et al.* Belimumab reduces autoantibodies, normalizes low complement, and reduces select B-cell populations in patients with systemic lupus erythematosus. *Arthritis Rheum.* published online doi:10.1002/art.34400 (24 January 2012).
143. Liu, Z. & Davidson, A. BAFF inhibition: a new class of drugs for the treatment of autoimmunity. *Exp. Cell Res.* **317**, 1270–1277 (2011).
144. Mackay, F. & Schneider, P. Cracking the BAFF code. *Nat. Rev. Immunol.* **9**, 491–502 (2009).
145. Stohl, W. *et al.* Belimumab reduces autoantibodies, normalizes low complement, and reduces select B-cell populations in patients with systemic lupus erythematosus. *Arthritis Rheum.* published online doi:10.1002/art.34400 (24 January 2012).

nature medicine

Melanoma exosomes educate bone marrow progenitor cells toward a pro-metastatic phenotype through MET

Héctor Peinado[1], Maša Alečković[2], Simon Lavotshkin[3], Irina Matei[1], Bruno Costa-Silva[1,4], Gema Moreno-Bueno[5], Marta Hergueta-Redondo[5], Caitlin Williams[1], Guillermo García-Santos[1], Cyrus M Ghajar[6], Ayuko Nitadori-Hoshino[1], Caitlin Hoffman[7], Karen Badal[1], Benjamin A Garcia[2], Margaret K Callahan[8], Jianda Yuan[9], Vilma R Martins[4], Johan Skog[10], Rosandra N Kaplan[11], Mary S Brady[12], Jedd D Wolchok[8,9,13], Paul B Chapman[8,13], Yibin Kang[2,14,15], Jacqueline Bromberg[8,13] & David Lyden[1,15,16]

Tumor-derived exosomes are emerging mediators of tumorigenesis. We explored the function of melanoma-derived exosomes in the formation of primary tumors and metastases in mice and human subjects. Exosomes from highly metastatic melanomas increased the metastatic behavior of primary tumors by permanently 'educating' bone marrow progenitors through the receptor tyrosine kinase MET. Melanoma-derived exosomes also induced vascular leakiness at pre-metastatic sites and reprogrammed bone marrow progenitors toward a pro-vasculogenic phenotype that was positive for c-Kit, the receptor tyrosine kinase Tie2 and Met. Reducing Met expression in exosomes diminished the pro-metastatic behavior of bone marrow cells. Notably, MET expression was elevated in circulating CD45$^-$C-KIT$^{low/+}$TIE2$^+$ bone marrow progenitors from individuals with metastatic melanoma. *RAB1A*, *RAB5B*, *RAB7* and *RAB27A*, regulators of membrane trafficking and exosome formation, were highly expressed in melanoma cells. *Rab27A* RNA interference decreased exosome production, preventing bone marrow education and reducing, tumor growth and metastasis. In addition, we identified an exosome-specific melanoma signature with prognostic and therapeutic potential comprised of TYRP2, VLA-4, HSP70, an HSP90 isoform and the MET oncoprotein. Our data show that exosome production, transfer and education of bone marrow cells supports tumor growth and metastasis, has prognostic value and offers promise for new therapeutic directions in the metastatic process.

Exosomes are small membrane vesicles (30–100 nm) derived from the luminal membranes of multivesicular bodies and constitutively released by fusion with the cell membrane[1–5]. In addition to diffusible factors, such as cytokines, growth factors and extracellular matrix molecules, exosomes mediate local and systemic cell communication through the horizontal transfer of information, such as mRNAs, microRNAs and proteins[2,5–15].

It is well recognized that bone marrow–derived cells (BMDCs) are crucial for the generation of a suitable microenvironment for the primary tumor and the development of metastasis[16] through a process called pre-metastatic niche formation[17,18]. Although secreted factors are known contributors to BMDC recruitment to both the primary tumor and to pre-metastatic niches[18–21], the role of exosomes in this process has not been evaluated. Exosomes may have a role in the crosstalk between the primary tumor and BMDCs, leading to the homing of both cell types to sites of metastasis[7,22,23].

Here we identify tumor-derived exosomes as new factors that promote metastatic niche formation by educating BMDCs toward a pro-vasculogenic and pro-metastatic phenotype through upregulation of the MET oncoprotein[24–29]. Our data show that a specific expression pattern of Ras-related (Rab) proteins[30,31] is associated with exosome production in melanoma. Moreover, using circulating exosomes isolated from subjects with stage 4 melanoma, we define a melanoma-specific exosome signature comprised of tyrosinase-related protein-2 (TYRP2), very late antigen 4 (VLA-4), heat shock protein 70 (HSP70), an HSP90 isoform and the MET oncoprotein. Notably, exosomal TYRP2 predicts disease progression in subjects with stage 3 melanoma. We also show that CD45$^-$C-KIT$^{low/+}$TIE2$^+$

[1]Children's Cancer and Blood Foundation Laboratories, Departments of Pediatrics, Cell and Developmental Biology, Weill Cornell Medical College, New York, New York, USA. [2]Department of Molecular Biology, Princeton University, Princeton, New Jersey, USA. [3]Department of Surgery, College of Physicians and Surgeons, Columbia University, New York, New York, USA. [4]International Center for Research and Education, A.C. Camargo Hospital, São Paulo, Brazil. [5]Departamento de Bioquímica, Universidad Autónoma de Madrid (UAM), Instituto de Investigaciones Biomédicas 'Alberto Sols', Consejo Superior de Investigaciones Científicas (CSIC)-UAM, IdiPAZ (Instituto de Investigación Sanitaria La Paz) & Fundación MD Anderson Cancer Center, Madrid, Spain. [6]Life Sciences Division, Lawrence Berkeley National Laboratory, Berkeley, California, USA. [7]Department of Neurosurgery, Weill Cornell Medical College, New York, New York, USA. [8]Department of Medicine, Memorial Sloan-Kettering Cancer Center, New York, New York, USA. [9]Department of Immunology, Ludwig Center for Cancer Immunotherapy, Sloan-Kettering Institute, New York, New York, USA. [10]Exosome Diagnostics Inc., New York, New York, USA. [11]Pediatric Oncology Branch, National Cancer Institute, US National Institutes of Health, Bethesda, Maryland, USA. [12]Department of Surgery, Memorial Sloan-Kettering Cancer Center, New York, New York, USA. [13]Weill Cornell Medical College, New York, New York, USA. [14]Genomic Instability and Tumor Progression Program, Cancer Institute of New Jersey, New Brunswick, New Jersey, USA. [15]Champalimaud Metastasis Programme, Lisbon, Portugal. [16]Department of Pediatrics, Memorial Sloan-Kettering Cancer Center, New York, New York, USA. Correspondence should be addressed to J.B. (bromberj@mskcc.org) or D.L. (dcl2001@med.cornell.edu).

Received 10 February; accepted 26 March; published online 27 May 2012; doi:10.1038/nm.2753

circulating bone marrow progenitors from individuals with metastatic melanoma highly express MET receptor. Our study shows that the MET oncoprotein is upregulated in bone marrow progenitor cells by tumor-derived exosomes, possibly by both direct and indirect mechanisms, promoting the education, mobilization and pro-metastatic behavior of BMDCs.

RESULTS

Exosomal proteins have diagnostic and prognostic value

To determine the relevance of circulating exosome concentrations in metastatic melanoma[32,33], we prospectively isolated and characterized exosomes from the plasma of human subjects with different clinical stages of melanoma. We isolated exosomes (100 nm particles) from plasma using standard methods and confirmed their identity by electron microscopy (**Fig. 1a**). We confirmed the presence of known exosome markers, including CD63, CD9 and major histocompatibility complex class I (MHC-I) (data not shown). Exosome number and size distribution quantified by NanoSight analysis did not differ based on clinical stage (**Supplementary Fig. 1a**). In contrast, exosome protein concentrations were higher in subjects with stage 4 disease compared to all other stages and to normal controls (**Supplementary Fig. 1b**). Furthermore, we found that individuals with stage 4 disease who had protein-poor exosomes (<50 μg ml^{-1}) had a survival advantage compared to those individuals with stage 4 disease who had protein-rich exosomes (>50 μg ml^{-1}) (**Fig. 1b**).

Exosomes from highly metastatic mouse (B16-F10) and human (SK-Mel-28, SK-Mel-202, SK-Mel-265 and SK-Mel-35) melanoma cell lines expressed typical exosome markers (**Supplementary Fig. 1c** and data not shown). We used mass spectrometry to identify additional human- and mouse-derived melanoma exosome proteins (**Supplementary Table 1**) that helped define a potential diagnostic signature for melanoma. Compared to control subjects, the amounts of TYRP2 (a melanoma-specific protein), VLA-4 and HSP70 were increased in the exosomes of subjects with stage 4 disease (**Fig. 1c,d**), whereas only TYRP2 was significantly higher ($P < 0.05$) in exosomes from subjects with stage 3 disease (**Fig. 1c,d**). Notably, 70% of subjects with stage 4 melanoma had exosomes that contained an isoform of HSP90, which has been reported to be key in cellular transformation[34] (**Fig. 1c**). In a retrospective analysis of individuals with stage 3 melanoma, we found that the amount of exosomal TYRP2 was significantly increased ($P < 0.001$) in individuals who eventually developed metastatic disease (**Fig. 1e** and data not shown). These data support analyzing circulating exosomes in patients to predict stage, prognosis (stage 3) and survival in subjects with metastatic disease.

Tumor exosomes alter organ tropism and metastatic potential

Exosomes from the highly malignant B16-F10, SK-Mel-28 and SK-Mel-202 melanoma cell lines expressed higher amounts (twofold to 20-fold) of protein than exosomes from poorly metastatic (B16-F1)[35] and nonmetastatic cell lines (melan-a) (**Fig. 2a**). Other less metastatic lung, breast and colon cancer cells also secreted lower amounts of exosomal proteins than B16-F10 cells (**Supplementary Fig. 2a**). To analyze the tissue distribution of the exosomes, we injected fluorescently labeled B16-F10 exosomes intravenously into naive mice. We detected the injected exosomes in the blood vessels of target organs 5 min later (**Fig. 2b**). Twenty-four hours after injection, we found B16-F10 exosomes in the interstitium of the lungs and in the bone marrow (**Fig. 2b**), livers and spleens of the mice (organotropic sites for B16-F10 metastasis) but not in the circulation (**Supplementary Table 2** and data not shown). To analyze vascular leakiness properties in the lung, an early event in pre-metastatic niche formation[36], we injected B16-F10 exosomes into mice, followed by injection of fluorescently labeled dextran 24 h later. The B16-F10 exosomes enhanced the lung endothelial permeability in the mice, as judged by the presence of extravasated dextran, compared to mice injected with conditioned media, control particles (**Fig. 2c**) or exosomes from nonmetastatic cell lines (**Supplementary Fig. 2b**).

To investigate the molecular pathways affected by exosome delivery, we performed gene expression profiling of lung tissue 24 h and 48 h after injecting B16-F10 exosomes into the tail veins of mice (**Supplementary Fig. 2c**). At both time points, we found approximately 130 differentially expressed genes in mice injected with B16-F10

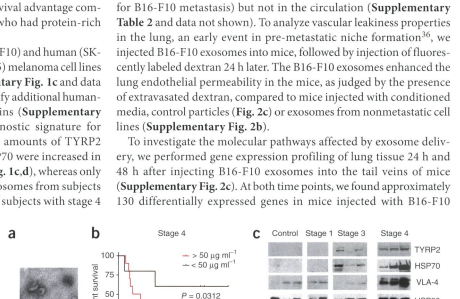

Figure 1 Analysis of protein expression in circulating exosomes from subjects with melanoma. (**a**) A representative electron microscopic image of exosomes derived from the plasma of a subject with melanoma. Scale bar, 100 nm. (**b**) Kaplan-Meier survival curves showing the cumulative survival probabilities in subjects with stage 4 melanoma over 42 months of follow up according to the total amount of protein (micrograms) in isolated circulating exosomes per milliliter of plasma analyzed ($n = 15$). Overall P values were calculated using a log-rank test. (**c**) Representative western blot of TYRP2, HSP70, VLA-4, HSP90 and heat shock cognate protein 70 (HSC70) in circulating exosomes isolated from the plasma of subjects with melanoma (at stage 1, 3 or 4, as indicated) and healthy controls. The arrow indicates a specific HSP90 isoform that was found in 70% of the stage 4 subjects with melanoma. Glyceraldehyde-3-phosphate dehydrogenase (GAPDH) was used as a loading control. (**d**) Statistical analysis of the western blot densitometry of signature proteins in circulating exosomes relative to GAPDH. Controls, $n = 9$; stage 1, $n = 2$; stage 3, $n = 7$; stage 4, $n = 18$. P values were calculated by analysis of variance (ANOVA). (**e**) Statistical analysis of the western blot densitometry for TYRP2 expression in circulating exosomes relative to GAPDH in a retrospective series of frozen plasma derived from subjects with stage 3 melanoma ($n = 29$) who had been followed for 4 years to evaluate disease progression (NED, no evidence of disease; POD, progression of disease). $P < 0.001$ using Mann-Whitney U test.

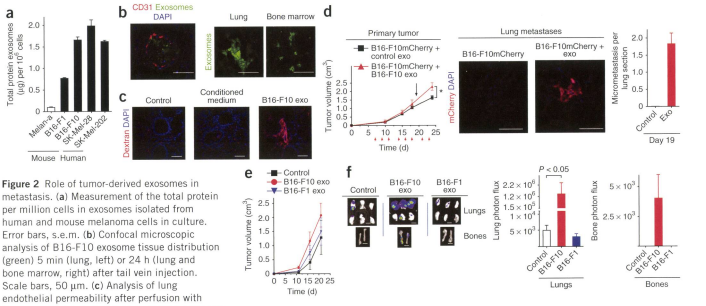

Figure 2 Role of tumor-derived exosomes in metastasis. (**a**) Measurement of the total protein per million cells in exosomes isolated from human and mouse melanoma cells in culture. Error bars, s.e.m. (**b**) Confocal microscopic analysis of B16-F10 exosome tissue distribution (green) 5 min (lung, left) or 24 h (lung and bone marrow, right) after tail vein injection. Scale bars, 50 μm. (**c**) Analysis of lung endothelial permeability after perfusion with fluorescently labeled dextran (red) 24 h after tail vein injection of B16-F10 exosomes (exo), conditioned medium or control particles. Scale bar, 50 μm. (**d**) Analysis of primary tumor growth (left) after subcutaneous flank injection of B16-F10mCherry cells in wild-type mice treated with 10 μg of B16-F10 exosomes for 3 weeks. $n = 6$ mice per group. Error bars, s.e.m. $^*P < 0.05$ by ANOVA. Red arrows indicate exosome injections. The black arrow denotes the time point (day 19) at which lung micrometastatic lesions were analyzed. Lung micrometastases (mCherry$^+$, middle, scale bars, 50 μm) quantified by immunofluorescence (right). (**e**) Analysis of primary tumor growth after subcutaneous flank injection of B16-F10–luciferase cells in mice pretreated with 5 μg of B16-F10 and B16-F1 exosomes as described in the text. Error bars, s.e.m. (**f**) Metastatic burden quantified by luciferin photon flux at 21 d after tumor injection (left). Scale bars, 200 μm. Quantification of total photon flux in lungs and bones (right). $n = 10$ mice per group. Error bars, s.e.m. $^*P < 0.05$ by ANOVA.

exosomes as compared to control-particle–injected mice. Many of these genes were related to extracellular matrix remodeling and inflammation, such as the genes encoding heat-shock proteins, as well as *S100A8* and *S100A9* (**Supplementary Table 3**), which are known effectors of pre-metastatic niche formation[37]; we confirmed these findings by quantitative real time PCR (**Supplementary Fig. 2d**). *TNFA* was upregulated 24 h after exosome injection (**Supplementary Fig. 2d**), suggesting that it could be involved in early events during the metastatic process (for example, vascular permeability)[38].

To further examine the role of tumor exosomes in primary tumor growth and metastasis, we intravenously injected mice with B16-F10–derived exosomes three times a week, starting 7 d after orthotopic injection of B16-F10mCherry cells. In contrast to the mice injected with control particles who had no evidence of micrometastatic disease, mice treated with exosomes showed lung micrometastasis at day 19 after tumor cell injection (**Fig. 2d**). Primary tumor growth was only enhanced in the exosome-injected mice 24 days after tumor cell injection (**Fig. 2d**). To analyze the differences between exosomes from highly compared to poorly metastatic melanomas, we injected equal and physiological concentrations of B16-F10– and B16-F1–derived exosomes intravenously (**Supplementary Fig. 3a**) into mice three times a week over 28 d, then subcutaneously implanted B16-F10 cells expressing luciferase (Online Methods). The exosome treatment did not affect primary tumor growth (**Fig. 2e**). However, mice injected with B16-F10 exosomes had a greater metastatic burden in the lungs (240-fold increase, as measured by luciferase intensity; **Fig. 2f**) compared to mice injected with control particles or mice treated with exosomes derived from the poorly metastatic B16-F1 cells (**Fig. 2f**). Furthermore, mice treated with B16-F10 exosomes developed metastasis with a greater tissue distribution, which included bone (**Fig. 2f**) and brain (data not shown), compared to either control-treated mice or B16-F1–exosome treated mice. These data suggest that qualitative differences in exosome content can mediate metastatic potential and organotropism.

Tumor exosomes enhance metastasis by bone marrow education

Given the key role of BMDCs in metastatic progression[17,39], we determined whether tumor-derived exosomes could educate BMDCs and influence metastatic progression (**Fig. 3a** and Online Methods). We transplanted lethally irradiated C57BL/6 mice with bone marrow from GFP-expressing mice that we had previously treated with B16-F10 exosomes (educated bone marrow) for 28 d or with synthetic exosomes or PBS (control bone marrow). After bone marrow reconstitution, we subcutaneously implanted the C57BL/6 mice with B16-F10 cells expressing mCherry. The mice transplanted with exosome-educated bone marrow had greater primary tumor growth than the mice transplanted with control bone marrow (**Fig. 3b**), indicating that pre-education of bone marrow cells with tumor exosomes was sufficient to accelerate tumor growth. The recruitment of BMDCs and tumor vascular density were enhanced by approximately 4.5-fold and threefold, respectively, in the primary tumors of mice transplanted with educated bone marrow compared with tumors of mice transplanted with control bone marrow (**Fig. 3c**).

After 28 days, we found an increase in the size and number of metastases at both typical (lungs and ipsilateral lymph nodes) and atypical (contralateral lymph nodes, mesentery and brain) sites in mice transplanted with exosome-educated bone marrow as compared to mice transplanted with control bone marrow (**Supplementary Table 4**). Mice transplanted with educated bone marrow had a threefold increase in metastatic burden, larger metastatic lesions in the lung and a twofold elevation in the number of metastasis-associated BMDCs as compared to mice transplanted with control bone marrow

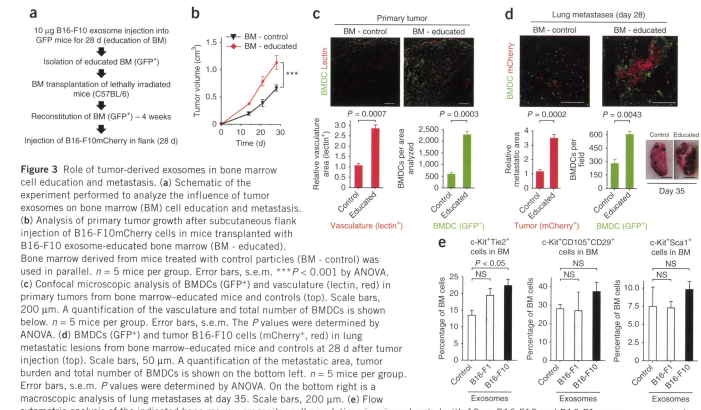

Figure 3 Role of tumor-derived exosomes in bone marrow cell education and metastasis. (**a**) Schematic of the experiment performed to analyze the influence of tumor exosomes on bone marrow (BM) cell education and metastasis. (**b**) Analysis of primary tumor growth after subcutaneous flank injection of B16-F10mCherry cells in mice transplanted with B16-F10 exosome-educated bone marrow (BM - educated). Bone marrow derived from mice treated with control particles (BM - control) was used in parallel. $n = 5$ mice per group. Error bars, s.e.m. $^{***}P < 0.001$ by ANOVA. (**c**) Confocal microscopic analysis of BMDCs (GFP$^+$) and vasculature (lectin, red) in primary tumors from bone marrow–educated mice and controls (top). Scale bars, 200 μm. A quantification of the vasculature and total number of BMDCs is shown below. $n = 5$ mice per group. Error bars, s.e.m. The P values were determined by ANOVA. (**d**) BMDCs (GFP$^+$) and tumor B16-F10 cells (mCherry$^+$, red) in lung metastatic lesions from bone marrow–educated mice and controls at 28 d after tumor injection (top). Scale bars, 50 μm. A quantification of the metastatic area, tumor burden and total number of BMDCs is shown on the bottom left. $n = 5$ mice per group. Error bars, s.e.m. P values were determined by ANOVA. On the bottom right is a macroscopic analysis of lung metastases at day 35. Scale bars, 200 μm. (**e**) Flow cytometric analysis of the indicated bone marrow progenitor cell populations in mice educated with 10 μg B16-F10 and B16-F1 exosomes or control particles three times a week for 28 d. $n = 5$ mice per group. Error bars, s.e.m. NS, not significant by ANOVA.

(**Fig. 3d**). Notably, BMDCs were present in metastatic (mCherry$^+$) and nonmetastatic regions (mCherry$^-$) in mice transplanted with exosome-educated bone marrow, although in the metastatic areas, the number of BMDCs per area was higher (**Supplementary Fig. 3b**). Moreover, education of bone marrow cells with B16-F10 exosomes also increased primary tumor growth 1.3-fold and metastatic burden tenfold in less metastatic models such as Lewis lung carcinoma (**Supplementary Fig. 4**), showing a crucial role for bone marrow cell education by tumor exosomes in regulating tumor metastasis.

To further define the mechanisms of the exosome education of BMDCs, we analyzed the effect of B16-F10 and B16-F1 exosomes on bone marrow progenitor cells. Twenty-eight days of B16-F10 exosome treatment in mice led to a twofold increase in the frequency of pro-angiogenic c-Kit$^+$Tie2$^+$ cells in the bone marrow, whereas c-Kit$^+$Sca1$^+$ hematopoietic stem cells were not affected by exosome treatment (**Fig. 3e**). Exosome education did not affect other bone marrow–derived cell populations, including CD11b$^+$, CD11b$^+$Gr1$^+$, F4/80$^+$ or VEGFR1$^+$ cells (data not shown), which are commonly mobilized by growth factors and chemokines[18,21,37].

Transfer of exosomal MET to bone marrow progenitors

Exosomes are known to promote the horizontal transfer of molecules to recipient cells[8,13,40]. Given the differential effects of B16-F1 compared to B16-F10 exosomes on metastatic potential together with previous studies suggesting differences in B16-F10 and B16-F1 membrane-derived vesicles[41], we identified proteins that were highly expressed in the B16-F10 exosomes but that were present in much lower amounts in the B16-F1 exosomes by proteomic profiling (**Supplementary Table 5**). Some candidates with known roles in tumorigenesis and metastasis include the Met oncoprotein, CD44, Hsp70 and annexin A6 (refs. 24,42). Given the key role of MET signaling in migration, invasion, angiogenesis and bone marrow cell mobilization[24,25,43,44], we focused our functional analyses on this proto-oncogene. We hypothesized that exosomes could horizontally transfer MET from melanoma to bone marrow progenitor cells and that this transfer could be a previously unknown mechanism for promoting metastatic progression. We verified that the amounts of Met and phosphorylated Met (pMet) were greater in both B16-F10 exosomes and cells compared to B16-F1 exosomes and cells, respectively (**Fig. 4a**). After 28 d of exosome education, *Met* expression was increased in bone marrow progenitor cells from mice injected with B16-F10 exosomes (**Fig. 4b**) but not in mice injected with the B16-F1 exosomes. Notably, *Cd44* expression in BMDCs was not affected by treatment with either B16-F10 or B16-F1 exosomes (**Fig. 4b**). These data suggest that exosome-mediated Met transfer is partially responsible for increased Met expression in bone marrow progenitor cells.

To determine the functional consequences of Met expression within exosomes, we reduced the amount of Met expression in B16-F10 tumor cells by 40% and the amount of pMet by 80% using *Met* shRNAs (B16-F10shMet; **Supplementary Fig. 5a**). Using fluorescently labeled exosomes isolated from B16-F10, B16-F10shMet and B16-F1 cells, we found a sixfold increase in c-Kit$^+$Met$^+$ bone marrow progenitors after treating bone marrow cells with B16-F10 exosomes as compared to treating cells with B16-F10shMet, B16-F1 exosomes or control particles (**Fig. 4c** and **Supplementary Fig. 5b**). Notably, exosome uptake quantified by flow cytometry was similar regardless of exosome origin and Met expression (**Fig. 4c**). To determine whether B16-F10 exosomes contribute to activation of the MET pathway in BMDCs, we analyzed the phosphorylation of downstream mediators of hepatocyte growth factor (HGF)-MET signaling, such as pS6 kinase (in the mammalian

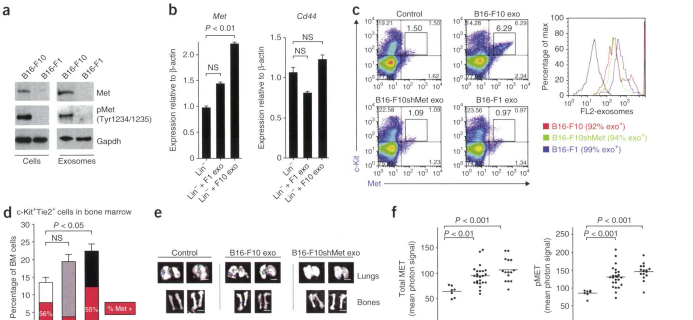

Figure 4 MET analysis in tumor and bone marrow cells. (**a**) Western blot analysis of Met and pMet in B16-F1 and B16-F10 exosomes and cells. pMet (Tyr1234/1235), Met phosphorylated at Tyr1234 and Tyr1235. (**b**) Quantitative real time PCR analysis of *Met* and *Cd44* in lineage-negative bone marrow cells after B16-F10 or B16-F1 exosome injection. Error bars, s.e.m. NS, not significant by ANOVA. Lin⁻, lineage negative (see Online Methods); F10, B16-F10; F1, B16-F1. (**c**) Flow cytometric analysis of c-Kit and Met expression on bone marrow cells after overnight incubation with fluorescently labeled exosomes with red fluorescent cell linker (PKH26⁺). Fluorescence in the red channel (FL2) indicates exosome uptake (right). (**d**) Flow cytometric analysis of Met expression in c-Kit⁺Tie2⁺ bone marrow cells (top) and Lin⁻c-Kit⁺Tie2⁺ circulating blood cells (bottom) of mice injected with 10 μg of B16-F10 and B16-F1 exosomes three times a week over 28 d (the red area indicates the percentage of Met⁺ cells). Error bars, s.e.m. NS, not significant by ANOVA. (**e**) Analysis of metastasis after subcutaneous flank injection of B16-F10–luciferase cells in mice pretreated with 5 μg of B16-F10 or B16-F10shMet exosomes or control particles three times a week over 28 d. Scale bars, 200 μm. Metastatic burden quantified by luciferin photon flux at 21 d after tumor injection (bottom). Error bars, s.e.m. *P* values were determined by ANOVA. (**f**) Multiplex protein analysis of MET and pMET (phosphorylated at Tyr1349) in the circulating exosomes isolated from a retrospective series of frozen plasma derived from subjects with melanoma and controls. Controls, $n = 7$; stage 3, $n = 24$; stage 4, $n = 15$. *P* values were determined by ANOVA. (**g**) Flow cytometric analysis depicting the percentage of MET⁺ bone marrow progenitor cells in the blood of individuals with melanoma. Controls, $n = 7$; stage 1–3, $n = 10$; stage 4, $n = 9$. Error bars, s.e.m. *P* values were determined by ANOVA.

target of rapamycin (mTOR) pathway) and pERK (in the mitogen-activated protein kinase (MAPK) pathway), which are known effectors of MET-mediated bone marrow progenitor cell mobilization[43,44]. Pretreatment of bone marrow cells with B16-F10 exosomes resulted in HGF-induced S6 and ERK phosphorylation, which was not seen in nontreated bone marrow or bone marrow pretreated with B16-F1 exosomes (**Supplementary Fig. 5c**). Additionally, we observed that a MET inhibitor (crizotinib) prevented HGF-induced phosphorylation of S6 kinase and ERK after treatment with B16-F10 exosomes, showing the specificity of this pathway (data not shown).

We then investigated the functional consequences of exosome-mediated MET signaling in bone marrow progenitor cells. Injection with B16-F10, but not B16-F1, exosomes increased Met expression in vasculogenic (c-Kit⁺Tie2⁺) and hematopoietic (c-Kit⁺Sca1⁺) progenitors in the circulation but not in the bone marrow (**Fig. 4d**, highlighted in red, and **Supplementary Fig. 5d**), suggesting that Met expression enhanced bone marrow cell mobilization. We made similar observations in mice transplanted with B16-F10 educated bone marrow, as described in **Figure 3** (data not shown). These data suggest that Met expression enhances bone marrow cell mobilization. To determine the effects of exosome-dependent MET signaling on primary tumor growth and metastasis, we implanted B16-F10 tumor cells in mice injected with exosomes from B16-F10 and B16-F10shMet cells, as well as control particles. Although we found no differences in primary tumor growth between the groups (data not shown), mice injected with the B16-F10shMet exosomes had less lung and

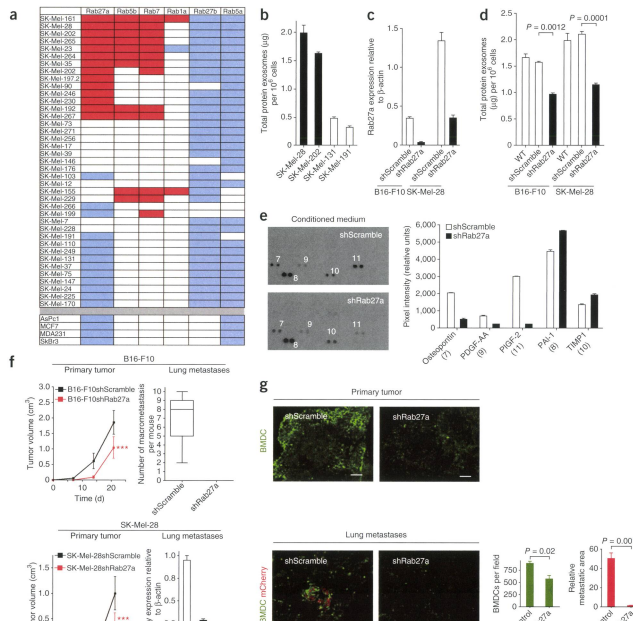

Figure 5 Disrupting *Rab27a* expression reduces exosome release, tumor growth and metastasis. (**a**) Quantitative real time PCR analysis of *RAB* genes in melanoma (SK-Mel-), breast cancer (MCF7, MDA-MB-231 and SkBr3) and pancreatic adenocarcinoma (AsPc1) human cell lines. Red denotes high (at least twofold), white denotes intermediate (less than twofold and >1.5-fold) and blue denotes low (≤1.5-fold) *RAB* expression in melanoma relative to breast cancer and pancreatic cell lines. (**b**) Measurement of the total amount of protein in the exosomes secreted per million human melanoma cells in culture. (**c**) Quantitative real time PCR analysis of *Rab27a* expression after shRNA knockdown of *Rab27a* in the B16-F10 and SK-Mel-28 cell lines. (**d**) Measurement of exosome protein per million cells after shRNA knockdown of *Rab27a* in the B16-F10 and SK-Mel-28 cell lines. Control scramble shRNA and parental cells were used as a reference. (**e**) Characterization and densitometric analysis of conditioned medium derived from B16-F10shScramble and B16-F10shRab27a cell lines. Numbers in parentheses below indicate the spots analyzed for the membrane (right image). (**f**) Analysis of primary tumor growth and metastasis in B16-F10shScramble, B16-F10shRab27a and SK-Mel-28 cell lines subcutaneously injected into the flanks of C57BL/6 (B16-F10shScramble and B16-F10shRab27a) and nonobese diabetic severe combined immunodeficient mice (SK-Mel-28). Metastases were macroscopically counted (B16-F10) or quantified by quantitative real time PCR for mCherry (SK-Mel-28). $n = 5$ mice per group. Error bars, s.e.m. $^{***}P < 0.001$ by ANOVA. (**g**) Analysis of BMDCs (GFP$^+$, green) and tumor cells (mCherry, red) in B16-F10shScramble and B16-F10shRab27a primary tumors (top, scale bar, 200 μm) and lungs (bottom, scale bar, 50 μm). Quantification of the metastatic area and the total number of BMDCs is shown on the right. $n = 5$ mice per group. Error bars, s.e.m. *P* values were determined by ANOVA.

bone metastasis compared to mice educated with B16-F10 exosomes (**Fig. 4e**). Moreover, the amounts of vasculogenic and hematopoietic precursors were lower in the bone marrow and peripheral blood of mice bearing B16-F10 tumors that were injected with B16-F10shMet exosomes compared to mice treated with B16-F10 exosomes (data not shown).

To determine the clinical relevance of our findings, we analyzed the amounts of MET and pMET in circulating exosomes isolated from subjects with stage 3 or 4 melanoma (from the same cohort as described in **Fig. 1**). We found higher amounts of total and pMET in both the individuals with stage 3 melanoma and those with stage 4 melanoma compared to normal controls (**Fig. 4f**). Moreover, MET protein expression analyzed by flow cytometry was higher in both bone marrow progenitor cells ($CD45^-C\text{-}KIT^{low/+}$) and pro-vasculogenic cells ($CD45^-C\text{-}KIT^{+/low}TIE2^+$) isolated from the blood of subjects with stage 4 disease compared to cells isolated from control subjects with stage 1–3 disease (**Fig. 4g** and **Supplementary Fig. 5e**). Our data suggest that MET expression in circulating exosomes and bone marrow progenitor cells could be new predictors or early markers of metastatic disease.

Rab27a regulates exosome production and metastasis

As Ras-related RAB proteins control exosome biogenesis[50], we analyzed the expression of *RAB* genes (*RAB1A*, *RAB5A*, *RAB5B*, *RAB7*, *RAB27A* and *RAB27B*) using a panel of 39 human-derived melanoma cell lines. Notably, those cell lines producing high concentrations of exosomes also had high expression of *RAB27A*, *RAB5B* and *RAB7* mRNA relative to those cell lines producing lower concentrations of exosomes (**Fig. 5a**,**b**). Given the key role of *RAB27* in exosome release[51], we reasoned that inactivating this gene would reduce exosome production. We selected the *Rab27a* isoform for knockdown, as it was selectively expressed in melanoma-derived cell lines (**Fig. 5a** and data not shown). We effectively reduced the expression of *Rab27a* in B16-F10 and SK-Mel-28 cells (**Fig. 5c**), which resulted in a 50% decrease in exosome secretion (**Fig. 5d** and **Supplementary Fig. 6a**), showing a role for Rab27a in exosome production by melanoma cells. Although we found no marked differences in total protein, protein content, exosome-specific markers or the amount of Met and pMet between the control and *Rab27a* knockdown cells and exosomes (**Supplementary Fig. 6b**,**c**), we did find a decrease in the secretion of placental growth factor 2 (PlGF-2), platelet-derived growth factor A chain homodimer (PDGF-AA) and osteopontin as a consequence of reducing the expression of *Rab27a* (**Fig. 5e**). Notably, *Rab27a* knockdown in B16-F10 and SK-Mel-28 cells reduced primary tumor growth, lung colonization and metastasis (**Fig. 5f**), which were associated with a decrease in the number of BMDCs recruited to these sites (**Fig. 5g** and **Supplementary Fig. 6d**). Consistent with our *in vitro* results (**Supplementary Fig. 6a**), the concentrations of circulating tumor-derived exosomes in mice bearing *Rab27a* knockdown tumors were reduced by 40–50 % (data not shown) and were therefore insufficient to educate and mobilize BMDCs.

By injecting increasing amounts of exosomes isolated from either B16-F10shScramble (B16-F10 cells plus scramble shRNA) or B16-F10shRab27a (B16-F10 cells plus Rab27a shRNA) cell lines in mice followed by flank injection of tumor cells, we observed a dose-dependent increase in metastatic burden (**Supplementary Fig. 7a**,**b**). These data suggest that quantitative differences in exosome production can alter metastatic potential. Because overexpression of Rab27a in the B16-F1, LLC and B16-F10 cell lines led to cell death (data not shown), we were unable to determine the sufficiency of Rab27a in exosome production and modulating metastasis. Collectively, these data suggest that *Rab27a* knockdown in melanoma models reduces exosome production and circulating exosome concentrations, thus preventing the recruitment of the BMDCs that are necessary for metastatic progression.

DISCUSSION

Accumulating evidence indicates that exosomes are mediators of metastasis[3,11,13,15,22,23,45,46]. Multiple cell types, including fibroblasts, endothelial cells and bone marrow progenitor cells, contribute to the generation of metastatic microenvironments[39,47] and may be influenced by the horizontal transfer of molecules (for example, proteins and microRNAs) by exosomes[8,40,48,49]. However, the molecular and cellular mechanisms underlying this association have not been determined. Here we show that exosomes have a role in tumor progression and metastatic niche formation that is distinct from that of tumor-derived growth factors, extracellular proteins and chemokines[18,20,21,37,50,51]. Tumor-derived exosomes promote the education and mobilization of BMDCs that support tumor vasculogenesis, invasion and metastasis. Notably, tumor-derived exosomes recruit BMDCs through upregulation of proinflammatory molecules at pre-metastatic sites. Specifically, preconditioning the bone marrow with exosomes from a highly metastatic cancer cell line (B16-F10) can increase the metastatic tumor burden and distribution in target tissues, even for tumors of different origins with a low metastatic capacity. Our work in tumor-derived exosome biology complements Paget and Ewing's theories of metastatic spread, offering an explanation of organotropic involvement in certain metastatic diseases[52,53].

By comparing the protein content of exosomes from highly metastatic and poorly metastatic melanoma cells, we identified MET signaling as a principal mediator of bone marrow progenitor cell education. We identified activated MET-related signaling proteins to be differentially expressed in exosomes from highly metastatic melanoma cells compared to poorly metastatic ones, which mediated provasculogenic and metastatic effects on bone marrow progenitor cells. The MET oncogene mediates cellular transformation and tumor cell proliferation, survival, motility, invasion and metastasis[26,28,29,44,54,55]. Here we propose a previously unknown role for exosome-packaged MET in metastatic melanoma. The unique cargo of exosomes from other tumor types may educate distinct bone marrow populations, thus directly affecting metastatic propensity and outcome. The bone marrow of mice educated with the poorly metastatic B16-F1 exosomes, which lack the MET receptor, reduced (though not statistically significant) the metastatic burden and organotropism of highly metastatic B16-F10 primary tumors, suggesting that nonmetastatic exosomes may educate bone marrow to prevent metastatic disease.

The molecular mechanisms of exosome biogenesis and secretion are not well described. We found that, among the 39 melanoma-derived cell lines studied, specific *RAB* genes involved in exosome secretion (*RAB1A*, *RAB5B*, *RAB7* and *RAB27A*) were highly expressed in cells lines secreting high concentrations of exosomes. Reducing the expression of RAB27A, a regulator of protein trafficking and melanoma proliferation[31,56], decreased exosome production and the release of proangiogenic factors (PlGF-2, osteopontin and PDGF-AA) from tumor cells, hindering BMDC mobilization, tumor growth and metastasis. Our data, together with other studies showing that overexpression of RAB27A correlates with breast cancer invasiveness and metastasis[57,58], suggest that RAB27A should be considered as a potential therapeutic target in cancer.

Our human studies identified a specific melanoma signature comprised of TYRP2, VLA-4, HSP70, an HSP90 isoform and MET in circulating exosomes from subjects with advanced melanoma, which

could be used as an indicator of metastatic disease and tumor burden. We found that the coexpression of TYRP2 and MET in exosomes, as well as an increased amount of protein per exosome, predicted disease progression. In addition, we showed that MET expression is elevated in circulating pro-vasculogenic progenitors in subjects with metastatic melanoma. Thus, our work identifies quantitative and qualitative signatures, along with specific bone marrow progenitor cell populations that are mobilized, as representative hallmarks of metastatic melanoma.

Although the membrane vesicles of cancer cells have been suggested to contribute to the horizontal propagation of oncoproteins and genetic material (RNA)[5,8,13,14,40,48], our study is the first, to our knowledge, to show that transfer of the MET oncoprotein from tumor-derived exosomes to bone marrow progenitor cells promotes the metastatic process *in vivo*. Notably, we show that exosomes can alter the bone marrow in a durable manner; these results suggest that genetic or epigenetic changes could be involved in this phenomenon, as bone marrow cells retain the educated phenotype after engraftment into a new host.

Here we propose a new mechanism that controls metastatic progression through the crosstalk between tumor-derived exosomes and bone marrow progenitor cells. Collectively, our data identify exosome-mediated transfer of the oncoprotein MET as a key regulator of bone marrow education and mobilization and metastatic progression.

METHODS

Methods and any associated references are available in the online version of the paper.

Accession codes. Microarray raw data tables have been deposited in the Gene Expression Omnibus (accession number GSE36584).

Note: Supplementary information is available in the online version of the paper.

ACKNOWLEDGMENTS

We dedicate this work to the memory of James A. Paduano. We thank M.J. Bissell, A. Cano, J. Wels and S.R. Granitto for critical reading of this paper and suggestions. We also thank the members of our laboratories for helpful discussions and the members of the Weill Cornell Medical College electron microscopy and microarray core facilities for their support. We thank V. Hearing, (US National Institutes of Health (NIH), National Cancer Institute (NCI)) for providing the antibody to TYRP2 and D.C. Bennett (St. George's University of London) for providing the melan-a cell line. Our work is supported by grants from the Children's Cancer and Blood Foundation (H.P. and D.L.), The Manning Foundation (B.C.-S. and D.L.), The Hartwell Foundation (D.L.), Pediatric Oncology Experimental Therapeutics Investigators Consortium (H.P. and D.L.), Stavros S. Niarchos Foundation (D.L.), Champalimaud Foundation (H.P., Y.K. and D.L.), The Nancy C. and Daniel P. Haerr Foundation (H.P. and D.L.), The Mary Kay Foundation (A.N.-H. and D.L.), American Hellenic Educational Progressive Association 5th District (D.L.), The Malcolm Hewitt Wiener Foundation (D.L.), The George Best Costacos Foundation (D.L.), NCI (D.L., grant NCI-R01CA 098234-01), National Foundation for Cancer Research (D.L.), Susan G. Komen for the Cure (H.P. and D.L.), NCI-U54-CA143836 training grant (C.M.G. and D.L.), Fundación para el Fomento en Asturias de la Investigación Científica Aplicada y la Tecnología (G.G.-S.), Fundación Universidad de Oviedo (G.G.-S.), The Beth C. Tortolani Foundation (H.P., D.L. and J.B.), Sussman Family Fund (J.B.), Charles and Marjorie Holloway Foundation (J.B.), Manhassat Breast Cancer Fund (J.B.), NIH-CA87637 (J.B.), Fundação de Amparo a Pesquisa do Estado de São Paulo (FAPESP, V.R.M. and B.C.-S.), NIH (Y.K., grants R01-CA134519 and R01-CA141062), National Science Foundation grant CBET-0941143 and an American Society for Mass Spectrometry research award (B.A.G.).

AUTHOR CONTRIBUTIONS

H.P. developed the hypothesis, designed the experimental approach, performed the experimental work, analyzed the data, coordinated the project and wrote the manuscript. S.L. conducted experimental work. I.M. performed flow cytometry studies and analysis. B.C.-S. conducted mouse work and proteomic characterization of exosomes. G.M.-B. conducted gene expression studies and analysis of microarray data. M.H.-R. conducted mouse work and bone marrow education studies. C.W. conducted mouse work and human studies. G.G.-S. developed bone marrow education assays. A.N.-H. and K.B. quantified exosomes in human plasma. M.A., B.A.G. and Y.K. performed mass spectrometry studies and contributed to data interpretation. C.H. obtained human blood specimens. M.K.C. and J.Y. contributed to the characterization of human plasma exosomes. J.S., R.N.K., V.R.M., M.S.B., J.D.W., P.B.C. and C.M.G. discussed the hypothesis and contributed to data interpretation and experimental design. J.B. coordinated the project, interpreted data and wrote the manuscript. D.L. conceived the hypothesis, led the project, interpreted the data and wrote the manuscript.

COMPETING FINANCIAL INTERESTS

The authors declare competing financial interests: details are available in the online version of the paper.

Published online at http://www.nature.com/doifinder/10.1038/nm.2753.
Reprints and permissions information is available online at http://www.nature.com/reprints/index.html.

1. Théry, C., Zitvogel, L. & Amigorena, S. Exosomes: composition, biogenesis and function. *Nat. Rev. Immunol.* **2**, 569–579 (2002).
2. Iero, M. *et al.* Tumour-released exosomes and their implications in cancer immunity. *Cell Death Differ.* **15**, 80–88 (2008).
3. Ratajczak, J., Wysoczynski, M., Hayek, F., Janowska-Wieczorek, A. & Ratajczak, M.Z. Membrane-derived microvesicles: important and underappreciated mediators of cell-to-cell communication. *Leukemia* **20**, 1487–1495 (2006).
4. Cocucci, E., Racchetti, G. & Meldolesi, J. Shedding microvesicles: artefacts no more. *Trends Cell Biol.* **19**, 43–51 (2009).
5. Valadi, H. *et al.* Exosome-mediated transfer of mRNAs and microRNAs is a novel mechanism of genetic exchange between cells. *Nat. Cell Biol.* **9**, 654–659 (2007).
6. van Niel, G., Porto-Carreiro, I., Simoes, S. & Raposo, G. Exosomes: a common pathway for a specialized function. *J. Biochem.* **140**, 13–21 (2006).
7. Peinado, H., Lavotshkin, S. & Lyden, D. The secreted factors responsible for pre-metastatic niche formation: old sayings and new thoughts. *Semin. Cancer Biol.* **21**, 139–146 (2011).
8. Ratajczak, J. *et al.* Embryonic stem cell-derived microvesicles reprogram hematopoietic progenitors: evidence for horizontal transfer of mRNA and protein delivery. *Leukemia* **20**, 847–856 (2006).
9. Nazarenko, I. *et al.* Cell surface tetraspanin Tspan8 contributes to molecular pathways of exosome-induced endothelial cell activation. *Cancer Res.* **70**, 1668–1678 (2010).
10. Webber, J., Steadman, R., Mason, M.D., Tabi, Z. & Clayton, A. Cancer exosomes trigger fibroblast to myofibroblast differentiation. *Cancer Res.* **70**, 9621–9630 (2010).
11. Liu, Y. *et al.* Contribution of MyD88 to the tumor exosome-mediated induction of myeloid derived suppressor cells. *Am. J. Pathol.* **176**, 2490–2499 (2010).
12. Xiang, X. *et al.* Induction of myeloid-derived suppressor cells by tumor exosomes. *Int. J. Cancer* **124**, 2621–2633 (2009).
13. Al-Nedawi, K. *et al.* Intercellular transfer of the oncogenic receptor EGFRvIII by microvesicles derived from tumour cells. *Nat. Cell Biol.* **10**, 619–624 (2008).
14. Hao, S. *et al.* Epigenetic transfer of metastatic activity by uptake of highly metastatic B16 melanoma cell-released exosomes. *Exp. Oncol.* **28**, 126–131 (2006).
15. Skog, J. *et al.* Glioblastoma microvesicles transport RNA and proteins that promote tumour growth and provide diagnostic biomarkers. *Nat. Cell Biol.* **10**, 1470–1476 (2008).
16. Sethi, N. & Kang, Y. Unravelling the complexity of metastasis—molecular understanding and targeted therapies. *Nat. Rev. Cancer* **11**, 735–748 (2011).
17. Psaila, B. & Lyden, D. The metastatic niche: adapting the foreign soil. *Nat. Rev. Cancer* **9**, 285–293 (2009).
18. Kaplan, R.N. *et al.* VEGFR1-positive haematopoietic bone marrow progenitors initiate the pre-metastatic niche. *Nature* **438**, 820–827 (2005).
19. Gao, D. *et al.* Bone marrow-derived endothelial progenitor cells contribute to the angiogenic switch in tumor growth and metastatic progression. *Biochim. Biophys. Acta* **1796**, 33–40 (2009).
20. Erler, J.T. *et al.* Hypoxia-induced lysyl oxidase is a critical mediator of bone marrow cell recruitment to form the premetastatic niche. *Cancer Cell* **15**, 35–44 (2009).
21. Hiratsuka, S., Watanabe, A., Aburatani, H. & Maru, Y. Tumour-mediated upregulation of chemoattractants and recruitment of myeloid cells predetermines lung metastasis. *Nat. Cell Biol.* **8**, 1369–1375 (2006).
22. Hood, J.L., San, R.S. & Wickline, S.A. Exosomes released by melanoma cells prepare sentinel lymph nodes for tumor metastasis. *Cancer Res.* **71**, 3792–3801 (2011).
23. Jung, T. *et al.* CD44v6 dependence of premetastatic niche preparation by exosomes. *Neoplasia* **11**, 1093–1105 (2009).
24. Trusolino, L., Bertotti, A. & Comoglio, P.M. MET signalling: principles and functions in development, organ regeneration and cancer. *Nat. Rev. Mol. Cell Biol.* **11**, 834–848 (2010).

25. Stella, G.M., Benvenuti, S. & Comoglio, P.M. Targeting the MET oncogene in cancer and metastases. *Expert Opin. Investig. Drugs* **19**, 1381–1394 (2010).
26. Boccaccio, C. & Comoglio, P.M. Invasive growth: a MET-driven genetic programme for cancer and stem cells. *Nat. Rev. Cancer* **6**, 637–645 (2006).
27. Cecchi, F., Rabe, D.C. & Bottaro, D.P. Targeting the HGF/Met signalling pathway in cancer. *Eur. J. Cancer* **46**, 1260–1270 (2010).
28. Peruzzi, B. & Bottaro, D.P. Targeting the c-Met signaling pathway in cancer. *Clin. Cancer Res.* **12**, 3657–3660 (2006).
29. Birchmeier, C., Birchmeier, W., Gherardi, E. & Vande Woude, G.F. Met, metastasis, motility and more. *Nat. Rev. Mol. Cell Biol.* **4**, 915–925 (2003).
30. Stenmark, H. Rab GTPases as coordinators of vesicle traffic. *Nat. Rev. Mol. Cell Biol.* **10**, 513–525 (2009).
31. Ostrowski, M. *et al.* Rab27a and Rab27b control different steps of the exosome secretion pathway. *Nat. Cell Biol.* **12**, 19–30 (2009).
32. Braeuer, R.R., Zigler, M., Villares, G.J., Dobroff, A.S. & Bar-Eli, M. Transcriptional control of melanoma metastasis: the importance of the tumor microenvironment. *Semin. Cancer Biol.* **21**, 83–88 (2011).
33. Fidler, I.J. Critical determinants of melanoma metastasis. *J. Investig. Dermatol. Symp. Proc.* **1**, 203–208 (1996).
34. Grammatikakis, N. *et al.* The role of Hsp90N, a new member of the Hsp90 family, in signal transduction and neoplastic transformation. *J. Biol. Chem.* **277**, 8312–8320 (2002).
35. Fidler, I.J. & Nicolson, G.L. Organ selectivity for implantation survival and growth of B16 melanoma variant tumor lines. *J. Natl. Cancer Inst.* **57**, 1199–1202 (1976).
36. Huang, Y. *et al.* Pulmonary vascular destabilization in the premetastatic phase facilitates lung metastasis. *Cancer Res.* **69**, 7529–7537 (2009).
37. Hiratsuka, S. *et al.* The S100A8-serum amyloid A3–TLR4 paracrine cascade establishes a pre-metastatic phase. *Nat. Cell Biol.* **10**, 1349–1355 (2008).
38. Lucas, R., Verin, A.D., Black, S.M. & Catravas, J.D. Regulators of endothelial and epithelial barrier integrity and function in acute lung injury. *Biochem. Pharmacol.* **77**, 1763–1772 (2009).
39. Joyce, J.A. & Pollard, J.W. Microenvironmental regulation of metastasis. *Nat. Rev. Cancer* **9**, 239–252 (2009).
40. Balaj, L. *et al.* Tumour microvesicles contain retrotransposon elements and amplified oncogene sequences. *Nat. Commun.* **2**, 180 (2011).
41. Taylor, D.D., Taylor, C.G., Jiang, C.G. & Black, P.H. Characterization of plasma membrane shedding from murine melanoma cells. *Int. J. Cancer* **41**, 629–635 (1988).
42. Zöller, M. CD44: can a cancer-initiating cell profit from an abundantly expressed molecule? *Nat. Rev. Cancer* **11**, 254–267 (2011).
43. Jalili, A., Shirvaikar, N., Marquez-Curtis, L.A., Turner, A.R. & Janowska-Wieczorek, A. The HGF/c-Met axis synergizes with G-CSF in the mobilization of hematopoietic stem/progenitor cells. *Stem Cells Dev.* **19**, 1143–1151 (2010).
44. Tesio, M. *et al.* Enhanced c-Met activity promotes G-CSF–induced mobilization of hematopoietic progenitor cells via ROS signaling. *Blood* **117**, 419–428 (2011).
45. Lima, L.G., Chammas, R., Monteiro, R.Q., Moreira, M.E. & Barcinski, M.A. Tumor-derived microvesicles modulate the establishment of metastatic melanoma in a phosphatidylserine-dependent manner. *Cancer Lett.* **283**, 168–175 (2009).
46. Logozzi, M. *et al.* High levels of exosomes expressing CD63 and caveolin-1 in plasma of melanoma patients. *PLoS ONE* **4**, e5219 (2009).
47. Guise, T. Examining the metastatic niche: targeting the microenvironment. *Semin. Oncol.* **37** (suppl. 2), S2–S14 (2010).
48. Aliotta, J.M. *et al.* Microvesicle entry into marrow cells mediates tissue-specific changes in mRNA by direct delivery of mRNA and induction of transcription. *Exp. Hematol.* **38**, 233–245 (2010).
49. Aliotta, J.M. *et al.* Alteration of marrow cell gene expression, protein production, and engraftment into lung by lung-derived microvesicles: a novel mechanism for phenotype modulation. *Stem Cells* **25**, 2245–2256 (2007).
50. Oskarsson, T. *et al.* Breast cancer cells produce tenascin C as a metastatic niche component to colonize the lungs. *Nat. Med.* **17**, 867–874 (2011).
51. Psaila, B., Kaplan, R.N., Port, E.R. & Lyden, D. Priming the 'soil' for breast cancer metastasis: the pre-metastatic niche. *Breast Dis.* **26**, 65–74 (2006).
52. Ewing, J. *Neoplastic Diseases: A Treatise on Tumours*, 3rd edn. (W.B. Saunders Co., Philadelphia, 1928).
53. Paget, G. The distribution of secondary growths in cancer of the breast. *Lancet* **133**, 571–573 (1889).
54. Scott, K.L. *et al.* Proinvasion metastasis drivers in early-stage melanoma are oncogenes. *Cancer Cell* **20**, 92–103 (2011).
55. Christensen, J.G., Burrows, J. & Salgia, R. c-Met as a target for human cancer and characterization of inhibitors for therapeutic intervention. *Cancer Lett.* **225**, 1–26 (2005).
56. Akavia, U.D. *et al.* An integrated approach to uncover drivers of cancer. *Cell* **143**, 1005–1017 (2010).
57. Wang, J.S., Wang, F.B., Zhang, Q.G., Shen, Z.Z. & Shao, Z.M. Enhanced expression of Rab27A gene by breast cancer cells promoting invasiveness and the metastasis potential by secretion of insulin-like growth factor-II. *Mol. Cancer Res.* **6**, 372–382 (2008).
58. Hendrix, A. *et al.* Effect of the secretory small GTPase Rab27B on breast cancer growth, invasion, and metastasis. *J. Natl. Cancer Inst.* **102**, 866–880 (2010).

nature medicine

β-catenin confers resistance to PI3K and AKT inhibitors and subverts FOXO3a to promote metastasis in colon cancer

Stephan P Tenbaum[1,14], Paloma Ordóñez-Morán[2,13,14], Isabel Puig[1,14], Irene Chicote[1], Oriol Arqués[1], Stefania Landolfi[3], Yolanda Fernández[4], José Raúl Herance[5], Juan D Gispert[5], Leire Mendizabal[6], Susana Aguilar[7,8], Santiago Ramón y Cajal[3], Simó Schwartz Jr[4], Ana Vivancos[6], Eloy Espín[9], Santiago Rojas[5], José Baselga[10,11], Josep Tabernero[12], Alberto Muñoz[2] & Héctor G Palmer[1]

The Wnt–β-catenin and PI3K-AKT-FOXO3a pathways have a central role in cancer. AKT phosporylates FOXO3a, relocating it from the cell nucleus to the cytoplasm, an effect that is reversed by PI3K and AKT inhibitors. Simultaneous hyperactivation of the Wnt–β-catenin pathway and inhibition of PI3K-AKT signaling promote nuclear accumulation of β-catenin and FOXO3a, respectively, promoting cell scattering and metastasis by regulating a defined set of target genes. Indeed, the anti-tumoral AKT inhibitor API-2 promotes nuclear FOXO3a accumulation and metastasis of cells with high nuclear β-catenin content. Nuclear β-catenin confers resistance to the FOXO3a-mediated apoptosis induced by PI3K and AKT inhibitors in patient-derived primary cultures and in corresponding xenograft tumors in mice. This resistance is reversed by XAV-939, an inhibitor of Wnt–β-catenin signaling. In the presence of high nuclear β-catenin content, activation of FOXO3a by PI3K or AKT inhibitors makes it behave as a metastasis inductor rather than a proapoptotic tumor suppressor. We show that it is possible to evaluate the β-catenin status of patients' carcinomas and the response of patient-derived cells to target-directed drugs that accumulate FOXO3a in the nucleus before deciding on a course of treatment. We propose that this evaluation could be essential to the provision of a safer and more effective personalized treatment.

Colon cancer is a leading cause of death worldwide[1]. Although surgical resection combined with adjuvant therapy is efficient at the early stages of disease, subsequent relapse and metastasis often occur. At these advanced stages, resistance to conventional therapies is frequent and treatments are ineffective[2]. To overcome this resistance, a new generation of target-directed drugs is being tested in clinical trials. Therefore, a better understanding of the molecular mechanisms responsible for patients' responses to these drugs is crucial to identify new predictive biomarkers and facilitate treatment decisions.

Abnormal activation of the wingless related MMTV integration site (Wnt)–β-catenin pathway by mutations is responsible for the initiation of more than 90% of colon cancers[3]. As a result, β-catenin accumulates in the nucleus, binds the T cell factor (TCF) or lymphoid enhancer factor (LEF) transcription factors and induces the expression of Wnt target genes that have key roles in tumor progression[4]. We and others have reported that binding of β-catenin to different transcription factors enhances the expression of alternative sets of target genes[5–7]. Forkhead box O3 (FOXO3a) is one of those transcription factors for which β-catenin acts as a transcriptional coactivator, enhancing the expression of common target genes[8]. However, the possible physiological relevance of the crosstalk between FOXO3a and β-catenin in cancer has not been addressed.

FOXO proteins control multiple processes in eukaryotic organisms by regulating the expression of specific sets of genes involved in stem-cell maintenance, stress resistance, longevity, differentiation or metabolism[9,10]. In cancer, FOXO transcription factors are considered to be tumor suppressors because they induce cell-cycle arrest and apoptosis[11].

[1]Vall d'Hebrón Institut d'Oncología (VHIO), Stem Cell and Cancer Laboratory, Barcelona, Spain. [2]Instituto de Investigaciones Biomédicas 'Alberto Sols', Consejo Superior de Investigaciones Cientificas-Universidad Autónoma de Madrid, Madrid, Spain. [3]Department of Pathology, Hospital Universitari Vall d'Hebrón, Universitat Autònoma de Barcelona, Barcelona, Spain. [4]Group of Drug Delivery and Targeting, Centro de Investigaciones en Bioquímica y Biología Molecular (CIBBIM)-Nanomedicine and Networking Biomedical Research Center on Bioengineering, Biomaterials and Nanomedicine (CIBER-BBN), Hospital Universitari Vall d'Hebrón, Institut de Recerca Vall d'Hebrón, Universitat Autònoma de Barcelona, Barcelona, Spain. [5]Parc de Recerca Biomèdica de Barcelona (PRBB), Centre d'Imatge Molecular (CRC) Corporació Sanitària, Barcelona, Spain. [6]VHIO, Genomics Cancer Group, Barcelona, Spain. [7]Centre for Respiratory Research, Rayne Institute, University College London, London, UK. [8]Hematopoietic Stem Cell Laboratory, London Research Institute, Cancer Research UK, London, UK. [9]General Surgery Service, Hospital Universitari Vall d'Hebrón, Barcelona, Spain. [10]Massachusetts General Hospital Cancer Center, Harvard Medical School, Charlestown, Massachusetts, USA. [11]Howard Hughes Medical Institute, Chevy Chase, Maryland, USA. [12]Medical Oncology Department, Hospital Universitari Vall d'Hebrón, Barcelona, Spain. [13]Present address: Swiss Institute for Experimental Cancer Research, École Polytechnique Fédérale de Lausanne, Lausanne, Switzerland. [14]These authors contributed equally to this work. Correspondence should be addressed to H.G.P. (hgpalmer@vhio.net).

Received 22 July 2011; accepted 10 April 2012; published online 20 May 2012; doi:10.1038/nm.2772

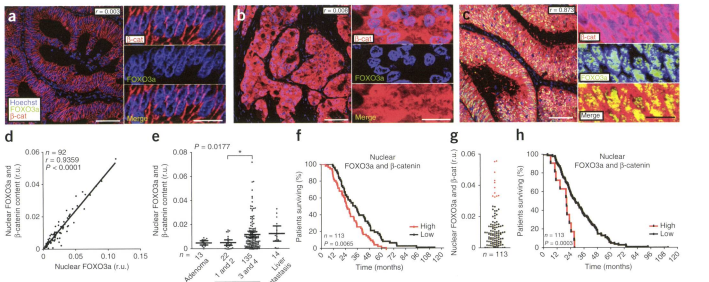

Figure 1 High nuclear concentrations of FOXO3a and β-catenin correlate with metastatic stage and shorter survival in patients with colon cancer. (**a**–**c**) Representative immunostained sections (left, scale bars, 100 μm) and the respective magnifications (right, scale bars, 20 μm) of tumors with low β-catenin (β-cat) and low FOXO3a expression (**a**), high β-catenin and low FOXO3a expression (**b**) and high β-catenin and high FOXO3a expression (**c**). FOXO3a is shown in green, β-catenin is shown in red, and Hoechst 33342 is shown in blue. The Spearman's coefficient of nuclear colocalization (*r*) is indicated (**b**,**c**). The merged magnified images lack blue channels, and yellow color indicates FOXO3a and β-catenin colocalization. (**d**) Plot depicting nuclear FOXO3a and β-catenin immunofluorescent signal intensity in human colon carcinomas. Correlation was evaluated by nonparametric Spearman test. The number of cases (*n*), coefficient of correlation (*r*) and *P* values are indicated. Relative units (r.u.) are calculated as described in the Online Methods. (**e**) Column scatter plot showing the amount of FOXO3a and β-catenin colocalization in tumors at different stages of colon-cancer progression. Horizontal lines indicate arithmetic mean values, and error bars show the 95% CI. The number of cases (*n*) and *P* values from nonparametric analysis of variance (ANOVA) analysis with Kruskal-Wallis test are indicated. Asterisk indicates a significant difference ($P < 0.05$) between groups as quantified by Dunn's multiple comparison test. (**f**) Kaplan-Meier survival analysis of patients with colon cancer separated into two groups by the median for the nuclear FOXO3a and β-catenin colocalization signal. The higher signal is shown in red ($n = 58$), and the lower signal is shown in black ($n = 55$). *P* values were calculated by log-rank (Mantel-Cox) test. (**g**) Plot representing the nuclear immunofluorescent signal for FOXO3a and β-catenin colocalization. Dots of the highest decile values are shown in red. (**h**) Kaplan-Meier survival analysis of patients with colon cancer separated into two groups by the highest decile for the nuclear FOXO3a and β-catenin colocalization signal. The higher signal is shown in red ($n = 11$), and the lower signal is shown in black ($n = 102$). *P* values were calculated by log-rank (Mantel-Cox) test.

Phosphorylation of FOXO proteins by activated v-akt murine thymoma viral oncogene homolog (AKT) or serum/glucocorticoid regulated kinase 1 (SGK1) induces their sequestration in the cytoplasm and the consequent inhibition of their transcriptional activity[12,13]. AKT is part of the rat sarcoma (RAS)-phosphoinositide-3-kinase (PI3K)-phosphatase and tensin homolog (PTEN)-AKT–mammalian target of rapamycin (mTOR) oncogenic pathway, which is frequently altered by activating mutations in colon and many other cancers[14]. Concerted efforts have been made in both academia and industry to identify specific anti-tumoral inhibitors of PI3K or AKT that relocate FOXO proteins back into the nucleus and thus restore their capacity to induce cell-cycle arrest and apoptosis[15]. In this study, we used the PI3K inhibitor NVP-BKM120 and the AKT signaling inhibitor-2 (API-2), which inhibit cell growth and induce apoptosis in human cancer cells in culture and in tumors growing in mice[16,17]. Phase 1 and 2 clinical trials with both compounds have been conducted in patients with solid metastatic cancers with promising results[18–20].

Considering the role of the Wnt–β-catenin and PI3K-AKT-FOXO3a pathways in tumorigenesis and the interaction of FOXO3a and β-catenin, we studied their crosstalk in colon cancer. We found that the joint action of the two transcription factors induced metastasis and that β-catenin conferred resistance to FOXO-induced apoptosis. Inhibitors of PI3K and AKT not only did not induce apoptosis *in vitro* or *in vivo*, but they also promoted metastasis when the concentration of nuclear β-catenin was high in colon-cancer cells. By studying the response of patient-derived colon-cancer–initiating cells to such target-directed drugs, we highlight the clinical relevance of our findings.

RESULTS

Nuclear FOXO3a and β-catenin concentrations in colon cancer

To assess the amount of nuclear FOXO3a and β-catenin in human colon cancer, we performed double immunofluorescent staining on paraffin sections of tumors at different stages. Nuclear FOXO3a accumulated alone in nonmalignant adenomas but always colocalized with β-catenin in the nuclei of tumoral cells in carcinomas and liver metastasis. We also detected carcinomas with high concentrations of nuclear β-catenin but low concentrations of nuclear FOXO3a. We found the highest nuclear concentrations of both factors in a subset of primary carcinomas at stages 3 or 4 from patients with metastatic disease (**Fig. 1a**–**e** and **Supplementary Fig. 1a**–**c**). Patients with high nuclear FOXO3a and β-catenin colocalization signals had, on average, an 8-month shorter survival time than patients with low colocalization signals. The median survival time was 33.7 months for patients with low nuclear FOXO3a and β-catenin signals and was 25.7 months for patients with high nuclear FOXO3a and β-catenin signals (hazard ratio (HR) 1.724, 95% CI 1.164–2.552). When we were more restrictive and analyzed the group of patients with the top 10% highest colocalization signals, the median survival was even shorter, 21.03 months, whereas it was 28.9 months for

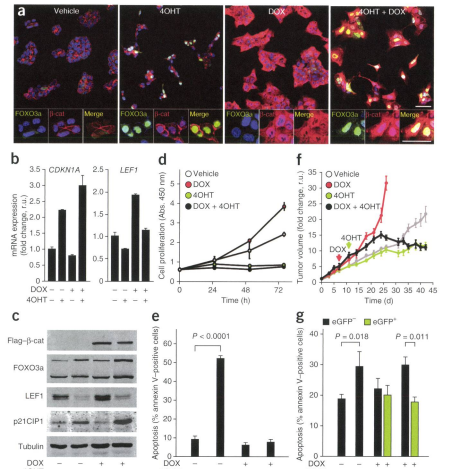

Figure 2 FOXO3a and β-catenin modulate colon cancer cell proliferation and apoptosis. (**a**) Immunofluorescence analysis of FOXO3a (green) and β-catenin (red) expression in DLD-1Fβ-C7 cells treated as indicated. Scale bar, top images, 50 μm. Below are magnifications of the upper images. Scale bar, bottom images, 20 μm. Nuclei were stained with Hoechst 33342 (blue). The merged magnification images lack the blue channel, and yellow color indicates FOXO3a and β-catenin colocalization. DOX, doxycycline. (**b**) Normalized relative *CDKN1A* and *LEF1* RNA expression levels in DLD-1Fβ-C7 cells treated with doxycycline, 4OHT or both measured by real-time RT-PCR. (**c**) The amounts of the indicated proteins in DLD-1Fβ-C7 cells as assessed by western blot. Flag-tag antibody detects exogenous Flag-tagged S33Y β-catenin. FOXO3a antibody recognizes endogenous protein (lower band) and FOXO3a3A-ER^{TM} fusion protein (upper band). Tubulin served as the loading control. (**d**) Graphic showing the proliferation of DLD-1Fβ-C7 cells treated as indicated. Abs., absorbance. (**e**) Chart depicting the percentage of apoptotic DLD-1Fβ-C7 cells in response to the indicated treatments as measured by flow cytometry. The *P* value corresponds to an unpaired *t* test. Error bars show ± s.d. of triplicates from three independent experiments (**b**,**d**,**e**). (**f**) Tumor growth in nude mice ($n = 8$, two tumors per mouse) injected subcutaneously with DLD-1Fβ cells and treated as indicated. Error bars show means ± s.d. of the volume of 16 tumors per treatment. (**g**) Graphic representing the percentage of apoptotic subpopulations positive (green bars) or negative for S33Y β-catenin–eGFP (black bars) of DLD-1Fβ cells in tumors ($n = 6$) growing in nude mice treated as indicated. Error bars show means ± s.d. of the volume of six tumors per treatment. *P* values correspond to unpaired *t* tests.

the other 90% of individuals who had lower colocalization signals (HR 6.392, 95% CI 2.322–17.6). Nuclear FOXO3a alone also correlated with metastatic stage and shorter median survival time (low FOXO3a content, 32.57 months, compared to high FOXO3a content, 25.37 months, HR 1.684, 95% CI 1.137–2.493). In contrast, β-catenin alone did not predict metastasis stage or survival time (HR 1.212, 95% CI 0.8331–1.765) (**Fig. 1f–h** and **Supplementary Fig. 1c–f**).

β-catenin diverts FOXO3a-induced apoptosis to metastasis

We expressed a tamoxifen-inducible (4-hydroxy-tamoxifen, 4OHT) AKT-insensitive mutant of FOXO3a (FOXO3a3A-ER^{TM})[21] and a stable β-catenin S33Y mutant that is inducible by doxycycline in a clone of DLD-1 human colon cancer cells (DLD-1Fβ-C7). The mutant β-catenin was expressed with a lentivirus, together with enhanced GFP (eGFP) using an internal ribosome entry site (IRES) (Online Methods). Exogenous FOXO3a and β-catenin proteins accumulated in the nucleus after the corresponding 4OHT or doxycycline treatments (**Fig. 2a** and **Supplementary Fig. 2**), reaching concentrations in the nucleus that were comparable to those caused by hydrogen peroxide, in the case of FOXO3a (**Supplementary Fig. 2a**,**b**,**d**), or, in the case of β-catenin, to those present in cancer cell lines with naturally occurring β-catenin accumulation, such as the HCT116 or SW480 human colon cancer cell lines (**Supplementary Fig. 2a**,**c**,**d**). β-catenin enhanced the induction of the known FOXO3a target gene *CDKN1A* (also known as p21CIP1) that resulted from treatment with 4OHT. Likewise, nuclear β-catenin accumulation resulting from doxycycline treatment induced the TCF target gene *LEF1*, whose expression was reduced by FOXO3a (4OHT) (**Fig. 2b**,**c**)[22,23]. FOXO3a alone reduced cell proliferation by accumulating cells in G1 phase of the cell cycle[24], whereas β-catenin alone increased cell proliferation. When both factors were expressed simultaneously in the nucleus, the cells had a reduced proliferation, similar to that seen with FOXO3a alone, indicating its dominant effect over β-catenin (**Fig. 2d** and **Supplementary Fig. 3a**,**b**). Separately, FOXO3a induced apoptosis, whereas β-catenin did not have a major effect. Nuclear accumulation of both factors resulted in a complete rescue of FOXO3a-induced apoptosis by β-catenin independently of proliferation, as this effect also occurred in cells arrested in G1 phase using pretreatment with mitomycin C (**Fig. 2e** and **Supplementary Fig. 3c–e**).

We injected a pool of DLD-1Fβ cells subcutaneously into nude mice that were all positive for FOXO3a3A-ER^{TM}, although only 62% of the mice expressed S33Y β-catenin and eGFP. This mixed pool of cells recapitulated a heterogeneity in the nuclear concentrations of β-catenin that was similar to that detected in human colon carcinomas (**Supplementary Figs. 4a–d** and **5a**,**b**). In mice treated with doxycycline, tumors accumulated high amounts of nuclear β-catenin and grew more rapidly, whereas those treated with 4OHT had increased nuclear FOXO3a content and grew more slowly compared to control

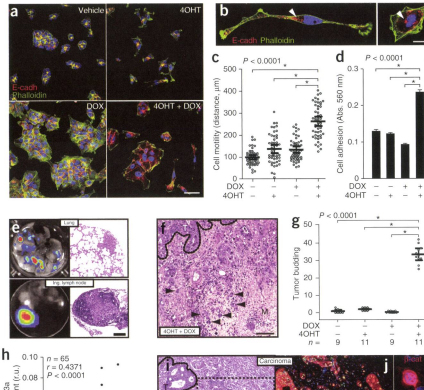

Figure 3 Nuclear FOXO3a and β-catenin drive cell scattering and metastasis. (**a**) Immunofluorescence analysis of DLD-1Fβ-C7 cells treated as indicated to detect E-cadherin (E-cadh) (red) and phalloidin-FITC–stained (phalloidin) actin filaments (green). Scale bar, 100 μm. (**b**) Immunofluorescence analysis of E-cadherin in DLD-1Fβ-C7 cells treated with 4OHT and doxycycline. Arrowheads indicate E-cadherin cytosolic aggregates. Scale bar, 10 μm. Nuclei were stained with Hoechst 33342 (blue; **a**,**b**). (**c**) Scatter plot representing the motility of DLD-1Fβ-C7 cells treated as indicated showing the distance covered by 50 individual cells in a time-lapse video recording one image every 20 min during 120 h. Horizontal bars indicate means, and error bars show the 95% CI. (**d**) Graphic representing adhesion to the substrate of DLD-1Fβ-C7 cells treated as indicated 5 min after seeding. Error bars show means ± s.d. of six replicates from two independent experiments. *P* values for non-parametric ANOVA analyses with Kruskal-Wallis test are shown. Asterisks indicate significant differences ($P < 0.0001$) between groups using Dunn's multiple comparison tests (**c**,**d**). (**e**) Bioluminescence imaging of organs obtained from necropsy of nude mice bearing orthotopic tumors from HT29Fβ cells injected in the cecum walls of the mice. Images overlaid with a gradual bioluminescent signal (blue to red) that originated from luciferase-expressing metastatic cells (left). H&E staining of the corresponding histological sections. Ing., inguinal. Scale bar, 100 μm. (**f**) H&E-stained histological section of the invasive front of a primary tumor xenograft from HT29Fβ cells growing in the cecum walls of nude mice treated with 4OHT and doxycycline described in **e**. Scale bar, 100 μm. (**g**) Column scatter plot presenting tumor budding in the primary tumors described in **e**. *n* indicates the number of tumors analyzed. Horizontal bars show the mean and the 95% CI. *P* values for non-parametric ANOVA analyses with Kruskal-Wallis test are shown. Asterisks indicate significant differences ($P < 0.0001$) between groups using Dunn's multiple comparison tests. (**h**) Dot plot representing the correlation of nuclear FOXO3a and β-catenin immunofluorescence signals with the incidence of tumor budding in 65 human primary colon carcinomas. Correlation was evaluated by non-parametric Spearman test, and *P* values were determined by non-parametric ANOVA analyses with a Kruskal-Wallis test. The number of cases (*n*), coefficient of correlation (*r*) and *P* values are indicated. Tumor budding and relative units (r.u.) of nuclear FOXO3a and β-catenin content were calculated as described in the Online Methods. (**i**) H&E-stained histological section of the invasive front of a primary human colon carcinoma. The black line delineates the tumor edge. T, tumor bulk; M, muscle. Black arrowheads indicate budding tumor cells. Scale bar, 100 μm. (**j**) Immunofluorescent staining of the invasive front of a human primary colon carcinoma for FOXO3a (green) and β-catenin (red). Nuclei were stained with Hoechst 33342 (blue). White arrowheads indicate budding tumor cells. The image on the left corresponds to the area in the dashed box in **i**, and on the right are magnifications. The merged magnified image lacks the blue channel, and yellow color indicates FOXO3a and β-catenin colocalization. Scale bar, left, 100 μm; right, 20 μm.

mice treated with vehicle (**Fig. 2f**). Combined treatment with doxycycline and 4OHT resulted in tumors with similar sizes at the end of the experiment as those treated with 4OHT alone. We observed that FOXO3a induced apoptosis only in DLD-1Fβ cells lacking β-catenin expression (eGFP^{-} cells) both in culture and in xenograft tumors (**Fig. 2g** and **Supplementary Fig. 4e**). Within the tumor tissue, this resulted in high amounts of cell death, which was partially rescued by β-catenin expression (**Supplementary Fig. 5c**,**d**). We confirmed that nuclear accumulation of FOXO3a and β-catenin was significantly ($P < 0.0001$) increased as a result of treatment with 4OHT and doxycycline, respectively (**Supplementary Fig. 5e**,**f**).

Cells accumulating high amounts of both FOXO3a and β-catenin scattered and lost their epithelial phenotype in subconfluent cell cultures and *in vivo*. Nuclear FOXO3a alone also promoted a change in cell shape, but this phenotype is typical of the cell detachment associated with apoptosis (**Fig. 2a** and **Supplementary Figs. 5f** and **6a**). We detected relocation of E-cadherin protein from cell-to-cell contacts to cytoplasmic aggregates in cells in which FOXO3a and β-catenin induced this scattering phenotype (**Figs. 2a** and **3a**,**b** and **Supplementary Figs. 5f** and **6a**,**b**,**e**,**f**). We did not detect E-cadherin protein fragments, a repression of E-cadherin expression or an increase in the concentrations of Snail1, zinc finger E-box binding homeobox 1 (Zeb1) or Slug in these cells as a result of accumulation of FOXO3a, β-catenin or both. This ruled out E-cadherin proteolysis or the canonical epithelial-to-mesenchymal transition as mechanisms of the cell-to-cell detachment (**Supplementary Fig. 6c**,**d**). Further, these morphological changes correlated with increased cell motility and adhesion to substrate (**Fig. 3c**,**d** and **Supplementary Fig. 6e**–**g**). Although a small proportion of cells developed an increased size and extended cytoplasm that resembled the morphology of senescent cells, they were negative for senescence-associated β-galactosidase activity (**Fig. 2a** and **Supplementary Fig. 6b**,**f**,**h**).

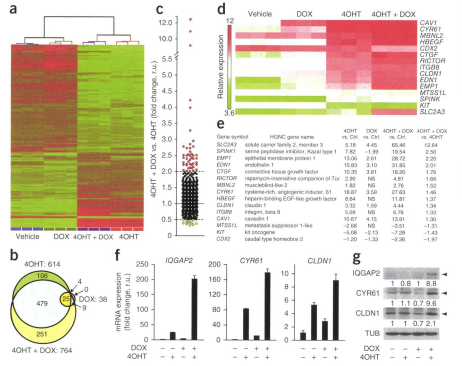

Figure 4 FOXO3a and β-catenin regulate a defined gene expression program. (**a**) Gene clustering diagram calculated using robust-multiarray–normalized expression values from the genome-wide microarray analysis. Triplicates of each treatment are indicated as colored rectangles at the bottom. Significance was calculated using two-tailed ANOVA with a significance cutoff of $P \leq 0.05$. Gene expression scaling, low (green) to high (red). (**b**) Venn diagram showing the number of genes regulated by the indicated treatments using a high-stringency analysis (with a Bonferroni cutoff $P \leq 0.05$) and having a twofold change compared to control in at least one of the conditions (**Supplementary Table 2**). (**c**) Plot representing changes in the relative expression of regulated genes comparing 4OHT and doxycycline with 4OHT alone. Red, higher than twofold induction; green, lower than twofold repression. (**d**) Metastasis signature. Heat map of robust-multiarray–normalized expression values for the genes involved in metastasis. Triplicates for each treatment are shown. Green, low expression; red, high expression. (**e**) Gene expression values of metastasis signature genes shown as a fold change compared to control vehicle-treated cells (Ctrl.) for the indicated treatments. The official gene symbols and HGNC gene names are listed. NS, not significant. (**f**) Main relative mRNA expression levels of *IQGAP2*, *CYR61* and *CLDN1* transcripts measured by real-time RT-PCR in DLD-1Fβ-C7 cells after the indicated treatments. Error bars, triplicate values ± s.d. obtained in three independent experiments. (**g**) Western blot analysis of the indicated proteins in DLD-1Fβ-C7 cells. Numbers below the blot indicate the relative amount of each protein compared to the amount of the protein in vehicle-treated cells. All values are corrected by the respective tubulin signal that served as the loading control. (**h**) Dot plot showing the immunofluorescent signal intensity for each indicated protein correlated to the nuclear FOXO3a and β-catenin colocalization signal intensity in 59 human colon carcinomas. Correlation was evaluated by non-parametric Spearman test. The number of patients (n), coefficient of correlation (r) and P values are indicated. Relative units (r.u.) were calculated as described in the Online Methods.

We then tested the metastatic potential of cells expressing high amounts of nuclear FOXO3a and β-catenin, but no tumor was formed when we injected 1×10^6 DLD1-Fβ cells in the cecum walls of 50 nude mice. Thus, we engineered the same inducible systems to express exogenous FOXO3a and β-catenin as those used in DLD1-Fβ cells in human HT29 colon cancer cells (HT29Fβ). Treatment with doxycycline and 4OHT promoted equivalent effects on proliferation, apoptosis and cell scattering in HT29Fβ cells as those previously observed in DLD-1Fβ cells (**Supplementary Fig. 7**). We then injected HT29Fβ cells into the cecum walls of immunodeficient nude mice to assess whether the scattering phenotype induced by FOXO3a and β-catenin was indicative of an enhanced metastatic potential. We used a pool of these cells, all of which expressed FOXO3a3A-ER^{TM} and a luciferase reporter but only 41% of which contained the S33Y β-catenin–IRES-eGFP construct (Online Methods).

We observed an increase in tumor bioluminescent signal in immunodeficient nude mice treated with doxycycline that decreased or even disappeared in mice treated with 4OHT and that was weak in mice treated with both drugs together (**Supplementary Fig. 8a,b**). We performed exhaustive necropsies and *ex vivo* analyses of the internal organs of these mice using luminometry. We used histology to analyze tissues positive for bioluminescence to confirm metastases. We saw metastases in significantly more mice that had combined nuclear accumulation of FOXO3a and β-catenin than in any other group of mice in the experiment ($P = 0.022$), with the lungs being the most significant dissemination site of the metastases ($P = 0.038$) (**Fig. 3e** and **Supplementary Fig. 8c,d**). A control experiment conducted with parental luciferase-expressing HT29 cells that did not express exogenous FOXO3a or β-catenin did not show any such differences in metastasis frequencies after analogous 4OHT or doxycycline treatments (**Supplementary Fig. 8e**). Treatment with 4OHT induced nuclear FOXO3a accumulation, leading to marked intratumoral cell death, which was rescued by β-catenin (**Supplementary Fig. 9a,b**).

E-cadherin relocation, loss of epithelial organization and cell scattering occurred only in the cell population that was positive for the S33Y β-catenin–eGFP mutant in mice treated with both 4OHT and doxycycline (**Supplementary Fig. 9b–d**). Tumor budding was significantly increased in primary carcinomas growing in

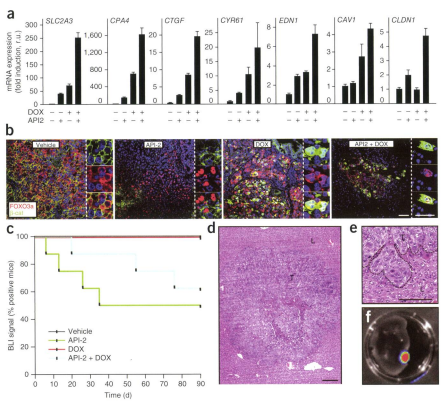

Figure 5 AKT inhibition by API-2 promotes metastasis of cells with high nuclear β-catenin content. (**a**) Relative mRNA levels of the indicated genes measured by real-time RT-PCR in DLD-1Fβ-C7 cells treated with API-2, doxycycline or both, as indicated. Error bars, ± s.d. of triplicates from three independent experiments. (**b**) Immunofluorescence analysis of FOXO3a (red) and β-catenin (green) expression in primary tumors growing in the cecum walls of nude mice. Scale bar, left images, 100 μm. Magnification of cells within the primary tumors (right). Scale bar, right images, 25 μm. Nuclei were stained with Hoechst 33342 (blue). (**c**) Kaplan-Meier analysis of bioluminescence (BLI) showing the percentage of nude mice injected in the cecum wall with HT29Fβ cells and treated as indicated that retained the signal over time. The number of mice used is listed in **Supplementary Table 5**. (**d**) H&E staining of liver metastasis from a cecum-injected mouse treated with API-2 and doxycycline. T, tumor; L, liver tissue. (**e**) A magnification of the image in **d** (top). The dashed line indicates the tumor-liver edge. *Ex vivo* image of infiltrated liver overlaid with gradual false-colored bioluminescent signal (blue, low; red, high) (bottom). Scale bar, **d**, 200 μm; **e**, 100 μm.

the cecum walls of mice treated with both 4OHT and doxycycline (**Fig. 3f**,**g**). We also found nuclear colocalization of FOXO3a and β-catenin in scattered cells at the invasive fronts of human colon carcinomas (**Fig. 3h**–**j**). By measuring the FOXO3a and β-catenin colocalization signal in the tumor bulk, we found that it had a positive correlation with tumor budding at the invasive front. Only a minor proportion of carcinomas had an increased accumulation of these factors at the invasive front, as has been previously described for β-catenin (**Supplementary Fig. 10**)[25].

FOXO3a and β-catenin co-regulate metastasis-relevant genes

Transcriptomic analyses showed that FOXO3a alone provoked a substantial change in the gene expression pattern of DLD-1Fβ cells[26], whereas β-catenin alone produced only a minor effect in these cells (**Fig. 4a**,**b** and **Supplementary Tables 1** and **2**). However, coexpression of β-catenin and FOXO3a enhanced the expression of many known or undescribed FOXO3a-induced target genes (**Fig. 4c**, **Supplementary Fig. 11a**,**b** and **Supplementary Tables 1** and **2**). In contrast, other genes involved in cell differentiation, such as *MUC13*, *VIL1* or *CDX2*, were repressed by nuclear FOXO3a, and the concomitant presence of nuclear β-catenin further enhanced such inhibition.

β-catenin enhances the expression of many FOXO3a target genes that are involved in cytoskeleton remodeling, cell shape and motility (**Supplementary Table 3**). The products of some of these genes are part of the protein complexes that control the stability of cell-to-cell contacts (**Supplementary Fig. 11c**,**d**)[27]. *IQGAP2* is one of these target genes that is involved in the stability of E-cadherin at adherent junctions[28,29]. The knockdown of IQGAP2 expression by shRNAi partially preserved the amount of E-cadherin that was associated with the actin cortex at cell-to-cell contacts in DLD1-Fβ-C7 cells treated with 4OHT and doxycycline. The induction of cell motility that was promoted by nuclear FOXO3a and β-catenin was also significantly reduced when we knocked down IQGAP2 ($P = 0.0467$). We also observed that IQGAP2 expression correlated with tumor budding in a set of 59 human colon carcinomas (**Supplementary Fig. 12**). We found IQGAP2 in association with E-cadherin aggregates in the cytoplasm of scattering DLD1-Fβ-C7 cells in culture or in subcutaneous xenografts as a result of FOXO3a and β-catenin nuclear colocalization and in cancer cells with disrupted epithelial organization in human colon carcinomas (**Supplementary Fig. 13**).

FOXO3a and β-catenin regulated a defined set of metastasis-relevant genes (**Fig. 4d**,**e** and **Supplementary Table 4**). In addition to *IQGAP2*, we also studied *CYR61* and *CLDN1*, which have both been reported to be associated with cell-to-cell disassembly and cell scattering, motility and metastasis[30,31]. The concentrations of nuclear FOXO3a alone or FOXO3a and β-catenin together correlated with the amount of protein expression of each of these three target genes in a set of 59 primary human colon carcinomas. The amount of nuclear β-catenin did not have any significant correlation with the protein expression of these genes (**Fig. 4f**–**h** and **Supplementary Figs. 14** and **15**).

A gene set enrichment analysis showed that FOXO3a regulated genes involved in apoptosis, whereas its coexpression with β-catenin also modulated genes controlling cell morphology, adhesion and motility. Nuclear β-catenin attenuated the upregulation of the proapoptotic genes *TNFSF10* and *BCL2L11*, and it synergized with FOXO3a to induce the upregulation of *FASLG* and the anti-apoptotic gene *HIPK3*. Moreover, β-catenin caused nuclear translocation of FAS-associated adaptor protein (FADD) and inhibited the poly (ADP-ribose) polymerase 1 (PARP1) cleavage that was induced by FOXO3a (**Supplementary Figs. 11a** and **16** and **Supplementary Table 3**).

AKT inhibition induces metastasis cooperating with β-catenin

The phosphorylation of FOXO3a by AKT translocates it from the nucleus to the cytoplasm. We therefore used the anti-tumoral drug API-2, which specifically inhibits AKT, to relocate FOXO3a back to

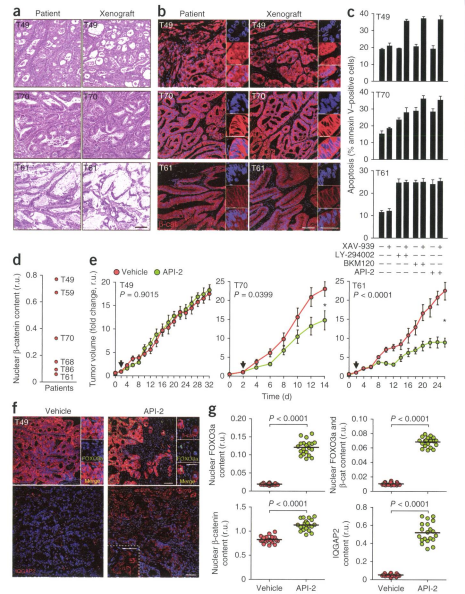

Figure 6 High nuclear β-catenin concentrations confer resistance to PI3K and AKT inhibitors in colon cancer patient-derived cells. (**a**) H&E staining of the primary carcinomas of the patients (left) and subcutaneous tumors (right, xenograft) generated in NOD-SCID mice from the corresponding patient-derived cells. Scale bar, 100 μm. (**b**) Immunofluorescent staining for β-catenin (red) in the primary carcinomas of the patients (left) and the corresponding subcutaneous xenograft tumors in mice (right). The smaller images on the right correspond to magnifications that show the amount of nuclear β-catenin. Nuclei were stained with Hoechst 33342 (blue). Scale bar, left images, 100 μm; right images, 50 μm. (**c**) Percentages of apoptotic cells in patient-derived sphere cultures treated as indicated. Apoptosis was measured by flow cytometry. Bars represent the mean of three independent experiments. Error bars, ± s.d. Cells were treated with the indicated compounds as described in the Online Methods. (**d**) Graph showing the amount of nuclear β-catenin measured by immunofluorescence in the primary colon carcinomas of each indicated patient. Relative units (r.u.) were calculated as described in the Online Methods. (**e**) Cancer cells derived from tumors from the three indicated patients were injected subcutaneously in NOD-SCID mice and treated with API-2 or vehicle ($n = 5$, two flanks per mouse). Arrows mark the initiation of treatment. The represented fold change was calculated by comparing the tumor volume at each given time point to the volume at the first day of treatment. Relative units (r.u.) were calculated as described in the Online Methods. Error bars, ± s.d. of ten tumors per treatment. *P* values correspond to non-parametric Mann-Whitney test. Asterisks indicate significant differences (with the *P* values indicated on the graphs) between the volumes of the tumors growing in mice treated with vehicle compared to mice treated with API-2. (**f**) Immunofluorescent staining for FOXO3a (green) and β-catenin (red) in histological sections of subcutaneous xenografted tumors from patient T49 treated as indicated (top images). The images on the right are magnifications that show the amounts of nuclear FOXO3a and β-catenin. Scale bar, left images, 100 μm; right images, 50 μm. Immunofluorescent staining for IQGAP2 (red) in the same xenograft tumors (bottom images). The insert shows a magnification of the cells with IQGAP2 accumulated in their cytoplasmic aggregates. Scale bar, main images, 100 μm; insert, 50 μm. Nuclei were stained with Hoechst 33342 (blue). (**g**) Column scatter plots showing the expression of each indicated protein in xenografted tumors from patient T49 treated as labeled. Five images were quantified for each of the four tumors treated. *P* values correspond to non-parametric Mann-Whitney test comparing the values of protein expression in each quantified picture. Relative units (r.u.) were calculated as described in the Online Methods.

the nucleus. Nuclear FOXO3a accumulation resulting from treatment with 4OHT or the AKT inhibitor API-2 promoted the scattering of DLD-1Fβ cells when concomitant high nuclear concentrations of β-catenin were induced by doxycycline. Some of the FOXO3a and β-catenin target genes defined in our metastasis signature were induced by API-2 and were further enhanced by β-catenin in DLD1-Fβ-C7 cells (**Figs. 4d**,**e** and **5a** and **Supplementary Fig. 17b**,**c**).

In tumors of HT29Fβ cells growing in the cecum walls of nude mice, treatment with API-2 and doxycycline induced the nuclear accumulation of FOXO3a and β-catenin, respectively, as well as the loss of the epithelial phenotype and the promotion of cell scattering (**Fig. 5b** and **Supplementary Fig. 17a**). Most crucially, although API-2 treatment reduced the primary tumor bioluminescence signal, it simultaneously promoted the development of metastasis when nuclear β-catenin was expressed. A significantly higher number of mice had metastases when treated with both API-2 and doxycycline compared to mice treated with vehicle ($P = 0.015$) (**Fig. 5c** and **Supplementary Table 5**). We found more mice affected in the lungs or lymph nodes or that had carcinomatosis as a result of treatment with both API-2 and doxycycline than as a result of vehicle treatment. Notably, API-2 treatment produced liver metastasis when β-catenin concentrations were high. We never detected this dissemination site previously in our HT29Fβ-cell model, and this site recapitulated the main organ affected in human patients with colon cancer (**Fig. 5d**–**f**).

β-catenin confers resistance to PI3K and AKT inhibitors

We observed a dose-dependent resistance to API-2–induced apoptosis that correlated with nuclear β-catenin content in DLD-1Fβ-C7 cells. HCT-116F cells with high endogenous amounts of mutant nuclear β-catenin or HT29Fβ cells with medium amounts were more resistant to NVP-BKM120– and API-2–induced apoptosis than DLD-1Fβ cells with any amount of nuclear β-catenin (**Supplementary Figs. 17b–h** and **18a,b** and **Supplementary Table 6**). In L8 colon cancer cells that are heterogeneous with respect to nuclear β-catenin concentrations and transcriptional activity, LY-249002, a pharmacological inhibitor of PI3K, preferentially induced apoptosis in the cell population with low expression of β-catenin (**Supplementary Fig. 19a–c**). Notably, the tankyrase inhibitor XAV-939, which reduces nuclear β-catenin concentrations and transcriptional activity, increased the sensitivity of HCT-116F cells to NVP-BKM120– and API-2–induced apoptosis (**Supplementary Figs. 17d,e**, **18b** and **19d–f**)[32].

We also analyzed the response to treatment of patient-derived colon cancer cells. Corresponding sphere cultures can regenerate carcinomas that preserve the same amounts of nuclear β-catenin and are histologically indistinguishable from the primary tumors of the patients after subcutaneous injection in nonobese diabetic severe combined immunodeficient (NOD-SCID) mice (**Fig. 6a,b** and **Supplementary Fig. 18c,d**). Treatment of sphere cultures with LY-294002 or NVP-BKM120 and API-2 induced the nuclear accumulation of FOXO3a and apoptosis in cells derived from patients T61, T68, T70 and T86, who originally presented with low nuclear β-catenin concentrations in their primary carcinomas. In contrast, sphere cultures derived from patients T49 and T59, who had high nuclear β-catenin concentrations, were innately resistant to the cell death mediated by these drugs. Notably, reduction of β-catenin concentrations by XAV-939 reverted such resistance (**Fig. 6c,d** and **Supplementary Fig. 18e–g**). In contrast, the sphere cultures were resistant to conventional chemotherapeutic agents such as 5-fluorouracil (5-FU) or oxaliplatin, and a combination treatment with these agents and XAV-939 did not sensitize the cultures to apoptosis (**Supplementary Fig. 18h**).

In vivo, treatment with API-2 inhibited the growth of the subcutaneous tumors generated in NOD-SCID mice when they were injected with cells derived from patient T61 (low β-catenin concentration), whereas mice injected with cells derived from patient T70 (intermediate β-catenin concentration) had only a partial response to API-2, and mice injected with cells derived from patient T49 (high β-catenin concentration) were resistant to API-2 treatment (**Fig. 6d,e**). The reduction of S6 ribosomal protein phosphorylation confirmed the efficacy of API-2 treatment in inhibiting PI3K-AKT pathway signaling *in vivo* (**Supplementary Fig. 20**). An analysis of the xenograft tumor derived from patient T49 revealed that API-2 treatment induced nuclear FOXO3a accumulation and increased cytoplasmatic IQGAP2 concentrations in tumor cell populations with disrupted epithelial organization. We also observed an enrichment of cells with high nuclear β-catenin concentrations in API-2–treated xenograft tumors from patient T49 compared to vehicle-treated control tumors (**Fig. 6f,g**).

DISCUSSION

Metastases are responsible for over 90% of deaths in patients with cancer, but the molecular mechanisms that drive this process are not well understood. Our data reveal previously unknown mechanisms by which FOXO3a and β-catenin can induce metastasis independently of the corresponding upstream pathways that control their nuclear accumulation[13,33].

Whereas some findings have related an abnormal activation of the Wnt–β-catenin pathway to metastasis[34], the contribution of PI3K-AKT-FOXO signaling to this process is not clear. On the one hand, mutational activation of PI3K and induction of AKT activity mediate metastasis[35], which might encourage the use of therapeutic inhibitors of PI3K and AKT. On the other hand, AKT can inhibit cell motility by blocking the transcriptional activity of nuclear factor of activated T cells (NFAT)[36]. Our results, which show that AKT inhibitors promote metastasis resulting from nuclear FOXO3a accumulation and cooperation with β-catenin, support the second notion.

Few studies have correlated FOXO3a function with metastasis or poor prognosis in cancer[37,38]. On the contrary, most studies have defined FOXO proteins as tumor suppressors, as they induce cell-cycle arrest and apoptosis[9,11]. Indeed, the combined knockdown of FOXO1, FOXO3 and FOXO4 in mice is responsible for tumor initiation[39]. However, our results reveal a previously unknown role for FOXO3a as an inducer of metastasis when acting in concert with β-catenin. We observed that the simultaneous nuclear accumulation of FOXO3a and β-catenin in primary tumors correlated with stages 3 and 4 of local or distant metastases and significantly shorter overall survival time of patients with colon cancer.

We show that to acquire such metastatic capacity, FOXO3a and β-catenin regulate functional sets of common target genes that are involved in reorganizing the cytoskeleton, destabilizing cell-to-cell contacts and increasing cell motility and migration, angiogenesis or evasion of the immune system. In particular, we revealed *IQGAP2* as a new target gene of FOXO3a–β-catenin complex that is required for destabilizing E-cadherin–containing adherens junctions, cell scattering and motility in colon carcinomas, indicating its role in metastasis.

AKT inhibition by API-2 induces nuclear FOXO3a accumulation and, in concert with nuclear β-catenin, promotes the expression of the aforementioned metastasis-related target genes and metastasis in mice. In fact, the nuclear accumulation of both factors correlates with tumor budding in human colon carcinomas.

Drug resistance is another crucial clinical feature that determines tumor relapse and patient survival. In particular, the mechanisms underlying resistance to new PI3K or AKT inhibitors are largely unknown[18,40,41]. Part of the anti-tumoral action of PI3K and AKT inhibitors is based on nuclear FOXO accumulation and subsequent cell-cycle arrest and apoptosis[42]. We show that nuclear β-catenin activity acts as a new mechanism of resistance to the FOXO3a-induced apoptosis promoted by inhibitors of PI3K or AKT. Thus, the induction of FOXO3a proapoptotic target genes such as *TNFSF10* (encoding TRAIL) or *BCL2L11* (encoding BIM)[43] is reduced by nuclear β-catenin, whereas FOXO3a and β-catenin cooperate synergistically to induce the anti-apoptotic kinase homeodomain interacting protein kinase 3 (HIPK3), which is responsible for FADD phosphorylation and confers resistance to death-receptor–mediated apoptosis[44,45].

Colon carcinomas are heterogeneous tissues containing cell populations with diverse biological properties and various amounts of nuclear β-catenin[3,25,46,47]. Cells with high nuclear β-catenin content behave as cancer stem cells[48,49] and are resistant to the FOXO3a-induced apoptosis that is promoted by inhibitors of PI3K or AKT. This resistant behavior leads to relapse and metastasis by inducing FOXO3a and β-catenin common target genes, supporting the concept of metastatic cancer stem cells (**Supplementary Fig. 21**)[49–52]. Indeed, sphere cultures derived from patients with colon cancer, which are enriched in cancer stem cells and which originated from tumors with high nuclear β-catenin content, were resistant to PI3K and AKT inhibitors *in vitro* and in subcutaneous xenograft tumors.

The information provided by these sphere cultures highlights the validity of studying target-directed therapies in cells derived from colon tumors immediately after surgical resection, as patients could therefore benefit from a personalized, experiment-based decision on the optimal treatment method. In the particular case of PI3K or AKT inhibitors, undesirable induction of FOXO3a and β-catenin target genes and promotion of metastasis could be predicted and avoided.

We show that the tankyrase inhibitor XAV-939 (ref. 32) sensitizes resistant cells specifically to the FOXO3a-induced apoptosis that is promoted by PI3K or AKT inhibitors. In contrast, XAV-939 does not have any benefit when combined with conventional chemotherapeutic agents such as 5-FU or oxaliplatin in cultures of colon-cancer–initiating cells. This points to a valid strategy to overcome drug resistance and metastasis by combining PI3K or AKT and Wnt–β-catenin inhibitory drugs. Currently used Wnt signaling inhibitors have reduced activity *in vivo*, and a new generation of tankyrase inhibitors with satisfactory *in vivo* activity must be developed to translate our results to clinical practice.

The benefit of some PI3K and AKT inhibitors is currently being tested in clinical trials in patients with colon cancer with advanced metastatic disease[15], and these inhibitors may be tested as part of adjuvant therapy in the future. Our findings call for the measurement of nuclear β-catenin concentrations as a biomarker of response to treatments that provoke FOXO3a nuclear accumulation to predict apoptosis or metastasis. This would be advisable for PI3K and AKT inhibitors and may be extended to other drugs such as cetuximab or receptor tyrosine kinase inhibitors that act upstream of a common oncogenic pathway.

METHODS

Methods and any associated references are available in the online version of the paper.

Note: Supplementary information is available in the online version of the paper.

ACKNOWLEDGMENTS

We thank W. Shao (Novartis Institutes for BioMedical Research, Inc.) for providing the experimental drug, XAV-939, and its inactive analog, LDW-643, and we thank K.F. Becker (Technische Universität München, Germany) for providing the antibody to Snail. We also thank P.J. Coffer (Utrecht, Netherlands) for providing the pcDNA3-FOXO3a(A3)-ER^{TM} expression plasmid, as well as H. Clevers (Utrecht, Netherlands) for providing L8 colon cancer cells. J. Seoane and G. Folch (VHIO, Barcelona, Spain) provided technical advice and reagents. We thank R. Luthra (Molecular Diagnostics Laboratory, MD Anderson Cancer Center, Houston, Texas, USA) for providing the CLIA panel of somatic mutations. We thank M.J. Larriba (Instituto de Investigaciones Biomédicas 'Alberto Sols', Consejo Superior de Investigaciones Cientificas-Universidad Autónoma de Madrid, Madrid, Spain) for providing the reagents necessary for the analysis of Zeb1 and Slug expression and M. Scaltriti (Massachusetts General Hospital Cancer Center, Harvard Medical School, Charlestown, Massachusetts, USA) for supplying the lentiviruses used to knock down IQGAP2 expression. We acknowledge R. Rycroft and A. Wren for their valuable assistance in the preparation of the English version of the manuscript. Experiments were supported by a VHIO starting grant and grants from Fondo de Investigaciones Sanitarias–Instituto de Salud Carlos III (ISCIII) (FIS-PI081356, RETICC-RD06/0020/0075 and RETICC-RD06/0020/0009), and Plan Nacional de Biomedicina, Ministerio de Ciencia e Innovación (SAF-18302). S.P.T. was supported by a Fundació Olga Torres Fellowship, I.P. was funded by the Fundación Científica de la Asociación Española Contra el Cancer (AECC), and H.G.P. was supported by the Miguel Servet Program, ISCIII.

AUTHOR CONTRIBUTIONS

S.P.T., P.O.-M. and I.P. contributed equally to the experiments. S.P.T. also contributed to writing the manuscript, and I.C. also performed experiments. O.A. helped to perform IQGAP2 knockdown experiments. S.L. classified human tumors according to histopathological criteria and built the tissue arrays. Y.F. performed and analyzed live imaging assays (IVIS), which were supervised by S.S. J.R.H., S.R. and J.D.G. participated in live imaging experiments. L.M. and A.V. performed mutational analysis of human colon carcinomas. S.A. cloned and tested lentiviral constructs. S.R.y.C. provided human specimens. E.E. performed surgery on patients with colon cancer. J.B. supervised the project. J.T. supervised the project and provided clinical follow up on all the patients included in the study. A.M. and H.G.P. wrote the manuscript and supervised the project. H.G.P. was responsible for designing all the experiments and analyzing and interpreting all data.

COMPETING FINANCIAL INTERESTS

The authors declare no competing financial interests.

Published online at http://www.nature.com/doifinder/10.1038/nm.2772.
Reprints and permissions information is available online at http://www.nature.com/reprints/index.html.

1. Jemal, A. *et al.* Global cancer statistics. *CA Cancer J. Clin.* **61**, 69–90 (2011).
2. Jänne, P.A. & Mayer, R.J. Chemoprevention of colorectal cancer. *N. Engl. J. Med.* **342**, 1960–1968 (2000).
3. Clevers, H. Wnt/β-catenin signaling in development and disease. *Cell* **127**, 469–480 (2006).
4. Reya, T. & Clevers, H. Wnt signalling in stem cells and cancer. *Nature* **434**, 843–850 (2005).
5. Pálmer, H.G. *et al.* Vitamin D(3) promotes the differentiation of colon carcinoma cells by the induction of E-cadherin and the inhibition of β-catenin signaling. *J. Cell Biol.* **154**, 369–387 (2001).
6. Olson, L.E. *et al.* Homeodomain-mediated β-catenin-dependent switching events dictate cell-lineage determination. *Cell* **125**, 593–605 (2006).
7. Pálmer, H.G., Anjos-Afonso, F., Carmeliet, G., Takeda, H. & Watt, F.M. The vitamin D receptor is a Wnt effector that controls hair follicle differentiation and specifies tumor type in adult epidermis. *PLoS ONE* **3**, e1483 (2008).
8. Essers, M.A. *et al.* Functional interaction between β-catenin and FOXO in oxidative stress signaling. *Science* **308**, 1181–1184 (2005).
9. Calnan, D.R. & Brunet, A. The FoxO code. *Oncogene* **27**, 2276–2288 (2008).
10. van der Horst, A. & Burgering, B.M. Stressing the role of FoxO proteins in lifespan and disease. *Nat. Rev. Mol. Cell Biol.* **8**, 440–450 (2007).
11. Myatt, S.S. & Lam, E.W. The emerging roles of forkhead box (Fox) proteins in cancer. *Nat. Rev. Cancer* **7**, 847–859 (2007).
12. Brunet, A. *et al.* Akt promotes cell survival by phosphorylating and inhibiting a Forkhead transcription factor. *Cell* **96**, 857–868 (1999).
13. Dehner, M., Hadjihannas, M., Weiske, J., Huber, O. & Behrens, J. Wnt signaling inhibits Forkhead box O3a-induced transcription and apoptosis through up-regulation of serum- and glucocorticoid-inducible kinase 1. *J. Biol. Chem.* **283**, 19201–19210 (2008).
14. Walther, A. *et al.* Genetic prognostic and predictive markers in colorectal cancer. *Nat. Rev. Cancer* **9**, 489–499 (2009).
15. Dienstmann, R., Rodon, J., Markman, B. & Tabernero, J. Recent developments in anti-cancer agents targeting PI3K, Akt and mTORC1/2. *Recent Pat. Anticancer. Drug Discov.* **6**, 210–236 (2011).
16. Yang, L. *et al.* Akt/protein kinase B signaling inhibitor-2, a selective small molecule inhibitor of Akt signaling with antitumor activity in cancer cells overexpressing Akt. *Cancer Res.* **64**, 4394–4399 (2004).
17. Zheng, Y. *et al.* Novel phosphatidylinositol 3-kinase inhibitor NVP-BKM120 induces apoptosis in myeloma cells and shows synergistic anti-myeloma activity with dexamethasone. *J Mol Med (Berl)* (2011).
18. Liu, P., Cheng, H., Roberts, T.M. & Zhao, J.J. Targeting the phosphoinositide 3-kinase pathway in cancer. *Nat. Rev. Drug Discov.* **8**, 627–644 (2009).
19. Hoffman, K. *et al.* Phase I–II study: triciribine (tricyclic nucleoside phosphate) for metastatic breast cancer. *Cancer Chemother. Pharmacol.* **37**, 254–258 (1996).
20. Bendell, J.C. *et al.* Phase I, dose-escalation study of BKM120, an oral pan-class I PI3K inhibitor, in patients with advanced solid tumors. *J. Clin. Oncol.* **30**, 282–290 (2012).
21. Dijkers, P.F., Medema, R.H., Lammers, J.W., Koenderman, L. & Coffer, P.J. Expression of the pro-apoptotic Bcl-2 family member Bim is regulated by the forkhead transcription factor FKHR-L1. *Curr. Biol.* **10**, 1201–1204 (2000).
22. Seoane, J., Le, H.V., Shen, L., Anderson, S.A. & Massague, J. Integration of Smad and forkhead pathways in the control of neuroepithelial and glioblastoma cell proliferation. *Cell* **117**, 211–223 (2004).
23. Hoogeboom, D. *et al.* Interaction of FOXO with β-catenin inhibits β-catenin/T cell factor activity. *J. Biol. Chem.* **283**, 9224–9230 (2008).
24. Kops, G.J. *et al.* Forkhead transcription factor FOXO3a protects quiescent cells from oxidative stress. *Nature* **419**, 316–321 (2002).
25. Brabletz, T. *et al.* Variable β-catenin expression in colorectal cancers indicates tumor progression driven by the tumor environment. *Proc. Natl. Acad. Sci. USA* **98**, 10356–10361 (2001).
26. Delpuech, O. *et al.* Induction of Mxi1-SR α by FOXO3a contributes to repression of Myc-dependent gene expression. *Mol. Cell. Biol.* **27**, 4917–4930 (2007).
27. Wells, C.D. *et al.* A Rich1/Amot complex regulates the Cdc42 GTPase and apical-polarity proteins in epithelial cells. *Cell* **125**, 535–548 (2006).
28. Yamashiro, S., Abe, H. & Mabuchi, I. IQGAP2 is required for the cadherin-mediated cell-to-cell adhesion in *Xenopus laevis* embryos. *Dev. Biol.* **308**, 485–493 (2007).

29. Natale, D.R. & Watson, A.J. Rac-1 and IQGAP are potential regulators of E-cadherin-catenin interactions during murine preimplantation development. *Gene Expr. Patterns* **2**, 17–22 (2002).
30. Tsai, M.S., Hornby, A.E., Lakins, J. & Lupu, R. Expression and function of CYR61, an angiogenic factor, in breast cancer cell lines and tumor biopsies. *Cancer Res.* **60**, 5603–5607 (2000).
31. Dhawan, P. *et al.* Claudin-1 regulates cellular transformation and metastatic behavior in colon cancer. *J. Clin. Invest.* **115**, 1765–1776 (2005).
32. Huang, S.M. *et al.* Tankyrase inhibition stabilizes axin and antagonizes Wnt signalling. *Nature* **461**, 614–620 (2009).
33. Cross, D.A., Alessi, D.R., Cohen, P., Andjelkovich, M. & Hemmings, B.A. Inhibition of glycogen synthase kinase-3 by insulin mediated by protein kinase B. *Nature* **378**, 785–789 (1995).
34. Brabletz, T., Jung, A., Dag, S., Hlubek, F. & Kirchner, T. β-catenin regulates the expression of the matrix metalloproteinase-7 in human colorectal cancer. *Am. J. Pathol.* **155**, 1033–1038 (1999).
35. Samuels, Y. *et al.* Mutant PIK3CA promotes cell growth and invasion of human cancer cells. *Cancer Cell* **7**, 561–573 (2005).
36. Yoeli-Lerner, M. *et al.* Akt blocks breast cancer cell motility and invasion through the transcription factor NFAT. *Mol. Cell* **20**, 539–550 (2005).
37. Chen, J. *et al.* Constitutively nuclear FOXO3a localization predicts poor survival and promotes Akt phosphorylation in breast cancer. *PLoS ONE* **5**, e12293 (2010).
38. Storz, P., Doppler, H., Copland, J.A., Simpson, K.J. & Toker, A. FOXO3a promotes tumor cell invasion through the induction of matrix metalloproteinases. *Mol. Cell. Biol.* **29**, 4906–4917 (2009).
39. Paik, J.H. *et al.* FoxOs are lineage-restricted redundant tumor suppressors and regulate endothelial cell homeostasis. *Cell* **128**, 309–323 (2007).
40. Juri, T., Gjorup, O. & Roberts, T.M. Tangled webs: evidence of cross-talk between c-Raf-1 and Akt. *Sci. STKE* **1999**, PE1 (1999).
41. Zunder, E.R., Knight, Z.A., Houseman, B.T., Apsel, B. & Shokat, K.M. Discovery of drug-resistant and drug-sensitizing mutations in the oncogenic PI3K isoform p110 α. *Cancer Cell* **14**, 180–192 (2008).
42. Gomes, A.R., Brosens, J.J. & Lam, E.W. Resist or die: FOXO transcription factors determine the cellular response to chemotherapy. *Cell Cycle* **7**, 3133–3136 (2008).
43. Obexer, P., Geiger, K., Ambros, P.F., Meister, B. & Ausserlechner, M.J. FKHRL1-mediated expression of Noxa and Bim induces apoptosis via the mitochondria in neuroblastoma cells. *Cell Death Differ.* **14**, 534–547 (2007).
44. Rochat-Steiner, V. *et al.* FIST/HIPK3: a Fas/FADD-interacting serine/threonine kinase that induces FADD phosphorylation and inhibits fas-mediated Jun NH(2)-terminal kinase activation. *J. Exp. Med.* **192**, 1165–1174 (2000).
45. Tourneur, L. & Chiocchia, G. FADD: a regulator of life and death. *Trends Immunol.* **31**, 260–269 (2010).
46. Shackleton, M., Quintana, E., Fearon, E.R. & Morrison, S.J. Heterogeneity in cancer: cancer stem cells versus clonal evolution. *Cell* **138**, 822–829 (2009).
47. Fodde, R. & Brabletz, T. Wnt/β-catenin signaling in cancer stemness and malignant behavior. *Curr. Opin. Cell Biol.* **19**, 150–158 (2007).
48. Clevers, H. The cancer stem cell: premises, promises and challenges. *Nat. Med.* **17**, 313–319 (2011).
49. Vermeulen, L. *et al.* Wnt activity defines colon cancer stem cells and is regulated by the microenvironment. *Nat. Cell Biol.* **12**, 468–476 (2010).
50. Brabletz, T., Jung, A., Spaderna, S., Hlubek, F. & Kirchner, T. Opinion: migrating cancer stem cells—an integrated concept of malignant tumour progression. *Nat. Rev. Cancer* **5**, 744–749 (2005).
51. Todaro, M. *et al.* Colon cancer stem cells dictate tumor growth and resist cell death by production of interleukin-4. *Cell Stem Cell* **1**, 389–402 (2007).
52. Van der Flier, L.G. *et al.* The intestinal Wnt/TCF signature. *Gastroenterology* **132**, 628–632 (2007).

nature medicine

Activation of AMP-activated protein kinase α2 by nicotine instigates formation of abdominal aortic aneurysms in mice *in vivo*

Shuangxi Wang[1,2,5], Cheng Zhang[1,2,5], Miao Zhang[1], Bin Liang[1], Huaiping Zhu[1], Jiyeon Lee[1], Benoit Viollet[3], Lijun Xia[4], Yun Zhang[2] & Ming-Hui Zou[1,2]

Smoking is the only modifiable risk factor that is associated with the development, expansion and rupture of abdominal aortic aneurysm (AAA). However, the causative link between cigarette smoke and AAA is unknown. Here we report a causative link between smoking and AAA *in vivo*. Acute infusion of angiotensin II (AngII) or nicotine, a major component of cigarette smoke, markedly increased the incidence of AAA in apolipoprotein E (apoE) knockout (*Apoe*$^{-/-}$) mice and in mice deficient in both apoE and the AMP-activated kinase α1 subunit (AMPK-α1) (*Apoe*$^{-/-}$; *Prkaa1*$^{-/-}$ mice). In contrast, genetic deletion of AMPK-α2 (*Apoe*$^{-/-}$; *Prkaa2*$^{-/-}$ mice) ablated nicotine- or AngII-triggered AAA *in vivo*. Mechanistically, we found that both nicotine and AngII activated AMPK-α2 in cultured vascular smooth muscle cells (VSMCs), resulting in the phosphorylation of activator protein 2α (AP-2α) and consequent matrix metallopeptidase 2 (MMP2) gene expression. We conclude that smoking (through nicotine) instigates AAA through AMPK-α2–mediated AP-2α–dependent MMP2 expression in VSMCs.

AAA is the most common form of aortic aneurysm. Ruptured AAAs are the thirteenth leading cause of death in the United States[1]. The exact cause of AAA is unknown. Among all the identified risk factors, smoking, which increases the risk of AAA 7.6-fold[2], is the only modifiable factor that has been associated with the development, expansion and rupture of AAA. However, no causative link has been proven between smoking and AAA.

Pathologically, AAAs are characterized by a dilatation of all the layers of the arterial wall as a result of loss of elastin, smooth muscle cell apoptosis and compensatory collagen deposition[3–5]. Reactive oxygen species (ROS) are thought to be a common link between inflammation, matrix degradation and AAA pathogenesis. For example, AngII increases the amount of NADPH oxidase-derived ROS[6], induces MMP protein and mRNA expression[7], and induces inflammation-mediated AAA formation in animal experiments[8]. Although increased amounts of ROS in AAA are well documented, the molecular mechanisms by which ROS induce AAA are not well characterized.

AMPK is a serine/threonine kinase consisting of α, β and γ subunits. The α subunit, for which two isoforms exist (AMPK-α1 and AMPK-α2), is responsible for the catalytic activity of the heterotrimer complex, whereas the β and γ regulatory subunits maintain its stability. AMPK, which is activated by AMP or ADP, is considered to be an energy sensor in the regulation of whole-body energy homeostasis. Recently, we and another group[9–12] found that AMPK can be activated by oxidants or hypoxia, including hydrogen peroxide and peroxynitrite; these agents activate AMPK through pathways that can be either dependent on or independent of LKB1 (refs. 12,13). Accordingly, oxidant-mediated AMPK activation in VSMCs inhibits cell proliferation and restenosis induced by AngII infusion or wire injury[13,14]. However, whether AMPK is involved in AAA formation is unknown. Here we report that nicotine, a major component of cigarette smoke, activates AMPK in VSMCs, resulting in aberrant expression of MMP2 and consequent AAA formation.

RESULTS

AMPK-α2 deletion suppresses nicotine-induced AAA formation

Nicotine is a major component of cigarette smoke and is rapidly absorbed into the bloodstream, with nicotine blood concentrations ranging from 40–100 ng ml^{-1} after each cigarette smoked[15]. In regular smokers, nicotine is present in the blood at 90–100 nM over the first 6 to 8 h of each day[16]. Although there is overwhelming epidemiological evidence linking smoking and AAA[2], there is no evidence that smoking or nicotine causes AAA formation in humans or animals. We first investigated whether nicotine infusion (at 1, 5 mg per kg of body weight per day for 6 weeks) increased the incidence of AAA in *Apoe*$^{-/-}$, *Apoe*$^{-/-}$; *Prkaa1*$^{-/-}$ and *Apoe*$^{-/-}$; *Prkaa2*$^{-/-}$ mice. None of the mice died during this time period, and nicotine infusion did not affect hemodynamic parameters or metabolic indices in the mice (**Supplementary Tables 1** and **2**).

[1]Department of Medicine, Division of Molecular Medicine, University of Oklahoma Health Sciences Center, Oklahoma City, Oklahoma, USA. [2]The Key Laboratory of Cardiovascular Remodeling and Function Research, Chinese Ministry of Education and Chinese Ministry of Health, Shandong University, Qilu Hospital, Jinan City, Shandong, China. [3]Institut Cochin, Université Paris Descartes, Centre National de la Recherche Scientifique (CNRS, UMR 8104), Paris, France. [4]Cardiovascular Biology Research Program, Oklahoma Medical Research Foundation, Oklahoma City, Oklahoma, USA. [5]These authors contributed equally to this work. Correspondence should be addressed to M.-H.Z. (ming-hui-zou@ouhsc.edu).

Received 9 December 2011; accepted 16 February 2012; published online 6 May 2012; doi:10.1038/nm.2711

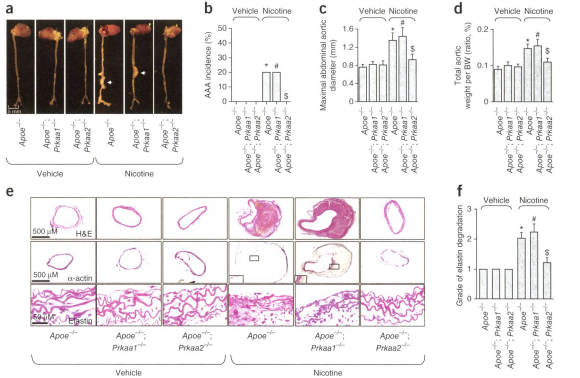

Figure 1 AMPK-α2 deficiency prevents nicotine-induced AAA formation in *Apoe*$^{-/-}$ mice. (**a**) Representative photographs showing the macroscopic features of aneurysms induced by nicotine. Vehicle or nicotine was administered to mice of the indicated genotypes. Arrows indicate typical AAAs. (**b**–**d**) The incidence of nicotine-induced AAA (**b**), maximal abdominal aortic diameter (**c**) and total aortic weights (**d**) in mice of the indicated genotypes after vehicle or nicotine infusion. BW, body weight. The ratios shown are the aortic weight (g) to the total body weight (g) of the mouse and are given as percentages. (**e**) Representative staining with H&E, elastin and α-actin in the suprarenal aortas of mice of the indicated genotypes after vehicle or nicotine infusion. The magnification of the two insets in the middle row is 40-fold. (**f**) Grade of elastin degradation in the aortic wall of mice of the indicated genotypes after vehicle or nicotine infusion. $^{*}P < 0.05$ compared to vehicle-infused *Apoe*$^{-/-}$ mice, $^{\#}P < 0.05$ compared to vehicle-infused *Apoe*$^{-/-}$; *Prkaa1*$^{-/-}$ mice, $^{\$}P < 0.05$ compared to nicotine-infused *Apoe*$^{-/-}$ mice. $n = 10$ in each group of *Apoe*$^{-/-}$, *Apoe*$^{-/-}$; *Prkaa1*$^{-/-}$ and *Apoe*$^{-/-}$; *Prkaa2*$^{-/-}$ mice infused with vehicle. $n = 15$ in the group of *Apoe*$^{-/-}$ mice infused with nicotine. $n = 12$ each for *Apoe*$^{-/-}$; *Prkaa1*$^{-/-}$ and *Apoe*$^{-/-}$; *Prkaa2*$^{-/-}$ mice infused with nicotine. The *P* values were obtained by a χ^2 test in **b** and by a one-way analysis of variance (ANOVA) plus a *post hoc* analysis using a Bonferroni test in **c**, **d** and **f**. The error bars in **c**, **d** and **f** are s.e.m.

None of the *Apoe*$^{-/-}$, *Apoe*$^{-/-}$; *Prkaa1*$^{-/-}$ or *Apoe*$^{-/-}$; *Prkaa2*$^{-/-}$ mice showed evidence of AAA when infused with vehicle (**Fig. 1a**–**d**). However, both low-dose (1 mg per kg of body weight per day) and high-dose (5 mg per kg of body weight per day) nicotine infusion for 6 weeks significantly increased the incidence of AAA, maximal aortic diameters and total aortic weights in *Apoe*$^{-/-}$ and *Apoe*$^{-/-}$; *Prkaa1*$^{-/-}$ mice (**Fig. 1a**–**d** and **Supplementary Fig. 1a**–**c**). Compared to mice infused with vehicle, nicotine infusion markedly increased the size of the aortic lumen and the wall thickness of both *Apoe*$^{-/-}$ and *Apoe*$^{-/-}$; *Prkaa1*$^{-/-}$ mice (**Fig. 1e**).

Apoe$^{-/-}$; *Prkaa2*$^{-/-}$ mice had a markedly reduced incidence of nicotine-induced AAA compared to *Apoe*$^{-/-}$ mice (**Fig. 1b**). The maximal aortic diameter and total aortic weight in nicotine-infused *Apoe*$^{-/-}$; *Prkaa2*$^{-/-}$ mice were also significantly less than those in nicotine-infused *Apoe*$^{-/-}$ mice (**Fig. 1c**,**d**), and nicotine infusion did not cause significant elastic lamina degradation and aortic expansion in *Apoe*$^{-/-}$; *Prkaa2*$^{-/-}$ mice (**Fig. 1e**,**f**). VSMCs were the major cellular component in the area of the AAA, as shown by α-actin staining (**Fig. 1e**). Taken together, these results indicate that deficiency of AMPK-α2 protects against nicotine-induced AAA formation in *Apoe*$^{-/-}$ mice *in vivo*.

AMPK-α2 deficiency attenuates AngII-induced AAA formation

AAA induced by AngII infusion is a well-characterized mouse model of the disease[17,18]. To further validate the role of AMPK-α2 in AAA, we examined the effects of a 4-week AngII infusion in *Apoe*$^{-/-}$, *Apoe*$^{-/-}$; *Prkaa1*$^{-/-}$ and *Apoe*$^{-/-}$; *Prkaa2*$^{-/-}$ mice. As shown in **Supplementary Tables 3** and **4**, AngII infusion increased blood pressure but had no effects on heart rate or any metabolic indices. When infused with saline, there was no difference in the gross morphology of aortas among *Apoe*$^{-/-}$, *Apoe*$^{-/-}$; *Prkaa1*$^{-/-}$ and *Apoe*$^{-/-}$; *Prkaa2*$^{-/-}$ mice (**Supplementary Fig. 2a**). Consistent with previous reports[3,8,19], the incidence of AAA induced by AngII infusion in the present study was 85% and 80% in *Apoe*$^{-/-}$ and *Apoe*$^{-/-}$; *Prkaa1*$^{-/-}$ mice, respectively (**Supplementary Fig. 2a**,**b**). Both the maximal abdominal aortic diameter (**Supplementary Fig. 2c**) and total aortic weight (**Supplementary Fig. 2d**) were markedly higher in AngII-treated *Apoe*$^{-/-}$ and *Apoe*$^{-/-}$; *Prkaa1*$^{-/-}$ mice compared to saline-treated control mice, consistent with previous reports[20–22]. Histological analysis showed that *Apoe*$^{-/-}$ and *Apoe*$^{-/-}$; *Prkaa1*$^{-/-}$ mice infused with AngII had larger aortic lumens and increased aortic wall thickness (**Supplementary Fig. 2e**) compared to saline-treated control mice and that the elastic laminas in AngII-treated mice were frequently disrupted and degraded (**Supplementary Fig. 2f**).

In contrast, only 17% of AngII-infused *Apoe*$^{-/-}$; *Prkaa2*$^{-/-}$ mice developed AAA (**Supplementary Fig. 2b**). The maximal abdominal aortic diameter (**Supplementary Fig. 2c**) and total aortic weight (**Supplementary Fig. 2d**) were markedly lower in AngII-treated

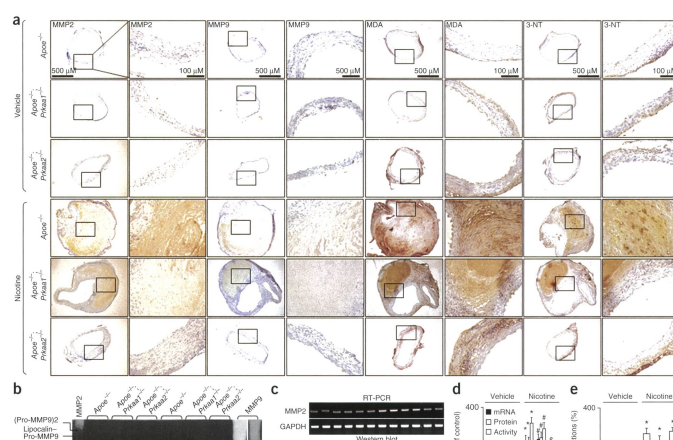

Figure 2 Nicotine infusion results in oxidative stress and enhances the expression of MMP2 and MMP9 through AMPK-α2 *in vivo*. (**a**) Representative immunostaining of MMP2, MMP9, MDA and 3-NT in the suprarenal aortas of vehicle- or nicotine-infused mice. (**b**–**d**) MMP2 and MMP9 activity (by zymography, **b**), MMP2 and GAPDH mRNA and protein expression (**c**) and quantitative data for MMP2 (**d**) in the aortas of vehicle- or nicotine-infused mice of the indicated genotypes. In **b**, the right two lanes were loaded with two different amounts of MMP9 protein. Pro-MMP9, full-length MMP9; Pro-MMP2, full-length MMP2; (Pro-MMP9)2, dimer of Pro-MMP9; Liposalin–Pro-MMP9, pro-MMP9 that binds to lipocalin. $^{*}P < 0.05$ compared to vehicle-infused *Apoe*$^{-/-}$ mice, $^{\#}P < 0.05$ compared to vehicle-infused *Apoe*$^{-/-}$; *Prkaa1*$^{-/-}$ mice, $^{\$}P < 0.05$ compared to nicotine-infused *Apoe*$^{-/-}$ mice. (**e**) ROS production as assessed by measurement of DHE levels by HPLC in the aortas of vehicle- or nicotine-infused mice of the indicated genotypes. $^{*}P < 0.05$ compared to control *Apoe*$^{-/-}$ mice. All results represent 5–10 mice per group. The *P* values in **d** and **e** were obtained by one-way ANOVA plus a *post hoc* analysis using a Bonferroni test. The error bars are s.e.m.

Apoe$^{-/-}$; *Prkaa2*$^{-/-}$ mice compared to AngII-treated *Apoe*$^{-/-}$ and *Apoe*$^{-/-}$; *Prkaa1*$^{-/-}$ mice. AngII infusion of *Apoe*$^{-/-}$; *Prkaa2*$^{-/-}$ mice did not affect aortic wall thickness and did not result in aortic expansion or elastic lamina degradation (**Supplementary Fig. 2e,f**). These results suggest that deficiency of AMPK-α2 reduces AngII-induced AAA formation *in vivo*.

AMPK-α2 deficiency abolishes MMP2 upregulation in AAA mice

MMPs have a key role in the initiation and progression of AAA[23,24]. In particular, VSMC-derived MMP2 and macrophage-derived MMP9 are crucial for AAA formation[25,26]. Thus, we next determined the relative contributions of MMP2 and MMP9 in nicotine-enhanced AAA formation. The expression of MMP2 was substantially increased in nicotine-infused *Apoe*$^{-/-}$ and *Apoe*$^{-/-}$; *Prkaa1*$^{-/-}$ mice (**Fig. 2a**). In contrast, *Apoe*$^{-/-}$; *Prkaa2*$^{-/-}$ mice had reduced MMP2 protein expression after nicotine infusion (**Fig. 2a**).

We next assessed MMP activity, mRNA levels and protein concentrations in isolated aortas from *Apoe*$^{-/-}$, *Apoe*$^{-/-}$; *Prkaa1*$^{-/-}$ and *Apoe*$^{-/-}$; *Prkaa2*$^{-/-}$ mice. We were able to detect both MMP2 and MMP9 activity in all three groups of mice; however, MMP2 seemed to be the most predominant MMP in both vehicle- and nicotine-treated *Apoe*$^{-/-}$, *Apoe*$^{-/-}$; *Prkaa1*$^{-/-}$ and *Apoe*$^{-/-}$; *Prkaa2*$^{-/-}$ mice (**Fig. 2b**). Nicotine infusion increased MMP2 activity markedly in *Apoe*$^{-/-}$ and *Apoe*$^{-/-}$; *Prkaa1*$^{-/-}$ mice and also did so to a lesser extent in *Apoe*$^{-/-}$; *Prkaa2*$^{-/-}$ mice. Nicotine infusion had minimal effects on MMP9 activity in the three groups of mice. Moreover, nicotine infusion significantly increased MMP2 protein concentrations and MMP2 mRNA levels in *Apoe*$^{-/-}$ and *Apoe*$^{-/-}$; *Prkaa1*$^{-/-}$ mice but not in *Apoe*$^{-/-}$; *Prkaa2*$^{-/-}$ mice (**Fig. 2c,d** and **Supplementary Fig. 3a**). Similarly, AngII infusion markedly increased the protein concentration and mRNA expression and activity of both MMP2 and MMP9 in *Apoe*$^{-/-}$ and *Apoe*$^{-/-}$; *Prkaa1*$^{-/-}$ mice but not in *Apoe*$^{-/-}$; *Prkaa2*$^{-/-}$ mice (**Supplementary Fig. 3b** and **4a,b**).

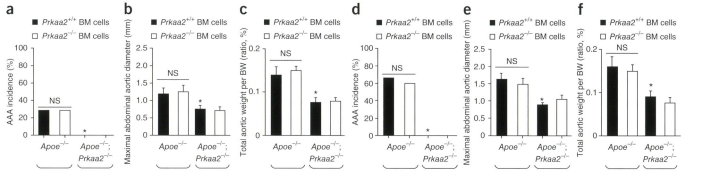

Figure 3 Bone marrow reconstitution shows a key role for vascular-specific AMPK-α2 deficiency in AAA formation. (**a**–**c**) The incidence of AAA (**a**), maximal abdominal aortic diameters (**b**) and total aortic weights (**c**) in nicotine-infused mice of the indicated genotypes. *$P < 0.05$ compared to nicotine-infused *Apoe*$^{-/-}$ mice reconstituted with *Apoe*$^{-/-}$; *Prkaa2*$^{+/+}$ bone-marrow cells. (**d**–**f**) The incidence of AAA (**d**), maximal abdominal aortic diameters (**e**) and total aortic weights (**f**) in AngII-infused mice of the indicated genotypes. BM, bone marrow; NS, not significant. *$P < 0.05$ compared to AngII-infused *Apoe*$^{-/-}$ mice reconstituted with *Apoe*$^{-/-}$; *Prkaa2*$^{+/+}$ bone marrow cells. NS, no significant difference. All results were obtained from 5–10 mice in each group. The *P* values were obtained by a χ^2 test in **a** and **d** and by one-way ANOVA plus a *post hoc* analysis using a Bonferroni test in **b**, **c**, **e** and **f**. The error bars in **b**, **c**, **e** and **f** are s.e.m.

Infusion with nicotine or AngII increases ROS *in vivo*

Increased amounts of ROS and associated vascular inflammation are considered to be key mediators of AngII-induced AAA formation[8]. Infusion with either nicotine or AngII markedly increased the amounts of malondialdehyde (MDA) and 3-nitrotyrosine (3-NT), two markers of oxidative stress[27], in the aortic tissue of *Apoe*$^{-/-}$, *Apoe*$^{-/-}$; *Prkaa1*$^{-/-}$ and *Apoe*$^{-/-}$; *Prkaa2*$^{-/-}$ mice (**Fig. 2a** and **Supplementary Fig. 4a**). Serum concentrations of inflammatory cytokines were also elevated in mice infused with AngII or nicotine (**Supplementary Tables 5** and **6**). We confirmed that nicotine or AngII resulted in an increased amount of ROS by assaying superoxide with dihydroethidium (DHE) by HPLC. Infusion with either nicotine or AngII increased DHE fluorescence in the aortic tissue of *Apoe*$^{-/-}$, *Apoe*$^{-/-}$; *Prkaa1*$^{-/-}$ and *Apoe*$^{-/-}$; *Prkaa2*$^{-/-}$ mice (**Fig. 2e** and **Supplementary Fig. 4c**). These data suggest that both AngII and nicotine trigger oxidative stress *in vivo*. Although ROS and inflammation are seen in *Apoe*$^{-/-}$; *Prkaa2*$^{-/-}$ mice, these mice do not develop AAA because of an AMPK-α2 deficiency.

Vascular AMPK-α2 deficiency is essential for AAA inhibition

Because AMPK-α1, rather than AMPK-α2, is the predominant AMPK isoform in macrophages and deletion of AMPK-α1 did not alter nicotine- or AngII-induced AAA formation, we reasoned that AMPK-α2 is likely acting in VSMCs to promote AAA formation. To test this hypothesis, we performed reciprocal bone marrow transplants between *Apoe*$^{-/-}$ and *Apoe*$^{-/-}$; *Prkaa2*$^{-/-}$ mice, in which bone marrow cells were transplanted into irradiated mice. After 42 d of engraftment, the transplanted mice were treated with nicotine (1 mg per kg of body weight per day for 42 days), which led to AAA formation in *Apoe*$^{-/-}$ mice transplanted with either *Prkaa2*$^{-/-}$ or *Prkaa2*$^{+/+}$ bone marrow cells, with a similar incidence of approximately 20% (**Fig. 3a**). However, AAA formation was not observed in *Apoe*$^{-/-}$; *Prkaa2*$^{-/-}$ mice transplanted with either *Prkaa2*$^{-/-}$ or *Prkaa2*$^{+/+}$ bone marrow cells (**Fig. 3a**), and there was no difference in the maximum abdominal aortic diameter (**Fig. 3b**) and total aortic weight (**Fig. 3c**) between the two groups of mice. Similarly to nicotine infusion, AngII infusion caused AAA formation and increased AAA incidence (**Fig. 3d**), maximum abdominal aortic diameter (**Fig. 3e**) and total aortic weight (**Fig. 3f**) in *Apoe*$^{-/-}$ mice transplanted with either *Prkaa2*$^{-/-}$ or *Prkaa2*$^{+/+}$ bone marrow cells but not in *Apoe*$^{-/-}$; *Prkaa2*$^{-/-}$ mice transplanted with the same bone marrow cells. Taken together, these data suggest that loss of AMPK-α2 expression in vascular cells, rather than bone-marrow–derived cells, is crucial for the development of AAA.

To obtain further support for the key role of VSMC-derived MMP2 in AAA formation, we acutely knocked down MMP2 expression using *in vivo* siRNA delivery. AngII or nicotine infusion increased pro-MMP2 protein concentrations in mice transfected with a control siRNA but not in mice transfected with the MMP2-targeted siRNA (**Supplementary Fig. 5a**). Accordingly, the amount of collagen IV, a direct substrate of MMP2, was reduced by AngII or nicotine infusion in control siRNA-transfected but not MMP2 siRNA-transfected mice (**Supplementary Fig. 5a**,**b**), and elastin degradation was also blocked in MMP2 siRNA-transfected mice (**Supplementary Fig. 5b**,**c**). These results indicate that MMP2, rather than MMP9, mediates AngII- and nicotine-induced elastin degradation in the aortic wall.

AMPK activation increases pro-MMP2 expression in VSMCs

We next determined whether AMPK in VSMCs modulates MMP2 expression. Exposure of human VSMCs to low concentrations (0.01–0.1 μM) of nicotine, equivalent to the blood concentrations present in habitual smokers, led to AMPK activation (**Supplementary Fig. 6a**,**b**). The degree of AMPK activation was similar to that caused by the potent AMPK activators 5-amino-4-imidazole carboxamide riboside (AICAR, 2 mM) or $ONOO^-$ (50 μM) (**Supplementary Fig. 6a**,**b**). Nicotine treatment also increased the phosphorylation of AMPK-α at Thr172, which activates AMPK, in a time-dependent manner (**Supplementary Fig. 6c**). Likewise, treatment with AngII also caused phosphorylation of AMPK at Thr172. Treatment with AngII also resulted in phosphorylation of the AMPK substrate, acetyl-CoA carboxylase (ACC), at Ser79 in a time-dependent manner (**Supplementary Fig. 6d**,**e**), consistent with previously published data[13].

We next tested the effects of nicotine or AngII on MMP2. Exposure of human VSMCs to AngII or nicotine markedly increased MMP2 mRNA and protein expression in whole-cell lysates and increased MMP2 activity in the culture medium (**Supplementary Fig. 3c**,**d** and **7a**,**b**). Compound C, an AMPK inhibitor, abolished the effects of AngII or nicotine on MMP2 (**Supplementary Fig. 7a**,**b**), indicating that AMPK mediates MMP2 expression induced by AngII or nicotine. Transfection of the VSMCs with AMPK-α2 siRNA, but not AMPK-α1

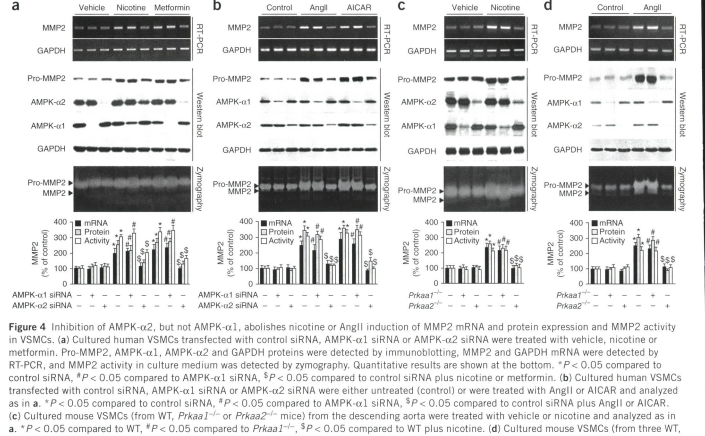

Figure 4 Inhibition of AMPK-α2, but not AMPK-α1, abolishes nicotine or AngII induction of MMP2 mRNA and protein expression and MMP2 activity in VSMCs. (**a**) Cultured human VSMCs transfected with control siRNA, AMPK-α1 siRNA or AMPK-α2 siRNA were treated with vehicle, nicotine or metformin. Pro-MMP2, AMPK-α1, AMPK-α2 and GAPDH proteins were detected by immunoblotting, MMP2 and GAPDH mRNA were detected by RT-PCR, and MMP2 activity in culture medium was detected by zymography. Quantitative results are shown at the bottom. $^{*}P < 0.05$ compared to control siRNA, $^{\#}P < 0.05$ compared to AMPK-α1 siRNA, $^{\$}P < 0.05$ compared to control siRNA plus nicotine or metformin. (**b**) Cultured human VSMCs transfected with control siRNA, AMPK-α1 siRNA or AMPK-α2 siRNA were either untreated (control) or were treated with AngII or AICAR and analyzed as in **a**. $^{*}P < 0.05$ compared to control siRNA, $^{\#}P < 0.05$ compared to AMPK-α1 siRNA, $^{\$}P < 0.05$ compared to control siRNA plus AngII or AICAR. (**c**) Cultured mouse VSMCs (from WT, *Prkaa1*$^{-/-}$ or *Prkaa2*$^{-/-}$ mice) from the descending aorta were treated with vehicle or nicotine and analyzed as in **a**. $^{*}P < 0.05$ compared to WT, $^{\#}P < 0.05$ compared to *Prkaa1*$^{-/-}$, $^{\$}P < 0.05$ compared to WT plus nicotine. (**d**) Cultured mouse VSMCs (from three WT, *Prkaa1*$^{-/-}$ or *Prkaa2*$^{-/-}$ mice) from the descending aorta were either untreated or were treated with AngII and analyzed as in **a**. $^{*}P < 0.05$ compared to WT, $^{\#}P < 0.05$ compared to *Prkaa1*$^{-/-}$, $^{\$}P < 0.05$ compared to WT plus AngII. $n = 3$ independent experiments for all quantitative data. The P values in **a**–**d** were obtained by one-way ANOVA plus a *post hoc* analysis using a Bonferroni test. The error bars in **a**–**d** are s.e.m.

siRNA, abolished the effects of nicotine, AngII, AICAR or metformin (an AMPK activator) on MMP2 protein and mRNA expression and MMP2 activity (**Fig. 4a**,**b** and **Supplementary Fig. 3e**,**f**). Moreover, treatment of primary VSMCs isolated from wild-type (WT) or *Prkaa1*$^{-/-}$ mice with AngII or nicotine upregulated MMP2 protein and mRNA expression and MMP2 activity, whereas treatment of VSMCs isolated from *Prkaa2*$^{-/-}$ mice did not have these effects (**Fig. 4c**,**d** and **Supplementary Fig. 3g**,**h**). Taken together, our results support the notion that AMPK-α2, but not AMPK-α1, is required for MMP2 expression in VSMCs.

MMP2 upregulation by nicotine or AngII is AP-2α dependent

The AP-2α transcription factor is required for MMP2 expression in endothelial cells[28], and mice with knockdown of AP-2α die at birth as a result of abnormal neural, craniofacial and vascular development[29,30], suggesting a crucial role of AP-2α in regulating angiogenesis. We hypothesized that nicotine- or AngII-induced MMP2 upregulation is mediated by AP-2α. Transfection of VSMCs with AP-2α–specific or AMPK-α2–specific siRNAs, but not control siRNA, inhibited nicotine-induced pro-MMP2 protein expression and MMP2 activity (**Fig. 5a**), implying that the upregulation of MMP2 by nicotine requires both AMPK-α2 and AP-2α. Similarly, transfection of VSMCs with AP-2α siRNA, but not control siRNA, abolished AngII-induced MMP2 upregulation (**Fig. 5b**).

Because AP-2α is required for nicotine- or AngII-induced MMP2 mRNA and protein expression, we reasoned that AngII and nicotine might activate AP-2α to increase its binding affinity for the *MMP2* gene promoter. In VSMCs stimulated with AngII or nicotine, we found an increased DNA affinity of AP-2α, as detected by the electrophoretic mobility shift assay (EMSA), and increased transcriptional activity of AP-2α, as assessed using a luciferase reporter gene (**Fig. 5c**–**f**). Inhibition of AMPK-α2 by either siRNA-mediated knockdown or compound C markedly suppressed AngII- or nicotine-induced AP-2α activation (**Fig. 5c**–**e**). Moreover, metformin increased and AMPK-α2 siRNA decreased the DNA binding affinity of AP-2α (**Fig. 5c**).

We next investigated whether AP-2α binds to the *MMP2* gene promoter in human VSMCs using chromatin immunoprecipitation (ChIP) analyses. In human VSMCs, the *MMP2* gene promoter was positively amplified in samples from AngII-treated cells after immunoprecipitation with primary antibody to AP-2α but not with control immunoglobulin G (IgG), and compound C attenuated this binding (**Fig. 5g**). We observed similar effects in nicotine-treated human VSMCs (**Fig. 5h**,**i**). Taken together, these data indicate that AMPK-α2 mediates nicotine- and AngII-induced AP-2α activation.

Nicotine and AngII promote the interaction of AMPK-α2 and AP-2α

As AP-2α is located in the nucleus, we determined whether AMPK-α1 and AMPK-α2 were also nuclear localized. Nicotine or AngII treatment of human VSMCs induced nuclear translocation of AMPK-α2 but not AMPK-α1, as assessed by a western blot analysis of separated cytoplasmic and nuclear fractions (**Fig. 6a**). Treatment of the cells with compound C inhibited the nicotine- or AngII-promoted AMPK-α2 nuclear translocation.

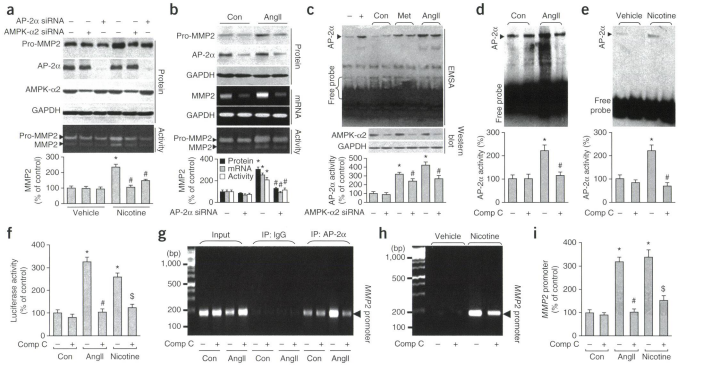

Figure 5 AP-2α mediates nicotine- or AngII-induced AMPK-α2–dependent MMP2 protein expression in VSMCs. (**a**) Cultured human VSMCs transfected with control siRNA, AMPK-α2 siRNA or AP-2α siRNA were treated with vehicle or nicotine. Pro-MMP2, AP-2α, AMPK-α2 and GAPDH proteins were detected by immunoblotting, and MMP2 activity in culture medium was detected by zymography. $^{*}P < 0.05$ compared to vehicle, $^{\#}P < 0.05$ compared to nicotine alone. (**b**) Cultured human VSMCs transfected with control siRNA or AP-2α siRNA were untreated (con) or were treated with AngII. Pro-MMP2, AP-2α and GAPDH proteins were detected by immunoblotting, MMP2 and GAPDH mRNA were detected by RT-PCR, and MMP2 activity in culture medium was detected by zymography. $^{*}P < 0.05$ compared to control siRNA, $^{\#}P < 0.05$ compared to control siRNA plus AngII. (**c**) Cultured human VSMCs transfected with control siRNA or AMPK-α2 siRNA were either untreated or were treated with AngII or metformin (Met). The DNA binding affinity of AP-2α was determined by EMSA running on nuclear extracts (top) and was quantitated (bottom). The negative control (–) was biotin-labeled DNA probe without extract, and the positive control (+) was biotin-labeled DNA probe with nuclear extract provided by the kit. AMPK-α2 and GAPDH protein were detected by immunoblotting (middle). $^{*}P < 0.05$ compared to control siRNA, $^{\#}P < 0.05$ compared to control siRNA plus metformin or AngII. (**d**–**i**) Cultured human VSMCs preincubated with or without compound C (comp C) were either untreated or treated with vehicle, nicotine or AngII, as indicated. AP-2α activity was detected by EMSA (**d**,**e**) or by a luciferase reporter assay (**f**); binding of AP-2α to the *MMP2* gene promoter was detected by ChIP analysis (**g**,**h**), and quantitative data from the ChIP analysis is shown in **i**. $^{*}P < 0.05$ compared to control or vehicle, $^{\#}P < 0.05$ compared to AngII or nicotine alone (**d**,**e**). In **f** and **i**, $^{*}P < 0.05$ compared to control without compound C, $^{\#}P < 0.05$ compared to AngII alone, $^{\$}P < 0.05$ compared to nicotine alone. For the ChIP analysis shown in **g**, the positive control was 10% of the total chromatin without immunoprecipitation (lanes 1–4, input); the negative control was chromatin immunoprecipitated with IgG and amplified with *MMP2* promoter primers (lanes 5–8), and AP-2α–specific antibody was used to detect the binding of AP-2α to the *MMP2* promoter (lanes 9–12). The expected PCR product is 200 bp in size. $n = 3$ independent experiments for all quantitative data. The *P* values in **a**, **f** and **i** were obtained by one-way ANOVA plus a *post hoc* analysis using a Bonferroni test. The error bars in **a**–**f** and **i** are s.e.m.

We confirmed the interaction of AMPK-α2 and AP-2α after treatment with either nicotine or AngII by immunoprecipitation experiments. Binding of AMPK-α2 to AP-2α was evident in immunoprecipitates pulled down by antibodies specific to either AP-2α or AMPK-α2 (**Fig. 6b**). However, we did not detect binding between AMPK-α1 and AP-2α (**Fig. 6b**). We further verified the nuclear translocation of AMPK-α2 and the colocalization of AMPK-α2 and AP-2α using immunofluorescence experiments (**Supplementary Fig. 8**). We also detected the interaction of AMPK-α2 and AP-2α using *in vitro* co-incubation and pulldown experiments (**Fig. 6c**). Together, these data suggest that AMPK-α2 directly affects AP-2α activity through a protein-protein interaction.

AMPK increases the phosphorylation of AP-2α at Ser219

Post-translational modifications of AP-2α, including serine phosphorylation, are known to regulate its transcriptional activity[31]. As AMPK is a threonine/serine protein kinase, we reasoned that AMPK might directly phosphorylate AP-2α. Treatment of human VSMCs with either AngII or nicotine resulted in an increase in the level of serine phosphorylation of AP-2α (**Fig. 6d**). Conversely, inhibition of AMPK by compound C markedly inhibited AngII- or nicotine-induced AP-2α serine phosphorylation (**Fig. 6d**). Moreover, AMPK-α2, but not a dominant-negative version of AMPK-α2, could phosphorylate recombinant AP-2α protein in an *in vitro* kinase assay, as detected by ^{32}P-ATP autoradiography, indicating that AP-2α is a direct target of AMPK-α2 (**Fig. 6e**).

We next determined which serine residue(s) in the AP-2α protein are phosphorylated by AMPK-α2. In comparison with an optimal AMPK substrate motif[32], an analysis of AP-2α revealed potential AMPK target motifs at Ser181, Ser219, Ser233, Ser252 and Ser320 in the regulatory and helix-span-helix domains (**Supplementary Fig. 9a**–**c**), which are similar to the target motifs in previously identified AMPK substrates[33–35]. We tested the ability of AMPK-α2 to carry out *in vitro* phosphorylation of peptides spanning residues 176–185, 214–223, 228–237, 247–256 or 315–324 of AP-2α. A canonical target sequence, the 'SAMS' sequence, was used as a positive control. Only the peptide spanning residues 214–223 of AP-2α was phosphorylated

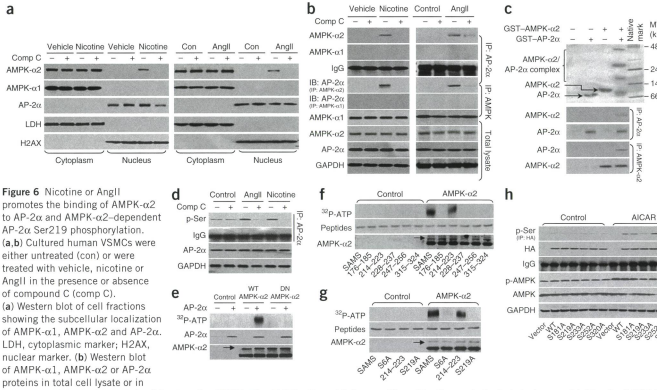

Figure 6 Nicotine or AngII promotes the binding of AMPK-α2 to AP-2α and AMPK-α2–dependent AP-2α Ser219 phosphorylation. (**a**,**b**) Cultured human VSMCs were either untreated (con) or were treated with vehicle, nicotine or AngII in the presence or absence of compound C (comp C). (**a**) Western blot of cell fractions showing the subcellular localization of AMPK-α1, AMPK-α2 and AP-2α. LDH, cytoplasmic marker; H2AX, nuclear marker. (**b**) Western blot of AMPK-α1, AMPK-α2 or AP-2α proteins in total cell lysate or in immunoprecipitates from total cell lysate using AMPK-α1–, AMPK-α2– or AP-2α–specific antibodies, as indicated. An immunoblotting for GAPDH in the total cell lysate and for IgG in the immunoprecipitates is also shown. IB, immunoblot; IP, immunoprecipitation. (**c**) GST–AMPK-α2 and GST–AP-2α proteins were incubated either alone or together in reaction buffer, and the mixture was then electrophoresed on a native gel; both proteins were then detected by Coomassie blue staining of the gel (top). The reaction mixture was also immunoprecipitated with the indicated antibodies, followed by immunoblotting using antibodies to AMPK-α2 or AP-2α (bottom). MW, molecular weight. 'Native mark', protein standards without heating. (**d**) Cultured human VSMCs were either untreated or were treated with AngII or nicotine in the presence or absence of compound C. Serine phosphorylation of AP-2α was detected by immunoprecipitation with antibodies to AP-2α followed by western blotting with antibodies to phosphorylated serine (p-Ser). Immunoblotting for IgG in the immunoprecipitates and for total AP-2α protein and GAPDH is also shown. (**e**) Cultured HEK293 cells were either untransfected (control) or transfected with WT AMPK-α2 or dominant-negative (DN) AMPK-α2. Immunoprecipitates obtained using antibody to AMPK-α2 were incubated with or without added AP-2α protein in kinase reaction buffer in the presence of ^{32}P-labeled ATP (^{32}P-ATP), and phosphorylation of AP-2α was visualized by autoradiography. Immunoblotting for AP-2α and AMPK-α2 is also shown. (**f**) The indicated peptides (SAMS peptide or peptides spanning the indicated amino acid residues of AP-2α) were incubated with or without AMPK-α2 protein in kinase reaction buffer in the presence of ^{32}P-ATP, and the phosphorylation of the peptides was visualized by autoradiography. Immunoblotting for AMPK-α2 is also shown. Peptides were visualized by Coomassie blue staining of the gel. (**g**) The indicated peptides (SAMS peptide, SAMS S6A peptide, an AP-2α peptide spanning residues 214–223 or the same AP-2α peptide with a S219A substitution) were incubated with or without AMPK-α2 protein in kinase reaction buffer in the presence of ^{32}P-ATP, and phosphorylation of the peptides was visualized by autoradiography. (**h**) HEK293 cells were transfected with vector, hemagglutinin (HA)-tagged, full-length WT AP-2α (WT) or the indicated HA-tagged site-directed mutants of AP-2α, and the cells were treated with or without AICAR. HA-specific antibodies were used for immunoprecipitation; serine phosphorylation of AP-2α was then detected by immunoblotting using antibodies to phosphorylated serine (p-Ser). Immunoblotting for HA, IgG, phosphorylated AMPKα (p-AMPKα), AMPKα and GAPDH are also shown. The arrow in **e**, **f** and **g** indicates the band corresponding to AMPK-α2. In all panels, representative data from three independent experiments are shown.

by AMPK-α2 protein (**Fig. 6f**). Furthermore, mutation of serine to alanine at Ser6 of the SAMS peptide or at Ser219 of the AP-2α peptide abolished AMPK-α2–induced phosphorylation (**Fig. 6g**).

To confirm Ser219 of AP-2α as the phosphorylation target of AMPK-α2, we generated five site-directed mutant constructs of AP-2α (S181A, S219A, S233A, S252A and S320A). In HEK293 cells transfected with WT AP-2α, treatment with AICAR, which induces phosphorylation of AMPK at Thr172, markedly increased AP-2α serine phosphorylation (**Fig. 6h**). Among the AP-2α mutant constructs, AICAR-induced AP-2α serine phosphorylation was abolished only in cells transfected with the AP-2α S219A mutant (**Fig. 6h**), confirming Ser219 as the target of AMPK-induced AP-2α serine phosphorylation.

We next tested whether Ser219 phosphorylation of AP-2α affects AP-2α activity and function. Transfection of human VSMCs with the AP-2α S219A mutant markedly abrogated AngII- or nicotine-induced upregulation of MMP2 expression and activity, AP-2α DNA binding affinity and AP-2α binding to the *MMP2* gene promoter (**Supplementary Fig. 10a**–**c**). These results suggest that Ser219 phosphorylation of AP-2α by AMPK-α2 promotes its binding to the *MMP2* promoter, resulting in aberrant MMP2 expression.

AMPK-α2 activation in human AAA and in smokers

To test the relevance of our findings in humans, we examined AMPK-α2 activity, AMPK Thr172 phosphorylation and ACC Ser79 phosphorylation in human AAA tissue. Aortic tissue of patients with AAA showed higher levels of AMPK-α2 activity, AMPK Thr172 phosphorylation and ACC Ser79 phosphorylation than did samples from control patients without AAA (**Supplementary Fig. 11a**,**b**).

To address whether cigarette smoking alters AMPK activity, we assessed AMPK-α2 activity, AMPK Thr172 phosphorylation and

ACC Ser79 phosphorylation in the blood of both active smokers and nonsmokers. In active smokers, the levels of AMPK-α2 activity, AMPK Thr172 phosphorylation and ACC Ser79 phosphorylation were higher than those in nonsmokers (**Supplementary Fig. 11c,d**), implying that smoking activates AMPK-α2 in humans.

DISCUSSION

Here we show that nicotine- or AngII-derived ROS triggers AMPK-α2 phosphorylation and subsequent nuclear translocation; AMPK-α2 then binds to and phosphorylates AP-2α at Ser219, resulting in aberrant expression of MMP2 and consequent extracellular matrix degradation (**Supplementary Fig. 12**). This mechanism not only provides a causal link between nicotine and AAA but also explains how proinflammatory factors such as ROS promote AAA formation.

We found that activation of AMPK-α2 by nicotine or AngII triggered AAA formation in *Apoe*$^{-/-}$ mice, such that AMPK-α2 deficiency had a marked protective effect. These results might help explain the clinical observation that diabetes is negatively associated with AAA formation[36], as hyperglycemia suppresses AMPK activity[37,38]; conversely, insulin treatment, which lowers blood glucose concentrations, promotes aortic diameter enlargement[39,40].

We also found that AP-2α is a direct substrate for phosphorylation by AMPK-α2 at Ser219. AP-2α is also phosphorylated by protein kinase A at Ser233 (ref. 31) and by protein kinase D at both Ser252 and Ser320 (ref. 41). AP-2α is crucial for mouse embryonic development, and mice lacking AP-2α die at birth[29]. In light of our findings, loss of MMP2 activity in AP-2α–deficient mice may be one of the factors contributing to the embryonic lethality of these mice.

After the acceptance of this paper, a recent publication reported that nicotine accelerates elastase- or AngII-stimulated AAA growth in mice[42]. The results from this study strongly support our findings that VSMC is a key target of nicotine in the initiation and progression of AAA. Moreover, we found that nicotine administration alone can trigger AAA formation and progression in mice. Our results are in line with earlier reports that nicotine, at concentrations relevant to those found in smokers, leads to increased levels of ROS and to AMPK activation in adipocytes[43], as well as with similar findings on the effects of AngII in VSMCs. Thus, our study extends these observations by showing that AMPK activation might be detrimental in the initiation and progression of AAA, contradicting the idea that AMPK activation is uniformly beneficial in cardiovascular diseases. For example, AMPK-α2 deficiency has been reported to cause accelerated atherosclerosis[44], and pharmacological activation of AMPK has been shown to attenuate wire-injury–induced vascular remodeling by inhibiting VSMC proliferation[13,14]. Although atherosclerosis, restenosis and AAA are associated with vascular inflammation and have many of the same predisposing risk factors, there are key differences among these conditions. For example, early atherosclerosis is primarily characterized by foam cell accumulation in the intima, a process that is mediated by proinflammatory factors. In contrast, AAA involves the degradation of the tunica media, in which enhanced activation of the proteolytic system, such as MMPs, has a crucial role[45]. Reduced VSMC proliferation has been found within fragmented media in human AAA biopsy specimens[46], and the inhibitory effects of AMPK activation on VSMC proliferation might accentuate the development of AAA. This is in contrast to the situation in atherosclerosis and restenosis, in which VSMC proliferation contributes to vascular remodeling[14]. The authors of a recent review[47] concluded that a plurality of studies indicate an independent effect of medications on aneurysms and atherosclerosis in animal models, further suggesting distinct pathogenic mechanisms.

Although both AngII and nicotine promoted AAA formation in *Apoe*$^{-/-}$ mice through a ROS–AMPK–α2–AP-2α–MMP2 pathway in VSMCs, the incidence and size of the aneurysms induced by AngII was markedly greater than those induced by nicotine for reasons that are unclear. Nicotine might cause a lower level of ROS generation than AngII does. Moreover, AngII has been reported to promote AAA through multiple mechanisms involving transforming growth factor β (TGF-β) and other growth factors[23,48]. Notably, MMP2 can promote the transcriptional activation of these growth factors as a group, and MMP2 can also interact with TGF-β relating to the processing of MMP2 activation[49]. Whether these pathways also contribute to nicotine-induced AAA warrants further investigation.

The results presented here have established a causal effect of nicotine on AAA *in vivo*, identifying nicotine as an active agent in smoke-triggered AAA. One common approach to the cessation of smoking is nicotine supplementation, such as with gum or patches. The rapid absorption of nicotine can increase plasma nicotine concentrations to as high as 5×10^{-7} M within 15 min (ref. 50), a concentration that, based on our findings, might increase AAA formation. Thus, we suggest that nicotine supplementation be cautiously reconsidered and that the duration of nicotine supplementation be minimized in populations with advanced age.

METHODS

Methods and any associated references are available in the online version of the paper.

Note: Supplementary information is available in the online version of the paper.

ACKNOWLEDGMENTS

We are grateful for helpful discussions with J. Du, X.L. Wang and C. Yan. We also thank D. Wang and M. McDaniel for technical support. This work was supported by US National Institutes of Health (NIH) grants (HL079584, HL074399, HL080499, HL089920, HL096032, HL105157 and HL110488 to M.-H.Z.). L.X's lab is supported by NIH grants (HL085607 and RR018758). This work was also supported by the National High-tech Research and Development Program of China (No.2012AA02A510) awarded to C.Z. and the National 973 Basic Research Program of China (number 2011CB503906) and the State Program of National Natural Science Foundation of China for Innovative Research Group (number 81021001) awarded to Y.Z. M.-H.Z. is a recipient of the National Established Investigator Award of the American Heart Association.

AUTHOR CONTRIBUTIONS

S.W. designed and conducted the experiments, analyzed data and wrote the manuscript. C.Z. and Y.Z. did the clinical experiments. M.Z. and L.X. did bone morrow transplantation. B.L. partially performed the pathological experiments. H.Z. and J.L. generated series mutants. B.V. provided the AMPK-deleted mice. M.-H.Z. conceived of the project, designed the experiments, analyzed data and wrote the manuscript.

COMPETING FINANCIAL INTERESTS

The authors declare no competing financial interests.

Published online at http://www.nature.com/doifinder/10.1038/nm.2711.
Reprints and permissions information is available online at http://www.nature.com/reprints/index.html.

1. Vorp, D.A. & Vande Geest, J.P. Biomechanical determinants of abdominal aortic aneurysm rupture. *Arterioscler. Thromb. Vasc. Biol.* **25**, 1558–1566 (2005).
2. Nordon, I.M., Hinchliffe, R.J., Loftus, I.M. & Thompson, M.M. Pathophysiology and epidemiology of abdominal aortic aneurysms. *Nat. Rev. Cardiol.* **8**, 92–102 (2011).
3. Satoh, K. *et al.* Cyclophilin A enhances vascular oxidative stress and the development of angiotensin II–induced aortic aneurysms. *Nat. Med.* **15**, 649–656 (2009).
4. Shah, P.K. Inflammation, metalloproteinases, and increased proteolysis: an emerging pathophysiological paradigm in aortic aneurysm. *Circulation* **96**, 2115–2117 (1997).
5. Thompson, R.W., Geraghty, P.J. & Lee, J.K. Abdominal aortic aneurysms: basic mechanisms and clinical implications. *Curr. Probl. Surg.* **39**, 110–230 (2002).

6. Rajagopalan, S. *et al.* Angiotensin II–mediated hypertension in the rat increases vascular superoxide production via membrane NADH/NADPH oxidase activation. Contribution to alterations of vasomotor tone. *J. Clin. Invest.* **97**, 1916–1923 (1996).
7. Browatzki, M. *et al.* Angiotensin II stimulates matrix metalloproteinase secretion in human vascular smooth muscle cells via nuclear factor-κB and activator protein 1 in a redox-sensitive manner. *J. Vasc. Res.* **42**, 415–423 (2005).
8. Thomas, M. *et al.* Deletion of p47phox attenuates angiotensin II–induced abdominal aortic aneurysm formation in apolipoprotein E–deficient mice. *Circulation* **114**, 404–413 (2006).
9. Mu, J., Brozinick, J.T. Jr., Valladares, O., Bucan, M. & Birnbaum, M.J. A role for AMP-activated protein kinase in contraction- and hypoxia-regulated glucose transport in skeletal muscle. *Mol. Cell* **7**, 1085–1094 (2001).
10. Choi, S.L. *et al.* The regulation of AMP-activated protein kinase by H(2)O(2). *Biochem. Biophys. Res. Commun.* **287**, 92–97 (2001).
11. Han, Y., Wang, Q., Song, P., Zhu, Y. & Zou, M.H. Redox regulation of the AMP-activated protein kinase. *PLoS ONE* **5**, e15420 (2010).
12. Zhang, M. *et al.* Thromboxane receptor activates the AMP-activated protein kinase in vascular smooth muscle cells via hydrogen peroxide. *Circ. Res.* **102**, 328–337 (2008).
13. Nagata, D. *et al.* AMP-activated protein kinase inhibits angiotensin II–stimulated vascular smooth muscle cell proliferation. *Circulation* **110**, 444–451 (2004).
14. Song, P. *et al.* AMPKα2 deletion exacerbates neointima formation by upregulating Skp2 in vascular smooth muscle cells. *Circ. Res.* **109**, 1230–1239 (2011).
15. Henningfield, J.E., Stapleton, J.M., Benowitz, N.L., Grayson, R.F. & London, E.D. Higher levels of nicotine in arterial than in venous blood after cigarette smoking. *Drug Alcohol Depend.* **33**, 23–29 (1993).
16. Benowitz, N.L. Cigarette smoking and cardiovascular disease: pathophysiology and implications for treatment. *Prog. Cardiovasc. Dis.* **46**, 91–111 (2003).
17. Lu, H., Rateri, D.L., Cassis, L.A. & Daugherty, A. The role of the renin-angiotensin system in aortic aneurysmal diseases. *Curr. Hypertens. Rep.* **10**, 99–106 (2008).
18. Daugherty, A. & Cassis, L.A. Mouse models of abdominal aortic aneurysms. *Arterioscler. Thromb. Vasc. Biol.* **24**, 429–434 (2004).
19. Wang, Y.X. *et al.* Fasudil, a Rho-kinase inhibitor, attenuates angiotensin II–induced abdominal aortic aneurysm in apolipoprotein E–deficient mice by inhibiting apoptosis and proteolysis. *Circulation* **111**, 2219–2226 (2005).
20. Daugherty, A. *et al.* Angiotensin II infusion promotes ascending aortic aneurysms: attenuation by CCR2 deficiency in *apoE*$^{-/-}$ mice. *Clin. Sci. (Lond.)* **118**, 681–689 (2010).
21. Gavrila, D. *et al.* Vitamin E inhibits abdominal aortic aneurysm formation in angiotensin II–infused apolipoprotein E–deficient mice. *Arterioscler. Thromb. Vasc. Biol.* **25**, 1671–1677 (2005).
22. Rateri, D.L. *et al.* Endothelial cell-specific deficiency of Ang II type 1a receptors attenuates Ang II–induced ascending aortic aneurysms in LDL receptor$^{-/-}$ mice. *Circ. Res.* **108**, 574–581 (2011).
23. Pearce, W.H. & Shively, V.P. Abdominal aortic aneurysm as a complex multifactorial disease: interactions of polymorphisms of inflammatory genes, features of autoimmunity, and current status of MMPs. *Ann. NY Acad. Sci.* **1085**, 117–132 (2006).
24. Aziz, F. & Kuivaniemi, H. Role of matrix metalloproteinase inhibitors in preventing abdominal aortic aneurysm. *Ann. Vasc. Surg.* **21**, 392–401 (2007).
25. Longo, G.M. *et al.* Matrix metalloproteinases 2 and 9 work in concert to produce aortic aneurysms. *J. Clin. Invest.* **110**, 625–632 (2002).
26. Pyo, R. *et al.* Targeted gene disruption of matrix metalloproteinase-9 (gelatinase B) suppresses development of experimental abdominal aortic aneurysms. *J. Clin. Invest.* **105**, 1641–1649 (2000).
27. Wang, S. *et al.* AMPKα2 deletion causes aberrant expression and activation of NAD(P)H oxidase and consequent endothelial dysfunction *in vivo*: role of 26S proteasomes. *Circ. Res.* **106**, 1117–1128 (2010).
28. Park, M.J. *et al.* Nerve growth factor induces endothelial cell invasion and cord formation by promoting matrix metalloproteinase-2 expression through the phosphatidylinositol 3-kinase/Akt signaling pathway and AP-2 transcription factor. *J. Biol. Chem.* **282**, 30485–30496 (2007).
29. Zhang, J. *et al.* Neural tube, skeletal and body wall defects in mice lacking transcription factor AP-2. *Nature* **381**, 238–241 (1996).
30. Schorle, H., Meier, P., Buchert, M., Jaenisch, R. & Mitchell, P.J. Transcription factor AP-2 essential for cranial closure and craniofacial development. *Nature* **381**, 235–238 (1996).
31. Garcia, M.A., Campillos, M., Marina, A., Valdivieso, F. & Vazquez, J. Transcription factor AP-2 activity is modulated by protein kinase A–mediated phosphorylation. *FEBS Lett.* **444**, 27–31 (1999).
32. Gwinn, D.M. *et al.* AMPK phosphorylation of raptor mediates a metabolic checkpoint. *Mol. Cell* **30**, 214–226 (2008).
33. Bungard, D. *et al.* Signaling kinase AMPK activates stress-promoted transcription via histone H2B phosphorylation. *Science* **329**, 1201–1205 (2010).
34. Egan, D.F. *et al.* Phosphorylation of ULK1 (hATG1) by AMP-activated protein kinase connects energy sensing to mitophagy. *Science* **331**, 456–461 (2011).
35. Kim, J., Kundu, M., Viollet, B. & Guan, K.L. AMPK and mTOR regulate autophagy through direct phosphorylation of Ulk1. *Nat. Cell Biol.* **13**, 132–141 (2011).
36. Golledge, J. *et al.* Reduced expansion rate of abdominal aortic aneurysms in patients with diabetes may be related to aberrant monocyte-matrix interactions. *Eur. Heart J.* **29**, 665–672 (2008).
37. Wang, S. *et al.* Acute inhibition of guanosine triphosphate cyclohydrolase 1 uncouples endothelial nitric oxide synthase and elevates blood pressure. *Hypertension* **52**, 484–490 (2008).
38. Choi, H.C. *et al.* Reactive nitrogen species is required for the activation of the AMP-activated protein kinase by statin *in vivo*. *J. Biol. Chem.* **283**, 20186–20197 (2008).
39. Miyama, N. *et al.* Hyperglycemia limits experimental aortic aneurysm progression. *J. Vasc. Surg.* **52**, 975–983 (2010).
40. Dua, M.M. *et al.* Hyperglycemia modulates plasminogen activator inhibitor-1 expression and aortic diameter in experimental aortic aneurysm disease. *Surgery* **148**, 429–435 (2010).
41. Nishikawa, K., Toker, A., Johannes, F.J., Songyang, Z. & Cantley, L.C. Determination of the specific substrate sequence motifs of protein kinase C isozymes. *J. Biol. Chem.* **272**, 952–960 (1997).
42. Maegdefessel, L. *et al.* MicroRNA-21 blocks abdominal aortic aneurysm development and nicotine-augmented expansion. *Sci. Transl. Med.* **4**, 122ra22 (2012).
43. An, Z. *et al.* Nicotine-induced activation of AMP-activated protein kinase inhibits fatty acid synthase in 3T3L1 adipocytes: a role for oxidant stress. *J. Biol. Chem.* **282**, 26793–26801 (2007).
44. Dong, Y. *et al.* Reduction of AMP-activated protein kinase α2 increases endoplasmic reticulum stress and atherosclerosis *in vivo*. *Circulation* **121**, 792–803 (2010).
45. Thompson, R.W. *et al.* Production and localization of 92-kilodalton gelatinase in abdominal aortic aneurysms. An elastolytic metalloproteinase expressed by aneurysm-infiltrating macrophages. *J. Clin. Invest.* **96**, 318–326 (1995).
46. Corey, S. & Moran *et al.* Association of osteoprotegerin with human abdominal aortic aneurysm progression. *Circulation.* **111**, 3119–3125 (2005).
47. Golledge, J., Muller, J., Daugherty, A. & Norman, P. Abdominal aortic aneurysm: pathogenesis and implications for management. *Arterioscler. Thromb. Vasc. Biol.* **26**, 2605–2613 (2006).
48. Dallas, S.L., Rosser, J.L., Mundy, G.R. & Bonewald, L.F. Proteolysis of latent transforming growth factor-β (TGF-β)-binding protein-1 by osteoclasts. A cellular mechanism for release of TGF-β from bone matrix. *J. Biol. Chem.* **277**, 21352–21360 (2002).
49. ten Dijke, P. & Arthur, H.M. Extracellular control of TGFβ signalling in vascular development and disease. *Nat. Rev. Mol. Cell Biol.* **8**, 857–869 (2007).
50. Tundulawessa, Y., Yongchaiyud, P., Churthong, W. & Tundulawessa, K. The bioequivalent and effect of nicotine formulation gum on smoking cessation. *J. Med. Assoc. Thai.* **93**, 574–579 (2010).

nature medicine

Peroxiredoxin family proteins are key initiators of post-ischemic inflammation in the brain

Takashi Shichita[1–3], Eiichi Hasegawa[1], Akihiro Kimura[1], Rimpei Morita[1], Ryota Sakaguchi[1], Ichiro Takada[1], Takashi Sekiya[1], Hiroaki Ooboshi[4], Takanari Kitazono[3], Toru Yanagawa[5], Tetsuro Ishii[5], Hideo Takahashi[6], Shuji Mori[6], Masahiro Nishibori[6], Kazumichi Kuroda[7], Shizuo Akira[8], Kensuke Miyake[9] & Akihiko Yoshimura[1,10]

Post-ischemic inflammation is an essential step in the progression of brain ischemia-reperfusion injury. However, the mechanism that activates infiltrating macrophages in the ischemic brain remains to be clarified. Here we demonstrate that peroxiredoxin (Prx) family proteins released extracellularly from necrotic brain cells induce expression of inflammatory cytokines including interleukin-23 in macrophages through activation of Toll-like receptor 2 (TLR2) and TLR4, thereby promoting neural cell death, even though intracellular Prxs have been shown to be neuroprotective. The extracellular release of Prxs in the ischemic core occurred 12 h after stroke onset, and neutralization of extracellular Prxs with antibodies suppressed inflammatory cytokine expression and infarct volume growth. In contrast, high mobility group box 1 (HMGB1), a well-known damage-associated molecular pattern molecule, was released before Prx and had a limited role in post-ischemic macrophage activation. We thus propose that extracellular Prxs are previously unknown danger signals in the ischemic brain and that its blocking agents are potent neuroprotective tools.

Stroke is one of the major causes of death and disability worldwide. The only globally approved treatment for ischemic stroke is tissue plasminogen activator, a time-dependent therapy that must be given within 4.5 h of stroke onset. Consequently, there is an unmet need for therapy that could be commenced beyond this time window and that would be aimed at brain tissue protection rather than clot dissolution[1–3].

Recent evidence suggests that various elements of the immune system are intimately involved in all stages of the ischemic cascade, from the acute intravascular events to the parenchymal processes leading to brain damage and tissue repair, which determine the fate of patients after stroke[4–6]. In mouse models, immune cells such as T cells and macrophages and their cytokines have been shown to have a pivotal role in the immunomodulation of post-ischemic inflammation[7–10]. We have reported that interleukin-23 (IL-23) produced from infiltrating macrophages induces IL-17–producing T cells. IL-17 is mainly produced from γδT cells and promotes delayed (day 3–4) ischemic brain damage[11,12].

Despite intensive study of post-ischemic inflammation, the molecular mechanisms that activate infiltrating macrophages remain unclear. TLRs are pivotal in triggering the inflammation of sterile organs[13,14]. HMGB1, heat shock proteins (HSPs), β-amyloid (Aβ) and others are well known as endogenous TLR ligands; that is, they are damage-associated molecular pattern molecules (DAMPs)[15–19]. Although HMGB1 is implicated in ischemic brain injury, it remains to be clarified whether HMGB1 is the major DAMP involved in the activation of infiltrating immune cells or whether other local DAMPs have roles in this process[20–23].

In this study, we identified Prx family proteins in brain lysate as strong inducers of inflammatory cytokines. The extracellular release of Prx proteins occurred 12 h after stroke onset, which coincided with the timing of macrophage infiltration and stimulated infiltrating macrophages via TLR2 and TLR4. Neutralization of Prx proteins rather than HMGB1 by specific antibodies suppressed inflammatory cytokine expression in the ischemic brain. Thus, extracellular Prx could be a previously unknown DAMP that triggers post-ischemic inflammation and an ideal therapeutic target for ischemic brain injury.

RESULTS

Peroxiredoxins are potent IL-23 inducers in brain lysate

To determine whether there are DAMPs that induce IL-23 in the brain, we cultured bone marrow–derived dendritic cells (BMDCs) with a brain homogenate supernatant (brain lysate) from mice. mRNA encoding IL-23 p19 and other cytokine mRNAs were rapidly induced in BMDCs by incubation with the brain lysate (**Fig. 1a** and

[1]Department of Microbiology and Immunology, School of Medicine, Keio University, Tokyo, Japan. [2]Precursory Research for Embryonic Science and Technology (PRESTO), Japan Science and Technology Agency, Tokyo, Japan. [3]Department of Medicine and Clinical Science, Graduate School of Medical Sciences, Kyushu University, Fukuoka, Japan. [4]Department of Internal Medicine, Fukuoka Dental College Medical and Dental Hospital, Fukuoka, Japan. [5]Faculty of Medicine, University of Tsukuba, Tsukuba, Japan. [6]Department of Pharmacology, Okayama University Graduate School of Medicine, Okayama, Japan. [7]Division of Microbiology, Nihon University School of Medicine, Tokyo, Japan. [8]Laboratory of Host Defense, WPI Immunology Frontier Research Center, Osaka University, Osaka, Japan. [9]Division of Infectious Genetics, Institute of Medical Science, University of Tokyo, Tokyo, Japan. [10]Core Research for Evolutional Science and Technology (CREST), Japan Science and Technology Agency, Tokyo, Japan. Correspondence should be addressed to A.Y. (yoshimura@a6.keio.jp).

Received 23 January; accepted 21 March; published online 20 May 2012; doi:10.1038/nm.2749

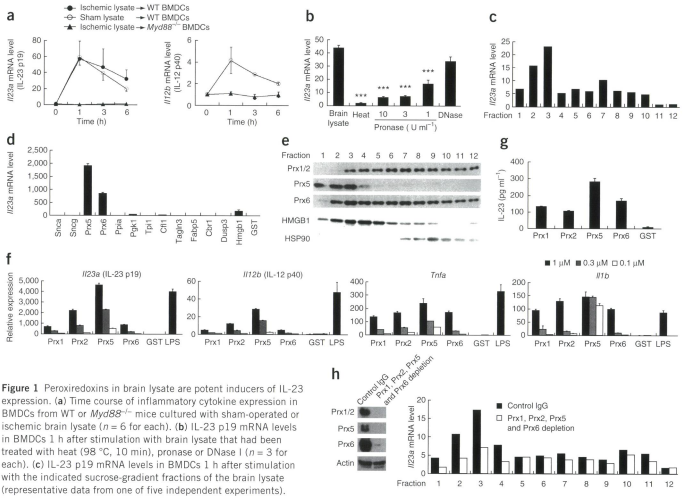

Figure 1 Peroxiredoxins in brain lysate are potent inducers of IL-23 expression. (**a**) Time course of inflammatory cytokine expression in BMDCs from WT or *Myd88*$^{-/-}$ mice cultured with sham-operated or ischemic brain lysate ($n = 6$ for each). (**b**) IL-23 p19 mRNA levels in BMDCs 1 h after stimulation with brain lysate that had been treated with heat (98 °C, 10 min), pronase or DNase I ($n = 3$ for each). (**c**) IL-23 p19 mRNA levels in BMDCs 1 h after stimulation with the indicated sucrose-gradient fractions of the brain lysate (representative data from one of five independent experiments). (**d**) IL-23 p19 mRNA levels in BMDCs 1 h after stimulation with the indicated recombinant GST-fusion proteins ($n = 3$ for each) that are detected in sucrose-gradient fractions 2 and 3 by LC-MS. (**e**) Western blot analysis of the indicated proteins in the sucrose-gradient fraction of the brain lysate. (**f**,**g**) mRNA levels of inflammatory cytokines (**f**) and IL-23 protein levels (**g**) induced in BMDC by the addition of recombinant Prxs or GST protein or lipopolysaccharide (LPS, 100 ng ml^{-1}) ($n = 3$ for each). (**h**) IL-23 p19–inducing activity of each sucrose gradient fraction after immunoprecipitation using control IgG or the Prx-specific antibody mixture. The depletion of Prxs was confirmed by western blot analysis (left; representative data from two independent experiments). Each mRNA expression level indicates relative expression compared to that in untreated BMDCs. ***$P < 0.001$ versus brain lysate (one-way analysis of variance (ANOVA) with Dunnett's correction; the error bars represent s.e.m.).

Supplementary Fig. 1). We detected IL-23 p19–inducing activity in both ischemic and sham-operated brain lysates, suggesting that IL-23 inducers were released by the homogenization process of the brain. Furthermore, IL-23 p19–inducing activity was completely dependent on myeloid differentiation factor 88 (MyD88), an adaptor protein for TLR signaling pathway, both *in vitro* and *in vivo*, as IL-23 mRNA induction disappeared in MyD88-deficient BMDCs (**Fig. 1a**) and in the infiltrating immune cells collected by Percoll-gradient centrifugation from the ischemic brains of MyD88-deficient mice (**Supplementary Fig. 2**). These results suggest that IL-23 p19 expression was induced in a TLR-dependent manner by DAMPs released from damaged brain tissue.

Next, we tried to identify the DAMPs in the brain lysate. We determined that the IL-23–inducing DAMPs must be proteins, given that the IL-23 p19–inducing activity was almost completely diminished by heat or pronase treatment (**Fig. 1b**). Fractionation of the brain lysate revealed that IL-23 p19–inducing activity was present in the cytosolic fraction, that the protein in question did not bind a DEAE-Sepharose column and that its molecular weight was over 10 kDa (**Supplementary Fig. 3a**,**b**). After sucrose density gradient centrifugation, fractions 2 and 3, which contained mostly 15–25 kDa proteins (**Supplementary Fig. 4**), showed high IL-23 p19–inducing activity (**Fig. 1c**). Further analysis by liquid chromatography–mass spectrometry (LC-MS) identified more than 15 proteins that appeared more often in fractions 2 and 3 than in fractions 1 and 4 (**Supplementary Table 1**). We generated recombinant GST-fusion versions of these proteins in bacteria. After extensive washing and filtration through a polymyxin B–Sepharose column, we detected almost no IL-23 p19–inducing activity in preparations containing GST alone or in several GST-fusion protein preparations (**Fig. 1d**). However, we found that Prx5 and Prx6 had potent IL-23 p19–inducing activity compared to HMGB1 (**Fig. 1d**).

Characterization of Prx family proteins as IL-23 inducers

On the basis of these observations, and also because Prx1 was reported to activate macrophages via TLR4 (ref. 24), we decided to investigate whether Prx family proteins contribute to IL-23 production in brain lysates. First, we generated specific antibodies to

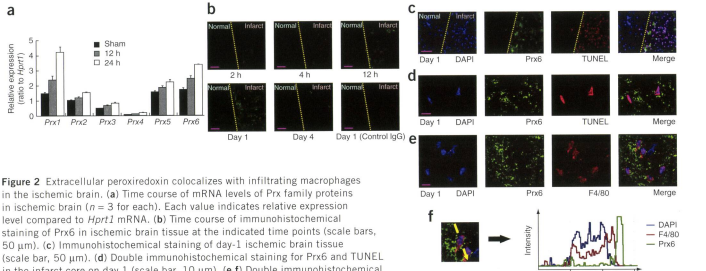

Figure 2 Extracellular peroxiredoxin colocalizes with infiltrating macrophages in the ischemic brain. (**a**) Time course of mRNA levels of Prx family proteins in ischemic brain ($n = 3$ for each). Each value indicates relative expression level compared to *Hprt1* mRNA. (**b**) Time course of immunohistochemical staining of Prx6 in ischemic brain tissue at the indicated time points (scale bars, 50 μm). (**c**) Immunohistochemical staining of day-1 ischemic brain tissue (scale bar, 50 μm). (**d**) Double immunohistochemical staining for Prx6 and TUNEL in the infarct core on day 1 (scale bar, 10 μm). (**e**,**f**) Double immunohistochemical staining for Prx6 and F4/80 in the infarct core on day 1 (scale bar, 10 μm). The graph in **f** shows a quantification of fluorescence intensity along the yellow arrow in left panel. The images were captured by using conventional fluorescence microscopy (**b**,**c**) or confocal laser microscopy (**d**–**f**). The error bars represent s.e.m.

Prx1 and Prx2 (Prx1/2), Prx5 and Prx6 by immunizing rabbits with recombinant Prx proteins. Our Prx1-specific antibody cross-reacted with Prx2 because of the high homology between Prx1 and Prx2, as previously reported[25] (**Supplementary Fig. 5**). Western blotting analysis revealed that Prx5 and Prx6 were most abundant in sucrose-gradient fractions 2 and 3 (**Fig. 1e**). Prx1 and Prx2 were broadly distributed but also detected in fractions 2 and 3. The highest incidence of HMGB1 and HSP90 in the sucrose density gradient was in fractions 4 and 9, respectively. These data suggest that Prx5, Prx6 and, to a lesser degree, Prx1/2 could contribute to the IL-23 induction achieved by fractions 2 and 3.

We then characterized the inflammatory cytokine–inducing activity of GST-free cleaved recombinant Prxs. Among these Prxs, recombinant Prx5 had the greatest activity in inducing the mRNA expression and production of IL-23 and other inflammatory cytokines, although other Prx family proteins could also induce both mRNA and protein expression of inflammatory cytokines in BMDCs (**Fig. 1f**,**g**). To confirm that Prxs are major inducers of IL-23 expression in the brain

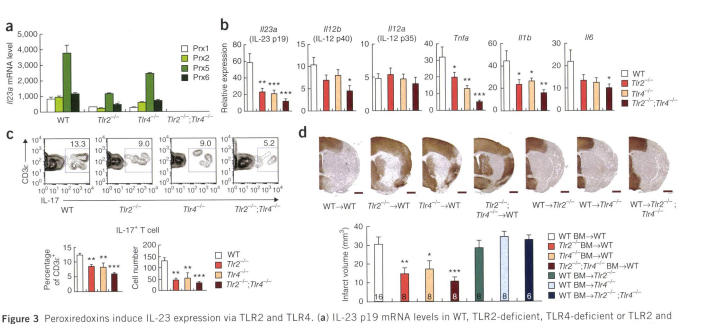

Figure 3 Peroxiredoxins induce IL-23 expression via TLR2 and TLR4. (**a**) IL-23 p19 mRNA levels in WT, TLR2-deficient, TLR4-deficient or TLR2 and TLR4 double-deficient BMDC 1 h after stimulation with 1 μM recombinant Prx proteins ($n = 4$ for each), shown relative to those in untreated BMDCs. (**b**) The mRNA levels of inflammatory cytokines in the infiltrating immune cells on day 1 after stroke onset ($n = 7$ for each). Each value indicates relative expression compared to that in sham-operated mice. (**c**) The ratio and the absolute number of IL-17$^+$ T cells on day 3 after stroke onset ($n = 8$ for WT and $n = 6$ for other samples). (**d**) Infarct volume (bottom) measured by MAP2 immunostaining of brain sections on day 4 after stroke onset in chimeric mice (top; scale bars, 1 mm). *Tlr2*$^{-/-}$ BM → WT means transfer of *Tlr2*$^{-/-}$ bone marrow cells into WT mice. The number of mice is shown on each bar. $^*P < 0.05$, $^{**}P < 0.01$, $^{***}P < 0.001$ versus WT mice (**b**,**c**) and WT bone marrow–transferred WT mice (**d**) (one-way ANOVA with Dunnett's correction; the error bars represent s.e.m.).

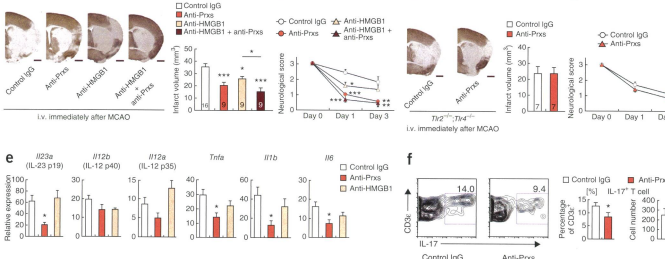

Figure 4 Extracellular release of Prxs contributes to the initiation of post-ischemic inflammation. (**a**,**b**) Infarct volume on day 4 after stroke onset (**a**) and neurological scores on days 1 and 3 after stroke onset (**b**) of mice treated with control IgG (500 μg per mouse), a mixture of antibodies specific for Prx1, Prx2, Prx5 and Prx6 (anti-Prxs; 500 μg per mouse), HMGB1-specific antibody (anti-HMGB1; 200 μg per mouse), or both Prx-specific antibodies and HMGB1-specific antibody immediately after stroke onset (scale bars, 1 mm). i.v., intravenous; MCAO, middle cerebral artery occlusion. (**c**,**d**) Infarct volume on day 4 after stroke onset (**c**) and neurological scores (**d**) on days 1 and 3 after stroke onset of TLR2 and TLR4 double-deficient mice treated with control IgG or the Prx-specific antibody mixture immediately after stroke onset ($n = 7$ for each) (scale bars, 1 mm). (**e**–**g**) mRNA levels of inflammatory cytokines in brain infiltrating immune cells on day 1 after stroke onset ($n = 11$ for control IgG, $n = 7$ for Prx-specific antibodies, and $n = 8$ for HMGB1-specific antibody) (**e**), the ratio and the absolute number of IL-17$^+$ T cells on day 3 after stroke onset ($n = 8$ for each) (**f**) and the absolute number of TUNEL$^+$ cells in the peri-infarct area on day 4 after stroke onset (scale bars, 50 μm; $n = 8$ for each) (**g**) in the mice treated with control IgG, Prx-specific antibody mixture or HMGB1-specific antibody immediately after stroke onset. Each mRNA expression level indicates relative expression compared to that in sham-operated mice. The number of mice is shown on each bar (**a**,**c**). $^*P < 0.05$, $^{**}P < 0.01$, $^{***}P < 0.001$ versus control IgG-administered mice (one-way ANOVA with Dunnett's correction (**a**,**b**,**e**) or two-sided Student's t test (**c**,**d**,**f**,**g**); the error bars represent s.e.m.).

lysate, we performed an antibody-depletion assay. We observed an apparent reduction of IL-23 p19–inducing activity in sucrose-gradient fractions 2 and 3 after depletion of Prx5 (**Fig. 1h**), whereas antibody depletion of HMGB1 had little effect (**Supplementary Fig. 6**). These results suggest that Prx family proteins in the brain lysate are major inducers of IL-23 expression.

Originally, Prx family proteins were described as antioxidative enzymes within cells that are neuroprotective by scavenging reactive oxygen species (ROS)[26–28]. Prxs contain one (Prx6) or two (Prx1–Prx5) conserved cysteine residues. Two-cysteine Prxs scavenge ROS in cooperation with thioredoxin[26,29,30]. However, once released from the cells, Prxs are considered to lose their antioxidant capacity because of oxidation of the cysteine residues, and the redox cycle of Prxs should not be possible[26,31]. Consistent with this notion, the disruption of cysteine residues by point mutations or iodoacetamide treatment did not affect the IL-23–inducing activity of Prx5 (**Supplementary Fig. 7**). Thus, extracellular Prxs, being independent of antioxidant activity, could function as inducers of IL-23 expression in BMDCs.

Extracellular Prxs colocalize with infiltrating macrophages

Recent reports have demonstrated that Prxs are released into the extracellular fluid after brain tissue death in rats and in humans after acute ischemic stroke[32,33]. We hypothesized that Prxs released from necrotic brain cells into the extracellular compartment function as a danger signal. The mRNA expression levels of Prxs were very high in normal brain tissue, comparable to those of the housekeeping gene hypoxanthine phosphoribosyltransferase 1 (*Hprt1*) and were increased further as a result of ischemic brain injury (**Fig. 2a**).

Immunohistochemical staining with our Prx-specific antibodies successfully detected Prx1/2 and Prx6 expression in normal brain tissues, as previously reported[34] (**Supplementary Fig. 8a**,**b**). Cerebral ischemic stress induced much stronger Prx6 expression in the infarct region than in the normal tissues (**Fig. 2b**). This increase in Prx6 expression was barely observable until 4 h after the reperfusion, and Prx6 expression was very evident on day 1 but had diminished by day 4 (**Fig. 2b**). Specific staining of Prx6 was confirmed by staining with a control nonspecific IgG, which did not exhibit any such staining patterns (**Fig. 2b**). We observed a similar increase in Prx1/2 protein staining upon ischemic stress on day 1 in wild-type (WT) mice; however, we obtained no detectable signals in *Prx1*$^{-/-}$ mice (**Supplementary Fig. 8c**), confirming the specificity of our immunohistostaining.

In the ischemic brain, we observed strong Prx6 expression in the TUNEL$^+$ infarct region (**Fig. 2c**). By using confocal laser microscopy, we found that Prx6-positive, debris-like granules were abundant around TUNEL$^+$ cells in the infarct core (**Fig. 2d**). These observations indicate that Prx6 was induced in injured ischemic cells and then released into the extracellular compartment from dying cells. Notably, Prx6$^+$ debris was often observed to be co-localized with the

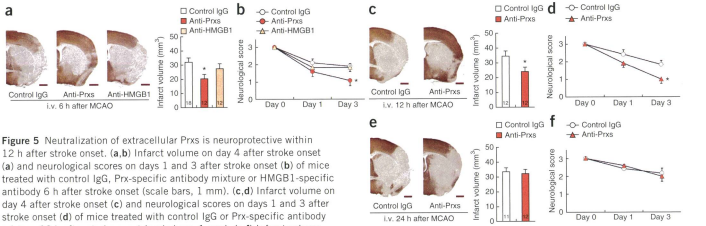

Figure 5 Neutralization of extracellular Prxs is neuroprotective within 12 h after stroke onset. (**a**,**b**) Infarct volume on day 4 after stroke onset (**a**) and neurological scores on days 1 and 3 after stroke onset (**b**) of mice treated with control IgG, Prx-specific antibody mixture or HMGB1-specific antibody 6 h after stroke onset (scale bars, 1 mm). (**c**,**d**) Infarct volume on day 4 after stroke onset (**c**) and neurological scores on days 1 and 3 after stroke onset (**d**) of mice treated with control IgG or Prx-specific antibody mixture 12 h after stroke onset (scale bars, 1 mm). (**e**,**f**) Infarct volume on day 4 after stroke onset (**e**) and neurological scores on days 1 and 3 after stroke onset (**f**) of mice treated with control IgG or Prx-specific antibody mixture 24 h after stroke onset (scale bars, 1 mm). The number of mice is shown on each bar (**a**,**c**,**e**). $^*P < 0.05$ versus control IgG–administered mice (one-way ANOVA with Dunnett's correction (**a**,**b**) or two-sided Student's *t* test (**c**–**f**); the error bars represent s.e.m.).

cell membranes of F4/80$^+$ macrophages (**Fig. 2e**,**f**), supporting our hypothesis that the extracellular release of Prx6 stimulates infiltrating macrophages.

Prxs induce IL-23 expression via TLR2 and TLR4

TLR2 and TLR4 have been implicated in ischemic brain injury[35]. Thus, we tried to determine the relationship between the IL-23–inducing activity of Prxs and TLR2 and TLR4. The recombinant Prx–mediated induction of IL-23 p19 expression was lower in TLR2- and TLR4-deficient BMDCs and completely absent in BMDCs doubly deficient in TLR2 and TLR4 as compared to WT BMDCs (**Fig. 3a**). In addition, we confirmed that Prx5 protein activated nuclear factor-κB through TLR4 in 293 cells expressing TLR4 (**Supplementary Fig. 9**). Therefore, Prxs induced IL-23 expression by activating both TLR2 and TLR4 *in vitro*.

Next, we examined inflammatory cytokine expression in the infiltrated mononuclear cells collected by Percoll-gradient centrifugation from the ischemic brain of mice deficient in TLR2, TLR4 or both. The expression levels of IL-23 p19, tumor necrosis factor-α (TNF-α) and IL-1β in the infiltrating immune cells on day 1 after stroke onset were largely dependent on both TLR2 and TLR4, but that of IL-12 p35 was not (**Fig. 3b**) (physiological data and cerebral blood flow (CBF) are shown in **Supplementary Tables 2** and **3**). Inflammatory cytokine expression was more severely reduced in TLR2 and TLR4 double-knockout mice than in TLR2 or TLR4 single-knockout mice (**Fig. 3b**), suggesting a functional redundancy between TLR2 and TLR4. In peripheral blood monocytes, we observed minimal expression of IL-23 p19, TNF-α and IL-1β (**Supplementary Fig. 10**), indicating that the activation of infiltrated cells via TLR2 and TLR4 occurred mainly in the ischemic brain rather than in the periphery.

The absolute number and the fraction of IL-17$^+$ T cells among infiltrated mononuclear cells on day 3 after stroke onset were also lower in TLR2 or TLR4 single-knockout mice and were further lowered in TLR2 and TLR4 double-knockout mice as compared to WT mice (**Fig. 3c**). However, TLR2 and TLR4 double deficiency did not significantly decrease the absolute number of interferon-γ$^+$ T cells (**Supplementary Fig. 11**); this observation is consistent with the minimal effect of TLR2 and TLR4 double deficiency on IL-12 expression. Bone marrow chimera experiments also confirmed that the infiltrating macrophages, but not residential microglia, were responsible for TLR2- and TLR4-mediated ischemic brain injury (**Fig. 3d**) and inflammatory cytokine expression (**Supplementary Fig. 12**) (CBF is shown in **Supplementary Table 4**). Thus, these data suggest that both TLR2 and TLR4 play essential parts in inducing post-ischemic inflammation by regulating the IL-23–IL-17 axis but not the IL-12–interferon-γ axis.

Extracellular Prxs trigger post-ischemic inflammation

Next, we investigated the therapeutic effects of neutralizing Prxs or HMGB1 by administrating antibodies immediately after stroke onset. The administration of a mixture of antibodies specific for Prx1, Prx2, Prx5 and Prx6, but not control IgG, had a neuroprotective effect associated with a significant reduction in infarct volume (**Fig. 4a**,**b**) (CBF and survival rate are shown in **Supplementary Table 5**). This reduction could still be observed on day 7 (**Supplementary Fig. 13**). We also confirmed that these Prx-specific antibodies were delivered to the ischemic brain tissue (**Supplementary Fig. 14**). Suppression of infarct volume growth by administering Prx-specific antibodies was dependent on TLR2, TLR4 and IL-23 (**Fig. 4c**,**d** and **Supplementary Fig. 15**). The administration of the Prx-specific antibody mixture decreased inflammatory cytokine expression in infiltrating immune cells on day 1 after stroke onset (**Fig. 4e**), as well as the absolute number and the fraction of IL-17–producing T cells on day 3 after stroke onset (**Fig. 4f** and **Supplementary Fig. 16**). The number of TUNEL$^+$ cells in the peri-infarct region on day 4 after stroke onset was also decreased by administration of the Prx-specific antibody mixture (**Fig. 4g**). These results were consistent with our hypothesis that extracellular Prxs induce the IL-23–IL-17 inflammatory pathway through TLR2 and TLR4 and promote post-ischemic inflammation and infarct volume growth.

HMGB1 is another important DAMP in ischemic brain injury[20]. We confirmed that HMGB1-specific antibody administered immediately after stroke onset reduced infarct volume (**Fig. 4a**). We obtained additive therapeutic effects by administering both Prx-specific antibodies and HMGB1-specific antibody (**Fig. 4a**,**b**). However, HMGB1-specific antibody had little effect on suppressing inflammatory cytokine expression on day 1 after stroke onset compared with the Prx-specific antibodies (**Fig. 4e**). This can be explained by the fact that extracellular release of HMGB1 is mostly diminished in the ischemic brain within 6 h after stroke onset[20], although the increase in blood cell infiltration mostly occurs 1 d after stroke onset[11].

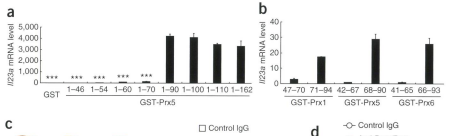

Figure 6 The conserved region of peroxiredoxins was essential for IL-23–inducing activity and the increase in infarct size. (**a**) IL-23 p19–inducing activities of C-terminal deletion mutants of Prx5 ($n = 3$ for each). The number of amino acid residues contained in each GST-fusion Prx5 peptide is shown on the x axis. (**b**) IL-23 p19–inducing activities of GST-fusion Prx1, Prx5, and Prx6 peptides ($n = 3$ for each). The number of amino acid residues contained in each Prx1, Prx5 and Prx6 peptide is shown on the x axis (GST-Prx1$_{47–70}$, GST-Prx5$_{42–67}$ and GST-Prx6$_{41–65}$ peptides contained the α2 helix region; GST-Prx1$_{71–94}$, GST-Prx5$_{68–90}$ and GST-Prx6$_{66–93}$ peptides contained the β_4 sheet and α_3 helix regions). IL-23 p19 mRNA levels were detected by means of quantitative RT-PCR in BMDCs 1 h after stimulation with 1 μM recombinant proteins and are shown relative to those of untreated BMDCs. (**c**,**d**) Infarct volume on day 4 after stroke onset (scale bars, 1 mm) (**c**) and neurological scores (**d**) on days 1 and 3 after stroke onset of mice treated with control IgG, a Prx5- and Prx6-specific antibody mixture (anti-Prx5/Prx6) or a Prx5$_{68–90}$- and Prx6$_{66–93}$-specific (common α_3 helix and β_4 sheet region) antibody mixture (anti-Prx5$_{68–90}$/Prx6$_{66–93}$) immediately after the induction of brain ischemia (300 μg per mouse). The number of mice is shown on each bar in **c**. $^*P < 0.05$, $^{**}P < 0.01$, $^{***}P < 0.001$ versus GST-Prx5$_{1–162}$ (**a**) and control IgG-treated mice (**c**,**d**) (one-way ANOVA with Dunnett's correction; the error bars represent s.e.m.).

Finally, we examined the effect of antibodies administered several hours after stroke onset to determine the therapeutic time window. Administration of the Prx-specific antibodies mixture 6 h after stroke onset significantly attenuated ischemic brain damage, whereas administration of the HMGB1-specific antibody was much less effective at this time point (**Fig. 5a**,**b**). The Prx-specific antibody mixture was therapeutic up to 12 h after stroke onset (**Fig. 5c**,**d**); however, we did not observe a therapeutic effect when it was administered 24 h after stroke onset (**Fig. 5e**,**f**). These results suggest that Prxs act later than HMGB1 in post-ischemic brain injury.

The conserved region of Prx is essential for IL-23 induction

As shown in **Figure 1f**, all Prx family proteins potently activate BMDCs. We thus suspected that a particular structure common to Prxs stimulates TLR2 and TLR4. By generating deletion mutants of Prx5, we found that the IL-23–inducing activity was located between amino acid residues 70 and 90 of Prx5 (**Fig. 6a**). This region is located at the surface of Prxs and contains β_4 sheet and α_3 helix regions that are well conserved among Prxs as well as among various species[36–38] (**Supplementary Fig. 17a**,**b**). A GST-fusion of this conserved region of Prx1, Prx5 and Prx6, but not other regions, resulted in similar IL-23–inducing activity to each other (**Fig. 6b** and **Supplementary Fig. 17c–e**).

Next, we generated specific antibodies to these conserved β_4 sheet and α_3 helix regions of Prx5 and Prx6 (Prx5$_{68–90}$ and Prx6$_{66–93}$). Although these two antibodies did not cross-react with each other (**Supplementary Fig. 18**), administration of a mixture of the Prx5$_{68–90}$-specific and Prx6$_{66–93}$-specific antibodies immediately after stroke onset significantly reduced the infarct volume on day 4 and the severity of neurological deficits on days 1 and 3 after stroke onset (**Fig. 6c**,**d**). These results suggest that this conserved region of Prxs is responsible for the induction of post-ischemic inflammation and could be an ideal target for developing neuroprotective therapy.

DISCUSSION

ROS and their inducers have been considered to be endogenous danger signals[39]. Unexpectedly, our study demonstrated that antioxidant proteins themselves can function as DAMPs under conditions of sterile inflammation. A recent study revealed that TLRs could be stimulated by DNA or formyl peptide complex released from mitochondria, which are evolutionary endosymbionts derived from bacteria[18]. Similarly, because Prxs are highly conserved among various species from bacteria to mammals, it is possible that these molecules function as DAMPs recognized by TLRs. As the conserved regions of Prxs were sufficient for induction of IL-23 expression, even partially degraded Prxs could function as DAMPs. Furthermore, the expression of Prx family proteins, in particular Prx5 and Prx6, is especially high in brain compared to other organs[30]. These are potential reasons for why Prxs could function as DAMPs in ischemic brain.

We showed that Prx-mediated post-ischemic inflammation was dependent on TLR2 and TLR4, which seem to be functionally redundant in the context of ischemic damage. Although it is rare that one TLR ligand activates multiple TLRs, HMGB1 has been shown to function as a DAMP through TLR2, TLR4 and TLR9 (refs. 15,40). The molecular mechanism underlying TLR2 and TLR4 activation by Prxs and other endogenous DAMPs remains to be clarified. It is also possible that other pattern recognition receptors (CD36, RAGE or SRA) in addition to TLRs are involved in the recognition of endogenous DAMPs and modification of TLR signaling[41–43].

Prx family proteins are antioxidant enzymes within cells, and are essential for cell survival in brain and other organ injuries[27,28,44]. Indeed, we observed the exacerbation of ischemic brain injury in *Prx1*$^{-/-}$ mice (data not shown). Yet this study revealed that once Prxs are released from necrotic brain cells into the extracellular compartment, these extracellular Prxs act as a neurotoxic danger signal via TLR2 and TLR4. Thus, we propose two opposing functions of Prx: one inside and one outside of brain cells (**Supplementary Fig. 19a**). These two opposing functions performed by a single molecule may be apposite for self-protection against injury and infection.

HMGB1 is another key DAMP that contributes to blood-brain barrier breakdown[20]. Although neutralization of HMGB1 is neuroprotective[45], extracellular HMGB1 may not be a good therapeutic target for reducing inflammation, given that the extracellular release of HMGB1 decreases rapidly in the ischemic core[20,46]. Our research demonstrates

that the extracellular release of Prxs is relatively slow and is a pivotal step in the activation of infiltrating macrophages, rather than release of HMGB1. In summary, we propose that there is a time lag as well as functional differences between HMGB1 and Prxs (**Supplementary Fig. 19b**). HMGB1 is a primary DAMP in the hyperacute phase of post-ischemic inflammation, whereas extracellular Prx is a second-ary one in the acute phase of brain ischemia. The extracellular Prxs could be a more potent therapeutic target than HMGB1 because their therapeutic time window would be longer than that of HMGB1.

METHODS

Methods and any associated references are available in the online version of the paper.

Note: Supplementary information is available in the online version of the paper.

ACKNOWLEDGMENTS

We thank N. Saito, N. Shiino and M. Asakawa for technical assistance. This work was supported by special grants-in-aid (A) and open research for young academics and specialists from the Ministry of Education, Culture, Sports, Science and Technology of Japan, PRESTO and CREST from the Japan Science and Technology Agency, an Intramural Research Grant (22-4) for Neurological and Psychiatric Disorders of the National Center of Neurology and Psychiatry (NCNP), the SENSHIN Research Foundation, the Takeda Science Foundation, the Uehara Memorial Foundation, the Mochida Memorial Foundation, the Scientific Research Fund from the Ministry of Health, Labor and Welfare of Japan (09156274) and the Program for Promotion of Fundamental Studies in Health Science of the National Institute of Biomedical Innovation.

AUTHOR CONTRIBUTIONS

T. Shichita designed and performed experiments, analyzed data and wrote the manuscript; E.H. and A.K. performed TLR-deficient mouse analysis; R.M., R.S. and T. Sekiya participated in data analysis and discussion; I.T. provided specific input on protein analysis; H.O. and T.K. provided technical advice about experimental design; T.Y. and T.I. provided crucial input on Prx1's functions; H.T., S.M. and M.N. provided the HMGB1-specific antibody and crucial input on HMGB1; K.K. provided specific input regarding LC-MS analysis; K.M. and S.A. provided TLR2 and/or TLR4-deficient mice; A.Y. initiated and directed the entire study, designed experiments and wrote the manuscript.

COMPETING FINANCIAL INTERESTS

The authors declare no competing financial interests.

Published online at http://www.nature.com/doifinder/10.1038/nm.2749.
Reprints and permissions information is available online at http://www.nature.com/reprints/index.html.

1. Moskowitz, M.A., Lo, E.H. & Iadecola, C. The science of stroke: mechanisms in search of treatments. *Neuron* **67**, 181–198 (2010).
2. Lo, E.H. Degeneration and repair in central nervous system disease. *Nat. Med.* **16**, 1205–1209 (2010).
3. Ooboshi, H. *et al.* Postischemic gene transfer of interleukin-10 protects against both focal and global brain ischemia. *Circulation* **111**, 913–919 (2005).
4. Macrez, R. *et al.* Stroke and the immune system: from pathophysiology to new therapeutic strategies. *Lancet Neurol.* **10**, 471–480 (2011).
5. Iadecola, C. & Anrather, J. The immunology of stroke: from mechanisms to translation. *Nat. Med.* **17**, 796–808 (2011).
6. Eltzschig, H.K. & Eckle, T. Ischemia and reperfusion—from mechanism to translation. *Nat. Med.* **17**, 1391–1401 (2011).
7. Hurn, P.D. *et al.* T- and B-cell-deficient mice with experimental stroke have reduced lesion size and inflammation. *J. Cereb. Blood Flow Metab.* **27**, 1798–1805 (2007).
8. Liesz, A. *et al.* Inhibition of lymphocyte trafficking shields the brain against deleterious neuroinflammation after stroke. *Brain* **134**, 704–720 (2011).
9. Yilmaz, G., Arumugam, T.V., Stokes, K.Y. & Granger, D.N. Role of T lymphocytes and interferon-gamma in ischemic stroke. *Circulation* **113**, 2105–2112 (2006).
10. Ren, X. *et al.* Regulatory B cells limit CNS inflammation and neurologic deficits in murine experimental stroke. *J. Neurosci.* **31**, 8556–8563 (2011).
11. Shichita, T. *et al.* Pivotal role of cerebral interleukin-17-producing γδT cells in the delayed phase of ischemic brain injury. *Nat. Med.* **15**, 946–950 (2009).
12. Konoeda, F. *et al.* Therapeutic effect of IL-12/23 and their signaling pathway blockade on brain ischemia model. *Biochem. Biophys. Res. Commun.* **402**, 500–506 (2010).
13. Tang, S.C. *et al.* Pivotal role for neuronal Toll-like receptors in ischemic brain injury and functional deficits. *Proc. Natl. Acad. Sci. USA* **104**, 13798–13803 (2007).
14. Chen, G.J. *et al.* Identification of a key pathway required for the sterile inflammatory response triggered by dying cells. *Nat. Med.* **13**, 851–856 (2007).
15. Yanai, H. *et al.* HMGB proteins function as universal sentinels for nucleic-acid-mediated innate immune responses. *Nature* **462**, 99–103 (2009).
16. Marsh, B.J., Williams-Karnesky, R.L. & Stenzel-Poore, M.P. Toll-like receptor signaling in endogenous neuroprotection and stroke. *Neuroscience* **158**, 1007–1020 (2009).
17. Stewart, C.R. *et al.* CD36 ligands promote sterile inflammation through assembly of a Toll-like receptor 4 and 6 heterodimer. *Nat. Immunol.* **11**, 155–161 (2010).
18. Zhang, Q. *et al.* Circulating mitochondrial DAMPs cause inflammatory responses to injury. *Nature* **464**, 104–107 (2010).
19. Rivest, S. Regulation of innate immune responses in the brain. *Nat. Rev. Immunol.* **9**, 429–439 (2009).
20. Zhang, J. *et al.* Anti-high mobility group box-1 monoclonal antibody protects the blood-brain barrier from ischemia-induced disruption in rats. *Stroke* **42**, 1420–1428 (2011).
21. Kim, J.B. *et al.* HMGB1, a novel cytokine-like mediator linking acute neuronal death and delayed neuroinflammation in the postischemic brain. *J. Neurosci.* **26**, 6413–6421 (2006).
22. Yang, Q.W. *et al.* HMBG1 mediates ischemia-reperfusion injury by TRIF-adaptor independent Toll-like receptor 4 signaling. *J. Cereb. Blood Flow Metab.* **31**, 593–605 (2011).
23. Hayakawa, K., Qiu, J. & Lo, E.H. Biphasic actions of HMGB1 signaling in inflammation and recovery after stroke. *Ann. NY Acad. Sci.* **1207**, 50–57 (2010).
24. Riddell, J.R., Wang, X.Y., Minderman, H. & Gollnick, S.O. Peroxiredoxin 1 stimulates secretion of proinflammatory cytokines by binding to TLR4. *J. Immunol.* **184**, 1022–1030 (2010).
25. Chesterman, E.S. *et al.* Investigation of Prx1 protein expression provides evidence for conservation of cardiac-specific posttranscriptional regulation in vertebrates. *Dev. Dyn.* **222**, 459–470 (2001).
26. Patenaude, A., Murthy, M.R. & Mirault, M.E. Emerging roles of thioredoxin cycle enzymes in the central nervous system. *Cell. Mol. Life Sci.* **62**, 1063–1080 (2005).
27. Hu, X. *et al.* Peroxiredoxin-2 protects against 6-hydroxydopamine–induced dopaminergic neurodegeneration via attenuation of the apoptosis signal-regulating kinase (ASK1) signaling cascade. *J. Neurosci.* **31**, 247–261 (2011).
28. Rashidian, J. *et al.* Essential role of cytoplasmic cdk5 and Prx2 in multiple ischemic injury models, *in vivo*. *J. Neurosci.* **29**, 12497–12505 (2009).
29. Wood, Z.A., Schröder, E., Robin Harris, J. & Poole, L.B. Structure, mechanism and regulation of peroxiredoxins. *Trends Biochem. Sci.* **28**, 32–40 (2003).
30. Seo, M.S. *et al.* Identification of a new type of mammalian peroxiredoxin that forms an intramolecular disulfide as a reaction intermediate. *J. Biol. Chem.* **275**, 20346–20354 (2000).
31. Toohey, J.I. Sulfhydryl dependence in primary explant hematopoietic cells. Inhibition of growth *in vitro* with vitamin B12 compounds. *Proc. Natl. Acad. Sci. USA* **72**, 73–77 (1975).
32. Chou, J.L. *et al.* Proteomic investigation of a neural substrate intimately related to brain death. *Proteomics* **11**, 239–248 (2011).
33. Dayon, L. *et al.* Brain extracellular fluid protein changes in acute stroke patients. *J. Proteome Res.* **10**, 1043–1051 (2011).
34. Jin, M.H. *et al.* Characterization of neural cell types expressing peroxiredoxins in mouse brain. *Neurosci. Lett.* **381**, 252–257 (2005).
35. Brea, D. *et al.* Toll-like receptors 2 and 4 in ischemic stroke: outcome and therapeutic values. *J. Cereb. Blood Flow Metab.* **31**, 1424–1431 (2011).
36. Hirotsu, S. *et al.* Crystal structure of a multifunctional 2-Cys peroxiredoxin heme-binding protein 23kDa/proliferation-associated gene product. *Proc. Natl. Acad. Sci. USA* **96**, 12333–12338 (1999).
37. Declercq, J.P. *et al.* Crystal structure of human peroxiredoxin 5, a novel type of mammalian peroxiredoxin at 1.5 A resolution. *J. Mol. Biol.* **311**, 751–759 (2001).
38. Choi, H.J. *et al.* Crystal structure of a novel human peroxidase enzyme at 2.0 A resolution. *Nat. Struct. Biol.* **5**, 400–406 (1998).
39. Chen, G.Y. & Nuñez, G. Sterile inflammation: sensing and reacting to damage. *Nat. Rev. Immunol.* **10**, 826–837 (2010).
40. Yu, M. *et al.* HMGB1 signals through Toll-like receptor (TLR) 4 and TLR2. *Shock* **26**, 174–179 (2006).
41. Triantafilou, M. *et al.* Membrane sorting of Toll-like receptor (TLR)-2/6 and TLR2/1 heterodimers at the cell surface determines heterotypic associations with CD36 and intracellular targeting. *J. Biol. Chem.* **281**, 31002–31011 (2006).
42. Yi, H. *et al.* Pattern recognition scavenger receptor SRAVCD204 down-regulates Toll-like receptor 4 signaling-dependent CD8 T-cell activation. *Blood* **113**, 5819–5828 (2009).
43. Akashi-Takamura, S. & Miyake, K. TLR accessory molecules. *Curr. Opin. Immunol.* **20**, 420–425 (2008).
44. Esmann, T. *et al.* Peroxiredoxin-6 protects against mitochondrial dysfunction and liver injury during ischemia-reperfusion in mice. *Am. J. Physiol. Gastrointest. Liver Physiol.* **296**, G266–G274 (2009).
45. Liu, K. *et al.* Anti-high mobility group box 1 monoclonal antibody ameliorates brain infarction induced by transient ischemia in rats. *FASEB J.* **21**, 3904–3916 (2007).
46. Qiu, J. *et al.* Early release of HMGB-1 from neurons after the onset of brain ischemia. *J. Cereb. Blood Flow Metab.* **28**, 927–938 (2008).

nature medicine

Retinaldehyde dehydrogenase 1 regulates a thermogenic program in white adipose tissue

Florian W Kiefer[1], Cecile Vernochet[2], Patrick O'Brien[1], Steffen Spoerl[1], Jonathan D Brown[1], Shriram Nallamshetty[1], Maximilian Zeyda[3,4], Thomas M Stulnig[3,4], David E Cohen[5], C Ronald Kahn[2] & Jorge Plutzky[1]

Promoting brown adipose tissue (BAT) formation and function may reduce obesity. Recent data link retinoids to energy balance, but a specific role for retinoid metabolism in white versus brown fat is unknown. Retinaldehyde dehydrogenases (Aldhs), also known as aldehyde dehydrogenases, are rate-limiting enzymes that convert retinaldehyde (Rald) to retinoic acid. Here we show that *Aldh1a1* is expressed predominately in white adipose tissue (WAT), including visceral depots in mice and humans. Deficiency of the *Aldh1a1* gene induced a BAT-like transcriptional program in WAT that drove uncoupled respiration and adaptive thermogenesis. WAT-selective *Aldh1a1* knockdown conferred this BAT program in obese mice, limiting weight gain and improving glucose homeostasis. Rald induced uncoupling protein-1 (*Ucp1*) mRNA and protein levels in white adipocytes by selectively activating the retinoic acid receptor (RAR), recruiting the coactivator PGC-1α and inducing *Ucp1* promoter activity. These data establish Aldh1a1 and its substrate Rald as previously unrecognized determinants of adipocyte plasticity and adaptive thermogenesis, which may have potential therapeutic implications.

Obesity is closely associated with many disorders, including atherosclerosis and type 2 diabetes[1,2]. Although excess caloric intake and decreased energy expenditure promote overall weight gain, visceral adiposity is particularly associated with cardiometabolic risk[3]. As such, unique factors may control the development and function of specific fat depots. Whereas WAT stores energy in the form of triglycerides, BAT oxidizes fatty acids and dissipates energy through uncoupled respiration and heat production[4–6]. WAT is the main adipose depot in humans; however, recent work has established both the presence of BAT in humans and its association with leanness[6,7]. These distinct aspects of adipocyte biology require further understanding and may represent a therapeutic strategy to combat obesity and its complications. Although the presence of brown adipocytes in WAT and factors determining white versus brown adipogenesis have received considerable attention[8–12], the exact origin of white and brown adipocytes and the potential for adipocyte plasticity in terms of white versus brown characteristics remains under debate[13,14].

Retinoids–vitamin A metabolites with diverse, essential biological functions–have recently been linked to the control of adipogenesis and energy homeostasis, with effects on obesity, diabetes and cardiovascular disease[15–19]. Retinoids exert these actions largely by activating RAR and the retinoid X receptor (RXR), nuclear hormone receptors that regulate gene expression[20,21]. Retinoid formation relies on a network of enzymes in which dietary vitamin A, or retinol, is first oxidized to Rald by alcohol and retinol dehydrogenases. Subsequently, Aldhs irreversibly convert Rald to retinoic acid—the rate-limiting step of retinoic acid formation[20–22].

We recently identified Rald as an active signaling metabolite in WAT and a modulator of adipogenesis in 3T3-L1 cells[16]. Deficiency in *Aldh1a1* (also known as *Raldh1*), the main postnatal Aldh isoform, results in higher Rald concentrations[16,23] and protects mice against diet-induced obesity and diabetes by increasing energy expenditure[16]. However, the mechanisms for this hypermetabolic phenotype, its dependency on high-fat feeding and its relevance to human adiposity has remained unclear.

Here we show that Aldh1a1 is a key determinant of WAT plasticity and the regulation of white versus brown adipocyte characteristics. In both mice and humans, *Aldh1a1* was expressed primarily in visceral WAT, and its expression level was highly associated with obesity. In mice fed standard chow, *Aldh1a1* deficiency strongly induced both expression of classic BAT markers and uncoupled respiration in WAT, increasing adaptive thermogenesis *in vivo*. Rald potently regulated transcription of *Ucp1* in white adipocytes through effects on RAR and not RXR, including peroxisome proliferator–activated receptor-γ coactivator (PGC-1α) recruitment; RAR antagonist treatment reversed the thermogenic phenotype in *Aldh1a1* deficiency. Notably, treatment of high-fat diet–fed mice with antisense oligonucleotides to *Aldh1a1* repressed *Aldh1a1* expression selectively in visceral WAT, induced a thermogenic program in WAT and conferred protection against cold exposure and obesity. These findings establish Aldh1a1 and its substrate Rald as previously unrecognized regulators of white adipose plasticity and adaptive thermogenesis and identify Aldh1a1 in visceral fat as a new potential target for treating obesity.

[1]Cardiovascular Division, Department of Medicine, Brigham and Women's Hospital, Harvard Medical School, Boston, Massachusetts, USA. [2]Joslin Diabetes Center, Harvard Medical School, Boston, Massachusetts, USA. [3]Christian Doppler-Laboratory for Cardio-Metabolic Immunotherapy, Vienna, Austria. [4]Clinical Division of Endocrinology and Metabolism, Department of Medicine, Medical University of Vienna, Austria. [5]Division of Gastroenterology, Department of Medicine, Brigham and Women's Hospital, Harvard Medical School, Boston, Massachusetts, USA. Correspondence should be addressed to J.P. (jplutzky@rics.bwh.harvard.edu).

Received 18 January; accepted 29 March; published online 6 May 2012; doi:10.1038/nm.2757

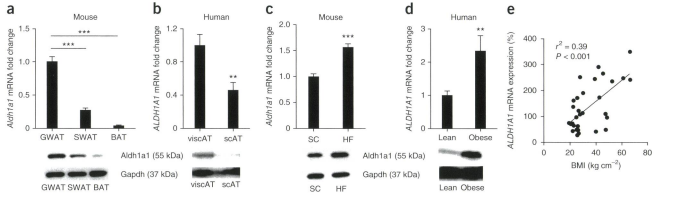

Figure 1 *Aldh1a1* is present primarily in visceral fat, and its expression correlates with obesity. (**a**) *Aldh1a1* mRNA and protein expression in different fat depots of female C57BL/6J mice ($n = 10$). (**b**) *ALDH1A1* mRNA and protein expression in visceral adipose tissue (viscAT) and subcutaneous adipose tissue (scAT) from nonobese male and female subjects ($n = 20$). (**c**) *Aldh1a1* mRNA and protein expression in GWAT from standard chow–fed (SC) lean and high-fat diet–fed (HF) obese C57BL/6J mice ($n = 8$ per group). (**d**) *ALDH1A1* mRNA and protein expression in viscAT from nonobese (body-mass index (BMI) = 25.2 ± 0.15 kg m^{-2}) and morbidly obese (BMI = 53.0 ± 0.55 kg m^{-2}) subjects; $n = 20$ per group. Representative western blots are shown. (**e**) Linear regression analysis between BMI and *ALDH1A1* mRNA expression in human viscAT ($n = 40$). $^{**}P < 0.01$, $^{***}P < 0.001$. Data are given as mean ± s.e.m.

RESULTS

Aldh1a1 is predominantly expressed in visceral fat

To consider the possible role of Aldh1a1 in specific adipose stores, we analyzed its mRNA expression and protein levels in different fat depots of standard chow–fed C57BL/6J mice and metabolically healthy human subjects of normal weight. In C57BL/6J mice, *Aldh1a1* expression was highest in perigonadal white adipose tissue (GWAT), a mouse visceral fat depot, significantly lower in inguinal subcutaneous white adipose tissue (SWAT) and barely detectable in interscapular BAT; Aldh1a1 protein levels followed a similar pattern (**Fig. 1a**). In humans, both *ALDH1A1* mRNA and protein were robustly present in visceral adipose tissue (viscAT), with significantly lower levels in abdominal subcutaneous adipose tissue (**Fig. 1b**).

Given that visceral adiposity is strongly implicated in the pathogenesis of obesity-related metabolic disorders, we investigated whether adipose *Aldh1a1* expression varied with obesity. *Aldh1a1* expression was significantly higher in GWAT and viscAT of C57BL/6J mice fed a high-fat diet and in morbidly obese human subjects, respectively, compared to lean controls (**Fig. 1c**,**d**). Moreover, regression analysis revealed a positive association between *ALDH1A1* mRNA expression in viscAT and body mass index ($r^2 = 0.39$, $P < 0.001$) in 40 human subjects (**Fig. 1e**). These results implicate Aldh1a1 in obesity and, specifically, in visceral adiposity.

Aldh1a1 deficiency induces a BAT gene program in WAT

Given this association of Aldh1a1 with obesity (**Fig. 1**) and the enhanced energy expenditure in *Aldh1a1*-deficient (*Aldh1a1*$^{-/-}$) mice fed a high-fat diet[16], we studied mitochondrial uncoupling in WAT and BAT as a mechanism for energy dissipation in *Aldh1a1* deficiency. *Ucp1* mRNA expression and protein content were significantly induced in GWAT of standard chow–fed *Aldh1a1*$^{-/-}$ versus C57BL/6J wild-type (WT) control mice; however, this induction was significantly lessened in SWAT, and *Ucp1* mRNA and protein remained unchanged in BAT (**Fig. 2a**,**b**). On immunohistochemistry images, lipid droplet size and adipocyte morphology appeared unaltered in *Aldh1a1*-deficient WAT, but *Ucp1* was strongly induced as compared to WT adipose tissue (**Fig. 2b**).

To further characterize fat in the presence or absence of Aldh1a1, we measured mRNA expression of known BAT markers including cell-death activator (*Cidea*), PGC-1α and PGC-1β (encoded by *Ppargc1a* and *Ppargc1b*, respectively), PR domain–containing 16 (*Prdm16*), cytochrome *c* (*Cycs*), cytochrome *c* oxidase subunit 4i1 (*Cox4i1*), transcription factor A (*Tfam*) and nuclear respiratory factor 1 (*Nrf1*) in GWAT, SWAT and BAT from chow-fed WT and *Aldh1a1*$^{-/-}$ mice. Expression of all BAT marker genes was significantly increased in *Aldh1a1*-deficient GWAT, with *Nrf1* being the only exception (**Fig. 2c**). In contrast, expression of this same gene panel was either unchanged or only modestly increased in SWAT and BAT of *Aldh1a1*$^{-/-}$ versus WT mice (**Fig. 2c**). We next tested whether altered mitochondrial biogenesis might explain this increase in BAT marker expression in white fat. In GWAT, SWAT and BAT, mitochondrial DNA content was unchanged between genotypes (**Fig. 2d**). Electron microscopy of GWAT revealed no differences in mitochondrial density or ultrastructure (**Supplementary Fig. 1a**). These data indicate that *Aldh1a1* deficiency increases BAT marker expression in visceral WAT without altering mitochondrial biogenesis.

Aldh1a1 deficiency activates a thermogenic program in WAT

To test whether increased *Ucp1* expression in GWAT from *Aldh1a1*$^{-/-}$ mice altered GWAT function, we assayed mitochondrial activity using citrate synthase activity, the rate-limiting step of the tricarboxylic acid cycle[24,25]. Citrate synthase activity was significantly increased in GWAT but not BAT from *Aldh1a1*$^{-/-}$ versus WT mice (**Fig. 3a**). Increased mitochondrial uncoupling drives oxidative phosphorylation, enhancing cellular respiration[4]. Oxygen consumption rates were significantly higher in *Aldh1a1*-deficient GWAT (1.7-fold) but not BAT (**Fig. 3b**) as compared to those in WT mice.

As uncoupled respiration dissipates energy through heat production, we next measured core body temperature in WT versus *Aldh1a1*$^{-/-}$ mice at room temperature (23 °C) and during 48 h of cold exposure (4 °C). At 23 °C, body temperature did not differ between genotypes. At 4 °C, body temperatures of WT mice dropped significantly; in contrast, mice lacking *Aldh1a1* were completely protected against cold exposure (**Fig. 3c**). Consistent with these findings, cold exposure markedly increased *Ucp1* expression in *Aldh1a1*-deficient GWAT and, to a minor extent, in SWAT, with no evidence for genotypic differences in BAT (**Fig. 3d**,**e**). Cold exposure induced the emergence of BAT-like Ucp1-positive multilocular adipocytes in *Aldh1a1*-deficient WAT (**Fig. 3e**).

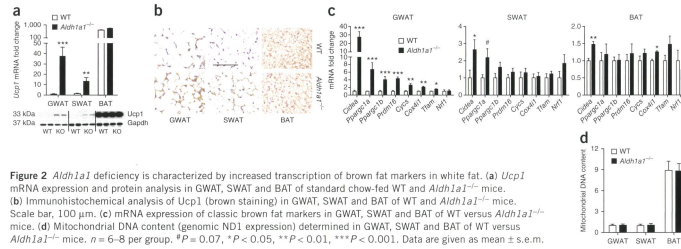

Figure 2 *Aldh1a1* deficiency is characterized by increased transcription of brown fat markers in white fat. (**a**) *Ucp1* mRNA expression and protein analysis in GWAT, SWAT and BAT of standard chow-fed WT and *Aldh1a1*$^{-/-}$ mice. (**b**) Immunohistochemical analysis of Ucp1 (brown staining) in GWAT, SWAT and BAT of WT and *Aldh1a1*$^{-/-}$ mice. Scale bar, 100 μm. (**c**) mRNA expression of classic brown fat markers in GWAT, SWAT and BAT of WT versus *Aldh1a1*$^{-/-}$ mice. (**d**) Mitochondrial DNA content (genomic ND1 expression) determined in GWAT, SWAT and BAT of WT versus *Aldh1a1*$^{-/-}$ mice. $n = 6$–8 per group. $^{\#}P = 0.07$, $^{*}P < 0.05$, $^{**}P < 0.01$, $^{***}P < 0.001$. Data are given as mean ± s.e.m.

We next asked whether altered adrenergic activation of BAT could have contributed to adaptive thermogenesis seen in *Aldh1a1* deficiency. Expression of β-adrenergic receptors (*Adrb1*, *Adrb2* and *Adrb3*) and the catecholamine-synthesizing enzyme tyrosine hydroxylase (*Th*) was unchanged in WT and *Aldh1a1*$^{-/-}$ BAT (**Supplementary Fig. 1b**,**c**). Likewise, baseline and isoproterenol-induced oxygen consumption in brown adipocytes and expression of BAT genes did not differ between genotypes (**Supplementary Fig. 1d**,**e**). These results argue for a role of Aldh1a1 in regulating uncoupled respiration and adaptive thermogenesis through effects in WAT but not BAT.

Rald promotes *Ucp1* transcription in white adipocytes

To investigate mechanisms for increased uncoupling in GWAT, we used chemical and targeted genetic approaches in mouse and human adipocyte models. The C3H10T1/2 (10T1/2) cell line is an established model of adipogenesis[26]. In undifferentiated 10T1/2 cells, *Aldh1a1* is not present but is robustly induced during adipogenesis (**Supplementary Fig. 2a**). Stimulation of 10T1/2 cells with the known Aldh inhibitor diethyl aminobenzaldehyde (DEAB, 1 μM)[27] during adipogenic differentiation significantly induced *Ucp1* gene and protein expression as compared to that in vehicle-treated cells (**Fig. 4a**). Similarly, stable repression of *Aldh1a1* mRNA in 10T1/2 cells by shRNA-expressing lentivirus (sh*Aldh1a1*, 80% knockdown without a compensatory increase in *Aldh1a2* or *Aldh1a3*; **Supplementary Fig. 2b**) induced *Ucp1* mRNA and protein fivefold as compared to lentiviral-treated control cells (shCtrl, **Fig. 4b**). Given that *Aldh1a1* deficiency increases endogenous Rald concentrations[16,23], we tested Rald as a *Ucp1* transcriptional regulator. Stimulation of 10T1/2 cells with all-*trans*-retinal (Rald, 1 μM) during adipogenic differentiation induced expression of *Ucp1* (100-fold) and other BAT markers including *Ppargc1b*, *Prdm16* and *Cidea*, whereas expression of the adipogenic genes peroxisome proliferator-activated receptor-γ (*Pparg*), fatty acid–binding protein 4 (*Fabp4*) and adiponectin (*Adipoq*) and lipid accumulation remained unaltered (**Fig. 4c** and **Supplementary Fig. 2c**,**d**). Similarly, Rald stimulation significantly

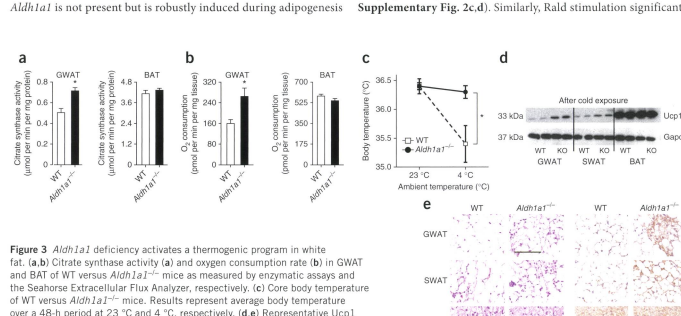

Figure 3 *Aldh1a1* deficiency activates a thermogenic program in white fat. (**a**,**b**) Citrate synthase activity (**a**) and oxygen consumption rate (**b**) in GWAT and BAT of WT versus *Aldh1a1*$^{-/-}$ mice as measured by enzymatic assays and the Seahorse Extracellular Flux Analyzer, respectively. (**c**) Core body temperature of WT versus *Aldh1a1*$^{-/-}$ mice. Results represent average body temperature over a 48-h period at 23 °C and 4 °C, respectively. (**d**,**e**) Representative Ucp1 western blot (**d**) and H&E and immunohistochemical Ucp1 staining (**e**) in GWAT, SWAT and BAT of WT versus *Aldh1a1*$^{-/-}$ (KO) mice after 48 h of cold stimulation. $n = 6$–8 per group, $^{*}P < 0.05$. Scale bar, 100 μm. Data are given as mean ± s.e.m.

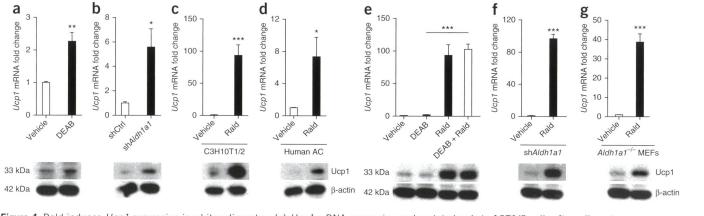

Figure 4 Rald induces *Ucp1* expression in white adipocytes. (**a**) *Ucp1* mRNA expression and protein levels in 10T1/2 cells after adipocyte differentiation in the presence or absence of the Aldh inhibitor DEAB (1 μM). (**b**) *Ucp1* mRNA and protein analysis in differentiated 10T1/2 cells stably transfected with scrambled (shCtrl) or *Aldh1a1*-targeting (sh*Aldh1a1*) shRNA. (**c**,**d**) *Ucp1* mRNA and protein analysis in 10T1/2 cells (**c**) and human stromal-vascular cells (**d**) from subcutaneous fat biopsies, differentiated into adipocytes in the presence or absence of Rald (1 μM). (**e**) *Ucp1* gene expression and protein content in differentiated 10T1/2 cells stimulated with DEAB (1 μM), Rald (1 μM) or both. (**f**,**g**) sh*Aldh1a1*-transfected 10T1/2 cells (**f**) and MEFs (**g**) isolated from *Aldh1a1*-deficient embryos were stimulated with Rald (1 μM) during adipogenic differentiation followed by *Ucp1* mRNA and protein analysis. $n = 5$ or 6 per condition, $^*P < 0.05$, $^{**}P < 0.01$, $^{***}P < 0.001$. Data are given as mean ± s.e.m.

increased *Ucp1* expression in differentiating human stromal-vascular cells from subcutaneous fat biopsies (**Fig. 4d**).

To test whether Rald conversion to retinoic acid accounted for the increased *Ucp1* expression seen, we studied Rald effects in three distinct *in vitro* models in which *Aldh1a1* expression or function was repressed or absent. Co-stimulation with Rald and the Aldh inhibitor DEAB increased *Ucp1* expression to the same extent as did Rald alone in differentiating 10T1/2 cells (**Fig. 4e**). Rald stimulation in sh*Aldh1a1*-treated 10T1/2 cells increased *Ucp1* mRNA and protein expression 100-fold (**Fig. 4f**), an effect similar to Rald stimulation of untransfected 10T1/2 cells (**Fig. 4c**). Finally, Rald stimulation (24 h) in *Aldh1a1*$^{-/-}$ mouse embryonic fibroblast (MEF)-derived adipocytes increased *Ucp1* gene expression 40-fold as compared to that in vehicle-treated cells (**Fig. 4g**). Together, these findings support Rald induction of *Ucp1* expression in white adipocytes independent of its conversion to retinoic acid.

Rald regulates *Ucp1* expression through RAR and PGC-1α

As retinoids regulate gene expression through retinoid receptor modulation, we next investigated retinoid receptor involvement in Rald effects on *Ucp1* expression. We stimulated differentiating 10T1/2 cells with Rald in the presence or absence of known antagonists to either RAR (AGN193109) or RXR (HX531)[28,29]. The RAR antagonist AGN193109 completely inhibited Rald-mediated expression of *Ucp1* and other BAT marker genes (*Ppargc1b*, *Prdm16* and *Cidea*), whereas HX531 did not alter *Ucp1* expression (**Fig. 5a** and **Supplementary Fig. 3a**,**b**). Notably, HX531 did significantly inhibit 9-*cis*-retinoic acid (9cisRA)-induced expression of the retinoic acid target gene *Cyp26a1*, verifying HX5131 as a functional RXR antagonist in this experimental model (**Supplementary Fig. 3c**). To further investigate RAR dependency through an alternative approach, we repeated 10T1/2 experiments in the presence of a validated siRNA to *Rara* (RARα), the main isoform expressed in these cells (data not shown) or control siRNA (siCtrl). Compared to siCtrl treatment, repression of *Rara* mRNA in 10T1/2 cells (60%, **Supplementary Fig. 3d**) significantly blunted Rald-mediated induction of *Ucp1* and additional BAT markers (*Ppargc1b*, *Prdm16* and *Cidea*) (**Fig. 5b** and **Supplementary Fig. 3e**,**f**). *Rxra* (RXRα) siRNA inhibited adipogenesis, resulting in extremely low *Ucp1* expression in all treatment groups (data not shown). Similar experiments in sh*Aldh1a1*-transfected 10T1/2 cells also showed that increased *Ucp1* expression was dependent on the presence of RAR but not RXR (**Fig. 5c**,**d** and **Supplementary Fig. 3g**).

To test *in vivo* whether the thermogenic phenotype observed in *Aldh1a1* deficiency is mediated through RAR, we injected *Aldh1a1*-deficient mice with the RAR antagonist AGN193109 (0.5 mg per kg of body weight per day, intraperitoneally (i.p.)) or vehicle for 2 weeks before cold exposure studies and *Ucp1* analysis. Core body temperature did not differ between groups at 23 °C ambient temperature. However, during cold exposure (4 °C), treatment of mice with RAR antagonist resulted in significantly lower body temperatures as compared to controls (**Fig. 5e**). Consistent with these temperature changes, AGN193109 treatment markedly reduced *Ucp1* expression in WAT but not in BAT (**Fig. 5f**), suggesting that the thermogenic program in *Aldh1a1* deficiency is RAR dependent.

Given these results, we next examined Rald interaction with RAR as a mechanism for increased *Ucp1* expression. PGC-1α is a transcriptional coactivator that induces *Ucp1* expression[30]. Using cell-free time-resolved fluorescence resonance energy transfer (TR-FRET) assays, we tested Rald-mediated recruitment of PGC-1α to either the RARα or RXRα ligand-binding domain (LBD). As expected, in response to their known natural ligands, all-*trans*–retinoic acid (ATRA) and 9cisRA potently recruited PGC-1α to RARα and RXRα, respectively. However, Rald alone also effectively recruited PGC-1α to RARα (half-maximal effective concentration (EC_{50}) 82 nM) but had virtually no effect on PGC-1α recruitment to RXRα in these cell-free assays, which lack the ability to convert Rald to retinoic acid (**Fig. 5g**). Stimulation with either ATRA or Rald significantly increased activity of a canonical retinoic acid response element (RARE) luciferase reporter in a concentration-dependent manner (**Fig. 5h**).

As the *Ucp1* promoter contains several RARE consensus sites[31], we examined whether Rald can directly activate a RARE-containing *Ucp1* promoter transfected into undifferentiated 10T1/2 cells, which lack retinoid-converting enzymes. Stimulation with cAMP (250 μM), a known *Ucp1* transcriptional activator[31], significantly increased *Ucp1* reporter activity (**Fig. 5i**). Notably, Rald and ATRA, but not their precursor retinol, increased luciferase activity in a

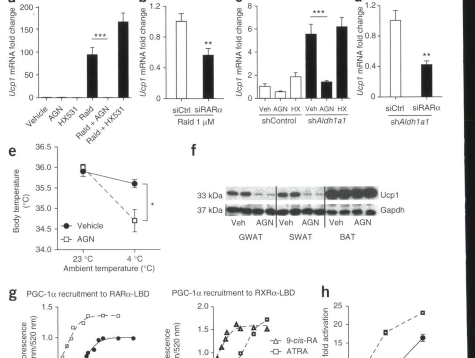

Figure 5 Rald-mediated *Ucp1* expression is RAR-dependent and involves PGC-1α recruitment. (**a**) *Ucp1* mRNA expression in 10T1/2 adipocytes stimulated with either the RAR antagonist AGN193109 (AGN), the RXR antagonist HX531, Rald (1 μM) or the combination of Rald + AGN or Rald + HX531 (each 1 μM). (**b**) *Ucp1* mRNA quantification in 10T1/2 adipocytes transiently transfected with scrambled (siCtrl) or *Rara* siRNA (siRARα) and stimulated with Rald (1 μM). (**c**) *Ucp1* mRNA quantification in shControl and sh*Aldh1a1*-transfected 10T1/2 adipocytes stimulated with AGN193109 or HX531 (both 1 μM). (**d**) *Ucp1* mRNA analysis in *Aldh1a1* knockdown 10T1/2 cells (sh*Aldh1a1*) transfected with siCtrl or siRARα. (**e**) Core body temperature in *Aldh1a1*$^{-/-}$ mice injected with the RAR antagonist AGN193109 or vehicle for 2 weeks. Results represent average body temperature over a 48-h period at 23 °C and 4 °C, respectively. (**f**) Western blot for Ucp1 in vehicle- and AGN-treated *Aldh1a1*$^{-/-}$ mice after cold exposure. (**g**) Ligand-dependent recruitment of PGC-1α to either the RARα-LBD or RXRα-LBD, respectively, as determined by cell-free TR-FRET assays. Dose-response curves for Rald, ATRA and 9-*cis*-retinoic acid (9-*cis*-RA) are shown. (**h**) Undifferentiated 10T1/2 cells, which lack Aldhs, were transfected with an RARE-luciferase construct (RARE-Luc) followed by stimulation (24 h) with increasing concentrations of Rald or ATRA and luciferase activity assays. (**i**) Undifferentiated 10T1/2 cells were transfected with a mouse 3.1-kb *Ucp1* promoter luciferase construct (*Ucp1*-Luc) and subsequently stimulated (24 h) with cAMP (250 μM), Rald, ATRA and retinol (each 1 μM). Normalized luciferase activities are shown as fold change. (**j**) RARα and PGC-1α recruitment to the *Ucp1* promoter region in Rald-stimulated (1 μM) 10T1/2 adipocytes analyzed by ChIP. Fold enrichment and a representative DNA gel pictures are given. $n = 5$ or 6 per condition, $^{*}P < 0.05$, $^{**}P < 0.01$, $^{***}P < 0.001$; Veh, vehicle. Data are given as mean ± s.e.m.

concentration-dependent manner (**Fig. 5i** and **Supplementary Fig. 3h**). Next, we used chromatin immunoprecipitation (ChIP) to study Rald-dependent transcription factor recruitment to the *Ucp1* promoter region in 10T1/2 cells. A robust RARα signal was present at the *Ucp1* promoter under basal conditions that did not increase further after Rald stimulation (**Fig. 5j**). The TR-FRET data above suggested that Rald may recruit PGC-1α to RARα already present on the *Ucp1* promoter. Indeed, similar ChIP studies showed that Rald stimulation enriched PGC-1α occupancy at the *Ucp1* promoter region five-fold (**Fig. 5j**). Taken together, these data suggest that Rald recruits PGC-1α to RARα at the *Ucp1* promoter, thus inducing *Ucp1* transcription.

Aldh1a1 antisense treatment induces a thermogenic porgam

To test whether acute, tissue-selective loss of Aldh1a1 *in vivo* alters *Ucp1* expression, thermogenesis and body weight, we injected a validated *Aldh1a1* antisense oligonucleotide (ASO) or a control ASO twice a week for 6 weeks (35 mg per kg of body weight per dose, i.p.) into C57BL/6J mice fed standard chow. The *Aldh1a1* ASO treatment significantly decreased *Aldh1a1* mRNA and protein levels selectively in liver and GWAT; *Aldh1a1* expression remained unchanged in SWAT, BAT, spleen, intestine and skeletal muscle as compared to treatment with control ASO (**Fig. 6a**,**b** and **Supplementary Fig. 4a**). *Aldh1a1* ASO treatment significantly increased *Ucp1* expression in GWAT but not SWAT or BAT (**Fig. 6c**,**d**). To test the functional impact of these effects, we measured core body temperature under ambient and cold-induced conditions. Core body temperature did not differ between mice treated with *Aldh1a1* ASO or control ASO at ambient temperature (23 °C). Exposure to 4 °C (48 h) decreased body temperature in mice treated with control ASO; in contrast, *Aldh1a1* ASO–treated mice were protected significantly against cold exposure (**Fig. 6e**).

To test whether GWAT-selective *Aldh1a1* repression could modulate established obesity, we fed C57BL/6J mice a high-fat diet for 8 weeks before treating them with *Aldh1a1* ASO and continuing the high-fat diet for an additional 9 weeks. *Aldh1a1* ASO treatment significantly limited weight gain in obese mice and decreased GWAT mass (**Fig. 6f**–**h**), resulting in improved insulin and glucose tolerance (**Fig. 6i** and **Supplementary Fig. 4b**), all as compared to a treatment

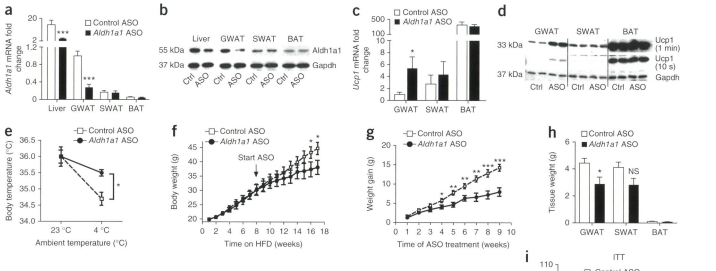

Figure 6 ASO-mediated *Aldh1a1* knockdown in GWAT promotes white-fat thermogenesis and limits diet-induced obesity. C57BL/6J mice on standard chow diet were injected with *Aldh1a1* ASO and control ASO (Ctrl ASO) for 6 weeks (two doses of 35 mg per kg of body weight per week, i.p., $n = 8$ per group). (**a**,**b**) *Aldh1a1* mRNA (**a**) and protein (**b**) expression in the indicated tissues of mice treated with *Aldh1a1* ASO or control ASO (Ctrl, Ctrl ASO; ASO, *Aldh1a1* ASO). (**c**,**d**) *Ucp1* mRNA (**c**) and protein (**d**) levels in GWAT, SWAT and BAT of mice treated with *Aldh1a1* ASO versus control ASO. (**e**) Core body temperature of mice treated with *Aldh1a1* ASO versus control ASO at 23 °C and at 4 °C over 48 h ($n = 6$ per group). (**f**–**i**) A cohort of C57BL/6J mice ($n = 16$) was fed a high-fat diet (HFD) for 8 weeks before initiation of *Aldh1a1* ASO or control ASO treatment ($n = 8$ per group), continued HFD, and measurement of body weight gain (**f**,**g**), fat depot mass (**h**) and insulin tolerance testing (at 17 weeks) (**i**). $^*P < 0.05$, $^{**}P < 0.01$, $^{***}P < 0.001$. Data are given as mean ± s.e.m. NS, not significant.

with control ASO. Thus, selective *Aldh1a1* repression in visceral fat confers induction of a thermogenic program that inhibits body weight gain and improves glucose homeostasis in obesity.

DISCUSSION

Understanding determinants of energy storage and utilization is crucial for addressing the epidemic of obesity and its complications. Energy dissipation through uncoupled respiration and increased thermogenesis are key components of energy balance. Promoting BAT or BAT-like characteristics may represent a therapeutic strategy for treating excess adiposity[32]. Despite this, activation of BAT differentiation and function remains poorly understood. Similarly, mechanisms that manipulate WAT to acquire BAT-like characteristics remain an alternative but even less well-characterized approach to enhancing energy expenditure and decreasing obesity[33].

Retinoids, and the enzymes that control retinoid formation, represent a complex, highly regulated system that controls fundamental biological processes, including fuel metabolism[15,17,21]. We previously reported that mice lacking *Aldh1a1*, the rate-limiting enzyme in Rald conversion to retinoic acid, show enhanced energy expenditure when fed a high-fat diet[16], suggesting that they have altered BAT activity. Here we report that *Aldh1a1* shows an adipose depot-specific expression pattern in mice fed a chow diet, with expression lowest in BAT and highest in visceral WAT. Moreover, genetic *Aldh1a1* deficiency increased expression of *Ucp1* and other classical BAT markers in mouse GWAT, with minimal changes in SWAT and BAT. *Aldh1a1* deficiency increased mitochondrial enzyme activity and oxygen consumption in GWAT, but not BAT, consistent with increased thermogenic capacity in white fat. Indeed, *Aldh1a1*$^{-/-}$ mice were completely resistant to cold exposure, establishing Aldh1a1 as a central regulator of WAT thermogenesis independent of BAT changes.

Other pathways that can induce brown-like transformation of white fat have been reported, although these mechanisms predominately altered subcutaneous fat, with the visceral depot considered less susceptible to acquiring BAT characteristics[34,35]. In GWAT of *Aldh1a1*$^{-/-}$ mice, the abundance of Ucp1-expressing unilocular white adipocytes under basal conditions and the increased presence of multilocular brown adipocytes after cold exposure suggest that *Aldh1a1* deficiency fosters thermogenic activation in visceral fat. This latent thermogenic potential of *Aldh1a1*-deficient visceral fat is unmasked in response to cold or high-fat feeding. Although the exact origins of BAT-like white adipocytes remains under debate, the lack of bona fide BAT cells, despite high *Ucp1* expression in *Aldh1a1*-deficient WAT at baseline, suggests 'browning' of white adipocytes rather than recruitment of BAT cells in this model. Our findings show that altered retinoid metabolism can promote functional plasticity of adipocytes, and identify Aldh1a1 as a previously unrecognized determinant of white versus brown fat transformation. This selective action of Aldh1a1 in GWAT may derive from the distinct expression pattern of this enzyme in different fat depots.

The effect of *Aldh1a1* deficiency on white versus brown characteristics in adipocyte seems to involve Rald's action as a transcriptional mediator that modulates retinoid receptor activity. Although other Aldh1a1 effects are difficult to exclude in contributing to the *in vivo* effects seen here, *Aldh1a1* deficiency is an established model of elevated endogenous Rald concentrations, especially in tissues with high *Aldh1a1* expression, such as WAT[16,23]. Rald can impair adipogenesis in 3T3-L1 cells and *in vivo* in response to high-fat feeding[16]. However, as studied here, in distinct pluripotent cell models and in the absence of the high-fat feeding, adipogenesis did not seem altered. We identify Rald as a positive transcriptional regulator of a classic BAT gene program including *Ucp1* in mouse and human

white adipocytes through RAR- but not RXR-dependent mechanisms. Rald recruited the coactivator PGC-1α to the *Ucp1* promoter in white adipocytes, a seminal event in BAT activation[30]. Those *in vitro* observations suggested that RAR activation might mediate the thermogenic phenotype in *Aldh1a1* deficiency. Indeed, *Aldh1a1*$^{-/-}$ mice treated with RAR antagonist had reduced Ucp1 expression in WAT and no longer manifested increased thermogenesis, consistent with RAR-dependent adaptive thermogenesis in this *in vivo* model. Previously, the RAR ligand retinoic acid has been shown to activate *Ucp1* transcription[31,36].

Our observation that Rald's effects on *Ucp1* transcription were similar in the presence or absence of the Rald-converting enzyme Aldh1a1 suggests Rald as a mediator in this model. In contrast to Rald, retinol failed to induce *Ucp1* promoter activity. The fact that both retinol and Rald can bind RAR in ligand-displacement assays[37], but only Rald activates *Ucp1* expression in these experimental models, argues for Rald-specific functional effects in WAT. Whether other Aldh1a1 effects or Ucp1-independent pathways might contribute to thermogenesis in *Aldh1a1* deficiency cannot be completely excluded. Similarly, the precise mechanisms through which Rald-RAR interaction potently induce a BAT-like thermogenic program in WAT warrants further investigation, but could include synergistic effects between Rald and retinoic acid, differential RXR and RAR modulation, or altered intracellular retinoid concentrations. In addition, intracellular or extracellular binding proteins, including retinol-binding protein-4 or cellular retinoic acid–binding protein II, which influence partitioning of retinoid ligands to specific nuclear receptors[38], may influence Rald effects. Indeed, we have previously observed reduced retinol-binding protein-4 plasma concentrations in *Aldh1a1*$^{-/-}$ mice[16], a pattern consistent with improved insulin sensitivity[39].

Dissipating energy stores by promoting thermogenic capacity in WAT has been proposed as an approach to treating obesity and its complications[33]. Although gene repression through antisense therapies has possible limitations[40], the impact of an *Aldh1a1* ASO on body-weight control and glucose metabolism in obese mice identifies Aldh1a1 as a therapeutic target. Although ASO-mediated reduction of hepatic *Aldh1a1* expression makes other effects, including altered glucose metabolism, difficult to exclude, selective *Aldh1a1* repression in GWAT through ASO treatment supports the prospect of specifically targeting visceral fat depots, including induction of BAT-like characteristics and thermogenesis.

Here we establish Aldh1a1 and its substrate Rald as previously unidentified determinants of functional plasticity in WAT that can activate a thermogenic program, promote energy dissipation and limit obesity. Disruption of Aldh1a1 expression or function in visceral fat could offer new opportunities in targeting and treating specific adipose depots and obesity-related complications.

METHODS

Methods and any associated references are available in the online version of the paper.

Note: Supplementary information is available in the online version of the paper.

ACKNOWLEDGMENTS

We thank H. Wang, G. Sukhova, E. Shvartz, T.A. Dang and V. Demchev for excellent technical support, R. Koza (Pennington Biomedical Research Center) for providing the *Ucp1* promoter luciferase construct, H. Kagechika (University of Tokyo) for providing HX531 and G. Duester (Burnham Medical Research Institute) for the *Aldh1a1*$^{-/-}$ mice and helpful discussions. This work was supported by the US National Institutes of Health grants HL048743, AR054604-03S1, 5P30DK057521-12 (J.P.); Mary K. Iacocca Professorship DK082659 and the National Institute of Diabetes and Digestive and Kidney Diseases DK056626 (C.R.K.); DK048873 and DK048873-14S2 (D.E.C.); the Austrian Science Fund (FWF): J3107-B19 (F.W.K.).

AUTHOR CONTRIBUTIONS

F.W.K. and J.P. designed the study; F.W.K., C.V., P.O., S.S., J.D.B., S.N. and M.Z. researched data; F.W.K. wrote the manuscript; C.V., J.D.B., S.N., M.Z., T.M.S., D.E.C., C.R.K. and J.P. reviewed the manuscript; D.E.C. and C.R.K. contributed to discussion.

COMPETING FINANCIAL INTERESTS

The authors declare no competing financial interests.

Published online at http://www.nature.com/doifinder/10.1038/nm.2757.
Reprints and permissions information is available online at http://www.nature.com/reprints/index.html.

1. Mensah, G.A. *et al.* Obesity, metabolic syndrome, and type 2 diabetes: emerging epidemics and their cardiovascular implications. *Cardiol. Clin.* **22**, 485–504 (2004).
2. Bray, G.A. & Bellanger, T. Epidemiology, trends, and morbidities of obesity and the metabolic syndrome. *Endocrine* **29**, 109–117 (2006).
3. Klein, S. *et al.* Waist circumference and cardiometabolic risk: a consensus statement from shaping America's health: Association for Weight Management and Obesity Prevention; NAASO, the Obesity Society; the American Society for Nutrition; and the American Diabetes Association. *Diabetes Care* **30**, 1647–1652 (2007).
4. Cannon, B. & Nedergaard, J. Brown adipose tissue: function and physiological significance. *Physiol. Rev.* **84**, 277–359 (2004).
5. Farmer, S.R. Molecular determinants of brown adipocyte formation and function. *Genes Dev.* **22**, 1269–1275 (2008).
6. Seale, P., Kajimura, S. & Spiegelman, B.M. Transcriptional control of brown adipocyte development and physiological function—of mice and men. *Genes Dev.* **23**, 788–797 (2009).
7. Cypess, A.M. *et al.* Identification and importance of brown adipose tissue in adult humans. *N. Engl. J. Med.* **360**, 1509–1517 (2009).
8. Tseng, Y.H. *et al.* New role of bone morphogenetic protein 7 in brown adipogenesis and energy expenditure. *Nature* **454**, 1000–1004 (2008).
9. Seale, P. *et al.* PRDM16 controls a brown fat/skeletal muscle switch. *Nature* **454**, 961–967 (2008).
10. Vegiopoulos, A. *et al.* Cyclooxygenase-2 controls energy homeostasis in mice by de novo recruitment of brown adipocytes. *Science* **328**, 1158–1161 (2010).
11. Hansen, J.B. *et al.* Retinoblastoma protein functions as a molecular switch determining white versus brown adipocyte differentiation. *Proc. Natl. Acad. Sci. USA* **101**, 4112–4117 (2004).
12. Fang, S. *et al.* Corepressor SMRT promotes oxidative phosphorylation in adipose tissue and protects against diet-induced obesity and insulin resistance. *Proc. Natl. Acad. Sci. USA* **108**, 3412–3417 (2011).
13. Cinti, S. Between brown and white: novel aspects of adipocyte differentiation. *Ann. Med.* **43**, 104–115 (2011).
14. Park, K.W., Halperin, D.S. & Tontonoz, P. Before they were fat: adipocyte progenitors. *Cell Metab.* **8**, 454–457 (2008).
15. Schwarz, E.J., Reginato, M.J., Shao, D., Krakow, S.L. & Lazar, M.A. Retinoic acid blocks adipogenesis by inhibiting C/EBPβ-mediated transcription. *Mol. Cell. Biol.* **17**, 1552–1561 (1997).
16. Ziouzenkova, O. *et al.* Retinaldehyde represses adipogenesis and diet-induced obesity. *Nat. Med.* **13**, 695–702 (2007).
17. Kane, M.A. *et al.* Crbp1 modulates glucose homeostasis and pancreas 9-*cis*-retinoic acid concentrations. *Mol. Cell. Biol.* **31**, 3277–3285 (2011).
18. Altucci, L., Leibowitz, M.D., Ogilvie, K.M., de Lera, A.R. & Gronemeyer, H. RAR and RXR modulation in cancer and metabolic disease. *Nat. Rev. Drug Discov.* **6**, 793–810 (2007).
19. Villarroya, F., Iglesias, R. & Giralt, M. Retinoids and retinoid receptors in the control of energy balance: novel pharmacological strategies in obesity and diabetes. *Curr. Med. Chem.* **11**, 795–805 (2004).
20. Ross, A.C. Overview of retinoid metabolism. *J. Nutr.* **123**, 346–350 (1993).
21. Ziouzenkova, O. & Plutzky, J. Retinoid metabolism and nuclear receptor responses: New insights into coordinated regulation of the PPAR-RXR complex. *FEBS Lett.* **582**, 32–38 (2008).
22. Duester, G., Mic, F.A. & Molotkov, A. Cytosolic retinoid dehydrogenases govern ubiquitous metabolism of retinol to retinaldehyde followed by tissue-specific metabolism to retinoic acid. *Chem. Biol. Interact.* **143–144**, 201–210 (2003).
23. Molotkov, A. & Duester, G. Genetic evidence that retinaldehyde dehydrogenase Raldh1 (*Aldh1a1*) functions downstream of alcohol dehydrogenase Adh1 in metabolism of retinol to retinoic acid. *J. Biol. Chem.* **278**, 36085–36090 (2003).
24. Wiegand, G. & Remington, S.J. Citrate synthase: structure, control, and mechanism. *Annu. Rev. Biophys. Biophys. Chem.* **15**, 97–117 (1986).

25. Trounce, I.A., Kim, Y.L., Jun, A.S. & Wallace, D.C. Assessment of mitochondrial oxidative phosphorylation in patient muscle biopsies, lymphoblasts, and transmitochondrial cell lines. *Methods Enzymol.* **264**, 484–509 (1996).
26. Tang, Q.Q., Otto, T.C. & Lane, M.D. Commitment of C3H10T1/2 pluripotent stem cells to the adipocyte lineage. *Proc. Natl. Acad. Sci. USA* **101**, 9607–9611 (2004).
27. Chute, J.P. *et al.* Inhibition of aldehyde dehydrogenase and retinoid signaling induces the expansion of human hematopoietic stem cells. *Proc. Natl. Acad. Sci. USA* **103**, 11707–11712 (2006).
28. Johnson, A.T., Wang, L., Gillett, S.J. & Chandraratna, R.A. High affinity retinoic acid receptor antagonists: analogs of AGN 193109. *Bioorg. Med. Chem. Lett.* **9**, 573–576 (1999).
29. Takahashi, B. *et al.* Novel retinoid X receptor antagonists: specific inhibition of retinoid synergism in RXR-RAR heterodimer actions. *J. Med. Chem.* **45**, 3327–3330 (2002).
30. Puigserver, P. *et al.* A cold-inducible coactivator of nuclear receptors linked to adaptive thermogenesis. *Cell* **92**, 829–839 (1998).
31. Alvarez, R. *et al.* A novel regulatory pathway of brown fat thermogenesis. Retinoic acid is a transcriptional activator of the mitochondrial uncoupling protein gene. *J. Biol. Chem.* **270**, 5666–5673 (1995).
32. Cypess, A.M. & Kahn, C.R. Brown fat as a therapy for obesity and diabetes. *Curr. Opin. Endocrinol. Diabetes Obes.* **17**, 143–149 (2010).
33. Langin, D. Recruitment of brown fat and conversion of white into brown adipocytes: strategies to fight the metabolic complications of obesity? *Biochim. Biophys. Acta* **1801**, 372–376 (2010).
34. Guerra, C., Koza, R.A., Yamashita, H., Walsh, K. & Kozak, L.P. Emergence of brown adipocytes in white fat in mice is under genetic control. Effects on body weight and adiposity. *J. Clin. Invest.* **102**, 412–420 (1998).
35. Seale, P. *et al.* Prdm16 determines the thermogenic program of subcutaneous white adipose tissue in mice. *J. Clin. Invest.* **121**, 96–105 (2011).
36. Silva, J.E. & Rabelo, R. Regulation of the uncoupling protein gene expression. *Eur. J. Endocrinol.* **136**, 251–264 (1997).
37. Repa, J.J., Hanson, K.K. & Clagett-Dame, M. All-*trans*-retinol is a ligand for the retinoic acid receptors. *Proc. Natl. Acad. Sci. USA* **90**, 7293–7297 (1993).
38. Schug, T.T., Berry, D.C., Shaw, N.S., Travis, S.N. & Noy, N. Opposing effects of retinoic acid on cell growth result from alternate activation of two different nuclear receptors. *Cell* **129**, 723–733 (2007).
39. Serum retinol binding protein 4 contributes to insulin resistance in obesity and type 2 diabetes. Yang, Q. *et al. Nature* **436**, 356–362 (2005).
40. Crooke, S.T. Progress in antisense technology. *Annu. Rev. Med.* **55**, 61–95 (2004).

nature medicine

Methylglyoxal modification of $Na_V1.8$ facilitates nociceptive neuron firing and causes hyperalgesia in diabetic neuropathy

Angelika Bierhaus[1,20], Thomas Fleming[1,20], Stoyan Stoyanov[1], Andreas Leffler[2,3], Alexandru Babes[4,5], Cristian Neacsu[5], Susanne K Sauer[4], Mirjam Eberhardt[4], Martina Schnölzer[6], Felix Lasischka[7], Winfried L Neuhuber[4], Tatjana I Kichko[4], Ilze Konrade[1,8], Ralf Elvert[9], Walter Mier[10], Valdis Pirags[11], Ivan K Lukic[1,12], Michael Morcos[1], Thomas Dehmer[13], Naila Rabbani[14], Paul J Thornalley[14], Diane Edelstein[15], Carla Nau[3], Josephine Forbes[16], Per M Humpert[1], Markus Schwaninger[17], Dan Ziegler[18], David M Stern[19], Mark E Cooper[16], Uwe Haberkorn[10], Michael Brownlee[15,20], Peter W Reeh[4] & Peter P Nawroth[1]

This study establishes a mechanism for metabolic hyperalgesia based on the glycolytic metabolite methylglyoxal. We found that concentrations of plasma methylglyoxal above 600 nM discriminate between diabetes-affected individuals with pain and those without pain. Methylglyoxal depolarizes sensory neurons and induces post-translational modifications of the voltage-gated sodium channel $Na_V1.8$, which are associated with increased electrical excitability and facilitated firing of nociceptive neurons, whereas it promotes the slow inactivation of $Na_V1.7$. In mice, treatment with methylglyoxal reduces nerve conduction velocity, facilitates neurosecretion of calcitonin gene-related peptide, increases cyclooxygenase-2 (COX-2) expression and evokes thermal and mechanical hyperalgesia. This hyperalgesia is reflected by increased blood flow in brain regions that are involved in pain processing. We also found similar changes in streptozotocin-induced and genetic mouse models of diabetes but not in $Na_V1.8$ knockout (*Scn10a*$^{-/-}$) mice. Several strategies that include a methylglyoxal scavenger are effective in reducing methylglyoxal- and diabetes-induced hyperalgesia. This previously undescribed concept of metabolically driven hyperalgesia provides a new basis for the design of therapeutic interventions for painful diabetic neuropathy.

Pain and hyperalgesia are key danger signals that are evoked by physical insults, noxious chemicals and inflammation. Such danger signals are also present in patients with diabetic neuropathy despite losses in sensory and autonomic functions in these individuals. Whereas the molecular mechanisms underlying inflammatory hyperalgesia are increasingly being unraveled, there is currently only a vague understanding of the mechanisms causing neuropathic pain in metabolic diseases such as diabetes[1]. In general, hyperglycemia has been emphasized as a major risk factor in these diseases; however, normalization of glucose concentrations has shown little benefit in affected individuals[1–3].

Elevated glucose concentrations lead to increased formation of the highly reactive dicarbonyl metabolite methylglyoxal[4], which is metabolized by glyoxalase 1 (GLO1) and GLO2 to the end product D-lactate[4–7]. As peripheral nerves have low GLO1 activity[8,9], it has been reasoned that they might be particularly vulnerable to methylglyoxal accumulation. As has been shown in the model organism *Caenorhabditis elegans*, the glyoxalase system is essential for neuronal integrity[10]. A recent study comparing the expression of GLO1 in various inbred mouse strains showed a negative correlation between GLO1 expression and mechanical hyperalgesia, implying that the balance between methylglyoxal and GLO1 might directly modulate pain perception[9].

Increased electrical excitability seems to be the underlying cause of the generation of orthotopic or ectopic impulses in experimental rat

[1]Department of Medicine I and Clinical Chemistry, University Hospital Heidelberg, Heidelberg, Germany. [2]Department of Anesthesiology and Intensive Care, Hannover Medical School, Hannover, Germany. [3]Department of Anesthesiology, Friedrich-Alexander-University Erlangen-Nuremberg, Erlangen, Germany. [4]Institute of Physiology and Pathophysiology, Friedrich-Alexander-University Erlangen-Nuremberg, Erlangen, Germany. [5]Department of Physiology and Biophysics, Faculty of Biology, University of Bucharest, Bucharest, Romania. [6]Functional Proteome Analysis B100, Core Facility Protein Analysis W120, German Cancer Research Center, Heidelberg, Germany. [7]Institute of Pathology, University Hospital Heidelberg, Heidelberg, Germany. [8]Stradins University, Riga Eastern Clinical University Hospital, Riga, Latvia. [9]Sanofi-Aventis Deutschland, Frankfurt, Germany. [10]Department of Nuclear Medicine, University Hospital Heidelberg, Heidelberg, Germany. [11]University of Latvia, Pauls Stradins Clinical University Hospital, Riga, Latvia. [12]Biosistemi d.o.o., Zagreb, Croatia. [13]Zentrum für Psychiatrie Südwürttemberg, Zwiefalten, Germany. [14]Warwick Medical School, Clinical Sciences Research Institute, University of Warwick, University Hospital, Coventry, UK. [15]Albert Einstein College of Medicine, Bronx, New York, USA. [16]Baker International Diabetes Institute, Heart and Diabetes Institute, Melbourne, Victoria, Australia. [17]Institute for Experimental und Clinical Pharmacology and Toxicology, University of Lübeck, Lübeck, Germany. [18]Institute for Clinical Diabetology, German Diabetes Center at the Heinrich Heine University Leibniz Center For Diabetes Research, Düsseldorf, Germany. [19]University of Tennessee College of Medicine, Memphis, Tennessee, USA. [20]These authors contributed equally to this work. Correspondence should be addressed to P.P.N. (peter.nawroth@med.uni-heidelberg.de).

Received 30 November 2011; accepted 22 March 2012; published online 13 May 2012; doi:10.1038/nm.2750

and human diabetic neuropathy[11,12]. Reduced potassium conductance and reduced Na^+/K^+ ATPase activity in diabetic nerves have been proposed as possible causes of increased excitability[12–14], but changes in neuronal voltage-gated sodium channels (VGSCs), which trigger, shape and propagate action potentials, could also directly explain the increased excitability. The effect of diabetes on VGSC gene expression has yielded results with some discrepancies that cannot account for the coexistence of positive and negative symptoms in diabetic neuropathy[15–17]. One particular VGSC, tetrodotoxin-resistant (TTXr) $Na_v1.8$, is exclusively expressed in pain-signaling neurons or nociceptors[18,19]; however, $Na_v1.8$ transcription and expression are decreased in diabetic rats[15,16] with increased TTXr sodium currents[16–20]. These seemingly contradictory findings led to a hypothesis that post-translational modifications in $Na_v1.8$ by methylglyoxal could increase either voltage sensitivity or functional channel availability, causing the hyperexcitability that is responsible for diabetic hyperalgesia and spontaneous pain.

In this study, we show that increased concentrations of methylglyoxal may account for metabolic hyperalgesia. The link between hyperalgesia and methylglyoxal is provided by nonenzymatic modifications of $Na_v1.8$, which, in turn, modify its function. Our data provide evidence for a previously unidentified pathway in which methylglyoxal directly induces hyperalgesia and may provide new therapeutic options for the treatment of painful metabolic neuropathy.

RESULTS

We found that plasma methylglyoxal discriminated patients with type 2 diabetes from healthy controls (**Fig. 1a**). Assessment of pain, determined by self report in the foot and graded on a ten point numerical scale, showed that the patients with diabetes could be subdivided into two groups: those with no pain and those with pain. Patients were considered to have pain when they reported more than seven points on the numeric scale. The mean pain scores for the two groups were 1.7 ± 1.2 and 7.7 ± 1.0 (mean ± s.e.m.) (for those with no pain and those with pain, respectively). Patients with pain also reported significantly more burning sensations and had a trend towards increased dysesthesia (**Fig. 1b**). The groups did not differ significantly in their neuropathy deficit score or in a range of metabolic variables (**Supplementary Table 1**). We subsequently found that diabetes-affected individuals with pain had significantly higher concentrations of plasma methylglyoxal (≥600 nM) compared to either healthy controls or diabetes-affected individuals with no pain (**Fig. 1a**), which is consistent with recent observations in patients with type 1 diabetes[21]. To establish whether these elevated concentrations of methylglyoxal could affect neuronal function, we exposed cultured mouse dorsal root ganglion (DRG) neurons from healthy wild-type (WT) mice to plasma from either healthy controls or diabetes-affected individuals with or without pain. We determined the induction of COX-2 as an indirect readout for altered neuronal function. Plasma from patients with pain induced significantly more COX-2 transcription in the neurons than plasma from controls or patients with no pain (**Fig. 1c**). Treatment with trypsin of the plasma from patients with pain did not prevent COX-2 expression in the neurons. The supplementation with exogenous methylglyoxal of plasma isolated from individuals with diabetes without pain to elevate the concentrations to those observed in patients with pain (≥ 600 nM) resulted in further increases in COX-2 transcription in the neuron (**Supplementary Fig. 1b**). As the activity of GLO1 is low in peripheral nerves and is even lower in peripheral nerves of diabetic mice[8,9] (**Fig. 1d**), we reasoned that neurons might be particularly likely to accumulate methylglyoxal.

Inhibition of GLO1 (ref. 22) by the cell-permeable inhibitor s-p-bromobenzylglutathione cyclopentyl diester in nondiabetic WT mice resulted in profound thermal hyperalgesia when the methylglyoxal plasma concentrations exceeded 600 nM (**Fig. 2a**). WT mice in which we induced diabetes with streptozotocin (STZ-induced diabetic WT mice) (8-week duration) showed a pronounced latency reduction in noxious heat withdrawal (**Fig. 2b**). Nondiabetic GLO1 knockdown ($Glo1^{-/+}$) mice[23] showed an equally pronounced latency reduction compared to STZ-induced diabetic WT mice. STZ-induction of diabetes in $Glo1^{-/+}$ mice (8-week

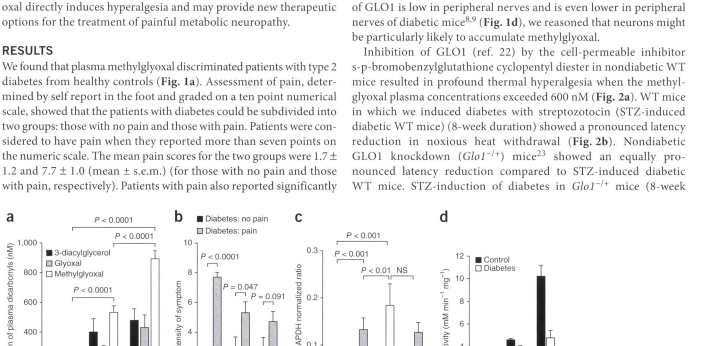

Figure 1 Methylglyoxal and pain in individuals with diabetes. (**a**) Plasma dicarbonyl concentrations in the patients with type 2 diabetes characterized in **Supplementary Table 1** with and without pain. Data represent the mean ± s.e.m. $n = 10$ patients per group (comparisons were made using analysis of variance (ANOVA)). (**b**) Intensity of neuropathy symptoms in the studied diabetes-affected individuals with and without pain as assessed by self report in the foot and graded on a ten point numerical scale. Data represent the mean ± s.e.m. $n = 10$ patients per group (unpaired, two-tailed Student's t test). (**c**) Quantification of COX-2 mRNA expression in DRGs isolated from healthy C57BL/6 WT mice treated with heat-inactivated plasma from healthy subjects (controls) or diabetes-affected individuals with and without pain. Where indicated, plasma samples from patients with diabetes and pain were pretreated with trypsin and neutralized using Soybean inhibitor. Data represent the mean of three independent experiments performed in triplicates ± s.d. $n = 3$ mice per group. GAPDH, glyceraldehyde-3-phosphate dehydrogenase; NS, not significant (unpaired, two-tailed Student's t test). (**d**) Organ survey for GLO1 activity in tissue extracts from healthy and STZ-induced diabetic WT mice. Data represent the mean ± s.d. $n = 10$ mice per group.

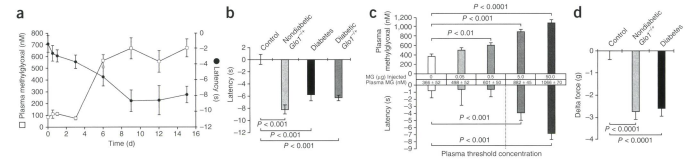

Figure 2 Exogenous methylglyoxal (MG) and STZ-induced diabetes induce thermal hyperalgesia. (**a**) Inhibition of GLO1 by the cell-permeable inhibitor S-p-bromobenzylglutathione cyclopentyl diester in healthy WT mice. Hyperalgesia was assessed by Hot Plate assay at day 0 before application of the inhibitor. Consecutive assessments of methylglyoxal plasma concentrations and thermal hyperalgesia were made at selected time points. Data represent the mean ± s.d. $n = 3$ mice per time point. (**b**) Thermal hyperalgesia in nondiabetic WT and GLO1 knockdown ($Glo1^{-/+}$) mice and diabetic WT mice 8 weeks after STZ-induced diabetes, as measured by Hot Plate assay. Data represent the mean ± s.e.m. $n = 20$–25 mice per group (ANOVA). (**c**) Responses to heat stimulation by Hot Plate assay in methylglyoxal-treated WT mice. Plasma was isolated for methylglyoxal analysis by HPLC. Data represent the mean ± s.d. ($n = 3$ mice per group) for methylglyoxal plasma concentrations and the mean ± s.e.m. ($n = 10$ mice per group) for hyperalgesia determination (ANOVA). (**d**) Mechanical hyperalgesia (tactile allodynia) in nondiabetic WT and $Glo1^{-/+}$ mice and STZ-induced diabetic WT mice, as determined by Frey filament test. Data represent the mean ± s.e.m. $n = 10$ mice per group (ANOVA).

duration) had no further sensitizing effect. Systemic administration of methylglyoxal resulted in an increase in methylglyoxal plasma concentrations and a dose-dependent thermal hyperalgesia response within 3 h of administration (**Fig. 2c** and **Supplementary Fig. 2a–c**). The methylglyoxal-induced sensitization to noxious heat was obscured when the hot plate temperature applied was 55 °C rather than 50 °C, implying that methylglyoxal lowered the heat threshold but did not disable the nocifensive response (**Supplementary Fig. 2d**). Diabetes, GLO1 deficiency and systemic methylglyoxal administration also induced pronounced mechanical hyperalgesia (**Fig. 2d** and **Supplementary Fig. 2e**).

Increased concentrations of methylglyoxal in diabetic mice are caused, in part, by reduced GLO1 transcription, expression and activity (**Supplementary Fig. 3a–c**). We achieved fully comparable results to those in the STZ-induced diabetic WT mice when we studied methylglyoxal concentrations in spontaneously diabetic BKS db/db mice[24] (**Supplementary Fig. 4**). The observed robust thermal and mechanical hyperalgesia in the STZ-induced diabetic WT mice after 8 weeks of hyperglycemia occurs at a time in which nonspecific STZ-derived inflammatory processes have dispersed[24] and no gross morphological changes in peripheral nerves are present on the ultrastructural level (data not shown). In STZ-induced diabetic WT mice, we found an induction of COX-2 immunoreactivity in the hindpaw epidermis (**Supplementary Fig. 3d**), which is consistent with the COX-2–inducing effect of patient plasma on DRG neurons (**Fig. 1c** and **Supplementary Fig. 1b**) and with excessive prostaglandin formation in diabetic rat skin[18]. Thus, non-neuronal and neuronal induction of COX-2, a marker of cellular activation and a producer of sensitizing eicosanoids[18], may be driven by increased concentrations of methylglyoxal.

Overexpression of GLO1 in STZ-induced diabetic WT mice (8-week duration) by somatic gene transfer resulted in an increase in sciatic GLO1 activity, decreased plasma methylglyoxal concentrations and reduced thermal hyperalgesia (**Fig. 3a–c**). This effect

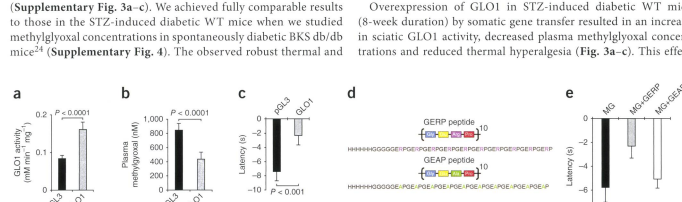

Figure 3 Overexpressing GLO1 or scavenging methylglyoxal by a synthetic peptide reduces thermal hyperalgesia in methylglyoxal-treated and diabetic mice. STZ-induced diabetic mice were treated every 2 d for 10 d with either GLO1-overexpressing vector (GLO1) or control vector (pGL3). (**a**) GLO1 activity in sciatic nerve tissue. Data represent the mean ± s.d. $n = 5$ mice per group (unpaired, two-tailed Student's t test). (**b**) Plasma methylglyoxal concentrations. Data represent the mean ± s.e.m. $n = 10$ mice per group (unpaired, two-tailed Student's t test). (**c**) Thermal hyperalgesia after 10 d of treatment with the GLO1-overexpressing vector by intravenous injection into the tail vein. Data represent the mean ± s.e.m. $n = 10$ mice per group (unpaired, two-tailed Student's t test). (**d**) A synthetic peptide, $GERP_{10}$ (GERP), was designed containing ten arginine residues per molecule to act as an effective *in vivo* scavenger of methylglyoxal. The peptide $GEAP_{10}$ (GEAP) served as an arginine-free control. (**e**) Healthy WT mice were injected with GERP or the control peptide GEAP before injection of methylglyoxal. Hyperalgesia was assessed 3 h after methylglyoxal injection by Hot Plate assay. Data represent the mean ± s.e.m. $n = 10$ mice per group (ANOVA). (**f**) The effects of GERP and GEAP on diabetes-induced hyperalgesia in STZ-induced diabetic WT mice. Data represent the mean ± s.e.m. $n = 10$ mice per group (ANOVA).

was independent of the pathway involving the advanced glycation endproducts (AGEs) and their receptor (the AGE-RAGE pathway), as systemic administration of carboxymethyl-lysine (800 nM, 3 h) did not induce thermal hyperalgesia (data not shown). Further, injection of methylglyoxal (5 μg, 3 h) into RAGE knockout (*Ager*$^{-/-}$) mice caused thermal hyperalgesia that was indistinguishable from that observed in the STZ-induced diabetic WT mice (data not shown). In contrast, treatment with either aminoguanidine, a scavenger of free methylglyoxal, or alagebrium (ALT-711), a compound that breaks AGE-derived crosslinks in proteins, inhibited methylglyoxal-induced hyperalgesia in methylglyoxal-treated WT mice (**Supplementary Fig. 5**), implying that *de novo* post-translational modifications of membrane proteins are responsible for the increased sensitivity and excitability of primary sensory neurons in these mice. To scavenge excessive concentrations of methylglyoxal *in vivo*, we designed an arginine-rich peptide ($GERP_{10}$) and a control peptide devoid of arginine ($GEAP_{10}$) (**Fig. 3d**). Systemic administration of $GERP_{10}$ reduced thermal hyperalgesia in both methylglyoxal-treated WT mice (**Fig. 3e**) and STZ-induced diabetic WT mice (**Fig. 3f**), with a half-life of approximately 80 h, whereas systemic administration of $GEAP_{10}$ had no effect in either of these groups.

To identify a possible protein target of post-translational modifications by methylglyoxal, we determined the expression of VGSCs in DRGs. Transient receptor potential V1 (TRPV1) and COX-2 expression served as positive controls for DRG expression[25,26]. Expression of $Na_V1.7$ and $Na_V1.9$ did not differ between the DRGs from nondiabetic WT and STZ-induced diabetic WT mice, whereas $Na_V1.8$ expression was slightly lower, but not significantly lower, in the STZ-induced diabetic WT mice compared to the nondiabetic WT mice[15,16] (**Fig. 4a**). Methylglyoxal-induced modifications of arginine residue(s) within the DIII-DIV linker of $Na_V1.8$ (comprising its inactivation gate) might alter the gating properties of $Na_V1.8$. Immunoprecipitations of DRGs isolated from rats treated with methylglyoxal, healthy WT mice treated with methylglyoxal, STZ-induced diabetic WT mice (8-week duration) and healthy *Glo1*$^{-/+}$ mice showed that modifications of $Na_V1.8$ by methylglyoxal were increased in the presence of

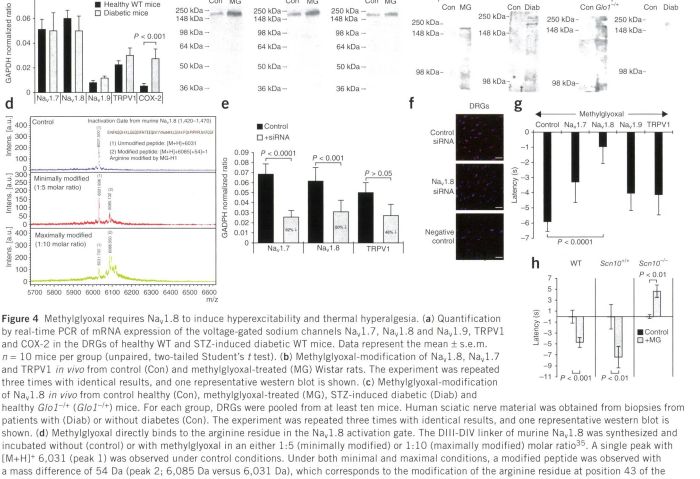

Figure 4 Methylglyoxal requires $Na_V1.8$ to induce hyperexcitability and thermal hyperalgesia. (**a**) Quantification by real-time PCR of mRNA expression of the voltage-gated sodium channels $Na_V1.7$, $Na_V1.8$ and $Na_V1.9$, TRPV1 and COX-2 in the DRGs of healthy WT and STZ-induced diabetic WT mice. Data represent the mean ± s.e.m. $n = 10$ mice per group (unpaired, two-tailed Student's t test). (**b**) Methylglyoxal-modification of $Na_V1.8$, $Na_V1.7$ and TRPV1 *in vivo* from control (Con) and methylglyoxal-treated (MG) Wistar rats. The experiment was repeated three times with identical results, and one representative western blot is shown. (**c**) Methylglyoxal-modification of $Na_V1.8$ *in vivo* from control healthy (Con), methylglyoxal-treated (MG), STZ-induced diabetic (Diab) and healthy *Glo1*$^{-/+}$ (*Glo1*$^{-/+}$) mice. For each group, DRGs were pooled from at least ten mice. Human sciatic nerve material was obtained from biopsies from patients with (Diab) or without diabetes (Con). The experiment was repeated three times with identical results, and one representative western blot is shown. (**d**) Methylglyoxal directly binds to the arginine residue in the $Na_V1.8$ activation gate. The DIII-DIV linker of murine $Na_V1.8$ was synthesized and incubated without (control) or with methylglyoxal in an either 1:5 (minimally modified) or 1:10 (maximally modified) molar ratio[35]. A single peak with $(M+H)^+$ 6,031 (peak 1) was observed under control conditions. Under both minimal and maximal conditions, a modified peptide was observed with a mass difference of 54 Da (peak 2; 6,085 Da versus 6,031 Da), which corresponds to the modification of the arginine residue at position 43 of the peptide by methylglyoxal to form the hydroimidazolone MG-H1. (**e**) Effects of *in vivo* siRNA treatment on the expression of $Na_V1.7$, $Na_V1.8$ and TRPV1 in healthy WT DRGs, as determined by real-time PCR. Data represent the mean ± s.d. $n = 3$ mice per group (unpaired, two-tailed Student's t test). (**f**) Effects of *in vivo* siRNA treatment for $Na_V1.8$ in healthy WT DRGs, as determined by immunocytochemistry. The experiment was repeated three times with identical results, and one representative staining is shown. Scale bars, 50 μm. (**g**) Effect of *in vivo* siRNA treatment for $Na_V1.7$, $Na_V1.8$ and $Na_V1.9$ on methylglyoxal-induced thermal hyperalgesia in mice. Data represent the mean ± s.e.m. $n = 10$ mice per group (unpaired, two-tailed Student's t test). (**h**) Effect of exogenous methylglyoxal on hyperalgesia in healthy WT mice, WT littermates of the $Na_V1.8$ knockout mice (*Scn10a*$^{+/+}$) and $Na_V1.8$ knockout mice (*Scn10a*$^{-/-}$). Data represent the mean ± s.d. $n = 5$ or 6 mice per group (unpaired, two-tailed Student's t test).

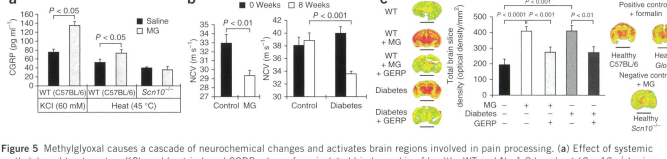

Figure 5 Methylglyoxal causes a cascade of neurochemical changes and activates brain regions involved in pain processing. (**a**) Effect of systemic methylglyoxal treatment on KCl- and heat-induced CGRP release from isolated hindpaw skin of healthy WT and $Na_V1.8$ knockout (*Scn10a*$^{-/-}$) mice after systemic methylglyoxal pretreatment. Data represent the mean ± s.e.m (two-tailed Student's *t* test). (**b**) Maximal dorsal tail NCV determined in healthy WT mice untreated (control) or pretreated with methylglyoxal ($n = 7$ mice in each group) and in healthy WT (control) and STZ-induced diabetic WT mice (diabetes) ($n = 12$ mice in each group). Data represent the mean ± s.d. (unpaired, two-tailed Student's *t* test). (**c**) CBF changes show increased brain activity. Sample colorized coronal sections showing differences in brain activation after heat stimulation; increased CBF is indicated in red. Each image is taken from a single brain section in the individual mice. Data represent the mean ± s.d., $n = 4$ mice per group (ANOVA), and one representative brain section is shown for each condition. Scale bars, 50 mm.

methylglyoxal, diabetes and the deficit in GLO1 (**Fig. 4b**). Further, in sciatic nerve tissue isolated from patients with or without diabetes who had amputations resulting from peripheral artery disease, we observed that the patients with diabetes had substantially more modifications of $Na_V1.8$ by methylglyoxal than the patients without diabetes (**Fig. 4c**). Incubation of a peptide, comprising the inactivation gate of $Na_V1.8$, with methylglyoxal followed by a mass spectrometry analysis confirmed that methylglyoxal binds to the arginine residue within the $Na_V1.8$ inactivation gate sequence (**Fig. 4d**). When we incubated plasma from diabetes-affected individuals with the peptide, peptide mapping confirmed methylglyoxal binding to the arginine residue in the $Na_V1.8$ inactivation gate (**Supplementary Fig. 6**).

Systemic treatment of WT mice with siRNA targeting $Na_V1.7$, $Na_V1.8$ or TRPV1 resulted in a significant inhibition of the respective mRNA (**Fig. 4e**,**f**). The $Na_V1.8$ knockdown was paralleled a by loss of methylglyoxal-induced thermal hyperalgesia (**Fig. 4g** and **Supplementary Fig. 7a**). In addition, the $Na_V1.8$ knockout mice were not only protected from methylglyoxal-induced hyperalgesia but actually showed hypoalgesia; we observed wild-type littermates of the $Na_V1.8$ knockout mice (*Scn10a*$^{+/+}$) to have a similar methylglyoxal-induced hyperalgesia to the C57BL/6 mice used throughout the study (**Fig. 4h** and **Supplementary Fig. 7b**).

We also found that *in vivo* pretreatment with methylglyoxal of healthy WT or $Na_V1.8$ knockout mice facilitated the potassium-induced and noxious-heat–induced release of the proinflammatory neuropeptide calcitonin gene-related peptide (CGRP) from cutaneous nociceptors *in vitro* (**Fig. 5a**), indicating increased responsiveness to both nonspecific and heat-transduced membrane depolarization of the skin nerve endings as a result of the pretreatment with methylglyoxal. Sensitization to heat, but not the heat response itself, was absent in skin flaps from the methylglyoxal-pretreated $Na_V1.8$ knockout mice. Methylglyoxal pretreatment and diabetes both significantly reduced the maximal tail nerve conduction velocity (NCV) (**Fig. 5b**) despite the absence of overt morphological changes (data not shown), a preclinical signature of the imminent large-fiber neuropathy.

We next determined the cerebral blood flow (CBF) changes in the pain-processing regions of the brain[27] in mice we stimulated with laser-evoked noxious heat. We visualized the blood flow distribution in these mice using pseudocolored frontal brain sections showing the resting and activated brain regions (**Fig. 5c**). We found increased heat responses in healthy WT mice pretreated with methylglyoxal and in STZ-induced diabetic WT mice compared to healthy WT mice, whereas the methylglyoxal-scavenging peptide $GERP_{10}$ showed an antihyperalgesic effect in the healthy WT methylglyoxal-pretreated and STZ-induced diabetic WT mice. $Na_V1.8$ knockout mice did not have an enhanced heat response after methylglyoxal pretreatment. Formalin injection in healthy WT mice, to induce pain without radiant heat, or healthy *Glo1*$^{-/+}$ mice plus heat stimulation showed an enhanced cerebral blood flow comparable to that in methylglyoxal-pretreated or STZ-induced diabetic WT mice. Notably, the areas of increased blood flow in all mouse brains studied (bregma, −1.72 to −2.41) correspond to the brain areas shown to be activated in rats (bregma, −2.3) with diabetes-induced neuropathic pain[28].

We used current-clamp recordings from cultured DRG neurons to characterize the direct effects of exogenous methylglyoxal on sensory neuron excitability (**Fig. 6**). Small- and medium-sized neurons from healthy WT and $Na_V1.8$ knockout mice did not differ in terms of resting membrane potential, current threshold and voltage threshold[29]. In the WT neurons, exposure to 100 μM methylglyoxal for 3 h resulted in a significant depolarizing shift by 8.2 mV in the resting membrane potential, a reduced current threshold for the activation of action potentials and a reduction in the depolarization required to reach the voltage threshold (**Fig. 6a**,**b**). The relative decrease in the current threshold in the WT neurons was larger (44%) than the decrease in voltage threshold (30%), which may indicate that the membrane resistance was increased by exposure to methylglyoxal. The rise time of the action potential was longer in WT methylglyoxal-treated (1.7 ms ± 0.1 ms (mean ± s.e.m)) than in control untreated WT neurons (1.3 ms ± 0.08 ms, $P < 0.01$), reflecting the lowered voltage threshold as a result of methylglyoxal treatment. Exposure of the WT neurons to a lower concentration of methylglyoxal (1 μM), corresponding to the plasma concentrations found in patients with diabetes and pain, for an extended period of time (12–14 h) also rendered their resting membrane potentials more depolarized (**Fig. 6c**; 4.3 mV, $P < 0.01$), however, their current and voltage thresholds were only reduced insignificantly. Additional pretreatment of these neurons with aminoguanidine, which inhibits protein modifications by methylglyoxal, was able to prevent the depolarizing effect of methylglyoxal, as well as the reduction of electrical thresholds (**Fig. 6c**).

Pretreatment of $Na_V1.8$ knockout neurons with methylglyoxal also resulted in a significant depolarizing shift by 5.2 mV of the resting membrane potential but did not induce a decrease in the current or voltage thresholds (**Fig. 6b**). Methylglyoxal pretreatment did not significantly change the amplitude or duration of either the

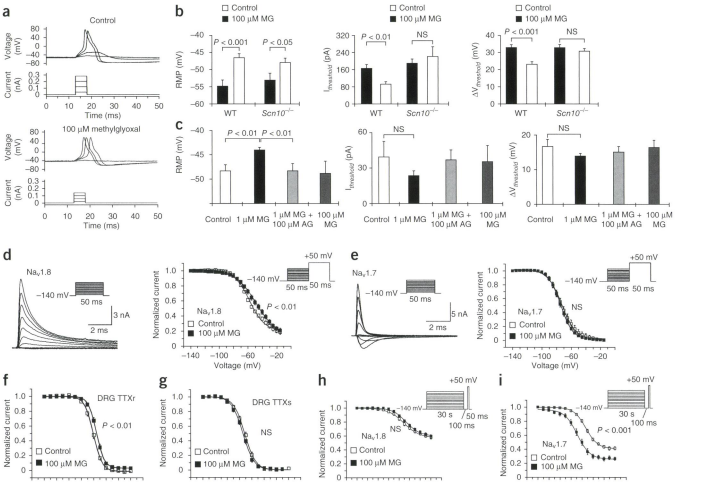

Figure 6 Effects of methylglyoxal on action potential generation and Na$^+$ currents in sensory neurons. (**a**) Examples of action potentials (upper traces) evoked by current pulses (lower traces) in neurons from WT mice stimulated with methylglyoxal. (**b**) The effect of methylglyoxal on the resting membrane potential, current threshold for pulses ($I_{threshold}$) and depolarization required to reach the threshold ($\Delta V_{threshold}$) in WT and $Na_V1.8$ knockout ($Scn10a^{-/-}$) neurons. Data represent the mean ± s.e.m. $n \geq 13$ neurons in each group. (**c**) The effects of methylglyoxal on the resting membrane potential, $I_{threshold}$ and $\Delta V_{threshold}$ in WT neurons in the presence and absence of aminoguanidine (AG). Data represent the mean ± s.e.m. $n \geq 13$ neurons per group. (**d**) A typical current trace of recombinant rat $Na_V1.8$ in ND7/23 cells activated by depolarizing steps (see insert) in the presence of TTX and voltage dependence of the steady-state fast inactivation of $Na_V1.8$ in ND7/23 cells ($n = 12/12$ (control/methylglyoxal treatment)). (**e**) A typical current trace of recombinant rat $Na_V1.7$ expressed in HEK293T cells, activated as shown in insert, but without any addition of TTX, showing the voltage dependence of the steady-state fast inactivation of $Na_V1.7$ ($n = 13/14$). NS, not significant. (**f**) The voltage dependence of the steady-state fast inactivation of TTXr Na$^+$ currents recorded in WT DRG neurons ($n = 14/15$). (**g**) The voltage dependence of the steady-state fast inactivation of TTXs currents recorded in $Na_V1.8$ knockout DRG neurons ($n = 11/11$). (**h**) The voltage dependence of the steady-state slow inactivation of heterologously expressed $Na_V1.8$ ($n = 12/10$). (**i**) The voltage dependence of the steady-state slow inactivation of heterologously expressed $Na_V1.7$ expressed in HEK293T cells ($n = 10/9$). NS, not significant. All datasets shown in this figure were analyzed by two-tailed Student's unpaired *t* test.

action potential or the afterhyperpolarization in WT or $Na_V1.8$ knockout neurons (data not shown). These data suggest that biophysical changes in $Na_V1.8$ function are responsible for the methylglyoxal-induced hyperexcitability of sensory neurons but not for their depolarization.

We further assessed the effects of methylglyoxal pretreatment (3 h) using voltage clamp recordings on recombinant rat $Na_V1.8$ and $Na_V1.7$ in ND7/23 and HEK293T cells, respectively (**Fig. 6d,e** and **Supplementary Fig. 8**). We found methylglyoxal to have no effect on the voltage dependence of activation (data not shown). However, the midpoint of the steady-state fast inactivation of $Na_V1.8$ was significantly shifted toward more depolarized potentials (from $V_{0.5}$ = −58 mV ± 0.5 mV (mean ± s.e.m.) to $V_{0.5}$ = −48.7 mV ± 0.9 mV, $n = 12$), an effect that signifies increased channel availability at voltages corresponding to the action potential threshold (**Fig. 6d**). We did not find this effect on fast inactivation when we applied methylglyoxal only briefly (3 min) before beginning the test protocol (data not shown). This is compatible with the time required for post-translational protein modifications to occur and excludes rapid, non-specific membrane effects. Methylglyoxal did not shift the steady-state fast inactivation of $Na_V1.7$ (**Fig. 6e**).

To reproduce the differential effects of methylglyoxal on the steady-state fast inactivation of $Na_V1.8$ and $Na_V1.7$ (**Fig. 6d,e** and **Supplementary Fig. 8**), we performed identical experiments on native TTXr and tetrodotoxin-sensitive (TTXs) Na$^+$ currents, which are the executive action potential generators in nociceptive DRG neurons[26].

We conducted the experiments in cultured DRG neurons of WT mice in the presence of TTX to monitor the effects on $Na_V1.8$ and of $Na_V1.8$ knockouts to monitor the effects on $Na_V1.7$ and other TTXs subunits.

We found a small but significant methylglyoxal-induced shift in the midpoint (from $V_{0.5} = -41$ mV ± 0.2 mV to $V_{0.5} = -36$ mV ± 0.2 mV, $n = 15$ (control) or 14 (methylglyoxal treatment)) of the steady-state fast inactivation for the TTXr currents (**Fig. 6f**) but not for the TTXs currents (**Fig. 6g**). Thus, methylglyoxal increased the known relative resistance of the TTXr action potential generator against fast inactivation, which may have contributed to the increased excitability. Using the same heterologous expression systems as described above, we then studied slow steady-state inactivation using recombinant VGSC.Whereas this voltage-dependent function of $Na_V1.8$ was not influenced by pretreatment with methylglyoxal (**Fig. 6h**), we did observe a significant shift toward more hyperpolarized potentials (from $V_{0.5} = -53$ mV ± 0.8 mV to $V_{0.5} = -68$ mV ± 0.6 mV, $n = 10$ (methylglyoxal treatment) or 9 (control)) with $Na_V1.7$ as a result of methylglyoxal pretreatment (**Fig. 6i**), reducing the availability of the $Na_V1.7$ channels at the resting membrane potential by half. As $Na_V1.7$ is known to be crucial for action potential triggering in nociceptive neurons, the slow inactivation of these ion channels could account for the methylglyoxal-induced hypoalgesia observed in the $Na_V1.8$ knockout mice (**Fig. 4g**). The contrary effects of methylglyoxal on $Na_V1.8$ and $Na_V1.7$ functions (sensitization and inactivation, respectively) argues against an indirect action of methylglyoxal, for example, by inducing COX-2 expression, which might enhance prostaglandin formation[30]. Although this and other inflammatory mediators increase the voltage sensitivity of $Na_V1.8$, they are not known to enhance the slow inactivation of $Na_V1.7$ (refs. 19,25).

DISCUSSION

Our data support a new mechanistic concept of painful peripheral neuropathy in diabetes. Post-translational modification of the nociceptor-specific sodium channel $Na_V1.8$ by methylglyoxal is associated with enhanced sensory neuron excitability and hyperalgesia, whereas methylglyoxal slows myelinated nerve conduction and drives $Na_V1.7$ into slow inactivation. As crystallographic and site-directed mutagenesis studies on these VGSCs are not yet available, the exact molecular link between methylglyoxal and changes in channel function is unknown. Other modifications secondary to treatment with methylglyoxal cannot be excluded as being responsible for the functional changes observed, such as the depolarizing effect. However, the biochemical and functional data presented here support the hypothesis that methylglyoxal-dependent modification(s) in $Na_V1.8$ have a role in diabetes-associated hyperalgesia that is independent of degenerative or regenerative changes in the nerve.

The concentration of plasma methylglyoxal is increased in patients with diabetes as a result of increased formation of methylglyoxal from excessive glycolysis[4] and decreased degradation and detoxification by the glyoxalase system. Other pathological states resulting in increased concentrations of methylglyoxal are uremia and ischemia-reperfusion. Although symptoms of painful diabetic neuropathy arise spontaneously, such as burning and prickling sensations in the feet, tactile allodynia is a classical sign of this condition, and burning pain can be provoked by warming the patients' feet[31]. Thus, the thermal and mechanical hypersensitivity in diabetic, healthy methylglyoxal-injected or GLO1-deficient mice can be considered to reflect, at least in part, the human symptoms.

To the best of our knowledge, methylglyoxal is the first endogenously produced small molecule (as opposed to cytokines, some of which induce systemic hyperalgesia) that induces thermal and mechanical hyperalgesia in healthy mice by acute systemic administration. Systemic application of methylglyoxal, however, gave rise to some ambiguity as to the target of its post-translational modification. CGRP release experiments, however, confirmed the induction of peripheral hypersensitivity by methylglyoxal and the dependence of this induction on $Na_V1.8$ expression. In diabetic neuropathy, the axonal transport of neuropeptide-containing dense core vesicles is impeded, which leads to reduced basal release from the skin nerve endings. However, stimulated neurosecretion is facilitated in diabetic neuropathy, suggesting an increased sensitivity, excitability or both[32]. These findings in the skin do not exclude additional effects of methylglyoxal on the nonpeptidergic subpopulation of nociceptors or on spinal terminals where further sensitization of synaptic transmission could occur[33].

The altered function of $Na_V1.8$ (reduced inactivation, as well as increased whole-cell excitability) is consistent with methylglyoxal binding to TTXr sodium channels and with the lack of methylglyoxal-induced hyperalgesia in $Na_V1.8$ knockout mice and siRNA-treated healthy WT mice. The prominent methylglyoxal-induced neuronal depolarization and the concomitant increase in membrane resistance both increase the chance for sensory functions, for example, heat-induced generator potentials or accidental spontaneous depolarization, to reach the relatively high voltage threshold of $Na_V1.8$ and generate action potentials[34]. Notably, methylglyoxal also causes a major slow inactivation of $Na_V1.7$, an essential VGSC and 'threshold channel' in nociceptive neurons. This inactivation of the TTXs sodium channel would be aggravated *in vivo* by the methylglyoxal-induced depolarization, and only unmyelinated nerve fibers, which have a high abundance of the inactivation-resistant $Na_V1.8$ in their endings, are expected to show increased excitability. In fact, the partial block of $Na_V1.7$ by methylglyoxal may explain why $Na_V1.8$ knockout mice show hypoalgesia in response to methylglyoxal, as hardly any action potential generator would be left in the nociceptors under these conditions. Similarly, postganglionic neurons of the autonomic nervous system, which are often affected by diabetic neuropathy and express $Na_V1.7$ but not $Na_V1.8$ (refs. 33,34), would fail under the condition of accumulating methylglyoxal. These opposing effects of methylglyoxal on TTXs compared to TTXr VGSCs could account for the coexistence of positive and negative clinical symptoms, such as burning feet and diabetic gastroparesis. Support for the general impairment of TTXs sodium channels by methylglyoxal comes from the marked slowing of NCV after systemic methylglyoxal administration.

Nociceptive neurons that express $Na_V1.8$ in their peripheral terminals gain one more 'profit' from the modifying actions of methylglyoxal, as $Na_V1.8$ is a faster repriming action potential generator than $Na_V1.7$ (ref. 18). Thus, the discharge rate in response to a given depolarization of the affected neuron can rise when the trigger function for discharge passes from the inactivated $Na_V1.7$ to the facilitated $Na_V1.8$. Modification of $Na_V1.8$ by methylglyoxal seems to be the root of primary hyperalgesia in animals, as well as the cause of pain in patients with diabetes. Although short-term diabetes in mice is not comparable to years of diabetes in humans, our findings suggest that methylglyoxal is a valid therapeutic target for the treatment of painful diabetic neuropathy, a medical condition for which few effective therapeutic options are available.

METHODS

Methods and any associated references are available in the online version of the paper.

Note: Supplementary information is available in the online version of the paper.

ACKNOWLEDGMENTS

The authors thank S. Kaymak for immunohistochemistry, A. Buhl and K. Leotta for assistance in the cerebral blood flow experiments, L. Werner for support with bregma gradings and X. Du and A. Erhardt for the daily care of the mice. A. Bierhaus, J.F., M.E.C., M.B. and P.P.N. were supported by a Centre grant from the Juvenile Diabetes Research Foundation (JDRF). This work was also supported in part by grants from the Deutsche Forschungsgemeinschaft (BI-1281/3-1 to A. Bierhaus; LU728/3-1 and NA 350/3-2 in KFO 130 to P.W.R., C. Nau and A.L.), the US National Institutes of Health (2R56DK33861-21 to M.B.), the European Foundation for the Study of Diabetes (EFSD/Lilly-Programme, to A. Bierhaus), the German Diabetes Association (DDG, Christian-Hagedorn-Award to A. Bierhaus), the Manfred-Lautenschläger-Stiftung for Diabetes (LSD, to P.P.N.), the Dietmar-Hopp-Stiftung (to A. Bierhaus, P.M.H. and P.P.N.) and the Network Aging Research (NAR, to A. Bierhaus). A. Babes and C.N. were supported by grant PN2 164/2007 from the Romanian Research Council (CNCSIS). A. Babes also received support from the Alexander von Humboldt Foundation.

AUTHOR CONTRIBUTIONS

A. Bierhaus planned, performed and supervised all experiments, was responsible for the data interpretation and wrote the manuscript. T.F. and S.S. performed most of the mouse experiments, and T.F. also did the biochemical analytics and cell culture experiments. A.L. and C. Nau performed the voltage clamp studies and were involved in data interpretation. A. Babes and C. Neacsu performed the current clamp studies and were involved in data interpretation. S.K.S., M.E. and T.I.K. performed CGRP-release experiments and single-fiber recordings in the skin-nerve preparation and were involved in data interpretation. M. Schnölzer, N.R. and P.J.T. were involved in the dicarbonyl analytics and data interpretation. F.L. provided biopsies of human sciatic nerves. W.L.N. performed electron microscopy. R.E. and I.K.L. performed the nerve conduction velocity experiments and the measurements of tactile allodynia. W.M., M. Schwaninger and U.H. supervised the cerebral blood flow measurements and were involved in data interpretation. T.D. was involved in the isolation and characterization of the DRG. D.E. generated the *Glo1*$^{-/+}$ mice. J.F. and M.E.C. provided ALT-711 and were involved in data interpretation. I.K., V.P. and M.M. performed the clinical studies. P.M.H. supervised the clinical studies and was involved in data interpretation. D.M.S. was involved in data interpretation and the writing of the manuscript. D.Z. provided the human skin biopsies and was involved in data interpretation. M.B. provided the *Glo1*$^{-/+}$ mice and was involved in data interpretation and the writing of the manuscript. P.W.R. supervised the electrophysiological part of the project and wrote the manuscript. P.P.N. supervised the project and wrote the manuscript. Senior coauthorship is shared by P.W.R. and P.P.N.

COMPETING FINANCIAL INTERESTS

The authors declare no competing financial interests.

Published online at http://www.nature.com/doifinder/10.1038/nm.2750.
Reprints and permissions information is available online at http://www.nature.com/reprints/index.html.

1. Tavee, J. & Zhou, L. Small fiber neuropathy: a burning problem. *Cleve. Clin. J. Med.* **76**, 297–305 (2009).
2. Nawroth, P.P., Rudofsky, G. & Humpert, P.M. Have we understood diabetes? New tasks for diagnosis and therapy. *Exp. Clin. Endocrinol. Diabetes* **118**, 1–3 (2010).
3. Calcutt, N.A. Potential mechanisms of neuropathic pain in diabetes. *Int. Rev. Neurobiol.* **50**, 205–228 (2002).
4. Thornalley, P.J. Dicarbonyl intermediates in the maillard reaction. *Ann. NY Acad. Sci.* **1043**, 111–117 (2005).
5. Brownlee, M. Biochemistry and molecular cell biology of diabetic complications. *Nature* **414**, 813–820 (2001).
6. Karachalias, N., Babaei-Jadidi, R., Ahmed, N. & Thornalley, P.J. Accumulation of fructosyl-lysine and advanced glycation end products in the kidney, retina and peripheral nerve of streptozotocin-induced diabetic rats. *Biochem. Soc. Trans.* **31**, 1423–1425 (2003).
7. Thornalley, P.J. Glyoxalase I—structure, function and a critical role in the enzymatic defence against glycation. *Biochem. Soc. Trans.* **31**, 1343–1348 (2003).
8. Bierhaus, A. & Nawroth, P.P. Multiple levels of regulation determine the role of the receptor for AGE (RAGE) as common soil in inflammation, immune responses and diabetes mellitus and its complications. *Diabetologia* **52**, 2251–2263 (2009).
9. Jack, M.M., Ryals, J.M. & Wright, D.E. Characterisation of glyoxalase I in a streptozocin-induced mouse model of diabetes with painful and insensate neuropathy. *Diabetologia* **54**, 2174–2182 (2011).
10. Morcos, M. *et al.* Glyoxalase-1 prevents mitochondrial protein modification and enhances lifespan in *Caenorhabditis elegans*. *Aging Cell* **7**, 260–269 (2008).
11. Suzuki, Y., Sato, J., Kawanishi, M. & Mizumura, K. Lowered response threshold and increased responsiveness to mechanical stimulation of cutaneous nociceptive fibers in streptozotocin-diabetic rat skin *in vitro*—correlates of mechanical allodynia and hyperalgesia observed in the early stage of diabetes. *Neurosci. Res.* **43**, 171–178 (2002).
12. Misawa, S. *et al.* Axonal potassium conductance and glycemic control in human diabetic nerves. *Clin. Neurophysiol.* **116**, 1181–1187 (2005).
13. Grafe, P., Bostock, H. & Schneider, U. The effects of hyperglycaemic hypoxia on rectification in rat dorsal root axons. *J. Physiol. (Lond.)* **480**, 297–307 (1994).
14. Quasthoff, S. The role of axonal ion conductances in diabetic neuropathy: a review. *Muscle Nerve* **21**, 1246–1255 (1998).
15. Craner, M.J., Klein, J.P., Renganathan, M., Black, J.A. & Waxman, S.G. Changes of sodium channel expression in experimental painful diabetic neuropathy. *Ann. Neurol.* **52**, 786–792 (2002).
16. Hong, S., Morrow, T.J., Paulson, P.E., Isorn, L.L. & Wiley, J.W. Early painful diabetic neuropathy is associated with differential changes in tetrodotoxin-sensitive and -resistant sodium channels in dorsal root ganglion neurons in the rat. *J. Biol. Chem.* **279**, 29341–29350 (2004).
17. Shah, B.S. *et al.* Beta3, a novel auxiliary subunit for the voltage gated sodium channel is upregulated in sensory neurones following streptozocin induced diabetic neuropathy in rat. *Neurosci. Lett.* **309**, 1–4 (2001).
18. Lampert, A., O'Reilly, A.O., Reeh, P. & Leffler, A. Sodium channelopathies and pain. *Pflugers Arch.* **460**, 249–263 (2010).
19. Silos-Santiago, I. The role of tetrodotoxin-resistant sodium channels in pain states: are they the next target for analgesic drugs? *Curr. Opin. Investig. Drugs* **9**, 83–89 (2008).
20. Hirade, M., Yasuda, H., Omatsu-Kanbe, M., Kikkawa, R. & Kitasato, H. Tetrodotoxin-resistant sodium channels of dorsal root ganglion neurons are readily activated in diabetic rats. *Neuroscience* **90**, 933–939 (1999).
21. Konrade, I. *et al.* Verminderte glyoxalase-1 aktivitat bei patienten mit schmerzhafter diabetischer neuropathie. *Diabetologie und Stoffwechsel* **2**, P98 (2007).
22. Thornalley, P.J. *et al.* Antitumour activity of S-p-bromobenzylglutathione cyclopentyl diester *in vitro* and *in vivo*. Inhibition of glyoxalase I and induction of apoptosis. *Biochem. Pharmacol.* **51**, 1365–1372 (1996).
23. El-Osta, A. *et al.* Transient high glucose causes persistent epigenetic changes and altered gene expression during subsequent normoglycemia. *J. Exp. Med.* **205**, 2409–2417 (2008).
24. Sullivan, K.A. *et al.* Mouse models of diabetic neuropathy. *Neurobiol. Dis.* **28**, 276–285 (2007).
25. Kellogg, A.P., Cheng, H.T. & Pop-Busui, R. Cyclooxygenase-2 pathway as a potential therapeutic target in diabetic peripheral neuropathy. *Curr. Drug Targets* **9**, 68–76 (2008).
26. Hong, S., Agresta, L., Guo, C. & Wiley, J.W. The TRPV1 receptor is associated with preferential stress in large dorsal root ganglion neurons in early diabetic sensory neuropathy. *J. Neurochem.* **105**, 1212–1222 (2008).
27. Morrow, T.J., Paulson, P.E., Danneman, P.J. & Casey, K.L. Regional changes in forebrain activation during the early and late phase of formalin nociception: analysis using cerebral blood flow in the rat. *Pain* **75**, 355–365 (1998).
28. Paulson, P.E., Wiley, J.W. & Morrow, T.J. Concurrent activation of the somatosensory forebrain and deactivation of periaqueductal gray associated with diabetes-induced neuropathic pain. *Exp. Neurol.* **208**, 305–313 (2007).
29. Renganathan, M., Cummins, T.R. & Waxman, S.G. Contribution of $Na_V1.8$ sodium channels to action potential electrogenesis in DRG neurons. *J. Neurophysiol.* **86**, 629–640 (2001).
30. Fuchs, D., Birklein, F., Reeh, P.W. & Sauer, S.K. Sensitized peripheral nociception in experimental diabetes of the rat. *Pain* **151**, 496–505 (2010).
31. Obrosova, I.G. Diabetic painful and insensate neuropathy: pathogenesis and potential treatments. *Neurotherapeutics* **6**, 638–647 (2009).
32. Sandkühler, J. Models and mechanisms of hyperalgesia and allodynia. *Physiol. Rev.* **89**, 707–758 (2009).
33. Rush, A.M., Cummins, T.R. & Waxman, S.G. Multiple sodium channels and their roles in electrogenesis within dorsal root ganglion neurons. *J. Physiol. (Lond.)* **579**, 1–14 (2007).
34. Rush, A.M. *et al.* A single sodium channel mutation produces hyper- or hypoexcitability in different types of neurons. *Proc. Natl. Acad. Sci. USA* **103**, 8245–8250 (2006).
35. Ahmed, N., Dobler, D., Dean, M. & Thornalley, P.J. Peptide mapping identifies hotspot site of modification in human serum albumin by methylglyoxal involved in ligand binding and esterase activity. *J. Biol. Chem.* **280**, 5724–5732 (2005).

nature medicine

Hepatic Hdac3 promotes gluconeogenesis by repressing lipid synthesis and sequestration

Zheng Sun[1,2], Russell A Miller[1,2], Rajesh T Patel[1,2], Jie Chen[3], Ravindra Dhir[1,2], Hong Wang[4], Dongyan Zhang[5], Mark J Graham[6], Terry G Unterman[7,8], Gerald I Shulman[5], Carole Sztalryd[4], Michael J Bennett[3,9], Rexford S Ahima[1,2], Morris J Birnbaum[1,2] & Mitchell A Lazar[1,2,10]

Fatty liver disease is associated with obesity and type 2 diabetes, and hepatic lipid accumulation may contribute to insulin resistance. Histone deacetylase 3 (Hdac3) controls the circadian rhythm of hepatic lipogenesis. Here we show that, despite severe hepatosteatosis, mice with liver-specific depletion of Hdac3 have higher insulin sensitivity without any changes in insulin signaling or body weight compared to wild-type mice. Hdac3 depletion reroutes metabolic precursors towards lipid synthesis and storage within lipid droplets and away from hepatic glucose production. Perilipin 2, which coats lipid droplets, is markedly induced upon Hdac3 depletion and contributes to the development of both steatosis and improved tolerance to glucose. These findings suggest that the sequestration of hepatic lipids in perilipin 2–coated droplets ameliorates insulin resistance and establish Hdac3 as a pivotal epigenomic modifier that integrates signals from the circadian clock in the regulation of hepatic intermediary metabolism.

Hepatosteatosis, the defining clinical hallmark of nonalcoholic fatty liver disease (NAFLD), is one of the most prevalent metabolic disorders throughout the world[1,2]. NAFLD has been shown to be highly correlated with insulin resistance in many epidemiological studies, leading to speculation of a cause and effect relationship between the two[3,4]. Insulin resistance in muscle and adipose tissue may increase the influx of carbohydrates and free fatty acids (FFAs) into the liver and thus promote hepatic *de novo* lipogenesis and triglyceride synthesis. Hyperinsulinemia, resulting from a compensation by the pancreas for systemic insulin resistance, also reinforces hepatic lipogenesis and therefore contributes additionally to the development of hepatosteatosis[2,5]. In addition, intrahepatic accumulation of triglycerides may generate various deleterious lipid intermediates, including diacylglycerols (DAG) and ceramide, which could activate several cytosolic protein kinases either directly or indirectly through inflammation, resulting in the modification and disruption of insulin signaling and causing lipotoxicity and insulin resistance[4,6].

These theories can have a major impact on the treatment of both NAFLD and diabetes. However, the use of insulin sensitizers to treat NAFLD in clinical trials has generated mixed outcomes[3,7]. Indeed, recent research has revealed that the interrelationship between hepatosteatosis and hepatic insulin resistance is complex[1,8]. For example, the role of insulin resistance in the pathogenesis of NAFLD is supported by the observation that in humans most hepatic lipid is derived from adipose-secreted FFAs and *de novo* lipogenesis rather than directly from the diet[9] and that insulin resistance precedes hepatosteatosis in several animal models of overnutrition-induced NAFLD[10]. And yet even in the face of this insulin resistance, intact insulin signaling through insulin receptors, phosphoinositide-3 kinases and Akt (also known as protein kinase B) is required to drive lipogenesis and hepatosteatosis, as has been shown using several knockout mouse models[11–14]. In addition, hepatic insulin hypersensitivity in the phosphatase and tensin homolog (Pten) liver-specific knockout mouse is sufficient to cause hepatosteatosis[15]. As for the role of hepatosteatosis in insulin resistance, DAG and other lipid intermediates have been shown to activate protein kinase C-ε (Prkce) and other cytosolic stress signals or inflammation, leading to the disruption of insulin signaling[6]. However, elevated total hepatic content of these lipid intermediates does not always cause hepatic insulin resistance, suggesting that the detailed composition of hepatic lipid species, as well as their spatial distribution, may matter in this process[1,8,16–18].

Although genetic factors contribute to the development of metabolic syndromes, environmental factors including diet, exercise and rotating work shifts are also key determinants[19,20]. The environment regulates the expression of genes involved in carbohydrate and lipid metabolism by altering the epigenome, including changes in the histone acetylation patterns in chromatin[21] that follow circadian rhythms[22,23]. Histone acetylation is governed by opposing functions

[1]Division of Endocrinology, Diabetes, and Metabolism, Department of Medicine, Perelman School of Medicine at the University of Pennsylvania, Philadelphia, Pennsylvania, USA. [2]The Institute for Diabetes, Obesity and Metabolism, Perelman School of Medicine at the University of Pennsylvania, Philadelphia, Pennsylvania, USA. [3]Department of Pathology and Laboratory Medicine, Children's Hospital of Philadelphia, Philadelphia, Pennsylvania, USA. [4]The Geriatric Research, Education and Clinical Center, Baltimore Veterans Affairs Health Care Center, Division of Endocrinology, Department of Medicine, School of Medicine, University of Maryland, Baltimore, Maryland, USA. [5]Department of Medicine, Yale University School of Medicine, New Haven, Connecticut, USA. [6]Isis Pharmaceuticals, Inc., Carlsbad, California, USA. [7]Section of Endocrinology, Diabetes and Metabolism, University of Illinois at Chicago, Chicago, Illinois, USA. [8]Jesse Brown Virginia Medical Center, Chicago, Illinois, USA. [9]Department of Pathology and Laboratory Medicine, Perelman School of Medicine at the University of Pennsylvania, Philadelphia, Pennsylvania, USA. [10]Department of Genetics, Perelman School of Medicine at the University of Pennsylvania, Philadelphia, Pennsylvania, USA. Correspondence should be addressed to M.A.L. (lazar@mail.med.upenn.edu).

Received 19 December 2011; accepted 16 March 2012; published online 6 May 2012; doi:10.1038/nm.2744

of two classes of enzymes: histone acetyltransferases and histone deacetylases (HDACs). Given the availability of many small molecules that activate or inhibit HDAC activities and the therapeutic potential of these small molecules in treating a variety of diseases, including metabolic disorders[24], it is of great interest and importance to understand the biology of individual HDACs in metabolic regulation.

We recently showed that Hdac3 colocalizes with nuclear receptor corepressor (Ncor1) in chromatin near genes involved in lipid metabolism in mouse liver in a circadian pattern, with the maximum occupancy occurring during the day and the minimum occurring at night[22]. This rhythm is orchestrated by nuclear receptor subfamily 1, group D, member 1 (Nr1d1), a nuclear receptor and key component of the molecular circadian clock machinery[22,25]. These findings, along with those of others, show that Hdac3 is crucial for the maintenance of hepatic lipid homeostasis[22,25,26]. However, it is unknown how hepatic Hdac3 regulates carbohydrate metabolism. Here we show that the severe hepatosteatosis caused by loss of Hdac3 in mouse liver engenders a notably insulin-hypersensitive state. Systematic characterization of the physiological function of hepatic Hdac3 in energy metabolism establishes Hdac3 as a pivotal regulator of hepatic glucose production through a previously unsuspected mechanism involving the rerouting of metabolites between lipid synthesis and glucose production pathways.

RESULTS

Hdac3 depletion is distinct from diet-induced hepatosteatosis

To delete Hdac3 specifically in the liver, we injected adult *Hdac3*$^{flox/flox}$ C57BL/6 mice[27] with adeno-associated virus (AAV) expressing either Cre recombinase or control GFP driven by the thyroxine-binding globulin (Tbg) promoter (AAV-Tbg-Cre or AAV-Tbg-GFP, respectively), which specifically targets hepatocytes and not Kupffer cells or endothelial cells[28]. We confirmed the hepatocyte-specific expression by immunohistochemistry of the livers from mice injected with AAV-Tbg-GFP (**Supplementary Fig. 1a**). Also by injecting mature mice, a direct assessment of hepatic Hdac3 function in the adult organ was achieved without any potential interference with proper embryonic or neonatal development that might alter adult hepatic function. This acute deletion approach also makes it possible to distinguish the direct effects of Hdac3 deletion from any secondary or compensatory effects. Depletion of hepatic Hdac3 was complete by 1 week after injection with AAV-Tbg-Cre compared to the AAV-Tbg-GFP control injection (**Fig. 1a**). Hepatic triglyceride content was significantly elevated twofold to threefold at 1 week after injection and was further increased fivefold to tenfold fold by 2–3 weeks after injection in the AAV-Tbg-Cre mice compared to the control AAV-Tbg-GFP mice (**Fig. 1b**). In contrast, mice with Hdac3 depleted in their macrophages using lysozyme M-Cre (LysM-Cre; *Hdac3*$^{flox/flox}$ mice)[27] did not develop fatty livers (**Supplementary Fig. 1b**). Accumulation of very small lipid droplets within the hepatocytes of AAV-Tbg-Cre mice was evident after H&E staining (**Fig. 1c**). Exogenous Flag-tagged Hdac3 protein, when introduced using AAV (AAV-Hdac3) at amounts similar to those of endogenous Hdac3 (**Fig. 1d**), was able to completely rescue hepatosteatosis, as assessed by triglyceride measurement and Oil Red O staining (**Fig. 1e,f**). These results show that the metabolic phenotype of the AAV-Tbg-Cre–injected mice was indeed a result of the lack of Hdac3 in hepatocytes.

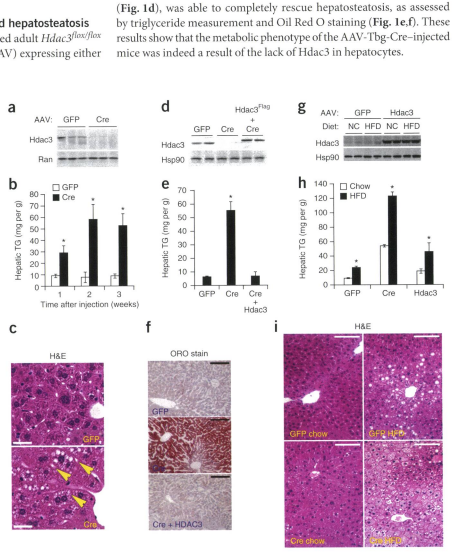

Figure 1 Liver-specific depletion of Hdac3 in adult mice causes quick-onset hepatosteatosis that is distinct from that caused by a HFD. (**a**) Western blot of total liver lysates at 1 week after AAV injection. GFP, treatment with AAV-Tbg-GFP; Cre, treatment with AAV-Tbg-Cre. Ran GTPase (Ran) was used as a loading control. (**b**) Hepatic triglyceride (TG) measurement. $n = 3$ mice per treatment. mg per g, mg triglyceride per g of liver weight. (**c**) H&E staining of livers at 2 weeks after the indicated AAV injection. Arrowheads indicate small lipid droplets. Scale bars, 25 μm. (**d**) Western blot of liver lysates from the rescue experiment. Cre + Hdac3, Flag-tagged Hdac3 delivered using an AAV plus injection with AAV-Tbg-Cre. Heat shock protein 90 (Hsp90) was used as a loading control. (**e**) Hepatic triglyceride measurements from the mice described in **d**. $n = 3$ mice per treatment. (**f**) Oil Red O (ORO) staining of livers from the mice described in **d**. Scale bars, 100 μm. (**g**) Western blot of total liver lysates. The lysates were from mice injected with AAV-Tbg-GFP or AAV-Tbg-Hdac3 (Hdac3), followed by feeding on normal chow (NC) or HFD for 6 weeks before being injected with AAV-Tbg-Cre and then maintained on their previous diet for another 2 weeks before tissue harvest. (**h**) Hepatic triglyceride measurements in livers from the mice described in **g**. $n = 3$ or 4 mice per treatment. (**i**) H&E staining of livers from the mice described in **g**. Scale bars, 100 μm. All error bars, s.e.m. $^*P < 0.05$ for the samples compared to the AAV-Tbg-GFP controls by Student's two-tailed t test.

To determine whether Hdac3 has a role in high-fat diet (HFD)-induced hepatosteatosis[10], we superimposed depletion (by AAV-Tbg-Cre) and overexpression of Hdac3 (by AAV-Hdac3) in mouse liver on a HFD feeding regimen. HFD feeding for 8 weeks did not alter the amounts of endogenous or overexpressed exogenous Hdac3 (**Fig. 1g**) and had a synergistic effect with Hdac3 depletion in terms of promoting hepatosteatosis (**Fig. 1h**). In addition, Hdac3 overexpression did not ameliorate HFD-induced hepatosteatosis (**Fig. 1h**), suggesting that HFD feeding and hepatic Hdac3 depletion probably result in hepatosteatosis through independent mechanisms. Consistent with this, the morphologic changes in the liver differed drastically in HDF feeding compared to Hdac3 depletion. Whereas Hdac3 depletion caused the formation of tiny lipid droplets that were barely discernable under low magnification, HFD feeding resulted in the accumulation of much bigger lipid droplets that were primarily restricted to the central vein areas (**Fig. 1i**). Depletion of Hdac3 in the setting of the HFD led to a striking reduction in the size of the lipid droplets (comparing mice injected with AAV-Tbg-Cre on the HFD to mice injected with AAV-Tbg-GFP on the HFD), even though the total lipid content was higher in the AAV-Tbg-Cre HFD group than the AAV-Tbg-GFP HFD group (**Fig. 1h,i**). Therefore, liver-specific depletion of Hdac3 in adult mice causes hepatosteatosis that is distinct from that caused by a HFD.

Glucose output and insulin sensitivity in the Hdac3-null liver

Despite the marked accumulation of triglycerides in the liver, mice lacking hepatic Hdac3 (AAV-Tbg-Cre mice) had lower fasting blood glucose concentrations at 2 weeks after injection compared to the AAV-Tbg-GFP control mice (**Fig. 2a**). This suggests that Hdac3 normally promotes hepatic glucose production during fasting. Mice without hepatic Hdac3 also had lower basal blood insulin concentrations (**Fig. 2b**) and were more tolerant to glucose and insulin than the AAV-Tbg control mice (**Fig. 2c,d**), suggesting insulin hypersensitivity in these mice. Although most of the studies were performed in males, we observed similar phenotypes in female mice (**Supplementary Fig. 2a,b**). These results are in line with a previous study reporting that mice with *in utero* depletion of hepatic Hdac3 using albumin-Cre (Alb-Cre; *Hdac3*$^{flox/flox}$ mice) develop hypoglycemia and hypoinsulinema, although that study was confounded by body-weight differences between genotypes and did not detect significant differences for whole-body glucose tolerance[26]. Here, depletion of hepatic Hdac3 in adult mice did not alter body weight at up to 4 weeks after injection of AAV-Tbg-Cre compared to injection of AAV-Tbg-GFP or compared to noninjected controls (**Fig. 2e** and data not shown).

The greater glucose tolerance in AAV-Tbg-Cre mice compared to AAV-Tbg-GFP mice was even more prominent when the mice were exposed to HFD (**Fig. 2f**), again without any accompanying differences in body-weight gain (**Supplementary Fig. 2c**) despite the severe hepatosteatosis in the livers of the Hdac3-depleted mice (**Supplementary Fig. 2d**). Hyperinsulinemic-euglycemic clamp studies using ^{3}H-glucose as a tracer revealed that insulin-mediated suppression of hepatic glucose production was significantly potentiated in the absence of hepatic Hdac3 compared to AAV-Tbg-GFP controls, resulting in a higher glucose infusion rate in the clamp state in the Hdac3-depleted mice (**Fig. 2g** and **Supplementary Fig. 2e,f**). The apparent lack of difference in basal hepatic glucose production in AAV-Tbg-GFP and AAV-Tbg-Cre mice is probably the result of the lower basal blood insulin concentrations in mice without hepatic Hdac3 compared to the AAV-Tbg-GFP control mice. Thus, the loss of hepatic Hdac3 results in insulin hypersensitivity and lower hepatic glucose production despite greater hepatic lipid accumulation.

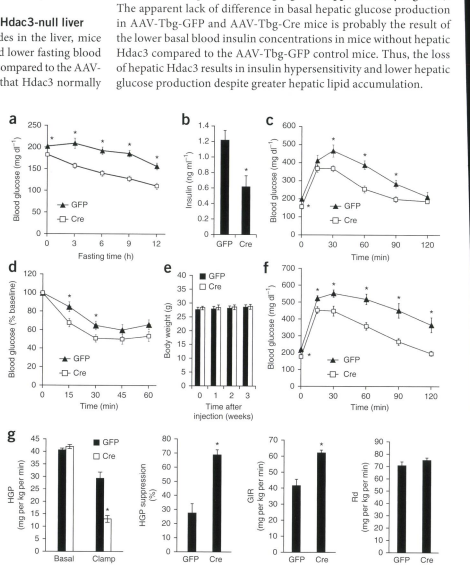

Figure 2 The Hdac3-depleted liver has impaired glucose production and is insulin hypersensitive. (**a**) Fasting blood glucose concentrations in mice fed on normal chow at 2 weeks after the indicated AAV injection. $n = 7$ or 8 mice per treatment. (**b**) Basal blood insulin concentrations in mice fed on normal chow at 5 p.m. 2 weeks after injection with the indicated AAV. $n = 7$ or 8 mice per treatment. (**c**) Results from the glucose tolerance test for mice fed on normal chow at 2 weeks after injection with the indicated AAV. $n = 7$ or 8 mice per treatment. (**d**) Results from the insulin tolerance test for mice fed on normal chow at 3 weeks after injection with the indicated AAV. $n = 7$ or 8 mice per treatment. (**e**) Body weight of mice fed on normal chow. $n = 7$ or 8 mice per treatment. (**f**) Results from the glucose tolerance test at 2 weeks after injection with the indicated AAV and after being fed a HFD for 4 weeks. $n = 8$ mice per treatment. (**g**) Hyperinsulinemic-euglycemic clamp at 3 weeks after injection with the indicated AAV and after being fed a HFD for 4 weeks. $n = 5$ mice per treatment. HGP, hepatic glucose production; GIR, glucose infusion rate; Rd, rate of disposal of glucose. All error bars, s.e.m. $^*P < 0.05$ for the comparison of the AAV-Tbg-GFP and AAV-Tbg-Cre groups by Student's two-tailed t test.

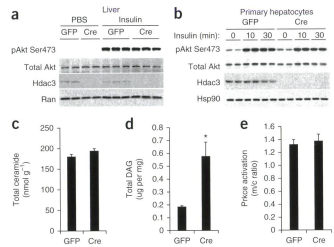

Figure 3 Molecular insulin signaling events are unchanged despite lipid accumulation in the Hdac3-depleted liver. (**a**) Western blot analysis of livers at 2 weeks after injection of the indicated AAV and after 18 h of fasting and subsequent injection of insulin (2 mU per g body weight) or PBS. pAkt, phosphorylated Akt. Ran was used as the loading control. (**b**) Western blot analysis of primary hepatocytes isolated from mice injected with the indicated AAV. Cells were serum starved, challenged with insulin for the indicated amount of time and then harvested. Hsp90 was used as the loading control. (**c**) Hepatic ceramide measured by liquid chromatography–tandem mass spectrometry. $n = 5$ mice per treatment. (**d**) Hepatic DAG measured by gas chromatography. $n = 5$ mice per treatment. (**e**) Results from the Prkce activation assay in the livers of mice in the indicated treatment groups. $n = 6$ mice per treatment. m/c, membrane compared to cytosolic Prkce protein concentration. All error bars, s.e.m. $^*P < 0.05$ compared to the AAV-Tbg-GFP control group by Student's two-tailed *t* test.

The prominent dissociation of hepatic steatosis from insulin resistance in Hdac3-depleted livers prompted us to further examine the insulin signaling pathway. We found that insulin-dependent phosphorylation of Akt was not altered as a result of Hdac3 depletion in either the livers or isolated primary hepatocytes of mice in response to different dosages of insulin (**Fig. 3a,b** and **Supplementary Fig. 3a,b**). Macrophage infiltration and expression of proinflammatory genes also remained unaltered in the Hdac3-depleted mice (**Supplementary Fig. 3c,d**). Total hepatic ceramide content was also not changed in these mice (**Fig. 3c**), although several ceramide species showed modest increases in concentration (**Supplementary Fig. 3e**). Hepatic DAG concentrations were indeed prominently elevated in AAV-Tbg-Cre mice (**Fig. 3d** and **Supplementary Fig. 3f**) but did not lead to Prkce activation (**Fig. 3e**), whereas HFD-induced hepatosteatosis did (**Supplementary Fig. 3g**). These results suggest that accumulated lipid species were somehow sequestered from activating cytosolic kinases such as Prkce and were restrained from inducing inflammatory responses, which may underlie the dissociation of hepatosteatosis from insulin resistance[29].

Hdac3 controls metabolic rerouting and lipid sequestration

From a metabolic kinetic perspective, hepatosteatosis is a result of an imbalance of hepatic triglyceride secretion, *de novo* lipogenesis, fatty acid oxidation and fatty acid uptake[5]. The hepatic triglyceride secretion rate, determined *in vivo* by measuring plasma triglyceride concentrations in a time course after blocking its turnover with the detergent Pluronic 407, was not affected by Hdac3 depletion (**Fig. 4a**). The hepatic *de novo* lipogenesis rate, measured *in vivo* by tracing newly synthesized oleate from deuterated water, was higher in Hdac3-depleted livers compared to livers from AAV-Tbg-GFP controls (**Fig. 4b**). Fatty acid oxidation and uptake were evaluated together in primary hepatocytes isolated from both groups of mice by measuring the production of ^{3}H-labeled water from ^{3}H-palmitate and the acquisition of ^{3}H-palmitate into the intracellular lipid pool, respectively. Hdac3-depleted hepatocytes showed a lower fatty acid oxidation rate compared to hepatocytes from the AAV-Tbg-GFP controls (**Fig. 4c**). Compared to the AAV-Tbg-GFP controls, we found more ^{3}H-palmitate in the intracellular lipid pool in the absence of Hdac3, with the net gain in fatty acid acquisition being roughly equal to the loss in fatty acid oxidation (**Fig. 4d**). Considering the unaltered triglyceride secretion in Hdac3-depleted mice, this suggests that the fatty acid uptake process *per se* was minimally affected by Hdac3 depletion.

In keeping with the metabolic tracing studies, a comprehensive gene expression analysis showed that Hdac3 deletion in the liver caused the prominent upregulation of genes that promote lipid sequestration, lipid synthesis and NADPH synthesis (**Fig. 4e** and Gene Expression Omnibus GSE25937). Upregulated expression of *Me1* (malic enzyme 1) and *Cs* (citrate synthase) suggests an enhanced pyruvate-malate cycle that supplies NADPH and acetyl-CoA for lipid synthesis (**Fig. 4e,f**). Upregulated *Pygl* (glycogen phosphorylase) and *G6pdx* and *G6pd2* (glucose-6-phosphate dehydrogenase), along with downregulated *Pfkfb3* (6-phosphofructo-2-kinase)[30,31], predict that glycogen would be consumed to feed into the pentose phosphate pathway, providing NADPH for lipid synthesis (**Fig. 4e,f**). Indeed, the hepatic glycogen content was significantly lower in the Hdac3-depleted livers compared to livers from the AAV-Tbg-GFP controls (**Fig. 4g** and **Supplementary Fig. 4a**). Mice without hepatic Hdac3 also had modestly higher FFA concentrations in their serum compared to the AAV-Tbg-GFP control mice (**Supplementary Fig. 4b**), potentially because of enhanced fat mobilization in adipose tissues as a result of lower blood insulin concentrations.

The expression of *Srebp* (sterol regulatory element-binding proteins) was not altered by Hdac3 depletion (**Supplementary Fig. 4c**). This, together with the finding that the genome-wide binding of Srebp proteins does not extensively overlap with the binding of Hdac3 in mouse liver[22,32,33], suggests that Srebp proteins probably did not contribute substantially to the hepatosteatosis phenotype in the Hdac3-depleted liver. Expression of other transcriptional regulators of lipogenesis, including *Lxr* (liver X receptors, also known as *Nr1h*) and *Mlxipl* (carbohydrate response element-binding protein), was unchanged as a result of Hdac3 depletion (**Supplementary Fig. 4c**), which is consistent with the conclusion that Hdac3 directly represses the transcription of the lipogenic genes to which it is recruited by Nr1d1 (ref. 22). The expression of genes involved in fatty acid oxidation (FAO) was unchanged or even upregulated by Hdac3 depletion (**Supplementary Fig. 4d**), despite lower FAO flux (**Fig. 4c**) and fasting serum ketone concentrations in Hdac3-depleted mice compared to AAV-Tbg-GFP controls (**Fig. 4h**). These observations, along with the lack of accumulation of acyl-CoA in the liver (**Fig. 4i**) or acylcarnitines in the plasma (**Supplementary Fig. 4e**) of Hdac3-depleted mice, suggest that the FAO pathway is not inherently defective but, rather, is dominated by the enhanced lipid synthesis pathway in the Hdac3-depleted liver. This domination could be accomplished through inhibition of the transport of acyl-CoA into mitochondria by glycerol-3-phosphate acyltransferase 1 (Gpam) and acetyl-CoA carboxylase 2 (Acacb)[5,34] (**Fig. 4f**).

The finding that the concentrations of acyl-CoA species were lower in Hdac3-depleted livers compared to AAV-Tbg-GFP control

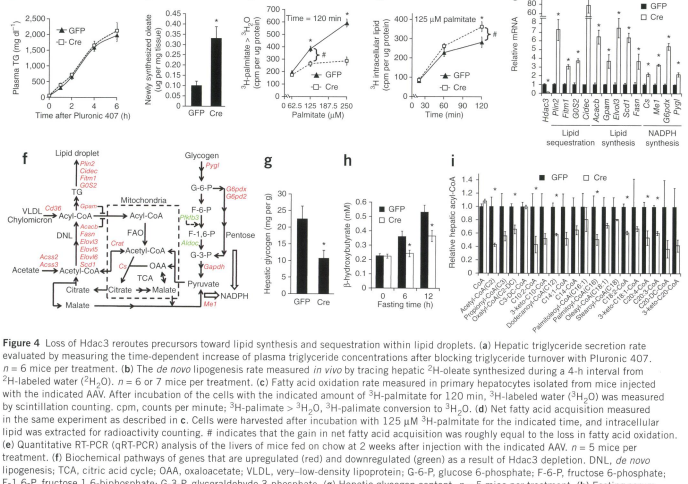

Figure 4 Loss of Hdac3 reroutes precursors toward lipid synthesis and sequestration within lipid droplets. (**a**) Hepatic triglyceride secretion rate evaluated by measuring the time-dependent increase of plasma triglyceride concentrations after blocking triglyceride turnover with Pluronic 407. $n = 6$ mice per treatment. (**b**) The *de novo* lipogenesis rate measured *in vivo* by tracing hepatic ^{2}H-oleate synthesized during a 4-h interval from ^{2}H-labeled water (^2H_2O). $n = 6$ or 7 mice per treatment. (**c**) Fatty acid oxidation rate measured in primary hepatocytes isolated from mice injected with the indicated AAV. After incubation of the cells with the indicated amount of ^{3}H-palmitate for 120 min, ^{3}H-labeled water (^3H_2O) was measured by scintillation counting. cpm, counts per minute; ^{3}H-palmitate > ^3H_2O, ^{3}H-palmitate conversion to ^3H_2O. (**d**) Net fatty acid acquisition measured in the same experiment as described in **c**. Cells were harvested after incubation with 125 μM ^{3}H-palmitate for the indicated time, and intracellular lipid was extracted for radioactivity counting. # indicates that the gain in net fatty acid acquisition was roughly equal to the loss in fatty acid oxidation. (**e**) Quantitative RT-PCR (qRT-PCR) analysis of the livers of mice fed on chow at 2 weeks after injection with the indicated AAV. $n = 5$ mice per treatment. (**f**) Biochemical pathways of genes that are upregulated (red) and downregulated (green) as a result of Hdac3 depletion. DNL, *de novo* lipogenesis; TCA, citric acid cycle; OAA, oxaloacetate; VLDL, very-low-density lipoprotein; G-6-P, glucose 6-phosphate; F-6-P, fructose 6-phosphate; F-1,6-P, fructose 1,6-biphosphate; G-3-P, glyceraldehyde 3-phosphate. (**g**) Hepatic glycogen content. $n = 5$ mice per treatment. (**h**) Fasting serum ketone body concentrations. $n = 7$ or 8 mice per treatment. (**i**) Hepatic acyl-CoA content measured by tandem mass spectrometry. $n = 4$. All error bars, s.e.m. $^*P < 0.05$ for the comparison of the AAV-Tbg-Cre and AAV-Tbg-GFP groups by Student's two-tailed *t* test.

livers despite the accumulation of triglycerides (**Fig. 4i**) suggests that these intermediates were shunted toward glycerolipid formation and the subsequent sequestration in lipid droplets in the Hdac3-depleted livers. Indeed, *Plin2* (perilipin 2), *Cidec* (cell-death–inducing DFFA-like effector c), *Fitm1* (fat storage-inducing transmembrane protein 1) and *G0S2* (G0/G1 switch gene 2), which encode proteins involved in lipolysis inhibition and lipid sequestration[16,35–37], were among the most prominently upregulated genes in the Hdac3-depleted liver (**Fig. 4e**). Their protein products were similarly upregulated and were associated with lipid droplets (**Supplementary Fig. 5a,b**) in a highly specific manner, as other proteins associated with lipid droplets, such as Plin3, Cideb and Cidea, were not significantly changed in response to Hdac3 depletion (**Supplementary Fig. 5b,c**). Thus, enhanced lipid sequestration causes a reduced availability of fatty acids to the FAO machinery in mitochondria, resulting in reduced FAO activity without an accumulation of acyl-CoA. In sharp contrast, HFD-induced fatty liver is associated with higher concentrations of hepatic acyl-CoA species[38–40] compared to chow-fed controls. When compared to Hdac3 depletion at the same degree of hepatosteatosis, HFD feeding caused less upregulated expression of the genes involved in lipid storage and sequestration (**Supplementary Fig. 6a,b**), highlighting the key role of intracellular lipid sequestration in combating lipotoxicity. Together, these results suggest that loss of Hdac3 derepresses metabolic genes and reroutes metabolites toward lipid synthesis and intracellular sequestration, which underlies hepatosteatosis.

Metabolic rerouting reduces hepatic glucose production

We next addressed the mechanism underlying the regulation of glucose metabolism by Hdac3. In primary hepatocytes isolated from fasted mice without hepatic Hdac3, glucose production from the precursors lactate and pyruvate was significantly lower compared to that seen in primary hepatocytes from AAV-Tbg-GFP control mice (**Fig. 5a**). In addition, the already high concentrations of intracellular triglyceride in Hdac3-depleted hepatocytes were further increased after exposure to lactate and pyruvate for 2 h (**Fig. 5a**), suggesting that these gluconeogenic precursors were rerouted into intracellular lipid pools instead of being used for glucose production. Indeed, the reduction in glucose output calculated in the number of carbon atoms was nearly 3 μmol per mg protein during the 2 h period, and the increase in intracellular triglyceride was about 2 μmol carbon atoms per mg protein (based on the mass of tripalmitin). Considering that only two out of the three carbons in lactate and pyruvate contribute to lipogenesis, these data strongly support the hypothesis that the reduced gluconeogenesis in the absence of Hdac3 is explained by enhanced lipogenesis.

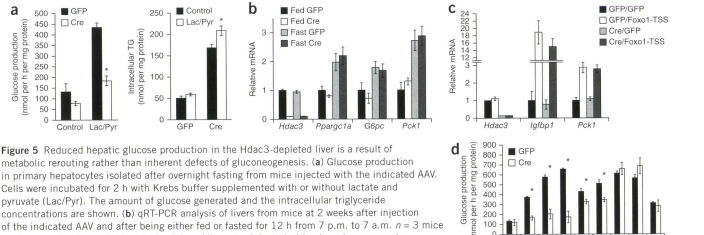

Figure 5 Reduced hepatic glucose production in the Hdac3-depleted liver is a result of metabolic rerouting rather than inherent defects of gluconeogenesis. (**a**) Glucose production in primary hepatocytes isolated after overnight fasting from mice injected with the indicated AAV. Cells were incubated for 2 h with Krebs buffer supplemented with or without lactate and pyruvate (Lac/Pyr). The amount of glucose generated and the intracellular triglyceride concentrations are shown. (**b**) qRT-PCR analysis of livers from mice at 2 weeks after injection of the indicated AAV and after being either fed or fasted for 12 h from 7 p.m. to 7 a.m. $n = 3$ mice per treatment. (**c**) qRT-PCR analysis of liver. Mice were injected with adenovirus expressing either GFP or Foxo1-TSS (where TSS is a mutant containing the mutations T24A, S256A and S319A) 9 d after injection with the indicated AAV. After another 5 d, mice were fasted for 12 h (7 p.m. to 7 a.m.) and then refed for 6 h, followed by tissue harvest. In the key, the GFP or Cre listed before the backslash indicates the initial AAV administered and the GFP or Foxo1-TSS after the slash indicates the adenovirus administered 9 d later. $n = 4$ mice per treatment. (**d**) Glucose production in primary hepatocytes. Lactate and pyruvate (Lac/Pyr) were added together at 2 mM/0.2 mM, 10 mM/1 mM or 30 mM/3 mM; glycerol and fructose was added individually at 10 mM and 25 mM, $n = 3$ mice per treatment. All error bars, s.e.m. $^*P < 0.05$ for the comparison of the AAV-Tbg-Cre and AAV-Tbg-GFP groups by Student's two-tailed t test.

Hdac3 was recently suggested to be directly involved in forkhead box O1 (Foxo1)-mediated transcriptional control of hepatic gluconeogenesis[41]. However, we found that deletion of Hdac3 in the liver did not alter the expression of key gluconeogenic genes, including *Ppargc1a* (peroxisome proliferator-activated receptor γ coactivator 1α), *G6pc* (glucose 6-phosphatase) and *Pck1* (phosphoenolpyruvate carboxykinase), under either fed or fasting conditions (**Fig. 5b**). To address whether Hdac3 is required specifically for Foxo1-mediated transcription, mice with or without hepatic Hdac3 were injected with adenovirus expressing constitutively active Foxo1. A gene expression analysis in the livers of these mice showed that the loss of Hdac3 did not interfere with Foxo1-dependent transcription of its target genes *Igfbp1* and *Pck1* (**Fig. 5c**). These data suggest that gluconeogenesis is not inherently defective in the Hdac3-depleted liver.

To circumvent the competition for substrates from lipogenesis, we sought to determine whether the lower glucose production in Hdac3-depleted hepatocytes compared to AAV-Tbg-GFP control hepatocytes could be rescued with substrates that are more direct precursors for gluconeogenesis but are less direct precursors for lipogenesis. Lactate and pyruvate were unable to rescue the lower glucose production even at high concentrations (**Fig. 5d**), presumably because of the enhanced pyruvate-malate cycle that is driven by continuous consumption of acetyl-CoA and NADPH in lipogenesis (**Fig. 4f**) and because of potentially limited pyruvate carboxylase activities resulting from low concentrations of acetyl-CoA (**Fig. 4i**). Glycerol significantly boosted glucose production in Hdac3-depleted hepatocytes but could not completely rescue it (**Fig. 5d**), which is in line with the fact that glycerol bypasses the citric acid cycle when it is used for gluconeogenesis but can also be directly used for fatty acid esterification. Fructose, a more direct glucose precursor, when used at a concentration (10–25 mM) well above its K_m for hexokinase (about 1–2 mM), completely rescued glucose production in Hdac3-depleted hepatocytes (**Fig. 5d**), excluding the possibility of any inherent defects in the last several steps of gluconeogenesis, including the step catalyzed by G6pc, in these cells. Exposing hepatocytes to a fatty acid synthase inhibitor, C75, also masked the difference in glucose production between Hdac3-depleted and control AAV-Tbg-GFP hepatocytes (**Fig. 5d**), supporting the notion that the metabolic rerouting toward lipid synthesis and sequestration contributes to the lower glucose production in Hdac3-depleted hepatocytes.

Lipid sequestration, steatosis and insulin resistance

Our studies in primary hepatocytes provided *in vitro* evidence that hepatic glucose production is dominated by the lipid synthesis and sequestration pathway when Hdac3 is depleted. To test this hypothesis *in vivo*, we sought to specifically inhibit lipid synthesis and sequestration in the liver. Several considerations prompted us to target Plin2: (i) the lipid-droplet–coating protein has been known to have an essential role in lipid sequestration and the inhibition of basal lipolysis[35]; (ii) our gene expression analysis showed that *Plin2* is among the most prominently upregulated genes in the Hdac3-depleted liver; (iii) it is known that Plin2 is required for hepatosteatosis and for upregulated lipogenic gene expression under prodiabetic conditions[42,43]; and (iv) antisense oligonucleotides (ASO) against *Plin2* are available for liver-specific knockdown[43].

We found that treatment of AAV-Tbg-Cre and AAV-Tbg-GFP control mice with ASO against *Plin2* blunted the prominent upregulation of Plin2 by Hdac3 deletion in liver (**Fig. 6a**). Consistent with previous findings[43], knockdown of Plin2 suppressed the hepatic *de novo* lipogenesis flux that was enhanced by Hdac3 deletion (**Fig. 6b**), suggesting that crosstalk exists between lipid storage and lipid synthesis. Plin2 knockdown clearly ameliorated the hepatosteatosis induced by Hdac3 depletion (**Fig. 6c,d**), and the steatotic areas that remained after Plin2 knockdown were primarily in regions that were proximal to central veins (**Fig. 6c**). Thus, enhanced lipogenesis and lipid sequestration contributed substantially to the development of hepatosteatosis after Hdac3 depletion. Of note, although Plin2 knockdown did not alter body weight in either the Hdac3-depleted or the AAV-Tbg-GFP control mice (**Fig. 6e**), it did blunt the improved tolerance to glucose (**Fig. 6f,g**) and insulin (**Fig. 6h,i**) in the hepatic Hdac3-depleted mice, strongly supporting the notion that lipid sequestration is a key causal factor in the dissociation of hepatosteatosis from insulin

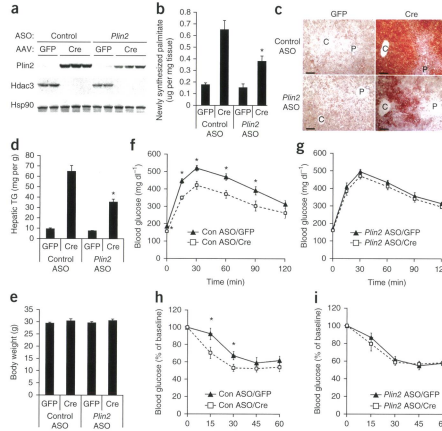

Figure 6 Lipid sequestration is required for the development of severe hepatosteatosis and improved glucose tolerance in mice without hepatic Hdac3. (**a**) Western blot analysis of total liver lysates from mice injected with either control ASO or ASO against *Plin2*, in addition to the indicated AAV vectors. Hsp90 was used as the loading control. (**b**) Hepatic *de novo* lipogenesis rate measured by tracing ^2H-palmitate synthesized from ^2H_2O. $n = 6$ mice per treatment. (**c**) ORO staining of liver. C, central vein; P, portal vein. Scale bars, 50 μm. (**d**) Hepatic triglyceride measurements. $n = 6$ mice per treatment. (**e**) Body weight measurements at 2 weeks after injection of the indicated AAV. $n = 7$ or 8 mice per treatment. (**f**,**g**) Results from the glucose tolerance test at 2 weeks after injection with the indicated AAV and ASO. $n = 7$ or 8 mice per treatment. Con ASO/GFP, control ASO plus AAV-Tbg-GFP; Con ASO/Cre, control ASO plus AAV-Tbg-Cre; *Plin2* ASO/GFP, ASO against *Plin2* plus AAV-Tbg-GFP; *Plin2* ASO/Cre, ASO against *Plin2* plus AAV-Tbg-Cre. (**h**,**i**) Insulin tolerance test at 2 weeks after injection with the indicated AAV. $n = 7$ or 8 mice per treatment. All error bars, s.e.m. $^*P < 0.05$ for the comparison of the AAV-Tbg-Cre and AAV-Tbg-GFP groups by Student's two-tailed *t* test.

resistance. Consistent with this, hepatic overexpression of Plin2 (**Supplementary Fig. 7a**,**b**) in wild-type mice caused hepatosteatosis (**Supplementary Fig. 7c**,**d**) that was associated with hypoglycemia (**Supplementary Fig. 7e**), hypoinsulinemia (**Supplementary Fig. 7f**) and improved whole-body insulin sensitivity (**Supplementary Fig. 7g**) without any associated changes in body weight (**Supplementary Fig. 7h**). Collectively, these data show that enhanced lipid synthesis and sequestration contribute to altered carbohydrate metabolism and insulin hypersensitivity in mice lacking hepatic Hdac3.

DISCUSSION

The liver is the central nexus of energy metabolism and governs the fate of substrates in response to nutritional and hormonal signals. Under normal physiological conditions, both hepatic glucose production and lipid synthesis have a circadian rhythm[20]. Our findings establish that the rhythmic rerouting of metabolic intermediates between the two synthetic pathways is directly regulated by the molecular circadian clock through the epigenomic modifier Hdac3 (**Supplementary Fig. 8**). During the day, when the nocturnal mouse is inactive and feeding less, Hdac3 is recruited to the genome and represses the expression of genes involved in lipid synthesis and sequestration, allowing for metabolic precursors to be directed toward gluconeogenesis to maintain normoglycemia. During the active and feeding night period, the virtual absence of Hdac3 at these genomic regions derepresses lipogenesis and reroutes metabolic intermediates toward lipid synthesis for energy storage at the expense of glucose production. This model is supported by the following findings: (i) depletion of Hdac3 in the liver results in the upregulation of genes involved in lipid synthesis and sequestration but does not alter the expression of key gluconeogenic genes; (ii) the chromatin occupancy of Hdac3 is predominantly on genes involved in lipid metabolism and has a circadian pattern, with the maximum occupancy occurring during fasting and minimum occupancy occurring during feeding[22]; (iii) hepatic glycogen concentrations are reduced by Hdac3 deletion, contrary to what would be expected if there was a primary defect in G6pc activity and an inability to generate glucose from glycogen[41,44]; (iv) glucose synthesis from the canonical precursors pyruvate and lactate is reduced in hepatocytes by Hdac3 depletion concurrently with an increase in lipid synthesis from the same precursors; (v) the low glucose production in Hdac3-depleted hepatocytes can be rescued by fructose, a six-carbon precursor of glucose, or by the inhibition of lipid synthesis, suggesting that gluconeogenesis is inherently intact but is dominated by the routing of three-carbon metabolites toward lipid synthesis; (vi) the low acetyl-CoA content is accompanied by an enhanced lipogenesis flux in the Hdac3-depleted liver, suggesting that acetyl-CoA is shunted toward lipogenesis, which may limit the activity of pyruvate carboxylase and thus reduce gluconeogenesis; (vii) the improved glucose and insulin tolerance in Hdac3 liver-specific knockout mice is attenuated by the suppression of the metabolic rerouting toward lipid synthesis and storage through knockdown of the lipid-sequestering and lipid-droplet–coating protein Plin2; and (viii) overexpression of Plin2 in the livers of wild-type mice results in hepatosteatosis and improved insulin sensitivity, mimicking the metabolic phenotype in mice without hepatic Hdac3

We here highlight the integrated nature of metabolism. Our results show that a given metabolic process can be modulated by the rerouting of metabolites without altering the enzymes that are immediately involved in that process, as exemplified by the indirect regulation of gluconeogenesis by Hdac3. Notably, a parallel and independent metabolic rerouting may be coordinated by hepatic Foxo proteins, which

are active in driving gluconeogenic gene expression during fasting and are inhibited by Akt-mediated phosphorylation and p300-mediated acetylation during feeding[45]. Constitutively active Foxo1 increases glucose production and seems to reduce hepatic lipid output, as evidenced by hypolipidemia[46,47]. Conversely, depletion of hepatic Foxo proteins decreases glucose production and tends to increase lipid synthesis, as evidenced by hepatosteatosis or hyperlipidemia[48,49]. In both situations, the effects of Foxo proteins on gluconeogenesis are through well-characterized direct transcriptional activation, whereas the effects of the Foxo proteins on lipid metabolism are less well defined and are still under debate. Of note, the acetylation of the Foxo proteins decreases their transactivation activity[45], and it has been shown that recombinant Hdac3 protein can deacetylate Foxo1 *in vitro*[41]. However, our findings that depletion of Hdac3 in the liver does not alter Foxo1-dependent transcription and does not cause the predicted accumulation of glycogen clearly indicate that the potential deacetylation of Foxo1 is not essential for the effects of Hdac3 on glucose metabolism *in vivo*. We speculate that Foxo-mediated transcriptional activation and Hdac3-mediated transcriptional repression may function collectively, but independently, to divert metabolic intermediates between glucose production and lipid synthesis during the fasting-feeding and light-dark cycles. Although Hdac3 clearly functions as an epigenomic modifier in the liver[22], it may also have non-histone protein targets, as well as deacetylase-independent functions.

In contrast to the circadian shifting between hepatic lipogenesis and gluconeogenesis under normal physiological conditions, pathological overnutrition provides excess metabolic intermediates that oversaturate and constantly activate both pathways. This leads to the coexistence of hepatosteatosis and insulin resistance. However, the concurrent insulin hypersensitivity and severe hepatosteatosis present in mice without hepatic Hdac3 clearly shows that hepatosteatosis and insulin resistance *per se* do not necessarily have a cause and effect relationship. Among the most prominently upregulated genes in the Hdac3-depleted liver are those encoding lipid-droplet–associated proteins, including *Plin2*, *Cidec*, *Fitm1* and *G0S2*, which negatively regulate lipolysis and the subsequent release of lipids in a cooperative manner[8,16,35–37,50,51]. Low acyl-CoA content is accompanied by a reduced FAO flux in the Hdac3-depleted liver, suggesting that acyl-CoA is shunted toward glycerolipid synthesis and the subsequent sequestration from mitochondrial oxidation machinery. Prkce activity and inflammation are not enhanced in the Hdac3-depleted liver, despite elevated total DAG and triglyceride contents, suggesting that these lipids are sequestered in lipid droplets and, hence, prevented from activating cytosolic kinases. Dampening the upregulation of Plin2 masked the insulin hypersensitivity in mice without hepatic Hdac3, whereas hepatic overexpression of Plin2 in wild-type mice resulted in steatosis and improved whole-body insulin sensitivity, supporting an essential role of intracellular lipid sequestration in preventing lipotoxicity and lipid-induced hepatic insulin resistance. Consistent with our findings, the insulin-sensitizing effect of Plin2 was observed previously in cultured hepatocytes in which depletion of Plin2 and other perilipin proteins decreased the cellular responses to insulin[52]. In addition, dissociation of hepatosteatosis from insulin resistance was observed in mice and humans that were deficient in either lipolysis or hepatic triglyceride secretion[8,18,53–55]. All these findings can be unified under the hypothesis that hepatic insulin resistance is determined by whether lipid droplets sequester lipid content well enough to prevent the cytosolic accumulation of deleterious lipid species.

Although hepatic lipogenesis is upregulated and required for the development of steatosis in both chow-fed mice lacking hepatic Hdac3 and wild-type mice on a HFD, a key difference between these two groups is in the balance between the capacity for lipid sequestration and the content of metabolic intermediates. In overnutrition mouse models (HFD or *ob/ob*), excess delivery of metabolic intermediates to the liver is the primary event, whereas increased hepatic lipid synthesis and storage is an adaptive response. However, the lipid sequestration capacity is insufficient relative to the overwhelming lipid content influx, leading to the accumulation of harmful lipid intermediates that promote insulin resistance. In this context, the ablation of Plin2 reduces lipid synthesis and thus reduces the generation of harmful lipid species, leading to improved insulin sensitivity[43,56]. In the Hdac3-deficient mouse model, the primary event of upregulated lipogenesis diverts metabolic precursors away from glucose production. In addition, reduced fatty acid oxidation and acetyl-CoA concentrations may contribute to a decrease in pyruvate carboxylase activity and thus limit the flux of pyruvate to glucose production. Collectively, these changes result in reduced glucose output and insulin hypersensitivity. Knockdown of Plin2 on this background reduces lipid synthesis and metabolic rerouting and therefore ameliorates insulin hypersensitivity. This highlights the concept that hepatic lipid accumulation has a diverse pathogenesis and requires specifically targeted therapies, which is crucial to consider in light of the failure of large therapeutic trials (such as the Action to Control Cardiovascular Risk in Diabetes (ACCORD) trial) that lump all diabetes together[57].

METHODS

Methods and any associated references are available in the online version of the paper.

Note: Supplementary information is available in the online version of the paper.

ACKNOWLEDGMENTS

We thank J. Millar and the Metabolic Tracer Resource at the Penn Institute for Diabetes, Obesity and Metabolism for the lipogenesis flux assay. We thank the Mouse Metabolic Phenotyping Core and the Viral Vector Core at Penn Diabetes Research Center (P30 DK19525) and the Penn Digestives Disease Center Morphology Core (P30 DK050306) at the University of Pennsylvania. We thank the Vanderbilt (DK59637) and Yale (U24 DK059635) Mouse Metabolic Phenotyping Centers and the Children's Hospital of Philadelphia Pathology Core. We thank B. Agarwal and S. Mullican for helpful discussion. This work was supported by US National Institutes of Health grants R37 DK43806 (M.A.L.), P01 DK49210 (M.A.L., M.J. Birnbaum and R.S.A.) and R01 DK40936 (G.I.S.), R01 DK075017 (C.S.), the Department of Veteran Affairs Merit Review Program (T.G.U.), grant F32 DK079572 (R.A.M.), the JPB Foundation and the Cox Institute for Medical Research.

AUTHOR CONTRIBUTIONS

Z.S. and M.A.L. conceived of the hypothesis and designed the experiments. Z.S., R.A.M., R.T.P., J.C., R.D., H.W. and D.Z. performed the experiments. Z.S., R.A.M., R.D., T.G.U., G.I.S., C.S., M.J. Bennett, R.S.A., M.J. Birnbaum and M.A.L. analyzed and interpreted the data. M.J.G. provided reagents. Z.S. and M.A.L. wrote the manuscript.

COMPETING FINANCIAL INTERESTS

The authors declare no competing financial interests.

Published online at http://www.nature.com/doifinder/10.1038/nm.2744.
Reprints and permissions information is available online at http://www.nature.com/reprints/index.html.

1. Cohen, J.C., Horton, J.D. & Hobbs, H.H. Human fatty liver disease: old questions and new insights. *Science* **332**, 1519–1523 (2011).
2. Browning, J.D. & Horton, J.D. Molecular mediators of hepatic steatosis and liver injury. *J. Clin. Invest.* **114**, 147–152 (2004).
3. Utzschneider, K.M. & Kahn, S.E. Review: the role of insulin resistance in nonalcoholic fatty liver disease. *J. Clin. Endocrinol. Metab.* **91**, 4753–4761 (2006).
4. Nagle, C.A., Klett, E.L. & Coleman, R.A. Hepatic triacylglycerol accumulation and insulin resistance. *J. Lipid Res.* **50** (suppl.), S74–S79 (2009).

5. Postic, C. & Girard, J. Contribution of *de novo* fatty acid synthesis to hepatic steatosis and insulin resistance: lessons from genetically engineered mice. *J. Clin. Invest.* **118**, 829–838 (2008).
6. Samuel, V.T., Petersen, K.F. & Shulman, G.I. Lipid-induced insulin resistance: unravelling the mechanism. *Lancet* **375**, 2267–2277 (2010).
7. Lonardo, A., Bellentani, S., Ratziu, V. & Loria, P. Insulin resistance in nonalcoholic steatohepatitis: necessary but not sufficient—death of a dogma from analysis of therapeutic studies? *Expert Rev. Gastroenterol. Hepatol.* **5**, 279–289 (2011).
8. Lass, A., Zimmermann, R., Oberer, M. & Zechner, R. Lipolysis—a highly regulated multi-enzyme complex mediates the catabolism of cellular fat stores. *Prog. Lipid Res.* **50**, 14–27 (2011).
9. Donnelly, K.L. *et al.* Sources of fatty acids stored in liver and secreted via lipoproteins in patients with nonalcoholic fatty liver disease. *J. Clin. Invest.* **115**, 1343–1351 (2005).
10. Larter, C.Z. & Yeh, M.M. Animal models of NASH: getting both pathology and metabolic context right. *J. Gastroenterol. Hepatol.* **23**, 1635–1648 (2008).
11. Biddinger, S.B. & Kahn, C.R. From mice to men: insights into the insulin resistance syndromes. *Annu. Rev. Physiol.* **68**, 123–158 (2006).
12. Taniguchi, C.M. *et al.* Divergent regulation of hepatic glucose and lipid metabolism by phosphoinositide 3-kinase via Akt and PKCλ/ζ. *Cell Metab.* **3**, 343–353 (2006).
13. Leavens, K.F., Easton, R.M., Shulman, G.I., Previs, S.F. & Birnbaum, M.J. Akt2 is required for hepatic lipid accumulation in models of insulin resistance. *Cell Metab.* **10**, 405–418 (2009).
14. Brown, M.S. & Goldstein, J.L. Selective versus total insulin resistance: a pathogenic paradox. *Cell Metab.* **7**, 95–96 (2008).
15. Stiles, B. *et al.* Liver-specific deletion of negative regulator Pten results in fatty liver and insulin hypersensitivity. *Proc. Natl. Acad. Sci. USA* **101**, 2082–2087 (2004).
16. Greenberg, A.S. *et al.* The role of lipid droplets in metabolic disease in rodents and humans. *J. Clin. Invest.* **121**, 2102–2110 (2011).
17. Matsuzaka, T. *et al.* Crucial role of a long-chain fatty acid elongase, Elovl6, in obesity-induced insulin resistance. *Nat. Med.* **13**, 1193–1202 (2007).
18. Brown, J.M. *et al.* CGI-58 knockdown in mice causes hepatic steatosis but prevents diet-induced obesity and glucose intolerance. *J. Lipid Res.* **51**, 3306–3315 (2010).
19. Tuomilehto, J. *et al.* Prevention of type 2 diabetes mellitus by changes in lifestyle among subjects with impaired glucose tolerance. *N. Engl. J. Med.* **344**, 1343–1350 (2001).
20. Bass, J. & Takahashi, J.S. Circadian integration of metabolism and energetics. *Science* **330**, 1349–1354 (2010).
21. Desvergne, B., Michalik, L. & Wahli, W. Transcriptional regulation of metabolism. *Physiol. Rev.* **86**, 465–514 (2006).
22. Feng, D. *et al.* A circadian rhythm orchestrated by histone deacetylase 3 controls hepatic lipid metabolism. *Science* **331**, 1315–1319 (2011).
23. Panda, S. *et al.* Coordinated transcription of key pathways in the mouse by the circadian clock. *Cell* **109**, 307–320 (2002).
24. Lawless, M.W., Norris, S., O'Byrne, K.J. & Gray, S.G. Targeting histone deacetylases for the treatment of immune, endocrine & metabolic disorders. *Endocr. Metab. Immune Disord. Drug Targets* **9**, 84–107 (2009).
25. Sun, Z., Feng, D., Everett, L.J., Bugge, A. & Lazar, M.A. Circadian epigenomic remodeling and hepatic lipogenesis: lessons from HDAC3. *Cold Spring Harb. Symp. Quant. Biol.* published online, doi:10.1101/sqb.2011.76.011494 (6 September 2011).
26. Knutson, S.K. *et al.* Liver-specific deletion of histone deacetylase 3 disrupts metabolic transcriptional networks. *EMBO J.* **27**, 1017–1028 (2008).
27. Mullican, S.E. *et al.* Histone deacetylase 3 is an epigenomic brake in macrophage alternative activation. *Genes Dev.* **25**, 2480–2488 (2011).
28. Bell, P. *et al.* Evaluation of adeno-associated viral vectors for liver-directed gene transfer in dogs. *Hum. Gene Ther.* **22**, 985–997 (2011).
29. Samuel, V.T. *et al.* Inhibition of protein kinase Cε prevents hepatic insulin resistance in nonalcoholic fatty liver disease. *J. Clin. Invest.* **117**, 739–745 (2007).
30. Calvo, M.N. *et al.* PFKFB3 gene silencing decreases glycolysis, induces cell-cycle delay and inhibits anchorage-independent growth in HeLa cells. *FEBS Lett.* **580**, 3308–3314 (2006).
31. Bolaños, J.P., Almeida, A. & Moncada, S. Glycolysis: a bioenergetic or a survival pathway? *Trends Biochem. Sci.* **35**, 145–149 (2010).
32. Seo, Y.-K. *et al.* Genome-wide analysis of SREBP-1 binding in mouse liver chromatin reveals a preference for promoter proximal binding to a new motif. *Proc. Natl. Acad. Sci. USA* **106**, 13765–13769 (2009).
33. Seo, Y.-K. *et al.* Genome-wide localization of SREBP-2 in hepatic chromatin predicts a role in autophagy. *Cell Metab.* **13**, 367–375 (2011).
34. Wendel, A.A., Lewin, T.M. & Coleman, R.A. Glycerol-3-phosphate acyltransferases: rate limiting enzymes of triacylglycerol biosynthesis. *Biochim. Biophys. Acta* **1791**, 501–506 (2009).
35. Brasaemle, D.L. Thematic review series: adipocyte biology. The perilipin family of structural lipid droplet proteins: stabilization of lipid droplets and control of lipolysis. *J. Lipid Res.* **48**, 2547–2559 (2007).
36. Gong, J., Sun, Z. & Li, P. CIDE proteins and metabolic disorders. *Curr. Opin. Lipidol.* **20**, 121–126 (2009).
37. Puri, V. *et al.* Fat-specific protein 27, a novel lipid droplet protein that enhances triglyceride storage. *J. Biol. Chem.* **282**, 34213–34218 (2007).
38. Samuel, V.T. *et al.* Mechanism of hepatic insulin resistance in non-alcoholic fatty liver disease. *J. Biol. Chem.* **279**, 32345–32353 (2004).
39. Hammond, L.E. *et al.* Mitochondrial glycerol-3-phosphate acyltransferase-1 is essential in liver for the metabolism of excess acyl-CoAs. *J. Biol. Chem.* **280**, 25629–25636 (2005).
40. Nilsson, A., Thomassen, M.S. & Christiansen, E. Long-chain Acyl-CoA levels in liver from rats fed high-fat diets: is it of significance for an increased peroxisomal β-oxidation? *Lipids* **19**, 187–194 (1984).
41. Mihaylova, M.M. *et al.* Class IIa histone deacetylases are hormone-activated regulators of FOXO and mammalian glucose homeostasis. *Cell* **145**, 607–621 (2011).
42. Chang, B.H.-J. *et al.* Protection against fatty liver but normal adipogenesis in mice lacking adipose differentiation-related protein. *Mol. Cell. Biol.* **26**, 1063–1076 (2006).
43. Imai, Y. *et al.* Reduction of hepatosteatosis and lipid levels by an adipose differentiation-related protein antisense oligonucleotide. *Gastroenterology* **132**, 1947–1954 (2007).
44. Mutel, E. *et al.* Control of blood glucose in the absence of hepatic glucose production during prolonged fasting in mice: induction of renal and intestinal gluconeogenesis by glucagon. *Diabetes* **60**, 3121–3131 (2011).
45. Vogt, P.K., Jiang, H. & Aoki, M. Triple layer control: phosphorylation, acetylation and ubiquitination of FOXO proteins. *Cell Cycle* **4**, 908–913 (2005).
46. Zhang, W. *et al.* FoxO1 regulates multiple metabolic pathways in the liver: effects on gluconeogenic, glycolytic, and lipogenic gene expression. *J. Biol. Chem.* **281**, 10105–10117 (2006).
47. Banks, A.S. *et al.* Dissociation of the glucose and lipid regulatory functions of FoxO1 by targeted knockin of acetylation-defective alleles in mice. *Cell Metab.* **14**, 587–597 (2011).
48. Haeusler, R.A., Han, S. & Accili, D. Hepatic FoxO1 ablation exacerbates lipid abnormalities during hyperglycemia. *J. Biol. Chem.* **285**, 26861–26868 (2010).
49. Tao, R. *et al.* Hepatic FoxOs regulate lipid metabolism via modulation of expression of the nicotinamide phosphoribosyltransferase gene. *J. Biol. Chem.* **286**, 14681–14690 (2011).
50. Kadereit, B. *et al.* Evolutionarily conserved gene family important for fat storage. *Proc. Natl. Acad. Sci. USA* **105**, 94–99 (2008).
51. Yang, X. *et al.* The G(0)/G(1) switch gene 2 regulates adipose lipolysis through association with adipose triglyceride lipase. *Cell Metab.* **11**, 194–205 (2010).
52. Bell, M. *et al.* Consequences of lipid droplet coat protein downregulation in liver cells: abnormal lipid droplet metabolism and induction of insulin resistance. *Diabetes* **57**, 2037–2045 (2008).
53. Kantartzis, K. *et al.* Dissociation between fatty liver and insulin resistance in humans carrying a variant of the patatin-like phospholipase 3 gene. *Diabetes* **58**, 2616–2623 (2009).
54. Minehira, K. *et al.* Blocking VLDL secretion causes hepatic steatosis but does not affect peripheral lipid stores or insulin sensitivity in mice. *J. Lipid Res.* **49**, 2038–2044 (2008).
55. Schonfeld, G., Yue, P., Lin, X. & Chen, Z. Fatty liver and insulin resistance: not always linked. *Trans. Am. Clin. Climatol. Assoc.* **119**, 217–223, discussion 223–224 (2008).
56. Chang, B.H.-J., Li, L., Saha, P. & Chan, L. Absence of adipose differentiation related protein upregulates hepatic VLDL secretion, relieves hepatosteatosis, and improves whole body insulin resistance in leptin-deficient mice. *J. Lipid Res.* **51**, 2132–2142 (2010).
57. Gerstein, H.C. *et al.* Effects of intensive glucose lowering in type 2 diabetes. *N. Engl. J. Med.* **358**, 2545–2559 (2008).

nature medicine

NF-κB–inducing kinase (NIK) promotes hyperglycemia and glucose intolerance in obesity by augmenting glucagon action

Liang Sheng[1], Yingjiang Zhou[1], Zheng Chen[1], Decheng Ren[1], Kae Won Cho[1], Lin Jiang[1], Hong Shen[1], Yoshiteru Sasaki[2] & Liangyou Rui[1]

The canonical inhibitor of nuclear factor κB kinase subunit β (IKK-β)–nuclear factor of κ light polypeptide gene enhancer in B cells 1 (NF-κB1) pathway has been well documented to promote insulin resistance; however, the noncanonical NF-κB–inducing kinase (NIK)–NF-κB2 pathway is not well understood in obesity. Additionally, the contribution of counter-regulatory hormones, particularly glucagon, to hyperglycemia in obesity is unclear. Here we show that NIK promotes glucagon responses in obesity. Hepatic NIK was abnormally activated in mice with dietary or genetic obesity. Systemic deletion of *Map3k14*, encoding NIK, resulted in reduced glucagon responses and hepatic glucose production (HGP). Obesity is associated with high glucagon responses, and liver-specific inhibition of NIK led to lower glucagon responses and HGP and protected against hyperglycemia and glucose intolerance in obese mice. Conversely, hepatocyte-specific overexpression of NIK resulted in higher glucagon responses and HGP. In isolated mouse livers and primary hepatocytes, NIK also promoted glucagon action and glucose production, at least in part by increasing cAMP response element-binding (CREB) stability. Therefore, overactivation of liver NIK in obesity promotes hyperglycemia and glucose intolerance by increasing the hyperglycemic response to glucagon and other factors that activate CREB.

Obesity is associated with chronic inflammation that is believed to contribute to the pathogenesis of type 2 diabetes[1,2]. Proinflammatory cytokines activate the canonical IKK-β–NF-κB1 and the Jun N-terminal kinase (JNK) pathways, which is believed to impair glucose metabolism by increasing insulin resistance[3–5]. Blood glucose concentrations are determined by a balance between insulin and counter-regulatory hormones (for example, glucagon, catecholamines, glucocorticoids or growth hormone)[6]. In the fasting state, glucagon is secreted by pancreatic α cells and increases HGP by stimulating hepatic glycogenolysis and gluconeogenesis[6]. Glucagon stimulates the phosphorylation and activation of CREB through the cAMP–protein kinase A pathway, and CREB in turn activates the transcription of key gluconeogenic enzymes, including phosphoenolpyruvate carboxykinase (PEPCK) and glucose-6-phosphatase (G6Pase)[7]. In rodents with type 1 diabetes, glucagon action is high and contributes to hyperglycemia and glucose intolerance[8–10]. Blood glucagon concentrations are elevated in rodents with insulin deficiency, and leptin treatments normalize hyperglucagonemia and hyperglycemia[8,9]. Deletion of glucagon receptors prevents streptozotocin (STZ)-induced hyperglycemia and glucose intolerance[10]. In a type 2 diabetes model, leptin treatments also attenuate hyperglucagonemia, leading to improvement in hyperglycemia and glucose intolerance[11]. Insulin suppresses glucagon secretion from α cells[12]; therefore, α cell insulin resistance may lead to hyperglucagonemia, which contributes to hyperglycemia in type 2 diabetes.

A subset of cytokines also stimulates the noncanonical NIK–NF-κB2 pathway; however, the metabolic function of this pathway has not been examined. It is also unclear whether inflammation alters glucagon responses. NIK, also called MAP3K14 (NM_003954), is an essential upstream serine/threonine kinase of the noncanonical NIK–NF-κB2 pathway[13]. NIK protein concentrations are extremely low in quiescent cells as a result of rapid degradation, and cytokines and oxidative stress increase NIK protein stability, leading to NIK activation[14]. NIK has been reported to regulate B and T cell development in mice[15,16]. In this study we show that liver NIK is aberrantly activated in obesity and increases HGP by promoting glucagon action in mice, thus contributing to hyperglycemia and glucose intolerance. NIK promotes glucagon action, at least in part, by increasing CREB stability.

RESULTS

NIK is abnormally activated in the livers of obese mice

We measured NIK activity in two commonly used mouse models of obesity: dietary obesity and genetic obesity with leptin deficiency (*ob/ob*). We immunopurified NIK protein from the livers of mice from these two models and subjected it to *in vitro* kinase assays using the glutathione-S transferase (GST)–IKK-α (amino acids 108–368) fusion protein as a substrate. GST–IKK-α contains an NIK phosphorylation site (IKK-α Ser176) and lacks catalytic activity[17]. NIK activity in the

[1]Department of Molecular and Integrative Physiology, University of Michigan Medical School, Ann Arbor, Michigan, USA. [2]Laboratory for Stem Cell Biology, Riken Center for Developmental Biology, Kobe, Japan. Correspondence should be addressed to L.R. (ruily@umich.edu).

Received 31 January; accepted 29 March; published online 13 May 2012; doi:10.1038/nm.2756

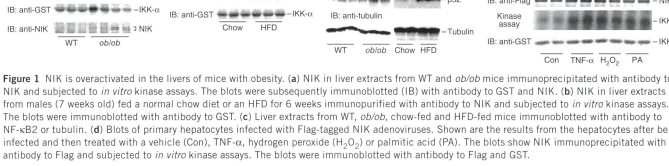

Figure 1 NIK is overactivated in the livers of mice with obesity. (**a**) NIK in liver extracts from WT and *ob/ob* mice immunoprecipitated with antibody to NIK and subjected to *in vitro* kinase assays. The blots were subsequently immunoblotted (IB) with antibody to GST and NIK. (**b**) NIK in liver extracts from males (7 weeks old) fed a normal chow diet or an HFD for 6 weeks immunopurified with antibody to NIK and subjected to *in vitro* kinase assays. The blots were immunoblotted with antibody to GST. (**c**) Liver extracts from WT, *ob/ob*, chow-fed and HFD-fed mice immunoblotted with antibody to NF-κB2 or tubulin. (**d**) Blots of primary hepatocytes infected with Flag-tagged NIK adenoviruses. Shown are the results from the hepatocytes after being infected and then treated with a vehicle (Con), TNF-α, hydrogen peroxide (H_2O_2) or palmitic acid (PA). The blots show NIK immunoprecipitated with antibody to Flag and subjected to *in vitro* kinase assays. The blots were immunoblotted with antibody to Flag and GST.

liver was tenfold higher in *ob/ob* mice (at 13 weeks of age) than in wild-type (WT) mice (**Fig. 1a**). Liver NIK activity was also 14-fold higher in mice fed a high-fat diet (HFD) than in mice fed a normal chow diet (**Fig. 1b**). We were able to detect NIK protein in the *ob/ob* mice (**Fig. 1a**) but not in the WT mice because of its rapid degradation[18,19]. The concentrations of the active form (p52) of NF-κB2 in the liver were higher in *ob/ob* mice than in WT mice and in HFD-fed mice than in chow-fed mice (**Fig. 1c**). In contrast, NIK activity in the skeletal muscles was similar between normal chow- and HFD-fed WT mice (**Supplementary Fig. 1a**).

Obesity is associated with chronic inflammation, oxidative stress and steatosis in the liver[1,2]. To determine whether these factors contribute to NIK activation, we examined the ability of tumor necrosis factor α (TNF-α) (which mimics inflammation), hydrogen peroxide (which mimics oxidative stress) and palmitic acid (which mimics steatosis) to stimulate NIK activity. We introduced recombinant NIK into mouse primary hepatocytes by NIK adenoviral infection, and we then treated the cells with each of the compounds. Treatment with TNF-α, hydrogen peroxide or palmitic acid increased both NIK autophosphorylation and the ability of NIK to phosphorylate GST–IKK-α (**Fig. 1d**). TNF-α, hydrogen peroxide and palmitic acid also stimulated endogenous NIK in hepatocytes (**Supplementary Fig. 1b**).

Inhibition of liver NIK improves glucose metabolism

To examine the metabolic function of NIK *in vivo*, we characterized previously generated NIK knockout mice[15]. The active form of NF-κB2 (p52) was abundant in WT but not knockout hepatocytes (**Supplementary Fig. 2a**). TNF-α similarly stimulated the degradation of inhibitor of κ light polypeptide gene enhancer in B cells (IκB) as well as the phosphorylation of IκB, p38 and JNK in both WT and knockout hepatocytes (**Supplementary Fig. 2b**). These results verify the previous findings that NIK is required for the noncanonical, but not the canonical, NF-κB pathways[15]. Notably, knockout mice had hypoglycemia (**Fig. 2a**) and greater glucose tolerance compared to WT littermates (**Fig. 2b**). HGP, estimated by pyruvate tolerance tests (PTT), was lower in knockout than in WT mice (**Fig. 2c**).

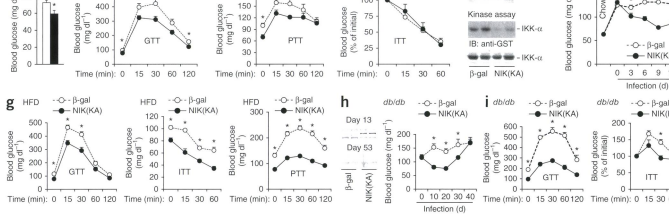

Figure 2 Inhibition of NIK in the liver decreases hyperglycemia and glucose intolerance in mice with obesity. (**a**–**d**) Blood glucose concentrations in WT and knockout (KO) males fed a normal chow diet. (**a**) Fasting blood glucose. WT, $n = 12$; knockout, $n = 16$ (all aged 7–8 weeks). (**b**) GTT. WT, $n = 8$; KO, $n = 11$ (aged 8 weeks). (**c**) PTT. WT, $n = 8$; KO, $n = 11$ (aged 8–9 weeks). (**d**) Insulin tolerance test (ITT). WT, $n = 9$; KO, $n = 10$ (aged 8 weeks). (**e**) Liver extracts from mice infected with β-galactosidase (β-gal) or Flag-tagged NIK(KA) adenoviruses and immunoblotted with antibody to Flag, as well as liver NIK immunopurified with antibody to NIK and subjected to *in vitro* kinase assays. (**f**,**g**) Blood glucose concentrations in C57BL/6 males (7 weeks old) fed an HFD and then infected with β-galactosidase or NIK(KA) adenoviruses. (**f**) Overnight fasting blood glucose. (**g**) GTT, ITT and PTT. β-galactosidase, $n = 9$ or 10; NIK(KA), $n = 10$. (**h**,**i**) Immunoblots and blood glucose concentrations from *db/db* males (8 weeks old) infected with β-galactosidase ($n = 8$) or NIK(KA) ($n = 9$) adenoviruses. (**h**) Liver extracts immunoblotted with antibody to Flag at the indicated times after infection (left). Overnight fasting blood glucose (right). (**i**) GTT and ITT. *$P < 0.05$ by two-tailed Student's t test. All data are mean ± s.e.m.

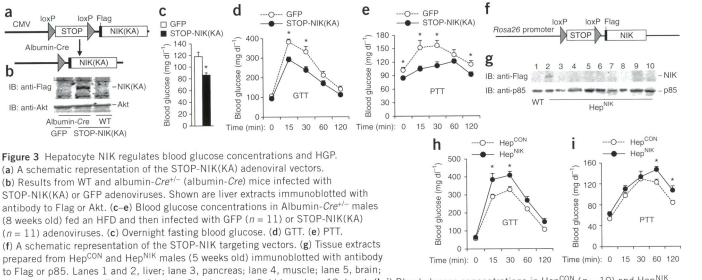

Figure 3 Hepatocyte NIK regulates blood glucose concentrations and HGP. (**a**) A schematic representation of the STOP-NIK(KA) adenoviral vectors. (**b**) Results from WT and albumin-*Cre*$^{+/-}$ (albumin-*Cre*) mice infected with STOP-NIK(KA) or GFP adenoviruses. Shown are liver extracts immunoblotted with antibody to Flag or Akt. (**c**–**e**) Blood glucose concentrations in Albumin-*Cre*$^{+/-}$ males (8 weeks old) fed an HFD and then infected with GFP ($n = 11$) or STOP-NIK(KA) ($n = 11$) adenoviruses. (**c**) Overnight fasting blood glucose. (**d**) GTT. (**e**) PTT. (**f**) A schematic representation of the STOP-NIK targeting vectors. (**g**) Tissue extracts prepared from Hep^{CON} and Hep^{NIK} males (5 weeks old) immunoblotted with antibody to Flag or p85. Lanes 1 and 2, liver; lane 3, pancreas; lane 4, muscle; lane 5, brain; lane 6, white fat; lane 7, brown fat; lane 8, spleen; lane 9, kidney; lane 10, heart. (**h**,**i**) Blood glucose concentrations in Hep^{CON} ($n = 10$) and Hep^{NIK} ($n = 7$) males fed a normal chow diet. (**h**) GTT. (**i**) PTT. *$P < 0.05$ by two-tailed Student's t test. Data are means ± s.e.m.

Plasma insulin concentrations (**Supplementary Fig. 2c**) and insulin tolerance (**Fig. 2d**) were relatively normal in the knockout mice.

To examine the role of liver NIK, we selectively inhibited NIK in the liver by adenovirally overexpressing kinase-inactive NIK(KA). NIK(KA) contains substitutions of Lys429 and Lys430 with alanines and acts as a dominant-negative mutant of NIK[20,21]. We detected the expression of Flag-tagged NIK(KA) and inhibition of NIK activity in the livers of mice infected with the NIK(KA) adenovirus but not when a β-galactosidase adenovirus control was used (**Fig. 2e**). We fed mice an HFD for 12 weeks and infected them with NIK(KA) or β-galactosidase adenoviruses. HFD promoted hyperglycemia; however, liver-specific inhibition of NIK significantly ameliorated the HFD-induced hyperglycemia (**Fig. 2f**), hyperinsulinemia (**Supplementary Fig. 3a**), glucose intolerance (**Fig. 2g**) and insulin resistance (**Fig. 2g**). HGP, estimated by PTT, was also lower in mice infected with NIK(KA) adenovirus than those infected with β-galactosidase adenovirus (**Fig. 2g**). The body weights and liver sizes were similar between the NIK(KA) and β-galactosidase groups (**Supplementary Fig. 3b**,**c**).

In *db/db* mice, which lack functional leptin receptors, blood glucose concentration was inversely correlated with NIK(KA) expression after infection with NIK(KA) adenovirus. We detected NIK(KA) in the livers of these mice 13 d after infection, but it was undetectable after 53 days (**Fig. 2h**). The blood glucose concentration in these mice was lowest at 10–20 d after NIK(KA) adenoviral infection and then increased progressively to reach concentrations at 40 d after infection that were similar to those in *db/db* mice that we infected with the β-galactosidase adenovirus (**Fig. 2h**). Glucose intolerance (**Fig. 2i**), insulin resistance (**Fig. 2i**) and hyperinsulinemia (**Supplementary Fig. 3d**) were also significantly lower in the NIK(KA) group than in the β-galactosidase group. Body weight and liver TNF-α expression were similar between the NIK(KA) and β-galactosidase groups (**Supplementary Fig. 3e**,**f**).

In *ob/ob* mice, liver-specific overexpression of NIK(KA) also reduced hyperglycemia (**Supplementary Fig. 3g**), glucose intolerance (**Supplementary Fig. 3h**), insulin resistance (**Supplementary Fig. 3i**) and HGP (**Supplementary Fig. 3j**). To further study NIK in hepatocytes, we generated STOP-NIK(KA) adenoviruses (**Fig. 3a**). In these adenoviruses, NIK(KA) expression was blocked by a STOP cassette and was able to be reactivated by Cre-mediated excision of the STOP cassette. To verify hepatocyte-specific expression of NIK(KA), we infected WT and albumin-*Cre*$^{+/-}$ mice with STOP-NIK(KA) or GFP adenoviruses. We detected NIK(KA) after infection with STOP-NIK(KA) adenovirus in the livers of albumin-*Cre*$^{+/-}$ but not WT mice (**Fig. 3b**). We fed the albumin-*Cre*$^{+/-}$ mice an HFD and infected them with STOP-NIK(KA) or GFP adenoviruses. Blood glucose concentrations (**Fig. 3c**), glucose intolerance (**Fig. 3d**) and HGP (**Fig. 3e**) were significantly lower in the STOP-NIK(KA) than the GFP groups. In contrast, STOP-NIK(KA) adenoviral infection neither lowered blood glucose concentrations nor improved glucose intolerance in WT mice (data not shown). Taken together, these data indicate that liver-specific inhibition of NIK decreases hyperglycemia and glucose intolerance in both dietary and genetic obesity independently of changes in body weight.

To determine whether activation of liver NIK is sufficient to alter glucose metabolism, we generated mice with hepatocyte-specific overexpression of Flag-tagged NIK (Hep^{NIK} mice) using previously generated STOP-NIK (Hep^{CON}) mice[22]. In Hep^{CON} mice with the genotype STOP-*Nik*$^{+/-}$; *Cre*$^{+/-}$, a STOP-*Map3k14* (also known as STOP-*Nik*) transgene was knocked in the *Rosa26* locus (**Fig. 3f**), and the STOP cassette blocked the expression of Flag-tagged NIK (**Fig. 3g**). To create the Hep^{NIK} mice (with the genotype STOP-*Nik*$^{+/-}$; *Cre*$^{+/-}$), we crossed Hep^{CON} mice with albumin-Cre mice. In Hep^{NIK} mice, Cre-mediated excision of the STOP sequences was restricted to the hepatocytes, resulting in modest expression of Flag-tagged NIK in the liver but not in the pancreas, muscle, brain, white fat, brown fat, spleen, kidney or heart (**Fig. 3g**). Glucose tolerance and pyruvate tolerance were impaired in Hep^{NIK} males fed a normal chow diet compared to Hep^{CON} mice on the same diet (**Fig. 3h**,**i**). Hep^{NIK} females fed an HFD also developed hyperglycemia and glucose intolerance (**Supplementary Fig. 4a**,**b**).

NIK promotes HGP by enhancing glucagon action

To directly measure HGP, we isolated livers from NIK knockout and WT mice and subjected them to *ex vivo* gluconeogenesis assays. In WT mice, the amount of hepatic gluconeogenesis was 1.4-fold higher in the fasting state than in the fed state (**Fig. 4a**). There was 92% less fasting-stimulated

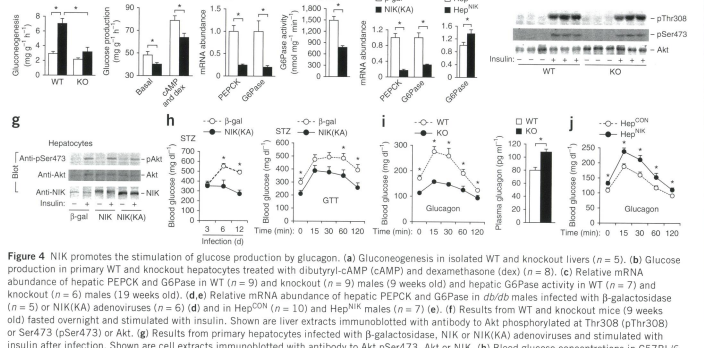

Figure 4 NIK promotes the stimulation of glucose production by glucagon. (**a**) Gluconeogenesis in isolated WT and knockout livers ($n = 5$). (**b**) Glucose production in primary WT and knockout hepatocytes treated with dibutyryl-cAMP (cAMP) and dexamethasone (dex) ($n = 8$). (**c**) Relative mRNA abundance of hepatic PEPCK and G6Pase in WT ($n = 9$) and knockout ($n = 9$) males (9 weeks old) and hepatic G6Pase activity in WT ($n = 7$) and knockout ($n = 6$) males (19 weeks old). (**d**,**e**) Relative mRNA abundance of hepatic PEPCK and G6Pase in *db/db* males infected with β-galactosidase ($n = 5$) or NIK(KA) adenoviruses ($n = 6$) (**d**) and in Hep^{CON} ($n = 10$) and Hep^{NIK} males ($n = 7$) (**e**). (**f**) Results from WT and knockout mice (9 weeks old) fasted overnight and stimulated with insulin. Shown are liver extracts immunoblotted with antibody to Akt phosphorylated at Thr308 (pThr308) or Ser473 (pSer473) or Akt. (**g**) Results from primary hepatocytes infected with β-galactosidase, NIK or NIK(KA) adenoviruses and stimulated with insulin after infection. Shown are cell extracts immunoblotted with antibody to Akt pSer473, Akt or NIK. (**h**) Blood glucose concentrations in C57BL/6 males (8 weeks old) injected intraperitoneally with STZ and infected with β-galactosidase ($n = 6$) or NIK(KA) ($n = 6$) adenoviruses. Randomly fed blood glucose concentrations and GTT are shown. (**i**) GTTs in WT ($n = 5$) and knockout ($n = 7$) males (14 weeks old) and overnight fasting plasma glucagon concentrations in WT ($n = 11$) and knockout ($n = 8$) males (14 weeks old). (**j**) GTTs in Hep^{CON} ($n = 10$) and Hep^{NIK} ($n = 9$) males (14 weeks old). *$P < 0.05$ by two-tailed Student's t test. Data are means ± s.e.m.

gluconeogenesis in knockout than in WT livers (**Fig. 4a**). Deletion of *Map3k14* also resulted in inhibition of glucose production in primary hepatocytes under both basal and dibutyryl-cAMP–stimulated and dexamethasone-stimulated conditions (**Fig. 4b**). Deletion of *Map3k14* led to lower expression of hepatic G6Pase (by 80%) and PEPCK (by 75%) and the catalytic activity of G6Pase (by 48%) (**Fig. 4c**). NIK(KA)-mediated, liver-specific inhibition of NIK also suppressed the expression of hepatic PEPCK and G6Pase in *db/db* mice (**Fig. 4d**). Conversely, hepatocyte-specific overexpression of NIK led to higher expression of G6Pase in both males (**Fig. 4e**) and females (**Supplementary Fig. 4c**).

To gain insights into the mechanism of NIK action, we examined insulin signaling. Deletion of *Map3k14* did not enhance the insulin-stimulated phosphorylation of thymoma viral proto-oncogene 1 (Akt) (**Fig. 4f**) or forkhead box O1 (FOXO1) (**Supplementary Fig. 4d**). Overexpression of NIK or NIK(KA) did not impair insulin-stimulated phosphorylation of Akt (**Fig. 4g**) or insulin receptor substrate 1 (IRS1) (**Supplementary Fig. 4e**). In mice with STZ-induced insulin deficiency, NIK(KA)-mediated, liver-specific inhibition of NIK improved hyperglycemia and glucose intolerance (**Fig. 4h**). Therefore, insulin probably does not mediate the regulation of HGP by NIK.

As glucagon seems to be responsible for hyperglycemia and glucose intolerance in STZ-treated mice[9,10], we examined glucagon responses in NIK genetic knockout mice. The hyperglycemic response to glucagon was significantly lower in knockout mice than in WT littermates (**Fig. 4i**), and knockout mice had compensatory hyperglucagonemia (**Fig. 4i**). Glucagon resistance in the knockout mice was reversed by liver-specific reconstitution of recombinant NIK (**Supplementary Fig. 4f**). Hepatocyte-specific overexpression of NIK enhanced the glucagon responses in Hep^{NIK} as compared to Hep^{CON} mice (**Fig. 4j**). In primary hepatocytes, NIK enhanced, whereas NIK(KA) impaired, glucagon-stimulated glucose production (**Supplementary Fig. 5**). In contrast, overexpression of kinase-inactive, dominant-negative IKK-β (KA) did not alter basal or glucagon-stimulated glucose production (**Supplementary Fig. 5**). Therefore, NIK enhances glucagon stimulation of HGP independently of IKK-β.

NIK mediates increased glucagon action in obesity

To examine glucagon responses in obesity, we performed glucagon tolerance tests (GTTs) in WT mice fed an HFD for 6 weeks. Blood glucose concentrations were significantly higher at each time point after glucagon injection in mice fed an HFD than in mice fed a normal chow diet (**Fig. 5a**). The glucagon-stimulated increase in blood glucose concentration was larger in HFD-fed than in chow-fed mice (**Fig. 5b**). Liver-specific inhibition of NIK significantly decreased the glucagon responses in mice infected with the NIK(KA) adenovirus compared to those infected with the β-galactosidase adenovirus (**Fig. 5c**).

As we found earlier that inflammation, oxidative stress or steatosis can induce NIK activity and that NIK promotes glucagon action, we next explored if these three conditions also enhance glucagon action and if this was dependent on NIK expression. Thus, we pretreated primary hepatocytes with TNF-α, hydrogen peroxide and palmitic acid before glucagon stimulation. TNF-α, hydrogen peroxide and palmitic acid all significantly increased both the basal and glucagon-stimulated glucose production in WT hepatocytes (**Fig. 5d**). Deletion of *Map3k14* greatly attenuated the ability of the three compounds to enhance glucagon responses in knockout compared to WT hepatocytes (**Fig. 5d**,**e**). Treatment with TNF-α, hydrogen peroxide and palmitic acid significantly increased glucagon-stimulated expression of PEPCK and G6Pase in WT hepatocytes (**Fig. 5f**). Deletion of *Map3k14* largely blocked the effects of these compounds in knockout hepatocytes (**Fig. 5g**).

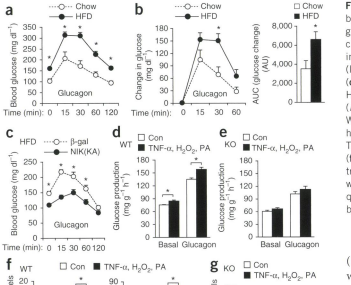

Figure 5 NIK mediates the enhancement of glucagon action induced by HFD and by TNF-α, hydrogen peroxide and palmitic acid. (**a**) Blood glucose concentrations in C57BL/6 males (8 weeks old) fed a normal chow diet ($n = 5$) or an HFD ($n = 9$) and then fasted and intraperitoneally injected with glucagon. (**b**) Glucagon-stimulated increase in blood glucose (left) and the areas under the curves (AUC) (right). AU, arbitrary units. (**c**) Blood glucose concentrations in C57BL/6 males (7 weeks old) fed an HFD and infected with β-galactosidase ($n = 10$) or NIK(KA) adenoviruses ($n = 10$). (**d**,**e**) Glucose production in primary hepatocytes prepared from WT (**d**) and knockout (**e**) mice pretreated with vehicle (Con) or TNF-α, hydrogen peroxide and palmitic acid and then treated with glucagon. The glucose production was normalized to total protein concentrations. (**f**,**g**) Relative mRNA levels in WT (**f**) and knockout (**g**) primary hepatocytes treated with TNF-α, hydrogen peroxide and palmitic acid, and then with glucagon. The expression of PEPCK and G6Pase was measured by quantitative PCR (qPCR) and normalized to β-actin expression. *$P < 0.05$ by two-tailed Student's t test. Data are means ± s.e.m.

NIK phosphorylates CREB and increases CREB stability

CREB mediates the stimulation of gluconeogenesis by glucagon[23–27]. CREB protein concentrations in both the liver and in purified hepatocytes were lower in NIK knockout mice than in WT littermates (**Fig. 6a**). CREB phosphorylation at Ser133 was also lower in knockout than in WT mice (**Fig. 6a**). Liver-specific restoration of CREB reversed glucagon resistance in the knockout mice (**Supplementary Fig. 6**). Conversely, liver CREB concentrations were higher in Hep^{NIK} than in Hep^{CON} mice (**Fig. 6b**). Liver CREB concentrations were also higher in mice with either dietary (HFD compared to chow diet) or genetic (*ob/ob* compared to WT) obesity (**Fig. 6c**); in agreement with these findings, liver NIK activity was abnormally high in HFD-fed and *ob/ob* mice (**Fig. 1**). Notably, hepatic CREB mRNA levels were similar between knockout and WT mice (**Supplementary Fig. 7a**,**b**) and between Hep^{CON} and Hep^{NIK} mice (**Supplementary Fig. 7c**).

We hypothesized that NIK increases CREB protein stability. To test this idea, we co-introduced into primary hepatocytes by adenoviral infection Flag-tagged CREB along with either β-galactosidase, NIK or NIK(KA). CREB mRNA levels were similar between cells infected with the β-galactosidase, NIK and NIK(KA) adenoviruses (**Supplementary Fig. 7d**); however, CREB protein concentrations were higher in NIK-expressing and lower in NIK(KA)-expressing cells

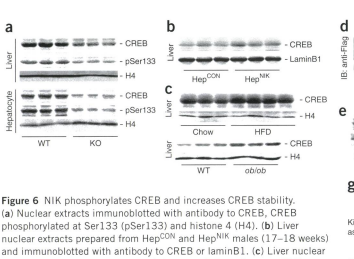

Figure 6 NIK phosphorylates CREB and increases CREB stability. (**a**) Nuclear extracts immunoblotted with antibody to CREB, CREB phosphorylated at Ser133 (pSer133) and histone 4 (H4). (**b**) Liver nuclear extracts prepared from Hep^{CON} and Hep^{NIK} males (17–18 weeks) and immunoblotted with antibody to CREB or laminB1. (**c**) Liver nuclear extracts prepared from WT males fed a normal chow diet or an HFD or from WT and *ob/ob* males (13 weeks old) and immunoblotted with antibody to CREB or H4. (**d**) Cell extracts from primary hepatocytes infected with Flag-tagged CREB adenoviruses and treated with a DMSO vehicle or MG132 and immunoblotted with antibody to Flag or tubulin. (**e**) Nuclear extracts from primary hepatocytes treated with DMSO or MG132 and immunoblotted with antibody to CREB or H4. (**f**) Cell extracts from primary hepatocytes co-infected with Flag-tagged CREB and Flag-tagged NIK, NIK(KA), or β-galactosidase adenoviruses and immunoprecipitated with antibody to Flag and subjected to *in vitro* kinase assays. The blots were immunoblotted with antibody to Flag. (**g**) *In vitro* NIK kinase assays of immunopurified myelocytomatosis oncogene (Myc)-tagged CREB and 13S-A. (**h**) Cell extracts from HepG2 cells cotransfected with NIK and Myc-tagged CREB or 13S-A plasmids and immunoblotted with antibody to Myc or tubulin. (**i**) Cell extracts from HepG2 cells cotransfected with NIK and Flag-tagged CREB, 3S-A or 4S-A plasmids and immunoblotted with antibody to Flag or tubulin.

compared to in β-galactosidase–expressing cells (**Supplementary Fig. 7e**). To determine whether proteasomes are involved in CREB degradation, we infected knockout and WT hepatocytes with CREB adenoviruses and treated them with MG132, a proteasome inhibitor. CREB concentrations were lower in knockout than in WT cells, and treatment with MG132 markedly increased the amount of recombinant CREB in knockout cells (**Fig. 6d**). MG132 also increased the amount of endogenous CREB in knockout hepatocytes (**Fig. 6e**). In agreement, CREB ubiquitination was higher in knockout than in WT hepatocytes (**Supplementary Fig. 7f**).

To determine whether NIK phosphorylates CREB, we performed *in vitro* kinase assays using immunopurified CREB, NIK and NIK(KA). CREB was robustly phosphorylated by NIK but not NIK(KA) (**Fig. 6f**). We identified Ser114 and Ser142 as phosphorylation sites in NIK-overexpressing hepatocytes using liquid chromatography–tandem mass spectrometry proteomics approaches. However, NIK did phosphorylate a CREB mutant lacking the Ser111, Ser114 and Ser142 sites (**Supplementary Fig. 8a**). We replaced Ser98, Ser108, Ser111, Ser114, Ser117, Ser121, Ser129, Ser142, Ser143, Ser156, Ser271, Ser340 and Thr100 (13 known phosphorylation sites) with alanines in CREB (termed here 13S-A). NIK was unable to phosphorylate 13S-A (**Fig. 6g**). To determine whether these 13 sites are involved in the regulation of CREB stability by NIK, we introduced CREB or 13S-A into HepG2 cells expressing low amounts of recombinant NIK. 13S-A migrated slightly faster than CREB in SDS-PAGE gels; NIK increased the abundance of CREB but not 13S-A proteins (**Fig. 6h**). However, NIK at high concentrations increased the amount of both CREB and 13S-A proteins (**Supplementary Fig. 8b,c**). NIK at low concentrations increased the abundance of 2S-A (Ser117 and Ser121 to alanines, Ser114 and Ser117 to alanines or Ser114 and Ser121 to alanines) (**Supplementary Fig. 8d**) but not 3S-A (Ser114, Ser117 and Ser121 to alanines) or 4S-A (Ser111, Ser114, Ser117 and Ser121 to alanines) proteins (**Fig. 6i**). In contrast, NIK at high concentrations increased the abundance of 3S-A proteins (**Supplementary Fig. 8e**). Therefore, NIK is able to increase CREB stability by both phosphorylation-dependent and phosphorylation-independent mechanisms.

DISCUSSION

We here identify NIK overactivation in the liver as a contributing factor to hyperglycemia and glucose intolerance in obesity. NIK was aberrantly activated in the livers of mice with either dietary or genetic obesity. Systemic deletion of *Map3k14* led to decreased blood glucose concentrations and improved glucose tolerance. In both dietary and genetic obesity, liver-specific inhibition of NIK markedly improved hyperglycemia and glucose intolerance. In agreement, hepatocyte-specific overexpression of NIK was sufficient to promote glucose intolerance.

We have discovered a new function of NIK in liver glucose metabolism. NIK promotes HGP by enhancing the hyperglycemic response to glucagon, a key counter-regulatory hormone. In mice, deletion of *Map3k14* resulted in a reduction in HGP, glucagon resistance and compensatory hyperglucagonemia. Similarly, liver-specific inhibition of NIK also decreased HGP and impaired glucagon responses. Conversely, hepatocyte-specific overexpression of NIK resulted in higher HGP and glucagon responses. In isolated livers and primary hepatocytes, deletion of *Map3k14* decreased both basal and glucagon-stimulated HGP. At molecular levels, NIK phosphorylated CREB and increased CREB protein stability by both phosphorylation-dependent and phosphorylation-independent mechanisms. Deletion of *Map3k14* decreased, whereas NIK overexpression increased, the amounts of hepatic CREB protein but not the levels of CREB mRNA. CREB mediates glucagon-stimulated hepatic gluconeogenesis[23–25]. Consistently, systemic deletion of *Map3k14* or liver-specific inhibition of NIK decreased, whereas hepatocyte-specific overexpression increased, the expression of gluconeogenic PEPCK and G6Pase, two CREB targets. Therefore, NIK is a newly identified positive regulator of hepatic gluconeogenesis, enhancing the action of glucagon and/or other factors that activate the protein kinase A (PKA)-CREB pathway. Notably, the transcriptional activity of 13S-A was slightly higher than that of WT CREB (data not shown), raising the possibility that phosphorylation of CREB by NIK may inhibit CREB activity. The NIK-induced increase in CREB stability may overcome the inhibition of CREB activity by NIK, promoting glucagon responses. However, our data do not exclude the possibility that NIK may regulate glucose metabolism by other mechanisms, in addition to increasing CREB stability and glucagon responses.

We show that obesity is associated with elevated glucagon responses. Liver-specific inhibition of NIK decreased glucagon responses, suggesting that overactivation of liver NIK is the major contributor to abnormal glucagon responses in obesity. Notably, TNF-α, hydrogen peroxide and palmitic acid activated NIK in hepatocytes, suggesting that inflammation, oxidative stress and/or steatosis contributes to NIK overactivation in obesity. Under normal conditions, NIK is recruited to the baculoviral IAP repeat containing 1 (cIAP1) and cIAP2 E3 ligases by a TNF receptor–associated factor 3 (TRAF3)-TRAF2 complex, leading to the ubiquitination and proteasome-mediated degradation of NIK[28–30]. Cytokine stimulation promotes the degradation of TRAF3, resulting in NIK stabilization and activation[29,30]. In future studies, it will be crucial to examine how inflammation, oxidative stress and steatosis promote the activation of hepatic NIK in obesity. We also found that TNF-α, hydrogen peroxide and palmitic acid enhanced glucagon-stimulated glucose production and the expression of gluconeogenic genes in an NIK-dependent manner in primary hepatocytes. These results suggest that hepatic inflammation, oxidative stress and/or steatosis activate NIK, which in turn promotes glucagon responses and HGP, thereby contributing to hyperglycemia and glucose intolerance in obesity.

In conclusion, we show that obesity is associated with the activation of the noncanonical NIK–NF-κB2 pathway in addition to the canonical IKK-β–NF-κB1 pathway in the liver. The NIK pathway increases HGP by enhancing glucagon and/or other counter-regulatory hormone responses, whereas the IKK-β pathway promotes insulin resistance. Both elevated counter-regulatory hormone responses and insulin resistance contribute to hyperglycemia and glucose intolerance in obesity. Thus, NIK may be a new therapeutic target for the treatment of type 2 diabetes.

METHODS

Methods and any associated references are available in the online version of the paper.

Note: Supplementary information is available in the online version of the paper.

ACKNOWLEDGMENTS

We thank H. Su, Z. Li, C. Duan, D. Morris and S. Wang for assistance and discussion. We thank R. Schreiber (Washington University School of Medicine, St. Louis, Missouri) for providing NIK knockout mice and K. Rajewsky (Immune Disease Institute, Harvard Medical School, Boston, Massachusetts) for providing STOP-NIK mice. Generation of the NIK knockout mice was supported by Amgen Inc., Thousand Oaks, California. This study was supported by grants DK 065122 and DK073601 from the US National Institutes of Health (NIH) and by research award 1-09-RA-156 from the American Diabetes Association. This work used the

cores supported by the Michigan Diabetes Research and Training Center (funded by NIH 5P60 DK20572), the University of Michigan's Cancer Center (funded by NIH 5 P30 CA46592), the University of Michigan Nathan Shock Center (funded by NIH P30AG013283) and the University of Michigan Gut Peptide Research Center (funded by NIH DK34933).

AUTHOR CONTRIBUTIONS

L.R. and L.S. designed the experiments and prepared the manuscript. L.S., Y.Z., Z.C., D.R., K.W.C., L.J. and H.S. performed experiments. Y.S. generated the STOP-NIK mice.

COMPETING FINANCIAL INTERESTS

The authors declare no competing financial interests.

Published online at http://www.nature.com/doifinder/10.1038/nm.2756.
Reprints and permissions information is available online at http://www.nature.com/reprints/index.html.

1. Hotamisligil, G.S. Inflammation and metabolic disorders. *Nature* **444**, 860–867 (2006).
2. Shoelson, S.E. & Goldfine, A.B. Getting away from glucose: fanning the flames of obesity-induced inflammation. *Nat. Med.* **15**, 373–374 (2009).
3. Arkan, M.C. *et al.* IKK-β links inflammation to obesity-induced insulin resistance. *Nat. Med.* **11**, 191–198 (2005).
4. Cai, D. *et al.* Local and systemic insulin resistance resulting from hepatic activation of IKK-β and NF-κB. *Nat. Med.* **11**, 183–190 (2005).
5. Yuan, M. *et al.* Reversal of obesity- and diet-induced insulin resistance with salicylates or targeted disruption of Ikkβ. *Science* **293**, 1673–1677 (2001).
6. Unger, R.H. & Cherrington, A.D. Glucagonocentric restructuring of diabetes: a pathophysiologic and therapeutic makeover. *J. Clin. Invest.* **122**, 4–12 (2012).
7. Jiang, G. & Zhang, B.B. Glucagon and regulation of glucose metabolism. *Am. J. Physiol. Endocrinol. Metab.* **284**, E671–E678 (2003).
8. Denroche, H.C. *et al.* Leptin therapy reverses hyperglycemia in mice with streptozotocin-induced diabetes, independent of hepatic leptin signaling. *Diabetes* **60**, 1414–1423 (2011).
9. Yu, X., Park, B.H., Wang, M.Y., Wang, Z.V. & Unger, R.H. Making insulin-deficient type 1 diabetic rodents thrive without insulin. *Proc. Natl. Acad. Sci. USA* **105**, 14070–14075 (2008).
10. Lee, Y., Wang, M.Y., Du, X.Q., Charron, M.J. & Unger, R.H. Glucagon receptor knockout prevents insulin-deficient type 1 diabetes in mice. *Diabetes* **60**, 391–397 (2011).
11. Cummings, B.P. *et al.* Subcutaneous administration of leptin normalizes fasting plasma glucose in obese type 2 diabetic UCD-T2DM rats. *Proc. Natl. Acad. Sci. USA* **108**, 14670–14675 (2011).
12. Maruyama, H., Hisatomi, A., Orci, L., Grodsky, G.M. & Unger, R.H. Insulin within islets is a physiologic glucagon release inhibitor. *J. Clin. Invest.* **74**, 2296–2299 (1984).
13. Thu, Y.M. & Richmond, A. NF-κB inducing kinase: a key regulator in the immune system and in cancer. *Cytokine Growth Factor Rev.* **21**, 213–226 (2010).
14. Sun, S.C. Non-canonical NF-κB signaling pathway. *Cell Res.* **21**, 71–85 (2011).
15. Yin, L. *et al.* Defective lymphotoxin-β receptor-induced NF-κB transcriptional activity in NIK-deficient mice. *Science* **291**, 2162–2165 (2001).
16. Murray, S.E. *et al.* NF-κB–inducing kinase plays an essential T cell–intrinsic role in graft-versus-host disease and lethal autoimmunity in mice. *J. Clin. Invest.* **121**, 4775–4786 (2011).
17. Ling, L., Cao, Z. & Goeddel, D.V. NF-κB–inducing kinase activates IKK-α by phosphorylation of Ser-176. *Proc. Natl. Acad. Sci. USA* **95**, 3792–3797 (1998).
18. Xiao, G., Fong, A. & Sun, S.C. Induction of p100 processing by NF-κB–inducing kinase involves docking IκB kinase α (IKKα) to p100 and IKKα-mediated phosphorylation. *J. Biol. Chem.* **279**, 30099–30105 (2004).
19. Xiao, G., Harhaj, E.W. & Sun, S.C. NF-κB–inducing kinase regulates the processing of NF-κB2 p100. *Mol. Cell* **7**, 401–409 (2001).
20. Malinin, N.L., Boldin, M.P., Kovalenko, A.V. & Wallach, D. MAP3K-related kinase involved in NF-κB induction by TNF, CD95 and IL-1. *Nature* **385**, 540–544 (1997).
21. Ninomiya-Tsuji, J. *et al.* The kinase TAK1 can activate the NIK-I κB as well as the MAP kinase cascade in the IL-1 signalling pathway. *Nature* **398**, 252–256 (1999).
22. Sasaki, Y. *et al.* NIK overexpression amplifies, whereas ablation of its TRAF3-binding domain replaces BAFF:BAFF-R–mediated survival signals in B cells. *Proc. Natl. Acad. Sci. USA* **105**, 10883–10888 (2008).
23. Herzig, S. *et al.* CREB regulates hepatic gluconeogenesis through the coactivator PGC-1. *Nature* **413**, 179–183 (2001).
24. Zhou, X.Y. *et al.* Insulin regulation of hepatic gluconeogenesis through phosphorylation of CREB-binding protein. *Nat. Med.* **10**, 633–637 (2004).
25. Koo, S.H. *et al.* The CREB coactivator TORC2 is a key regulator of fasting glucose metabolism. *Nature* **437**, 1109–1111 (2005).
26. He, L. *et al.* Metformin and insulin suppress hepatic gluconeogenesis through phosphorylation of CREB binding protein. *Cell* **137**, 635–646 (2009).
27. Yoon, J.C. *et al.* Control of hepatic gluconeogenesis through the transcriptional coactivator PGC-1. *Nature* **413**, 131–138 (2001).
28. Liao, G., Zhang, M., Harhaj, E.W. & Sun, S.C. Regulation of the NF-κB–inducing kinase by tumor necrosis factor receptor-associated factor 3-induced degradation. *J. Biol. Chem.* **279**, 26243–26250 (2004).
29. Vallabhapurapu, S. *et al.* Nonredundant and complementary functions of TRAF2 and TRAF3 in a ubiquitination cascade that activates NIK-dependent alternative NF-κB signaling. *Nat. Immunol.* **9**, 1364–1370 (2008).
30. Zarnegar, B.J. *et al.* Noncanonical NF-κB activation requires coordinated assembly of a regulatory complex of the adaptors cIAP1, cIAP2, TRAF2 and TRAF3 and the kinase NIK. *Nat. Immunol.* **9**, 1371–1378 (2008).

nature medicine

Jejunal nutrient sensing is required for duodenal-jejunal bypass surgery to rapidly lower glucose concentrations in uncontrolled diabetes

Danna M Breen[1,2], Brittany A Rasmussen[1,3], Andrea Kokorovic[1,3], Rennian Wang[4,5], Grace W C Cheung[1,3] & Tony K T Lam[1–3,6]

Gastrointestinal bypass surgeries restore metabolic homeostasis in patients with type 2 diabetes and obesity[1], but the underlying mechanisms remain elusive. Duodenal-jejunal bypass surgery (DJB), an experimental surgical technique that excludes the duodenum and proximal jejunum from nutrient transit[1,2], lowers glucose concentrations in nonobese type 2 diabetic rats[2–5]. Given that DJB redirects and enhances nutrient flow into the jejunum and that jejunal nutrient sensing affects feeding[6,7], the repositioned jejunum after DJB represents a junction at which nutrients could regulate glucose homeostasis. Here we found that intrajejunal nutrient administration lowered endogenous glucose production in normal rats through a gut-brain-liver network in the presence of basal plasma insulin concentrations. Inhibition of jejunal glucose uptake or formation of long chain fatty acyl-coA negated the metabolic effects of glucose or lipid, respectively, in normal rats, and altered the rapid (2 d) glucose-lowering effect induced by DJB in streptozotocin (STZ)-induced uncontrolled diabetic rats during refeeding. Lastly, in insulin-deficient autoimmune type 1 diabetic rats and STZ-induced diabetic rats, DJB lowered glucose concentrations in 2 d independently of changes in plasma insulin concentrations, food intake and body weight. These data unveil a glucoregulatory role of jejunal nutrient sensing and its relevance in the early improvement of glycemic control after DJB in rat models of uncontrolled diabetes.

DJB is an experimental procedure that was developed to investigate the underlying mechanisms responsible for the metabolic benefits of the Roux-en-Y gastric bypass surgery (RYGB). DJB lowers glucose concentrations in nonobese rodents[2–5] and humans[8,9] with type 2 diabetes. However, the precise mechanisms that underlie the glucose-lowering effect induced by DJB and its clinical relevance remain elusive.

The small intestine activates neuronal and metabolic feedback systems to counteract energy excess and glucose imbalance[10–14]. Duodenal nutrient sensing lowers food intake in rodents and humans via a gut-brain axis[15,16] and lowers endogenous glucose production in rodents via a gut-brain-liver axis[17,18]. It remains a possibility that other segments of the small intestine could regulate peripheral homeostasis. In fact, intrajejunal lipid infusion lowers food intake in rodents and humans[6,7]. The underlying mechanisms of jejunal lipid sensing remain unclear, but a gut-brain contribution is implicated[19,20], although this has been challenged[7]. In light of these findings, we propose that jejunal nutrient sensing mechanisms regulate glucose homeostasis and that their identification will begin to unveil mechanisms responsible for the diabetes resolution after DJB.

We first examined whether the jejunum regulates peripheral glucose metabolism in response to intrajejunal infusion of nutrients, such as glucose or lipids (**Fig. 1a**). Rats were subjected to a pancreatic clamp to obtain basal measurements of glucose metabolism (**Fig. 1b** and **Supplementary Tables 1–3**). Given that carbohydrates are a major source of ingested nutrients, we first assessed whether jejunal glucose sensing affects glucose metabolism (**Fig. 1b**). Intrajejunal glucose administration for 50 min increased the glucose infusion rate and decreased endogenous glucose production (**Fig. 1c,d** and **Supplementary Fig. 1a**) during the clamp, whereas plasma insulin concentrations were maintained at basal levels (**Supplementary Table 1**) and whole-body glucose uptake remained constant (**Supplementary Fig. 1b**). Whole-body glucose uptake was unaltered by all subsequent intrajejunal treatments (**Supplementary Fig. 1b,d,f**). To assess whether intrajejunal glucose infusion reduced endogenous glucose production via portal glucose sensing, we infused an equal amount of glucose into the hepatic portal vein (as compared to intrajejunal infusion) for 50 min (**Supplementary Fig. 2a**). Portal glucose infusion had no effect on whole-body glucose metabolism in the presence of basal insulin concentrations (**Supplementary Fig. 2b–e**), indicating that the metabolic response of intrajejunal glucose infusion was localized to the jejunum.

We next co-infused phlorizin, a sodium-dependent glucose transporter inhibitor[21], with glucose intrajejunally to evaluate the necessity of jejunal glucose uptake from the lumen in glucose regulation. Phlorizin negated the ability of jejunal glucose to increase the glucose

[1]Toronto General Research Institute, University Health Network, Toronto, Ontario, Canada. [2]Department of Medicine, University of Toronto, Toronto, Ontario, Canada. [3]Department of Physiology, University of Toronto, Toronto, Ontario, Canada. [4]Department of Physiology, University of Western Ontario, London, Ontario, Canada. [5]Department of Pharmacology, University of Western Ontario, London, Ontario, Canada. [6]Banting and Best Diabetes Centre, University of Toronto, Toronto, Ontario, Canada. Correspondence should be addressed to T.K.T.L. (tony.lam@uhnres.utoronto.ca).

Received 8 December 2011; accepted 19 March 2012; published online 20 May 2012; doi:10.1038/nm.2745

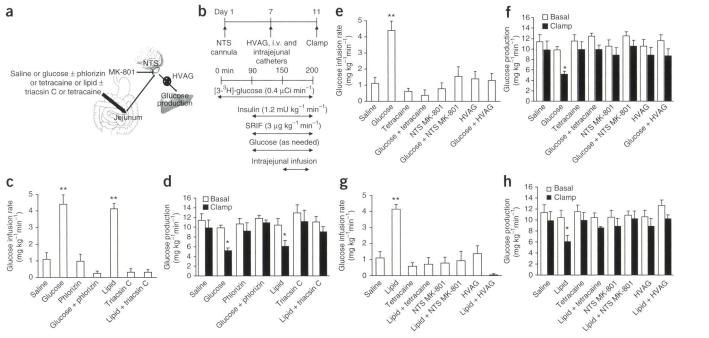

Figure 1 Jejunal nutrient-sensing mechanisms lower glucose production via a neuronal network. (**a**) Schematic representation of the working hypothesis. (**b**) Experimental procedure and clamp protocol. NTS, nucleus of the solitary tract; HVAG, hepatic vagotomy; SRIF, somatostatin. i.v., intravenous. (**c**,**d**) The glucose infusion rate (**c**) and the rate of endogenous glucose production (**d**) during the clamp with intrajejunal glucose, lipid, glucose and phlorizin or lipid and triacsin C (**c**, $^{**}P < 0.01$ glucose versus other groups, $^{**}P < 0.01$ lipid versus other groups; **d**, $^{*}P < 0.05$ glucose versus other groups, $^{*}P < 0.05$ lipid versus other groups). (**e**–**h**) The glucose infusion rate (**e**,**g**) and the rate of endogenous glucose production (**f**,**h**) during the clamp with intrajejunal glucose or lipid infusion alone or in combination with jejunal tetracaine infusion, MK-801 infusion into the NTS or HVAG (**e**–**h**, $^{*}P < 0.05$ versus other groups, $^{**}P < 0.01$ versus other groups). Values are shown as means ± s.e.m. (one-way analysis of variance (ANOVA)). $n = 5$ or 6 rats per group.

infusion rate (**Fig. 1c**) and to reduce endogenous glucose production (**Fig. 1d**). Plasma glucagon concentrations were unaltered among the groups (for basal: saline: 66 ± 8 pg ml^{-1}; glucose: 55 ± 5 pg ml^{-1}; glucose plus phlorizin: 69 ± 6 pg ml^{-1}; for clamp: saline: 74 ± 15 pg ml^{-1}; glucose: 57 ± 7 pg ml^{-1}; glucose plus phlorizin: 70 ± 12 pg ml^{-1}). Systemic intravenous phlorizin administered at the same dose as jejunal phlorizin did not prevent an intrajejunal glucose infusion from increasing the glucose infusion rate (**Supplementary Fig. 3b**) and inhibiting endogenous glucose production (**Supplementary Fig. 3c**,**d**), thus ruling out any nonintestinal effects of jejunal phlorizin. In addition, intraduodenal or ileal phlorizin infusion (**Supplementary Fig. 4a**; same dose as jejunal phlorizin) failed to negate the ability of intrajejunal glucose to increase the glucose infusion rate (**Supplementary Fig. 4b**) and inhibit endogenous glucose production (**Supplementary Fig. 4c**,**d**). These data indicate that selective activation of jejunal glucose sensing lowers endogenous glucose production in the presence of basal plasma insulin concentrations.

We next infused Intralipid, a fat emulsion, as a source of long-chain fatty acids (LCFAs) into the jejunum and evaluated the potential glucoregulatory impact (**Fig. 1a**,**b**). Intrajejunal lipid infusion for 50 min increased the glucose infusion rate and decreased endogenous glucose production, whereas concurrent infusion of triacsin C, an acyl-CoA synthetase inhibitor, abolished this effect (**Fig. 1c**,**d** and **Supplementary Fig. 1a**), indicating that the formation of jejunal LCFA-CoAs is required for jejunal lipid sensing to lower endogenous glucose production. A gut-brain-liver axis that mediates duodenal lipid sensing to lower endogenous glucose production[17] was evaluated for its potential involvement in jejunal nutrient sensing (**Fig. 1a**). We repeated the intrajejunal glucose or lipid infusion protocol in rats that received: (i) jejunal co-infusion of the anesthetic tetracaine to inhibit jejunal vagal innervation, (ii) MK-801 (NMDA receptor blocker) infusion into the nucleus of the solitary tract or (iii) hepatic branch vagotomy. All treatments fully reversed the ability of intrajejunal glucose or lipid to lower endogenous glucose production (**Fig. 1e**–**h** and **Supplementary Fig. 1c**,**e**), indicating that jejunal nutrient sensing triggers a neuronal network to lower endogenous glucose production.

Given that jejunal nutrient sensing inhibits endogenous glucose production in normal rats and that DJB redirects and enhances nutrient flow into the remaining distal jejunum and lowers glucose concentrations in nonobese type 2 diabetic rodents[2–5] and humans[8,9], we next tested whether jejunal nutrient sensing is required for DJB to lower plasma glucose concentrations in uncontrolled diabetes (**Figs. 2** and **3**).

We performed DJB or sham surgery as previously described[2] in normal and nonobese STZ-induced diabetic rats (**Fig. 2a**). We measured the effect of sham or DJB surgery on plasma glucose concentrations at 2 d after surgery to rule out any potential secondary effects on weight loss (**Fig. 2b**). STZ-injected rats were hyperglycemic (**Fig. 2c**) and insulin deficient (**Fig. 2e**) before DJB surgery. Two days after surgery, DJB had a minimal effect on plasma glucose concentrations in nondiabetic rats. Notably, although plasma glucose concentrations were lowered in the STZ-treated, sham-operated (STZ-sham) group at 2 d, DJB further reduced and normalized plasma glucose concentrations compared to sham in STZ-induced diabetic rats (**Fig. 2c**). This effect was not associated with changes in food intake (**Fig. 2d**) or body weight (**Supplementary Fig. 5**), although we did observe a trend of an increase in food intake in STZ-sham rats as compared to other groups.

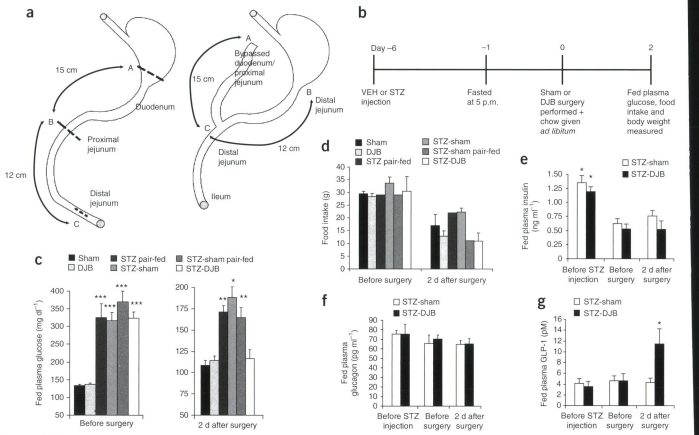

Figure 2 DJB surgery lowers glucose concentrations in uncontrolled diabetic rats. (**a**) Schematic representation of the sham and DJB operation procedure. (**b**) Experimental procedure. (**c**) Plasma glucose in normal and STZ-induced diabetic rats before (left) and at 2 d after (right) sham or DJB surgery (***$P < 0.001$ versus other groups before surgery; **$P < 0.01$, *$P < 0.05$ versus other groups at 2 d after surgery). (**d**) Food intake in normal and STZ-induced diabetic rats before and at 2 d after sham or DJB surgery. (**e**–**g**) Fed plasma insulin (**e**), glucagon (**f**) and active glucagon-like peptide-1 (GLP-1) (**g**) before STZ injection, after STZ injection (before surgery) and at 2 d after surgery (**e**, *$P < 0.05$ versus other groups; **g**, *$P < 0.05$ versus other groups). Values are shown as mean ± s.e.m. (one-way ANOVA). $n = 5$–8 rats per group.

When we matched STZ-sham and STZ-treated, DJB-operated (STZ-DJB) groups for food intake, plasma glucose concentrations remained elevated in the STZ-sham compared to STZ-DJB rats (**Fig. 2c**), indicating that DJB lowered plasma glucose concentrations independently of changes in food intake. Also, the fact that plasma glucose concentrations were similarly reduced to ~175 mg dl^{-1} in pair-fed STZ-treated rats and STZ-sham rats (2 d) (**Fig. 2c**) indicated that the sham operation may have reduced plasma glucose concentrations to ~175 mg dl^{-1} at day 2 as a secondary result of reduced food intake (**Fig. 2d**). We detected no changes in plasma insulin (**Fig. 2e**) or glucagon (**Fig. 2f**) concentrations at 2 d in the STZ-DJB group compared to the STZ-sham group. However, active GLP-1 plasma concentrations were higher in the STZ-DJB group compared to STZ-sham (**Fig. 2g**). These results indicate that DJB rapidly (in 2 d) lowers plasma glucose concentrations in STZ-induced uncontrolled diabetes, and this glucose lowering is independent of changes in insulin concentrations, food intake and body weight.

We then tested whether jejunal nutrient sensing mediates this early improvement of glycemia induced by DJB in uncontrolled diabetes. We inserted a jejunal catheter at the time of DJB in STZ-treated rats (**Fig. 3a**) into the same location used for intrajejunal infusion studies in normal rats (**Fig. 1a**,**b**). We subsequently performed a fasting-refeeding experiment to activate nutrient-sensing mechanisms while intrajejunally administering phlorizin, triacsin C or both to disrupt jejunal nutrient-sensing mechanisms (**Fig. 3b**). We monitored plasma glucose for 50 min during refeeding in an attempt to match the duration of intrajejunal nutrient infusion (**Fig. 1b**). Consistent with the glucose-lowering effect of DJB in STZ-induced diabetic rats (**Fig. 2c**), the glucose control of nutrient-sensing mechanisms activated by refeeding was intact in STZ-DJB diabetic rats that received intrajejunal vehicle infusion (**Fig. 3c**), resulting in plasma glucose concentrations (~120 mg dl^{-1}) comparable to those in STZ-DJB rats at 2 d after surgery (**Fig. 2c**). In contrast, intrajejunal infusion of phlorizin or triacsin C alone, or in combination disrupted glucose homeostasis during refeeding to a similar degree (**Fig. 3c**) independently of changes in food intake (**Fig. 3d**), resulting in plasma glucose concentrations (~175 mg dl^{-1}) comparable to those in STZ-sham rats at 2 d after surgery (**Fig. 2c**).

To additionally evaluate whether jejunal nutrient sensing is intact in STZ-DJB rats at 2 d after surgery, we infused glucose into the jejunum of STZ-induced diabetic rats in an unclamped setting. We restricted food intake to 5 g in these STZ-treated rats the night before the experiment to reduce glucose concentrations to ~180 mg dl^{-1} (**Fig. 3e**) in an attempt to match the glucose concentrations of STZ-sham rats 2 days after surgery (**Fig. 2c**). Intrajejunal glucose infusion for 50 min normalized plasma glucose concentrations (**Fig. 3e**) and endogenous glucose production (**Fig. 3f**) independently of changes in plasma insulin and glucagon concentrations (**Fig. 3g**,**h**) in these STZ-treated rats.

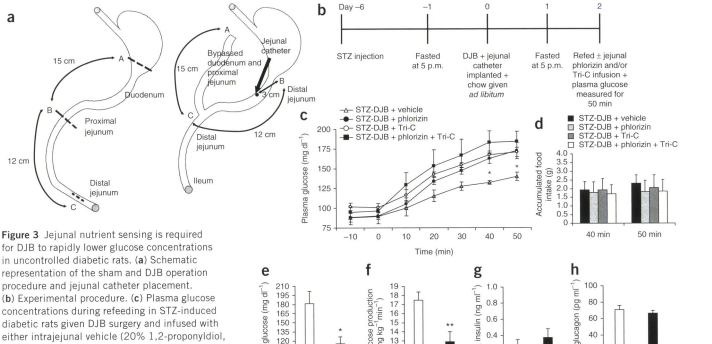

Figure 3 Jejunal nutrient sensing is required for DJB to rapidly lower glucose concentrations in uncontrolled diabetic rats. (**a**) Schematic representation of the sham and DJB operation procedure and jejunal catheter placement. (**b**) Experimental procedure. (**c**) Plasma glucose concentrations during refeeding in STZ-induced diabetic rats given DJB surgery and infused with either intrajejunal vehicle (20% 1,2-propanyldiol, 0.001% DMSO and 0.9% NaCl), phlorizin, triacsin C (Tri-C) or phlorizin plus triacsin C (*$P < 0.05$ versus all other treatment groups). (**d**) Accumulated food intake during the refeeding protocol. (**e**–**g**) Plasma glucose (**e**), endogenous glucose production (**f**), plasma insulin concentration (**g**) and plasma glucagon concentrations (**h**) after intrajejunal saline or glucose infusion in nonclamped conditions in STZ-diabetic rats that underwent jejunal and vascular cannulation only (*$P < 0.05$, **$P < 0.01$ versus jejunal saline). Values are shown as means ± s.e.m. (Student's *t* test or one-way ANOVA). $n = 5$–8 rats per group.

These findings indicate that jejunal nutrient sensing is required for the rapid (2-d) glucose-lowering effect induced by DJB in nonobese, uncontrolled diabetes. The accumulation of LCFA-CoAs in the brain and the liver mediates lipid and glucose sensing to regulate hepatic glucose metabolism[14]. The fact that intrajejunal infusion of phlorizin together with triacsin C as compared to phlorizin or triacsin C alone did not further disrupt glucose homeostasis in STZ-DJB rats indicates that jejunal glucose- and lipid-sensing mechanisms may converge as they do in the brain and the liver. In addition, in light of the above data and the fact that intrajejunal infusion of phlorizin and triacsin C together did not disrupt glucose homeostasis when normal rats underwent fasting-refeeding (**Supplementary Fig. 6a**–**d**), we propose that the rapid glucose-lowering effect of jejunal nutrient sensing in uncontrolled diabetes is revealed apparent after DJB.

To investigate whether the glucose-lowering effect of DJB was transient and whether it would remain in STZ-induced diabetic rats when the confounding glucose-lowering effect induced at 2 d after surgical operation (**Fig. 2c**) was eliminated, we allowed STZ-sham and STZ-DJB rats to recover for up to 14 d (**Fig. 4**). Two weeks after surgery, there was no significant difference between the plasma glucose concentrations in nondiabetic DJB-operated and sham-operated rats (**Fig. 4a**,**b**). Notably, plasma glucose concentrations in STZ-induced diabetic rats remained normal at 14 d after DJB surgery, whereas the plasma glucose concentrations in STZ-sham rats reached presurgical glucose values (~400 mg dl^{-1}) (**Fig. 4b**). The STZ-sham rats became hyperphagic after 14 d compared to the STZ-DJB rats, whose food intake had returned to presurgical levels (**Fig. 4c**). We observed no changes in body weight between surgical groups after 14 d (**Fig. 4c**).

To better evaluate whether DJB lowers glucose concentrations in uncontrolled type 1 diabetes, we performed DJB in nonobese, diabetes-prone BioBreeding (BB-dp) rats. BB-dp rats spontaneously develop autoimmune type 1 diabetes and recapitulate many features of human type 1 diabetes, including severe hypoinsulinemia (reviewed in ref. 22). DJB or sham surgery was performed in BB-dp rats 2 d after the onset of hyperglycemia (plasma glucose > 300 mg dl^{-1}), hypoinsulinemia (**Fig. 4g**) and hyperglucagonemia (**Fig. 4h**). Plasma glucose remained elevated in control sham-operated rats, comparable to concentrations observed before surgery (**Fig. 4d**), and the majority of the sham-operated rats did not survive beyond 6 d after surgery. In contrast, DJB lowered plasma glucose concentrations within 2 d of surgery (**Fig. 4d**), independently of changes in food intake and body weight (**Fig. 4e**,**f**), as well as plasma insulin, glucagon and active GLP-1 concentrations (**Fig. 4g**–**i**). Of note, the glucose-lowering effect induced by DJB in BB-dp rats was sustained past the 2-d time point and remained 6 d after DJB (**Fig. 4d**). In contrast to the case at 2 d, when plasma insulin concentrations were similar between sham-operated and DJB-operated rats, at 6 d after surgery plasma insulin concentrations were increased in the rats that received DJB as compared to sham-operated rats (**Fig. 4g**). Also, sham operation or DJB reduced food intake and body weight to a similar extent in BB-dp rats at both 2 d and 6 d (**Fig. 4e**,**f**). Lastly, four out of the five BB-dp–DJB rats survived for at least 3 weeks (data not shown).

To begin evaluating whether jejunal nutrient sensing mediates DJB to lower plasma glucose concentrations in STZ-induced diabetic rats after 14 d (**Fig. 4b**), we infused glucose into the jejunum of

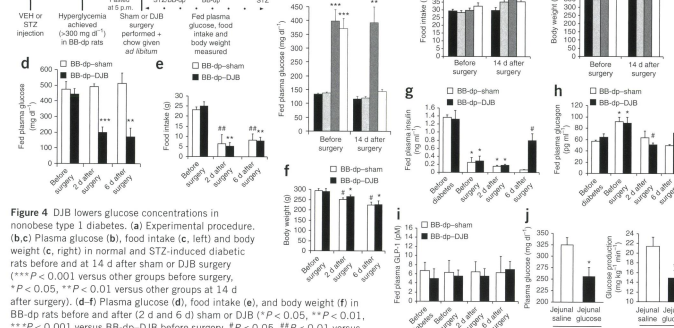

Figure 4 DJB lowers glucose concentrations in nonobese type 1 diabetes. (**a**) Experimental procedure. (**b**,**c**) Plasma glucose (**b**), food intake (**c**, left) and body weight (**c**, right) in normal and STZ-induced diabetic rats before and at 14 d after sham or DJB surgery (***$P < 0.001$ versus other groups before surgery, *$P < 0.05$, **$P < 0.01$ versus other groups at 14 d after surgery). (**d**–**f**) Plasma glucose (**d**), food intake (**e**), and body weight (**f**) in BB-dp rats before and after (2 d and 6 d) sham or DJB (*$P < 0.05$, **$P < 0.01$, ***$P < 0.001$ versus BB-dp–DJB before surgery, #$P < 0.05$, ##$P < 0.01$ versus BB-dp–sham before surgery). (**g**–**i**) Fed plasma insulin (**g**), glucagon (**h**) and active GLP-1 (**i**) before and after surgery in BB-dp rats (*$P < 0.05$ versus before diabetes; **g**, #$P < 0.05$ versus BB-dp–sham 6 d after surgery; **h**, #$P < 0.05$ versus BB-dp–DJB before surgery). (**j**) Plasma glucose (left) and endogenous glucose production (right) after intrajejunal saline or glucose infusion in nonclamped conditions in STZ-induced diabetic rats that underwent jejunal and vascular cannulation only (*$P < 0.05$ versus jejunal saline). Values are shown as mean ± s.e.m. (Student's *t* test or one-way ANOVA). $n = 5$–8 rats per group.

STZ-induced diabetic rats with plasma glucose concentrations (~325 mg dl^{-1}; **Fig. 4j**) elevated to a similar extent as in STZ-sham rats at day 14 (**Fig. 4b**) under nonclamp conditions. Intrajejunal glucose administration for 50 min lowered (but did not normalize) plasma glucose concentrations and endogenous glucose production (**Fig. 4j**) in these STZ-induced diabetic rats. These findings indicate that jejunal nutrient sensing may partly contribute to the chronic (14-d) glucose-lowering effect induced by DJB in uncontrolled diabetes.

We here report that jejunal nutrient sensing is required for the early improvement of glycemia induced by DJB in nonobese, uncontrolled diabetes. In addition, DJB normalized glucose levels within 2 d of surgery in both insulin-deficient, STZ-induced diabetic rats and in autoimmune type 1 diabetic rats independently of changes in plasma insulin concentrations, food intake and body weight, whereas the glucose-lowering effect induced by DJB in both uncontrolled diabetic models remained beyond 2 d. Bariatric surgery lowers glucose concentrations in type 2 diabetes[23,24]. However, only a few studies to date have demonstrated that DJB lowers glucose concentrations in nonobese type 2 diabetic rodents[2–5] and humans[8,9]. We here propose that the redirection and enhancement of nutrient flow into the jejunum that are triggered shortly after a meal mediate the rapid glucose-lowering effect induced by DJB in uncontrolled diabetes. Thus, our current findings indicate a therapeutic potential of gastrointestinal bypass procedures for both type 1 and type 2 diabetes.

Although the underlying mechanisms responsible for the glucose-lowering effect induced by DJB in type 2 and type 1 diabetes remain to be explored, a few sets of observations are worth noting. First, bariatric surgery induces a rapid glucose-lowering effect in type 2 diabetes[25,26], whereas DJB also lowers glucose concentrations in nonobese type 2 diabetic rats[2–5] and humans[8,9] as well as in nonobese uncontrolled diabetic rats (this study) independent of a reduction in food intake and body weight.

Second, consistent with the fact that jejunal nutrient sensing, which mediates the early improvement (2 d) in glucose homeostasis by DJB in uncontrolled diabetes, is achieved through a reduction in endogenous glucose production (this study), a stomach-sparing proximal intestinal bypass operation (a variant of DJB) has previously been shown to improve glucose homeostasis by a selective reduction in endogenous glucose production in high-fat diet–fed mice[28]. Similarly in high-fat diet–fed rats, a selective improvement on hepatic insulin sensitivity is seen with RYGB[29]. Thus, these findings indicate that the inhibition of endogenous glucose production induced by jejunal nutrient sensing mediates the rapid (2 d) glucose-lowering effect induced by DJB in uncontrolled diabetes. However, it is notable that changes in glucose use and/or mechanisms that are activated independently of jejunal nutrient sensing may be responsible for the chronic (14 d) glucose-lowering effect induced by DJB in uncontrolled diabetes. Future studies are warranted to clarify the underlying mechanisms responsible for the acute versus chronic glucose-lowering effect induced by DJB in diabetes. In addition, it would be important to determine the concentration of glucoregulatory hormones at 14 d after DJB in STZ-treated rats. This should begin to shed light on the mechanisms involved in the sustained lowering of plasma glucose concentrations induced by DJB. The relative contribution of jejunal versus portal nutrient sensing in triggering the central nervous system to reduce endogenous glucose production in DJB-diabetic rodents[28] also remain to be clarified.

Third, although we documented hypoinsulinemia in both models of uncontrolled diabetes, we still detected insulin in the plasma. This finding indicates that a considerable amount of beta cells may still persist at this stage. Given that plasma insulin concentrations were increased in BB-dp rats at 6 d after DJB, it remains to be assessed whether DJB enhances insulin secretion to lower plasma glucose concentrations in nonobese, uncontrolled diabetes.

Fourth, although RYGB increases plasma GLP-1 concentrations in association with a glucose improvement in obese type 2 diabetes[1], DJB reduces endogenous glucose production in high-fat diet–fed mice independent of GLP-1 action[28]. We here found that at 2 d after surgery DJB normalized glucose concentrations in STZ-induced uncontrolled diabetic rats in association with a rise in plasma GLP-1 concentrations. However, the normalization of glucose concentrations induced by DJB in autoimmune type 1 diabetic rats was independent of changes in GLP-1 concentrations. Thus, the functional relevance of GLP-1 in mediating the rapid glucose-lowering effect induced by DJB in diabetes remains to be clarified.

Last, DJB affects the mixing of bile with nutrients in the duodenum and may consequently alter bile acid metabolism. In fact, the higher serum bile acid levels observed in patients after RYGB are postulated to mediate the improvement of glucose metabolism[30]. In light of the fact that biliary excretory function is altered in STZ-induced diabetes[31], the potential involvement of bile acid metabolism in the ability of DJB to improve glucose homeostasis in uncontrolled diabetic models warrants future investigation.

In summary, we here provide evidence indicating that activation of jejunal nutrient-sensing mechanisms mediates the ability of DJB to rapidly lower glucose concentrations in insulin-deficient, uncontrolled diabetes independently of weight loss. In parallel, DJB normalizes glucose concentrations in autoimmune type 1 diabetic rats. These findings further support the emerging use of gastrointestinal surgery for the treatment of diabetes and unveil sensing mechanisms in the jejunum as potential therapeutic targets for this condition.

METHODS

Methods and any associated references are available in the online version of the paper.

Note: Supplementary information is available in the online version of the paper.

ACKNOWLEDGMENTS

We are extremely grateful to P.Y.T. Wang for excellent technical assistance. This work was supported by a research grant to T.K.T.L. from the Canadian Institutes of Health Research (MOP-82701). D.M.B. is supported by a post-doctoral fellowship from the University Health Network and the Banting and Best Diabetes Centre (BBDC), University of Toronto. B.A.R. is supported by a BBDC graduate scholarship. A.K. and G.W.C.C. were supported by Canadian Institutes of Health Research and BBDC graduate scholarships. T.K.T.L. holds the John Kitson McIvor (1915–1942) Endowed Chair in Diabetes Research and the Canada Research Chair in Obesity at the Toronto General Research Institute and the University of Toronto.

AUTHOR CONTRIBUTIONS

D.M.B. conducted and designed experiments, performed data analyses and wrote the manuscript; B.A.R., A.K. and G.W.C.C. assisted in experiments; R.W. assisted in setting up the DJB surgical procedure; and T.K.T.L. supervised the project, designed experiments and edited the manuscript.

COMPETING FINANCIAL INTERESTS

The authors declare no competing financial interests.

Published online at http://www.nature.com/doifinder/10.1038/nm.2745.
Reprints and permissions information is available online at http://www.nature.com/reprints/index.html.

1. Rubino, F., Schauer, P.R., Kaplan, L.M. & Cummings, D.E. Metabolic surgery to treat type 2 diabetes: clinical outcomes and mechanisms of action. *Annu. Rev. Med.* **61**, 393–411 (2010).
2. Rubino, F. & Marescaux, J. Effect of duodenal-jejunal exclusion in a non-obese animal model of type 2 diabetes: a new perspective for an old disease. *Ann. Surg.* **239**, 1–11 (2004).
3. Wang, T.Y. *et al.* Ileal transposition controls diabetes as well as modified duodenal jejunal bypass with better lipid lowering in a nonobese rat model of type II diabetes by increasing GLP-1. *Ann. Surg.* **247**, 968–975 (2008).
4. Pacheco, D. *et al.* The effects of duodenal-jejunal exclusion on hormonal regulation of glucose metabolism in Goto-Kakizaki rats. *Am. J. Surg.* **194**, 221–224 (2007).
5. Kindel, T.L., Yoder, S.M., Seeley, R.J., D'Alessio, D.A. & Tso, P. Duodenal-jejunal exclusion improves glucose tolerance in the diabetic, Goto-Kakizaki rat by a GLP-1 receptor-mediated mechanism. *J. Gastrointest. Surg.* **13**, 1762–1772 (2009).
6. Drewe, J., Gadient, A., Rovati, L.C. & Beglinger, C. Role of circulating cholecystokinin in control of fat-induced inhibition of food intake in humans. *Gastroenterology* **102**, 1654–1659 (1992).
7. Ogawa, N. *et al.* The vagal afferent pathway does not play a major role in the induction of satiety by intestinal fatty acid in rats. *Neurosci. Lett.* **433**, 38–42 (2008).
8. Cohen, R.V. *et al.* Duodenal-jejunal bypass for the treatment of type 2 diabetes in patients with body mass index of 22–34 kg/m^2: a report of 2 cases. *Surg. Obes. Relat. Dis.* **3**, 195–197 (2007).
9. Cohen, R.V. *et al.* Glycemic control after stomach-sparing duodenal-jejunal bypass surgery in diabetic patients with low body mass index. *Surg. Obes. Relat. Dis.* published online, doi:10.1016/j.soard.2012.01.017 (2 February 2012).
10. Bachman, M.K. & Flier, J.S. The gut and energy balance: visceral allies in the obesity wars. *Science* **307**, 1909–1914 (2005).
11. Cummings, D.E. & Overduin, J. Gastrointestinal regulation of food intake. *J. Clin. Invest.* **117**, 13–23 (2007).
12. Murphy, K.G. & Bloom, S.R. Gut hormones and the regulation of energy homeostasis. *Nature* **444**, 854–859 (2006).
13. Coll, A.P., Farooqi, I.S. & O'Rahilly, S. The hormonal control of food intake. *Cell* **129**, 251–262 (2007).
14. Lam, T.K. Neuronal regulation of homeostasis by nutrient sensing. *Nat. Med.* **16**, 392–395 (2010).
15. Greenberg, D., Smith, G.P. & Gibbs, J. Intraduodenal infusions of fats elicit satiety in sham-feeding rats. *Am. J. Physiol.* **259**, R110–R118 (1990).
16. Matzinger, D. *et al.* The role of long chain fatty acids in regulating food intake and cholecystokinin release in humans. *Gut* **46**, 688–693 (2000).
17. Wang, P.Y. *et al.* Upper intestinal lipids trigger a gut-brain-liver axis to regulate glucose production. *Nature* **452**, 1012–1016 (2008).
18. Cheung, G.W., Kokorovic, A., Lam, C.K., Chari, M. & Lam, T.K. Intestinal cholecystokinin controls glucose production through a neuronal network. *Cell Metab.* **10**, 99–109 (2009).
19. Lal, S., Kirkup, A.J., Brunsden, A.M., Thompson, D.G. & Grundy, D. Vagal afferent responses to fatty acids of different chain length in the rat. *Am. J. Physiol. Gastrointest. Liver Physiol.* **281**, G907–G915 (2001).
20. Randich, A. *et al.* Jejunal administration of linoleic acid increases activity of neurons in the paraventricular nucleus of the hypothalamus. *Am. J. Physiol. Regul. Integr. Comp. Physiol.* **286**, R166–R173 (2004).
21. Ehrenkranz, J.R., Lewis, N.G., Kahn, C.R. & Roth, J. Phlorizin: a review. *Diabetes Metab. Res. Rev.* **21**, 31–38 (2005).
22. Mordes, J.P., Bortell, R., Blankenhorn, E.P., Rossini, A.A. & Greiner, D.L. Rat models of type 1 diabetes: genetics, environment and autoimmunity. *ILAR J.* **45**, 278–291 (2004).
23. Cohen, R., Pinheiro, J.S., Correa, J.L. & Schiavon, C.A. Laparoscopic Roux-en-Y gastric bypass for BMI < 35 kg/m^2: a tailored approach. *Surg. Obes. Relat Dis.* **2**, 401–404 (2006).
24. Kim, Z. & Hur, K.Y. Laparoscopic mini-gastric bypass for type 2 diabetes: the preliminary report. *World J. Surg.* **35**, 631–636 (2011).
25. Thaler, J.P. & Cummings, D.E. Minireview: Hormonal and metabolic mechanisms of diabetes remission after gastrointestinal surgery. *Endocrinology* **150**, 2518–2525 (2009).
26. Rubino, F. Is type 2 diabetes an operable intestinal disease? A provocative yet reasonable hypothesis. *Diabetes Care* **31** (suppl. 2), S290–S296 (2008).
27. Cox, J.E., Kelm, G.R., Meller, S.T., Spraggins, D.S. & Randich, A. Truncal and hepatic vagotomy reduce suppression of feeding by jejunal lipid infusions. *Physiol. Behav.* **81**, 29–36 (2004).
28. Troy, S. *et al.* Intestinal gluconeogenesis is a key factor for early metabolic changes after gastric bypass but not after gastric lap-band in mice. *Cell Metab.* **8**, 201–211 (2008).
29. Chambers, A.P. *et al.* Weight-independent changes in blood glucose homeostasis after gastric bypass or vertical sleeve gastrectomy in rats. *Gastroenterology* **141**, 950–958 (2011).
30. Patti, M.E. *et al.* Serum bile acids are higher in humans with prior gastric bypass: potential contribution to improved glucose and lipid metabolism. *Obesity (Silver Spring)* **17**, 1671–1677 (2009).
31. Watkins, J.B. III & Dykstra, T.P. Alterations in biliary excretory function by streptozotocin-induced diabetes. *Drug Metab. Dispos.* **15**, 177–183 (1987).

nature medicine

A high-throughput drug screen for *Entamoeba histolytica* identifies a new lead and target

Anjan Debnath[1], Derek Parsonage[2], Rosa M Andrade[3,4], Chen He[3], Eduardo R Cobo[3], Ken Hirata[3], Steven Chen[5], Guillermina García-Rivera[6], Esther Orozco[6], Máximo B Martínez[6], Shamila S Gunatilleke[1], Amy M Barrios[7], Michelle R Arkin[5], Leslie B Poole[2], James H McKerrow[1] & Sharon L Reed[3,4]

***Entamoeba histolytica*, a protozoan intestinal parasite, is the causative agent of human amebiasis. Amebiasis is the fourth leading cause of death and the third leading cause of morbidity due to protozoan infections worldwide[1], resulting in ~70,000 deaths annually. *E. histolytica* has been listed by the National Institutes of Health as a category B priority biodefense pathogen in the United States. Treatment relies on metronidazole[2], which has adverse effects[3], and potential resistance of *E. histolytica* to the drug is an increasing concern[4,5]. To facilitate drug screening for this anaerobic protozoan, we developed and validated an automated, high-throughput screen (HTS). This screen identified auranofin, a US Food and Drug Administration (FDA)-approved drug used therapeutically for rheumatoid arthritis, as active against *E. histolytica* in culture. Auranofin was ten times more potent against *E. histolytica* than metronidazole. Transcriptional profiling and thioredoxin reductase assays suggested that auranofin targets the *E. histolytica* thioredoxin reductase, preventing the reduction of thioredoxin and enhancing sensitivity of trophozoites to reactive oxygen-mediated killing. In a mouse model of amebic colitis and a hamster model of amebic liver abscess, oral auranofin markedly decreased the number of parasites, the detrimental host inflammatory response and hepatic damage. This new use of auranofin represents a promising therapy for amebiasis, and the drug has been granted orphan-drug status from the FDA.**

Screening large chemical libraries to identify amebicidals has been hindered by the throughput of labor-intensive traditional assays that rely on microscopic visualization[6], radioisotopes[7] and/or extensive staining methods[8]. We developed and employed an automated HTS that is suitable for rapid and more efficient screening of large, diverse inhibitor libraries for activity against *E. histolytica*. The challenges of developing the HTS platform for *E. histolytica* included the facts that it is an anaerobe and that no rapid readout assay is available. We solved these issues by using GasPak EZ Anaerobe Gas Generating Pouch Systems and the CellTiter-Glo Luminescent Cell Viability Assay. The GasPak was not needed during robotic transfers, making this assay fully compatible with workstation-based automation. We developed the assay with exponentially growing *E. histolytica* trophozoites plated at 50,000 parasites per milliliter in 96-well[8] or 30,000 parasites per milliliter in 384-well microtiter plates. We maintained anaerobic conditions using GasPak during growth. As ATP is an essential cofactor for biogenesis in *E. histolytica*, we used the CellTiter-Glo luciferase-based assay to validate the correlation between the number of viable trophozoites and their ATP levels. The relationship between numbers of parasites seeded into 96- and 384-well plates and relative luminescence from CellTiter-Glo assaying of parasites showed a linear correlation ($R^2 = 0.86$ and $R^2 = 0.9$) (**Fig. 1a**,**b**). Trophozoites readily tolerated up to 0.5% DMSO, used to dissolve the compounds, with no effect on growth rate (data not shown). In our system, the half-maximal effective concentration (EC_{50}) for metronidazole, defined as that concentration of compound necessary to reduce the culture density to 50% of that of a DMSO-treated culture, was 5 μM. We used this HTS assay to evaluate the amebicidal activity of potential drug candidates, with parasites plated at 50,000 parasites per milliliter in a 96-well microtiter plate at a single concentration of 5 μM of the test compound.

We performed the screen with a 910-member Iconix library, consisting of both FDA-approved and unapproved bioactive compounds. The use of drugs already approved for human use opens the possibility to reprofile or repurpose[9] drugs to treat amebiasis in a rapid and cost-effective manner; using approved compounds allows for shortened development timelines and decreased risk, as such compounds have already passed regulatory clinical trials with full toxicological and pharmacokinetic profiles[9].

We identified 11 compounds as 'active', causing statistically significant growth inhibition (>50%; **Fig. 1c** and **Table 1**). The assay showed excellent discrimination between active and inactive compounds with a Z' (a dimensionless calculation used to assess the quality of a

[1]Sandler Center for Drug Discovery, University of California–San Francisco, San Francisco, California, USA. [2]Department of Biochemistry, Wake Forest School of Medicine, Winston-Salem, North Carolina, USA. [3]Department of Pathology, University of California–San Diego, San Diego, California, USA. [4]Department of Medicine, University of California–San Diego, San Diego, California, USA. [5]Small Molecule Discovery Center, University of California–San Francisco, San Francisco, California, USA. [6]Department of Experimental Pathology, Centro de Investigación y de Estudios Avanzados del Instituto Politécnico Nacional, Mexico City, Mexico. [7]Department of Medicinal Chemistry, University of Utah, Salt Lake City, Utah, USA. Correspondence should be addressed to S.L.R. (slreed@ucsd.edu) or A.D. (anjan.debnath@ucsf.edu).

Received 3 October 2011; accepted 30 March 2012; published online 20 May 2012; doi:10.1038/nm.2758

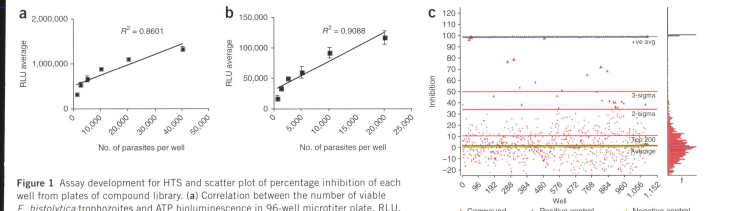

Figure 1 Assay development for HTS and scatter plot of percentage inhibition of each well from plates of compound library. (**a**) Correlation between the number of viable *E. histolytica* trophozoites and ATP bioluminescence in 96-well microtiter plate. RLU, relative light unit. (**b**) Correlation between the number of viable *E. histolytica* trophozoites and ATP bioluminescence in 384-well microtiter plate. Values plotted in **a** and **b** are the means and s.d. of triplicate wells. The lines represent the linear regression for plotted data. (**c**) Scatter plot of percentage inhibition of each well from 12 96-well plates of the Iconix library. Eleven compounds yielded both 50% inhibition and 3 s.d. above the mean of the population of compounds tested in the primary screen at 5 μM. +ve avg, mean inhibition of positive controls; 3-sigma, 50% inhibition and 3 s.d. above the mean of the population of compounds tested; 2-sigma, 2 s.d. above the mean of the population of compounds tested; top 200, top 200 active compounds above the mean of the population of compounds tested; average, mean of the population of compounds tested. Right graph represents the histogram of the compounds tested.

high-throughput assay) of 0.96 ± 0.13 in the screening experiment using 12 different plates containing the Iconix library compounds. Among the 11 compounds, auranofin had the highest amebicidal activity with an EC_{50} of 0.5 μM, tenfold better than that of metronidazole. Auranofin purchased from another manufacturer and three auranofin analogs also inhibited growth of *E. histolytica* trophozoites (**Supplementary Table 1**). Two purine analogs, cladribine and fludarabine, showed 79% and 77% growth inhibition, respectively, at 5 μM but are not promising for further development because of reported adverse effects in humans. We also identified trifluoperazine, a compound with known amebicidal activity[10], as a primary hit, confirming the sensitivity of our whole-cell HTS assay format.

Auranofin is an FDA-approved oral, gold-containing drug that has been in clinical use to treat rheumatoid arthritis for 25 years and is sold as Ridaura (Prometheus). The published pharmacokinetic data of auranofin come from studies in humans with rheumatoid arthritis after long-term therapy. Auranofin is rapidly metabolized, so only the released elemental gold can be detected in human blood or tissues. Following an oral dose, 25% of auranofin (gold) is absorbed into blood, of which 60% is bound by plasma proteins[11]. Steady-state mean blood gold concentrations in humans are 0.68 ± 0.45 μg ml^{-1} (according to the package insert from the manufacturer) or approximately 3.5 μM, more than 7 times the *in vitro* EC_{50} for *E. histolytica*. Auranofin was approved for the long-term treatment of unresponsive rheumatoid arthritis in adults with courses for a minimum of 6 months at oral doses of 3 mg once or twice daily (not adjusted for weight). The manufacturer indicates the following complications in patients treated for at least 1 year with auranofin: 47% of patients had at least one loose stool, 24% a rash, 14% an episode of abdominal pain, 13% stomatitis, 10% nausea, 3% anemia and 2% elevated liver function tests at some point. The likelihood of gold toxicity is extremely small in the standard, short-term (7–10 d) therapy for amebiasis.

Recently, auranofin has been shown to rapidly kill juvenile and adult *Schistosoma mansoni* in culture at concentrations achievable in patients with rheumatoid arthritis (5 μM)[12] and the bloodstream and procyclic stages of *Trypanosoma brucei* with half-maximal inhibitory concentration (IC_{50}) in the lower nanomolar range[13]. Concentrations as low as 2.5 μM also kill larval worms of *Echinococcus granulosus in vitro*[14]. Auranofin also strongly inhibits the growth of malarial parasite *Plasmodium falciparum in vitro*[15] and kills the promastigote stage of *Leishmania infantum in vitro* at micromolar concentrations[16].

Although auranofin has been used clinically for 25 years, its mechanism of action is poorly understood. To identify the basis of auranofin's activity against *E. histolytica*, we undertook a transcriptional profiling study using *E. histolytica* oligonucleotide microarrays[17]. Incubation of *E. histolytica* with 1 μM auranofin for only 3 h induced downregulation of genes encoding crucial proteins involved in mitosis (Rae1 (ref. 18)) and nucleotide metabolism (nucleoside diphosphate kinase[19]), whereas the genes encoding the signal transduction proteins ADP-ribosylation factor and Ras1p were upregulated[20] (**Supplementary Table 2**). However, these transcripts are also induced by other forms of cellular stress[21]. Furthermore, there was a marked upregulation of the gene encoding a protein similar to arsenite-inducible RNA-associated protein (AIRAP) (**Supplementary Table 2**). The differential expression of these down- and upregulated transcripts in auranofin-treated *E. histolytica* was validated by real-time quantitative reverse transcription PCR (qRT-PCR) (**Supplementary Fig. 1** and **Supplementary Table 3**).

AIRAP is unique among known arsenite-induced genes in that its expression is not upregulated in response to other oxidants and is only modestly induced by exposure to metals, such as zinc[22], although gold has not been tested. Our finding that the transcript for a gene similar to that encoding AIRAP in *E. histolytica* was highly upregulated by treatment with low concentrations of auranofin thereby identifies a

Table 1 Hits obtained after screening the Iconix library

Compound	Percentage inhibition (5 μM)
Auranofin	100
Sporidesmin A	99
Cycloheximide	98
Cladribine	79
Fludarabine	77
Homochlorcyclizine	73
Trifluoperazine	69
Idarubicin	65
4,4′-diethylaminoethoxyhexestrol	58
Clomiphene	54
Amiodarone	51

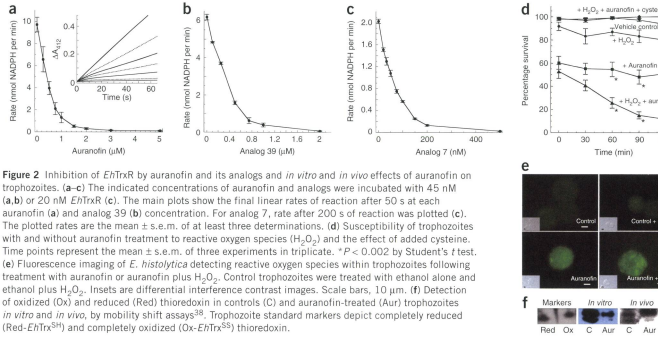

Figure 2 Inhibition of *Eh*TrxR by auranofin and its analogs and *in vitro* and *in vivo* effects of auranofin on trophozoites. (**a**–**c**) The indicated concentrations of auranofin and analogs were incubated with 45 nM (**a**,**b**) or 20 nM *Eh*TrxR (**c**). The main plots show the final linear rates of reaction after 50 s at each auranofin (**a**) and analog 39 (**b**) concentration. For analog 7, rate after 200 s of reaction was plotted (**c**). The plotted rates are the mean ± s.e.m. of at least three determinations. (**d**) Susceptibility of trophozoites with and without auranofin treatment to reactive oxygen species (H_2O_2) and the effect of added cysteine. Time points represent the mean ± s.e.m. of three experiments in triplicate. *$P < 0.002$ by Student's *t* test. (**e**) Fluorescence imaging of *E. histolytica* detecting reactive oxygen species within trophozoites following treatment with auranofin or auranofin plus H_2O_2. Control trophozoites were treated with ethanol alone and ethanol plus H_2O_2. Insets are differential interference contrast images. Scale bars, 10 μm. (**f**) Detection of oxidized (Ox) and reduced (Red) thioredoxin in controls (C) and auranofin-treated (Aur) trophozoites *in vitro* and *in vivo*, by mobility shift assays[38]. Trophozoite standard markers depict completely reduced (Red-*Eh*Trx^{SH}) and completely oxidized (Ox-*Eh*Trx^{SS}) thioredoxin.

new gene in *E. histolytica* selectively inducible by auranofin exposure. It is noteworthy that both arsenite and auranofin are reported to be inhibitors of thioredoxin reductase (TrxR)[23,24] and metabolic inhibitors of selenium metabolism[25]. This led us to hypothesize that *E. histolytica* TrxR is the probable target of auranofin. Because *E. histolytica* resides in either aerobic (liver) or anaerobic (colon) environments in its mammalian hosts, the parasite must have a means to minimize damage caused by reactive oxygen species produced by the host immune assault. In most organisms, there are two largely independent systems to detoxify reactive oxygen species, one based on glutathione and the other based on thioredoxin. Each of these systems has a dedicated NADPH-dependent flavoenzyme, glutathione reductase and TrxR, to maintain the reduced state of glutathione and thioredoxin, respectively[26–28]. However, *E. histolytica* lacks both glutathione reductase activity and glutathione synthetic enzymes[29]; its TrxR is involved in prevention, intervention and repair of damage caused by oxidative stress[30].

There is a single TrxR-encoding gene in the *E. histolytica* genome (*EHI_155440*). *E. histolytica* TrxR (*Eh*TrxR) belongs to the low-molecular-weight TrxR family[31] and is similar to bacterial and yeast enzymes, including the TrxR from *Escherichia coli* (**Supplementary Fig. 2**). In contrast, most higher eukaryotes have a high-molecular-weight TrxR that is typically a selenocysteine protein; this enzyme in *S. mansoni*, known as TGR, has both selenium and an appended glutaredoxin domain[24] (**Supplementary Fig. 3**). We hypothesized that *Eh*TrxR would not contain selenium and that auranofin would bind the active-site cysteines. We were able to readily purify active, His-tagged *Eh*TrxR from solubilized *E. coli* by nickel-affinity chromatography[30] for use in inhibition studies.

We examined the activities of auranofin and its two most active analogs for inhibition of recombinant *Eh*TrxR. Low-micromolar concentrations of auranofin and analog 39 and nanomolar concentrations of analog 7 were inhibitory (**Fig. 2a**–**c**). The assays were nonlinear for the first 50 s (shown for auranofin in the inset of **Fig. 2a** at concentrations of 0, 0.25, 0.5, 0.75, 1, 2 and 5 μM, in order of decreasing slope), unlike control reactions without auranofin; inhibition increased with time until a linear, inhibited rate was established after 50 s of reaction (**Fig. 2a**). Examination of the rates after 50 s indicated that 0.4 μM auranofin caused 50% inhibition. The EC_{50} values for analog 39 and analog 7 were 0.33 and 0.055 μM, respectively. Preincubation of the inhibitor with reduced *Eh*TrxR did not remove the lag phase in inhibition, as seen by the nonlinearity of the data acquired up to 50 s (data not shown).

Because TrxR is crucial for protecting amebic trophozoites from oxidant attack, we compared the susceptibility of trophozoites with and without auranofin treatment to reactive oxygen species (H_2O_2). After incubation of trophozoites with 2 μM auranofin for 18 h, the remaining viable trophozoites (~50%) were significantly more sensitive to killing by 300 μM H_2O_2 than control trophozoites in medium alone ($P < 0.002$) (**Fig. 2d**). Killing by auranofin (2 μM) and H_2O_2 was reversed by the presence of 2 mg ml^{-1} of cysteine (**Fig. 2d**). Cysteine is the major reductant in *E. histolytica*[32], and its apparent protective effect may be through direct reduction of thioredoxin or inhibition of auranofin binding to cysteine residues in TrxR. We detected the presence of reactive oxygen species after 2 μM auranofin treatment with fluorescence generated by the oxidation of dichlorodihydrofluorescein added to the medium[33] (**Fig. 2e**). However, the same concentration of metronidazole, although producing stress, did not increase intracellular reactive oxygen species (**Supplementary Fig. 4**). Moreover, we observed increased amounts of oxidized thioredoxin in auranofin-treated trophozoites, both *in vitro* and *in vivo*, indicating that TrxR may be a target for auranofin (**Fig. 2f**).

Recently, the crystal structure of *S. mansoni* TGR that had been incubated with auranofin before crystallization was solved[24]. The structure revealed gold (Au(I)) rather than auranofin as an adduct between pairs of cysteines (Cys-Au-Cys) in two different sites and also bound to the proposed NADPH binding site of the reductase in a third location. The C terminus of TGR containing a selenocysteine residue was not observed in the structure and may have bound a fourth gold atom. The authors of that study proposed that the selenocysteine at the penultimate position of TGR accelerated the release of gold from auranofin to form the inactivated enzymes; benzeneselenol added to a

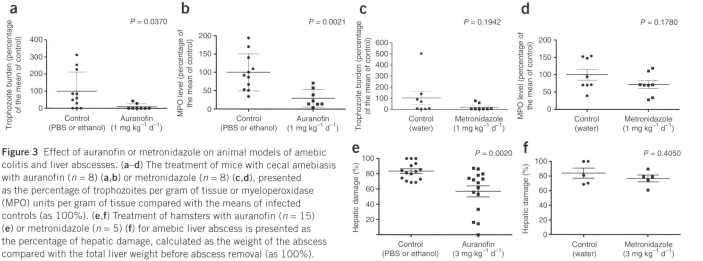

Figure 3 Effect of auranofin or metronidazole on animal models of amebic colitis and liver abscesses. (**a**–**d**) The treatment of mice with cecal amebiasis with auranofin ($n = 8$) (**a**,**b**) or metronidazole ($n = 8$) (**c**,**d**), presented as the percentage of trophozoites per gram of tissue or myeloperoxidase (MPO) units per gram of tissue compared with the means of infected controls (as 100%). (**e**,**f**) Treatment of hamsters with auranofin ($n = 15$) (**e**) or metronidazole ($n = 5$) (**f**) for amebic liver abscess is presented as the percentage of hepatic damage, calculated as the weight of the abscess compared with the total liver weight before abscess removal (as 100%).

C-terminally truncated TGR or to glutathione reductase increased the rate of inactivation by auranofin[24]. The crystal structure of reduced *L. infantum* trypanothione reductase complexed with NADPH and auranofin also demonstrated that gold binds two active cysteine residues of trypanothione reductase[16].

*Eh*TrxR is of very similar size and domain topology as *E. coli* TrxR, a well-studied enzyme[34]. Both proteins have an active site dithiol/disulfide center (Cys-Ala-Thr-Cys for *Ec*TrxR, Cys-Ala-Ile-Cys for *Eh*TrxR) plus either two or four additional cysteine residues, respectively (**Supplementary Fig. 2**). By analogy with the *S. mansoni* TGR, addition of auranofin could cause gold atoms to bind the NADPH-binding site of *Eh*TrxR, the active-site thiols, the four cysteine residues near the C terminus of the enzyme or some combination of these sites.

Because of auranofin's *in vitro* activity against *E. histolytica* trophozoites and oral availability, we tested its efficacy in two animal models of amebiasis. We adapted a mouse amebic colitis model in which trophozoites invade and colonize mouse cecal tissue after surgical inoculation[35,36]. We co-cultured amebic trophozoites with cecal bacteria and surgically inoculated them into the cecum of C3H/HeJ mice. We delivered auranofin or metronidazole by gavage 24 h after infection at a concentration of 1 mg per kg body weight per day for 7 d (ref. 37). Both the parasite burden and the inflammatory response as measured by activity of myeloperoxidase in cecal tissue were significantly decreased by auranofin ($P = 0.037$ and $P = 0.0021$, respectively) (**Fig. 3a**,**b**) but not by metronidazole (**Fig. 3c**,**d**). Auranofin (**Fig. 3e**) was more effective than an equivalent dose of metronidazole (**Fig. 3f**) in a hamster model of amebic liver abscess where treatment started 4 d after infection. A single oral dose of 3 mg per kg body weight per day of auranofin for 7 d significantly decreased hepatic damage in hamsters ($P = 0.002$) (**Fig. 3e**). These findings suggest that auranofin may be an entirely new class of drug to treat amebiasis and potentially other parasitic infections. On the basis of these results, the FDA has approved an orphan-drug designation of auranofin for treatment of amebiasis.

In summary, we have shown that it is feasible to screen large numbers of compounds in an HTS format for effectiveness against *E. histolytica*, and robust and reproducible results can be generated from this HTS. The discovery of the amebicidal activity of the FDA-approved drug auranofin offers a promising drug-repositioning opportunity for the treatment of amebiasis.

METHODS

Methods and any associated references are available in the online version of the paper.

Accession codes. Microarray data are deposited in ArrayExpress with accession code E-MEXP-3494.

Note: *Supplementary information is available in the online version of the paper.*

ACKNOWLEDGMENTS

This work was supported by the Sandler Foundation and US National Institute of Allergy and Infectious Diseases grant 5U01AI077822; we also acknowledge support from R01 GM050389. *E. histolytica* microarray slides were kindly provided by S.L. Stanley Jr. (Stony Brook University, New York), and the *E. histolytica* thioredoxin–specific antibody was a kind gift from S. Adrian-Guerrero (Universidad Nacional del Litoral). We thank G. Hwang and C. Le for their help with the mouse surgery and K. Ang and J. Gut for sharing their expertise.

AUTHOR CONTRIBUTIONS

A.D. and J.H.M. designed the HTS screening studies and arrays. A.D. performed HTS and array experiments. D.P. and L.B.P. performed the enzymatic assays. R.M.A. performed the oxidant studies. C.H., E.R.C., K.H., G.G.-R., E.O. and M.B.M. did the *in vivo* studies. K.H. purified recombinant *Eh*TrxR. S.C. and M.R.A. provided compound libraries and edited the manuscript. S.S.G. and A.M.B. synthesized auranofin analogs. S.L.R. designed the *Eh*TrxR and oxidant studies. A.D., L.B.P., J.H.M. and S.L.R. wrote the manuscript.

COMPETING FINANCIAL INTERESTS

The authors declare no competing financial interests.

Published online at http://www.nature.com/doifinder/10.1038/nm.2758.
Reprints and permissions information is available online at http://www.nature.com/reprints/index.html.

1. World Health Organization. The World Health Report 1998: life in the 21st century: a vision for all. <http://www.who.int/whr/1998/en/whr98_en.pdf>. (1998).
2. Freeman, C.D., Klutman, N.E. & Lamp, K.C. Metronidazole. A therapeutic review and update. *Drugs* **54**, 679–708 (1997).
3. Krogstad, D.J. & Cedeno, J.R. Problems with current therapeutic regimens. in *Amebiasis: Human Infection by Entamoeba Histolytica* (ed. Ravdin, J.I.) 741–748 (John Wiley & Sons, New York, 1988).
4. Samarawickrema, N.A., Brown, D.M., Upcroft, J.A., Thammapalerd, N. & Upcroft, P. Involvement of superoxide dismutase and pyruvate:ferredoxin oxidoreductase in mechanisms of metronidazole resistance in *Entamoeba histolytica*. *J. Antimicrob. Chemother.* **40**, 833–840 (1997).
5. Wassmann, C., Hellberg, A., Tannich, E. & Bruchhaus, I. Metronidazole resistance in the protozoan parasite *Entamoeba histolytica* is associated with increased expression of iron-containing superoxide dismutase and peroxiredoxin and decreased expression of ferredoxin 1 and flavin reductase. *J. Biol. Chem.* **274**, 26051–26056 (1999).

6. Seifert, K. *et al.* Effects of miltefosine and other alkylphosphocholines on human intestinal parasite *Entamoeba histolytica*. *Antimicrob. Agents Chemother.* **45**, 1505–1510 (2001).
7. Ghosh, S. *et al.* Effects of bisphosphonates on the growth of *Entamoeba histolytica* and *Plasmodium* species *in vitro* and *in vivo*. *J. Med. Chem.* **47**, 175–187 (2004).
8. Singh, S., Athar, F. & Azam, A. Synthesis, spectral studies and in vitro assessment for antiamoebic activity of new cyclooctadiene ruthenium(II) complexes with 5-nitrothiophene-2-carboxaldehyde thiosemicarbazones. *Bioorg. Med. Chem. Lett.* **15**, 5424–5428 (2005).
9. Ashburn, T.T. & Thor, K.B. Drug repositioning: identifying and developing new uses for existing drugs. *Nat. Rev. Drug Discov.* **3**, 673–683 (2004).
10. Makioka, A., Kumagai, M., Ohtomo, H., Kobayashi, S. & Takeuchi, T. Effect of calcium antagonists, calcium channel blockers and calmodulin inhibitors on the growth and encystation of *Entamoeba histolytica* and *E. invadens*. *Parasitol. Res.* **87**, 833–837 (2001).
11. Gottlieb, N.L. Pharmacology of auranofin: overview and update. *Scand. J. Rheumatol. Suppl.* **63**, 19–28 (1986).
12. Kuntz, A.N. *et al.* Thioredoxin glutathione reductase from *Schistosoma mansoni*: an essential parasite enzyme and a key drug target. *PLoS Med.* **4**, e206 (2007).
13. Lobanov, A.V., Gromer, S., Salinas, G. & Gladyshev, V.N. Selenium metabolism in *Trypanosoma*: characterization of selenoproteomes and identification of a kinetoplastida-specific selenoprotein. *Nucleic Acids Res.* **34**, 4012–4024 (2006).
14. Bonilla, M. *et al.* Platyhelminth mitochondrial and cytosolic redox homeostasis is controlled by a single thioredoxin glutathione reductase and dependent on selenium and glutathione. *J. Biol. Chem.* **283**, 17898–17907 (2008).
15. Sannella, A.R. *et al.* New uses for old drugs. Auranofin, a clinically established antiarthritic metallodrug, exhibits potent antimalarial effects *in vitro*: Mechanistic and pharmacological implications. *FEBS Lett.* **582**, 844–847 (2008).
16. Ilari, A. *et al.* A gold-containing drug against parasitic polyamine metabolism: the X-ray structure of trypanothione reductase from *Leishmania infantum* in complex with auranofin reveals a dual mechanism of enzyme inhibition. *Amino Acids* **42**, 803–811 (2012).
17. Davis, P.H., Schulze, J. & Stanley, S.L. Jr. Transcriptomic comparison of two *Entamoeba histolytica* strains with defined virulence phenotypes identifies new virulence factor candidates and key differences in the expression patterns of cysteine proteases, lectin light chains and calmodulin. *Mol. Biochem. Parasitol.* **151**, 118–128 (2007).
18. Blower, M.D., Nachury, M., Heald, R. & Weis, K.A. Rae1-containing ribonucleoprotein complex is required for mitotic spindle assembly. *Cell* **121**, 223–234 (2005).
19. Parks, R.E. Jr. *et al.* Purine metabolism in primitive erythrocytes. *Comp. Biochem. Physiol. B* **45**, 355–364 (1973).
20. Créchet, J.B., Cool, R.H., Jacquet, E. & Lallemand, J.Y. Characterization of *Saccharomyces cerevisiae* Ras1p and chimaeric constructs of Ras proteins reveals the hypervariable region and farnesylation as critical elements in the adenylyl cyclase signaling pathway. *Biochemistry* **42**, 14903–14912 (2003).
21. Arnaud-Dabernat, S. *et al.* Nm23-M2/NDP kinase B induces endogenous c-myc and nm23-M1/NDP kinase A overexpression in BAF3 cells. Both NDP kinases protect the cells from oxidative stress-induced death. *Exp. Cell Res.* **301**, 293–304 (2004).
22. Sok, J. *et al.* Arsenite-inducible RNA-associated protein (AIRAP) protects cells from arsenite toxicity. *Cell Stress Chaperones* **6**, 6–15 (2001).
23. Lu, J., Chew, E.H. & Holmgren, A. Targeting thioredoxin reductase is a basis for cancer therapy by arsenic trioxide. *Proc. Natl. Acad. Sci. USA* **104**, 12288–12293 (2007).
24. Angelucci, F. *et al.* Inhibition of *Schistosoma mansoni* thioredoxin-glutathione reductase by auranofin: structural and kinetic aspects. *J. Biol. Chem.* **284**, 28977–28985 (2009).
25. Talbot, S., Nelson, R. & Self, W.T. Arsenic trioxide and auranofin inhibit selenoprotein synthesis: implications for chemotherapy for acute promyelocytic leukaemia. *Br. J. Pharmacol.* **154**, 940–948 (2008).
26. Townsend, D.M., Tew, K.D. & Tapiero, H. The importance of glutathione in human disease. *Biomed. Pharmacother.* **57**, 145–155 (2003).
27. Lillig, C.H. & Holmgren, A. Thioredoxin and related molecules—from biology to health and disease. *Antioxid. Redox Signal.* **9**, 25–47 (2007).
28. Sayed, A.A. *et al.* Identification of oxadiazoles as new drug leads for the control of schistosomiasis. *Nat. Med.* **14**, 407–412 (2008).
29. Fahey, R.C., Newton, G.L., Arrick, B., Overdank-Bogart, T. & Aley, S.B. *Entamoeba histolytica*: a eukaryote without glutathione metabolism. *Science* **224**, 70–72 (1984).
30. Arias, D.G., Gutierrez, C.E., Iglesias, A.A. & Guerrero, S.A. Thioredoxin-linked metabolism in *Entamoeba histolytica*. *Free Radic. Biol. Med.* **42**, 1496–1505 (2007).
31. Hirt, R.P., Muller, S., Embley, T.M. & Coombs, G.H. The diversity and evolution of thioredoxin reductase: new perspectives. *Trends Parasitol.* **18**, 302–308 (2002).
32. Jeelani, G. *et al.* Two atypical L-cysteine-regulated NADPH-dependent oxidoreductases involved in redox maintenance, L-cystine and iron reduction and metronidazole activation in the enteric protozoan *Entamoeba histolytica*. *J. Biol. Chem.* **285**, 26889–26899 (2010).
33. Sen, A., Chatterjee, N.S., Akbar, M.A., Nandi, N. & Das, P. The 29-kilodalton thiol-dependent peroxidase of *Entamoeba histolytica* is a factor involved in pathogenesis and survival of the parasite during oxidative stress. *Eukaryot. Cell* **6**, 664–673 (2007).
34. Williams, C.H. *et al.* Thioredoxin reductase: two modes of catalysis have evolved. *Eur. J. Biochem.* **267**, 6110–6117 (2000).
35. Houpt, E.R. *et al.* The mouse model of amebic colitis reveals mouse strain susceptibility to infection and exacerbation of disease by CD4$^+$ T cells. *J. Immunol.* **169**, 4496–4503 (2002).
36. He, C. *et al.* A novel *Entamoeba histolytica* cysteine proteinase, EhCP4, is key for invasive amebiasis and a therapeutic target. *J. Biol. Chem.* **285**, 18516–18527 (2010).
37. Markiewicz, V.R., Saunders, L.A., Geus, R.J., Payne, B.J. & Hook, J.B. Carcinogenicity study of auranofin, an orally administered gold compound in mice. *Fundam. Appl. Toxicol.* **11**, 277–284 (1988).
38. Bersani, N.A., Merwin, J.R., Lopez, M.I., Pearson, G.D. & Merrill, G.F. Protein electrophoretic mobility shift assay to monitor redox state of thioredoxin in cells. *Methods Enzymol.* **347**, 317–326 (2002).

nature medicine

The ephrin receptor tyrosine kinase A2 is a cellular receptor for Kaposi's sarcoma–associated herpesvirus

Alexander S Hahn[1,8], Johanna K Kaufmann[1,8,9], Effi Wies[1,8,9], Elisabeth Naschberger[2], Julia Panteleev-Ivlev[1], Katharina Schmidt[1], Angela Holzer[1], Martin Schmidt[1], Jin Chen[3,4], Simone König[5], Armin Ensser[1], Jinjong Myoung[6], Norbert H Brockmeyer[7], Michael Stürzl[2], Bernhard Fleckenstein[1] & Frank Neipel[1]

Kaposi's sarcoma–associated herpesvirus (KSHV) is the causative agent of Kaposi's sarcoma[1], a highly vascularized tumor originating from lymphatic endothelial cells, and of at least two different B cell malignancies[2,3]. A dimeric complex formed by the envelope glycoproteins H and L (gH-gL) is required for entry of herpesviruses into host cells[4]. We show that the ephrin receptor tyrosine kinase A2 (EphA2) is a cellular receptor for KSHV gH-gL. EphA2 co-precipitated with both gH-gL and KSHV virions. Infection of human epithelial cells with a GFP-expressing recombinant KSHV strain, as measured by FACS analysis, was increased upon overexpression of EphA2. Antibodies against EphA2 and siRNAs directed against EphA2 inhibited infection of endothelial cells. Pretreatment of KSHV with soluble EphA2 resulted in inhibition of KSHV infection by up to 90%. This marked reduction of KSHV infection was seen with all the different epithelial and endothelial cells used in this study. Similarly, pretreating epithelial or endothelial cells with the soluble EphA2 ligand ephrinA4 impaired KSHV infection. Deletion of the gene encoding EphA2 essentially abolished KSHV infection of mouse endothelial cells. Binding of gH-gL to EphA2 triggered EphA2 phosphorylation and endocytosis, a major pathway of KSHV entry[5,6]. Quantitative RT-PCR and *in situ* histochemistry revealed a close correlation between KSHV infection and EphA2 expression both in cultured cells derived from human Kaposi's sarcoma lesions or unaffected human lymphatic endothelium, and *in situ* in Kaposi's sarcoma specimens, respectively. Taken together, our results identify EphA2, a tyrosine kinase with known functions in neovascularization and oncogenesis, as an entry receptor for KSHV.

Herpesvirus entry involves several viral glycoproteins and cellular receptors[4,7]. KSHV uses cell surface heparan sulfate[8–11] or DC-SIGN[12] for attachment. Subsequently, KSHV binding to integrins activates several downstream effectors[13,14] followed by endocytosis[5,6]. The cysteine transporter xCT was identified as a fusion receptor for KSHV[15]. However, the viral glycoproteins responsible for interactions with xCT have not been identified. In the case of KSHV, gB and gH-gL seem to comprise the minimal fusion machinery[16]. We previously reported that the gH-gL complex binds an unknown receptor on the heparan sulfate–negative mouse fibroblast cell line sog9 (ref. 11).

To identify this putative KSHV receptor, we surface-biotinylated sog9 cells[17], lysed them and subjected the lysate to immunoprecipitation with a soluble variant of gH lacking the transmembrane and intracellular part fused to the Fc fragment of human IgG (gHΔTM-Fc) that was co-expressed in complex with gL (gHΔTM-Fc/gL) (**Fig. 1a**). We identified by mass spectrometry a membrane protein of ~110 kDa that specifically interacted with this glycoprotein complex as EphA2 (**Supplementary Table 1**). Immunoprecipitation with gHΔTM-Fc/gL from 293T human embryonic kidney cells expressing Myc- and His-tagged EphA2 lacking the intracellular domain (EphA2ΔICMycHis) confirmed this interaction (**Fig. 1b**). Soluble EphA2 also bound to 293T cells expressing KSHV gH-gL (**Supplementary Fig. 1**). However, only KSHV gH-gL precipitated EphA2 whereas gH-gL from the related rhesus monkey rhadinovirus (RRV) did not (**Fig. 1c**). Co-sedimentation experiments were performed using KSHV virions concentrated from the supernatant of the KSHV-positive primary effusion lymphoma (PEL) cell line BC3 to further prove that EphA2 is associated with gH-gL in the virion envelope. The recombinantly expressed hemagglutinin-tagged ectodomain of EphA2 (EphA2-HA) was incubated with precleared supernatant from BC3 cells that were either induced to produce KSHV virions or left uninduced (mock). KSHV virions were then pelleted by centrifugation and subjected to western blot analysis. The virion envelope protein gpK8.1 did not bind directly to EphA2 (data not shown). Due to alternative splicing and glycosylation, different forms of the viral envelope glycoprotein gpK8.1 are expressed in cells lytically infected with KSHV. The predominant

[1]Virologisches Institut, Universitätsklinikum Erlangen, Erlangen, Germany. [2]Abteilung für Molekulare und Experimentelle Chirurgie, Universitätsklinikum Erlangen, Erlangen, Germany. [3]Departments of Medicine, Cancer Biology, Cell and Developmental Biology, Vanderbilt-Ingram Cancer Center, Vanderbilt University, Nashville, Tennessee, USA. [4]Veterans Affairs Medical Center, Tennessee Valley Healthcare System, Nashville, Tennessee, USA. [5]Integrated Functional Genomics, Interdisciplinary Center of Clinical Research, University of Münster, Münster, Germany. [6]Novartis Institutes for Biomedical Research, Emeryville, California, USA. [7]Department for Dermatology, St. Josef-Hospital, Bochum, Germany. [8]Present addresses: New England Primate Research Center, Harvard Medical School, Southborough, Massachusetts, USA (A.H. and E.W.); German Cancer Research Center, Heidelberg, Germany (J.K.K.). [9]These authors contributed equally to this work. Correspondence should be addressed to F.N. (frank.neipel@viro.med.uni-erlangen.de).

Received 28 November 2011; accepted 17 April 2012; published online 27 May 2012; doi:10.1038/nm.2805

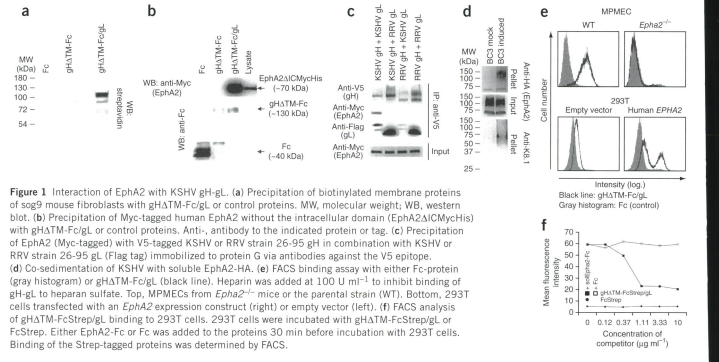

Figure 1 Interaction of EphA2 with KSHV gH-gL. (**a**) Precipitation of biotinylated membrane proteins of sog9 mouse fibroblasts with gHΔTM-Fc/gL or control proteins. MW, molecular weight; WB, western blot. (**b**) Precipitation of Myc-tagged human EphA2 without the intracellular domain (EphA2ΔICMycHis) with gHΔTM-Fc/gL or control proteins. Anti-, antibody to the indicated protein or tag. (**c**) Precipitation of EphA2 (Myc-tagged) with V5-tagged KSHV or RRV strain 26-95 gH in combination with KSHV or RRV strain 26-95 gL (Flag tag) immobilized to protein G via antibodies against the V5 epitope. (**d**) Co-sedimentation of KSHV with soluble EphA2-HA. (**e**) FACS binding assay with either Fc-protein (gray histogram) or gHΔTM-Fc/gL (black line). Heparin was added at 100 U ml^{-1} to inhibit binding of gH-gL to heparan sulfate. Top, MPMECs from *Epha2*$^{-/-}$ mice or the parental strain (WT). Bottom, 293T cells transfected with an *EphA2* expression construct (right) or empty vector (left). (**f**) FACS analysis of gHΔTM-FcStrep/gL binding to 293T cells. 293T cells were incubated with gHΔTM-FcStrep/gL or FcStrep. Either EphA2-Fc or Fc was added to the proteins 30 min before incubation with 293T cells. Binding of the Strep-tagged proteins was determined by FACS.

variant of gpK8.1 that is present in cellular membranes migrates with an apparent molecular weight of 35–37 kDa. In contrast, a protein of 68–72 kDa is selectively incorporated into the virion envelope[18]. Co-sedimentation of EphA2-HA with a gpK8.1 protein of 68–72 kDa[18] and not the cell-membrane variant of 35 kDa demonstrated association of EphA2 with virions (**Fig. 1d**). Having shown that soluble EphA2 is able to bind both isolated gH-gL (**Fig. 1b**,**c** and **Supplementary Fig. 1**) and KSHV (**Fig. 1d**), we next examined whether gH-gL is able to bind membrane-bound EphA2. We added heparin to the recombinantly expressed gH-gL glycoprotein complex to inhibit binding of gH-gL to heparan sulfate[11]. We incubated mouse pulmonary microvascular endothelial cells (MPMECs) from either an *Epha2*-knockout mouse or the parental mouse strain (WT) with gHΔTM-Fc/gL. Binding of gHΔTM-Fc/gL to WT MPMECs in the presence of heparin was clearly detectable, whereas MPMECs from an *Epha2*-knockout mouse[19] did not bind gHΔTM-Fc/gL (**Fig. 1e**). Overexpression of EphA2 greatly increased binding of gHΔTM-Fc/gL to 293T cells (**Fig. 1e**), whereas competition with soluble EphA2-Fc reduced binding of gHΔTM-Fc/gL to these cells (**Fig. 1f**). This finding is particularly noteworthy because heparin was not used here (**Fig. 1f**), and both gH alone and the gH-gL complex bind cell-surface heparan sulfates with high affinity[11].

The inhibition of the interaction of gHΔTM-Fc/gL with the cell surface by soluble EphA2 (**Fig. 1f**) raised the question of whether soluble EphA2 is able to influence KSHV infection. To address this question we used the recombinant KSHV strain rKSHV.219 (ref. 20). rKSHV.219 carries the gene encoding GFP under the control of a cellular constitutive promoter. This allows the detection of KSHV-infected cells by fluorescence microscopy or FACS analysis. When we incubated rKSHV.219 with EphA2-Fc before infection of human lymphatic endothelial cells (LECs), primary Kaposi's sarcoma spindle cells (M7/2 (ref. 21)) and two established Kaposi's sarcoma cell lines (KSImm[22] and SLK[23]), EphA2-Fc inhibited KSHV infection in a dose-dependent manner by up to 97% (**Fig. 2a** and **Supplementary Fig. 2**). Half-maximal inhibition of KSHV infection was achieved at a concentration of <0.2 μg ml^{-1}, which corresponds to approximately 1 nM of dimeric EphA2-Fc (**Fig. 2a**). A recombinant herpesvirus saimiri serving as a control was unaffected by EphA2-Fc (**Supplementary Fig. 3a**).

In addition to blocking the EphA2 binding site(s) on KSHV virions with soluble EphA2 (**Fig. 2a** and **Supplementary Fig. 2**),we also blocked EphA2 on primary human umbilical vein endothelial cells (HUVECs) and primary human LECs with a polyclonal antibody against EphA2 before KSHV infection, resulting in a significant reduction of KSHV infection (**Fig. 2b**, $P < 0.001$). In contrast to KSHV infection, infection with herpesvirus saimiri was not inhibited by EphA2-specific antibody (**Supplementary Fig. 3b**). Overexpression of EphA2 in two human epithelial cell lines (293T and H1299) resulted in increased KSHV infection (**Supplementary Fig. 4**). We confirmed the relevance of EphA2 in infection of endothelial cells by RNAi (**Fig. 2c**); siRNA against EphA2 specifically reduced infection of LECs by approximately 70% (nonsense siRNA siNon versus siEphA2, Student's *t* test, $P < 0.05$). Silencing of EphA2 was verified by FACS analysis (**Supplementary Fig. 5**).

We performed additional control experiments using (i) soluble EphA2 without the Fc tag, (ii) the closely related protein EphA5, (iii) the soluble EphA2 ligand ephrinA4-Fc, which induces EphA2 signaling, (iv) preincubation of the cells, rather than KSHV, with EphA2 and (v) soluble integrins and heparin for comparison (**Fig. 2d**,**e**). The GFP-expressing rKSHV.219 was used again. We determined infection rates by FACS analysis for GFP expression and by quantitative real time-PCR (qRT-PCR) for the KSHV latency-associated nuclear antigen-1 (LANA-1) transcript. Preincubation of KSHV with EphA2-Fc or monomeric EphA2, in contrast to preincubation with the closely related EphA5, resulted in a significant reduction of infection that was comparable to the inhibitory effect of the virion-attachment inhibitor heparin, as did preincubation of the cells with ephrinA4-Fc (**Fig. 2d**). Surprisingly, in contrast to data from other groups[5–7,14], preincubation of KSHV with integrin $\alpha_5\beta_1$ or integrin $\alpha_V\beta_3$ did not inhibit KSHV infection, and pretreatment of SLK cells with antibody LM609, specific for integrin $\alpha_V\beta_3$, had only a very moderate effect

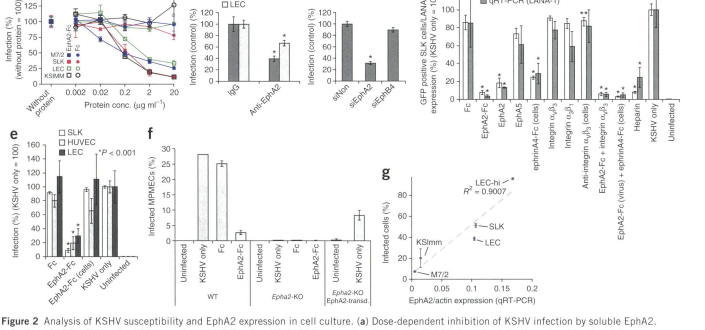

Figure 2 Analysis of KSHV susceptibility and EphA2 expression in cell culture. (**a**) Dose-dependent inhibition of KSHV infection by soluble EphA2. Infection of LECs, SLK cells, KSImm cells and M7/2 cells. rKSHV.219 was preincubated with EphA2-Fc or Fc. Infection rate without protein was set to 100% (SLK and KSImm $n = 6$, LEC and M7/2 $n = 3$, error bars represent s.d.). (**b**) Inhibition of KSHV infection by antibodies against EphA2. HUVECs and LECs were incubated with antibody to EphA2 or rabbit IgG and infected with rKSHV.219. Relative infection rates are shown ($n = 7$, error bars represent s.e.m.; $^*P < 0.001$). (**c**) Infection of LECs after EphA2 knockdown. siNon was set to 100% relative infection ($n = 4$, error bars represent s.e.m.; $^*P < 0.001$). (**d**) rKSHV.219 or, where indicated, the SLK target cells were pre-incubated with the indicated reagents at 2 μg ml^{-1} (integrins and anti-integrin $\alpha_v\beta_3$ at 10 μg ml^{-1}; heparin at 166 IU ml^{-1}). Infection was determined by both FACS and qRT-PCR. KSHV only was set to 100% (FACS $n = 6$, qRT-PCR $n = 3$, error bars represent s.d.). Asterisks indicate statistically significant differences compared to KSHV only ($^*P < 0.001$; $^{**}P < 0.01$). (**e**) Infection of endothelial cells. Either the viral inoculum or the cells were preincubated with EphA2-Fc (2 μg ml^{-1}) or Fc (KSHV only = 100%, $n = 3$, error bars represent s.d.). Asterisks indicate statistically significant differences compared to KSHV only ($P < 0.001$). (**f**) Infection of MPMECs from either WT or an *EphA2*-knockout (KO) mouse or *EphA2*-knockout cells transduced with a mouse EphA2 cDNA as a control. Where indicated, KSHV was preincubated with EphA2-Fc or control protein (2 μg ml^{-1}. $n = 3$, error bars represent s.d.) (**g**) Correlation of EphA2 mRNA expression as determined by qRT-PCR and KSHV infection in human primary cells and cell lines (R^2 = square correlation coefficient; SLK and KSImm $n = 6$, otherwise $n = 3$).

(**Fig. 2d**). The discrepancy between these results and previously published work[5–7,14] may reflect cell-specific usage of integrins by KSHV, and the role of integrins in the infection of endothelial cells and cells derived from Kaposi's sarcoma has not been examined so far. In summary, these data indicated that the observed inhibition of KSHV infection is specific for EphA2. However, it remained to be shown that this inhibitory effect is mediated by the interaction of EphA2-Fc with the KSHV virion and not the cell. Thus, we incubated either KSHV or the cells with EphA2-Fc 30 min prior to infection. We used soluble Fc as a control. Compared to both Fc pretreatment or the buffer control (KSHV only), only pretreatment of the viral inoculum with EphA2-Fc at 2 μg ml^{-1} resulted in a statistically significant reduction in KSHV infection (**Fig. 2e**). In contrast to the EphA2 ligand ephrinA4-Fc (**Fig. 2d**), soluble EphA2-Fc did not result in reduced infection when added to the cells (**Fig. 2e**). This shows that inhibition of infection by EphA2 requires the interaction of EphA2 with the KSHV virion.

Infection of MPMECs with rKSHV.219 resulted in 25% infected cells at 3 d after infection. Preincubation of the virus with EphA2-Fc reduced infection by about 90% (**Fig. 2f**). MPMECs from an *Epha2*-knockout mouse were almost completely resistant to KSHV infection (**Fig. 2f**). When we reconstituted EphA2 expression in these knockout cells by a retroviral expression vector[19], MPMECs from the *EphA2*$^{-/-}$ mouse regained permissiveness (**Fig. 2f**).

Although many cell lines can be infected by KSHV, permissiveness for KSHV entry varies as reflected by the percentage of cells infected using a constant MOI[24], as does expression of EphA2. We measured EphA2 mRNA expression levels by qRT-PCR in ten different types of primary human cells and human cell lines. EphA2-Fc (2 μg ml^{-1}) diminished KSHV infection by at least 50% in all cell lines examined (**Supplementary Fig. 6**). Plotting EphA2 mRNA expression against the infection rate revealed a linear correlation (Pearson's $r = 0.95$, $P = 0.014$) for cells of lymphatic endothelial origin (**Fig. 2g**). Notably, the permissiveness of two different batches of LECs varied about twofold (LEC and LEC-hi), which was reflected by the corresponding EphA2 expression.

To assess the effect of KSHV on EphA2 activation, we incubated 293T cells with concentrated supernatants either from 293 cells producing recombinant KSHV strain rKSHV.219 or uninfected control cells. EphrinA1-Fc was used as a positive control. Both rKSHV.219 and the natural EphA2 ligand ephrinA1 recombinantly expressed in fusion to the Fc (ephrinA1-Fc) increased EphA2 phosphorylation (**Fig. 3a** and **Supplementary Fig. 7**). EphA2 phosphorylation was reverted when KSHV was preincubated with EphA2-Fc (**Fig. 3b**). Next, we stimulated cellular EphA2 with gHΔTM-Fc/gL. Crosslinking of gHΔTM-Fc/gL through an Fc-specific antibody was required for activation of EphA2 (data not shown), mimicking higher-order clustering of envelope glycoproteins. Treatment of cells with crosslinked gHΔTM-Fc/gL or ephrinA1-Fc resulted in a marked increase in EphA2 phosphorylation, as detected by western blot (**Fig. 3c**). To determine whether these effects are of biological importance for KSHV entry, we transiently overexpressed either full-length EphA2 or

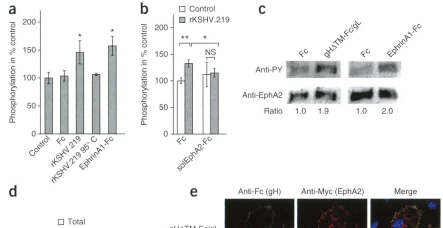

Figure 3 Phosphorylation and endocytosis of EphA2 in response to KSHV and gH-gL. (**a**) Phosphorylation of EphA2 as determined by ELISA after stimulation with KSHV. rKSHV.219 ($n = 5$), heat-denatured rKSHV.219 ($n = 2$), a control preparation with supernatant from KSHV-uninfected cells ($n = 5$) or Fc (5 μg ml^{-1}, $n = 5$). EphrinA1-Fc (5 μg ml^{-1}) served as a positive control ($n = 5$). The KSHV-negative control preparation was set to 100% (error bars represent s.d., $^*P < 0.005$). (**b**) Inhibition of EphA2 phosphorylation in response to KSHV by soluble EphA2. 293T cells were stimulated with concentrated rKSHV.219 or control as in **a**. Fc or EphA2-Fc were added to 5 μg ml^{-1} 30 min before incubation with the cells. EphA2 phosphorylation was determined by ELISA (control preparation with Fc-protein = 100%; $n = 3$, error bars represent s.d., $^*P < 0.05$, $^{**}P < 0.005$; NS, not significant). (**c**) EphA2 phosphorylation as determined by western blotting after stimulation with preclustered gHΔTM-Fc/gL or ephrinA1-Fc as a positive control. (**d**) Infection of 293T cells transfected with empty vector, an expression plasmid for EphA2 or EphA2ΔIC. KSHV infection (GFP) and the transfected proteins (Cy5 fluorescence) were analyzed by FACS. Open bars represent rKSHV.219 infection in the total population; gray bars within the population of cells staining positive for the transfected constructs. Empty-vector–transfected cells were set to 100%. ($n = 3$, error bars represent s.d., $^*P < 0.05$). (**e**) Immunofluorescence analysis of EphA2 and gHΔTM-Fc/gL localization. gHΔTM-Fc/gL was crosslinked for 30 min with Alexa 488–conjugated antibody to human Fc. HeLa cells transfected with an EphA2-Myc expression plasmid were incubated with the crosslinked gHΔTM-Fc/gL for 1 h at 4 °C, then washed, shifted to 37 °C and fixed with 3% paraformaldehyde after 0 min (top row) or 60 min at 37 °C (second row, enlarged insets in the third row), and analyzed by immunofluorescence. The scale bar in the top left panel is 25 μm and applies to all other images.

EphA2 without the intracellular kinase domain (EphA2ΔICMycHis) in 293T cells. We confirmed equal surface expression by FACS analysis (**Supplementary Fig. 8**). Overexpression of full-length EphA2, but not EphA2ΔICMycHis, enhanced KSHV infection in the total cell population by more than 70% (**Fig. 3d**). We detected a threefold increase in KSHV infection when the analysis was limited to those cells positive for the Myc-tagged EphA2 constructs (**Fig. 3d**).

To ascertain whether EphA2 is able to mediate uptake of gHΔTM-Fc/gL, we transiently expressed Myc-tagged EphA2 in HeLa cells. We incubated the cells with cross-linked gHΔTM-Fc/gL at 4 °C before analyzing the localization of both EphA2 and gHΔTM-Fc proteins by immunofluorescence. Directly after incubation at 4 °C, EphA2 and gHΔTM-Fc/gL colocalized at the membrane, whereas after a shift to 37 °C for 60 min both proteins colocalized at vesicular structures within the cell (**Fig. 3e**). We performed additional experiments to confirm that gHΔTM-Fc/gL is endocytosed in a fashion analogous to ephrinA1-Fc (**Supplementary Fig. 9**).

Finally, we examined EphA2 expression in tissue sections from individuals with Kaposi's sarcoma. We stained for the latent KSHV antigen LANA-1 and for EphA2 in consecutive sections of tissues from the skin ($n = 14$) or the lung ($n = 1$) from 15 individuals with AIDS and Kaposi's

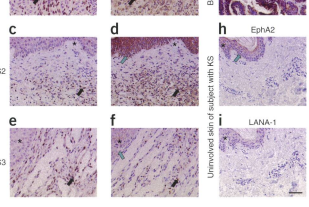

Figure 4 EphA2 and LANA-1 expression in KS. (**a**–**f**) Immunohistochemical detection of LANA-1 and EphA2 in two different Kaposi's sarcoma skin lesions (KS1, KS2) and one lung Kaposi's sarcoma (KS3). (**g**) EphA2 expression in breast cancer, used as a positive control. (**h**,**i**) EphA2 and LANA-1 expression in uninvolved tissue sections of the skin of a subject with Kaposi's sarcoma . Similar tissue areas of consecutive sections are indicated by asterisks. Areas with Kaposi's sarcoma spindle cells, showing prominent nuclear LANA-1 staining and cytoplasmic EphA2 staining in consecutive sections, are indicated by black arrows. Teal arrows indicate EphA2 expression in the epidermis overlaying Kaposi's sarcoma (**b**,**d**), in the tumor cells of breast cancer (**g**) or the epidermal layer of uninvolved skin (**h**). The scale bar in **i** is 50 μm and applies to all other panels.

sarcoma. In all Kaposi's sarcoma tissues, LANA-1 and EphA2 were expressed in the Kaposi's sarcoma spindle cells (**Fig. 4a–f**). Kaposi's sarcoma skin tissues showed increased numbers of KSHV-positive cells compared to uninvolved skin from the same individual (**Fig. 4a,c**), and we detected increased EphA2 staining in the respective consecutive sections (**Fig. 4b,d**). We also detected numerous KSHV-infected cells in lung Kaposi's sarcoma tissue (**Fig. 4e**). In lung Kaposi's sarcoma, EphA2 staining resembled the distribution of LANA-1 and both proteins were less homogeneously distributed than in skin Kaposi's sarcoma tissue (**Fig. 4f**). We used breast carcinoma tissue as a positive control for EphA2 detection (**Fig. 4g**). Uninvolved skin tissues from the same KS patient stained only slightly positive for EphA2 in the epithelial cells of the epidermis (**Fig. 4h**) and stained negative for LANA-1 (**Fig. 4i**). Thus, the percentage of KSHV-infected, LANA-1–positive cells was reflected by the percentage of EphA2-expressing cells. Whereas hardly any EphA2-positive cells were detectable in uninvolved and KSHV-negative skin, the expression of EphA2 was greatly increased in Kaposi's sarcoma specimens from lung and skin, which was paralleled by the number of KSHV-infected cells. In contrast to cells in uninvolved skin, the epidermal cells of the skin overlaying Kaposi's sarcoma tissue were strongly positive for EphA2, suggesting an induction of EphA2 expression in the Kaposi's sarcoma–associated micromilieu (**Fig. 4b,d**).

This study has shown that EphA2 directly interacts with gH and gL of KSHV. Moreover, interference with this interaction by antibodies against EphA2, by soluble EphA2 ligands, by siRNA-mediated knockdown of EphA2 or by competition with soluble EphA2, but not by closely related Eph proteins, unequivocally inhibited KSHV infection, whereas overexpression of EphA2 enhanced it. Moreover, we showed a strong correlation between EphA2 expression and KSHV infection both in cultured Kaposi's sarcoma–derived cells and in Kaposi's sarcoma tissues (**Figs. 2g** and **4**, respectively). Knockout of both *Epha2* alleles in mice essentially abrogated KSHV infection of mouse endothelial cells (**Fig. 2f**). Recently, EphA2 was identified as a cellular co-factor for hepatitis C virus (HCV) entry[25], organizing other receptors on the cell surface to facilitate virus entry. Thus, the role for EphA2 in the case of HCV infection is mechanistically different, as it seems not to function as a receptor. Still, phosphorylation of EphA2 (**Fig. 3a–c**) may contribute to KSHV entry by membrane-organizing effects similar to those described for HCV[25].

Herpesviral gH-gL proteins mediate entry and fusion, sometimes in a cell-specific manner[26–30] and in concert with other viral glycoproteins[4]. Unexpectedly, the crystal structures of gH-gL from two herpesviruses, herpes simplex virus and Epstein-Barr virus, did not resemble other viral fusion proteins[31,32]. KSHV gH-gL has been shown to be required for fusion[16], but further work will be required to define the exact steps of viral entry involving KSHV gH-gL and EphA2. EphA2 ligand binding results in receptor clustering and endocytosis[33,34], as does binding of preclustered gH-gL (**Fig. 3e** and **Supplementary Fig. 9**). Thus, KSHV mimics ligand-induced activation of EphA2 and may profit from this endocytotic stimulus.

We clearly demonstrate a crucial role of EphA2 in KSHV infection of endothelial cells, the cells from which Kaposi's sarcoma originates[35], and show that EphA2 is highly expressed in Kaposi's sarcoma tissue sections (**Fig. 4a–f**). EphA2, EphA4 and EphB2 are known to be phosphorylated in Kaposi's sarcoma tissues[36,37], and EphA2 activation is an important factor in angiogenesis[36,38]. In turn, Kaposi's sarcoma is an angiogenic tumor characterized by chronic, ongoing KSHV infection and neovascularization. The known proangiogenic properties of EphA2 together with the findings of this study support the hypothesis that KSHV interaction with EphA2 is implicated in Kaposi's sarcoma pathogenesis. Therapeutic synergies between inhibiting viral entry and blocking angiogenesis by targeting EphA2 may be beneficial in the treatment of this disease.

METHODS

Methods and any associated references are available in the online version of the paper.

Note: Supplementary information is available in the online version of the paper.

ACKNOWLEDGMENTS

This work was supported by the Akademie der Wissenschaften und der Literatur (Mainz), the European Community research project TargetHerpes, Deutsche Forschungsgemeinschaft center grant 643 and graduate school grant 1071 "viruses of the immune system." M. Stürzl, E.N. and F.N. were supported by the interdisciplinary center for clinical research at the University Hospital of the University of Erlangen. M. Stürzl and E.N. were supported by the German Cancer Aid. We thank L. Wall for experimental assistance and R.C. Desrosiers for helpful discussions and critical reading of the manuscript. KSImm cells were kindly provided by A. Albini (Science and Technology Pole, IRCCS MultiMedica). 4G10 mouse hybridoma supernatant was kindly provided by B. Biesinger (Virologisches Institut, Universitätsklinikum Erlangen).

AUTHOR CONTRIBUTIONS

A.S.H. and F.N. designed the study. A.S.H., J.K.K. and E.W. performed the key experiments. J.P.-I., K.S., M. Schmidt and A.H. performed real-time PCR experiments, cell culture and infection assays. S.K. performed mass spectrometry and analyzed the data. J.C., A.E., J.M. and N.H.B. contributed key reagents. E.N. and M. Stürzl helped with endothelial cell cultures and performed immunohistochemistry experiments. A.S.H. and F.N. wrote the manuscript. B.F. contributed expertise and helped write the paper.

COMPETING FINANCIAL INTERESTS

The authors declare competing financial interests: details are available in the online version of the paper.

Published online at http://www.nature.com/doifinder/10.1038/nm.2805.
Reprints and permissions information is available online at http://www.nature.com/reprints/index.html.

1. Chang, Y. *et al.* Identification of herpesvirus-like DNA sequences in AIDS- associated Kaposi's sarcoma. *Science* **266**, 1865–1869 (1994).
2. Cesarman, E., Chang, Y., Moore, P.S., Said, J.W. & Knowles, D.M. Kaposi's sarcoma–associated herpesvirus-like DNA sequences in AIDS-related body-cavity–based lymphomas. *N. Engl. J. Med.* **332**, 1186–1191 (1995).
3. Soulier, J. *et al.* Kaposi's sarcoma-associated herpesvirus-like DNA sequences in multicentric Castleman's disease. *Blood* **86**, 1276–1280 (1995).
4. Campadelli-Fiume, G. *et al.* The multipartite system that mediates entry of herpes simplex virus into the cell. *Rev. Med. Virol.* **17**, 313–326 (2007).
5. Akula, S.M. *et al.* Kaposi's sarcoma–associated herpesvirus (human herpesvirus 8) infection of human fibroblast cells occurs through endocytosis. *J. Virol.* **77**, 7978–7990 (2003).
6. Raghu, H., Sharma-Walia, N., Veettil, M.V., Sadagopan, S. & Chandran, B. Kaposi's sarcoma-associated herpesvirus utilizes an actin polymerization–dependent macropinocytic pathway to enter human dermal microvascular endothelial and human umbilical vein endothelial cells. *J. Virol.* **83**, 4895–4911 (2009).
7. Chandran, B. Early events in Kaposi's sarcoma-associated herpesvirus infection of target cells. *J. Virol.* **84**, 2188–2199 (2010).
8. Birkmann, A. *et al.* Cell surface heparan sulfate is a receptor for human herpesvirus 8 and interacts with envelope glycoprotein K8.1. *J. Virol.* **75**, 11583–11593 (2001).
9. Wang, F.Z., Akula, S.M., Pramod, N.P., Zeng, L. & Chandran, B. Human herpesvirus 8 envelope glycoprotein K8.1A interaction with the target cells involves heparan sulfate. *J. Virol.* **75**, 7517–7527 (2001).
10. Akula, S.M., Pramod, N.P., Wang, F.Z. & Chandran, B. Human herpesvirus 8 envelope-associated glycoprotein B interacts with heparan sulfate–like moieties. *Virology* **284**, 235–249 (2001).
11. Hahn, A. *et al.* Kaposi's sarcoma-associated herpesvirus gH/gL: Glycoprotein export and interaction with cellular receptors. *J. Virol.* **83**, 396–407 (2009).
12. Rappocciolo, G. *et al.* DC-SIGN is a receptor for human herpesvirus 8 on dendritic cells and macrophages. *J. Immunol.* **176**, 1741–1749 (2006).
13. Sharma-Walia, N., Naranatt, P.P., Krishnan, H.H., Zeng, L. & Chandran, B. Kaposi's sarcoma-associated herpesvirus/human herpesvirus 8 envelope glycoprotein gB induces the integrin-dependent focal adhesion kinase-Src-phosphatidylinositol 3-kinase-Rho GTPase signal pathways and cytoskeletal rearrangements. *J. Virol.* **78**, 4207–4223 (2004).

14. Naranatt, P.P., Akula, S.M., Zien, C.A., Krishnan, H.H. & Chandran, B. Kaposi's sarcoma–associated herpesvirus induces the phosphatidylinositol 3-kinase–PKC-ζ–MEK-ERK signaling pathway in target cells early during infection: implications for infectivity. *J. Virol.* **77**, 1524–1539 (2003).
15. Kaleeba, J.A.R. & Berger, E.A. Kaposi's sarcoma-associated herpesvirus fusion-entry receptor: cystine transporter xCT. *Science* **311**, 1921–1924 (2006).
16. Pertel, P.E. Human herpesvirus 8 glycoprotein B (gB), gH, and gL can mediate cell fusion. *J. Virol.* **76**, 4390–4400 (2002).
17. Banfield, B.W., Leduc, Y., Esford, L., Schubert, K. & Tufaro, F. Sequential isolation of proteoglycan synthesis mutants by using herpes simplex virus as a selective agent: evidence for a proteoglycan-independent virus entry pathway. *J. Virol.* **69**, 3290–3298 (1995).
18. Zhu, L., Puri, V. & Chandran, B. Characterization of human herpesvirus-8 K8.1A/B glycoproteins by monoclonal antibodies. *Virology* **262**, 237–249 (1999).
19. Brantley-Sieders, D.M. *et al.* EphA2 receptor tyrosine kinase regulates endothelial cell migration and vascular assembly through phosphoinositide 3-kinase-mediated Rac1 GTPase activation. *J. Cell Sci.* **117**, 2037–2049 (2004).
20. Vieira, J. & O'Hearn, P.M. Use of the red fluorescent protein as a marker of Kaposi's sarcoma–associated herpesvirus lytic gene expression. *Virology* **325**, 225–240 (2004).
21. Stürzl, M. *et al.* Identification of interleukin-1 and platelet-derived growth factor-B as major mitogens for the spindle cells of Kaposi's sarcoma: a combined *in vitro* and *in vivo* analysis. *Oncogene* **10**, 2007–2016 (1995).
22. Albini, A. *et al.* The beta-core fragment of human chorionic gonadotrophin inhibits growth of Kaposi's sarcoma-derived cells and a new immortalized Kaposi's sarcoma cell line. *AIDS* **11**, 713–721 (1997).
23. Herndier, B.G. *et al.* Characterization of a human Kaposi's sarcoma cell line that induces angiogenic tumors in animals. *AIDS* **8**, 575–581 (1994).
24. Kaleeba, J.A.R. & Berger, E.A. Broad target cell selectivity of Kaposi's sarcoma–associated herpesvirus glycoprotein-mediated cell fusion and virion entry. *Virology* **354**, 7–14 (2006).
25. Lupberger, J. *et al.* EGFR and EphA2 are host factors for hepatitis C virus entry and possible targets for antiviral therapy. *Nat. Med.* **17**, 589–595 (2011).
26. Vleck, S.E. *et al.* Structure–function analysis of varicella-zoster virus glycoprotein H identifies domain-specific roles for fusion and skin tropism. *Proc. Natl. Acad. Sci. USA* **108**, 18412–18417 (2011).
27. Chesnokova, L.S., Nishimura, S.L. & Hutt-Fletcher, L.M. Fusion of epithelial cells by Epstein-Barr virus proteins is triggered by binding of viral glycoproteins gHgL to integrins $\alpha_v\beta_6$ or $\alpha_v\beta_8$. *Proc. Natl. Acad. Sci. USA* **106**, 20464–20469 (2009).
28. Chesnokova, L.S. & Hutt-Fletcher, L.M. Fusion of EBV with epithelial cells can be triggered by $\alpha_v\beta_6$ in addition to $\alpha_v\beta_5$ and $\alpha_v\beta_8$ and integrin binding triggers a conformational change in gHgL. *J. Virol.* **85**, 13214–13223 (2011).
29. Vanarsdall, A.L., Chase, M.C. & Johnson, D.C. Human cytomegalovirus glycoprotein gO complexes with gH-gL, promoting interference with viral entry into human fibroblasts but not entry into epithelial cells. *J. Virol.* **85**, 11638–11645 (2011).
30. Ryckman, B.J., Chase, M.C. & Johnson, D.C. HCMV gH/gL/UL128–131 interferes with virus entry into epithelial cells: evidence for cell type-specific receptors. *Proc. Natl. Acad. Sci. USA* **105**, 14118–14123 (2008).
31. Chowdary, T.K. *et al.* Crystal structure of the conserved herpesvirus fusion regulator complex gH-gL. *Nat. Struct. Mol. Biol.* **17**, 882–888 (2010).
32. Matsuura, H., Kirschner, A.N., Longnecker, R. & Jardetzky, T.S. Crystal structure of the Epstein-Barr virus (EBV) glycoprotein H/glycoprotein L (gH/gL) complex. *Proc. Natl. Acad. Sci. USA* **107**, 22641–22646 (2010).
33. Walker-Daniels, J., Riese, D.J. & Kinch, M.S. c-Cbl–dependent EphA2 protein degradation is induced by ligand binding. *Mol. Cancer Res.* **1**, 79–87 (2002).
34. Zhuang, G., Hunter, S., Hwang, Y. & Chen, J. Regulation of EphA2 receptor endocytosis by SHIP2 lipid phosphatase via phosphatidylinositol 3-kinase-dependent Rac1 activation. *J. Biol. Chem.* **282**, 2683–2694 (2007).
35. Wang, H.W. *et al.* Kaposi sarcoma herpesvirus–induced cellular reprogramming contributes to the lymphatic endothelial gene expression in Kaposi sarcoma. *Nat. Genet.* **36**, 687–693 (2004).
36. Ogawa, K. *et al.* The ephrin-A1 ligand and its receptor, EphA2, are expressed during tumor neovascularization. *Oncogene* **19**, 6043–6052 (2000).
37. Scehnet, J.S. *et al.* The role of Ephs, ephrins and growth factors in Kaposi sarcoma and implications of ephrinB2 blockade. *Blood* **113**, 254–263 (2009).
38. Cheng, N. *et al.* Blockade of EphA receptor tyrosine kinase activation inhibits vascular endothelial cell growth factor–induced angiogenesis. *Mol. Cancer Res.* **1**, 2–11 (2002).

nature medicine

ApoB-containing lipoproteins regulate angiogenesis by modulating expression of VEGF receptor 1

Inbal Avraham-Davidi[1], Yona Ely[1], Van N Pham[2], Daniel Castranova[2], Moshe Grunspan[1], Guy Malkinson[1], Liron Gibbs-Bar[1], Oded Mayseless[1], Gabriella Allmog[1], Brigid Lo[2], Carmen M Warren[3], Tom T Chen[3], Josette Ungos[2,9], Kameha Kidd[2,9], Kenna Shaw[2,9], Ilana Rogachev[4], Wuzhou Wan[5], Philip M Murphy[5], Steven A Farber[6], Liran Carmel[7], Gregory S Shelness[8], M Luisa Iruela-Arispe[3], Brant M Weinstein[2] & Karina Yaniv[1]

Despite the clear major contribution of hyperlipidemia to the prevalence of cardiovascular disease in the developed world, the direct effects of lipoproteins on endothelial cells have remained obscure and are under debate. Here we report a previously uncharacterized mechanism of vessel growth modulation by lipoprotein availability. Using a genetic screen for vascular defects in zebrafish, we initially identified a mutation, *stalactite* (*stl*), in the gene encoding microsomal triglyceride transfer protein (*mtp*), which is involved in the biosynthesis of apolipoprotein B (ApoB)-containing lipoproteins. By manipulating lipoprotein concentrations in zebrafish, we found that ApoB negatively regulates angiogenesis and that it is the ApoB protein particle, rather than lipid moieties within ApoB-containing lipoproteins, that is primarily responsible for this effect. Mechanistically, we identified downregulation of vascular endothelial growth factor receptor 1 (VEGFR1), which acts as a decoy receptor for VEGF, as a key mediator of the endothelial response to lipoproteins, and we observed VEGFR1 downregulation in hyperlipidemic mice. These findings may open new avenues for the treatment of lipoprotein-related vascular disorders.

We identified a zebrafish mutant, which we named *stalactite* (*stl*), with excessive sprouting angiogenesis, in a *Tg(fli1:eGFP)*[y1] (refs. 1, 2) transgenic-based forward genetic screen for vascular-specific mutations. *stl* mutants have ectopic angiogenic segments that extend ventrally from the subintestinal vessels (SIVs) (**Fig. 1a**,**b**), a vascular bed that initially forms bilaterally over the dorsal-lateral aspect of the large zebrafish yolk cell (**Supplementary Fig. 1**). A quantitative analysis (**Supplementary Fig. 1**) revealed both greater numbers and longer lengths of ventral SIV sprouts in *stl* mutants (**Fig. 1c**) compared to their wild-type (WT) siblings. At slightly later stages of development, we also found excessive angiogenic branching in the dorsal part of the intersegmental vessels (ISVs) in *stl* mutants compared to their WT siblings (**Fig. 1d**,**e**). We counted endothelial nuclei in the yolk areas of WT and *stl*; *Tg(fli1:nEGFP)*[y7] embryos to determine whether formation of ectopic sprouts in *stl* mutants involves overproliferation of endothelial cells. The total number of endothelial cells in the yolk area was 42% higher in *stl* mutants than in their WT siblings, with excess cells being found exclusively in the ectopic ventral sprouts of the mutant embryos (**Fig. 1f**,**g**). *stl* mutants also had defects in yolk absorption (**Supplementary Fig. 1**), and *stl* mutant larvae died by approximately 6 days post fertilization (dpf).

To examine the molecular nature of the *stl* phenotype, we positionally cloned the defective locus. We genetically mapped the mutation to an interval in linkage group 1 that contains the gene encoding microsomal triglyceride transfer protein (*mtp*). Sequence analysis of *mtp* complementary DNA (cDNA) from *stl* mutants and their wild-type siblings revealed a change in a conserved leucine residue (Leu475) to a proline in the mutants (**Supplementary Fig. 2**). MTP, an intraluminal protein found within the endoplasmic reticulum of the liver and intestine, is required for the assembly and secretion of proatherogenic, ApoB-containing lipoproteins such as chylomicrons, very-low-density lipoproteins and low-density lipoproteins (LDLs)[3]. After their assembly into mature particles, ApoB-containing lipoproteins are secreted into the blood and lymph stream. Although the MTP-ApoB pathway was originally thought to be unique to the liver and intestine, the findings that the mouse yolk sac expresses Mtp and that mice homozygous for an *Mtp* gene disruption die at embryonic day 10.5 (ref. 4) underscores the key role of the synthesis and secretion of ApoB-containing lipoproteins during early embryogenesis. The yolk syncytial layer (YSL) of zebrafish (the functional counterpart of the yolk sac of higher vertebrates) expresses *mtp* starting at the gastrula stage[5] and forms ApoB-related lipoproteins, which enter the circulatory

[1]Department of Biological Regulation, Weizmann Institute of Science, Rehovot, Israel. [2]Laboratory of Molecular Genetics, National Institute of Child Health and Human Development, US National Institutes of Health (NIH), Bethesda, Maryland, USA. [3]Department of Molecular, Cell and Developmental Biology, University of California Los Angeles, Los Angeles, California, USA. [4]Department of Plant Sciences, Weizmann Institute of Science, Rehovot, Israel. [5]Laboratory of Molecular Immunology, National Institute of Allergy and Infectious Diseases, NIH, Bethesda, Maryland, USA. [6]Department of Embryology, Carnegie Institution for Science, Baltimore, Maryland, USA. [7]Department of Genetics, The Alexander Silberman Institute of Life Sciences, The Hebrew University of Jerusalem, Edmond J. Safra Campus, Givat Ram, Jerusalem, Israel. [8]Department of Pathology, Wake Forest University School of Medicine, Winston-Salem, North Carolina, USA. [9]These authors contributed equally to this work. Correspondence should be addressed to K.Y. (karina.yaniv@weizmann.ac.il).

Received 13 December 2011; accepted 2 April 2012; published online 13 May 2012; doi:10.1038/nm.2759

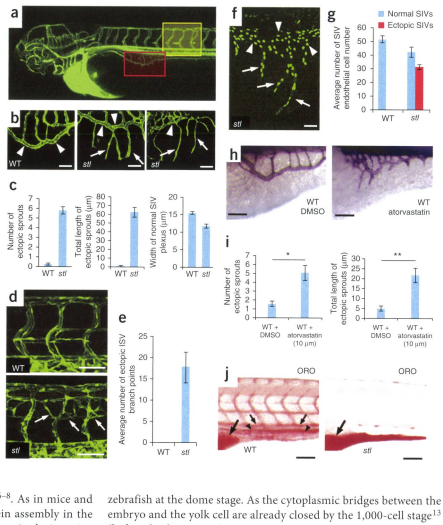

Figure 1 *stl* is a zebrafish mutant with excessive angiogenesis. (**a**) Confocal angiography of a 3.5-dpf zebrafish illustrating the SIVs (boxed in red) and the ISVs (boxed in yellow). (**b**) Confocal images of SIVs (shown boxed in red in **a**) in 3.5-dpf WT *Tg(fli1:eGFP)*[y1] (right) and 3.5-dpf and 5-dpf *stl* mutant larvae (middle and left, respectively). Ectopic segments (arrows) extend from the subintestinal vein (arrowheads). (**c**) Quantification of the ectopic sprouting phenotype in *stl* mutants ($n_{WT} = 87$, $n_{stl} = 107$). (**d**) Confocal images of ISVs (shown boxed in yellow in **a**) in the midtrunks of 5-dpf *Tg(fli1:eGFP)*[y1] WT (top) and *stl* mutant (bottom) larvae. Ectopic sprouts in the *stl* mutants are indicated with arrows. (**e**) Quantification of the average number of ectopic ISV branch points in WT larvae and *stl* mutants ($n_{WT} = 16$, $n_{stl} = 27$). (**f**) Confocal image of SIVs in a 3.5-dpf *stl*; *Tg(fli1:nEGFP)*[y7] zebrafish with the endothelial cell nuclei visible in the normal plexus (arrowheads) and in ectopic sprouts (arrows). (**g**) Quantification of the average number of endothelial cell nuclei in the yolk area of WT and *stl* mutant larvae ($n_{WT} = 12$, $n_{stl} = 14$). $P = 7.3 \times 10^{-6}$ by *t* test. (**h**) Alkaline phosphatase staining of SIVs in WT larvae treated with DMSO (left) or atorvastatin (right). (**i**) Quantification of the average number (left) ($n_{WT+DMSO} = 41$, $n_{WT+atorvastatin} = 38$) and average total length (right) ($n_{WT+DMSO} = 39$, $n_{WT+atorvastatin} = 35$) of ectopic SIV segments. $^{*}P = 1.4 \times 10^{-4}$, $^{**}P = 7.7 \times 10^{-5}$ by *t* test. (**j**) Transmitted light images of 5-dpf ORO-stained WT (left) and *stl* mutant (right) larvae. The yolk is indicated by large arrows. The main vessels are indicated by small arrows and arrowheads. Scale bars, **b**, **f**, **h** and **j**, 30 μm; **d**, 60 μm. All values are mean ± s.e.m.

system and deliver nutrient lipids to the tissues[6–8]. As in mice and humans, zebrafish MTP is involved in lipoprotein assembly in the YSL and is also found at later stages of development in the intestine and liver[5,9]. In addition, zebrafish have structural and functional homologs of mammalian ApoAI, ApoCII, ApoE, phospholipase A2 (PLA2) and lipoprotein lipase (LPL)[10,11].

Four additional lines of evidence confirm that a mutation in *mtp* is responsible for the *stl* phenotype. First, injection of antisense morpholino oligonucleotides targeting *mtp*[6] reproducibly phenocopied the angiogenesis and yolk absorption phenotypes seen in *stl* mutants (**Supplementary Fig. 3a**,**b**,**d**). Second, injection of *mtp* mRNA into *stl* mutants suppressed ectopic sprouting, and mRNA-rescued larvae survived for at least 10 dpf (**Supplementary Fig. 3a**,**c**,**e**). Third, downregulation of *apoB* using *apoB* morpholino oligonucleotides led to ectopic SIV branching that was reminiscent of that seen in the *stl* mutants (**Supplementary Fig. 3f**). However, we did not observe this proangiogenic response upon downregulation of *apoA1* (**Supplementary Fig. 3g**). Finally, reduction of LDL concentrations in WT embryos using atorvastatin[12] efficiently phenocopied the phenotype of excess angiogenesis seen in *stl* mutants (**Fig. 1h**,**i**). Together, these results confirm the specificity of the MTP-ApoB pathway in causing excess angiogenesis.

The restricted expression of the *mtp* transcript in the yolk syncytium, liver and intestine[5] and the lack of vascular *mtp* expression (**Supplementary Fig. 3h**) strongly suggest that the role of this gene in vessel development is not cell autonomous. To confirm this notion, we injected *mtp* mRNA into the yolk syncytium of WT and *stl* mutant zebrafish at the dome stage. As the cytoplasmic bridges between the embryo and the yolk cell are already closed by the 1,000-cell stage[13] (before the dome stage), reagents injected into the yolk cell after this stage are restricted exclusively to the yolk syncytium. As expected for a YSL-specific defect, injection of *mtp* mRNA at the dome stage yielded efficient rescue of the excessive angiogenesis phenotype in *stl* mutants (**Supplementary Fig. 3e**).

In humans, mutations in *MTP* are the proximate cause of abetalipoproteinemia[14–16], an autosomal-recessive defect in the production of ApoB-containing lipoproteins that results in a virtual absence of LDL in the blood. To confirm that the effects of *mtp* downregulation on lipoprotein production and secretion are conserved in zebrafish, we stained WT and *stl* mutant zebrafish larvae with Oil Red O (ORO)[6]. *stl* mutants had a clear absence of lipids in their vasculature when compared to their WT siblings (**Fig. 1j**). To further confirm the lipoprotein-depletion phenotype, we performed a detailed lipid profile analysis of the *stl* mutants. Taking advantage of the fact that exogenously supplied, radioactively labeled fatty acids are properly processed by zebrafish larvae and are found as expected in the triglyceride fraction[17], we used thin-layer chromatography to confirm that the concentrations of triglycerides are strongly reduced in *stl* mutants (**Supplementary Fig. 4**). We also found reduced concentrations of cholesterol using gas chromatography–mass spectrometry (GC-MS) (**Supplementary Fig. 4**).

To further characterize the effects of lipoproteins on angiogenesis *in vivo*, we generated a zebrafish model of lipoprotein overload in the circulation by downregulating the *apoCII* gene[18,19]. ApoCII is a

component of ApoB-containing lipoproteins and is required for the activation of the enzyme LPL in capillaries. LPL activation leads to triglyceride hydrolysis and the release of free fatty acids for use by cells (reviewed in ref. 20). In humans, mutations in *APOCII* result in the accumulation of unprocessed lipoproteins in the circulation (hyperlipoproteinemia type IB and hypertriglyceridemia) and in increased risk of early atherosclerosis[21–23]. We reasoned that whereas morpholino knockdown of *apoCII* early in development would lead to a global reduction in lipid delivery, the endothelial cells of these morphants would nevertheless be exposed to elevated concentrations of plasma lipoproteins, mimicking the hyperlipidemia seen in *APOCII* mutant humans. Injection of *apoCII* morpholino oligonucleotides into *Tg(fli1:eGFP)*^{y1} embryos resulted in increased intravascular concentrations of lipoproteins, as assessed by ORO staining at 4 dpf (**Fig. 2a**; compare with **Fig. 1j**). This increase was accompanied by a marked reduction in total triglyceride and cholesterol levels (**Supplementary Fig. 4**). In contrast to the excess angiogenesis phenotype seen in *stl* mutants, however, we found no ectopic SIV sprouts in *apoCII* (**Fig. 2b,c**) or *lpl* morphants (**Supplementary Fig. 4**), confirming that global lipoprotein starvation *per se* does not lead to excessive angiogenesis. On the contrary, high lipoprotein concentrations in the circulation of *apoCII* morphants resulted in a poorly developed vasculature that was characterized by short and partially lumenized ISVs (**Fig. 2d–f**). These results are consistent with previous findings describing premature vascular disease[24] and general endothelial dysfunction[25] under hyperlipoproteinemic conditions in humans[26].

To further show that the angiogenic phenotypes seen in *stl* and *apoCII* morphants result from a direct response of endothelial cells to lipoprotein concentrations and not from alternative cues trigged by fatty-acid depletion, we investigated the ability of exogenously supplied fatty acids to restore a normal vasculature. The addition of short-, intermediate- or long-chain fatty acids to the embryo culture media did not rescue the vascular phenotype of *stl* mutants (**Fig. 2g,h**) or *apoCII* morphants (**Fig. 2i,j** and data not shown), even when applied at high concentrations (**Supplementary Fig. 4**), consistent with the notion that the angiogenic phenotypes result from a direct response of the endothelial cells to lipoprotein concentrations.

To elucidate the mechanisms underlying the effects of lipoproteins on vascular growth, we began by searching for endothelial-specific mRNAs whose expression was affected by changes in lipoprotein concentrations. Quantitative real time PCR (**Fig. 3a**) and *in situ* hybridization (**Supplementary Fig. 5**) revealed that *vegfr1* mRNA levels were lower in *mtp* morpholino oligonucleotide–injected embryos than in uninjected siblings at 24 h post fertilization (hpf). This reduction was specific for *vegfr1*, as we found little change in the levels of *vegfr2* or *vegfr3* mRNAs or in the mRNA levels of other vascular genes in the *mtp* morphants (**Fig. 3a** and **Supplementary Fig. 5**). VEGFR1 protein concentrations were also strongly downregulated in *stl* mutants but were substantially upregulated in *apoCII* morphants, in which endothelial cells face high concentrations of ApoB lipoproteins (**Fig. 3b**). We found similar effects on VEGFR1 levels in endothelial cells *in vitro*. Treatment of cultured human umbilical vein endothelial cells (HUVECs) with LDL elicited an increase in VEGFR1 but not VEGFR2 concentrations (**Fig. 3b**). In addition, hyperlipidemic *Apoe*- or *Ldlr*-null mice (reviewed in refs. 27,28) also showed increased endothelial-specific Vegfr1 expression compared to control WT mice (**Fig. 3c–e**), confirming conservation of this pathway in higher vertebrates.

Previous studies have shown that VEGFR1 has an inhibitory role in angiogenesis, acting as a 'sink' for the VEGF ligand[29–31]. Downregulation of *vegfr1* by an ATG-blocking morpholino oligonucleotide resulted in excessive sprouting and branching from the

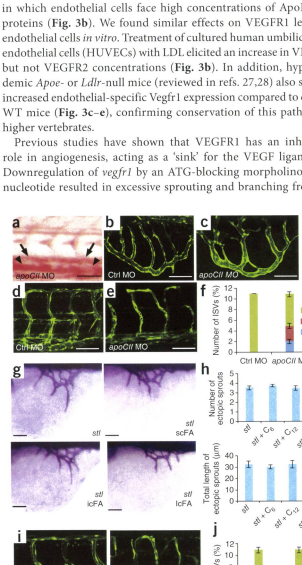

Figure 2 The excessive angiogenesis phenotype is not caused by global lipid starvation. (**a**) Transmitted light image of a 4-dpf ORO-stained larva injected with *apoCII* morpholino oligonucleotides (MOs). The dorsal aorta and the cardinal vein are indicated by arrows and arrowheads, respectively. (**b**–**e**) Confocal imaging of SIVs (**b**,**c**) and ISVs (**d**,**e**) in 3.5-dpf *Tg(fli1:eGFP)*^{y1} larvae injected with a control morpholino oligonucleotide (ctrl) (**b**,**d**) or an *apoCII* morpholino oligonucleotide (**c**,**e**). (**f**) Quantification of the ISV phenotypes of control ($n = 17$) or *apoCII* morpholino-oligonucleotide–injected ($n = 15$) zebrafish embryos. The bars show the percentages of ISVs that have failed to sprout (0, blue), ISVs that have grown only up to the horizontal myosepturn halfway up the trunk (0.5, red) and ISVs that have grown all the way to the dorsal trunk to form the dorso-lateral anastomotic vessel (1, green). (**g**) Alkaline phosphatase staining of SIVs in 3.5-dpf *stl* mutants either not treated (left, top) or treated with short-chain fatty acids (C_6) (scFA) (right, top), intermediate-chain fatty acids (C_{12}) (icFA) (left, bottom) or long-chain fatty acids (C_{18}) (lcFA) (right, bottom). (**h**) Quantification of the ectopic sprouting phenotype. *stl*, untreated *stl* mutants; *stl* + C_6, *stl* mutants plus short-chain fatty acids; *stl* + C_{12}, *stl* mutants plus intermediate-chain fatty acids; *stl* + C_{18}, *stl* mutants plus long-chain fatty acids. $n_{control} = 27$, $n_{C6} = 29$, $n_{C12} = 21$, $n_{C18} = 17$. $P_{top} = 0.517$, $P_{bottom} = 0.5058$ by analysis of variance. (**i**) Confocal images of trunk ISVs in embryos injected with control morpholino oligonucleotides (left) or *apoCII* morpholino oligonucleotides (right) and treated with short-chain fatty acids. (**j**) Quantification of the phenotype of trunk ISVs in embryos injected with *apoCII* morpholino oligonucleotides that were soaked either in normal medium ($n = 15$) or in medium supplemented with short-chain fatty acids ($n = 17$). Trunk ISVs were classified as in **f**. $P = 0.839$ by χ^2 test for injection of *apoCII* morpholino oligonucleotide compared to *apoCII* morpholino oligonucleotide plus short-chain fatty acids. Scale bars, **a**,**b**,**c** and **g**, 30 μm; **d**,**e** and **i**, 60 μm. Data in **f**,**h**, and **j** are mean ± s.e.m.

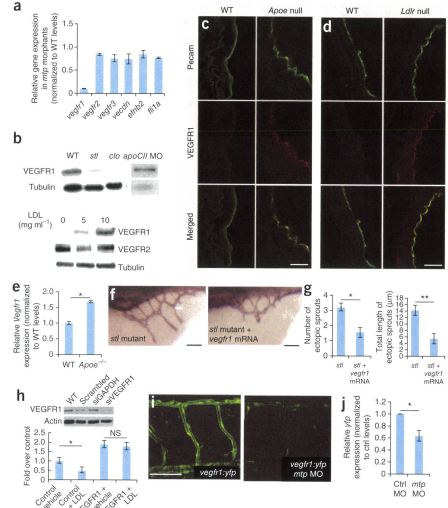

Figure 3 Lipoprotein concentrations regulate the expression of VEGFR1. (**a**) The expression of the indicated mRNAs in 24-hpf embryos injected with *mtp* morpholino oligonucleotides (MO) ($n_{\text{control MO}} = 50$, $n_{mtp\ MO} = 30$). (**b**) Western blots detecting VEGFR1 and tubulin in extracts from 3-dpf zebrafish (top)($n_{\text{control MO}} = 30$, $n_{apoCII\ MO} = 30$, $n_{stl} = 30$, $n_{clo} = 20$). Western blots detecting VEGFR1, VEGFR2 and tubulin in lysates from HUVECs cultured in LDL^- medium with or without the addition of LDL (bottom). The data shown are representative of three independent experiments. (**c**,**d**) Confocal images of aortic roots in WT C57BL/6 (left, **c**) and *Apoe*-null (right, **c**) littermates and of abdominal aortas in WT C57BL/6 (left, **d**) and *Ldlr*-null (right, **d**) littermates stained with Pecam-specific (top) or VEGFR1-specific (middle) antibodies. Merged images are presented at the bottom. Scale bars, 25 μm. (**e**) Semiquantitative RT-PCR measurements of *Vegfr1* mRNA expression in aortic arches dissected from WT ($n = 5$) and *Apoe*-null ($n = 5$) mice. $^*P = 4 \times 10^{-14}$ by *t* test. (**f**) Transmitted light images of alkaline-phosphatase–stained SIVs in a 3.5-dpf *stl* mutant not injected (left) or injected with *vegfr1* mRNA (right). (**g**) Quantification of the ectopic sprouting phenotype ($n_{stl} = 26$, $n_{stl+vegfr1\ \text{mRNA}} = 23$). $^*P = 1.6 \times 10^{-4}$, $^{**}P = 2.6 \times 10^{-4}$ by *t* test. (**h**) Western blots detecting VEGFR1 and actin in lysates from HUVECs exposed to the indicated siRNAs (top). siGAPDH, siRNA targeting glyceraldehyde-3-phosphate dehydrogenase (GAPDH); siVEGFR1, siRNA targeting VEGFR1. Migration area of HUVECs treated with either LDL or vehicle as a response to a 200-μm wound (bottom). Bars represent mean ± s.e.m. (**i**) Confocal images of *Tg(flt1:YFP)*^{hu4624} (left) and *mtp* morpholino-oligonucleotide–injected *Tg(flt1:YFP)*^{hu4624} (right) embryos. (**j**) *yfp* mRNA expression levels in 48-hpf WT and *mtp* morpholino-oligonucleotide–injected *Tg(flt1:YFP)*$^{hu4624/+}$ embryos ($n_{Tg(flt1:YFP)^{hu4624/+}} = 98$, $n_{Tg(flt1:YFP)^{hu4624/+}\ mtp\ \text{MO}} = 73$). $^*P = 0.0248$ by *t* test. Scale bar in **f**, 30 μm; **i**, 60 μm. NS, not significant. All data (**a**,**e**,**g**,**h**,**j**) are mean ± s.e.m.

SIV plexus and trunk ISVs, resembling the phenotype of *stl* mutants (**Supplementary Fig. 5**). We reasoned that if lipoprotein depletion promotes angiogenesis by downregulation of VEGFR1, we should be able to rescue the proangiogenic phenotype of the *stl* mutants by restoring VEGFR1 expression. Indeed, injection of *vegfr1* mRNA into *stl* mutant embryos suppressed ectopic SIV sprouting (**Fig. 3f**,**g**). Furthermore, siRNA-mediated downregulation of *VEGFR1* (**Fig. 3h**) abolished the ability of cultured HUVECs to respond to LDL levels in both wound-healing and Boyden-chamber (data not shown) assays.

The changes in *vegfr1* mRNA levels observed in *stl* mutants (**Fig. 3a**) and *Apoe*-null mice (**Fig. 3e**) could have resulted from either transcriptional regulation or post-transcriptional modifications altering the stability of the *vegfr1* transcript. To distinguish between these two possibilities, we took advantage of a transgenic zebrafish line that expresses yellow fluorescent protein (YFP) under the regulation of the *vegfr1* promoter[32]. In these animals, YFP expression recapitulates the pattern of endogenous *vegfr1* expression[32]. However, the YFP cassette possesses its own 3′ untranslated region (Online Methods); hence, YFP expression would not be subject to post-transcriptional modifications mediated by the 3′ untranslated region of the *vegfr1* gene. We hypothesized that if APOB lipoproteins regulate *vegfr1* mRNA expression at the transcriptional level, downregulation of *mtp* will result in a significant decrease in the levels of *yfp* mRNA. If in turn, *vegfr1* downregulation involves alterations in its mRNA stability, the levels of *yfp* mRNA will remain unchanged upon *mtp* morpholino oligonucleotide injection. *mtp* knockdown resulted in a significant ($P = 0.0248$) decrease in YFP expression (**Fig. 3i**,**j**), providing evidence that ApoB-containing lipoproteins inhibit *vegfr1* expression at the transcriptional level. Whether this regulation is direct or indirect remains to be determined.

Because the vascular phenotype of *stl* mutants was not triggered by global lipid starvation (**Fig. 2**), we hypothesized that lowered concentrations of lipoproteins in mutant animals, directly sensed by endothelial cells, exert a proangiogenic response. To test this hypothesis, we first examined whether exogenously supplied LDL could suppress ectopic sprouting in *stl* mutants when applied intravascularly. Injection of LDL labeled with the lipophilic carbocyanine dye DiI into 2.5-dpf *stl* mutants resulted in a strong reduction in both the

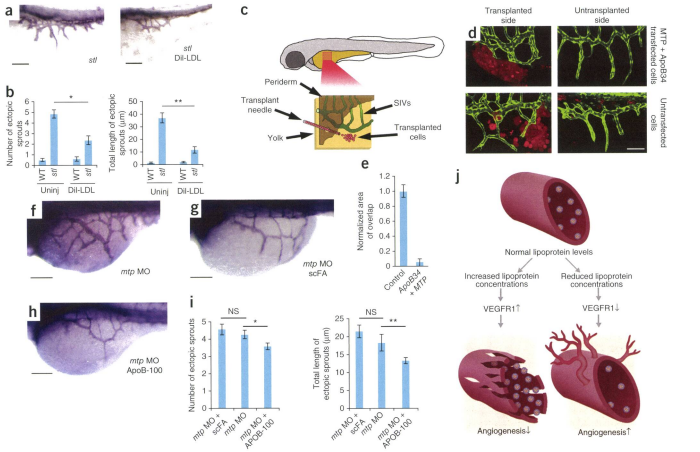

Figure 4 ApoB particles regulate angiogenesis by directly acting on endothelial cells. (**a**) Alkaline phosphatase staining of SIVs of 3.5-dpf *stl* mutants either not injected (right) ($n = 26$) or injected intravascularly with Dil-LDL (left) ($n = 14$). (**b**) Quantification of the ectopic sprouting phenotype. $^*P = 0.0001$, $^{**}P = 0.75$ by t test. Uninj, uninjected. (**c**) Diagram illustrating the procedure used for transplanting lipoprotein-secreting HEK293 cells into the yolk area of zebrafish embryos. (**d**) Confocal images of the SIVs (green) of 3.5-dpf *Tg(fli1:eGFP)*^{y1} zebrafish transplanted with HEK293 cells transfected with plasmids encoding MTP and ApoB34 (top; $n = 3$) or with untransfected control cells (bottom; $n = 3$) (red) on one side of the yolk ball. Untransplanted (right) and transplanted (left) sides of the same embryo are shown. (**e**) Quantification of the area of overlap between the SIV endothelium and HEK293 cells in 3.5-dpf transplanted zebrafish, normalized to the total length of the interface between the two cell populations. (**f**–**h**) Alkaline phosphatase staining of SIVs of 4.5-dpf *stl* mutants either not injected ($n = 16$) (**f**) or injected intravascularly with short chain fatty acid ($n = 10$) (**g**) or a delipidated form of ApoB-100 ($n = 24$) (**h**). (**i**) Quantification of the ectopic sprouting phenotype. $^*P = 0.0411$, $^{**}P = 4.6 \times 10^{-5}$ by t test. (**j**) Schematic model illustrating the effects of circulating ApoB-containing lipoproteins on angiogenesis. Scale bars, **a**,**f**–**h**, 30 μm; **d**, 60 μm. NS, not significant. Data in **b**,**e** and **i** are mean ± s.e.m.

number and length of the ectopic SIV sprouts (**Fig. 4a**,**b**), suggesting that circulating lipoproteins can activate antiangiogenic mechanisms in endothelial cells.

To further confirm the cell-autonomous nature of the endothelial response, we designed an *in vivo* approach to allow for the localized delivery of exogenous ApoB particles in the proximity of angiogenic vessels. Lipoprotein-secreting HEK293 cells cotransfected with vectors encoding the human forms of MTP and ApoB34 (ref. 33) (**Supplementary Fig. 6a**) or untransfected HEK293 control cells were transplanted into the perivitelline space on one side of 2.5-dpf *stl*; *Tg(fli1:eGFP)*^{y1} embryos in close proximity to the forming SIVs (**Fig. 4c**). ApoB34 is a truncated form of ApoB that has been shown to be properly assembled and secreted in the presence of MTP[33]. We chose to use this construct as it is the shorter form of ApoB whose secretion is MTP dependent. Lipoprotein-secreting cells impeded the migration of endothelial cells and the growth of ectopic sprouts in the area of transplantation (**Fig. 4d**). Ectopic SIV sprouting, however, was not affected on the untransplanted side of the same embryos (**Fig. 4d**), confirming that the localized transplantation did not result in systemic rescue of the *stl* phenotype. Non–lipoprotein-secreting cells, in contrast, did not impede endothelial migration or sprouting (**Fig. 4d**). Quantitative analysis revealed a much lower amount of endothelial migration onto lipoprotein-producing when compared to non–lipoprotein-producing cells (**Fig. 4e** and **Supplementary Fig. 6b**). We also found a similar direct inhibitory effect of LDL on the migration of HUVECs and human aortic endothelial cells (HAECs) *in vitro* using either Boyden-chamber (**Supplementary Fig. 7a**) or wound-healing (**Supplementary Fig. 7b**) assays. We observed these effects even at concentrations of LDL that did not affect cell proliferation (**Supplementary Fig. 7c**). It is notable, however, that LDL concentrations that are considered pathological in humans (>160 mg dl^{-1}) result in endothelial cell death *in vitro* (ref. 34 and data not shown). Taken together, these results indicate that endothelial cells respond in a cell-autonomous manner to changes in ApoB-containing lipoprotein concentrations. Although it is unclear whether this response involves the interaction of lipoproteins with the luminal

or abluminal surface of endothelial cells, direct contact between the lipoprotein and endothelial cells seems to be needed, as lipoprotein-secreting cells that were not placed in close proximity to developing vessels did not induce inhibitory effects (data not shown). Further studies will be required to ascertain whether there are luminal and abluminal receptors within endothelial cells for lipoprotein present in different areas of the vessel microenvironment.

We next asked which component of ApoB-containing lipoproteins elicits an endothelial response. Taking advantage of the fact that *stl* mutants lack secreted ApoB-containing lipoproteins, we attempted to rescue the vascular phenotype of the mutants by restoring lipid or protein components individually (**Fig. 4f–i**). Although an intravascular supply of free fatty acids did not rescue the ectopic branching phenotype of the mutants, injection of a delipidated form of ApoB-100 (Online Methods) substantially reduced the number and length of the ectopic angiogenic sprouts (**Fig. 4f–i**). ApoB-100 is the full-length form of the endogenous *apoB* gene, encoding a 550-kDa protein, that is essential for the assembly and secretion of ApoB-containing lipoproteins from the liver (very–low-density lipoprotein, LDL and intermediate-density lipoprotein). These results strongly support the idea that the ApoB protein itself, but not the lipid moieties within the lipoprotein, acts on endothelial cells to regulate angiogenesis.

Endothelial-lipoprotein interactions have direct relevance to atherogenesis, thrombosis and other cardiovascular diseases. The results presented here reveal an intrinsic capacity of ApoB-containing lipoproteins to control vascular growth by regulating the expression of VEGFR1 in endothelial cells (**Fig. 4j**).

Previous data has hinted at direct interactions between LDL and VEGF receptors *in vitro*[35,36], but the molecular mechanisms regulating this interplay have remained unclear. Here we show that expression of VEGFR1 is regulated *in vivo* by the availability of ApoB-containing lipoproteins. Moreover, we show that this regulation is achieved primarily at the transcriptional level. However, the molecular pathways responsible for this regulation are unknown, including which receptors within the endothelial cells mediate the uptake of lipoproteins or provide signals in response to lipoprotein particle abundance. The finding that endothelial cells of *Ldlr*-null mice express elevated amounts of Vegfr1 highlights the potential role of alternative lipoprotein receptors in mediating the endothelial response.

Recent evidence suggests a potentially crucial role for the nutritional state of tissues in vessel growth[37–39]. By taking advantage of our new zebrafish models of hypolipidemia and hyperlipidemia, we show that the effects of ApoB-containing lipoproteins on angiogenesis are not trigged by a reduced delivery of fatty acids to tissues or to global lipid starvation, as *apoC1l* deficiency in zebrafish embryos did not phenocopy the vascular phenotype that resulted from the loss of MTP. Furthermore, the high plasma concentrations of triglyceride-rich ApoB-containing lipoproteins in these animals inhibited angiogenesis, as did exogenous delivery of LDL. This effect, however, required the presence of ApoB, as intravascular delivery of a delipidated form of ApoB-100, but not of free fatty acids, efficiently reverted the excessive angiogenesis phenotype of *stl* mutants. Although we cannot exclude the possibility that the fate of delipidated ApoB in circulation might involve its association with endogenous plasma lipid moieties, our results support the notion that ApoB itself provides the crucial signal for the antiangiogenic effects.

Several pathological conditions involve dramatic alterations in lipoprotein concentrations, resulting in a wide variety of vascular-related diseases. Our results have uncovered a new mechanism for the regulation of developmental angiogenesis by ApoB-containing lipoproteins that seems to be reactivated during pathological conditions of hyperlipidemia. These findings may provide an explanation for the endothelial dysfunction that precedes the formation of atherogenic plaques, as well as for the impaired collateral vessel growth that is observed in patients with hypercholesterolemia. Furthermore, these findings raise key questions about the potential effects of circulating lipoproteins during tumor-related angiogenesis.

METHODS

Methods and any associated references are available in the online version of the paper.

Note: Supplementary information is available in the online version of the paper.

ACKNOWLEDGMENTS

The authors would like to thank G. Palardy, R. Miyares, N. Nevo, I. Harel, T. Berkutzki, I. Raviv, R. Oren and C. Rot for technical assistance; A. Aharoni for help with GC-MS analyses; E. Zelzer (Weizmann Institute, Israel) for providing the *Ldlr*-null mice, K. Tordjman (Sourasky Medical Center, Israel) for providing the *ApoE*-null mice, S. Schulte-Merker (Hubrecht Institute) for providing the *vegfr1* plasmid and the *Tg(fli1:YFP)*^{hu4624} transgenic line; J. Berliner (University of California Los Angeles, California) for providing human aortic endothelial cells (HAECs); D. Haratz, I. Groskop and A. Shaish for advice regarding lipid analyses; A. Harmelin and N. Stettner for animal care; and I.B. Dawid, E. Tzahor, A. Gross, B. Shilo and J. Torres-Vazquez for critical reading of the manuscript. The authors are grateful to all the members of the Yaniv and Weinstein labs for discussion, technical assistance and continuous support. This work was supported in part by Israel Science Foundation 748/2009 (to K.Y.), Marie Curie Actions–International Reintegration grants FP7-PEOPLE-2009-RG 256393 (to K.Y.), the Yeda-Sela Center (to K.Y.), the Israel Cancer Research Foundation Postdoctoral Fellowship (to I.A.-D.), US National Institutes of Health (NIH) RO1CA126935 (to M.L.I.-A.), NIH T32HL069766 (training grant for T.T.C. and C.M.W.) and NIH HL049373 (to G.S.S.). S.A.F. is funded by the NIH (R56DK093399 and R01GM063904), the Carnegie Institution for Science endowment and the G. Harold and Leila Y. Mathers Charitable Foundation. B.M.W. is supported by the intramural program of the National Institute of Child Health and Human Development, NIH, and by the Foundation Leducq.

AUTHOR CONTRIBUTIONS

I.A.-D. conducted experiments, data analyses and wrote the manuscript. Y.E., V.N.P., M.G., G.M., L.G.-B. and O.M. performed zebrafish experiments. G.A. managed the fish facility. D.C., B.L., I.U., K.K. and K.S. contributed to the F3 mutagenesis screen. C.M.W. and T.T.C. performed *in vitro* studies. I.R. performed lipidomics analyses. W.W. and P.M.M. provided the *ApoE*-null mice. S.A.F. provided advice in lipids studies. L.C. conducted statistical analyses and developed software for quantification. G.S.S. supervised *in vitro* experiments and provided advice in lipids studies. M.L.I.-A. supervised *in vitro* studies. B.M.W. supervised the initial zebrafish studies and provided advice throughout the project. K.Y. conducted experiments and data analyses, wrote the manuscript and supervised the project.

COMPETING FINANCIAL INTERESTS

The authors declare no competing financial interests.

Published online at http://www.nature.com/doifinder/10.1038/nm.2759.
Reprints and permissions information is available online at http://www.nature.com/reprints/index.html.

1. Yaniv, K. *et al.* Live imaging of lymphatic development in the zebrafish. *Nat. Med.* **12**, 711–716 (2006).
2. Lawson, N.D. & Weinstein, B.M. *In vivo* imaging of embryonic vascular development using transgenic zebrafish. *Dev. Biol.* **248**, 307–318 (2002).
3. Hussain, M.M. *et al.* Microsomal triglyceride transfer protein in plasma and cellular lipid metabolism. *Curr. Opin. Lipidol.* **19**, 277–284 (2008).
4. Raabe, M. *et al.* Knockout of the abetalipoproteinemia gene in mice: reduced lipoprotein secretion in heterozygotes and embryonic lethality in homozygotes. *Proc. Natl. Acad. Sci. USA* **95**, 8686–8691 (1998).
5. Marza, E. *et al.* Developmental expression and nutritional regulation of a zebrafish gene homologous to mammalian microsomal triglyceride transfer protein large subunit. *Dev. Dyn.* **232**, 506–518 (2005).
6. Schlegel, A. & Stainier, D.Y. Microsomal triglyceride transfer protein is required for yolk lipid utilization and absorption of dietary lipids in zebrafish larvae. *Biochemistry* **45**, 15179–15187 (2006).

7. Stoletov, K. *et al.* Vascular lipid accumulation, lipoprotein oxidation, and macrophage lipid uptake in hypercholesterolemic zebrafish. *Circ. Res.* **104**, 952–960 (2009).
8. Schlegel, A. & Stainier, D.Y. Lessons from "lower" organisms: what worms, flies, and zebrafish can teach us about human energy metabolism. *PLoS Genet.* **3**, e199 (2007).
9. Shelton, J.M., Lee, M.H., Richardson, J.A. & Patel, S.B. Microsomal triglyceride transfer protein expression during mouse development. *J. Lipid Res.* **41**, 532–537 (2000).
10. Babin, P.J. & Gibbons, G.F. The evolution of plasma cholesterol: direct utility or a "spandrel" of hepatic lipid metabolism? *Prog. Lipid Res.* **48**, 73–91 (2009).
11. Babin, P.J. *et al.* Both apolipoprotein E and A-I genes are present in a nonmammalian vertebrate and are highly expressed during embryonic development. *Proc. Natl. Acad. Sci. USA* **94**, 8622–8627 (1997).
12. Thorpe, J.L., Doitsidou, M., Ho, S.Y., Raz, E. & Farber, S.A. Germ cell migration in zebrafish is dependent on HMGCoA reductase activity and prenylation. *Dev. Cell* **6**, 295–302 (2004).
13. Amack, J.D. & Yost, H.J. The T box transcription factor no tail in ciliated cells controls zebrafish left-right asymmetry. *Curr. Biol.* **14**, 685–690 (2004).
14. Berriot-Varoqueaux, N., Aggerbeck, L.P., Samson-Bouma, M. & Wetterau, J.R. The role of the microsomal triglyceride transfer protein in abetalipoproteinemia. *Annu. Rev. Nutr.* **20**, 663–697 (2000).
15. Shoulders, C.C. *et al.* Abetalipoproteinemia is caused by defects of the gene encoding the 97 kDa subunit of a microsomal triglyceride transfer protein. *Hum. Mol. Genet.* **2**, 2109–2116 (1993).
16. Rader, D.J. & Brewer, H.B. Jr. Abetalipoproteinemia. New insights into lipoprotein assembly and vitamin E metabolism from a rare genetic disease. *J. Am. Med. Assoc.* **270**, 865–869 (1993).
17. Farber, S.A. *et al.* Genetic analysis of digestive physiology using fluorescent phospholipid reporters. *Science* **292**, 1385–1388 (2001).
18. Pickart, M.A. *et al.* Genome-wide reverse genetics framework to identify novel functions of the vertebrate secretome. *PLoS ONE* **1**, e104 (2006).
19. Anderson, J.L., Carten, J.D. & Farber, S.A. Zebrafish lipid metabolism: from mediating early patterning to the metabolism of dietary fat and cholesterol. *Methods Cell Biol.* **101**, 111–141 (2011).
20. Breckenridge, W.C. Apolipoprotein C–II deficiency. *Adv. Exp. Med. Biol.* **201**, 211–226 (1986).
21. Hegele, R.A. *et al.* An apolipoprotein CII mutation, CIILys19—Thr' identified in patients with hyperlipidemia. *Dis. Markers* **9**, 73–80 (1991).
22. Sethuraman, G. *et al.* Familial homozygous hypercholesterolemia: report of two patients and review of the literature. *Pediatr. Dermatol.* **24**, 230–234 (2007).
23. Hegele, R.A. Plasma lipoproteins: genetic influences and clinical implications. *Nat. Rev. Genet.* **10**, 109–121 (2009).
24. Connelly, P.W., Maguire, G.F. & Little, J.A. Apolipoprotein CIISt. Michael. Familial apolipoprotein CII deficiency associated with premature vascular disease. *J. Clin. Invest.* **80**, 1597–1606 (1987).
25. Landmesser, U., Hornig, B. & Drexler, H. Endothelial dysfunction in hypercholesterolemia: mechanisms, pathophysiological importance, and therapeutic interventions. *Semin. Thromb. Hemost.* **26**, 529–537 (2000).
26. Henry, P.D. Hypercholesterolemia and angiogenesis. *Am. J. Cardiol.* **72**, 61C–64C (1993).
27. Fazio, S. & Linton, M.F. Mouse models of hyperlipidemia and atherosclerosis. *Front. Biosci.* **6**, D515–D525 (2001).
28. Wouters, K., Shiri-Sverdlov, R., van Gorp, P.J., van Bilsen, M. & Hofker, M.H. Understanding hyperlipidemia and atherosclerosis: lessons from genetically modified *Apoe* and *Ldlr* mice. *Clin. Chem. Lab. Med.* **43**, 470–479 (2005).
29. Hiratsuka, S., Minowa, O., Kuno, J., Noda, T. & Shibuya, M. Flt-1 lacking the tyrosine kinase domain is sufficient for normal development and angiogenesis in mice. *Proc. Natl. Acad. Sci. USA* **95**, 9349–9354 (1998).
30. Kearney, J.B. *et al.* Vascular endothelial growth factor receptor Flt-1 negatively regulates developmental blood vessel formation by modulating endothelial cell division. *Blood* **99**, 2397–2407 (2002).
31. Chappell, J.C., Taylor, S.M., Ferrara, N. & Bautch, V.L. Local guidance of emerging vessel sprouts requires soluble Flt-1. *Dev. Cell* **17**, 377–386 (2009).
32. Bussman, J. *et al.* Arteries provide essential guidance cues for lymphatic endothelial cells in the zebrafish trunk. *Development* **137**, 2653–2657 (2010).
33. Shelness, G.S., Hou, L., Ledford, A.S., Parks, J.S. & Weinberg, R.B. Identification of the lipoprotein initiating domain of apolipoprotein B. *J. Biol. Chem.* **278**, 44702–44707 (2003).
34. Hessler, J.R., Robertson, A.L. Jr. & Chisolm, G.M. III. LDL-induced cytotoxicity and its inhibition by HDL in human vascular smooth muscle and endothelial cells in culture. *Atherosclerosis* **32**, 213–229 (1979).
35. Usui, R., Shibuya, M., Ishibashi, S. & Maru, Y. Ligand-independent activation of vascular endothelial growth factor receptor 1 by low-density lipoprotein. *EMBO Rep.* **8**, 1155–1161 (2007).
36. Yla-Herttuala, S. & Alitalo, K. On the relationship of LDL and VEGFR1: not just a family affair. *EMBO Rep.* **8**, 1127–1128 (2007).
37. Arany, Z. *et al.* HIF-independent regulation of VEGF and angiogenesis by the transcriptional coactivator PGC-1α. *Nature* **451**, 1008–1012 (2008).
38. Fraisl, P., Baes, M. & Carmeliet, P. Hungry for blood vessels: linking metabolism and angiogenesis. *Dev. Cell* **14**, 313–314 (2008).
39. Hagberg, C.E. *et al.* Vascular endothelial growth factor B controls endothelial fatty acid uptake. *Nature* **464**, 917–921 (2010).

TECHNICAL REPORTS

nature medicine

Development of a new hydrogen peroxide–based vaccine platform

Ian J Amanna[1,3], Hans-Peter Raué[2,3] & Mark K Slifka[2]

Safe and effective vaccines are crucial for maintaining public health and reducing the global burden of infectious disease. Here we introduce a new vaccine platform that uses hydrogen peroxide (H_2O_2) to inactivate viruses for vaccine production. H_2O_2 rapidly inactivates both RNA and DNA viruses with minimal damage to antigenic structure or immunogenicity and is a highly effective method when compared with conventional vaccine inactivation approaches such as formaldehyde or β-propiolactone. Mice immunized with H_2O_2-inactivated lymphocytic choriomeningitis virus (LCMV) generated cytolytic, multifunctional virus-specific CD8$^+$ T cells that conferred protection against chronic LCMV infection. Likewise, mice vaccinated with H_2O_2-inactivated vaccinia virus or H_2O_2-inactivated West Nile virus showed high virus-specific neutralizing antibody titers and were fully protected against lethal challenge. Together, these studies demonstrate that H_2O_2-based vaccines are highly immunogenic, provide protection against a range of viral pathogens in mice and represent a promising new approach to future vaccine development.

Routine vaccination represents one of the most effective approaches to safeguard public health against infectious disease. All currently licensed antiviral vaccines fall into one of two broad categories: replicating, live, attenuated vaccines and noninfectious whole or subunit vaccines. Formaldehyde, the most common reagent used for vaccine production, was first identified by serendipity in the 1920s as a chemical means for inactivation of bacterial toxins[1]. β-propiolactone (BPL, first described in 1955 (ref. 2)), is second only to formaldehyde as the most commonly used inactivation method for vaccine development. Despite the routine use of formaldehyde, vaccinologists have known for decades that it is a cross-linking agent that can damage key antigenic epitopes, leading to reduced immunogenicity or even exacerbated disease under certain circumstances[3]. One example of vaccine-induced exacerbation of disease is the case of the formaldehyde-inactivated respiratory syncytial virus (RSV) vaccine developed in the 1960s[4]. Though the vaccine was well tolerated, severe complications arose following exposure to wild-type RSV, leading to 16 hospitalizations and the deaths of two children[4]. Recent studies indicate that formaldehyde destroys key neutralizing epitopes, resulting in exacerbated disease following wild-type challenge[5]. Similarly, clinical trials involving formaldehyde-inactivated measles vaccine failed to protect against wild-type infection and instead led to an atypical form of the disease[6]. This was also associated with an inadequate antiviral antibody response, linked to formaldehyde-induced alteration of the measles hemolysin (F protein)[6]. Inactivation of viruses with BPL may also trigger adverse immune reactions, including the induction of allergic responses through chemical modifications of vaccine components[7,8]. It is unclear whether this was a factor in a recent phase 1 clinical trial in which one of 20 subjects developed urticaria shortly after booster vaccination with a 4.8-μg dose of BPL-inactivated yellow fever vaccine[9]. Bearing these concerns in mind, there is clearly an unmet need for identifying new and improved strategies for preparing inactivated vaccines.

H_2O_2 is an oxidizing agent that is well established as a potent antimicrobial agent and antiseptic[10]. The belief that strong oxidizing agents irreversibly damage the basic molecular structure of proteins may be one reason why H_2O_2 has not previously been tested as a means for producing inactivated viral vaccines[11]. However, inactivation of microbes with H_2O_2 (as well as other oxidizing agents such as superoxide and nitric oxide) represents a key element of the innate mammalian immune system and functions in endosomal compartments to inactivate intracellular pathogens[12]. In addition, H_2O_2 has also been used to detoxify pertussis toxin[13]. In these current studies we have used three unrelated virus model systems to show that H_2O_2-based vaccines can protect against chronic or lethal viral infection, and we believe that this approach represents a new concept in vaccine development.

RESULTS

H_2O_2 inactivates pathogens while maintaining antigenicity

To determine the feasibility of H_2O_2-based vaccine development, we first examined the inactivating potential of H_2O_2 against a spectrum of viral pathogens. A 3% aqueous solution of H_2O_2 inactivated both RNA and DNA viruses with up to a 6-$\log_{10}$ reduction in titer observed in less than 2 h (**Fig. 1a**). One mechanism for virus inactivation is through genomic damage caused by hydroxyl radicals that attack carbon double bonds in the nucleosides or abstract hydrogen atoms, both of which are processes that lead to carbon radicals with the potential for further downstream oxidation, and this ultimately results

[1]Najit Technologies, Beaverton, Oregon, USA. [2]Oregon National Primate Research Center, Oregon Health & Sciences University, Beaverton, Oregon, USA. [3]These authors contributed equally to this work. Correspondence should be addressed to M.K.S. (slifkam@ohsu.edu).

Received 27 April 2011; accepted 25 October 2011; published online 27 May 2012; doi:10.1038/nm.2763

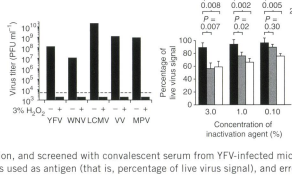

Figure 1 H_2O_2 inactivates viruses without substantial damage to antigenic epitopes. (**a**) H_2O_2 was used to inactivate a group of viruses including YFV, WNV, LCMV, VV and monkeypox virus (MPV). After 2 h of incubation with or without H_2O_2, infectious virus was measured by plaque assay. The limit of detection is indicated by the dashed line. (**b**,**c**) Purified YFV was treated with H_2O_2, β-propiolactone, or formaldehyde (Form.) for 2 h (**b**) or 16 h (**c**) at 20–24 °C and compared to untreated, live virus for retained antigenicity. ELISA plates were coated with each purified virus preparation, and screened with convalescent serum from YFV-infected mice ($n = 3$). ELISA results were normalized to the levels observed when live virus was used as antigen (that is, percentage of live virus signal), and error bars represent s.d.

in single- or double-strand breaks that destroy viability[14]. For the viruses described here, H_2O_2-based inactivation followed first-order rate kinetics, with half-life decay rates of <4 min. This is in contrast to formaldehyde, with which complete virus inactivation often requires 2–3 weeks of treatment[15–17].

To broadly assess the consequences of H_2O_2 inactivation on antigenicity, we compared yellow fever virus (YFV) inactivated by H_2O_2 to YFV inactivated by formaldehyde or BPL (**Fig. 1b**,**c**). Samples of purified virus that underwent these three different forms of inactivation were coated onto ELISA plates and we used YFV-immune serum from mice infected with YFV-17D (220 d after infection), to probe the samples and determine end-point antibody titers. We chose YFV-immune serum to assess the reactivity of antibodies to native YFV that would be generated during live viral infection. After 2 h of treatment (**Fig. 1b**), virus inactivation by H_2O_2 had only a minor effect on antigenicity and maintained 87–98% of the maximum antibody binding response observed with live virus. This is in contrast to the effects observed with BPL and formaldehyde, which significantly reduced the antigenicity of YFV at 3.0% and 1.0% concentrations (**Fig. 1b**). At 0.1%, H_2O_2 still performed significantly better than formaldehyde ($P = 0.005$), whereas 0.1% BPL was not significantly different from 0.1% H_2O_2 ($P = 0.30$). In practice, however, both BPL[18] and formaldehyde[15–17] are used for more extended periods of time to provide complete virus inactivation. Therefore, we exposed samples to H_2O_2, BPL, or formaldehyde at concentrations of 3.0%, 1.0% or 0.10% for 16 h before determining viral antigenicity. Similar to the results observed after 2 h of exposure, H_2O_2 maintained significantly greater antibody binding compared to formaldehyde or BPL (**Fig. 1c**). We observed analogous results showing retained antigenicity in preliminary experiments in which we used YFV-immune serum from YFV-17D–infected human subjects or YFV-17D–infected rhesus macaques (data not shown). Although this ELISA approach does not distinguish between neutralizing and non-neutralizing epitopes, these studies indicate that H_2O_2-based inactivation of a virus is less damaging to native antibody binding sites than other currently used approaches to virus inactivation such as BPL or formaldehyde.

H_2O_2-LCMV vaccination induces CD8$^+$ T cell–mediated immunity

One concern with inactivated vaccines is that many are suboptimal at inducing protective CD8$^+$ T cell responses[19]. To determine whether the H_2O_2-based vaccine approach is capable of generating effective antiviral CD8$^+$ T cell responses, we chose the LCMV model, wherein protective immunity is mediated by CD8$^+$ T cells[20]. We vaccinated mice with purified H_2O_2-inactivated LCMV-Armstrong and compared them to mice acutely infected with LCMV-Armstrong (**Fig. 2**). At 8 d after vaccination, the frequency of LCMV-specific CD8$^+$ T cells reached about 1–2% of the total splenic CD8$^+$ T cell response (**Fig. 2a**), similar to what is observed following live vaccination with recombinant vaccinia virus (VV) expressing LCMV nucleoprotein (NP)[21] or glycoprotein (GP)[22]. Comparable levels of HLA-A*0201-restricted CD8$^+$ T cell immunity have been observed in HLA-A*0201-transgenic mice vaccinated with H_2O_2-inactivated West Nile virus (WNV) (M.S. Diamond (Washington University–St. Louis), personal communication), indicating these results are not unique to the H-2L^d–restricted NP118 epitope or to the LCMV model system. At 8 d after LCMV-Armstrong infection, 40–50% of splenic CD8$^+$ T cells were specific for LCMV NP118 and expressed interferon-γ (IFN-γ) after 6 h stimulation with peptide directly *ex vivo* (**Fig. 2a**). However, CD8$^+$ T cells generated by live viral infection were significantly less efficient at co-expressing tumor necrosis factor-α (TNF-α) when compared to T cells generated by H_2O_2-LCMV vaccination (62 ± 9% IFN-γ$^+$TNF-α$^+$CD8$^+$ T cells versus 89 ± 5% IFN-γ$^+$TNF-α$^+$CD8$^+$ T cells, respectively; $P = 0.0002$). Notably, there was also more than a tenfold difference in the ability to produce interleukin-2 (IL-2) after peptide stimulation, with 51 ± 5% of IFN-γ$^+$CD8$^+$ T cells from H_2O_2-LCMV–vaccinated mice co-expressing IL-2 compared to only 3 ± 1% of virus-specific T cells from LCMV-Armstrong–infected mice ($P = 0.0001$, **Fig. 2a**).

To examine the proliferative capacity of H_2O_2-LCMV vaccine–induced CD8$^+$ T cells *in vivo*, we challenged mice with 2×10^5 plaque-forming units (PFU) of LCMV-Armstrong at 28 d after vaccination and determined virus-specific CD8$^+$ T cell frequencies before challenge (that is, day 28) and 4 d after challenge (that is, day 32). H_2O_2-LCMV–vaccinated mice showed a >40-fold increase in LCMV NP118–specific T cells within 4 d after challenge, reaching frequencies of 22 ± 6% of the CD8$^+$ T cell compartment (**Fig. 2b**). This expansion eclipsed the CD8$^+$ T cell responses observed at this early time point in naïve mice during primary infection (0.11 ± 0.04%, $P = 0.0002$) and was higher than that observed in LCMV-immune mice that were challenged in parallel (10 ± 2%, $P = 0.005$). Although LCMV-specific memory T cells expressed little or no granzyme B at 28 d after infection or vaccination, they rapidly upregulated granzyme B expression within 96 h after acute viral challenge (**Fig. 2c**). Of note, H_2O_2-LCMV vaccine–induced CD8$^+$ T cells expressed higher amounts of granzyme B after secondary challenge than did LCMV-specific T cells elicited by prior acute viral infection (**Fig. 2c**). These results indicate that vaccine-induced CD8$^+$ T cells rapidly upregulate cytolytic proteins, but it was unclear from these studies whether they have direct cytolytic activity in the absence of infection. To address this question, we used an *in vivo* cytotoxic T lymphocyte (CTL) assay

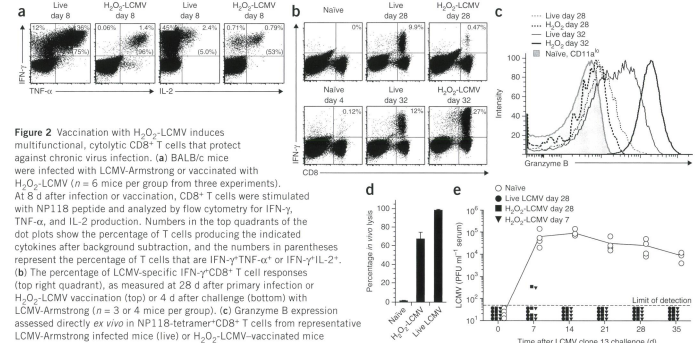

Figure 2 Vaccination with H_2O_2-LCMV induces multifunctional, cytolytic $CD8^+$ T cells that protect against chronic virus infection. (**a**) BALB/c mice were infected with LCMV-Armstrong or vaccinated with H_2O_2-LCMV ($n = 6$ mice per group from three experiments). At 8 d after infection or vaccination, $CD8^+$ T cells were stimulated with NP118 peptide and analyzed by flow cytometry for IFN-γ, TNF-α, and IL-2 production. Numbers in the top quadrants of the dot plots show the percentage of T cells producing the indicated cytokines after background subtraction, and the numbers in parentheses represent the percentage of T cells that are IFN-γ$^+$TNF-α$^+$ or IFN-γ$^+$IL-2$^+$. (**b**) The percentage of LCMV-specific IFN-γ$^+$$CD8^+$ T cell responses (top right quadrant), as measured at 28 d after primary infection or H_2O_2-LCMV vaccination (top) or 4 d after challenge (bottom) with LCMV-Armstrong ($n = 3$ or 4 mice per group). (**c**) Granzyme B expression assessed directly *ex vivo* in NP118-tetramer$^+$$CD8^+$ T cells from representative LCMV-Armstrong infected mice (live) or H_2O_2-LCMV–vaccinated mice (H_2O_2) at 28 d after infection or vaccination or at 4 d after challenge with LCMV-Armstrong (day 32). (**d**) *In vivo* lysis of peptide-coated targets at 8 d after H_2O_2-LCMV vaccination or LCMV-Armstrong infection, compared to naïve controls ($n = 4$ mice per group). Error bars represent s.d. (**e**) At 28 d after LCMV-Armstrong infection or at 7 d or 28 d after H_2O_2-LCMV vaccination, mice were challenged with LCMV clone 13, and viremia was monitored by plaque assay ($n = 4$ mice per group).

to measure antiviral CTL activity at 8 d after H_2O_2-LCMV vaccination or infection. We observed robust major histocompatibility complex (MHC) class I–restricted, LCMV NP118–specific CTL responses in H_2O_2-LCMV vaccinated mice (**Fig. 2d**), indicating that viral infection was not required for the development of cytolytic activity *in vivo*.

To determine protective efficacy, we challenged H_2O_2-LCMV vaccinated mice with 2×10^6 PFU of LCMV clone 13. This viral variant of LCMV causes chronic infection in naïve mice that lasts for several weeks or months and provides a rigorous test for $CD8^+$ T cell–mediated protection[20] (**Fig. 2e**). As expected, mice that had previously cleared acute LCMV-Armstrong infection were protected from chronic LCMV clone 13 infection. Mice that were vaccinated once with H_2O_2-inactivated LCMV at either 7 d or 28 d before challenge were also protected against chronic infection (**Fig. 2e**). Similar to LCMV-Armstrong immune mice and mice vaccinated with recombinant *Listeria monocytogenes* expressing LCMV NP in previous studies[23], H_2O_2-LCMV–vaccinated mice had reduced virus titers by >99% or had fully cleared LCMV within 7 d after challenge, whereas unvaccinated mice remained viremic for at least 35 d (**Fig. 2e**). *In vivo* depletion of $CD8^+$ T cells before LCMV clone 13 challenge completely abrogated protection against chronic infection, indicating that vaccine-induced immunity was mediated by $CD8^+$ T cells (data not shown). Together, these results demonstrate that multifunctional $CD8^+$ T cells can be elicited with a H_2O_2-inactivated vaccine and provide protective immunity against chronic viral infection.

H_2O_2-based vaccines elicit neutralizing antibody responses

Neutralizing antibody responses are the hallmark of protective immunity for most licensed vaccines[24,25], and the H_2O_2 vaccine platform is well suited for inducing neutralizing antibody responses because it does not seem to damage native viral epitopes to the extent observed with other methods of inactivation (**Fig. 1b,c**). However, the only method to formally determine immunogenicity is through *in vivo* vaccination studies using appropriate model systems in which neutralizing antibody responses have an important role in protection. The live, attenuated smallpox vaccine (consisting of VV) is often described as the 'gold standard' in vaccine efficacy, having achieved total eradication of its target virus, variola. Prior studies have demonstrated that VV-induced neutralizing antibodies are both necessary and sufficient for protection against lethal orthopoxvirus (for example, monkeypox) infection[26]. To determine how H_2O_2-based vaccines might compare in this model system, we measured neutralizing

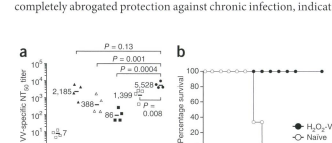

Figure 3 Induction of protective orthopoxvirus-specific neutralizing antibody responses following H_2O_2-VV immunization. (**a**) BALB/c mice ($n = 4$ per group) were vaccinated with live VV, MVA or purified VV inactivated with ultraviolet light (UV), 1% formaldehyde (Form.) for 2 h or 1% H_2O_2 for 2 h. Each group of mice was boosted 28 d later with the same vaccine preparation, and neutralizing antibody titers (NT_{50}) were determined 28 d after secondary immunization. The black bars indicate group geometric mean NT_{50} titers with statistical comparisons determined using analysis of variance (ANOVA). (**b**) Naïve mice or mice that received primary H_2O_2-VV immunization 28 d previously ($n = 6$–8 mice per group) were challenged intranasally with 10 LD_{50} of VV.

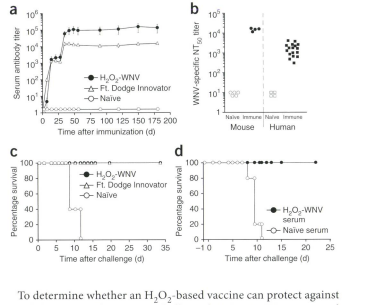

Figure 4 Vaccination with H_2O_2-WNV induces strong neutralizing antibody responses and protects against lethal WNV infection. (**a**) BALB/c mice ($n = 4$ mice per group) were vaccinated with H_2O_2-WNV or the Ft. Dodge WNV Innovator horse vaccine and boosted with the same vaccine at 28 d after primary vaccination. WNV-specific IgG responses ± the s.e.m. were determined by ELISA. (**b**) Virus-specific neutralizing antibody levels were determined for mice vaccinated with H_2O_2-WNV (2 months after booster vaccination) and compared to the levels observed after natural WNV infection in human subjects (~1 year after exposure). (**c**) Naïve mice and mice vaccinated with H_2O_2-WNV or Ft. Dodge WNV Innovator (75 d after booster vaccination) were challenged with 20 LD_{50} of WNV-NY99 ($n = 4$ mice per group). (**d**) Naïve mice received immune serum from H_2O_2-WNV–vaccinated mice or naïve serum from unvaccinated mice 1 d before challenge with 20 LD_{50} of WNV-NY99 ($n = 3$–5 mice per group).

antibody responses against VV in mice vaccinated subcutaneously with either live VV, live modified vaccinia Ankara (MVA, which is replication deficient in humans and mice), or purified VV inactivated with either H_2O_2, formaldehyde or ultraviolet (UV) irradiation. At 28 d after booster vaccination, we determined antibody responses to VV. H_2O_2-VV immunization induced significantly higher virus-specific neutralizing antibody responses than vaccines produced by other inactivation approaches, and the response most closely mimicked the immunity induced by live viral infection (**Fig. 3a**). In addition to the subcutaneous administration experiment, we infected another group of mice with 1×10^6 PFU of VV by the intraperitoneal route, and they generated half-maximal plaque reduction neutralization (NT_{50}) responses with a geometric mean value of 5,858, but this was not significantly different from the antibody responses elicited by H_2O_2-VV immunization ($NT_{50} = 5{,}528$, $P = 0.99$; data not shown). To determine whether H_2O_2-VV induced protective immunity, we challenged mice immunized with H_2O_2-VV with a lethal dose of VV, and 100% of the vaccinated animals survived (**Fig. 3b**). These studies indicate that H_2O_2-inactivated VV not only stimulates high titers of neutralizing antibodies ($NT_{50} = 5{,}528$), but also protects against a rigorous model of encephalitic disease.

Similar to the protective role of antibody against orthopoxvirus infection[26], the key role of humoral immunity in controlling flavivirus infection is also well documented[27,28]. Although there is no WNV vaccine licensed for human use, there is an effective formaldehyde-inactivated horse vaccine, the Ft. Dodge Innovator[29]. For comparison, we immunized mice with H_2O_2-WNV or the Ft. Dodge Innovator and measured virus-specific antibody titers. Both groups mounted similar WNV-specific antibody responses after primary vaccination (**Fig. 4a**). After booster vaccination, H_2O_2-WNV–immunized mice showed antibody responses that were nearly tenfold higher than those induced in mice given the horse vaccine (**Fig. 4a**). Antiviral antibody titers peaked within 28 d after booster vaccination and then stabilized with no evidence of decline during the ensuing 6 months of observation (**Fig. 4a**). For a point of reference, we compared neutralizing antibody levels in H_2O_2-WNV–immunized mice with those observed in human subjects who recovered from WNV infection (**Fig. 4b**). Within 2 months after booster vaccination (that is, the plateau phase of the response, **Fig. 4a**), H_2O_2-WNV–vaccinated mice developed neutralizing titers of $14{,}400 \pm 2{,}442$ by NT_{50}. In comparison, human subjects who contracted WNV naturally had a geometric mean $NT_{50} = 1{,}400 \pm 1{,}115$ when measured at ~1 year after infection. Although it is unknown what level of immunity is required for protection in humans, those who survive WNV infection are believed to be immune for life, and H_2O_2-WNV vaccination of mice elicits antibody responses that seem to meet or exceed the levels of immunity that develop after natural infection in humans.

To determine whether an H_2O_2-based vaccine can protect against lethal flavivirus infection, we challenged H_2O_2-WNV–immunized mice and age-matched naïve controls with 200 PFU of WNV-NY99, representing 20 times the half-maximal lethal dose (20 LD_{50}) of WNV-NY99 by intraperitoneal injection (**Fig. 4c**). Similarly to C57BL/6 mice, naïve BALB/c mice showed weight loss starting at day 6 after WNV infection, with a mean survival time of 9.9 ± 1.6 d. All H_2O_2-WNV–vaccinated mice survived virulent WNV-NY99 challenge with no signs of disease or weight loss (**Fig. 4c** and data not shown). Unlike C57BL/6 mice, which lose consistent susceptibility to peripheral WNV challenge after ~12 weeks of age[30], unvaccinated BALB/c mice remain susceptible to lethal WNV infection and thus provide an excellent model for determining long-term, vaccine-mediated immunity. Indeed, in this strain of mice we observed full protective immunity against WNV-NY99 challenge at >280 d after vaccination (data not shown), indicating the induction of long-term protective immunity by the H_2O_2-based vaccine platform. Both neutralizing antibody and $CD8^+$ T cells are important for protection against WNV infection[30]. Therefore, to determine whether vaccine-induced neutralizing antibodies are sufficient to provide protection in this model, we transferred 300 µl of immune serum from H_2O_2-WNV–vaccinated mice (60–90 d after vaccination) into naïve recipient mice and challenged them with a lethal dose of WNV-NY99 (**Fig. 4d**). Serum was transferred by intraperitoneal injection, and for this reason the mice were challenged by the subcutaneous route 1 d later with 1,000 PFU (20 LD_{50} by subcutaneous injection). Mice that received the same amount of naïve serum before WNV challenge died or required euthanasia, whereas 100% of the mice that received WNV-specific immune serum from H_2O_2-WNV–vaccinated mice were protected and showed no signs of disease or weight loss (data not shown). Together, these results demonstrate that full protective immunity against a lethal WNV infection can be attained by vaccination with a H_2O_2-inactivated vaccine and that the protective immunity achieved by this approach can be mediated by neutralizing antibodies.

DISCUSSION

In these studies, we demonstrate that H_2O_2 is effective at inactivating viruses for vaccine production. Exposure to H_2O_2 resulted in minimal damage to viral epitopes and provided improved antigenicity and immunogenicity when compared to other standard approaches used for virus inactivation. Immunization with H_2O_2-inactivated

viruses resulted in effective $CD8^+$ T cell responses with enhanced antiviral function as well as strong neutralizing antibody responses that protected against lethal VV or WNV infection. Together, these results indicate that the use of H_2O_2 represents a new approach to preparing inactivated antiviral vaccines with improved potency and protective efficacy.

The ability of H_2O_2-inactivated LCMV vaccination to induce antiviral $CD8^+$ T cell responses was particularly noteworthy. Within 8 d after vaccination, the frequency of LCMV-specific $CD8^+$ T cells reached levels similar to those observed following infection with recombinant VV expressing LCMV NP^{21} or GP^{22}. It is unclear whether MHC class I presentation is due to truncated or residual translation of viral proteins in the absence of productive replication or whether cross-presentation of virus particles is the underlying mechanism. Further mechanistic analysis is underway, but the results presented here indicate that the H_2O_2 platform induces cytolytic, multifunctional T cells (**Fig. 2**) and is similar to live recombinant vaccines at inducing protective antigen-specific $CD8^+$ T cell responses.

The majority of licensed vaccines provide protective immunity via the induction of neutralizing antibodies[24]. Thus, any new approach to vaccine development will require the capacity to induce strong and effective antiviral antibody responses. To assess retained viral antigenicity, we examined antibody binding after 2–16 h exposure to varying concentrations of H_2O_2, formaldehyde or BPL. Inactivated hepatitis vaccines are produced using 0.025% formaldehyde at 37 °C for 15 d (ref. 15), and complete inactivation of Japanese encephalitis virus requires ~0.02% formaldehyde at 37 °C for several weeks[17]. We chose 0.1% formaldehyde because it is within the same general range of concentration used for these other vaccines (albeit under less harsh conditions than 37 °C for 2 or more weeks), and it matched the routine time and concentration of 0.1% BPL used for comparison. Moreover, 0.01% H_2O_2, BPL and formaldehyde were insufficient to provide complete virus inactivation within 16 h at 20–24 °C (data not shown) and were not examined further. To assess immunogenicity and protective efficacy, we compared H_2O_2-VV to the live, attenuated smallpox vaccine (that is, VV infection) and found that H_2O_2-inactivated VV immunization induced neutralizing antibodies that were comparable to those elicited by the live vaccine and protected mice against lethal VV infection. To further evaluate the ability of H_2O_2 to function as a vaccine platform, we examined immunity against WNV. Our results indicate that H_2O_2-WNV vaccination induces virus-specific neutralizing antibody responses that equal or exceed the levels observed following natural WNV infection and that full protective immunity against lethal challenge can be elicited by direct vaccination or by adoptive transfer of immune serum from H_2O_2-WNV–vaccinated mice. Induction of vaccine-mediated antiviral antibody responses that exceed those observed after live viral infection is not unprecedented. For example, virus-like particle-based human papillomavirus (HPV) vaccines induce HPV-specific antibody responses that are more than tenfold higher than those observed after natural HPV infection[31]. Our data showing H_2O_2-WNV vaccine–mediated protection, together with the studies performed with VV (**Fig. 3**), support the potential of H_2O_2-inactivated vaccines for inducing protective immunity against a variety of viral pathogens in which humoral immunity is involved in host defense.

For many years, the standard approach to preparing inactivated vaccines has been to inactivate the pathogens with formaldehyde or BPL[3,7]. In particular, the utility of formaldehyde as the standard mode of pathogen inactivation for vaccine development has been questioned[3]. Other inactivation approaches such as psoralens, ethylenimine and nonionic detergents have also been tested for development of various vaccines, but these are believed to have disadvantages similar to formaldehyde or BPL in terms of chemical modification of immunogenic proteins[3,7]. In contrast, we have found that H_2O_2 represents a new and versatile platform for the development of inactivated vaccines. In the studies presented here, we used the H_2O_2 vaccine platform to demonstrate protective immunity against chronic viral infection (LCMV clone 13), and lethal viral challenge in two independent model systems, VV and WNV. The current commercial use of H_2O_2 for sterilizing manufacturing equipment and the availability of assay kits for determining H_2O_2 identity and potency (for example, the PeroXOquant kit from Thermo Scientific) add to the feasibility of using H_2O_2 for vaccine production. Moreover, the ability of H_2O_2 to inactivate a wide spectrum of pathogens, including viruses[32], bacteria[33], parasites[33] and potentially even bacterial spores[34], may allow expansion into new areas of vaccine research, fulfilling previously unmet needs for combating a number of human pathogens.

METHODS

Methods and any associated references are available in the online version of the paper.

ACKNOWLEDGMENTS

We thank E. Poore and M. Dubois for the growth of YFV and E. Hammarlund for the growth of monkeypox virus. This work was supported by US National Institutes of Health grants R56 AI076506 (to M.K.S.), UO1 AI082196 (to M.K.S.) and R43 AI079898 (to I.J.A. and M.K.S.) and Oregon National Primate Research Center grant 8P51 OD011092-53 (to M.K.S.).

AUTHOR CONTRIBUTIONS

M.K.S. conceived of the project. H.-P.R. performed the *in vivo* experiments, data analysis and figure preparation for the LCMV studies. I.J.A. performed the experiments, data analysis and figure preparation for the VV, YFV and WNV studies. I.J.A., H.-P.R. and M.K.S. wrote the manuscript, discussed the results and reviewed the manuscript before submission.

COMPETING FINANCIAL INTERESTS

The authors declare competing financial interests: details are available in the online version of the paper.

Published online at http://www.nature.com/doifinder/10.1038/nm.2763.
Reprints and permissions information is available online at http://www.nature.com/reprints/index.html.

1. Plotkin, S.L. & Plotkin, S.A. A short history of vaccination. in *Vaccines* (eds. Plotkin, S.A., Orenstein, W.A. & Offit, P.A.) 1–16 (Saunders/Elsevier, Philadelphia, 2008).
2. Logrippo, G.A. & Hartman, F.W. Antigenicity of β-propiolactone–inactivated virus vaccines. *J. Immunol.* **75**, 123–128 (1955).
3. Brown, F. Review of accidents caused by incomplete inactivation of viruses. *Dev. Biol. Stand.* **81**, 103–107 (1993).
4. Kim, H.W. *et al.* Respiratory syncytial virus disease in infants despite prior administration of antigenic inactivated vaccine. *Am. J. Epidemiol.* **89**, 422–434 (1969).
5. Delgado, M.F. *et al.* Lack of antibody affinity maturation due to poor Toll-like receptor stimulation leads to enhanced respiratory syncytial virus disease. *Nat. Med.* **15**, 34–41 (2009).
6. Annunziato, D. *et al.* Atypical measles syndrome: pathologic and serologic findings. *Pediatrics* **70**, 203–209 (1982).
7. Stauffer, F., El-Bacha, T. & Da Poian, A.T. Advances in the development of inactivated virus vaccines. *Recent Pat. Antiinfect. Drug Disc.* **1**, 291–296 (2006).
8. Swanson, M.C. *et al.* IgE and IgG antibodies to β-propiolactone and human serum albumin associated with urticarial reactions to rabies vaccine. *J. Infect. Dis.* **155**, 909–913 (1987).
9. Monath, T.P. *et al.* An inactivated cell-culture vaccine against yellow fever. *N. Engl. J. Med.* **364**, 1326–1333 (2011).
10. Guenter, T.E. Hydrogen peroxide. in *Encyclopedia of Chemical Processing and Design*, Vol. 27 (ed. McKetta, J.J.) 27–43 (Marcel Dekker, New York, 1988).
11. Sykes, G. The theory and mode of action of disinfection. in *Disinfection and Sterilization*, Ch. 2 (Lippincott, Philadelphia, 1965).
12. Valko, M. *et al.* Free radicals and antioxidants in normal physiological functions and human disease. *Int. J. Biochem. Cell Biol.* **39**, 44–84 (2007).

13. Siber, G.R. *et al.* Safety and immunogenicity of hydrogen peroxide-inactivated pertussis toxoid in 18-month-old children. *Vaccine* **9**, 735–740 (1991).
14. Terminiì, J. Hydroperoxide-induced DNA damage and mutations. *Mutat. Res.* **450**, 107–124 (2000).
15. Fiore, A.E., Finestone, S.M. & Bell, B.P. Hepatitis A vaccine. in *Vaccines* (eds. Plotkin, S.A., Orenstein, W.A. & Offit, P.A.) 177–203 (Saunders/Elsevier, Philadelphia, 2008).
16. Plotkin, S.A. & Vidor, E. Poliovirus vaccine—inactivated. in *Vaccines* (eds. Plotkin, S.A., Orenstein, W.A. & Offit, P.A.) 605–630 (Saunders/Elsevier, Philadelphia, 2008).
17. Srivastava, A.K. *et al.* A purified inactivated Japanese encephalitis virus vaccine made in Vero cells. *Vaccine* **19**, 4557–4565 (2001).
18. Monath, T.P. *et al.* Inactivated yellow fever 17D vaccine: development and nonclinical safety, immunogenicity and protective activity. *Vaccine* **28**, 3827–3840 (2010).
19. Robinson, H.L. & Amara, R.R. T cell vaccines for microbial infections. *Nat. Med.* **11**, S25–S32 (2005).
20. Lau, L.L., Jamieson, B.D., Somasundaram, T. & Ahmed, R. Cytotoxic T-cell memory without antigen. *Nature* **369**, 648–652 (1994).
21. Hassett, D.E., Slifka, M.K., Zhang, J. & Whitton, J.L. Direct *ex vivo* kinetic and phenotypic analyses of $CD8^+$ T cell responses induced by DNA immunization. *J. Virol.* **74**, 8286–8291 (2000).
22. Schwarz, K. *et al.* Efficient homologous prime-boost strategies for T cell vaccination based on virus-like particles. *Eur. J. Immunol.* **35**, 816–821 (2005).
23. Slifka, M.K. *et al.* Antiviral cytotoxic T-cell memory by vaccination with recombinant Listeria monocytogenes. *J. Virol.* **70**, 2902–2910 (1996).
24. Plotkin, S.A. Correlates of protection induced by vaccination. *Clin. Vaccine Immunol.* **17**, 1055–1065 (2010).
25. Amanna, I.J., Messaoudi, I. & Slifka, M.K. Protective immunity following vaccination: how is it defined? *Hum. Vaccin.* **4**, 316–319 (2008).
26. Edghill-Smith, Y. *et al.* Smallpox vaccine-induced antibodies are necessary and sufficient for protection against monkeypox virus. *Nat. Med.* **11**, 740–747 (2005).
27. Eckels, K.H. & Putnak, R. Formalin-inactivated whole virus and recombinant subunit flavivirus vaccines. *Adv. Virus Res.* **61**, 395–418 (2003).
28. Amanna, I.J. & Slifka, M.K. Wanted, dead or alive: new viral vaccines. *Antiviral Res.* **84**, 119–130 (2009).
29. Ng, T. *et al.* Equine vaccine for West Nile virus. *Dev. Biol. (Basel)* **114**, 221–227 (2003).
30. Shrestha, B., Ng, T., Chu, H.J., Noll, M. & Diamond, M.S. The relative contribution of antibody and $CD8^+$ T cells to vaccine immunity against West Nile encephalitis virus. *Vaccine* **26**, 2020–2033 (2008).
31. Giannini, S.L. *et al.* Enhanced humoral and memory B cellular immunity using HPV16/18 L1 VLP vaccine formulated with the MPL/aluminium salt combination (AS04) compared to aluminium salt only. *Vaccine* **24**, 5937–5949 (2006).
32. Neighbor, N.K. *et al.* The effect of microaerosolized hydrogen peroxide on bacterial and viral poultry pathogens. *Poult. Sci.* **73**, 1511–1516 (1994).
33. Channon, J.Y. & Blackwell, J.M. A study of the sensitivity of *Leishmania donovani* promastigotes and amastigotes to hydrogen peroxide. I. Differences in sensitivity correlate with parasite-mediated removal of hydrogen peroxide. *Parasitology* **91**, 197–206 (1985).
34. DeQueiroz, G.A. & Day, D.F. Disinfection of *Bacillus subtilis* spore-contaminated surface materials with a sodium hypochlorite and a hydrogen peroxide-based sanitizer. *Lett. Appl. Microbiol.* **46**, 176–180 (2008).

nature medicine

Monoclonal TCR-redirected tumor cell killing

Nathaniel Liddy[1,4], Giovanna Bossi[1,4], Katherine J Adams[1,4], Anna Lissina[2], Tara M Mahon[1], Namir J Hassan[1], Jessie Gavarret[1], Frayne C Bianchi[1], Nicholas J Pumphrey[1], Kristin Ladell[2], Emma Gostick[2], Andrew K Sewell[2], Nikolai M Lissin[1], Naomi E Harwood[1], Peter E Molloy[1], Yi Li[1], Brian J Cameron[1], Malkit Sami[1], Emma E Baston[1], Penio T Todorov[1], Samantha J Paston[1], Rebecca E Dennis[1], Jane V Harper[1], Steve M Dunn[1], Rebecca Ashfield[1], Andy Johnson[1], Yvonne McGrath[1], Gabriela Plesa[3], Carl H June[3], Michael Kalos[3], David A Price[2], Annelise Vuidepot[1], Daniel D Williams[1], Deborah H Sutton[1] & Bent K Jakobsen[1]

T cell immunity can potentially eradicate malignant cells and lead to clinical remission in a minority of patients with cancer. In the majority of these individuals, however, there is a failure of the specific T cell receptor (TCR)–mediated immune recognition and activation process. Here we describe the engineering and characterization of new reagents termed immune-mobilizing monoclonal TCRs against cancer (ImmTACs). Four such ImmTACs, each comprising a distinct tumor-associated epitope-specific monoclonal TCR with picomolar affinity fused to a humanized cluster of differentiation 3 (CD3)-specific single-chain antibody fragment (scFv), effectively redirected T cells to kill cancer cells expressing extremely low surface epitope densities. Furthermore, these reagents potently suppressed tumor growth *in vivo*. Thus, ImmTACs overcome immune tolerance to cancer and represent a new approach to tumor immunotherapy.

Harnessing the power of adaptive immunity to combat cancer has been a long-term goal of translational immunotherapy. However, although many avenues in this field have been explored over the past couple of decades, a definitive advance has remained elusive.

To date, monoclonal antibodies (mAbs) derived from B cell antigen receptors have dominated immunotherapeutic efforts with their unique ability to target the required epitope *in vivo* at high affinities and with fine specificity[1]. Indeed, over the years, mAbs have been engineered to reduce immunogenicity[2], increase affinity[3] and deliver various 'payloads' to the site of malignant tumors[4]. Such payloads include the natural crystallizable fragment (Fc) receptor, which initiates antibody-dependent cellular cytotoxicity[5,6], cytotoxic drugs, prodrugs, toxins and radioisotopes[7]. Furthermore, bispecific mAbs have been produced in various forms to target cancer antigens with one arm and activate T cells with the other[8]. In such cases, a CD3-specific moiety activates T cells in a polyclonal manner. The efficacy of these bispecific formats has been varied, with the most successful candidates being the bispecific T cell-engaging (BiTE) mAbs[4,9,10]. In addition, trispecific mAbs have been developed, which target overexpressed or tissue-specific tumor antigens and CD3, yet maintain the natural Fc receptor to elicit a full range of Fc-mediated responses[11,12]. Although mAb-based therapies show great promise in certain situations, they are largely limited in scope to membrane-integral protein targets and therefore restricted primarily to tissue-specific or lineage-expressed antigens.

In contrast to mAbs, which bind antigen in unrestricted formats, TCRs specifically recognize endogenously processed peptides bound to major histocompatibility complex (pMHC) antigens presented on the cell surface. However, the natural affinity of such interactions is several orders of magnitude weaker than mAb binding to protein antigens. Furthermore, self-derived antigens, such as those that are typically overexpressed in various tumors, are targeted with even lower affinities than exogenous pathogen-derived antigens[13]. These generic differences presumably reflect the effects of thymic selection, which operate to minimize autoreactivity. Recent advances, however, have enabled the production of soluble monoclonal TCRs (mTCRs) that target defined pMHC class I (pMHCI) antigens with greatly enhanced affinities and without any apparent loss of specificity[14–17]. Such developments overcome the biophysical limitations that otherwise hamper TCR-based immunotherapeutic approaches and potentially enable the targeting of any cell based on its proteomic characteristics. Here we describe the generation, optimization and characterization of ImmTACs. These new reagents, each comprising a high-affinity mTCR fused to a humanized CD3-specific scFv, redirect and activate T cells to lyse tumor cells *in vitro* and *in vivo*. The exquisite potency, sensitivity, specificity and *in vivo* efficacy of these reagents is reported here for pMHCI epitopes derived from four tumor-associated antigens: (i) gp100, a melanocyte differentiation antigen[18]; (ii) MAGE-A3, a cancer testis antigen expressed by a wide variety of tumors[19]; (iii) Melan-A/MART-1, a lineage-specific antigen expressed by a large proportion of primary and metastatic melanomas[20,21]; and (iv) NY-ESO-1, a cancer testis antigen expressed in multiple myeloma, melanoma and a range of other cancers[22]. The data indicate that ImmTACs represent a powerful new approach to combat cancer.

[1]Immunocore Ltd., Abingdon, Oxon, UK. [2]Cardiff University School of Medicine, Heath Park, Cardiff, UK. [3]University of Pennsylvania School of Medicine, Philadelphia, Pennsylvania, USA. [4]These authors contributed equally to this work. Correspondence should be addressed to B.K.J. (bent.jakobsen@immunocore.com).

Received 21 January 2011; accepted 17 October 2011; published online 6 May 2012; doi:10.1038/nm.2764

RESULTS

Production of affinity-matured mTCRs and ImmTACs

To generate a range of ImmTACs, we first produced wild-type mTCRs as soluble disulfide-linked proteins[14] from CD8$^+$ T cell clones with the following tumor-associated epitope specificities: (i) gp100$_{280–288}$: YLEPGPVTA–HLA-A*0201 (ref. 23); (ii) MAGE-A3$_{168–176}$: EVDPIGHLY–HLA-A*0101 (ref. 24); (iii) Melan-A/MART-1$_{26–35}$: EAAGIGILTV–HLA-A*0201 (ref. 25); and (iv) NY-ESO-1$_{157–165}$: SLLMWITQC–HLA-A*0201 (ref. 26). These wild-type mTCRs bound their corresponding cognate pMHCI antigens with dissociation constant (K_D) values of 26 μM, 248 μM, 18 μM and 11 μM, respectively, as determined by surface plasmon resonance (SPR) equilibrium-binding measurements. We then generated high-affinity mTCRs using directed molecular evolution and phage display selection, with the mutagenesis targeting primarily the complementarity-determining regions of the parent receptors[15]. The generation and characterization of the high-affinity NY-ESO-1 mTCR was described previously[15,27].

Next, we engineered hybrid proteins with the capacity to redirect and activate T cells, in each case comprising a humanized CD3-specific scFv fused to the high-affinity mTCR β chain by a flexible linker. We expressed the α and β chains of the resultant ImmTACs separately in *Escherichia coli*, refolded them *in vitro* and then purified them using a process similar to that described previously for unfused mTCRs[14]. The mTCR component of each ImmTAC bound its cognate pMHCI antigen for many hours (**Fig. 1a–d**) with biophysical parameters similar to those observed for the corresponding unfused protein, thereby indicating that the integrity of the mTCR binding surface was not compromised by the process of fusing the CD3-specific scFv to the mTCR β chain. Furthermore, binding of the CD3-specific scFv component to immobilized CD3-εγ protein was similar for all ImmTAC reagents (data not shown).

ImmTACs target tumor cells and activate CD8$^+$ T cells

To quantify naturally presented antigens on tumor cell lines, we used fluorochrome-labeled mTCRs in single molecule fluorescence microscopy experiments. Epitope levels were found to range from 10 to 150 copies per cell (data not shown[27]). We then evaluated the specificity and biological activity of the ImmTACs using interferon-γ (IFN-γ) enzyme-linked immunosorbent spot (ELISpot) assays to measure the activation of unstimulated purified CD8$^+$ T cells *in vitro*. Representative data from these experiments are shown in **Figure 1a–d**. In all cases, CD8$^+$ T cells were only activated in the presence of antigen-relevant tumor cells and the corresponding ImmTAC.

Extensive *in vitro* testing against a panel of primary human cell lines confirmed the exquisite specificity of these reagents (**Supplementary Table 1** and data not shown). In dose-response experiments, all four ImmTACs produced half-maximal effective concentration (EC_{50}) values in the range of 100 pM or lower, which is consistent with the K_D values for the corresponding ImmTAC-pMHCI interactions. This indicates a remarkable degree of sensitivity, especially considering the extremely low densities of the naturally presented cognate pMHCI molecules on the tumor cell surface.

T cell activation potency depends on ImmTAC-pMHCI affinity

To further investigate the relationship between biological activity and ImmTAC-pMHCI affinity, we studied seven different variants of the gp100-specific ImmTAC (ImmTAC-gp100) with K_D values spanning over six orders of magnitude for their ability to activate unstimulated purified CD8$^+$ T cells in the presence of T2 target cells presenting a range of gp100$_{280–288}$ peptide antigen concentrations in the context of HLA-A*0201 (**Fig. 1e**). The two ImmTACs with the highest affinities for pMHCI (K_D values of 0.32 nM and 0.03 nM) were able to activate

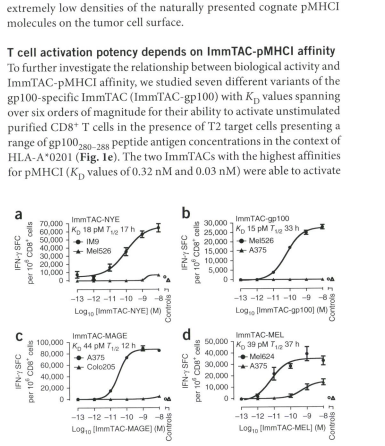

Figure 1 The biological activity and biophysical characteristics of ImmTAC molecules with different specificities. (**a–d**) IFN-γ ELISpot assays showing the activation of purified CD8$^+$ T cells mediated by titrated concentrations of ImmTAC molecules in the presence of tumor cells expressing endogenous levels of cognate antigen (closed circles). Antigen-negative tumor cells matched for expression of the relevant HLA class I molecule (closed triangles) were used in parallel titrations under identical conditions as specificity controls. The shape-matched open symbols represent the corresponding ImmTAC-negative controls. (**a**) For ImmTAC-NYE, IM9 EBV-transformed B-lymphoblastoid cells (NY-ESO-1$^+$) and Mel526 cells (NY-ESO-1$^-$) were used. (**b**) For ImmTAC-gp100, Mel526 melanoma cells (gp100$^+$) and A375 melanoma cells (gp100$^-$) were used. (**c**) For ImmTAC-MAGE, A375 melanoma cells (MAGE-A3$^+$) and Colo205 cells (MAGE-A3$^-$) were used. (**d**) For ImmTAC-MEL, Mel624 melanoma cells (Melan-A/MART-1$^+$) and A375 melanoma cells (Melan-A/MART-1$^-$) were used. The equilibrium binding (K_D) and half-life ($T_{1/2}$) values determined by SPR are shown for each ImmTAC-pMHCI interaction. In most cases, the relevant heteroclitic peptide was used for SPR measurements because of increased protein stability when complexed to pMHCI as a soluble molecule. (**e**) IFN-γ ELISpot assays showing activation of purified CD8$^+$ T cells in the presence of T2 cells pulsed with various concentrations of the gp100$_{280–288}$ heteroclitic peptide YLEPGPVTV and different ImmTAC-gp100 variants, color coded by affinity according to the inset key, each at a concentration of 100 pM. The epitope numbers per cell determined by single-cell three-dimensional fluorescence microscopy at different concentrations of exogenous peptide were 0–1 at 10^{-11} M, 2–10 at 10^{-10} M and 15–45 at 10^{-9} M; the latter corresponds to the number of antigens typically detected on tumor cells (indicated with an asterisk). (**f**) IFN-γ ELISpot assays showing activation of purified CD8$^+$ T cells in the presence of Mel526 melanoma cells expressing natural levels of wild-type gp100$_{280–288}$ complexed to HLA-A*0201 and a dose titration of different ImmTAC-gp100 variants, color coded by affinity according to the inset key. Data are means ± s.e.m.

$CD8^+$ T cells in the presence of target cells loaded with 10^{-10} M peptide, which equates to 2–10 pMHCI epitopes per cell. At higher K_D values, we observed a progressive reduction in potency. Indeed, the wild-type reagent (K_D = 30 μM) and a minimally modified variant (K_D = 8 μM) did not activate $CD8^+$ T cells at any of the peptide concentrations tested.

In additional experiments, we examined the ability of ImmTACs with varying affinities for pMHCI to activate $CD8^+$ T cells in the presence of melanoma tumor cells (Mel526) presenting naturally processed cognate epitopes (<70 epitopes per cell; data not shown). All ImmTAC variants responded in a dose-dependent manner, although to markedly different extents (**Fig. 1f**). The two ImmTACs with the highest affinities were again the most sensitive, activating $CD8^+$ T cells at concentrations as low as 10^{-11} M, with cellular EC_{50} values in the 40 pM range. We found progressive increases in the cellular EC_{50} values as the affinities of the ImmTAC-pMHCI interactions decreased, with the wild-type and minimally modified reagents showing only limited activation at concentrations of 10^{-8} M. Thus, the potency of ImmTACs is dependent on the affinity of the interaction with cognate pMHCI antigen.

ImmTACs elicit polyfunctional memory $CD8^+$ T cell responses

To determine the effects of ImmTAC reagents under more physiological conditions, we conducted polychromatic flow cytometry experiments on peripheral blood mononuclear cells (PBMCs) directly *ex vivo*. In ImmTAC titration experiments using peptide-pulsed PBMCs, substantial numbers of $CD8^+$ T cells were activated in a sensitive and dose-dependent manner to elicit multiple effector functions, including degranulation and the production of IFN-γ, tumor necrosis factor (TNF) and interleukin-2 (IL-2) (**Fig. 2a** and data not shown). The activated $CD8^+$ T cells were distributed throughout the various memory compartments defined according to standard phenotypic parameters (**Fig. 2b** and data not shown).

Polyfunctional $CD8^+$ T cell responses with similar phenotypic profiles were also elicited when we incubated PBMCs with relevant ImmTAC reagents and Mel526 melanoma cells expressing natural amounts of antigen (**Fig. 2c** and data not shown). Notably, many of the responding $CD8^+$ T cells showed a terminally differentiated phenotype characterized by expression of the senescence marker CD57 (data not shown); CD57 identifies $CD8^+$ T cells with maximal lytic capacity[28], a desirable feature for an immunotherapeutic agent designed to target tumor cells. Contemporaneously, we found activation within the $CD4^+$ T cell compartment. In particular, $CD4^+$ T cells produced substantial amounts of TNF and IL-2 in these experiments (**Fig. 2d–f**). This coordinated activation of synergistic T cell subsets could operate to enhance ImmTAC-driven cellular immune efficacy within the tumor microenvironment[29].

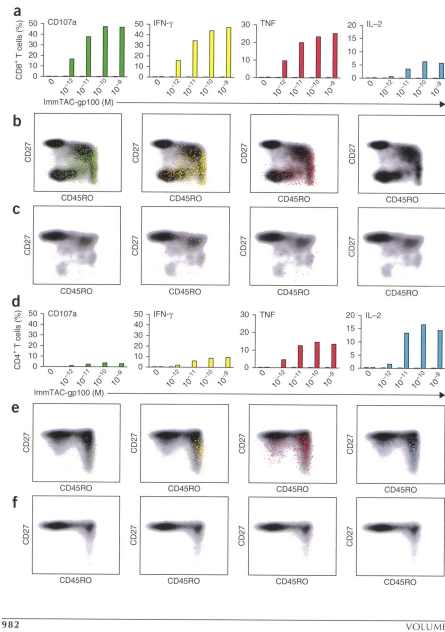

Figure 2 Efficient activation of multiple $CD8^+$ T cell effector functions by ImmTAC-gp100. Results are shown for target PBMCs, pulsed with the $gp100_{280-288}$ heteroclitic peptide YLEPGPVTV or mock pulsed with medium alone, or target Mel526 melanoma cells incubated with fresh PBMCs in the presence or absence of ImmTAC-gp100 at the indicated concentrations. The surface mobilization of lysosomal-associated membrane protein 1 (CD107a) (green) and the intracellular production of the cytokines IFN-γ (yellow), TNF (red) and IL-2 (turquoise) are shown. (**a**) The dose-response relationship between the concentration of ImmTAC-gp100 and the percentage of $CD8^+$ T cells activated to express each individual function in the presence of peptide-pulsed PBMCs. The colored bars represent activation in response to the peptide-pulsed targets; the black bars, which in most cases merge with the *x* axis, represent activation in response to the mock-pulsed targets. (**b**,**c**) The phenotypic profile of $CD8^+$ T cells activated with ImmTAC-gp100 at a concentration of 10^{-11} M in the presence of peptide-pulsed PBMCs (**b**) or Mel526 cells (**c**). The colored dots depict individual cells that elicited a distinct function, as indicated in **a**, superimposed on cloud plots showing the phenotypic profile of the overall $CD8^+$ T cell population; events shown in **b** correspond to those shown in **a** at a concentration of 10^{-11} M and are color coded to match. (**d–f**) $CD4^+$ T cell activation data from the same experiments and with the same details described in **a–c**.

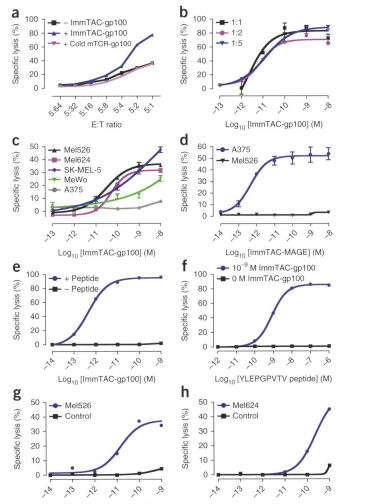

Figure 3 Redirected lysis of tumor cells and peptide-pulsed targets by $CD8^+$ T cells in the presence of ImmTAC molecules. (**a**) Lysis of Mel624 melanoma cells over a period of 4 h by a $CD8^+$ T cell clone (MEL187.c5) specific for the Melan-A/MART-1_{26-35} epitope at different E:T ratios (black squares). Enhanced lysis by redirection in the presence of 1 nM ImmTAC-gp100 (blue triangles) and inhibition of redirected lysis mediated by ImmTAC-gp100 with 100 nM cold mTCR-gp100 (purple inverted triangles) are shown. (**b**) Redirected lysis of Mel624 cells over a period of 24 h by a $CD8^+$ T cell clone specific for $BRLF1_{259-267}$ (176.c4.1) at E:T ratios of 1:1 (black squares), 1:2 (purple circles) and 1:5 (blue inverted triangles) in the presence of titrated doses of ImmTAC-gp100. (**c**) Redirected lysis of four $gp100^+$, HLA-A^*0201^+ melanoma cell lines over a period of 24 h by purified $CD8^+$ T cells in the presence of titrated doses of ImmTAC-gp100. Mel526 cells (black triangles), Mel624 cells (purple squares), SK-MEL-5 cells (blue diamonds), MeWo cells (green inverted triangles) and control A375 ($gp100^-$, HLA-A^*0201^+) cells (gray circles) are shown. (**d**) Redirected lysis of A375 (MAGE-$A3^+$, HLA-A^*0101^+) melanoma cells over a period of 24 h by purified $CD8^+$ T cells in the presence of titrated doses of ImmTAC-MAGE (blue circles). The HLA-A^*0101^- melanoma cell line Mel526 was used as a control (black inverted triangles). (**e**) Redirected lysis of PBMCs pulsed with (blue circles) or without (black squares) the $gp100_{280-288}$ heteroclitic peptide YLEPGPVTV in the presence of titrated doses of ImmTAC-gp100 and autologous PBMCs. A 16-h time point is shown. (**f**) Redirected lysis of PBMCs pulsed with various concentrations of the $gp100_{280-288}$ heteroclitic peptide YLEPGPVTV in the presence (blue circles) or absence (black squares) of 10^{-9} M ImmTAC-gp100 and autologous PBMCs. A 16 h time point is shown. (**g**) Redirected lysis of Mel526 cells (blue circles) or control (TO) cells (black squares) over a period of 16 h in the presence of titrated doses of ImmTAC-gp100 and PBMCs. (**h**) Redirected lysis of Mel624 cells (blue circles) or control (TO) cells (black squares) over a period of 16 h in the presence of titrated doses of ImmTAC-NYE and PBMCs. Lysis was determined on the basis of LDH release (**a**–**d**) or flow cytometric quantification of labeled target cell elimination (**e**–**h**). Data are means ± s.e.m.

ImmTACs redirect T cells to lyse tumor cells

To be effective *in vivo*, activated $CD8^+$ T cells must be redirected by ImmTACs to lyse tumor cells irrespective of their primary specificity. To investigate this process more thoroughly, we first examined the ability of ImmTAC-gp100 to enhance the killing of melanoma cells by a $CD8^+$ T cell clone specific for Melan-A/MART-1 (MEL187.c5). The MEL187.c5 clone killed Mel624 cells *in vitro*, even at low effector-to-target (E:T) ratios, although with levels of specific lysis below 50% after 4 h (**Fig. 3a**). In the presence of ImmTAC-gp100, which binds a different epitope on the same tumor cells, substantially more tumor cells were lysed by the same clone under otherwise identical conditions. Furthermore, a 100-fold excess of the high-affinity gp100-specific mTCR blocked this enhanced killing, resulting in levels of lysis similar to those found in the presence of the MEL187.c5 clone alone. Thus, the enhancement of lytic function mediated by ImmTACs is the direct result of binding to the cognate pMHCI epitopes expressed on the cell surface and does not occur as a nonspecific effect.

In dose-response experiments conducted over a range of E:T ratios, ImmTAC-gp100 was able to redirect the lytic activity of a $CD8^+$ T cell

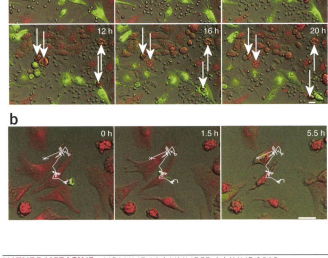

Figure 4 Visualization of the redirected lysis of Mel642 melanoma cells by PBMCs or $CD8^+$ T cells in the presence of ImmTAC-gp100. (**a**) Images from time lapse video microscopy showing the redirected lysis of Mel624 melanoma cells (red) by PBMCs (gray) in the presence of 0.1 nM ImmTAC-gp100. In the same wells, SK-MEL-28 cells ($gp100^+$, HLA-A^*0201^-) were not lysed (green). Arrows indicate selected cells that were lysed. Scale bar, 50 μm. (**b**) Images from time lapse video microscopy showing serial killing of three Mel624 melanoma cells (red) by a single $CD8^+$ T cell (clone 176.c4.1) without tumor specificity (green) in the presence of 0.1 nM ImmTAC-gp100. The white line tracks the path of the single $CD8^+$ T cell over a period of 5.5 h. Scale bar, 75 μm. The real-time videos containing the images in **a** and **b** can be seen in **Supplementary Video 1a** and **1b**, respectively.

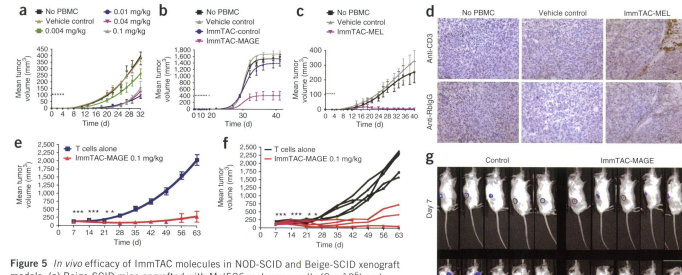

Figure 5 *In vivo* efficacy of ImmTAC molecules in NOD-SCID and Beige-SCID xenograft models. (**a**) Beige-SCID mice engrafted with Mel526 melanoma cells (2×10^6) and PBMCs (5×10^6) were treated with ImmTAC-gp100 at the doses indicated in the key according to the schedule depicted by the asterisks. As controls, Mel526 cells were engrafted without (black squares) or with (brown triangles) PBMCs and mice were dosed with vehicle (PBS). $N = 8$ mice per group. At doses of 0.1, 0.04 and 0.01 mg/kg, the differences between groups compared to controls were highly significant from day 8 to day 25 ($P < 0.001$ at all time points, Mann-Whitney U-test) and remained significant through day 32. (**b**) NOD-SCID mice engrafted with A375 melanoma cells (2.5×10^6) and PBMCs (2.5×10^6) were treated with ImmTAC-MAGE at 0.01 mg/kg (purple inverted triangles) or control ImmTAC at 0.01 mg/kg (blue circles) according to the schedule depicted by the asterisks. As controls, A375 cells were engrafted without (black squares) or with (gray triangles) PBMCs and mice were dosed with vehicle (PBS). $N = 12$ mice per group. Differences between the ImmTAC-MAGE group and the controls were highly significant at all time points from day 22 to day 41 ($P < 0.001$, Mann-Whitney U-test). (**c**) NOD-SCID mice engrafted with Mel526 melanoma cells (1×10^6) and PBMCs (1×10^6) were treated with ImmTAC-MEL at 0.04 mg/kg (purple inverted triangles) according to the schedule depicted by the asterisks. As controls, Mel526 cells were engrafted without (black squares) or with (gray triangles) PBMCs and mice were dosed with vehicle (PBS). $N = 8$ mice per group. Differences between the ImmTAC-MEL group and the controls were significant at all time points from day 24 to day 40 ($P < 0.05$, Mann-Whitney U-test). (**d**) Representative immunohistochemistry staining of Mel526 xenograft tumors from the experiments shown in **c** after day 40. Rabbit mAbs specific for CD3 (anti-CD3, top) or immunoglobulin G (IgG) (anti-RbIgG, bottom) as a control were used. (**e**–**g**) IL-2Rγc^{null} NOD-SCID mice implanted with OV79 cells engineered to express luciferase, then injected with 1×10^7 freshly expanded CD3$^+$ cells after 7 d, were treated with ImmTAC-MAGE at 0.1 mg/kg according to the schedule depicted by the asterisks. Untreated mice were used as controls. $N = 5$ mice per group. (**e**) Serial tumor volume measurements in the control untreated (blue squares) and ImmTAC-MAGE–treated (red triangles) groups. Differences between the ImmTAC-MAGE group and the controls were highly significant from day 28 to day 42 ($P < 0.01$, Mann-Whitney U-test) and remained significant through day 63 ($P < 0.05$, Mann-Whitney U-test). (**f**) Serial tumor volume measurements in individual control untreated (black) and ImmTAC-MAGE–treated (red) mice. The tumor volume measurements in **e** and **f** corresponded with the calculated photon flux measurements (data not shown). (**g**) Imaging data from control untreated (left) and ImmTAC-MAGE–treated (right) mice at day 7 (top) and day 42 (bottom). Control untreated mice were euthanized at day 63 because of tumor burden; ImmTAC-MAGE–treated mice survived considerably longer, with one mouse apparently being cured of tumors at day 90 after implantation (data not shown). Data are means ± s.e.m.

clone (176.c4.1) specific for a BRLF1 epitope derived from Epstein-Barr virus (EBV); melanoma cells were not killed by this clone because they do not present the cognate antigen (**Fig. 3b**). Notably, the EC_{50} values at all of the E:T ratios used in these experiments were similar (2–14 pM). Furthermore, the levels of lysis that we observed at the lower E:T ratios indicate that a single CD8$^+$ T cell must be capable of serially killing several target cells over a period of 24 h in the presence of an ImmTAC reagent.

To extend our experiments to nonclonal systems, we examined the ability of ImmTAC-gp100 to redirect the lytic activity of unstimulated purified CD8$^+$ T cells against various melanoma tumor cell lines expressing <70 copies of the HLA-A*0201–restricted gp100$_{280–288}$ epitope per cell (**Fig. 3c**). The resulting dose-response curves varied according to the tumor cell lines used, but the EC_{50} values in the experiments using Mel526 or Mel624 cells were 50 pM or less. Control A375 cells, which express HLA-A*0201 but not gp100, were not killed. The MAGE-A3–specific ImmTAC (ImmTAC-MAGE) displayed similar potency and specificity, inducing the killing of A375 melanoma cells (MAGE-A3$^+$, HLA-A*0101$^+$) with an EC_{50} value of 0.5 pM; in the presence of Mel526 cells, which do not express HLA-A*0101, ImmTAC-MAGE was inert, even at the highest concentrations used (**Fig. 3d**).

In experiments conducted with PBMCs isolated directly *ex vivo*, ImmTAC reagents induced specific lysis in a dose-dependent manner (**Fig. 3e,f**). Furthermore, PBMCs were effectively redirected *ex vivo* to lyse tumor cells in dose titrations of ImmTAC-gp100 and the NY-ESO-1–specific ImmTAC (ImmTAC-NYE) (**Fig. 3g,h**). We then used real-time imaging to visualize tumor cell lysis (**Fig. 4a**). Over a period of 20 h, Mel624 cells (gp100$^+$, HLA-A*0201$^+$) were targeted by T cells within the PBMC population and killed in the presence of ImmTAC-gp100, as shown by their altered morphology; in contrast, SK-MEL-28 cells (gp100$^+$, HLA-A*0201$^-$) maintained a healthy morphology in these conditions. Thus, ImmTACs are highly potent and specific in the direct *ex vivo* setting, enabling the effective antigen-dependent lysis of tumor cells with no detectable background reactivity in the presence of PBMCs presenting physiological levels of self-antigens across a range of cell lineages.

To extend these observations, we studied the ability of individual CD8$^+$ T cells to kill multiple targets in the presence of

ImmTAC-gp100. Representative data are shown in **Figure 4b**, which illustrates a single EBV-specific $CD8^+$ T cell (clone 176.c4.1) killing three Mel624 cells over a period of 5.5 h. These data confirm that ImmTAC reagents can induce serial killing, a feature that might contribute to their potency.

ImmTACs control tumor growth *in vivo*

To determine whether ImmTAC reagents could affect tumor growth *in vivo*, we used a xenograft model in which we engrafted nonobese diabetic severe combined immunodeficient (NOD-SCID) or Beige-SCID mice subcutaneously with tumor cells (Mel526 or A375) and unstimulated PBMCs. In a dose-response study, we treated the mice intravenously with ImmTAC-gp100 1 h after engraftment and then every 24 h for the next 4 d; the dosage of ImmTAC-gp100 in these experiments was 0.1, 0.04, 0.01 or 0.004 mg per kg body weight (mg/kg). All four doses of ImmTAC-gp100 in this schedule inhibited tumor growth over the study period of 32 d, with the highest doses (0.1, 0.04 and 0.01 mg/kg) resulting in significant reductions in tumor size compared to the control groups, which lacked either PBMCs or the ImmTAC reagent (**Fig. 5a**). There was no detectable inhibition of tumor growth in the absence of ImmTAC-gp100.

In a second study using the same system, we administered ImmTAC-MAGE at a dose of 0.01 mg/kg 1 h after engraftment; we then administered nine further doses on alternate days. As a control, we used an irrelevant ImmTAC in an identical parallel dosing schedule (**Fig. 5b**). Over the 42 d of the study period, ImmTAC-MAGE significantly inhibited tumor growth; in contrast, the irrelevant ImmTAC was unable to inhibit tumor growth compared to the vehicle-treated control mice. These results confirm that the CD3-specific scFv portion of the ImmTAC reagents does not exert any detectable anti-tumor effect in the absence of specific target-cell binding and show that ImmTACs must bind both effector and target cells together to be effective.

In a third study, we engrafted mice as described above and administered the Melan-A/MART-1–specific ImmTAC (ImmTAC-MEL), which completely inhibited tumor growth over a period of 40 d at a dose of 0.04 mg/kg administered 1 h after engraftment and then every 24 h for an additional 4 d (**Fig. 5c**). In addition, immunohistochemistry studies revealed the presence of $CD3^+$ cells in and around the vasculature of the tumors in the mice treated with ImmTAC-MEL; this was not apparent in the vehicle-treated control mice (**Fig. 5d**).

To determine whether ImmTACs could localize to the site of established tumors and mediate their regression *in vivo*, we used NOD-SCID mice lacking the IL-2 γc receptor ($IL\text{-}2R\gamma c^{null}$) implanted with OV79 cells (MAGE-A3$^+$, HLA-A*01$^+$) engineered to express luciferase. In this model, eight doses (0.1 mg/kg) of ImmTAC-MAGE administered intravenously (i.v.) after the transfer of expanded $CD3^+$ cells significantly delayed tumor growth and improved survival in all recipient mice compared to untreated controls (**Fig. 5e–g**). Further, tumor regression was apparent in two out of five mice treated with ImmTAC-MAGE.

DISCUSSION

T cells monitor intracellular events throughout the body by scanning peptide fragments that are presented on cell surfaces by MHC molecules. These peptides are generated by proteolysis within the cell and represent an abbreviated code that serves as a display mechanism for cellular activity. T cells survey and decode this array of peptides through a highly diverse repertoire of antigen receptors (TCRs) generated on a common immunoglobulin superfamily scaffold. The human T cell repertoire is selected at an early age, and, unlike antibodies, TCRs cannot undergo additional affinity maturation. Further, in the process of TCR selection, the immune system must strike a precarious balance between the dangers of failing to detect abnormal cells and the potentially devastating consequences of releasing self-reactive T cells into the periphery. The resultant T cell repertoire, comprising approximately 25 million distinct TCRs[30], is a compromise that often fails to detect and effectively eliminate malignant cells.

Here we developed new reagents (ImmTACs) that can overcome the limitations of natural TCR-mediated recognition and redirect the full arsenal of T cell effector functions to kill tumors expressing even very low epitope numbers on their cell surfaces. We produced four such ImmTACs, each comprising a humanized CD3-specific scFv fused to a high-affinity mTCR specific for a tumor-associated pMHCI antigen, to couple enhanced epitope targeting with potent T cell activation. The following salient features emerged: (i) ImmTACs activate $CD8^+$ T cells in a dose-dependent manner at cellular EC_{50} values in the low picomolar range, consistent with the K_D values of the corresponding monomeric mTCR-pMHCI interactions; (ii) the potency of ImmTAC-mediated $CD8^+$ T cell activation is a function of mTCR-pMHCI affinity; (iii) polyclonal $CD8^+$ T cell activation triggered by ImmTACs elicits a polyfunctional response that includes cytokine production and lytic activity; (iv) target lysis is specific and is limited to cells that express cognate pMHCI molecules; and (v) ImmTACs display *in vivo* efficacy in mouse tumor models that is associated with the localization of T cells to the tumor site and improved survival.

The majority of tumor-associated pMHCI antigens *in vivo* are likely to be presented at low densities on the cell surface. Indeed, we have previously used soluble high-affinity mTCRs to quantify the number of cognate antigens expressed on the surfaces of tumor cells; using this approach, we showed that individual melanoma and myeloma cells present an average of 10–50 copies of the NY-ESO-$1_{157-165}$ epitope per cell[27]. In addition, we have determined that other tumor-associated peptide antigens in association with their restricting MHCI molecules are similarly presented at extremely low levels on the surfaces of melanoma cells, averaging 20–70 copies per cell for both gp$100_{280-288}$ and MAGE-$A3_{168-176}$, and 60–150 copies per cell for Melan-A/MART-1_{26-35} (unpublished data). Furthermore, $CD8^+$ T cells require at least oligovalent engagement for full activation to occur[31]. Given these considerations, we designed ImmTAC molecules based on high-affinity mTCRs to enable the accurate and specific targeting of low-density pMHCI ligands, with the presentation of the activating moiety effectively tethered to the target cell surface in a stable form. The observation that mTCRs are not internalized when bound (data not shown) was integral to the success of this strategy, as was the selection of CD3-specific scFv as the activating moiety, which possesses two crucial features: (i) it activates $CD8^+$ T cells in a polyclonal manner regardless of primary specificity; and (ii) it binds CD3 with an affinity that is several orders of magnitude lower than the mTCR-pMHCI interaction, thereby preventing loss of specific targeting as a result of decoy binding. In addition, this approach exploits both the natural antigen presentation pathway that uses peptide fragments to flag intracellular events and the natural receptor structures that have evolved to recognize such pMHCI antigens, thereby enabling an exquisite degree of specificity. The resulting ImmTAC molecules were able to induce the lysis of tumor cell lines presenting naturally processed epitopes on the cell surface and, in peptide titration experiments, were capable of activating $CD8^+$ T cells in the presence of pMHCI densities as low as 2–10 copies per cell.

We established the efficacy of ImmTACs *in vivo* by showing that these reagents inhibited the outgrowth of xenograft tumors in NOD-SCID and Beige-SCID mouse models. This effect extended to established tumors, even leading to tumor regression in some cases. The dosing regimens we used were based on the therapeutic window derived from *in vitro* experiments (0.1–1 nM). We observed tumor growth inhibition at doses as low as 0.004 mg/kg, with maximal efficacy occurring at doses in the range of 0.04–0.1 mg/kg. Notably, immunohistochemistry studies revealed specific ImmTAC-mediated accumulation of $CD3^+$ cells at tumor sites; this site-specific localization was apparent at the end of the study periods, thereby revealing a persistent effect that is compatible with ongoing immune activity many days after the final administration of the ImmTAC reagent. Considering the observation that ImmTACs induce polyfunctional $CD8^+$ T cell responses comprising both lytic activity and the production of soluble factors, it is tempting to speculate that the initial redirection event acts as a catalyst that precipitates the recruitment of additional immune effectors to the tumor site[32]. Subsequent amplification of the response through epitope spreading and ImmTAC-mediated activation of $CD4^+$ T cells could then serve to generate a self-sustaining tumor-specific immune reactivity, potentially minimizing the necessity for prolonged dosing schedules. However, the precise cellular composition of the ImmTAC-associated tumor infiltrates remains to be fully elucidated, and a more direct role for $CD4^+$ T cell subsets is highly plausible[33].

Immunotherapeutic anti-cancer strategies that rely on the naturally available T cell repertoire have previously been used with limited success. For example, although some patients with late-stage melanoma have shown responses to the adoptive transfer of expanded, autologous tumor-infiltrating T cells, response rates to this form of therapy are generally disappointing and unpredictable[34]. Similarly, although some clinical benefits have been observed with vaccination-based anti-cancer approaches, it has been difficult to elicit definitive reductions in tumor burden[35]. More recently, gene-transfer studies with modified TCRs have been undertaken in an attempt to circumvent the restrictions of the naturally available autologous T cell repertoire. In such studies, autologous T cells transduced with affinity-enhanced TCRs specific for tumor-associated antigens were adoptively transferred into patients with melanoma; 30% of the patients transfused with these human TCRs experienced objective cancer regression[36]. Here we developed and validated a new class of TCR-based immunotherapeutics, termed ImmTACs, that harness the power of picomolar-affinity mTCRs to circumvent the limitations of the natural TCR repertoire in the face of malignant processes. These reagents are potent, highly specific and show *in vivo* activity against cancer. Two features of these reagents are particularly remarkable: (i) ImmTACs target cells presenting less than 50 epitopes, which extends the boundaries of therapeutic protein engineering; and (ii) the anticipated dose of any given ImmTAC for use in humans will be less than 10 mg. Furthermore, in contrast to cell-based therapies that require extensive *ex vivo* lymphocyte manipulations on an individual basis, ImmTACs can be formulated as 'off-the-shelf' drugs for administration following defined dosing schedules to any patient with the relevant *HLA* allele and an antigen-positive tumor. Based on these favorable characteristics, ImmTACs have now entered early phase clinical trials.

METHODS

Methods and any associated references are available in the online version of the paper.

Note: Supplementary information is available in the online version of the paper.

ACKNOWLEDGMENTS

We would like to thank Sanofi Pasteur for funding affinity maturation of the gp100 and MAGE-A3 mTCRs; C. Yee (Fred Hutchinson Cancer Research Centre, Seattle, Washington, USA), P. Coulie (University of Louvain, Brussels, Belgium) and V. Cerundolo (Weatherall Institute of Molecular Medicine, University of Oxford, UK) for providing T cell clones; Southern Research and Cellvax for conducting mouse xenograft experiments; Southern Research for immunohistochemistry staining; R. Liu for assistance with mouse imaging and tumor measurements; K. Haines (Translational and Correlative Studies Laboratory, University of Pennsylvania School of Medicine, Philadelphia, Pennsylvania, USA) for technical support; and A. Secreto, C. Keefer and G. Danet-Desnoyers (Stem Cell and Xenograft Core, University of Pennsylvania School of Medicine, Philadelphia, Pennsylvania, USA) for assistance with the established tumor xenograft studies.

AUTHOR CONTRIBUTIONS

N.L., N.E.H., P.E.M. and E.G. isolated wild-type mTCRs and carried out the phage display process under the supervision of Y.L.; A.V. and Y.L. were involved in ImmTAC construct optimization; T.M.M., J.G., A.V., E.E.B., N.J.P., N.M.L. and B.J.C. were involved in protein production and biochemical testing; G.B., K.J.A., A.L., N.J.H., K.L., S.J.P., J.V.H. and R.E.D. performed *in vitro* experiments under the supervision of D.D.W., R.A., D.H.S., A.K.S. and D.A.P. Large-scale production, stability testing, quality control and biochemical testing of ImmTACs was conducted by F.C.B., M.S., A.J., E.E.B., P.T.T. and S.M.D. under the supervision of Y.M. Mouse xenograft experiments were designed, coordinated and conducted by G.P., C.H.J., M.K. and D.D.W. Data analysis and interpretation were performed by D.H.S. and D.A.P.; D.H.S. and D.A.P. wrote the paper. B.K.J. conceived the idea and directed the project. All authors contributed to discussions.

COMPETING FINANCIAL INTERESTS

The authors declare competing financial interests: details are available in the online version of the paper.

Published online at http://www.nature.com/doifinder/10.1038/nm.2764.
Reprints and permissions information is available online at http://www.nature.com/reprints/index.html.

1. Köhler, G. & Milstein, C. Continuous cultures of fused cells secreting antibody of predefined specificity. *Nature* **256**, 495–497 (1975).
2. Isaacs, J.D. *et al.* Humanised monoclonal antibody therapy for rheumatoid arthritis. *Lancet* **340**, 748–752 (1992).
3. Maynard, J. & Georgiou, G. Antibody engineering. *Annu. Rev. Biomed. Eng.* **2**, 339–376 (2000).
4. Kufer, P., Lutterbuse, R. & Baeuerle, P.A. A revival of bispecific antibodies. *Trends Biotechnol.* **22**, 238–244 (2004).
5. Clynes, R.A., Towers, T.L., Presta, L.G. & Ravetch, J.V. Inhibitory Fc receptors modulate *in vivo* cytoxicity against tumor targets. *Nat. Med.* **6**, 443–446 (2000).
6. Cartron, G. *et al.* Therapeutic activity of humanized anti-CD20 monoclonal antibody and polymorphism in IgG Fc receptor $Fc\gamma RIIIa$ gene. *Blood* **99**, 754–758 (2002).
7. von Mehren, M., Adams, G.P. & Weiner, L.M. Monoclonal antibody therapy for cancer. *Annu. Rev. Med.* **54**, 343–369 (2003).
8. Withoff, S., Helfrich, W., de Leij, L.F. & Molema, G. Bi-specific antibody therapy for the treatment of cancer. *Curr. Opin. Mol. Ther.* **3**, 53–62 (2001).
9. Bargou, R. *et al.* Tumor regression in cancer patients by very low doses of a T cell–engaging antibody. *Science* **321**, 974–977 (2008).
10. Baeuerle, P.A., Kufer, P. & Bargou, R. BiTE: teaching antibodies to engage T-cells for cancer therapy. *Curr. Opin. Mol. Ther.* **11**, 22–30 (2009).
11. Kiewe, P. *et al.* Phase I trial of the trifunctional anti-HER2 x anti-CD3 antibody ertumaxomab in metastatic breast cancer. *Clin. Cancer Res.* **12**, 3085–3091 (2006).
12. Sebastian, M. *et al.* Treatment of malignant pleural effusion with the trifunctional antibody catumaxomab (Removab) (anti-EpCAM x anti-CD3): results of a phase 1/2 study. *J. Immunother.* **32**, 195–202 (2009).
13. Cole, D.K. *et al.* Human TCR-binding affinity is governed by MHC class restriction. *J. Immunol.* **178**, 5727–5734 (2007).
14. Boulter, J.M. *et al.* Stable, soluble T-cell receptor molecules for crystallization and therapeutics. *Protein Eng.* **16**, 707–711 (2003).
15. Li, Y. *et al.* Directed evolution of human T-cell receptors with picomolar affinities by phage display. *Nat. Biotechnol.* **23**, 349–354 (2005).
16. Holler, P.D. *et al. In vitro* evolution of a T cell receptor with high affinity for peptide/MHC. *Proc. Natl. Acad. Sci. USA* **97**, 5387–5392 (2000).
17. Chlewicki, L.K., Holler, P.D., Monti, B.C., Clutter, M.R. & Kranz, D.M. High-affinity, peptide-specific T cell receptors can be generated by mutations in CDR1, CDR2 or CDR3. *J. Mol. Biol.* **346**, 223–239 (2005).

18. Adema, G.J. *et al.* Melanocyte lineage-specific antigens recognized by monoclonal antibodies NKI-beteb, HMB-50, and HMB-45 are encoded by a single cDNA. *Am. J. Pathol.* **143**, 1579–1585 (1993).
19. Gaugler, B. *et al.* Human gene MAGE-3 codes for an antigen recognized on a melanoma by autologous cytolytic T lymphocytes. *J. Exp. Med.* **179**, 921–930 (1994).
20. Coulie, P.G. *et al.* A new gene coding for a differentiation antigen recognized by autologous cytolytic T lymphocytes on HLA-A2 melanomas. *J. Exp. Med.* **180**, 35–42 (1994).
21. Kawakami, Y. *et al.* Cloning of the gene coding for a shared human melanoma antigen recognized by autologous T cells infiltrating into tumor. *Proc. Natl. Acad. Sci. USA* **91**, 3515–3519 (1994).
22. Chen, Y.T. *et al.* A testicular antigen aberrantly expressed in human cancers detected by autologous antibody screening. *Proc. Natl. Acad. Sci. USA* **94**, 1914–1918 (1997).
23. Cox, A.L. *et al.* Identification of a peptide recognized by five melanoma-specific human cytotoxic T cell lines. *Science* **264**, 716–719 (1994).
24. Celis, E. *et al.* Induction of anti-tumor cytotoxic T lymphocytes in normal humans using primary cultures and synthetic peptide epitopes. *Proc. Natl. Acad. Sci. USA* **91**, 2105–2109 (1994).
25. Kawakami, Y. *et al.* Identification of the immunodominant peptides of the MART-1 human melanoma antigen recognized by the majority of HLA-A2–restricted tumor infiltrating lymphocytes. *J. Exp. Med.* **180**, 347–352 (1994).
26. Jäger, E. *et al.* Simultaneous humoral and cellular immune response against cancer-testis antigen NY-ESO-1: definition of human histocompatibility leukocyte antigen (HLA)-A2–binding peptide epitopes. *J. Exp. Med.* **187**, 265–270 (1998).
27. Purbhoo, M.A. *et al.* Quantifying and imaging NY-ESO-1/LAGE-1–derived epitopes on tumor cells using high affinity T cell receptors. *J. Immunol.* **176**, 7308–7316 (2006).
28. Chattopadhyay, P.K. *et al.* The cytolytic enzymes granyzme A, granzyme B, and perforin: expression patterns, cell distribution, and their relationship to cell maturity and bright CD57 expression. *J. Leukoc. Biol.* **85**, 88–97 (2009).
29. Schietinger, A., Philip, M., Liu, R.B., Schreiber, K. & Schreiber, H. Bystander killing of cancer requires the cooperation of CD4$^+$ and CD8$^+$ T cells during the effector phase. *J. Exp. Med.* **207**, 2469–2477 (2010).
30. Arstila, T.P. *et al.* A direct estimate of the human αβ T cell receptor diversity. *Science* **286**, 958–961 (1999).
31. Purbhoo, M.A., Irvine, D.J., Huppa, J.B. & Davis, M.M. T cell killing does not require the formation of a stable mature immunological synapse. *Nat. Immunol.* **5**, 524–530 (2004).
32. Price, D.A., Klenerman, P., Booth, B.L., Phillips, R.E. & Sewell, A.K. Cytotoxic T lymphocytes, chemokines and antiviral immunity. *Immunol. Today* **20**, 212–216 (1999).
33. Quezada, S.A. *et al.* Tumor-reactive CD4$^+$ T cells develop cytotoxic activity and eradicate large established melanoma after transfer into lymphopenic hosts. *J. Exp. Med.* **207**, 637–650 (2010).
34. Rosenberg, S.A. & Dudley, M.E. Adoptive cell therapy for the treatment of patients with metastatic melanoma. *Curr. Opin. Immunol.* **21**, 233–240 (2009).
35. Benowitz, S. Rethinking cancer vaccine trials: would new measures of success make a difference? *J. Natl. Cancer Inst.* **100**, 237–238 (2008).
36. Johnson, L.A. *et al.* Gene therapy with human and mouse T-cell receptors mediates cancer regression and targets normal tissues expressing cognate antigen. *Blood* **114**, 535–546 (2009).

fnrs
LA LIBERTÉ DE CHERCHER

Fonds Fund
InBev-Baillet Latour

FWO
VLAANDEREN
Fonds Wetenschappelijk Onderzoek
Research Foundation – Flanders

NOMINATIONS ARE INVITED

for the prestigious

InBev-BAILLET LATOUR HEALTH PRIZE

of

€250,000

(Two hundred and fifty thousand euros)

THEME FOR 2013: CANCER

Previous recipient in that field: Robert A. Weinberg, USA

Recipient 2012 (Neurosciences): Gero Miesenböck, UK

This annual award is intended to recognize outstanding scientific achievements in biomedical research for the benefit of human health and to encourage the laureate in the pursuit of his/her career. The Prize is open to scientists of all nationalities who have not received an equivalent Prize for their personal use. Exceptionally, the Prize may be shared between two persons who have collaborated over a long period. The laureate will be selected by an international Jury in February 2013.

The themes for the following years will be:
Cardiovascular Diseases, Metabolic Disorders,
Infectious Diseases and Immunology, Neurosciences.

For more information go to www.inbevbailletlatour.com (Medical research)

Deadline for nominations : September 14, 2012

Regulations and nomination forms can be obtained by e-mail from prix@frs-fnrs.be

NM224698R

a nature conference

Nature Genetics and the Wellcome Trust present:

The Genomics of Common Diseases 2012

Nature Genetics in association with the Wellcome Trust is pleased to announce the sixth annual Genomics of Common Diseases meeting, which will address the following topics across a range of common diseases: exome and whole genome sequencing, clinical and targeted sequencing, regulatory and functional genomics, cancer genomics, clinical translation and pharmacogenetics, statistical analyses of sequencing datasets, population and evolutionary genetics and infectious disease and host genetics.

September 19-22, 2012
Bolger Center, Potomac, MD, USA

KEYNOTE SPEAKERS

Thomas Hudson (Ontario Institute for Cancer Research, Canada)
Neil Risch (University of California, San Francisco, USA)
Sarah Tishkoff (University of Pennsylvania School of Medicine, USA)

SPEAKERS

Antonis Antoniou
Les Biesecker
John Blangero
Mary Carrington
Stephen Chanock
Paul de Bakker
Claire Fraser-Liggett
Manolis Kellis
Patricia Munroe
Benjamin Neale
Alkes Price
Jonathan Pritchard
Dan Roden
Nicholas Schork
Christine Seidman
Jay Shendure
Adam Siepel
Pamela Sklar
Nicole Soranzo
Shamil Sunyaev
Cisca Wijmenga
Ramnik Xavier

ORGANIZERS:

Orli Bahcall (*Nature Genetics*, USA)
Aravinda Chakravarti (Johns Hopkins University School of Medicine, USA)
Peter Donnelly (University of Oxford, UK)
Michael Dunn (Wellcome Trust, UK)
Michel Georges (University of Liège, Belgium)
Terri Manolio (National Human Genome Research Institute, National Institutes of Health, USA)
Mark McCarthy (University of Oxford, UK)
Nazneen Rahman (Institute of Cancer Research, UK)
Mary Relling (St. Jude Children's Research Hospital, USA)

For more information and to register visit:

www.nature.com/natureconferences/gcd2012

Abstract submission deadline- June 28, 2012

nature genetics

wellcome trust

nature OUTLOOK

Published in the 26 April issue of *Nature* and available free online for six months

The struggle to gain ground

The war against the malaria parasite has raged for millennia, and still claims hundreds of thousands of lives each year. Past attempts to eradicate malaria have failed. What will it take to finally subdue this deadly disease?

Access the Outlook free online for six months.
nature.com/nature/outlook/malaria_2012

Scan this tag to access the Outlook on your smartphone

Produced with support from: MMV Medicines for Malaria Venture · sigma-tau GROUP · VESTERGAARD FRANDSEN DISEASE CONTROL TEXTILES

If you would be interested in partnering with *Nature* on a similar project please contact: sponsorship@nature.com

nature publishing group npg